MOLECULAR MECHANISMS OF VOLTAGE-GATING IN ION CHANNELS

EDITED BY: Gildas Loussouarn and Mounir Tarek
PUBLISHED IN: Frontiers in Pharmacology

frontiers Research Topics

frontiers

ISSN 1664-8714
ISBN 978-2-88971-588-6
DOI 10.3389/978-2-88971-588-6

About Frontiers

Frontiers is more than just an open-access publisher of scholarly articles: it is a pioneering approach to the world of academia, radically improving the way scholarly research is managed. The grand vision of Frontiers is a world where all people have an equal opportunity to seek, share and generate knowledge. Frontiers provides immediate and permanent online open access to all its publications, but this alone is not enough to realize our grand goals.

Frontiers Journal Series

The Frontiers Journal Series is a multi-tier and interdisciplinary set of open-access, online journals, promising a paradigm shift from the current review, selection and dissemination processes in academic publishing. All Frontiers journals are driven by researchers for researchers; therefore, they constitute a service to the scholarly community. At the same time, the Frontiers Journal Series operates on a revolutionary invention, the tiered publishing system, initially addressing specific communities of scholars, and gradually climbing up to broader public understanding, thus serving the interests of the lay society, too.

Dedication to Quality

Each Frontiers article is a landmark of the highest quality, thanks to genuinely collaborative interactions between authors and review editors, who include some of the world's best academicians. Research must be certified by peers before entering a stream of knowledge that may eventually reach the public - and shape society; therefore, Frontiers only applies the most rigorous and unbiased reviews.
Frontiers revolutionizes research publishing by freely delivering the most outstanding research, evaluated with no bias from both the academic and social point of view. By applying the most advanced information technologies, Frontiers is catapulting scholarly publishing into a new generation.

What are Frontiers Research Topics?

Frontiers Research Topics are very popular trademarks of the Frontiers Journals Series: they are collections of at least ten articles, all centered on a particular subject. With their unique mix of varied contributions from Original Research to Review Articles, Frontiers Research Topics unify the most influential researchers, the latest key findings and historical advances in a hot research area! Find out more on how to host your own Frontiers Research Topic or contribute to one as an author by contacting the Frontiers Editorial Office: frontiersin.org/about/contact

MOLECULAR MECHANISMS OF VOLTAGE-GATING IN ION CHANNELS

Topic Editors:
Gildas Loussouarn, Université de Nantes, France
Mounir Tarek, Centre National de la Recherche Scientifique (CNRS), France

Citation: Loussouarn, G., Tarek, M., eds. (2021). Molecular Mechanisms of Voltage-Gating in Ion Channels. Lausanne: Frontiers Media SA.
doi: 10.3389/978-2-88971-588-6

Table of Contents

frontiers in Pharmacology

EDITORIAL
published: 15 September 2021
doi: 10.3389/fphar.2021.768153

Editorial: Molecular Mechanisms of Voltage-Gating in Ion Channels

Gildas Loussouarn[1]* *and Mounir Tarek*[2]

[1]L'Institut Du Thorax, Inserm UMR 1087/CNRS UMR 6291, Nantes, France, [2]Université de Lorraine, LPCT, CNRS UMR 7019, Nancy, France

Keywords: voltage-gated ion channel, patch - clamp technique, toxins, cryo-EM, VSD gate coupling

Editorial on the Research Topic

Molecular Mechanisms of Voltage-Gating in Ion Channels

Voltage-gated ion channels are transmembrane proteins conducting ions according to the electrochemical gradient, when opened by voltage. Hence, in these channels, at least one of the channel gates regulating the ion flux is controlled by the transmembrane potential. They are frequently ion specific and therefore selectively permeable to sodium (Na_V channels), potassium (K_V channels), calcium (Ca_V channels) or chloride (CLC channels) ions. Depending on the channels, opening of the activation gate is triggered by membrane depolarization (e.g. K_V, Na_V and Ca_V channels) or hyperpolarization (HCN channels for instance). In addition, in many voltage-gated channels, a so-called inactivation gate is also present. Compared to the activation gate, the latter is, when voltage-dependent, oppositely coupled to the potential: In K_V, Na_V and Ca_V channels, upon membrane depolarization, the inactivation gate closes whereas the activation gate opens.

Various voltage-dependent channels have been identified, depending on the excitable cell types in which they are expressed and their physiological role. They are characterized by their conductance, ion selectivity, pharmacology and voltage-sensitivity. These properties are mainly dictated by the amino-acid sequence and structure of the pore forming subunit(s), the presence of accessory subunit(s), the membrane composition and the intra- and extracellular ions concentrations. Many mutations have been identified in these channels, impacting their functions and provoking diseases named channelopathies.

In 2012, we hosted a Research Topic on the Molecular Mechanisms of Voltage Dependency (Loussouarn and Tarek, 2012), bringing together scientists to collaborate and showcase the latest developments in the field. Since this Frontiers Research Topic, the development of new approaches, such as the use of cryo-electron microscopy (cryo-EM) at the atomic scale and the original approach of split channels, to name a few, has led to a more precise understanding of the mechanisms of voltage-gating, their targeting by toxins, and also their physio-pathological implications. Given the wealth of recent electrophysiological, biochemical, optical, and structural data regarding ion channel voltage-dependence, we felt there was clearly a need for putting together a new Research Topic that would include up to date Reviews and Original Research describing molecular details of the functioning of these complex voltage-gated channels.

The review of Brewer et al. underlines how ion channel structures and models reveal critical differences in the atomic details of KCNQ1, hERG, and $Na_V1.5$ structures associated with their distinct voltage-gating and implication in Long QT syndrome, and also their pharmacological profiles. Such structural data may help defining the pathogenicity of the hundreds of variants in absence of functional data. It also mentions an important point: Molecular Dynamics represents a useful tool in refining cryo-EM structures, which are often of lower resolution in the periphery of protein core structures.

OPEN ACCESS

Edited and reviewed by:
Michael Pusch,
National Research Council (CNR), Italy

***Correspondence:**
Gildas Loussouarn
Gildas.Loussouarn@univ-nantes.fr

Specialty section:
This article was submitted to Frontiers in Pharmacology, a section of the journal Frontiers in Pharmacology of Ion Channels and Channelopathies

Received: *31 August 2021*
Accepted: *03 September 2021*
Published: *15 September 2021*

Citation:
Loussouarn G and Tarek M (2021) Editorial: Molecular Mechanisms of Voltage-Gating in Ion Channels. Front. Pharmacol. 12:768153. doi: 10.3389/fphar.2021.768153

Among the critical differences recapitulated by Brewer et al., cryo-EM was instrumental to reveal the presence of a variation in the overall organization of voltage-gated channels, which is the presence of a non-domain-swapped *vs.* a domain-swapped structure. The non-domain-swapped structure (in which the voltage sensor of subunit A leans against the pore-forming helices of subunit A, B against B, etc.) first identified in K_V10.1 channel and confirmed in hERG/K_V11.1 has a major molecular impact: it prevents the role of the S4-S5 linker as a mechanical lever, and may explain why K_V10.1 and K_V11.1 channels, when artificially split at the level this S4-S5 linker, are still voltage-gated (Barros et al.). These observations are greatly compatible with the ligand-receptor suggested by our work on K_V10.2 and K_V11.2 (Malak et al., 2019; Malak et al., 2017). It remains puzzling then that such a ligand-receptor model also applies to the domain-swapped K_V7.1 channel (Choveau et al., 2011), suggesting that key elements are still missing to understand the molecular mechanism of voltage gating.

Another article of our Research Topic also underlines the role of Structural Biology data, enriched by Molecular Dynamics, to confirm and refine the succession of electrostatic interactions of S4 residues with S1 to S3 countercharges during voltage-gated activation, and the role of voltage sensor domain (VSD) hydration in ion channel functioning (Groome and Bayless-Edwards). Importantly, some mutations of countercharges present in VSD are implicated in neural, cardiac and skeletal muscle disorders. For example, in hERG, mutation of these countercharges accelerates deactivation, slow deactivation being crucial for proper repolarization of the ventricular action potential (Shi et al.). VSD also seems to play a role in hysteresis of channel gating. Hysteresis is a property of channel gating making it dependent on its "history," resulting, for hERG, in a shifted voltage-dependence of deactivation towards hyperpolarized potentials as compared to the voltage-dependence of activation. Structural determinants of this property have been reviewed for hERG in Shi et al., suggesting a contribution of both the S4-S5 linker and the VSD to hERG gating hysteresis. Hysteresis has been more generally and very didactically reviewed in Villalba-Galea and Chiem, including physiological implications. For instance, hysteresis prevents HCN activation during the repolarization phase of the sinoatrial node action potential.

Regarding voltage-gated channel modulators targeting hydrophobic binding sites, the review of Van Theemsche et al. compiled the residues implicated in K_V channel modulation by various lipophilic molecules. Mapping them on available structural data, they suggest three lipophilic drugs/toxin binding sites, a first step toward the classification of hydrophobic binding sites in the large and complex family of K_V channels.

Finally, we are glad that our Research Topic motivated the submission of original articles. Kudaibergenova et al. compared the molecular mechanisms of ivabradine and dofetilide block of hERG channel. Li et al. correlated the clinical response to mexiletine of LQT3 patients carrying various mutation on *SCN5A* (coding for Na_V1.5), to the extent of inhibition of the late Na current by mexiletine, in cells expressing these mutated Na_V1.5 channels. Chang et al., described the off-target effect of remdesivir, an antiviral drug that was recently tested in SARS-CoV2 infected patients, on voltage-gated potassium currents present in pituitary tumor (GH3) and T lymphoblast (Jurkat) cells. Inwardly rectifying channels are not voltage-gated channels strictly speaking, but pore block by polyamines, the molecular mechanism of rectification in these channels, is a voltage-dependent process. For that reason and because tools are the same to study inwardly rectifying channels and voltage-gated channels, we also included a study that used Molecular Dynamics to get further insights on the mechanism of voltage dependent block by the polyamine putrescine (Chen et al.).

AUTHOR CONTRIBUTIONS

GL and MT wrote the manuscript.

FUNDING

GL is funded by the "Fondation d'entreprise Genavie."

REFERENCES

Choveau, F. S., Rodriguez, N., Abderemane Ali, F., Labro, A. J., Rose, T., Dahimène, S., et al. (2011). KCNQ1 Channels Voltage Dependence through a Voltage-dependent Binding of the S4-S5 Linker to the Pore Domain. *J. Biol. Chem.* 286, 707–716. doi:10.1074/jbc.M110.146324

Loussouarn, G., and Tarek, M. (2012). Mechanisms of Ion Channels Voltage-Dependency: All about Molecular Sensors, Gates, Levers, Locks, and Grease. *Front. Pharmacol.* 3, 174. doi:10.3389/fphar.2012.00174

Malak, O. A., Es-Salah-Lamoureux, Z., and Loussouarn, G. (2017). hERG S4-S5 Linker Acts as a Voltage-dependent Ligand that Binds to the Activation Gate and Locks it in a Closed State. *Sci. Rep.* 7, 113. doi:10.1038/s41598-017-00155-2

Malak, O. A., Gluhov, G. S., Grizel, A. V., Kudryashova, K. S., Sokolova, O. S., and Loussouarn, G. (2019). Voltage-dependent Activation in EAG Channels Follows a Ligand-Receptor rather Than a Mechanical-Lever Mechanism. *J. Biol. Chem.* 294, 6506–6521. doi:10.1074/jbc.RA119.007626

Conflict of Interest: The authors declare that the research was conducted in the absence of any commercial or financial relationships that could be construed as a potential conflict of interest.

frontiers in Pharmacology

REVIEW
published: 28 February 2020
doi: 10.3389/fphar.2020.00160

Roles for Countercharge in the Voltage Sensor Domain of Ion Channels

James R. Groome[1]* *and Landon Bayless-Edwards*[1,2]

[1] Department of Biological Sciences, Idaho State University, Pocatello, ID, United States, [2] Oregon Health and Sciences University School of Medicine, Portland, OR, United States

Voltage-gated ion channels share a common structure typified by peripheral, voltage sensor domains. Their S4 segments respond to alteration in membrane potential with translocation coupled to ion permeation through a central pore domain. The mechanisms of gating in these channels have been intensely studied using pioneering methods such as measurement of charge displacement across a membrane, sequencing of genes coding for voltage-gated ion channels, and the development of all-atom molecular dynamics simulations using structural information from prokaryotic and eukaryotic channel proteins. One aspect of this work has been the description of the role of conserved negative countercharges in S1, S2, and S3 transmembrane segments to promote sequential salt-bridge formation with positively charged residues in S4 segments. These interactions facilitate S4 translocation through the lipid bilayer. In this review, we describe functional and computational work investigating the role of these countercharges in S4 translocation, voltage sensor domain hydration, and in diseases resulting from countercharge mutations.

Keywords: countercharge, crystallography, electrostatic, ion channel, molecular dynamics, channelopathy, sliding helix model, voltage sensor domain

OPEN ACCESS

Edited by:
Gildas Loussouarn, Université de Nantes, France

Reviewed by:
Fredrik Elinder, Linköping University, Sweden
Leo C. T. Ng, Northwestern University, United States

***Correspondence:**
James R. Groome
groojame@isu.edu

Specialty section:
This article was submitted to Pharmacology of Ion Channels and Channelopathies, a section of the journal Frontiers in Pharmacology

Received: *22 November 2019*
Accepted: *07 February 2020*
Published: *28 February 2020*

Citation:
Groome JR and Bayless-Edwards L (2020) Roles for Countercharge in the Voltage Sensor Domain of Ion Channels. Front. Pharmacol. 11:160. doi: 10.3389/fphar.2020.00160

VOLTAGE-GATED ION CHANNELS AND ELECTRICAL EXCITABILITY

The seminal work of Hodgkin and Huxley (1952) described voltage-dependent gating particles that determine membrane permeability to sodium and potassium ions during an action potential. Their experimental work culminated in a mathematical description of the action potential based on activation gates for sodium (m) and potassium (n) ions, and an inactivation gate for sodium (h). This paradigm describing the ionic basis for the action potential has since been upheld and augmented with biophysical explanations of the molecular phenomena through which voltage-gated ion channels (VGICs) dictate membrane excitability.

The description of the structure of DNA and the discovery of the genetic code allowed molecular biology to become an integral part of research into VGIC function. Genes for ion channels and other proteins involved in electrical signaling were cloned using strategies of peptide purification from a diversity of electrically excitable tissues [reviewed by (Dolphin, 2018)], and by employing unique phenotypes of *Drosophila* mutants to generate probes for gene cloning [i.e., *Shaker* potassium channel (Papazian et al., 1987)], and *para* sodium channel [reviewed by (Papazian et al., 1988; Ganetzky, 2000)].

A striking pattern emerged in the amino acid sequences predicted from gene sequences for VGICs. Regularly spaced positively charged amino acid residues were observed within the fourth segment (S4) of hydrophobicity (Noda et al., 1984; **Figure 1**). Subsequent models of channel structure that were put forth included postulates regarding the interaction of positive and negative charges, and a helical screw mechanism of S4 translocation in channel activation (Greenblatt et al., 1985; Guy and Seetharamulu, 1986). With functional reconstitution of ion channel proteins in mammalian cells or *Xenopus* oocytes (Noda et al., 1986; Stuhmer et al., 1988; Timpe et al., 1988; Leonard et al., 1989), investigations of the structure to function relationships in VGICs focused first on the role of S4 segments in channel activation and fast inactivation (Stuhmer et al., 1989; Zagotta et al., 1989; Papazian et al., 1991). Progress in our understanding of the mechanisms of voltage-gating in ion channels has since been facilitated with advanced electrophysiological techniques, crystallography, and computational work. In this review, we examine the research efforts that describe the contributions made by negative countercharges of S1 to S3 segments to the voltage-gating of ion channels.

Homology of Voltage Sensor Domains: Positively and Negatively Charged Residues

Voltage-gated channels show considerable homology in S1–S4 segments that comprise the voltage sensor domain (VSD). Alignments for a sample of voltage-gated sodium, calcium, and potassium channel VSDs are shown in **Figure 1**. Loci of conserved negatively charged (acidic) or polar residues are observed in S1–S3 segments. These residues represent putative countercharges to conserved, positively charged residues observed in the S4 segment.

An extensive analysis of VSDs from over 6,500 sequence alignments across taxa (**Figure 2A**; Palovcak et al., 2014) highlights the conservation of acidic or polar charges in S1–S3, positive charges in S4, and the degree of sequence identity. **Figure 2B** shows the location of conserved countercharges in relation to a central hydrophobic constriction site (HCS) that separates the outer and inner vestibules of the VSD. Countercharges above the HCS are located in an extracellular negatively charged region (ENC), with those nearer to the cytoplasmic region located in the intracellular negatively charged region (INC). Also shown is a conserved S2 aromatic residue located in a putative, gating charge transfer center (GCTC); this aromatic residue may act as a steric barrier to S4 translocation (Tao et al., 2010; Schwaiger et al., 2013). Current models of that S4 movement postulate that S4 arginine residues pass through an aqueous gating pore in the HCS region of the VSD [reviewed by (Groome et al., 2018)]. Side chains of S1–S3 countercharges face toward the guanidyl groups of the conserved S4 arginine residues (**Figure 2C**). The high degree of conservation of countercharge residues suggests that they play an important role or roles in channel function. Interactions of

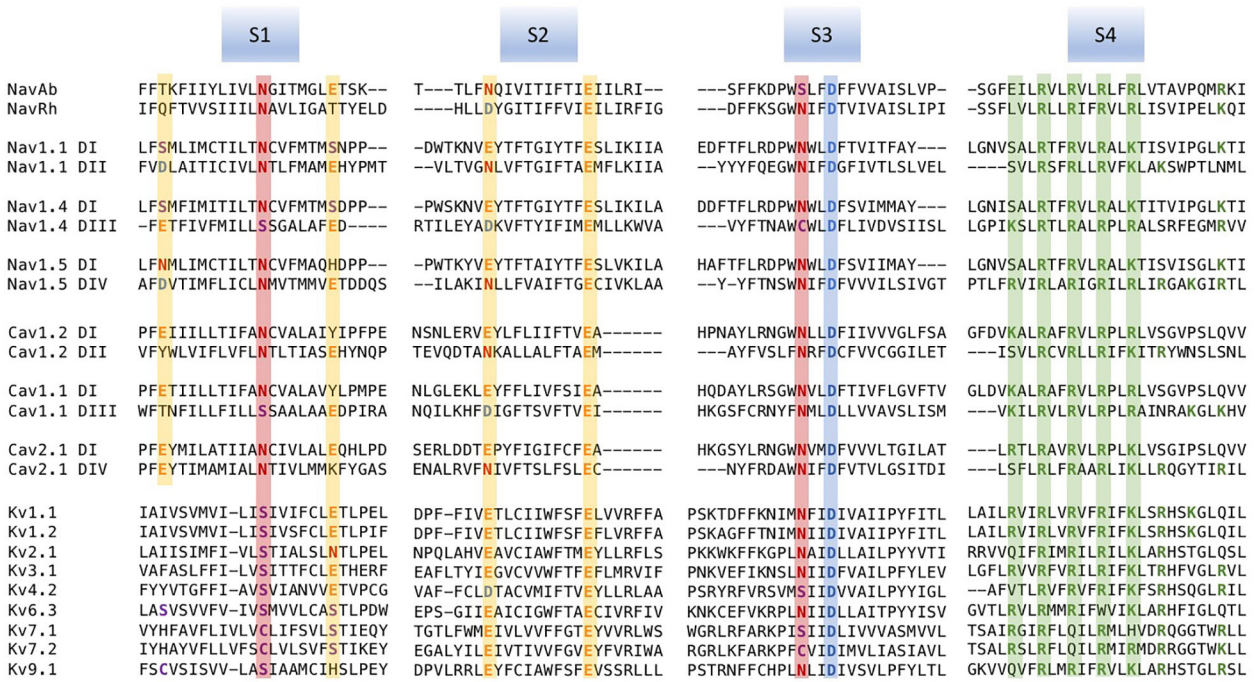

FIGURE 1 | Multiple sequence alignments of voltage sensor domains (VSDs) (S1–S4) from a sample of voltage-gated ion channel (VGIC) alpha subunit domains. Prokaryotic sodium channels are Na_vAb from *Arcobacter butzleri* (Payandeh et al., 2011), and the NaChBac orthologue Na_vRh from *alpha proteobacterium* (Zhang et al., 2012). The remaining sequences are human. For each alignment, putative consensus negative charge regions are highlighted with boxes colored according to frequently observed residues (glutamate, yellow; asparagine, red; aspartate, blue). The first five positively charged residues in S4 are shown in green.

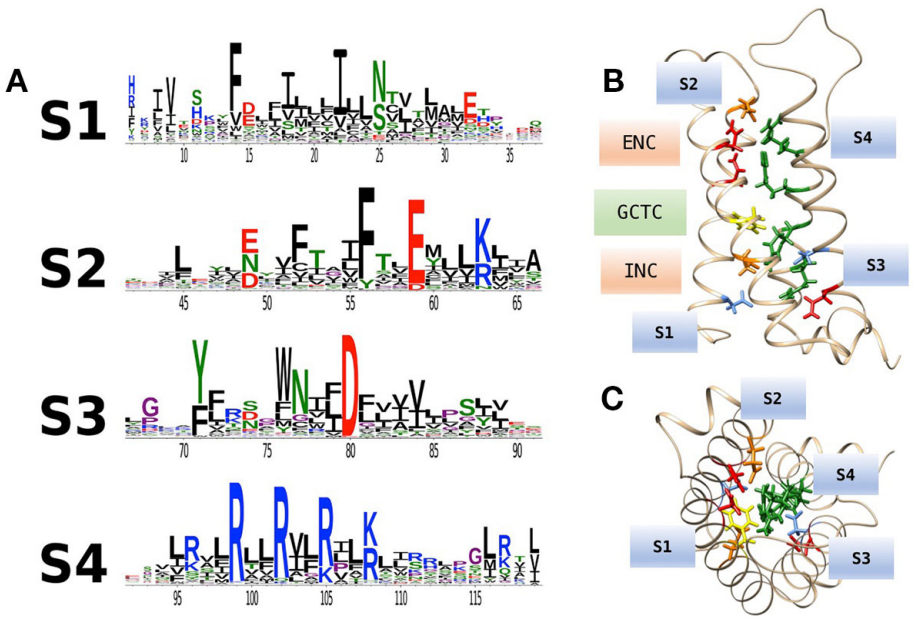

FIGURE 2 | (A) Conservation of amino acid residues in voltage sensor domains (VSDs) across taxa, highlighting the evolutionary conservation of polar or acidic residues in S1–S3 (putative countercharges), positively charged arginine or lysine residues in S4, and conserved aromatic residues. With permission from J. Gen. Physiol. and first author (Palovcak et al., 2014). **(B)** Homology model of hNa$_v$1.4 domain IV VSD based on prokaryotic structural information [3RVY.pdb, (Payandeh et al., 2011)] showing locations of consensus S1–S3 countercharges in the extracellular negatively charged (ENC) and intracellular negatively charged (INC) regions. A conserved aromatic in S2 (yellow) is also shown as part of the gating charge transfer center (GCTC). **(C)** Top view of the VSD showing side chains of S1–S3 countercharges facing the S4 arginine guanidyl groups.

these countercharges with S4 residues have been investigated in a set of functional experiments described below, that support roles for countercharges in protein folding and S4 translocation.

VSD S1–S3 Negative Charges Contribute to Voltage-Gating: Functional Studies

Experiments to describe gating charge movements associated with sodium channel function in the squid giant axon (Armstrong and Bezanilla, 1973; Armstrong and Bezanilla, 1977) were followed by characterization of gating charge movement in *Shaker* potassium channels (Perozo et al., 1992; Perozo et al., 1994; Bezanilla et al., 1994). The biophysical basis for displacement of the gating charge, and thus voltage-sensitivity, is S4 translocation in response to altered membrane potential [reviewed by (Bezanilla, 2000; Bezanilla, 2018)]. Investigations of the role of the S4 segment as the voltage sensor have employed mutagenesis including mutant cycle analysis, toxins to trap resting or activated states, thiosulfonate reagents to determine S4 residue accessibility, fluorescence measurements, and molecular dynamics simulations [reviewed by (Groome, 2014)]. Pertinent to this review, a series of investigations have supported the premise that sequential, salt-bridge (countercharge/S4 residue) interactions facilitate transitions from the resting to fully activated state of VGICs. Here, we describe the functional experiments that provide support for that role of countercharges in voltage-gating.

Pairwise Electrostatic Interactions of Countercharges and S4 Residues: Potassium Channels

Countercharge residues that interact with S4 arginines were first identified in potassium channels [**Table 1**, and reviewed by (Fedida and Hesketh, 2001; Papazian et al., 2002; Kuang et al., 2015)]. In a series of papers, Papazian and colleagues showed that electrostatic interactions between S4 residues and negative countercharges in S2 and S3 were crucial in the folding or maturation of the fully functional tetrameric *Shaker* channel (Papazian et al., 1995; Seoh et al., 1996; Tiwari-Woodruff et al., 1997; Schulteis et al., 1998). Protein maturation in *Shaker* was dependent on short-range electrostatic interactions between S2 ENC residue E283 and S4 residues R368 (R3) and R371 (R4), and between INC residues E293 (S2) and D316 (S3) and S4 residue K374 (K5).

Comparison of the effects of single (charge-reversing) *versus* double (charge-swapping) mutations reveled pairwise interactions in the functional *Shaker* channel between E283 and R368 (intermediate, closed state activation) and between E283 and R371 [open-state activation; (Tiwari-Woodruff et al., 2000)]. A closed, resting state interaction was suggested between E283 and R362 (R1) by comparing the amplitude of omega current in single and double mutations using an R1S construct (Tombola et al., 2005; Tombola et al., 2007). Studies of EAG potassium channels confirmed interactions of countercharge and S4 arginine residues during activation. Silverman et al. (2003) showed that a unique,

TABLE 1 | Specific countercharge/S4 residue interactions identified in potassium channels.

Channel	Countercharge locus	S4 locus	Experimental approach	Functional interaction	Reference
Shaker	S2 ENC (E283)	R3 (R368) R4 (R371)	Charge swapping	Folding (maturation)	Tiwari-Woodruff et al., 1997
	S2 INC (E293) S3 INC (D316)	K5 (K374)	Charge swapping	Folding (maturation)	Papazian et al., 1995 Tiwari-Woodruff et al., 1997
	S2 ENC (E283)	R3 (R368) R4 (R371)	Charge swapping	Intermediate (deactivated) state Activated state	Tiwari-Woodruff et al., 2000
	S2 ENC (E283)	R1 (R362)	Double mutations, omega current	Resting state	Tombola et al., 2005 Tombola et al., 2007
EAG	S2 ENC (D274)	R3 (R353) R4 (R356)	Ni^{2+} inhibition	Activated state	Silverman et al., 2003
hERG	S1 INC (D411)	K5 (K538)	Mutant cycle analysis	Intermediate (deactivated) state	Zhang et al., 2005 Dou et al., 2017
	S2 ENC (D456)	K1 (K525)	Mutant cycle analysis	Intermediate (deactivated) state	Zhang et al., 2005

For each channel, residues are identified in ENC (extracellular negatively charged) or INC (intracellular negatively charged) regions of S1–S3 segments, locus in S4 segment, and with interpreted role of their paired interaction.

inhibitory effect of divalent ion (Ni^{2+}) on the S2 ENC mutant D274A was reversed by pairing that mutant with R353Q (R3). Pairing D274A with R356Q (R4) did not reverse Ni^{2+} inhibition. Finally, the observation that Ni^{2+} inhibition was reversed in the triple D274A/R353Q/R356Q mutation suggested stepwise translocation of R353 and R356 to promote their interaction with D274. These results supported a two-stage model of S4 activation mediated by interaction of an S2 ENC residue with S4 arginine residues R3 and R4, as in *Shaker* channels.

In studies of human EAG channels (hERG), mutant cycle analysis showed that the S1 INC countercharge D411 and S2 ENC countercharge D456 interact with S4 residues K538 (K5) and K525 (K1), respectively, dictating early closed-state transitions (Zhang et al., 2005; Dou et al., 2017). Results using a similar approach suggested that S2 and S3 countercharges D460 and D509 may influence S4 translocation later in the activation pathway (Liu et al., 2003; Zhang et al., 2005). Taken together, results from these studies on potassium channels were consistent with a model of voltage-gating in which, from a resting conformation with R1 in the GCTC (Lin et al., 2011), sequential pairwise interactions of countercharge residues with S4 residues mediate channel activation.

Pairwise Electrostatic Interactions of Countercharges and S4 Residues: Sodium Channels

Cloning of the prokaryotic sodium channel NaChBac (Ren et al., 2001) provided an advantage to study specific electrostatic interactions in the VSD of sodium channels. Like potassium channels, functional NaChBac is comprised of a homotetramer from the channel gene coding for one domain, providing robust effect with mutagenesis and more direct interpretation of the effect of these mutations on channel function.

In studies with NaChBac, cysteine substitution of countercharge and S4 residue pairs allowed for interpretation of their putative interaction (**Table 2**). For cysteine substitutions in close proximity, disulfide bond formation resulted in loss of channel availability. A key element of these experiments was the observation that reducing agents such as beta-mercaptoethanol or TCEP (tris 2-carboxyethyl phosphine) were able to rescue channel function by breaking the disulfide linkage. For mutations in which partial loss of channel opening was observed, interactions were determined from results showing that oxidizing agents such as hydrogen peroxide more fully abolished sodium currents, and with subsequent treatment with reducing agents that restored channel function. Double-mutant

TABLE 2 | Specific countercharge/S4 residue interactions identified in NaChBac sodium channels.

Channel	Countercharge locus	S4 locus	Experimental approach	Functional interaction	Reference
NaChBac	S2 ENC (D60)	R3 (R119)	Cysteine substitution disulfide locking	Activated state	DeCaen et al., 2008
	S2 ENC (D60) S2 INC (D70)	R4 (R122)	Cysteine substitution disulfide locking	Intermediate Activated states	DeCaen et al., 2009
	S1 ENC (E43)	T0 (T110) R1 (R113)	Cysteine substitution disulfide locking	Resting state	DeCaen et al., 2011
	S1 ENC (E43)	R2 (R116) R3 (R119)	Cysteine substitution disulfide locking	Intermediate Activated states	DeCaen et al., 2011
	S2 ENC (D60)	T0 (T110)	Cysteine substitution	Resting state	Yarov-Yarovoy et al., 2012
	S1 ENC (E43)	R1 (R113) R2 (R116) R3 (R119) R4 (R122)	Mutant cycle analysis	Intermediate Activated states	
	S1 ENC (E43)	R1 (R113) R2 (R116)	Mutant cycle analysis	Resting state Activated state	Paldi and Gurevitz, 2010

Residues are identified in extracellular negatively charged (ENC) or intracellular negatively charged (INC) regions of S1–S3 segments, locus in S4 segment, and with interpreted role of their paired interaction.

cycle analysis of the free energy change required for activation was used in these experiments to corroborate interactions [for review see (Bosshard et al., 2004)].

These experiments showed that NaChBac S2 residues D60 (ENC) and D70 (INC) interact with R119 (R3) and/or R122 (R4) during activation (DeCaen et al., 2008; DeCaen et al., 2009). Subsequent studies employing disulfide locking (DeCaen et al., 2011), and/or mutant cycle analysis (Paldi and Gurevitz, 2010; Yarov-Yarovoy et al., 2012) revealed interactions between a highly conserved ENC S1 residue (E43) and S4 residues T110 (T0), R113 (R1) in the resting state, and with R116 (R2), R119 (R3), and R122 (R4) during intermediate to fully activated states of the channel. A combined set of results was compared in Rosetta models illustrating the pairwise interaction of countercharge/S4 residue interactions from resting to activated states (Yarov-Yarovoy et al., 2012), with an interpretation of VSD gating similar to that suggested by the aforementioned experiments in potassium channels.

Scanning Mutagenesis of Countercharge Mutations in Eukaryotic Channels

With the reports of crystal structures for prokaryotic sodium channels (Payandeh et al., 2011; Payandeh et al., 2012; Zhang et al., 2012) supporting the functional characterization of countercharge/S4 residue interactions in NaChBac, research attention was given to eukaryotic sodium channels. Here, both molecular dynamics simulations (Gosselin-Badaroudine et al., 2012) and scanning mutagenesis (Groome and Winston, 2013; Pless et al., 2014) probed each of the four domains of the skeletal muscle sodium channel ($Na_V1.4$) for domain-specific roles of countercharges in activation and fast inactivation. Groome and Winston (2013) found that effects on activation probability were notable for mutations in domain II, while effects on fast inactivation kinetics were characteristic in domain IV (**Figure 3**). Using unnatural amino acid substitutions to precisely target the relative impact of charge content *versus* structure for gating contributions of countercharge residues, Pless et al. (2014) showed that mutations of ENC residues in domains I and II produce effects dependent on charge, whereas the effects of INC mutations are independent of charge alteration. These results were similar to those observed for *Shaker* channel mutations at ENC *versus* INC loci (Pless et al. (2011), and these authors presented the possibility that INC charges influence S4 movement through hydration of the inner vestibule of the VSD. Clearly, the significant differences observed in the functional effects of S1 to S3 mutations across domains, or at different loci (ENC *versus* INC) should be considered in the interpretation of the role(s) of countercharges in voltage-gating.

Countercharges in Calcium and Proton Channels

Domain specific roles for voltage sensors in calcium channels have also been identified (Pantazis et al., 2014; Tuluc et al., 2016a). One source of functional variability across domains in Ca_V channels may be related to an outer countercharge observed in DIIS3 and DIVS3 segments (Coste de Bagneaux et al., 2018). In $Ca_V1.1$, aspartate D1196, identified as D4 in the extracellular region of DIVS3, interacts with DIVS4 arginines R1 and R2, albeit differentially in distinct splice variants (Tuluc et al., 2016b). Specifically, the alternative splice variant $Ca_V1.1e$ excluding 19 amino acids in the DIVS3-S4 linker enhances activation, suggesting that in $Ca_V1.1a$, the DIVS3-S4 linker disrupts D4 interaction with R1 and R2. Differential effects of DIVS3 D4 mutations in $Ca_V1.2$ and $Ca_V1.3$ are not solely dependent on the intact linker (Coste de Bagneaux et al., 2018) but also support a role for this countercharge in channel gating, and provide insight into domain-specific voltage-sensitivity in these channels.

VSD S1–S3 negative charges have roles in gating and selectivity in the voltage-gated proton channel H_V1. Countercharge/S4 residue interactions during H_V1 gating are suggested by mutant cycle

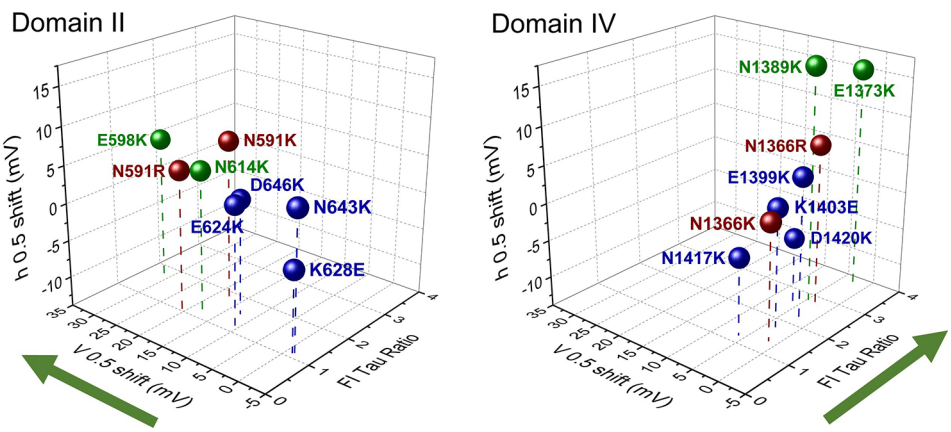

FIGURE 3 | Scanning mutagenesis of putative countercharges in domains II and IV of the skeletal muscle sodium channel $Na_V1.4$. Charge-reversing mutations in domain II decrease activation probability (indicated by shift in $V_{0.5}$), while those in domain IV slow the entry of channels into a fast-inactivated state (indicated by the ratio of time constant (tau) of mutation with respect to that of wild type, at 20 mV). These effects are consistent with the hypothesis that countercharges facilitate certain domain-specific functions highlighted by green arrows (DII activation, DIV fast inactivation). Adapted from Groome and Winston (2013). Colors indicate countercharge loci as extracellular negatively charged (ENC) (green, red), or intracellular negatively charged (INC) (blue).

analysis of the effects of single and double cysteine mutations (Chamberlain et al., 2014), and molecular dynamics simulations have defined salt-bridge interactions between countercharge and S4 residues during H_V1 activation (Gianti et al., 2016). Interestingly, mutation of negative charge D112 in S1 results in channels that are non-functional (D112V), that display a shift in permeability to anions (i.e., D112H), or that maintain proton selectivity (D112E; Musset et al., 2012). The proton selectivity function of D112 might be based on its salt-bridge formation with S4 residue R211 (Chamberlain et al., 2015; Dudev et al., 2015). D112 and other countercharges in Hv1 S1–S3 appear to facilitate proton conduction through a mechanism in which proton binding sites are comprised of three pairs of acidic countercharges, with conformational change in the VSD promoting exchange of protons between sites (van Keulen et al., 2017). Proton-mediated disruption of the cation-pi interaction of S2 aromatic residue F150 with R211 has been proposed as a key determinant in the closed to open transition of the channel, facilitating the S2 E153 to S1 D112 proton exchange across the VSD permeation pathway.

Structural Studies Illuminate Voltage Sensor Topology and Electrostatic Interactions

Following the successful crystallization of the KcSA potassium channel (Doyle et al., 1998), efforts to determine the atomic structure of VGICs intensified, and led to alternative hypotheses about the mechanism through which S4 voltage-sensing segments promote channel activation. The first full length structure of a voltage-gated potassium channel (K_VAP) was solved with crystallography at a resolution of 3.2 Å (Jiang et al., 2003). In addition, an isolated VSD was solved at a resolution of 1.9 Å and whose structure revealed a salt-bridge between the S4 residue R133 (R5) with the S2 ENC countercharge D62. Importantly, the authors hypothesized that the second helical region in S3, along with the S4 helix, formed a voltage-sensor paddle that moved through the lipid membrane in response to membrane depolarization. Crystallization of the eukaryotic potassium channel $K_V1.2$ (Long et al., 2005a; Long et al., 2005b) and the chimera $K_V1.2/2.1$ (Long et al., 2007) partially reconciled the paddle hypothesis of charge displacement with functional data that supported vertical displacement of the S4 helix [reviewed by (Horn, 2002; Gandhi and Isacoff, 2002; Elinder et al., 2007)]. As described later, structural data for K_V VSDs were utilized in molecular dynamics simulations (Delemotte et al., 2011; Jensen et al., 2012) that supported a mechanism of voltage-gating dependent on multiple salt-bridge interactions facilitating intermediate states of channel activation.

The crystal structure of the prokaryotic sodium channel Na_VAb (Payandeh et al., 2011) revealed the proximity of ENC and INC countercharges with specific S4 residues. Importantly, Kv1.2/2.1 and Na_VAb structures showed the S4 segment in nearly identical positions (Long et al., 2007; Payandeh et al., 2011), confirming the vertical position of the S4 segment in the activated state. Countercharge to S4 arginine residue interactions have been revealed with crystallographic data from Na_VAb, Na_VRh, and Na_VMs (Payandeh et al., 2011; Payandeh et al., 2012; Zhang et al., 2012; Sula et al., 2017; Wisedchaisri et al., 2019). It has also been hypothesized that negatively charged residues tune the hydrophilicity of the inner and outer vestibules of the VSD (Palovcak et al., 2014), while the central, hydrophobic region separates these vestibules and focuses the electric field (Starace and Bezanilla, 2004; Ahern and Horn, 2005; Chanda and Bezanilla, 2008; Lacroix et al., 2014).

Recently, improvements in cryo-electron microscopy (cryo-EM) have allowed for rapid advances in structure determination of large membrane proteins, including eukaryotic sodium and calcium channels. Shen et al. (2017) used cryo-EM to determine the structure of Na_VPaS, the cockroach isoform of $Na_V1.4$, at 3.8 Å. Shortly thereafter, the structure of $EeNa_V1.4$, the electric eel construct of $Na_V1.4$, was solved to 4.0 Å and in complex with the accessory β1 subunit (Yan et al., 2017). Many of the countercharge/S4 residue interactions described in the structures of prokaryotic sodium channels are reiterated in these eukaryotic structures, and in the cryo-EM structure of $Ca_V1.1$ (Wu et al., 2016). When the structure of the human $Na_V1.4$ channel/β1 subunit was solved to 3.2 Å (Pan et al., 2018), an expanded set of interactions between S1 and S3 countercharges and S4 residues was presented, and suggested a role for polar residues in stabilizing VSDs across domains. Together, these cryo-EM structures have provided a structural framework to complement functional investigations of domain-specific functions of eukaryotic VSDs (Chanda and Bezanilla, 2002; Goldschen-Ohm et al., 2013; Tuluc et al., 2016a) and of domain-specific effects of S1–S3 countercharge mutations (Groome and Winston, 2013; Pless et al., 2014).

Molecular Dynamics Simulations Bridge Structural and Functional Work

Molecular dynamics simulations have been used extensively in computational approaches to investigate ion channel function, by providing a view of time-dependent interactions within the VSD in response to applied membrane potential on the system [for reviews see (Delemotte et al., 2009; Cournia et al., 2015; Howard et al., 2018)]. These mathematical simulations solve the equations for motion in three dimensions for atoms with a defined mass and charge. As parameters such as membrane potential and amino acid sequence can be easily manipulated, these simulations allow researchers to test specific hypotheses about countercharge interactions with S4 residues, as the S4 segment vertically transverses the electric field. However, these simulations are computationally limited to short timescales, making it difficult to simulate an entire conformational transition.

Molecular dynamics simulations of VSDs conducted following the publication of voltage-gated potassium channel structures (Jiang et al., 2003; Long et al., 2005a; Long et al., 2005b; Long et al., 2007) probed the activated state of the voltage sensor. Several research groups were interested in hydration of the intracellular and extracellular vestibules, as well an interaction between the voltage sensor and surrounding lipid environment. Treptow and Tarek (2006) found that the outer S4 arginine residues are accessible to water in the activated state, and Jogini and Roux (2007) proposed that S4 arginine residues interact with both negatively charged lipid phosphate groups and S2

countercharges. While their continuum electrostatic calculations showed that the membrane potential varies greatly across the membrane, the greatest membrane potential was focused on the center of the voltage sensor, a hypothesis that has been supported functionally (Starace and Bezanilla, 2004; Ahern and Horn, 2005). Simulations of S4 dynamics in response to an applied membrane potential suggested that the S4 segment transverses the membrane in a screw-like motion (Nishizawa and Nishizawa, 2008), with salt-bridges (Treptow et al., 2009) and hydrogen bonding networks (Bjelkmar et al., 2009) stabilizing intermediate states. These simulations supported a model of vertical translocation of the S4 helix through the membrane, and groups began focusing on defining the intermediate states of the voltage sensor and interactions that occurred within each state.

Due to computational limitations, simulating each intermediate state of the VSD required biasing simulations based on initial starting structure (Yarov-Yarovoy et al., 2006; Wood et al., 2012), a directed path of S4 helix motion through the membrane (Delemotte et al., 2011; Schwaiger et al., 2011) or enhanced sampling techniques (Delemotte et al., 2015). Resting state models have been built by multiple groups. Yarov-Yarovoy et al. (2006); Pathak et al. (2007), and Henrion et al. (2012) used a *de novo* and homology modeling approach, Delemotte et al. (2011) used a combination of harmonic restraints and steered molecular dynamics, Vargas et al. (2011) computed an average structure over multiple simulations, and Jensen et al. (2012) ran a long time-scale simulation to reach a resting state structure. Although the methodologies to produce them were unique, these models showed a high degree of similarity, with the S4 helix rotated and translated inwardly, and R1 located between the S2 ENC and INC countercharges, and near the conserved S2 aromatic residue of the GCTC. A consensus model of the resting state was then proposed (Vargas et al., 2012). While simulations have suggested that the S4 segment adopts a 3_{10} helical secondary structure to favor the resting state and align S4 arginine side chains with those of negative countercharges (Villalba-Galea et al., 2008; Khalili-Araghi et al., 2010; Schow et al., 2010; Schwaiger et al., 2011), the functional contribution of 3_{10} helical structure to VGIC gating remains to be clearly elucidated (Kubota et al., 2014; Bassetto et al., 2019).

Computational approaches to VSD activation have confirmed and refined the description of intermediate states. Nishizawa and Nishizawa (2008) initially hypothesized that the free energy landscape between intermediate states would be "ragged," indicating multiple pathways of transition between states due to the large number of electrostatic interactions taking place. This hypothesis was confirmed by Delemotte et al. (2015), who characterized the transition between the resting and a partially activated state using well-tempered metadynamics. They showed that R1 must transit across the hydrophobic septum prior to the transition of R3 engaged with intracellular lipid phosphate groups, to R3 engaged with the INC S2 countercharge. Although this single most favorable pathway between a resting and intermediate state was found, their results did show a rough free energy landscape, as previously hypothesized. However, when the free energy was plotted as a function of gating charge, a smooth free energy landscape was produced, with two well-defined energy wells corresponding to the resting and intermediate states. It is important to note that the bulk of these simulations were completed using the Kv1.2 channel as a model. Thus, although many of these findings can be translated to other channel types, it is yet unknown how the differences between VSDs affect dynamics. For example, the cryo-EM structure of $hNa_V1.4$ (Pan et al., 2018) suggests unique electrostatic interactions within each VSD, and differences in the extent of voltage sensor activation across domains.

To further explore the differences in interactions between domains of $hNa_V1.4$, we have conducted a network analysis from short time-scale molecular dynamics simulations (Bayless-Edwards, 2019). **Figure 4** shows each S4 segment translocated intracellularly from an initial activated structure (Pan et al., 2018) to produce both an intermediate state and a potential resting state structure, using methods similar to those of Wood et al. (2012). gRINN (get Residue Interaction eNergies and Networks) was used to complete the network analysis (Sercinoglu and Ozbek, 2018). Our results support the presence of unique electrostatic interactions in each domain over multiple conformations. The strongest interactions are between acidic countercharges with S4 residues, consistent with other simulations (Gosselin-Badaroudine et al., 2012) and functional experiments in sodium channels (Groome and Winston, 2013; Pless et al., 2014).

Water Permeability Within and Across the Voltage Sensor Domain

Solvation of the VSD is an essential component in models of voltage-gating in which positively charged S4 arginine residues traverse the membrane through an aqueous environment (Freites and Tobias, 2015). Water permeation within the VSD is often measured by calculating either the solvent-accessible surface or the simulated average water occupancy along the z-axis of the membrane. As is expected by the hourglass shape of the VSD comprising inner and outer vestibules, water occupancy is highest at the edges of the membrane and decreases to the hydrophobic septum (Freites et al., 2006; Schow et al., 2010; Gosselin-Badaroudine et al., 2012). Chakrapani et al. (2010) used site-directed spin-labeling to quantify the hydrophilicity of outer and inner vestibules of the VSD and incorporated these environmental restraints into molecular dynamics simulations of NaChBac. Their results showed that S4 arginines R1 and R2 move through a hydrophilic environment toward their interaction with phospholipid heads of the bilayer as the S2 ENC (D60)/S4 R3 salt-bridge interaction is formed with activation of the channel. The significance of hydration in voltage-gating is further emphasized with the finding that S4 aspartate substitutions in the *Shaker* channel are remarkably tolerated with respect to gating function (Diaz-Franulic et al., 2018), and by the corollary observation that mutation of S1–S3 residues comprising the hydrophobic plug have dramatic effects on gating charge movement (Lacroix et al., 2014, and reviewed by Bezanilla, 2018).

In diseases such as hypokalemic periodic paralysis and dilated cardiomyopathy, mutation of S4 arginines can lead to

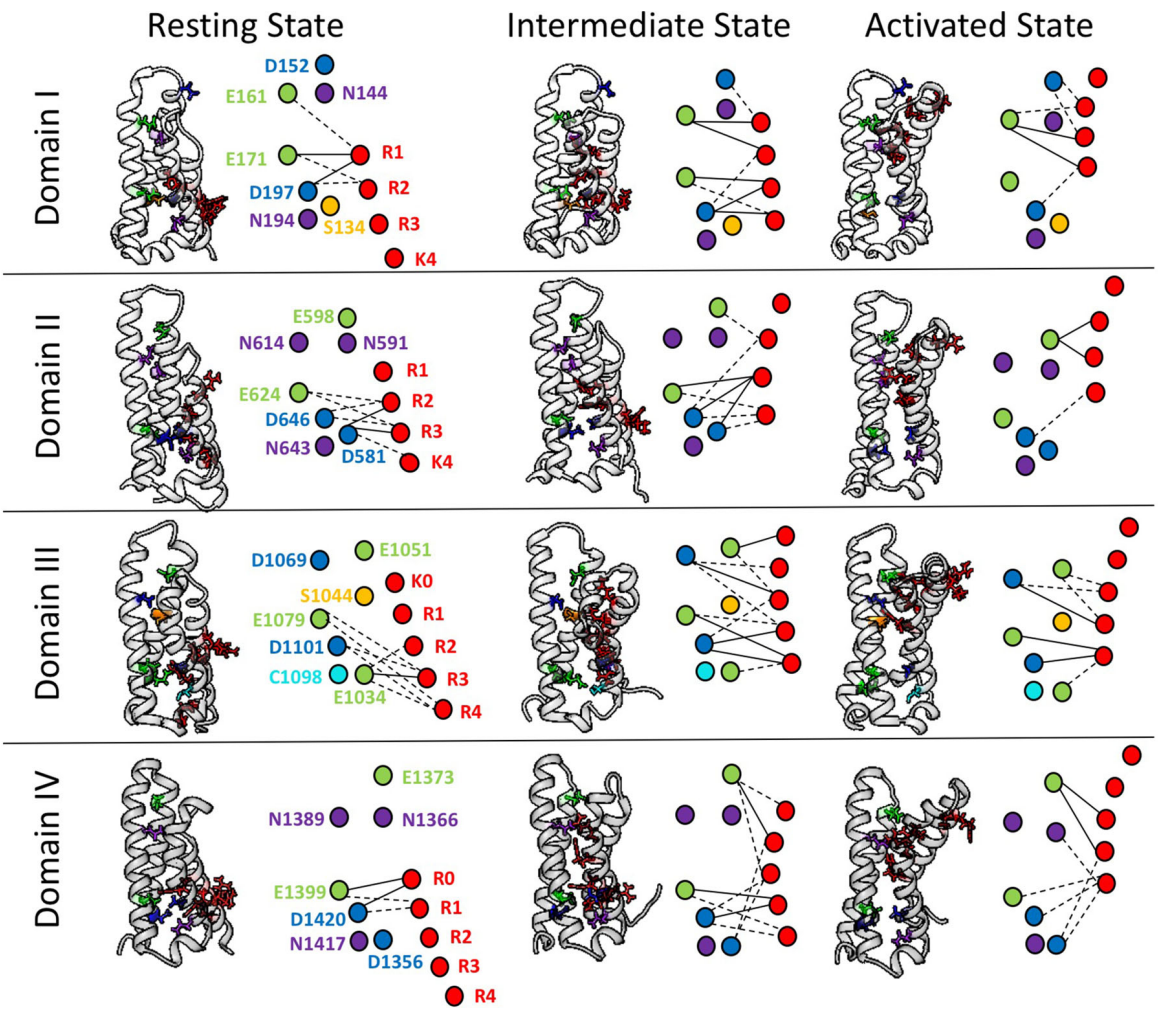

FIGURE 4 | Electrostatic interactions between countercharges (aspartate, blue; glutamate, green; asparagine, purple; serine, yellow, cysteine, cyan) and each of four to five positively charged residues in S4 segments (arginine or lysine, red) in domains I–IV of the skeletal muscle sodium channel $Na_V1.4$. Nodes indicate charged and polar residues within the voltage sensor, while edge width indicates strength of interaction. The profile of interactions is given for a presumptive resting state, intermediate closed state, and activated state. Reproduced with permission from Idaho State University Libraries (Bayless-Edwards, 2019).

permeation of protons or cations between the inner and outer vestibules of the VSD, a finding supported using both molecular dynamics simulations (Jensen et al., 2012; Monteleone et al., 2017) and cryo-EM (Jiang et al., 2018). This omega current is a characteristic effect of mutations in these diseases, and is a significant factor in pathogenesis [reviewed by Groome et al., 2018)]. Interestingly, the width of the hydrophobic region varies between sodium channel domains (Gosselin-Badaroudine et al., 2012), and the large hydrophobic septum in DIV may explain the lack of observed omega current associated with DIVS4 channelopathy mutations (Francis et al., 2011), even with periodic paralysis as a contributing element to the phenotype (Poulin et al., 2018).

It has been hypothesized that mutations near the hydrophobic septum disrupt not only steric inhibition of water molecules and ions (Jiang et al., 2018), but also hydrogen bonding (Monteleone et al., 2017; Poulin et al., 2018) and electrostatic interactions (Bayless-Edwards et al., 2018). This hypothesis is consistent with the premise that charged and polar residues play an important role in the hydration of ion channel vestibules in VSDs (Pless et al., 2011; Palovcak et al., 2014). An interesting set of questions remain as to the nature and extent of contributions of polar, countercharge residues to specific aspects of voltage-gating. For example, mutations of VSD polar residues do elicit substantial effects on channel activation, fast inactivation, and slow inactivation (Gamal El-Din et al., 2013; Groome and Winston, 2013; Pless et al., 2014; Groome et al., 2019). The domain-specific VSD conformations underlying these channel functions are an important target for investigation (Yarov-Yarovoy and DeCaen, 2019) and a

determination of the impact of hydration provided by polar countercharges in voltage-gating may provide some unique insight.

Countercharge Mutations in Disease

Inherited mutations in the genes for VGICs comprise a set of channelopathies including epilepsy and migraine syndromes, pain, cardiac arrhythmia syndromes, myotonia, periodic paralysis, and congenital myasthenia (for reviews see Catterall, 2012; Bezzina et al., 2015; Cannon, 2015). These mutations may result in a truncated protein, disrupt trafficking or assembly with accessory subunits, or produce gating defects. Channelopathy mutations have been studied in heterologous expression to characterize their biophysical impact on membrane excitability, and in transgenics to test their impact on physiology and behavior [reviewed by (Cannon, 2018; Catterall, 2018)].

A number of variants predicting VSD countercharge mutations associated with disease phenotypes have been identified, with missense mutations for these channelopathies given in **Table 3**. Noteworthy on this list are the prevalence of SCN1A mutations identified in genetic screening of patients with intractable epilepsy syndromes. These countercharge mutations have yet to be functionally characterized in heterologous expression (Brunklaus et al., 2020). However, several countercharge mutations identified in cardiac arrhythmia or skeletal muscle syndromes have been characterized, and are described here.

Functional Characterization of Countercharge Channelopathy Mutations

Channelopathy mutations identified in patients with Brugada syndrome and/or overlapping phenotypes such as dilated cardiomyopathy confer loss of function in the cardiac sodium channel $hNa_V1.5$ (SCN5A; for reviews see Garcia-Elias and Benito, 2018; Asatryan, 2019). A few of these mutations are at countercharge loci, and for which biophysical characterization has been reported. Loss of function may be explained to some extent with observed reduction in current density, as in DIS2 ENC mutation E161Q (Meregalli et al., 2009). In contrast, N1541D (DIVS1 ENC) elicits specific gating defects including enhanced probability of fast inactivation, and slowed recovery from open-state fast inactivation (Dharmawan et al., 2019). Interestingly, each of these gating defects are reiterated in the homologous $Na_V1.4$ mutation N1366D (Groome and Winston, 2013).

The SCN5A DIIIS3 INC mutation D1275N produces mild, loss of function gating defects including impaired activation and enhanced fast inactivation when studied in heterologous expression (Groenewegen et al., 2003; Hayano et al., 2017). However, D1275N promotes significant cardiac defects such as slowed conduction, heart block, atrial fibrillation, ventricular tachycardia, and dilated cardiomyopathy when inserted in transgenic mice (Watanabe et al., 2011) or zebrafish (Huttner et al., 2013). Two SCN5A channelopathy mutations have been characterized at D1595 (DIVS3 INC). First, D1595N has been linked to atrioventricular block (Wang et al., 2002). The mutation reduces current density and enhances fast and slow inactivation consistent with the cardiac

TABLE 3 | Voltage-gated ion channel (VGIC) countercharge S1–S3 mutations identified in human disease phenotypes.

Gene	S1 mutation	S2 mutation	S3 mutation	Phenotype	Reference
SCN1A			DI: N191K/Y	EIEE6	Depienne et al., 2009; Depienne et al., 2010 Huang et al., 2017
			DI: D194G/N	EIEE6	Depienne et al., 2009 Azmanov et al., 2010 Kodera et al., 2013
	DIII: E1221K			EIEE6	Zuberi et al., 2011
	DIII: S1231R/T			EIEE6	Fujiwara et al., 2003 Kearney et al., 2006
	DIII: E1238D			EIEE6	Harkin et al., 2007
		DIII: E1266A		EIEE6	Zuberi et al., 2011
			DIII: D1288N	EIEE6	Zuberi et al., 2011
	DIV: D1544A/G			EIEE6	Depienne et al., 2009 Zuberi et al., 2011
	DIV: E1561K			EIEE6	Depienne et al., 2009
			DIV: N1605I/S	EIEE6	Parrini et al., 2017 Zuberi et al., 2011
			DIV: D1608G/Y	EIEE6	Wang et al., 2012 Marini et al., 2007
SCN2A	DI: N132K			EIEE11	Matalon et al., 2014
		DI: E169G		EIEE11	Nakamura et al., 2013 Parrini et al., 2017
	DIII: E1211K			EIEE11	Ogiwara et al., 2009 Wong et al., 2015
SCN4A		DIII: D1069N		CM	Zaharieva et al., 2016
	DIV: N1366S			PMC	Ke et al., 2017
SCN5A		DI: E161K/Q		BRGDA/ PFHB	Smits et al., 2002; Smits et al., 2005 Meregalli et al., 2009 Kapplinger et al., 2010
	DIII: E1225K			BRGDA/ LQT-3	Smits et al., 2002 Tester et al., 2005
		DIII: D1243N		BRGDA	Kapplinger et al., 2010
		DIII: E1253G		BRGDA	Kapplinger et al., 2010
			DIII: D1275N	BRGDA/ AS/DCM	Groenewegen et al., 2003 Hayano et al., 2017
	DIV: N1541D			BRGDA/ AF/SND	Dharmawan et al., 2019
	DIV: E1548K			BRGDA	Kapplinger et al., 2010
		DIV: E1574K		BRGDA	Kapplinger et al., 2010
			DIV: D1595N/H	DCM/SND/ AV Block	Wang et al., 2002 McNair et al., 2004 Nguyen et al., 2008

(Continued)

TABLE 3 | Continued

Gene	S1 mutation	S2 mutation	S3 mutation	Phenotype	Reference
KCNQ1	C136F			LQT-1	Tester et al., 2005
		E160K/V		LQT-1	Splawski et al., 2000
					Tester et al., 2005
					Kapplinger et al., 2009
			S199A	LQT-1	Kapplinger et al., 2009
			D202H/N	LQT-1	Napolitano et al., 2005
					Kapplinger et al., 2009
KCNH2	T421M			LQT-2	Tester et al., 2005
					Kapplinger et al., 2009
	S428L			LQT-2	Napolitano et al., 2005
		D456Y		LQT-2	Tester et al., 2005
		D466Y		LQT-2	Kapplinger et al., 2009
			D501H/N	LQT-2	Napolitano et al., 2005
					Jongbloed et al., 2002
					Kapplinger et al., 2009
KCNA1			N225D	HM	Glaudemans et al., 2009

EIEE, early infantile epileptic encephalopathy; CM, congenital myopathy; PMC, paramyotonia congenita; BRGDA, Brugada syndrome; PFHB, progressive familial heart block; LQT, long QT syndrome; AS, atrial standstill; DCM, dilated cardiomyopathy; SND, sinus node dysfunction; HM, hypomagnesemia.

muscle phenotype as shown in action potential modeling. Histidine substitution at this locus (D1595H) is identified in patients with arrhythmic dilated cardiomyopathy (Olson et al., 2005), and enhances fast inactivation (Nguyen et al., 2008).

In the skeletal muscle sodium channel $hNa_V1.4$ (SCN4A), the mutation D1069N (DIIIS2 ENC) has been identified in family members presenting with congenital myopathy (Zaharieva et al., 2016). The mutation produces a right shift in the midpoint of the activation curve, consistent with loss of function (hypoexcitability). In contrast, N1366S (DIVS1 ENC), identified in a family diagnosed with paramyotonia congenita, produces gain of function effects including enhanced activation, slowed entry into the fast-inactivated state, and accelerated recovery (Ke et al., 2017). These effects are consistent with a hyperexcitable skeletal muscle fiber phenotype that characterizes the disease. Thus, functional characterizations of countercharge mutations have extended the genotype to phenotype correlation for loss or gain of function in SCN5A and SCN4A channelopathies.

Countercharge Roles in Voltage-Gating: Concluding Remarks

Common sequence motifs in VSDs include the positively charged S4 region, and conserved aromatic, acidic, or polar amino acid residues in S1–S3 segments. Investigations of the mechanism of voltage-gating in VGICs have supported the hypothesis that VSD negatively charged residues act as countercharges to facilitate S4 translocation in an energetically unfavorable membrane environment. Functional experiments have revealed pairwise interactions between countercharge/S4 residues that play an important role in protein folding, the resting state of the channel, and in outward movement of the S4 segment in the steps leading to channel opening. Determinations of protein structure at atomic resolution supports such countercharge/S4 residue interactions, and have facilitated in-depth analyses of their choreography, using molecular dynamics simulations. These simulations have also been instrumental in present efforts to elucidate the mechanisms by which countercharge residues regulate VSD hydration and to explore the role of hydration in ion channel function. An expanding genetic database has revealed that countercharge mutations comprise a portion of published variants of ion channel genes in patients presenting with neural, cardiac, or skeletal muscle disorders. Genotype to phenotype correlation for countercharge mutations is an important aspect of continued research of the biophysical mechanisms of channelopathies.

AUTHOR CONTRIBUTIONS

JG and LB-E contributed equally to the writing of this review article.

FUNDING

This work was supported by the NIH under 1R15NS093579-01A1 to JG and Idaho INBRE (through an Institutional Development Award from the National Institute of General Medical Sciences) under Grant P20GM103408.

ACKNOWLEDGMENTS

The research presented in Figure 4 (Bayless-Edwards, 2019) made use of the Idaho National Laboratory High Performance Computing Center, which is supported by the Office of Nuclear Energy of the U.S. DOE and the Nuclear Science User Facilities under Contract No. DE-AC07-05ID14517.

REFERENCES

Ahern, C. A., and Horn, R. (2005). Focused electric field across the voltage sensor of potassium channels. *Neuron* 48 (1), 25–29. doi: 10.1016/j.neuron.22056.08.020

Armstrong, C. M., and Bezanilla, F. (1973). Currents related to movement of the gating particles of the sodium channels. *Nature* 242 (5398), 459–461. doi: 10.1038/242459a0

Armstrong, C. M., and Bezanilla, F. (1977). Inactivation of the sodium channel. II. Gating current experiments. *J. Gen. Physiol.* 70 (5), 567–590. doi: 10.1085/jgp.70.5.567

Asatryan, B. (2019). Cardiac sodium channel dysfunction and dilated cardiomyopathy: a contemporary reappraisal of pathophysiological concepts. *J. Clin. Med.* 8 (7), E1029. doi: 10.3390/jcm8071029

Azmanov, D. N., Zhelyaskova, S., Dimova, P. S., Radionova, M., Bojinova, V., Florez, L., et al. (2010). Mosaicism of a missense SCN1A mutation and Dravet syndrome in a Roma/Gypsy family. *Epileptic Disord.* 12 (2), 117–124. doi: 10.1684/epd.2010.0311

Bassetto, C. A. Z.Jr., Carvalho-de-Souza, J. L., and Bezanilla, F. (2019). Metal bridge in S4 segment supports helix transition in Shaker channel. *Biophys. J.* 117, 1–12. doi: 10.1016/j.bpj.2019.08.035.

Bayless-Edwards, L., Winston, V., Lehmann-Horn, F., Arinze, P., Groome, J. R., and Jurkat-Rott, K. (2018). $Na_V1.4$ DI-S4 periodic paralysis mutation R222W enhances inactivation and promotes leak current to attenuate action potentials and depolarize muscle fibers. *Sci. Rep.* 8, 10372. doi: 10.1038/s41598-018-28594-5

Bayless-Edwards, L. (2019). *From molecule to cell: using electrophysiology and multiscale modelling to understand how $Na_V1.4$ controls electrical excitability. [Master's thesis]*. (Pocatello, ID: Idaho State University).

Bezanilla, F., Perozo, E., and Stefani, E. (1994). Gating of Shaker K+ channels: II. The components of gating currents and a model of channel inactivation. *Biophys. J.* 66 (4), 1011–1021. doi: 10.1016/S0006-3495(94)80882-3

Bezanilla, F. (2000). The voltage sensor in voltage-dependent ion channels. *Physiol. Rev.* 80 (2), 555–592. doi: 10.1151/physrev.2000.80.2.555

Bezanilla, F. (2018). Gating currents. *J. Gen. Physiol.* 150 (7), 911–932. doi: 10.1085/jgp.201812157

Bezzina, C. R., Lahrouchi, N., and Priori, S. G. (2015). Genetics of sudden cardiac death. *Circ. Res.* 116 (12), 1919–1936. doi: 10.1161/CIRCRESAHA.116.304030

Bjelkmar, P., Niemela, P. S., Vattulainen, I., and Lindahl, E. (2009). Conformational changes and slow dynamics through microsecond polarized atomistic molecular simulation of an integral Kv1.2 ion channel. *PLoS Computat. Biol.* 5 (2), e1000289. doi: 10.1371/journal.pcbi.1000289

Bosshard, H. R., Marti, D. N., and Jelesarov, I. (2004). Protein stabilization of salt bridges: concepts, experimental approaches and clarification of some misunderstandings. *J. Mol. Recognit.* 17 (1), 1–16. doi: 10.1002/jmr.657

Brunklaus, A., Schorge, S., Smith, A. D., Ghanty, I., Stewart, K., Gardiner, S., et al. (2020). SCN1A variants from bench to bedside – improved prediction from functional characterization. *Hum. Mutat.* 41, 363–374. doi: 10.1002/humu.23943. in press.

Cannon, S. C. (2015). Channelopathies of skeletal muscle excitability. *Compr. Physiol.* 5 (2), 761–790. doi: 10.1002/cphy.c140062

Cannon, S. C. (2018). "Sodium channelopathies of skeletal muscle," in *Voltage-gated sodium channels: structure, function and channelopathies*, vol. 246 . Ed. M. Chahine Handbook of Experimental Pharmacology (Switzerland: Springer International Publishing AG), 309–330. doi: 10.10017/164_2017_52

Catterall, W. A. (2012). Voltage-gated sodium channels at 60: structure, function and pathophysiology. *J. Physiol.* 590 (11), 2577–2589. doi: 10.1113/jphysiol.2011.224204

Catterall, W. A. (2018). Dravet syndrome: a sodium channel interneuronopathy. *Curr. Opin. Physiol.* 2, 42–50. doi: 10.1016/j.cophys.2017.12.007

Chakrapani, S., Sompornpisut, P., Intharathep, P., Roux, B., and Perozo, E. (2010). The activated state of a sodium channel voltage sensor in a membrane environment. *Proc. Natl. Acad. Sci. U. S. A.* 107 (12), 5435–5440. doi: 10.1073/pnas.0914109107

Chamberlain, A., Qiu, F., Rebolledo, S., Wang, Y., Noskov, S. Y., and Larsson, H. P. (2014). Hydrophobic plug functions as a gate in voltage-gated proton channels. *Proc. Natl. Acad. Sci. U. S. A.* 111 (2), E273–E282. doi: 10.1073/pnas.1318018111

Chamberlain, A., Qiu, F., Wang, Y., Noskov, S. Y., and Larsson, H. P. (2015). Mapping the gating and permeation pathways in the voltage-gated proton channel Hv1. *J. Mol. Biol.* 427 (1), 131–145. doi: 10.1016/j.jmb.2014.11.018

Chanda, B., and Bezanilla, F. (2002). Tracking voltage-dependent conformational changes in skeletal muscle sodium channel during activation. *J. Gen. Physiol.* 120 (5), 629–645. doi: 10.1085/jgp.20028679

Chanda, B., and Bezanilla, F. (2008). A common pathway for charge transport through voltage-sensing domains. *Neuron* 57 (3), 345–351. doi: 10.1016/j.neuron.2008.01.015

Coste de Bagneaux, P., Campiglio, M., Benedetti, B., Tuluc, P., and Flucher, B. E. (2018). Role of putative voltage-sensor countercharge D4 in regulating gating properties of Cav1.2 and Cav1.3 calcium channels. *Channels* 12 (1), 249–261. doi: 10.1080/19336950.2018.1482183

Cournia, Z., Allen, T. W., Andricioaei, I., Antonny, B., Baum, D., Brannigan, G., et al. (2015). Membrane protein structure, function and dynamics: a perspective from experiments and theory. *J. Mem. Biol.* 248 (4), 611–640. doi: 10.1007/s00232-015-9802-0

DeCaen, P. G., Yarov-Yarovoy, V., Zhao, Y., Scheuer, T., and Catterall, W. A. (2008). Disulfide-locking of a sodium channel voltage sensor reveals ion pair formation during activation. *Proc. Natl. Acad. Sci. U. S. A.* 105 (39), 15142–15147. doi: 10.1073/pnas.0806486105

DeCaen, P. G., Yarov-Yarovoy, V., Sharp, E. M., Scheuer, T., and Catterall, W. A. (2009). Sequential formation of ion pairs during activation of a sodium channel voltage sensor. *Proc. Natl. Acad. Sci. U. S. A.* 106 (52), 22498–22503. doi: 10.1073/pnas.0912307106

DeCaen, P. G., Yarov-Yarovoy, V., Scheuer, T., and Catterall, W. A. (2011). Gating charge interactions with the S1 segment during activation of a Na+ channel voltage sensor. *Proc. Natl. Acad. Sci. U. S. A.* 108 (46), 18825–18830. doi: 10.1073/pnas.1116449108

Delemotte, L., Dehez, F., Treptow, W., and Tarek, M. (2009). Modeling membranes under a transmembrane potential. *J. Phys. Chem. B.* 112 (18), 5547–5550. doi: 10.1021/jp710846y

Delemotte, L., Tarek, M., Klein, M. L., Amaral, C., and Treptow, W. (2011). Intermediate states of the Kv1.2 voltage sensor from atomistic molecular dynamics simulations. *Proc. Natl. Acad. Sci. U. S. A.* 108 (15), 6019–6114. doi: 10.1073/pnas.1102724108

Delemotte, L., Kasimova, M. A., Klein, M. L., Tarek, M., and Carnevale, V. (2015). Free-energy landscape of ion channel voltage-sensor domain activation. *Proc. Natl. Acad. Sci. U. S. A.* 112 (1), 124–129. doi: 10.1073/pnas.1416959112

Depienne, C., Trouillard, O., Saint-Martin, C., Gourfinkel-An, I., Bouteiller, D., Carpentier, W., et al. (2009). Spectrum of SCN1A gene mutations associated with Dravet syndrome: analysis of 333 patients. *J. Med. Genet.* 46 (3), 183–191. doi: 10.1136/jmg.2008.062323

Depienne, C., Trouillard, O., Gourfinkel-An, I., Saint-Martin, C., Bouteiller, D., Barthez-Carpentier, M. A., et al. (2010). Mechanisms for variable expressivity of inherited SCN1A mutations causing Dravet syndrome. *J. Med. Genet.* 47 (6), 404–410. doi: 10.1136/jmg.2009.074328

Dharmawan, T., Nakajima, T., Iizuka, T., Tamura, S., Matsui, H., Kaneko, Y., et al. (2019). Enhanced closed-state inactivation of mutant cardiac sodium channels (SCN5A N1541D and R1632C) through different mechanisms. *J. Mol. Cell. Cardiol.* 130, 88–95. doi: 10.1016/j.yjmcc.2019.02.023

Diaz-Franulic, I., Gonzalez-Perez, V., Moldenhauer, H., Navarro-Quezada, N., and Naranjo, D. (2018). Gating-induced large aqueous volumetric remodeling and aspartate tolerance in the voltage sensor domain of Shaker K+ channels. *Proc. Natl. Acad. Sci. U. S. A.* 115 (32), 8203–8208. doi: 10.1073/pnas.1806578115

Dolphin, A. C. (2018). Voltage-gated calcium channels: their discovery, function and importance as drug targets. *Brain Neurosci. Adv.* 2, 1–8. doi: 10.1177/2398212818794805

Dou, Y., Macdonald, L. C., Wu, Y., and Fedida, D. (2017). The fast component of hERG gating charge: an interaction between D411 in the S1 and S4 residues. *Biophys. J.* 113 (9), 1979–1991. doi: 10.1016/j.bpj.2017.09.004

Doyle, D. A., Morais Cabral, J., Pfuetzner, R. A., Kuo, A., Gulbis, J. M., Cohen, S. L., et al. (1998). The structure of the potassium channel: molecular basis of K+ conduction and selectivity. *Science* 280 (5360), 69–77. doi: 10.1126/science.280.5360.69

Dudev, T., Musset, B., Morgan, D., Cherny, V. V., Smith, S. M., Mazmanian, K., et al. (2015). Selectivity mechanism of the voltage-gated proton channel, HV1. *Sci. Rep.* 5, 10320. doi: 10.1038/srpe10320

Elinder, F., Nilsson, J., and Arhem, P. (2007). On the opening of voltage-gated ion channels. *Physiol. Behav.* 92 (1-2), 1–7. doi: 10.1016/j.physbeh.2007.05.058

Fedida, D., and Hesketh, J. C. (2001). Gating of voltage-gated potassium channels. *Progr. Biophys. Mol. Biol.* 75 (3), 165–199. doi: 10.1016/S0079-6107(01)00006-2

Francis, D. G., Rybalchenko, V., Struyk, A., and Cannon, S. C. (2011). Leaky sodium channels from voltage sensor mutations in periodic paralysis, but not paramyotonia. *Neurol* 76 (19), 1635–1641. doi: 10.1212/WNL.0b013e318219fb57

Freites, J. A., and Tobias, D. J. (2015). Voltage-sensing in membranes: from macroscopic currents to molecular motions. *J. Membr. Biol.* 248 (3), 419–430. doi: 10.1007/s00232-015-0805-x

Freites, J. A., Tobias, D. J., and White, S. H. (2006). A voltage-sensor water pore. *Biophys. J.* 91 (11), L90–L92. doi: 10.1529/biophysj.106.096065

Fujiwara, T., Sugawara, T., Mazaki-Miyazaki, E., Takahashi, Y., Fukushima, K., Watanabe, M., et al. (2003). Mutations of sodium channel a subunit type I (SCN1A) in intractable childhood epilepsies with frequent generalized tonic-clonic seizures. *Brain* 126, 531–546. doi: 10.1093/brain/awg053

Gamal El-Din, T. M., Martinez, G. Q., Payandeh, J., Scheuer, T., and Catterall, W. A. (2013). A gating charge interaction required for late slow inactivation of the bacterial sodium channel Na_VAb. *J. Gen. Physiol.* 142 (3), 181–190. doi: 10.1085/jgp.201311012

Gandhi, C. S., and Isacoff, E. Y. (2002). Molecular models of voltage sensing. *J. Gen. Physiol.* 120 (4), 455. doi: 10.1085/jgp.20028678

Ganetzky, B. (2000). Genetic analysis of ion channel dysfunction in Drosophila. *Kidney Int.* 57 (3), 766–771. doi: 10.1016/j.1523-1755.2000.00913.x

Garcia-Elias, A., and Benito, B. (2018). Ion channel disorders and sudden cardiac death. *Int. J. Mol. Sci.* 19 (3), E692. doi: 10.3390/ijms19030692

Gianti, E., Delemotte, L., Klein, M., and Carvnevale, V. (2016). On the role of water density fluctuations in the inhibition of a proton channel. *Proc. Natl. Acad. Sci. U. S. A.* 113 (52), E8359–E8368. doi: 10.1073/pna.1609964114

Glaudemans, B., van der Wijst, J., Scola, R. H., Lorenzoni, P. J., Heister, A., van der Kemp, A. W., et al. (2009). A missense mutation in the Kv1.1 voltage-gated potassium channel-encoding gene KCNA1 is linked to human autosomal dominant hypomagnesemia. *J. Clin. Invest.* 119 (4), 936–942. doi: 10.1172/JCI36948

Goldschen-Ohm, M. P., Capes, D. L., Oelstrom, K. M., and Chanda, B. (2013). Multiple pore conformations driven by asynchronous movements of voltage sensors in a eukaryotic sodium channel. *Nat. Commun.* 4, 1350. doi: 10.1038/ncomms2356

Gosselin-Badaroudine, P., Delemotte, L., Moreau, A., Klein, M. L., and Chahine, M. (2012). Gating pore currents and the resting state of $Na_V1.4$ voltage sensor domains. *Proc. Natl. Acad. Sci. U. S. A.* 109 (47), 19250–19255. doi: 10.1073/pnas.1217990109

Greenblatt, R. E., Blatt, Y., and Montal, M. (1985). The structure of the voltage-sensitive sodium channel: inferences from computer-aided analysis of the Electrophorus electricus channel primary structure. *FEBS* 193 (2), 125–134. doi: 10.1016/0014-5793(85)80136-8

Groenewegen, W. A., Firouzi, M., Bezzina, C. R., Vliex, S., van Langen, I. M., Sandkuijl, L., et al. (2003). A cardiac sodium channel mutation cosegregates with a rare connexin40 genotype in familial atrial standstill. *Circ. Res.* 92 (1), 14–22. doi: 10.1161/01.RES.0000050585.07097.D7

Groome, J. R., and Winston, V. (2013). S1-S3 counter charges in the voltage sensor module of a mammalian sodium channel regulate fast inactivation. *J. Gen. Physiol.* 141 (5), 601–618. doi: 10.1085/jgp.201210935

Groome, J. R., Moreau, A., and Delemotte, L. (2018). "Gating pore currents in sodium channels," in *Handbook of Experimental Pharmacology*, vol. 246 . Ed. M. Chahine Voltage-gated sodium channels: structure, function and channelopathies (Switzerland: Springer International Publishing AG), 371–399. doi: 10.1007/164_2017_54

Groome, J. R., Bayless-Edwards, L., Wheeler, A., and Camp, R. (2019). Domain I countercharges limit slow inactivation in $hNa_V1.4$ channels. *Biophys. J.* 116 (Supplement Issue3), 390a. doi: 10.1016/j.bpj.2018.11.2113

Groome, J. R. (2014). "The voltage sensor module in sodium channels," in *Handbook of Experimental Pharmacology*, vol. 221 . Ed. P. Ruben Voltage gated sodium channels (Berlin, Heidelberg: Springer International Publishing AG), 7–31. doi: 10.1007/978-3.642-41588-3_2

Guy, H. R., and Seetharamulu, P. (1986). Molecular model of the action potential sodium channel. *Proc. Natl. Acad. Sci. U. S. A.* 83, 508–512. doi: 10.1073/pnas.83.2.508

Harkin, L. A., McMahon, J. M., Iona, X., Dibbens, L., Pelekanos, J. T., Zuberi, S. M., et al. (2007). The spectrum of SNC1A-related infantile epileptic encephalopathies. *Brain* 130 (3), 843–852. doi: 10.1093/brain/awm002

Hayano, M., Makiyama, T., Kamakura, T., Watanabe, H., Sasaki, K., Funakoshi, S., et al. (2017). Development of a patient-derived induced pluripotent stem cell model for the investigation of SCN5A-D1275N-related cardiac sodium channelopathy. *Circ. J.* 81 (12), 1783–1791. doi: 10.1253/circj.CJ-17-0064

Henrion, U., Renhorn, J., Borjesson, S. I., Nelson, E. M., Schwaiger, C. S., Bjelkmar, P., et al. (2012). Tracking a complete voltage-sensor cycle with metal-ion bridges. *Proc. Natl. Acad. Sci. U. S. A.* 109 (22), 8552–8557. doi: 10.1073/pnas.1116938109

Hodgkin, A. L., and Huxley, A. F. (1952). A quantitative description of membrane current and its application to conduction and excitation in nerve. *J. Physiol.* 117, 500–544. doi: 10.1113/jphysiol.1952.sp004764

Horn, R. (2002). Coupled movements in voltage-gated ion channels. *J. Gen. Physiol.* 120 (4), 449–453. doi: 10.1085/jgp.20028658

Howard, R. J., Carnevale, V., Delemotte, L., Hellmich, U. A., and Rothberg, B. S. (2018). Permeating disciplines: overcoming barriers between molecular simulations and classical structure-function approaches in biological transport. *Biochim. Biophys. Acta Biomembr.* 1860 (4), 927–942. doi: 10.1016/j.bbamem.2017.12.013

Huang, W., Liu, M., Yan, S. F., and Yan, N. (2017). Structure-based assessment of disease-related mutations in human voltage-gated sodium channels. *Protein Cell* 8 (6), 401–438. doi: 10.1007/s13238-017-0372-z

Huttner, I. G., Trivedi, G., Jacoby, A., Mann, S. A., Vandenberg, J. I., and Fatkin, D. (2013). A transgenic zebrafish model of a human cardiac sodium channel mutation exhibits bradycardia, conduction-system abnormalities and early death. *J. Mol. Cell. Cardiol.* 61, 123–132. doi: 10.1016/j.yjmcc.2013.06.005

Jensen, M. Ø., Jojini, V., Borhani, D. W., Leffler, A. E., Dror, R. O., and Shaw, D. E. (2012). Mechanism of voltage gating in potassium channels. *Science* 336 (6078), 229–233. doi: 10.1126/science.1216533

Jiang, Y., Lee, A., Chen, J., Ruta, V., Cadene, M., Chait, B. T., et al. (2003). X-ray structure of a voltage-gated K+ channel. *Nature* 423 (6935), 33–41. doi: 10.1038/nature01580

Jiang, D., Gamal El-Din, T. M., Ing, C., Lu, P., Pomes, R., Zheng, N., et al. (2018). Structural basis for gating pore current in periodic paralysis. *Nature* 557 (7706), 590–594. doi: 10.1038/s41586-018-0120-4

Jogini, V., and Roux, B. (2007). Dynamics of the Kv1.2 voltage-gated potassium channel in a membrane environment. *Biophys. J.* 93 (9), 3070–3082. doi: 10.1529/biophysj.107.112540

Jongbloed, R., Marcelis, C., Velter, C., Doevendans, P., Geraedts, J., and Smeets, H. (2002). DHPLC analysis of potassium ion channel genes in congenital long QT syndrome. *Hum. Mutat.* 20 (5), 382–391. doi: 10.1002/humu.10131

Kapplinger, J. D., Tester, D. J., Salisbury, B. A., Carr, J. L., Harris-Kerr, C., Pollevick, G. D., et al. (2009). Spectrum and prevalence of mutations from the first 2,500 consecutive unrelated patients referred for the FAMILION® long QT syndrome genetic test. *Heart Rhythm.* 6 (9), 1297–1303. doi: 10.1016/j.hrthm.2009.05.021

Kapplinger, J. D., Tester, D. J., Alders, M., Benito, B., Berthet, M., Brugada, J., et al. (2010). An international compendium of mutations in the SCN5A-encoded cardiac sodium channel in patients referred for Brugada syndrome genetic testing. *Heart Rhythm.* 7 (1), 33–46. doi: 10.1016/j.hrthm.2009.090.069

Ke, Q., Ye, J., Tang, S., Wang, J., Luo, B., Ji, F., et al. (2017). N1366S mutation of human skeletal muscle sodium channel causes paramyotonia congenita. *J. Physiol.* 595 (22), 6837–6850. doi: 10.1113/JP274877

Kearney, J. A., Wiste, A. K., Stephani, U., Trudeau, M. S., Siegel, A., RamachandranNair, R., et al. (2006). Recurrent *de novo* mutations of SCN1A in severe myoclonic epilepsy of infancy. *Ped. Neurol.* 34 (2), 116–120. doi: 10.1016/j.pediatrneurol.2005.07.009

Khalili-Araghi, F., Jogini, V., Yarov-Yarovoy, V., Tajkhorshid, E., Roux, B., and Schulten, K. (2010). Calculation of the gating charge for $K_V1.2$ voltage-activated potassium channel. *Biophys. J.* 98 (10), 2189–2198. doi: 10.1016/bpj.2010.02.056

Kodera, H., Kato, M., Nord, A. S., Walsh, T., Lee, M., Yamanaka, G., et al. (2013). Targeted capture and sequencing for detection of mutations causing early onset epileptic encephalopathy. *Epilepsia* 54 (7), 1262–1269. doi: 10.1111/epi.12203

Kuang, Q., Purhonen, P., and Hebert, H. (2015). Structure of potassium channels. *Cell. Mol. Life Sci.* 72 (19), 3677–3693. doi: 10.1007/s00018-015-1948-5

Kubota, T., Lacroix, J. J., Bezanilla, F., and Correa, A. M. (2014). Probing α-3_{10} transitions in a voltage-sensing S4 helix. *Biophys. J.* 107 (5), 1117–1128. doi: 10.1016/j.bpj.2014.07.042

Lacroix, J. J., Hyde, H. C., Campos, F. V., and Bezanilla, F. (2014). Moving gating charges through the gating pore in a Kv channel voltage sensor. *Proc. Natl. Acad. Sci. U. S. A.* 111 (19), E1950–E1959. doi: 10.1073/pnas.1406161111

Leonard, R. J., Karschin, A., Jayashree-Aiyar, S., Davidson, N., Tanouye, M. A., Thomas, L., et al. (1989). Expression of Drosophila Shaker potassium channels in mammalian cells infected with recombinant vaccina virus. *Proc. Natl. Acad. Sci. U. S. A.* 86 (19), 7629–7633. doi: 10.1073/pnas.86.19.7629

Lin, M.-C. A., Hsieh, J.-Y., Mock, A. F., and Papazian, D. M. (2011). R1 in the Shaker S4 occupies the gating charge transfer center in the resting state. *J. Gen. Physiol.* 138 (2), 155–163. doi: 10.1085/jgp.201110642

Liu, J., Zhang, M., Jiang, M., and Tseng, G.-N. (2003). Negative charges in the transmembrane domains of the HERG K channel are involved in the activation- and deactivation-gating processes. *J. Gen. Physiol.* 121 (6), 599–614. doi: 10.1085/jgp.200308788

Long, S. B., Campbell, E. B., and MacKinnon, R. (2005a). Voltage sensor of $K_V1.2$: structural basis of electromechanical coupling. *Science* 309 (5736), 903–908. doi: 10.1126/science.1116270

Long, S. B., Campbell, E. B., and MacKinnon, R. (2005b). Crystal structure of a mammalian voltage-dependent Shaker family K+ channel. *Science* 309 (5736), 897–903. doi: 10.1126/science.1116269

Long, S. B., Tao, X., Campbell, E. B., and MacKinnon, R. (2007). Atomic structure of a voltage-dependent K+ channel in a lipid membrane-like environment. *Nature* 450 (7168), 376–382. doi: 10.1038/nature06265

Marini, C., Mei, D., Temudo, T., Ferrari, A. R., Buti, D., Dravet, C., et al. (2007). Idiopathic epilepsies with seizures precipitated by fever and SCN1A abnormalities. *Epilepsia* 48 (9), 1678–1685. doi: 10.1111/j.1528-1167.2007.01122x

Matalon, D., Goldberg, E., Medne, L., and Marsh, E. D. (2014). Confirming an expanded spectrum of SCN2A mutations: a case series. *Epileptic Disord.* 16 (1), 13–18. doi: 10.1684/epd.2014.0641

McNair, W. P., Ku, L., Taylor, M. R. G., Fain, P. R., Dao, D., Wolfel, E., et al. (2004). SCN5A mutation associated with dilated cardiomyopathy, conduction disorder, and arrhythmia. *Circulation* 110, 2163–2167. doi: 10.1161/01.CIR.0000144458_58660.BB

Meregalli, P. G., Tan, H. L., Probst, V., Koopmann, T. T., Tanck, M. W., Bhuiyan, Z. A., et al. (2009). Type of SCN5A-mutation determines clinical severity and degree of conduction slowing in loss-of-function sodium channelopathies. *Heart Rhythm.* 6 (3), 341–348. doi: 10.1016/j.hrthm.2008.11.009

Monteleone, S., Lieb, A., Pinggera, A., Negro, G., Fuchs, J. E., Hofer, F., et al. (2017). Mechanisms responsible for w-pore currents in Cav calcium channel voltage-sensing domains. *Biophys. J.* 113 (7), 1485–1495. doi: 10.1016/j.bpj.2017.08.010

Musset, B., Smith, S. M. E., Rajan, S., Morgan, D., Cherny, V. V., and DeCoursey, T. E. (2012). Aspartate is the selectivity filter of the human voltage gated proton channel. *Nature* 480 (7376), 273–277. doi: 10.1038/nature10557

Nakamura, K., Kato, M., Osaka, H., Yamashita, S., Nakagawa, E., Haginoya, K., et al. (2013). Clinical spectrum of SCN2A mutations expanding to Ohtahara syndrome. *Neurol* 81 (11), 992–998. doi: 10.1212/WNL.0b013e3182a43e57

Napolitano, C., Priori, S. G., Schwartz, P. J., Bloise, R., Ronchetti, E., Nastoli, J., et al. (2005). Genetic testing in the long QT syndrome: development and validation of an efficient approach to genotyping in clinical practice. *JAMA* 294 (23), 2975–2980. doi: 10.1001/jama.294.23.2975

Nguyen, T. P., Wang, D. W., Rhodes, T. H., and George, A. L.Jr. (2008). Divergent biophysical defects caused by mutant sodium channels in dilated cardiomyopathy with arrhythmia. *Circ. Res.* 102 (3), 364–371. doi: 10.1161/CIRCRESAHA.107.164673

Nishizawa, M., and Nishizawa, K. (2008). Molecular dynamics simulations of Kv channel voltage sensor helix in a lipid membrane with applied electric field. *Biophys. J.* 95 (4), L1729–L1744. doi: 10.1529/biophysj.108.130658

Noda, M., Shimizu, S., Tanabe, T., Takai, T., Kayano, T., Ikeda, T., et al. (1984). Primary structure of Electrophorus electricus sodium channel deduced from cDNA sequence. *Nature* 312 (5990), 121–127. doi: 10.1038/312121a0

Noda, M., Ikeda, T., Suzuki, H., Takeshima, H., Takahashi, T., Kuno, M., et al. (1986). Expression of functional sodium channels from cloned DNA. *Nature* 322 (6082), 826–828. doi: 10.1038/322826a0

Ogiwara, I., Ito, K., Sawaishi, Y., Osaka, H., Mazaki, E., Inoue, I., et al. (2009). De novo mutations of voltage-gated sodium channel alphaII gene SCN2A in intractable epilepsies. *Neurol* 73 (13), 1046–1053. doi: 10.1212/WNL.0b013e3181b0cebc

Olson, T. M., Michels, W., Ballew, J. D., Reyna, S. P., Karst, M. L., Herron, K. J., et al. (2005). Sodium channel mutations and susceptibility to heart failure and atrial fibrillation. *JAMA* 293 (4), 447–454. doi: 10.1001/jama.293.4.447

Paldi, T., and Gurevitz, M. (2010). Coupling between residues on S4 and S1 defines the voltage-sensor resting conformation in NaChBac. *Biophys. J.* 99 (2), 456–463. doi: 10.1016/bpj.2010.04.053

Palovcak, E., Delemotte, L., Klein, M. L., and Carnevale, V. (2014). Evolutionary imprint of activation: the design principles of VSDs. *J. Gen. Physiol.* 143 (2), 145–156. doi: 10.1085/jgp.201311103

Pan, X., Li, Z., Zhou, Q., Shen, H., Wu, K., Huang, X., et al. (2018). Structure of the human voltage-gated sodium channel $Na_V1.4$ in complex with beta1. *Science* 362 (6412), eaau2486. doi: 10.1126/science.aau2486

Pantazis, A., Savalli, N., Sigg, D., Neely, A., and Olcese, R. (2014). Functional heterogeneity of the four voltage sensors of a human L-type calcium channel. *Proc. Natl. Acad. Sci. U. S. A.* 111 (51), 18381–18386. doi: 10.1073/pnas.1411127112

Papazian, D. M., Schwarz, T. L., Tempel, B. L., Jan, Y. N., and Jan, L. Y. (1987). Cloning of genomic and complementary DNA from Shaker, a putative potassium gene from Drosophila. *Science* 237 (4816), 749–753. doi: 10.1126/science.2441470

Papazian, D. M., Schwarz, T. L., Tempel, B. L., Timpe, L. C., and Jan, L. Y. (1988). Ion channels in Drosophila. *Ann. Rev. Physiol.* 50, 379–394. doi: 10.1146/annurev.ph.50.030188.002115

Papazian, D. M., Timpe, L. C., Jan, Y. N., and Jan, L. Y. (1991). Alteration of voltage-dependence of Shaker potassium channel by mutations in the S4 sequence. *Nature* 349 (6307), 305–310. doi: 10.1038/349305a0

Papazian, D. M., Shao, X. M., Seoh, S.-A., Mock, A. F., Huang, Y., and Wainstock, D. H. (1995). Electrostatic interactions of S4 voltage sensor in Shaker K+ channel. *Neuron* 14 (6), 1293–1301. doi: 10.1016/0896-6273(95)90276-7

Papazian, D. M., Silverman, W. R., Lin, M. C., Tiwari-Woodruff, S. K., and Tang, C. Y. (2002). Structural organization of the voltage sensor in voltage-dependent K+ channels. *Noavartis Found. Symp.* 245, 178–190. doi: 10.1002/0470868759.ch13

Parrini, E., Marini, C., Mei, D., Galuppi, A., Cellini, E., Pucatti, D., et al. (2017). Diagnostic targeted resequencing in 349 patients with drug-resistant pediatric epilepsies identifies causative mutations in 30 different genes. *Hum. Mutat.* 38, 216–225. doi: 10.1002/humu.23149

Pathak, M. M., Yarov-Yarovoy, V., Agarwal, G., Roux, B., Barth, P., Kohout, S., et al. (2007). Closing in on the resting state of the shaker K+ channel. *Neuron* 56 (4), 124–140. doi: 10.1016/j.neuron.2007.09.023

Payandeh, J., Scheuer, T., Zheng, N., and Catterall, W. A. (2011). The crystal structure of a voltage-gated sodium channel. *Nature* 475 (7356), 353–358. doi: 10.1038/nature10238

Payandeh, J., Gamal El-Din, T. M., Scheuer, T., Zheng, N., and Catterall, W. A. (2012). Crystal structure of a voltage-gated sodium channel in two potentially inactivated states. *Nature* 486 (7401), 135–139. doi: 10.1038/nature11077

Perozo, E., Papazian, D. M., Stefani, E., and Bezanilla, F. (1992). Gating currents in Shaker K+ channels. Implications for activation and inactivation models. *Biophys. J.* 62 (1), 160–168. doi: 10.1016/S0006-3495(92)81802-7

Perozo, E., Santacruz-Toloza, L., Stefani, E., Bezanilla, F., and Papazian, D. M. (1994). S4 mutations alter gating currents of Shaker K channels. *Biophys. J.* 66, 345–354. doi: 10.1016/s0006-3495-(94)80783-0

Pless, S. A., Galpin, J. D., Niciforovic, A. P., and Ahern, C. A. (2011). Contributions of counter-charge in a potassium channel voltage-sensor domain. *Nat. Chem. Biol.* 7 (9), 617–623. doi: 10.1038/nchembio.622

Pless, S. A., Elstone, F. D., Niciforovic, A. P., Galpin, J. D., Yang, R., Kurata, H. T., et al. (2014). Asymmetric functional contributions of acidic and aromatic side chains in sodium channel voltage-sensor domains. *J. Gen. Physiol.* 143 (5), 645–656. doi: 10.1085/jgp.201311036

Poulin, H., Gosselin-Badaroudine, P., Vicart, S., Habbout, K., Sternberg, D., Giuliano, S., et al. (2018). Substitutions of the S4DIV R2 residue (R1451) in $Na_V1.4$ lead to complex forms of paramyotonia congenita and periodic paralyses. *Sci. Rep.* 8, 2041. doi: 10.1038/s41598-018-20468-0

Ren, D., Navarro, B., Xu, H., Yue, L., Shi, Q., and Clapham, D. E. (2001). A prokaryotic voltage-gated sodium channel. *Science* 294 (5550), 2372–2375. doi: 10.1126/science.1065635

Schow, E. V., Frietes, J. A., Gogna, K., White, S. H., and Tobias, D. J. (2010). Down-state model of the voltage-sensing domain of a potassium channel. *Biophys. J.* 98 (112), 2857–2866. doi: 10.1016/j.bpj.2010.03.031

Schulteis, C. T., Nagaya, N., and Papazian, D. M. (1998). Subunit folding and assembly steps are interspersed during Shaker potassium channel biogenesis. *J. Biol. Chem.* 273 (40), 26210–26217. doi: 10.1074/jbc.273.40.26210

Schwaiger, C. S., Bjelkmar, P., Hess, B., and Lindahl, E. (2011). 3_{10}-helix conformation facilitates the transition of a voltage sensor S4 segment toward the down state. *Biophys. J.* 100 (6), 1446–1454. doi: 10.1016/j.bpj.2011.02.003

Schwaiger, C. S., Liin, S. I., Elinder, F., and Lindahl, E. (2013). The conserved phenylalanine in the K+ channel voltage-sensor domain creates a barrier with unidirectional effects. *Biophys. J.* 104 (1), 75–84. doi: 10.1016/j.bpj.2012.11.3827

Seoh, S.-A., Sigg, D., Papazian, D. M., and Bezanilla, F. (1996). Voltage-sensing residues in the S2 and S4 segments of the Shaker K+ channel. *Neuron* 16, 1159–1167. doi: 10.1016/s0896-6273(00)80142-7

Sercinoglu, O., and Ozbek, P. (2018). gRINN: a tool for calculation of residue interaction energies and protein energy network analysis of molecular dynamics simulations. *Nucleic Acids Res.* 46 (W1), W554–W526. doi: 10.1093/nar/gky381

Shen, H., Zhou, Q., Pan, X., Li, Z., Wu, J., and Yan, N. (2017). Structure of a eukaryotic voltage-gated sodium channel at near-atomic resolution. *Science* 355 (6328), eaa14326. doi: 10.1126/scienceaa14326

Silverman, W. R., Roux, B., and Papazian, D. M. (2003). Structural basis of two-stage voltage dependent activation in K+ channels. *Proc. Natl. Acad. Sci. U. S. A.* 100 (5), 2935–2940. doi: 10.1073/pnas.0636603100

Smits, J. P., Eckardt, L., Probst, V., Bezzina, C. R., Schott, J. J., Remme, C. A., et al. (2002). Genotype-phenotype relationship in Brugada syndrome: electrocardiographic features differentiate SCN5A-related patients from non-SCN5A-related patients. *J. Am. Coll. Cardiol.* 40 (2), 350–356. doi: 10.1016/s0735-1097(02)01962-9

Smits, J. P., Koopmann, T. T., Wilders, R., Veldkamp, M. W., Opthof, T., Bhuiyan, Z. A., et al. (2005). A mutation in the human cardiac sodium channel E161K

contributes to sick sinus syndrome, conduction disease, and Brugada syndrome in two families. *J. Mol. Cell. Cardiol.* 38 (6), 969–981. doi: 10.1016/j.yjmcc.2005.02.024

Splawski, I., Shen, J., Timothy, K. W., Lehmann, M. H., Priori, S., Robinson, J. L., et al. (2000). Spectrum of mutations in long-QT syndrome genes KVLQT1, HERG, SCN5A, KCNE1, and KCNE2. *Circ* 102, 1178–1185. doi: 10.1161/01.cir.102.10.1178

Starace, D. M., and Bezanilla, F. (2004). A proton pore in a potassium channel voltage sensor reveals a focused electric field. *Nature* 427 (6974), 548–553. doi: 10.1038/nature02270

Stuhmer, W., Stocker, M., Sakmann, B., Seeburg, P., Baumann, A., Grupe, A., et al. (1988). Potassium channels expressed from rat brain DNA have delayed rectifier properties. *FEBS Lettr.* 242 (1), 199–206. doi: 10.1016/0014-5793(88)8105-9

Stuhmer, W., Conti, F., Suzuki, H., Wang, X. D., Noda, M., Yahagi, N., et al. (1989). Structural parts involved in the activation and inactivation of the sodium channel. *Nature* 339 (6226), 597–603. doi: 10.1038/339597a0

Sula, A., Booker, J., Ng, L. C. T., Naylor, C. E., DeCaen, P. G., and Wallace, B. A. (2017). The complete structure of an activated open sodium channel. *Nat. Commun.* 8, 14205. doi: 10.1038/ncomms14205

Tao, X., Lee, A., Limapichat, W., Dougherty, D. A., and MacKinnon, R. (2010). A gating charge transfer center in voltage sensors. *Science* 328 (5974), 67–73. doi: 10.1126/science.1185954

Tester, D. J., Will, M. L., Haglund, C. M., and Ackermann, M. J. (2005). Compendium of cardiac sodium channel mutations in 541 consecutive unrelated patients referred for long QT syndrome genetic testing. *Heart Rhythm.* 2 (5), 507–517. doi: 10.1016/j.hrthm.2005.01.020

Timpe, L. C., Schwarz, T. L., Tempel, B. L., Papazian, D. M., Jan, Y. N., and Jan, L. Y. (1988). Expression of functional potassium channels from Shaker cDNA in Xenopus oocytes. *Nature* 331 (6152), 143–145. doi: 10.1038/331143a0

Tiwari-Woodruff, S. K., Schulteis, C. T., Mock, A. F., and Papazian, D. M. (1997). Electrostatic interactions between transmembrane segments mediate folding of Shaker K+ channel subunits. *Biophys. J.* 72 (4), 1489–1500. doi: 10.1016/S0006-3495(97)78797-6

Tiwari-Woodruff, S. K., Lin, M.-A., Schulteis, C. T., and Papazian, D. M. (2000). Voltage-dependent structural interactions in the Shaker K+ channel. *J. Gen. Physiol.* 115 (2), 123–138. doi: 10.1085/jgp.115.2.123

Tombola, F., Pathak, M. M., and Isacoff, E. Y. (2005). Voltage-sensing arginines in a potassium channel permeate and occlude cation-selective pores. *Neuron* 45 (3), 379–388. doi: 10.1016/j.neuron.2004.12.047

Tombola, F., Pathak, M. M., Gorostiza, P., and Isacoff, E. Y. (2007). The twisted ion-permeation pathway of a resting voltage-sensing domain. *Nature* 445 (7127), 546–549. doi: 10.1038/nature05396

Treptow, W., and Tarek, M. (2006). Environment of the gating charges in the Kv1.2 shaker potassium channel. *Biophys. J.* 90 (9), L64–L66. doi: 10.1529/biophysj.106.080754

Treptow, W., Tarek, M., and Klein, M. L. (2009). Initial response of the potassium channel voltage sensor to a transmembrane potential. *J. Am. Chem. Soc* 131 (6), 2107–2109. doi: 10.1021/ja807330g

Tuluc, P., Benedetti, B., Coste de Bagneaux, P., Grabner, M., and Flucher, B. E. (2016a). Two distinct voltage-sensing domains control voltage-sensitivity and kinetics of current activation in Cav1.1 calcium channels. *J. Gen. Physiol.* 147 (6), 437–439. doi: 10.1085/jgp.201511568

Tuluc, P., Yarov-Yarovoy, V., Benedetti, B., and Flucher, B. E. (2016b). Molecular interactions in the voltage sensor controlling gating properties of Ca_V calcium channels. *Structure* 24 (2), 262–271. doi: 10.1016/j.str.2015.11.011

van Keulen, S. C., Gianti, E., Carnevale, V., Klein, M. L., Rothlisberger, U., and Delemotte, L. (2017). Does proton conduction in the voltage-gated H+ channel hHv1 involve Grotthuss-like hopping *via* acidic residues? *J. Phys. Chem. B* 121, 3340–3351. doi: 10.1021/acs.jpcb.6b08339

Vargas, E., Bezanilla, F., and Roux, B. (2011). In search of a consensus model of the resting state of a voltage-sensing domain. *Neuron* 72 (5), 713–720. doi: 10.1016/j.neuron.2011.09.024

Vargas, E., Yarov-Yarovoy, V., Khalili-Araghi, F., Catterall, W. A., Klein, M. L., Tarek, M., et al. (2012). An emerging consensus on voltage-dependent gating from computational modeling and molecular dynamics simulations. *J. Gen. Physiol.* 140 (6), 587–594. doi: 10.1085/jgp.201210873

Villalba-Galea, C. A., Sandtner, W., Starace, D. M., and Bezanilla, F. (2008). S4-based voltage sensors have three major conformations. *Proc. Natl. Acad. Sci. U. S. A.* 105 (46), 17600–17607. doi: 10.1073/pnas.0807387105

Wang, D. W., Viswanathan, P. C., Balser, J. R., George, A. L.Jr., and Benson, D. W. (2002). Clinical, genetic, and biophysical characterization of SCN5A mutations associated with atrioventricular conduction block. *Circ* 105 (3), 341–346. doi: 10.1161/hc0302.102592

Wang, J.-W., Shi, X.-Y., Kurahashi, H., Hwang, S.-K., Ishii, A., Higurashi, N., et al. (2012). Prevalence of SCN1A mutations in children with suspected Dravet syndrome and intractable childhood epilepsy. *Epilepsy Res.* 102 (3), 195–200. doi: 10.1016/j.eplepsyres.2012.06.006

Watanabe, H., Yang, T., Stroud, D. M., Lowe, J. S., Harris, L., Atack, T. C., et al. (2011). Striking *in vivo* phenotype of a disease-associated human SCN5A mutation producing minimal changes *in vitro*. *Circ* 124 (9), 1001–1011. doi: 10.1161/CIRCULATIONAHA.110.987248

Wisedchaisri, G., Tonggu, L., McCord, E., Gamal El-Din, T. M., Wang, L., Zheng, N., et al. (2019). Resting-state structure and gating mechanism of a voltage-gated sodium channel. *Cell* 178 (4), 993–1003. doi: 10.1016/j.cell.2019.06.031

Wong, V. C., Fung, C. W., and Kwong, A. K. (2015). SCN2A mutation in a Chinese boy with infantile spasm – response to modified Atkins diet. *Brain Dev.* 37 (7), 729–732. doi: 10.1016/j.braindev.2014.10.008

Wood, M. L., Schow, E. V., Freites, J. A., White, S. H., Tombola, F., and Tobias, D. J. (2012). Water wires in atomistic models of the Hv1 proton channel. *Biochim. Biophys. Acta* 1818 (2), 286–293. doi: 10.1016/j.bbamem.2011.07.045

Wu, J., Yan, Z., Li, Z., Qian, X., Lu, S., Dong, M., et al. (2016). Structure of the voltage-gated calcium channel Ca(v)1.1 at 3.6 Å resolution. *Nature* 537 (7619), 191–196. doi: 10.1038/nature19321

Yan, Z., Zhou, Q., Wang, L., Wu, J., Zhao, Y., Huang, G., et al. (2017). Structure of the $Na_V1.4$-beta1 complex from electric eel. *Cell* 170 (3), 470–482. doi: 10.1016/j.cell.2017.06.039

Yarov-Yarovoy, V., and DeCaen, P. G. (2019). The sodium channel voltage sensor slides to rest. *Trends Pharmacol. Sci.* 40 (10), 718–720. doi: 10.1016/j.tips.2019.08.009

Yarov-Yarovoy, V., Baker, D., and Catterall, W. A. (2006). Voltage sensor conformations in the open and closed states in ROSETTA structural models of K(+) channels. *Proc. Natl. Acad. Sci. U. S. A.* 103 (19), 7292–7297. doi: 10.1073/pnas.0602350103

Yarov-Yarovoy, V., DeCaen, P. G., Westenbroek, R. E., Pan, C. Y., Scheuer, T., Baker, D., et al. (2012). Structural basis for gating charge movement in the voltage sensor of a sodium channel. *Proc. Natl. Acad. Sci. U. S. A.* 109 (2), E93–E102. doi: 10.1073/pnas.1118434109

Zagotta, W. N., Toshi, T., and Aldrich, R. W. (1989). Gating of single Shaker potassium channels in Drosophila muscle and in Xenopus oocytes injected with Shaker mRNA. *Proc. Natl. Acad. Sci. U. S. A.* 86 (18), 7243–7247. doi: 10.1073/pnas.86.18.7243

Zaharieva, I. T., Thor, M. G., Oates, E. C., van Karnebeek, C., Hendson, G., Blom, E., et al. (2016). Loss-of-function mutations in SCN4A cause severe foetal hypokinesia or 'classical' congenital myopathy. *Brain* 139 (3), 674–691. doi: 10.1093/brain/awv352

Zhang, M., Liu, J., Jiang, M., Wu, D.-M., Sonawane, K., Guy, H. R., et al. (2005). Interactions between charged residues in the transmembrane segments of the voltage-sensing domain in the hERG channel. *J. Mem. Biol.* 207 (3), 169–181. doi: 10.1007/s00232-005-0812-1

Zhang, X., Ren, W., DeCaen, P., Yan, C., Tao, X., Tang., L., et al. (2012). Crystal structure of an orthologue of the NaChBac voltage-gated sodium channel. *Nature* 486 (7401), 130–134. doi: 10.1038/nature11054

Zuberi, S. M., Brunklaus, A., Birch, R., Reavey, E., Duncan, J., and Forbes, G. H. (2011). Genotype-phenotype associations in SCN1A-epilepsies. *Neurol* 76 (7), 594–600. doi: 10.1212/WNL.0b013e31820c309b

Conflict of Interest: The authors declare that the research was conducted in the absence of any commercial or financial relationships that could be construed as a potential conflict of interest.

frontiers in Pharmacology

REVIEW
published: 28 February 2020
doi: 10.3389/fphar.2020.00139

Modulation of hERG K^+ Channel Deactivation by Voltage Sensor Relaxation

Yu Patrick Shi[†‡], *Samrat Thouta*[†‡] *and Thomas W. Claydon*[*]

Department of Biomedical Physiology and Kinesiology, Simon Fraser University, Burnaby, BC, Canada

OPEN ACCESS

Edited by:
Gildas Loussouarn, Université de Nantes, France

Reviewed by:
Jamie Vandenberg, Victor Chang Cardiac Research Institute, Australia
Matthew Perry, Victor Chang Cardiac Research Institute, Australia

***Correspondence:**
Thomas W. Claydon
thomas_claydon@sfu.ca

[†]Present address:
Yu Patrick Shi, Department of Molecular and Cellular Physiology, Stanford University School of Medicine, Stanford, CA, United States
Samrat Thouta, Michael Smith Laboratories and Djavad Mowafaghian Centre for Brain Health, University of British Columbia, Vancouver, BC, Canada

[‡]*These authors have contributed equally to this work*

Specialty section:
This article was submitted to Pharmacology of Ion Channels and Channelopathies, a section of the journal Frontiers in Pharmacology

Received: *25 November 2019*
Accepted: *31 January 2020*
Published: *28 February 2020*

Citation:
Shi YP, Thouta S and Claydon TW (2020) Modulation of hERG K^+ Channel Deactivation by Voltage Sensor Relaxation. Front. Pharmacol. 11:139. doi: 10.3389/fphar.2020.00139

The hERG (human-ether-à-go-go-related gene) channel underlies the rapid delayed rectifier current, I_{kr}, in the heart, which is essential for normal cardiac electrical activity and rhythm. Slow deactivation is one of the hallmark features of the unusual gating characteristics of hERG channels, and plays a crucial role in providing a robust current that aids repolarization of the cardiac action potential. As such, there is significant interest in elucidating the underlying mechanistic determinants of slow hERG channel deactivation. Recent work has shown that the hERG channel S4 voltage sensor is stabilized following activation in a process termed relaxation. Voltage sensor relaxation results in energetic separation of the activation and deactivation pathways, producing a hysteresis, which modulates the kinetics of deactivation gating. Despite widespread observation of relaxation behaviour in other voltage-gated K^+ channels, such as *Shaker*, Kv1.2 and Kv3.1, as well as the voltage-sensing phosphatase *Ci*-VSP, the relationship between stabilization of the activated voltage sensor by the open pore and voltage sensor relaxation in the control of deactivation has only recently begun to be explored. In this review, we discuss present knowledge and questions raised related to the voltage sensor relaxation mechanism in hERG channels and compare structure-function aspects of relaxation with those observed in related ion channels. We focus discussion, in particular, on the mechanism of coupling between voltage sensor relaxation and deactivation gating to highlight the insight that these studies provide into the control of hERG channel deactivation gating during their physiological functioning.

Keywords: hERG, relaxation, voltage sensor, gating, deactivation, mode-shift

OVERVIEW

The mechanisms by which membrane depolarization triggers the voltage sensing unit to undergo conformational changes that lead to opening of the voltage-gated potassium (Kv) channel pore are of significant interest. Recent findings have shown that prolonged activation of Kv channels leads to further reconfiguration of the S4 voltage sensor into a stable activated relaxed state. This relaxation imparts hysteresis, or mode-shift behavior, where the voltage-dependence of S4 return and subsequent pore closure occurs at more hyperpolarized membrane potentials than are required to activate S4 and open the pore. Voltage sensor relaxation was recently demonstrated in hERG channels, and is likely a contributor to slow deactivation gating. The significance of relaxation and

stabilization of the activated hERG voltage sensor have only recently begun to be recognized as potential orchestrators of the unique and critical I_{Kr} repolarizing current during the cardiac action potential. This review aims to highlight this role by describing current understanding of the role of voltage sensor relaxation in the slow deactivation gating of hERG channels. To begin, we first provide a brief overview of the structure-function aspects of hERG channels, followed by detailed review of the mechanistic determinants of voltage sensor relaxation and its connection to slow deactivation gating in hERG channels.

Structure of the hERG Channel

Recent cryogenic electron microscopy (cryo-EM) structures of the hERG channel and the related eag1 channel in a depolarized conformation have provided direct and highly valuable insight into understanding the gating properties of hERG channels and their role in the heart and drug discovery (Whicher and MacKinnon, 2016; Wang and MacKinnon, 2017). The *KCNH2* gene encodes the pore-forming α-subunit of the voltage-gated K^+ channel, Kv11.1, commonly referred to as hERG. The hERG channel is tetrameric, with each subunit comprised of six α-helical transmembrane segments (S1–S6) and large intracellular N- and C-terminus domains (**Figure 1**). Voltage sensitivity of the hERG channel is predominantly imparted by the S1–S4 transmembrane segments, with S4 containing six positively charged amino acids and S1–S3 segments possessing several negatively charged amino acids thought to act as counter-charges. The impetus for conformational changes leading to pore opening is the movement of the positively charged amino acids of S4 in response to the force exerted upon them by the electric field across the membrane. Since the transmembrane segments of hERG resemble those of the eag1 family member, Kv10.1, it is reasonable to presume that the three-dimensional structure of the hERG S4 segment is likely to be a 3_{10} helix (Whicher and MacKinnon, 2016), although the dynamic structure of the S1–S4 voltage sensing domain (VSD) during open to closed transitions is not known. The VSD of hERG has previously been suggested to be coupled to the pore domain (PD), formed by S5 and S6, *via* the S4–S5 linker, a short flexible connecting sequence known to be important in electromechanical coupling of VSD motions with the pore in other Kv channels (Tristani-Firouzi et al., 2002; Ferrer et al., 2006; Van Slyke et al., 2010; Cheng and Claydon, 2012; Ng et al., 2012; Hull et al., 2014). However, the recent cryo-EM structures of eag1 and hERG channels have questioned this. The structures revealed that the S4–S5 linker is a short loop that is not domain swapped (i.e., the S4–S5 linker of one subunit interacts with the C-terminal portion of the S6 helix in the same subunit, rather than the adjacent subunit) and thus, may not function as a mechanical lever. The S6 segment of hERG channels also lacks a proline-valine-proline (PVP) motif that would narrow the pore region and which, in other channels, is suggested to orient the S6 to allow it to interact with the S4–S5 linker. The lack of this structure combined with the short non-domain swapped S4–S5 linker contributes to the idea that eag family channels may have unconventional means of electromechanical coupling (Thouta et al., 2014; Lörinczi et al., 2015; Whicher and MacKinnon, 2016; Malak et al., 2017; Malak et al., 2019). An alternative model of

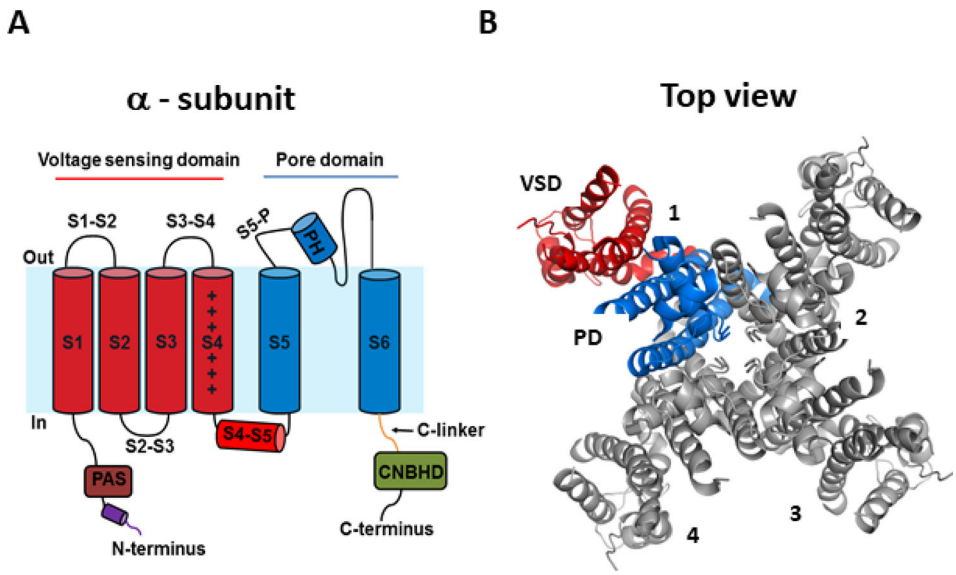

FIGURE 1 | hERG channel structure. **(A)** Schematic of a single α-subunit of the hERG channel comprising of six α-helical transmembrane segments (S1–S6). The voltage sensing domain (VSD) (S1–S4) and pore domain (PD) (S5–S6) are highlighted in red and blue, respectively. Important features of the hERG channels include a short S4–S5 linker, an intracellular N-terminus containing a PAS domain shown in brown, a cap region shown in purple, and the C-terminus containing a C-linker shown in green and a cNBHD domain shown in gray. **(B)** Top view of the cryogenic electron microscopy (cryo-EM) structure of the hERG channel assembled as a tetramer with the central conducting pore formed by pore domains from all four subunits. For clarity, only one subunit is highlighted (5VA1.pdb) (Wang and MacKinnon, 2017).

gating translation from the VSD to the PD (Whicher and MacKinnon, 2016; Wang and MacKinnon, 2017) proposes that the deactivated (down state) of the S4 voltage sensor interacts directly with the C-linker to induce a bend in S6 to close the pore gate. The up or depolarized conformation of S4 would enable rotation of the C-linker such that it loosens the S6 thereby relieving the high-energy bend to open the pore. The involvement of the cytosolic domains in the translation of voltage sensing to the pore region is an intriguing possibility that requires further functional testing to establish whether this is the means by which VSD movement is translated to the PD in hERG channels. Certainly, the cytosolic N- and C-terminal domains play a critical role in gating of hERG channels and contain structurally well conserved domains among closely related channels (Adaixo et al., 2013). The well-structured distal N-terminus contains a Per-Arnt-Sim (PAS) domain (residues 1–136) participates in functionally important interactions with the S4–S5 linker and the C-terminus to regulate channel deactivation (Fernández-Trillo et al., 2011; Adaixo et al., 2013; de la Peña et al., 2015; de la Peña et al., 2018). The main physical feature of the hERG C-terminus is the cyclic nucleotide-binding homology domain (cNBHD) which shares homology with that in cyclic nucleotide-gated (cNG) and hyperpolarization-activated cyclic nucleotide-gated (HCN) channels. However, the cNBHD does not appear to be directly regulated by binding of cyclic nucleotides (Brelidze et al., 2012; Marques-Carvalho et al., 2012; Brelidze et al., 2013) as a result of the binding pocket being occupied by an "intrinsic ligand" (Brelidze et al., 2012; Marques-Carvalho et al., 2012; Brelidze et al., 2013; Zhao et al., 2017), which mediates interactions between the PAS domain and cNBHD to regulate channel closing (Zhao et al., 2017; Codding and Trudeau, 2019). Further structures of closed channel state would undoubtedly contribute to our understanding of the dynamic structure of hERG channels.

Gating of the hERG Channel

Compared to other Kv channels, such as the archetypal *Shaker* channel, hERG channels exhibit unusual gating properties. hERG channels activate and deactivate slowly, but inactivate and recover from inactivation rapidly and with a strong dependence on voltage (Sanguinetti et al., 1995; Trudeau et al., 1995) (**Figure 2A**). The result is that upon membrane depolarization, only a small outward current is generated, because the transition from closed to open states is slow (e.g., hERG activates in ~60 ms at +60 mV, whereas *Shaker* activates in <2 ms) (Hoshi et al., 1994; Wang et al., 1997) and channels inactivate rapidly (hERG inactivates in 1–2 ms at +60 mV) (Schönherr and Heinemann, 1996; Smith et al., 1996; Spector, 1996; Rasmusson et al., 1998). Upon membrane repolarization, however, channels recover rapidly from inactivation into the open state giving rise to a resurgent current before slow channel deactivation (**Figure 2B**). This resurgent current provides a significant contribution to cardiac repolarization associated with the termination of the action potential. Despite their critical role in determining cardiac excitability, the molecular bases of these unusual gating properties remain poorly understood. Below, we

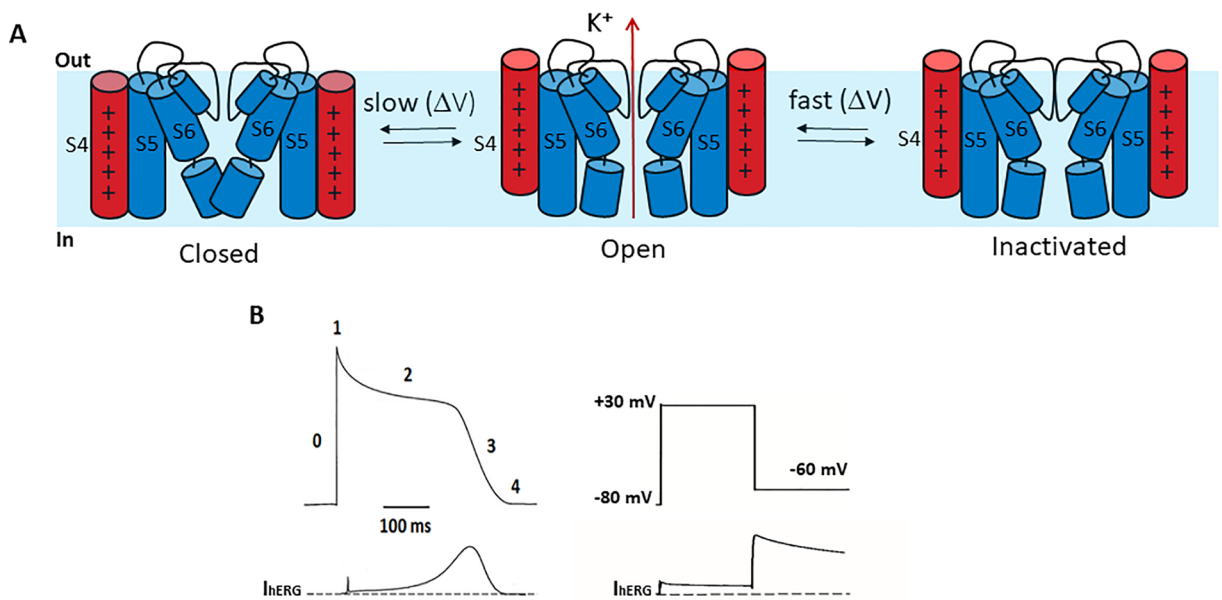

FIGURE 2 | hERG channel gating. **(A)** Schematic of the hERG channel gating scheme representing the state transitions between the closed and open stated being slower than transitions between open and inactivated states. **(B)** Left. A stylized ventricular cardiac action potential waveform (top) with five distinct phases and the corresponding current conducted by hERG channels (bottom). Right. In a step voltage clamp experiment, depolarization to +30 mV activates and quickly inactivates hERG channels, producing a small outward current. Upon repolarization to –60 mV hERG channels quickly recover from inactivation, producing a large resurgent current that decays slowly due to slow deactivation.

briefly highlight current knowledge pertaining to each gating step, since these are reviewed in detail elsewhere (Cheng and Claydon, 2012; Vandenberg et al., 2012).

Activation

The physiological significance of slow hERG channel activation is a reduced channel availability and reduced repolarizing current during the early phases of the cardiac action potential. Several studies measuring gating currents and/or fluorescence reports of VSD movement suggest that the unusually slow activation in hERG channels results from slow voltage sensor movement that is the rate limiting step (Smith and Yellen, 2002; Piper et al., 2003; Piper et al., 2005; Van Slyke et al., 2010; Thouta et al., 2014), although some fraction of S4 charge appears to move rapidly (Wang et al., 2013; Goodchild and Fedida, 2014). The molecular determinants of slow VSD activation in hERG channels remains poorly understood. Like other K_v channels, the hERG channel contains a series of basic residues in the S4 voltage sensor that traverse the electric field upon changes in membrane voltage (Bezanilla et al., 1991; Starace and Bezanilla, 2004; Ahern and Horn, 2005) and this induces opening of the channel pore (Lu et al., 2002; Long, 2005). The hERG channel VSD comprises fewer charges than *Shaker*-like channels, with six basic residues: K525, R528, R531, R534, R537, and K538. Mutation scanning shows that mutation of K525, R528, and R531 perturbed activation gating, suggesting that these sidechains influence gating charge translocation (Subbiah et al., 2004; Piper et al., 2005). This is supported by the state-dependent accessibility of these sites to membrane-impermeable thiol-modifying reagents during activation (Zhang et al., 2004; Elliott et al., 2009). Limiting slope analysis estimates of the number of elemental gating charges moved per channel tetramer during activation (~8 e_o) (Zhang et al., 2004) are also consistent with these observations. Interestingly, this suggests more limited movement of the hERG S4 segment than in *Shaker* channels, where MTSET accessibility studies show the translocation of four outermost arginines, consistent with the movement of ~12–14 e_o across the electric field (Aggarwal and MacKinnon, 1996; Seoh et al., 1996). Of the outer three hERG S4 charges, K525 is particularly important in stabilizing closed channel states in a manner that involves non-electrostatic functional interactions with a gating charge transfer center formed by F463 and D466 within the voltage sensing unit (Liu et al., 2003; Subbiah et al., 2004; Cheng et al., 2013). The presence of lysine at this site is peculiar to hERG channels and may contribute to slow gating. The presence of K538, at the base of the S4 segment alongside R537, is equally unusual and is important in stabilizing closed channel states *via* functional interactions with the gating charge transfer center (Cheng and Claydon, 2012; Cheng et al., 2013). These observations are supported by the cryo-EM hERG structure (Wang and MacKinnon, 2017) and lead to the suggestion that overcoming the energetics of stabilizing interactions between the K525 outermost S4 charge and the gating charge transfer center, and the shuttling of S4 charges through the transfer center, may limit hERG channel activation kinetics, although this remains to be directly demonstrated.

Inactivation

Slow activation of hERG channels is accompanied by an unusual fast inactivation process that occurs more rapidly than activation and is voltage-dependent. hERG channel inactivation is P/C-type in nature in that it is slowed in the presence of external tetraethylammonium and largely unaffected by deletion of N-terminus (Schönherr and Heinemann, 1996), and sensitive to ion occupancy of the selectivity filter (Schönherr and Heinemann, 1996) suggesting that inactivation of hERG channels involves a collapse of the selectivity filter (Smith et al., 1996). The recent hERG cryo-EM structure highlighted subtle rearrangements of the selectivity filter that might correlate with rapid hERG inactivation gating (Wang and MacKinnon, 2017). In particular, the unique position of F627 within the selectivity filter may play a key dynamic role, which may be demonstrated by future functional investigation.

The voltage-dependence of inactivation does not appear to derive from positively charged S4 residues (Zhang et al., 2004) and evidence of distinct origins of the voltage-dependence of activation and inactivation comes from an alanine scan of hERG S4 residues, which highlighted a discrete cluster of residues that perturbed inactivation when mutated without significant effect on activation gating (Piper et al., 2005). The most comprehensive description of the molecular determinants of inactivation involves a global model with complex rearrangements throughout the channel that are initiated by K^+ efflux from the pore. In this Japanese puzzle box model a precise sequence of moves that involves interconnected but separate components is required to open and close the inactivation gate (Wang et al., 2011).

Deactivation

Another hallmark feature of hERG channel gating is slow deactivation, which is important for producing the resurgent current during repolarization of the cardiac action potential (Sanguinetti et al., 1995; Smith et al., 1996). Regulation of slow deactivation in hERG channels is complex, and is modulated by multiple regions of the channel. Mutations within the distal N-terminus Cap domain, consisting of residues 1–26, accelerate deactivation suggesting that this domain is essential for normal hERG deactivation gating (Cabral et al., 1998; Wang et al., 1998; Gustina and Trudeau, 2009; Muskett et al., 2011; Ng et al., 2011). The recent hERG cryo-EM structure shows that the N-terminus is indeed structurally integrated within the VSD-PD interface (Wang and MacKinnon, 2017). Consistent with this, application of a PAS domain fragment (1–135) restores slow deactivation to N-terminally deleted (Δ2–354) fast deactivating hERG channels (Cabral et al., 1998; Gustina and Trudeau, 2009; Gustina and Trudeau, 2011; Gustina and Trudeau, 2012; Gianulis et al., 2013; Gustina and Trudeau, 2013) and this is dependent on interactions between the PAS and cNBHD (Gustina and Trudeau, 2011; Gianulis et al., 2013). The N-terminus may also interact with the S4–S5 linker to regulate deactivation gating

(Wang et al., 1998; Li et al., 2010; Van Slyke et al., 2010; de la Peña et al., 2011).

Slow deactivation is also influenced by the transmembrane core of the channel. Mutation of the negative S4 counter charge residues in S1–S3 all accelerated deactivation kinetics leading to the proposal for a "master-switch" in hERG channels that maintains slow deactivation (Liu et al., 2003). In this model, each of the negative residues need to be present to keep the master-switch in the ON position, and mutations or conditions that turn OFF the master-switch set the channel in a fast deactivation mode (Liu et al., 2003). A potential candidate for this master-switch has been suggested to be the PAS domain in the N-terminus (Liu et al., 2003). Another potential regulator for slow deactivation is voltage sensor relaxation and is an intrinsic property of the VSD in response to depolarization that stabilizes the activated VSD in a relaxed, stable conformation. In doing so, more energy is required to return the voltage sensor than to activate it, thus inducing a hyperpolarizing-shift in the voltage-dependence of deactivation compared to that for activation, and a slowing of the deactivation kinetics. Recent studies suggest a role for the N-terminus in stabilizing the activated voltage sensor in a relaxed state (Tan et al., 2012; Goodchild et al., 2015; Thouta et al., 2017). As an important contributor to slow deactivation, voltage sensor relaxation could perhaps act as a master-switch that is influenced by mutations within the transmembrane core, as well as the N-terminus. In the following sections, we discuss current understanding of relaxation in hERG channels and the mechanisms by which stabilizing voltage sensor transitions might be coupled to the pore to control closing.

Hysteresis of Gating in Voltage-Dependent Ion Channels

Hysteresis is a phenomenon by which a system displays differing responses depending on its history. In other words, hysteretic behavior is thought to give a system "memory." Such hysteretic behavior is observed in numerous chemical, physical, biological, and engineering systems. One example of the physiological importance of hysteresis is in the regulation of activation, deactivation and inactivation gating of voltage-gated Na^+ (Nav) channels and Kv channels to control action potential firing, which has been expertly reviewed elsewhere (Villalba-Galea, 2017). Hysteresis in ion channels has also been suggested to play a critical role in the normal heartbeat (Männikkö et al., 2005), rhythmic firing of pacemaking neurons (Bruening-Wright and Larsson, 2007), the regulation of cellular excitability (Chatelain et al., 2012; Corbin-Leftwich et al., 2016), and temperature sensitization (Liu et al., 2011; Liu and Qin, 2015).

Hysteresis in voltage-gated ion channels can be observed during each activation and deactivation cycle. An early observation in squid giant axon Nav channels showed a hyperpolarizing-shift of the voltage-dependence of gating charge return compared with that of gating charge activation when the membrane was held for some time at a depolarized potential (Bezanilla et al., 1982). In this case, this hysteresis behavior indicated a change in the energy landscape during deactivation such that the return of charge to rest occurred *via* an alternative kinetic pathway than that during activation. The measured observation is that the voltage sensor required stronger repolarization to return to its resting position and to close the pore gate than was required to activate it (**Figure 3A**).

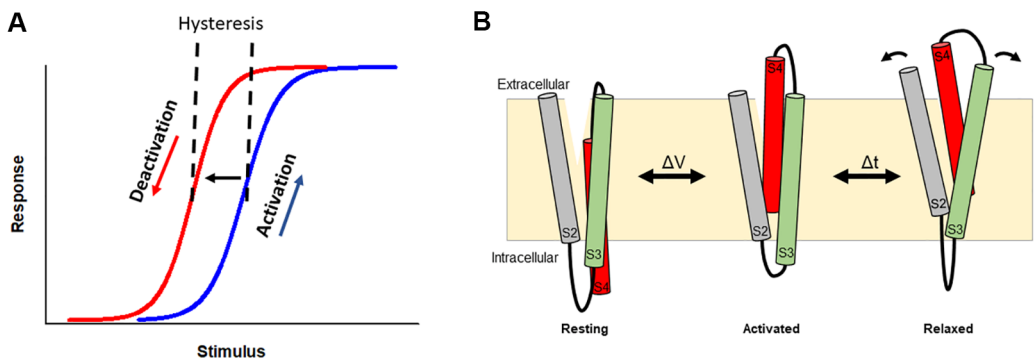

FIGURE 3 | Hysteresis in hERG channels due to voltage sensor relaxation. **(A)** In a hysteretic system, the response of the system differs in response to activating and deactivating stimuli. In hERG channels, depolarization activates (blue) channels, which then shift to a different mode (i.e., enter the relaxed state), from which deactivation follows a different response upon repolarization (red). This produces a hysteresis. **(B)**. Cartoon representation of stabilization the S4 voltage sensor into a relaxed conformation during voltage sensor relaxation. Arrows represent hypothetic reorganization of helices during relaxation as a result of interactions involving acidic residues in S2–S3. **(C)**. The Shi et al. model of voltage sensor gating adopts the formulation of the Piper *et al*. gating charge model and includes addition of description of hysteresis behavior of the hERG channel voltage sensor as a result of voltage sensor relaxation (Shi et al., 2019).

Similar hysteresis behavior has been reported in a broad collection of channels including sodium channels of the squid giant axon and NaChBac (Bezanilla et al., 1982; Kuzmenkin et al., 2004), calcium channels (Brum and Rios, 1987; Brum et al., 1988; Shirokov et al., 1992), potassium channels, such as KcSA (Tilegenova et al., 2017), *Shaker* (Haddad and Blunck, 2011; Lacroix et al., 2011; Labro et al., 2012; Priest et al., 2013), Kv1.2 (Labro et al., 2012), Kv3.1 (Labro et al., 2015), Kv7.2/7.3 (Corbin-Leftwich et al., 2016), Kv11.1(hERG) (Piper et al., 2003; Tan et al., 2012; Hull et al., 2014; Goodchild et al., 2015; Thouta et al., 2017; Shi et al., 2019), Kv12.1 (Dierich et al., 2018), and HCN channels (Elinder et al., 2006; Bruening-Wright and Larsson, 2007). In HCN channels, the term mode-shift has been used to describe the hysteresis in the voltage-dependence of activation and deactivation in response to prolonged depolarization (Elinder et al., 2006), and the terms hysteresis and mode-shift are often used to describe the separation between the voltage-dependence of Kv channel activation and deactivation. Here we use the term hysteresis to describe the separation of the voltage-dependence of activation and deactivation, and mode-shift to describe the mechanism for the hysteretic behavior.

The mechanistic basis that underlies hysteretic behavior in K^+ channels has only recently been explored. Initially, the time course of development of the mode-shift was correlated with that of P/C-type inactivation, suggesting that P/C-type inactivation is required for mode-shift to occur (Bezanilla et al., 1982; Olcese et al., 1997). In KcsA channels, mode-shift of gating has also been suggested to be an intrinsic property of the PD caused by structural changes at the selectivity filter associated with P/C-type inactivation (Tilegenova et al., 2017). Other studies showed that mutations in the S4–S5 linker and S6 of *Shaker* channels which uncouple the VSD from the PD impede mode-shift, suggesting that mode-shift arises from the mechanical load placed on the voltage VSD by the PD (Batulan et al., 2010; Haddad and Blunck, 2011). However, there is also plausible evidence that mode-shift behavior is an intrinsic property of the voltage sensor. For example, hysteresis is observed in proteins that comprise a voltage sensor-like domain without a canonical pore, such as Hv1 proton channels (Villalba-Galea, 2014), *Shaker* channels with the PD deleted (Zhao and Blunck, 2016), and *Ciona intestinalis* voltage sensor-containing phosphatase (*Ci*-VSP) (Villalba-Galea et al., 2008). In the latter, a site-specific fluorophore tag reporting voltage sensor dynamics revealed a slow component of fluorescence change that is kinetically distinct from that reporting charge movement. This suggested that the voltage sensors adopt an alternate conformation following activation, which the authors termed the relaxed state of the voltage sensor (**Figure 3B**). Additional studies in *Shaker* channels demonstrated that the mode-shift is caused by prolonged depolarization, which shifts the voltage sensor into this more stable relaxed state, a process termed voltage sensor relaxation (Lacroix et al., 2011; Labro et al., 2012; Priest et al., 2013). In support of this idea, voltage sensor relaxation in *Shaker* channels is also sensitive to both the length and composition of the S3–S4 linker (Priest et al., 2013). These observations emphasize an intrinsic predilection of the voltage sensing unit to relax into a stable activated state from which S4 return requires the input of additional energy.

Mode-Shift and Voltage Sensor Relaxation in hERG Channels

hERG channel gating displays a prominent hysteresis in the voltage-dependencies of activation and deactivation of both the movement of the voltage sensor (voltage sensor mode-shift) and the gating of the pore (ionic mode-shift). Interestingly, mode-shift in hERG channels occurs on a physiological time scale suggesting that the dynamic switching of voltage-dependencies of activation and deactivation gating may contribute to the amplitude and timing of the repolarizing I_{Kr} current during the cardiac action potential (Piper et al., 2003; Tan et al., 2012; Goodchild et al., 2015; Thouta et al., 2017; Shi et al., 2019). In *Shaker* and Kv1.2 channels, the time-dependence of voltage sensor stabilization and mode-shift were measured by applying depolarizing steps of increasing duration and observing the progressive slowing of charge return (Lacroix et al., 2011; Labro et al., 2012). Charge return slowed in a biphasic manner with the faster phase kinetically associated with pore opening and therefore was suggested to reflect stabilization of the activated voltage sensor by the open pore. The second component of charge return slowing occurred over 2–4 s and was attributed to reconfiguration of the voltage sensor into the relaxed state. In Kv3.1 channels a very rapid component of charge return that kinetically precedes pore gate opening was observed, and this was attributed to an ultra-fast relaxation mechanism in these channels (Labro et al., 2015). In hERG channels, increasing depolarization duration slows charge return (Goodchild and Fedida, 2014; Goodchild et al., 2015; Thouta et al., 2017; Shi et al., 2019). The slowing of voltage sensor return showed a biphasic dependence upon depolarizing step duration similar to that in *Shaker* and Kv1.2 channels, with a fast phase (tau = 34 ms) and a slower component (tau = 2.5 s) (Thouta et al., 2017). These data highlight two important points. The first is that the fast phase correlates kinetically with pore gate opening, which is slower in hERG than in *Shaker* channels. These findings therefore support the assertion that stabilization of the activated voltage sensor occurs in response to opening of the pore gate. The second is that the time course of the slower component of voltage sensor stabilization is similar in hERG, *Shaker*, and Kv1.2 channels despite marked differences in inactivation properties: *Shaker* and Kv1.2 inactivation occurs on the timescale of seconds and is voltage-independent, whereas hERG inactivation is strongly voltage-dependent and occurs with a tau of a few milliseconds. These observations have led to the suggestion that relaxation is unrelated to inactivation in hERG channels, an idea that is consistent with studies showing a lack of correlation between inactivation and mode-shift in hERG mutant channels that either reduce (S631A) or abolish (S620T) inactivation (Piper et al., 2003; Tan et al., 2012).

Stabilization of the activated hERG voltage sensor by the open pore and by its transition into the relaxed state most likely contributes to the observed voltage sensor mode-shift by

retarding charge return upon repolarization. A similar hysteresis is observed in the voltage-dependencies of ionic current flow through the pore during activation and deactivation. One question worth considering is to what extent relaxation and stabilization of the voltage sensor contribute to these hysteretic behaviors. When voltage steps of physiological duration were applied to measure activation and deactivation, hERG channels showed a profound ionic hysteresis with the voltage-dependence of ionic current activation and deactivation separated by ~65 mV on the voltage axis. However, longer voltage step durations that allow the slow transitions to reach steady-state, produced an ionic hysteresis of ~15 mV (Thouta et al., 2017). Similar experiments capturing pseudo steady-state gating charge movement revealed a voltage sensor hysteresis of ~40 mV, much greater than that of ionic current through the pore. This observation has led to the suggestion that, upon repolarization, pore closing is energetically more favorable than the return of the voltage sensor to its resting state. The consequence of this is that the pore may close while some of the voltage sensors in the tetramer remain in their extruded position. Approximations suggest that ~25% of charge (functionally equivalent to one voltage sensor per channel tetramer) is needed to return to close the pore (Thouta et al., 2017).

Together, the evidence from hERG channels support a model in which depolarization stabilizes voltage sensors in an activated configuration producing hysteretic behavior, and that return of a single voltage sensor to the resting state is sufficient to close the channel pore gate. In this model, pore gate opening slows the return of the voltage sensor involving some form of coupling between the PD and VSD, followed by a further slower stabilization of the activated voltage sensor into the relaxed state, which is an intrinsic property of the sensor itself. In the next section, we consider evidence indicating potential structural interactions that underlie these mechanistic behaviors.

Structural Determinants of hERG Voltage Sensor Stabilization and Relaxation

The S1–S2 and S3–S4 Extracellular Linkers

In *Shaker* channels the S3–S4 linker plays a role in stabilizing the activated configuration of the voltage sensor in response to prolonged depolarization (Priest et al., 2013). Reducing the length of the 31 residue linker increased the extent of voltage sensor relaxation and a role for a negatively charged cluster of residues at the N-terminal margin of the linker was also noted. Although the extent of voltage sensor relaxation has not been quantified in many channels, available data suggested a strong inverse correlation between S3 and S4 linker length and the extent of voltage senor relaxation (Priest et al., 2013). However, modifications to the hERG S3–S4 linker have little influence on mode-shift behavior (Thouta et al., 2017). Neither increasing the length, nor alteration of the amino acid composition of the short native linker, altered the hysteresis in hERG channels. Similar findings were observed with alterations to the S1–S2 linker. These observations suggest that in hERG channels the extracellular linkers do not play a role in stabilizing the activated configuration of the voltage sensor as they appear to do in *Shaker* channels. This may be due to the unique configuration of S4 gating charges as discussed below.

The S4–S5 Linker

In *Shaker* channels specific interactions between residues in the S4–S5 linker and the pore contribute to mode-shift behavior (Haddad and Blunck, 2011). In hERG channels, information about the influence of the S4–S5 linker on mode-shift and relaxation is less comprehensive. Such information is particularly relevant given the shorter linker length and its non-domain swapped connection of the VSD with the PD in hERG channels. Functional studies of hERG channels split within the S4–S5 linker such that tetramers are formed by independent and uncoupled VSD and PD show perturbations in deactivation gating, with less impact on activation gating (Lörinczi et al., 2015). This observation suggests that slow deactivation gating in hERG channels is incumbent upon communication involving the S4–S5 linker. This is consistent with observations that perturbations within the S4–S5 linker dramatically influence the open-closed equilibrium in hERG channels (Sanguinetti and Xu, 1999; Tristani-Firouzi et al., 2002; Ferrer et al., 2006; Alonso-Ron et al., 2008; Van Slyke et al., 2010; Hull et al., 2014). However, while mutations within the hERG S4–S5 linker are well known to accelerate deactivation gating, available evidence from G546L mutant channels shows that voltage sensor mode-shift remains intact in these channels (Hull et al., 2014). Interestingly, while increasing depolarizing durations slows voltage sensor return in G546L mutant channels, the pattern of slowing is monophasic, rather than biphasic, lacking the fast phase of slowing attributed to pore induced stabilization of the activated voltage sensor (Thouta et al., 2017). This finding leads to the suggestion that S4–S5 linker perturbation interferes with pore-to-voltage sensor coupling in the control of deactivation. Such an influence of the S4–S5 linker on the coupling between the pore gate and the activated voltage sensor is consistent with the voltage sensing mechanism suggested for eag channel gating in which the S4–S5 linker alters the interaction between S4 and the inner S6, directing S4 toward the C-linker that loosens the helical bundle and opens the pore (Whicher and MacKinnon, 2016). Thus, both functional and structural data portray a key role for the S4–S5 linker in communicating between the pore and the voltage sensor to control hERG channel deactivation gating. These findings may also be interpreted to suggest that the mechanisms of voltage sensor stabilization by the open pore gate and by relaxation are separable, and also that pore gate stabilization of the voltage sensor contributes minimally to the observed hysteresis in the voltage-dependencies of voltage sensor activation and return in hERG channels.

The Voltage Sensor Domain (S1–S4)

Outward translocation of the hERG voltage sensor upon activation involves the formation of stabilizing electrostatic interactions between basic residues in S4 and extracellular acidic counter charges in S1 (D411), S2 (D456 and D460), and S3 (D509) (Liu et al., 2003; Zhang et al., 2005; Piper et al., 2008).

Double mutant cyclic analysis revealed energetic coupling between R531 and D456, D460, and D509 during activation and with D411 and D466 through a cooperative ionic-pairing interaction mechanism (Piper et al., 2008). Accessibility studies have also revealed that D460 and D509 stabilize the activated state (Liu et al., 2003), which is consistent with observations that neutralization of any of the acidic charges accelerates deactivation kinetics, likely by disrupting electrostatic interactions with S4 basic residues (Liu et al., 2003; Fernandez et al., 2005; Piper et al., 2008; Shi et al., 2014). Interestingly, disruption of the electrostatic pairing involving D509, either by protonation or alanine substitution, destabilizes the relaxed state of the voltage sensor leading to the loss of hysteresis and accelerated deactivation (Shi et al., 2019). This suggests that external acidic residues form stabilizing electrostatic interactions that are critical in recruiting the voltage sensor into the relaxed conformation and that these consequently control pore closure. Taken together with the observed role of the S4–S5 linker in coupling pore motions to stabilization of the S4 described in the previous section, these findings indicate dual regulation, i.e., at both extracellular and intracellular ends, of S4 movement that contributes to mode-shift behavior in hERG channels and their unique slow deactivation properties. Further studies will determine whether all S4 counter charges play a similar stabilizing role, as well as the specific roles played by each S4 gating charge.

The N-Terminus

The N-terminus is well recognized as an integral component of deactivation gating in hERG channels that stabilizes the open state of the channel (Cabral et al., 1998; Wang et al., 1998; Wang et al., 2000; Muskett et al., 2011; Ng et al., 2011; Gustina and Trudeau, 2011). However, the mechanism by which this occurs still lacks definition. Using voltage clamp fluorimetry (VCF) to track voltage sensor movement, Tan et al. showed that while deletion of the distal N-terminus (or even single point mutations, R4A, R5A, G6A) accelerated voltage sensor return upon repolarization, perturbation of the N-terminus did not alter mode-shift of the voltage sensor (Tan et al., 2012). This finding is consistent with an intrinsic mechanism of voltage sensor stabilization and that coupling of the pore with the voltage senor was disturbed by the N-terminal perturbations. Indeed, the authors proposed that the N-terminus serves as an adaptor, mediating communication between the voltage sensor and pore gate. Initial measurements of voltage sensor movement from gating currents reported that N-terminus perturbations might reduce voltage sensor mode-shift (Goodchild et al., 2015); however, subsequent longer duration recordings enabling steady-state measurements showed that the mode-shift of gating charge movement in hERG channels lacking the distal N-terminus (Δ2–135) is similar to that in WT channels (Thouta et al., 2017). In this study, slowing of charge return upon increasing depolarizing step duration measured in Δ2–135 channels showed a biphasic function with similar early and late components of charge return slowing to that seen in full-length channels. These observations suggest that both the stabilization of the voltage sensor by the open pore gate and the intrinsic voltage sensor relaxation process are preserved in hERG channels lacking the N-terminus. It is a clear and consistent observation, however, that perturbation of the N-terminus enhances the kinetics of voltage sensor return (Tan et al., 2012; Goodchild et al., 2015; Thouta et al., 2017). This observation supports the idea proposed by Tan et al. that closure of the pore during deactivation can be modified at the interface of the voltage sensor and pore gate by the N-terminus independent of changes in voltage sensor configuration and demonstrates that coupling of the voltage sensor with the pore gate is an important mediator of deactivation in addition to relaxation of the voltage sensor (see section below on hERG activator compounds) (Tan et al., 2012).

Targeted Modulation of hERG Voltage Sensor Relaxation

The Relaxed State of the Voltage Sensor Is Destabilized by Extracellular Protons

hERG channel deactivation kinetics are sensitive to changes in the extracellular proton concentration and numerous studies have shown that acidosis accelerates deactivation rate (Anumonwo et al., 1999; Bérubé et al., 1999; Jiang et al., 1999; Terai et al., 2000; Bett and Rasmusson, 2003; Du et al., 2010; Zhou and Bett, 2010; Du et al., 2011; Van Slyke et al., 2012; Shi et al., 2014; Shi et al., 2019). pH reductions within the physiological range (as low as pH 6.5) accelerated both the fast and the slow components of deactivation with a *pKa* of ~6.8 (Bett and Rasmusson, 2003; Shi et al., 2019) with little effect channel conductance, and other voltage-dependent gating parameters (Jiang et al., 1999; Bett and Rasmusson, 2003; Shi et al., 2019). Until recently, the mechanism by which protons modulate deactivation was unknown although studies had ruled out involvement of extracellular histidine residues (Jiang et al., 1999; Van Slyke et al., 2012), the N-terminus, and P/C-type inactivation, and shown the action to be mediated by an extracellular site (Jiang et al., 1999).

Measurements of voltage sensor relaxation from fluorescence reports of voltage sensor movement and gating current recordings recently provided a plausible mechanism for the action of protons on hERG channel deactivation (Shi et al., 2019). These studies showed that acidic pH (pH 6.5) abolished voltage sensor mode-shift behavior. In particular, elevated external protons produced a depolarizing-shift of the voltage-dependence of the return of the voltage sensor upon repolarization without altering that of voltage sensor activation. This evidence suggested that the relaxed conformation of the hERG voltage sensor was destabilized by protons, such that less energy was required to return the voltage sensor to rest leading to an acceleration of pore gate closure at a given voltage during deactivation (Shi et al., 2019).

A key site of action for this effect of external protons may be three acidic residues, D456, D460, and D509, which form a cation binding pocket that coordinates Zn^{2+}, Mg^{2+}, Ca^{2+}, Cd^{2+}, as well as H^{+} (Ho et al., 1998; Jo et al., 1999; Fernandez et al., 2005; Lin and Papazian, 2007; Abbruzzese et al., 2010;

Kazmierczak et al., 2013; Shi et al., 2014; Shi et al., 2019). These sites may also interact with positive S4 gating charges as discussed in an earlier section. Consistent with a role for this site, neutralization of D509 abolished voltage sensor mode-shift at pH 7.4 mimicking the effect of external protons, which exerted no further effects on the voltage-dependence or kinetics of voltage sensor gating (Shi et al., 2019). This suggested that protons destabilize the relaxed state of the voltage sensor by disrupting electrostatic interactions formed between D509 and basic residues in the S4 voltage sensor. In the hERG cryo-EM structure, D509 is located at the external end of S3 close to the unresolved flexible S3–S4 linker, and readily accessible to extracellular aqueous solvents (Liu et al., 2003). Unlike in *Shaker* and *Ci*-VSP, where entry into the relaxed state may be tracked during long depolarizations as a slow fluorescence change from fluorophores attached at the top of the voltage sensor (Villalba-Galea et al., 2008; Haddad and Blunck, 2011), voltage sensor relaxation in hERG channels is not associated with overt fluorescence reports or gating charge. Therefore, entry into the relaxed state may involve subtle reconfiguration of the hERG voltage sensor that is not associated with charge movement across the membrane electric field or significant environment change experienced by a fluorophore label attached to the top of S4. Instead, transition into the relaxed state may involve, for example, widening of a water-filled cleft at the extracellular face of S2, S3, and S4 transmembrane segments, where water molecules may act to bridge H-bond or electrostatic interactions between D509 and positive charges in the S4 to stabilize the relaxed state. Higher resolution structures near the extracellular portion of S4 will undoubtedly contribute to better understanding of this as a possible mechanism. Similarly, information on the involvement of the other two acidic residues, D456 and D460, in stabilization of the relaxed voltage sensor will also contribute to a more complete picture. Moreover, given that divalent cations share a similar site of action, it is quite plausible that such ions would, like protons, destabilize relaxation. Indeed, various divalent ions are known to accelerate deactivation kinetics (Anumonwo et al., 1999; Fernandez et al., 2005; Lin and Papazian, 2007; Abbruzzese et al., 2010; Shi et al., 2014).

hERG Channel Activators May Alter Coupling Between the Voltage Sensor and Pore Gate

hERG channels are highly promiscuous in their ability to bind and be blocked by a wide range of drugs with varied structure and function. This causes acquired long QT syndrome (LQTS), and presents a significant challenge to new drug development. However, this promiscuity has led to the discovery and development of potential therapeutic activator compounds that aim to enhance or rescue lost hERG channel function as a result of inherited or acquired LQTS (Kang et al., 2005; Perry et al., 2007; Perry and Sanguinetti, 2008; Wu et al., 2016). A number of such small molecule compounds have been identified and some, such as RPR260243, niflumic acid, and ginsenoside Rg3, slow hERG deactivation gating (known as Type 1 activators) resulting in increased hERG current during cardiac repolarization. RPR260243, slows deactivation kinetics by interacting with L553 and F557 at the cytosolic end of S5 and S6 (Kang et al., 2005; Perry et al., 2007; Perry and Sanguinetti, 2008). In doing so, RPR260243 likely stabilizes the open conformation of the pore leading to slower deactivation (Gardner and Sanguinetti, 2015; Wu et al., 2015). Gating current measurements show that RPR260243 had no effects on the kinetics and voltage-dependence of hERG voltage sensor movements (Abbruzzese et al., 2010), suggesting that the activator exerts its effect by altering the coupling between the voltage sensor and pore closure during membrane repolarization. Thus, these findings further support the VSD-PD interface as a critical site of modulation of deactivation gating. Interestingly, another activator, NS1643, which is a type 2 compound that increases hERG current primarily by inducing a depolarizing-shift of the voltage-dependence of inactivation, may interact within the voltage sensing unit (Guo et al., 2015). Molecular simulations placed NS1643 close to L529 in S4 in a position that could plausibly interfere with S4 gating charge stabilizing interactions with the gating charge transfer center. It remains to be seen whether NS1643 modifies the stability of the relaxed voltage sensor configuration. As such, there may be therapeutic potential in rational design of small molecule activators of hERG channels that target sites known to modulate voltage sensor relaxation and/or its coupling to the pore gate to safely restore hERG channel dysfunction.

Kinetic Modeling of hERG Channel Relaxation

One of the earliest kinetic models constructed to describe I_{Kr} current in ventricular myocytes used first-order Hodgkin and Huxley formalism with the absence of an inactivated state (Zeng et al., 1995). Shortly thereafter, a model describing hERG channel activation and inactivation properties was developed (Wang et al., 1997), and the robustness of this Wang model is demonstrated by its continued usage. The Wang model was adopted to model I_{Kr} in the ten Tusscher human ventricular action potential waveform (ten Tusscher, 2003), although there have been several subsequent variations/refinements of the linear model, most notably to include a direct transition from the last closed state directly to the inactivated state (Clancy and Rudy, 2001; Mazhari et al., 2001; Oehmen et al., 2002). A detailed comparison of available models suggested that the most informative model was the original 5-state linear Wang model, since the forward rate of the final closed state to inactivated state transition is so low in other models that is it not required (Bett et al., 2011). Piper et al. provided the first Markov model to describe hERG channel gating current kinetics (Piper et al., 2003). This study showed that hERG on- and off-gating currents present a fast (0.5 ms) and a slow (53 ms) component. To model this behavior, two transitions, S0–S1 (fast component) and S1–S2 (slow component), were used in the gating scheme and these were treated independently for the four subunits with a positive cooperativity factor incorporated

for the second transition, prior to channel opening. A derivation of this model was also used to simulate and recapitulate gating currents in the presence of Cd^{2+} (Abbruzzese et al., 2010).

Recently, a similar model of gating current kinetics was used to describe hERG channel voltage sensor relaxation (Shi et al., 2019) (**Figure 3C**). In this model, two independent transitions per subunit are followed by a voltage-dependent concerted transition to the activated state, and a subsequent voltage-independent transition into the relaxed state. The model recapitulates the main features of hERG gating currents including voltage sensor mode-shift behavior. Moreover, acceleration of the rate out of the relaxed state to mimic the destabilization of relaxation observed at low pH, selectively abolished mode-shift behavior without other gating consequences, recapitulating the experimentally observed voltage sensor behavior. From this model, acceleration of de-relaxation, or exit from relaxed state, was sufficient to reduce voltage sensor mode-shift and supported the hypothesis that destabilization of the relaxed state of the voltage sensor may drive voltage sensor return leading to accelerated deactivation (Shi et al., 2019). One limitation to this model is the absence of description of ionic activation and inactivation gating of the channel, which are needed to develop a more complete model of gating transitions of the hERG channel voltage sensor in conjunction with pore gating during voltage sensor stabilization and relaxation. This might involve an approach used previously in *Shaker* and Kv1.2 channels to construct models that describe transitions of voltage sensor domains corresponding to those of the pore (Labro et al., 2012), which may be applicable for adaptation into a hERG scheme.

SUMMARY

Hysteresis of hERG channel voltage-dependent gating and the role of dynamic changes in voltage-sensitivity in the control of physiological function is only beginning to be uncovered. In this review we have discussed current knowledge pertaining to the mechanistic determinants of hysteretic behavior in hERG channels and how this might influence deactivation gating and therefore resurgent repolarizing current during the cardiac action potential. We have discussed the role of different channel regions in precipitating reconfiguration of the voltage sensor into a stabilized relaxed state and highlighted the importance of an extracellular site within the voltage sensor that contributes to this stabilization. We have also discussed evidence suggesting that intracellular modulators that regulate deactivation kinetics may do so by altering coupling between the voltage sensor and pore gate during repolarization. These discussions highlight what is known about the complex interactions that regulate movement of the voltage sensor and its coupling to the pore in the control of the physiologically critical slow deactivation of hERG channels and how they might be manipulated for potential therapeutic benefit. The discussion also highlights that much remains to be discovered about how the dynamic structural stability of the voltage sensor is modulated and influenced by a complex combination of extracellular ionic interactions and intracellular coupling to the pore. It remains to be determined, for example, how these complex interactions contribute to the slow activation of hERG channels, the fast and slow components of ON gating current, and the fast and slow components of channel deactivation. Further structural information, for example from closed hERG channels, will undoubtedly provide further mechanistic insight, as would functional studies investigating voltage sensor dynamics using fluorophore reporters or gating charge translocation measurements in isolated voltage sensor domains and comparing this with dynamics in VSD-PD coupled channels. Such future research will help to understand the complex structural determinants of hERG channel gating.

AUTHOR CONTRIBUTIONS

YS and ST contributed equally. YS, ST, and TC wrote and approved the manuscript.

FUNDING

This work was supported by a Canadian Institutes of Health Research Project Grant (PJT-156168) held by TC. Open access funds were provided by Simon Fraser University.

REFERENCES

Abbruzzese, J., Sachse, F. B., Tristani-Firouzi, M., and Sanguinetti, M. C. (2010). Modification of hERG1 channel gating by Cd^{2+}. *J. Gen. Physiol.* 136, 203–224. doi: 10.1085/jgp.201010450

Adaixo, R., Harley, C. A., Castro-Rodrigues, A. F., and Morais-Cabral, J. H. (2013). Structural properties of PAS domains from the KCNH potassium channels. *PloS One* 8, e59265. doi: 10.1371/journal.pone.0059265

Aggarwal, S. K., and MacKinnon, R. (1996). Contribution of the S4 segment to gating charge in the Shaker K^+ channel. *Neuron* 16, 1169–1177. doi: 10.1016/S0896-6273(00)80143-9

Ahern, C. A., and Horn, R. (2005). Focused electric field across the voltage sensor of potassium channels. *Neuron* 48, 25–29. doi: 10.1016/j.neuron.2005.08.020

Alonso-Ron, C., De La Peña, P., Miranda, P., Domínguez, P., and Barros, F. (2008). Thermodynamic and kinetic properties of amino-terminal and S4-S5 loop HERG channel mutants under steady-state conditions. *Biophys. J.* 94, 3893–3911. doi: 10.1529/biophysj.107.116731

Anumonwo, J. M. B., Horta, J., Delmar, M., Taffet, S. M., and Jalife, J. (1999). Proton and zinc effects on HERG currents. *Biophys. J.* 77, 282–298. doi: 10.1016/S0006-3495(99)76889-X

Bérubé, J., Chahine, M., and Daleau, P. (1999). Modulation of HERG potassium channel properties by external pH. *Pflugers Arch. Eur. J. Physiol.* 438, 419–422. doi: 10.1007/s004240050930

Batulan, Z., Haddad, G. A., and Blunck, R. (2010). An intersubunit interaction between S4-S5 linker and S6 is responsible for the slow off-gating component in Shaker K^+ channels. *J. Biol. Chem.* 285, 14005–14019. doi: 10.1074/jbc.M109.097717

Bett, G. C. L., and Rasmusson, R. L. (2003). Functionally-distinct proton-binding in HERG suggests the presence of two binding sites. *Cell Biochem. Biophys.* 39, 183–193. doi: 10.1385/CBB:39:3:183

Bett, G. C. L., Zhou, Q., and Rasmusson, R. L. (2011). Models of HERG gating. *Biophys. J.* 101, 631–642. doi: 10.1016/j.bpj.2011.06.050

Bezanilla, F., Taylor, R. E., and Fernández, J. M. (1982). Distribution and kinetics of membrane dielectric polarization. 1. Long-term inactivation of gating currents. *J. Gen. Physiol.* 79, 21–40. doi: 10.1085/jgp.79.1.21

Bezanilla, F., Perozo, E., Papazian, D., and Stefani, E. (1991). Molecular basis of gating charge immobilization in Shaker potassium channels. *Sci. (80)* 254, 679–683. doi: 10.1126/science.1948047

Brelidze, T. I., Carlson, A. E., Sankaran, B., and Zagotta, W. N. (2012). Structure of the carboxy-terminal region of a KCNH channel. *Nature* 481, 530–533. doi: 10.1038/nature10735

Brelidze, T. I., Gianulis, E. C., DiMaio, F., Trudeau, M. C., and Zagotta, W. N. (2013). Structure of the C-terminal region of an ERG channel and functional implications. *Proc. Natl. Acad. Sci.* 110, 11648–11653. doi: 10.1073/pnas.1306887110

Bruening-Wright, A., and Larsson, H. P. (2007). Slow conformational changes of the voltage sensor during the mode shift in hyperpolarization-activated cyclic-nucleotide-gated channels. *J. Neurosci.* 27, 270–278. doi: 10.1523/JNEUROSCI.3801-06.2007

Brum, G., and Rios, E. (1987). Intramembrane charge movement in frog skeletal muscle fibres. Properties of charge 2. *J. Physiol.* 387, 489–517. doi: 10.1113/jphysiol.1987.sp016586

Brum, G., Ríos, E., and Stéfani, E. (1988). Effects of extracellular calcium on calcium movements of excitation-contraction coupling in frog skeletal muscle fibres. *J. Physiol.* 398, 441–473. doi: 10.1113/jphysiol.1988.sp017052

Cabral, J. H. M., Lee, A., Cohen, S. L., Chait, B. T., Li, M., and Mackinnon, R. (1998). Crystal structure and functional analysis of the HERG potassium channel N terminus. *Cell* 95, 649–655. doi: 10.1016/S0092-8674(00)81635-9

Chatelain, F. C., Bichet, D., Douguet, D., Feliciangeli, S., Bendahhou, S., Reichold, M., et al. (2012). TWIK1, a unique background channel with variable ion selectivity. *Proc. Natl. Acad. Sci. U. S. A* 109, 5499–5504. doi: 10.1073/pnas.1201132109

Cheng, Y. M., and Claydon, T. W. (2012). Voltage-dependent gating of hERG potassium channels. *Front. Pharmacol.* 3, 83. doi: 10.3389/fphar.2012.00083

Cheng, Y. M., Hull, C. M., Niven, C. M., Qi, J., Allard, C. R., and Claydon, T. W. (2013). Functional interactions of voltage sensor charges with an S2 hydrophobic plug in hERG channels. *J. Gen. Physiol.* 142, 289–303. doi: 10.1085/jgp.201310992

Clancy, C. E., and Rudy, Y. (2001). Cellular consequences of HERG mutations in the long QT syndrome: precursors to sudden cardiac death. *Cardiovasc. Res.* 50, 301–313. doi: 10.1016/S0008-6363(00)00293-5

Codding, S. J., and Trudeau, M. C. (2019). The hERG potassium channel intrinsic ligand regulates N- and C-terminal interactions and channel closure. *J. Gen. Physiol.* 151, 478–488. doi: 10.1085/jgp.201812129

Corbin-Leftwich, A., Mossadeq, S. M., Ha, J., Ruchala, I., Le, A. H. N., and Villalba-Galea, C. A. (2016). Retigabine holds KV7 channels open and stabilizes the resting potential. *J. Gen. Physiol.* 147, 229–241. doi: 10.1085/jgp.201511517

de la Peña, P., Alonso-Ron, C., Machín, A., Fernández-Trillo, J., Carretero, L., Domínguez, P., et al. (2011). Demonstration of physical proximity between the N terminus and the S4-S5 linker of the human ether-à-go-go-related gene (hERG) potassium channel. *J. Biol. Chem.* 286, 19065–19075. doi: 10.1074/jbc.M111.238899

de la Peña, P., Machín, A., Fernández-Trillo, J., Domínguez, P., and Barros, F. (2015). Interactions between the N-terminal tail and the gating machinery of hERG K^+ channels both in closed and open/inactive states. *Pflugers Arch. Eur. J. Physiol.* 467, 1747–1756. doi: 10.1007/s00424-014-1612-1

de la Peña, P., Domínguez, P., and Barros, F. (2018). Gating mechanism of Kv11.1 (hERG) K^+ channels without covalent connection between voltage sensor and pore domains. *Pflugers Arch.* 470, 517–536. doi: 10.1007/s00424-017-2093-9

Dierich, M., Evers, S., Wilke, B. U., and Leitner, M. G. (2018). Inverse modulation of neuronal Kv 12.1 and kv 11.1 channels by 4-aminopyridine and NS1643. *Front. Mol. Neurosci.* 11, 1–13. doi: 10.3389/fnmol.2018.00011

Du, C. Y., Adeniran, I., Cheng, H., Zhang, Y. H., El Harchi, A., McPate, M. J., et al. (2010). Acidosis impairs the protective role of hERG K^+ channels against premature stimulation. *J. Cardiovasc. Electrophysiol.* 21, 1160–1169. doi: 10.1111/j.1540-8167.2010.01772.x

Du, C. Y., El Harchi, A., McPate, M. J., Orchard, C. H., and Hancox, J. C. (2011). Enhanced inhibitory effect of acidosis on hERG potassium channels that incorporate the hERG1b isoform. *Biochem. Biophys. Res. Commun.* 405, 222–227. doi: 10.1016/j.bbrc.2011.01.014

Elinder, F., Männikkö, R., Pandey, S., and Larsson, H. P. (2006). Mode shifts in the voltage gating of the mouse and human HCN2 and HCN4 channels. *J. Physiol.* 575, 417–431. doi: 10.1113/jphysiol.2006.110437

Elliott, D. J. S., Dondas, N. Y., Munsey, T. S., and Sivaprasadarao, A. (2009). Movement of the S4 segment in the herg potassium channel during membrane depolarization. *Mol. Membr. Biol.* 26, 435–447. doi: 10.3109/09687680903321081

Fernández-Trillo, J., Barros, F., Machín, A., Carretero, L., Domínguez, P., and de la Peña, P. (2011). Molecular determinants of interactions between the N-terminal domain and the transmembrane core that modulate hERG K^+ channel gating ed. Attali B. *PloS One* 6, e24674. doi: 10.1371/journal.pone.0024674

Fernandez, D., Ghanta, A., Kinard, K. I., and Sanguinetti, M. S. (2005). Molecular mapping of a site Cd^{2+}-induced modification of human ether-à-go-go-related gene (hERG) channel activation. *J. Physiol.* 567, 737–755. doi: 10.1113/jphysiol.2005.089094

Ferrer, T., Rupp, J., Piper, D. R., and Tristani-Firouzi, M. (2006). The S4-S5 linker directly couples voltage sensor movement to the activation gate in the human ether-à-go-go-related gene (hERG) K^+ channel. *J. Biol. Chem.* 281, 12858–12864. doi: 10.1074/jbc.M513518200

Gardner, A., and Sanguinetti, M. C. (2015). C-linker accounts for differential sensitivity of ERG1 and ERG2 K^+ channels to RPR260243-induced slow deactivation. *Mol. Pharmacol.* 88, 19–28. doi: 10.1124/mol.115.098384

Gianulis, E. C., Liu, Q., and Trudeau, M. C. (2013). Direct interaction of eag domains and cyclic nucleotide-binding homology domains regulate deactivation gating in hERG channels. *J. Gen. Physiol.* 142, 351–366. doi: 10.1085/jgp.201310995

Goodchild, S. J., and Fedida, D. (2014). Gating charge movement precedes ionic current activation in hERG channels. *Channels* 8, 84–89. doi: 10.4161/chan.26775

Goodchild, S. J., Macdonald, L. C., and Fedida, D. (2015). Sequence of gating charge movement and pore gating in hERG activation and deactivation pathways. *Biophys. J.* 108, 1435–1447. doi: 10.1016/j.bpj.2015.02.014

Guo, J., Cheng, Y. M., Lees-Miller, J. P., Perissinotti, L. L., Claydon, T. W., Hull, C. M., et al. (2015). NS1643 Interacts around L529 of hERG to alter voltage sensor movement on the path to activation. *Biophys. J.* 108, 1400–1413. doi: 10.1016/j.bpj.2014.12.055

Gustina, A. S., and Trudeau, M. C. (2009). A recombinant N-terminal domain fully restores deactivation gating in N-truncated and long QT syndrome mutant hERG potassium channels. *Proc. Natl. Acad. Sci. U. S. A* 106, 13082–13087. doi: 10.1073/pnas.0900180106

Gustina, A. S., and Trudeau, M. C. (2011). hERG potassium channel gating is mediated by N- and C-terminal region interactions. *J. Gen. Physiol.* 137, 315–325. doi: 10.1085/jgp.201010582

Gustina, A. S., and Trudeau, M. C. (2012). HERG potassium channel regulation by the N-terminal eag domain. *Cell Signal* 24, 1592–1598. doi: 10.1016/j.cellsig.2012.04.004

Gustina, A. S., and Trudeau, M. C. (2013). The eag domain regulates hERG channel inactivation gating *via a* direct interaction. *J. Gen. Physiol.* 141, 229–241. doi: 10.1085/jgp.201210870

Haddad, G., and Blunck, R. (2011). Mode shift of the voltage sensors in Shaker K^+ channels is caused by energetic coupling to the pore domain. *J. Gen. Physiol.* 137, 455–472. doi: 10.1085/jgp.201010573

Ho, W. K., Kim, I., Lee, C. O., and Earm, Y. E. (1998). Voltage-dependent blockade of HERG channels expressed in Xenopus oocytes by external Ca^{2+} and Mg^{2+}. *J. Physiol.* 507, 631–638. doi: 10.1111/j.1469-7793.1998.631bs.x

Hoshi, T., Zagotta, W. N., and Aldrich, R. W. (1994). Shaker potassium channel gating. I: Transitions near the open state. *J. Gen. Physiol.* 103, 249–278. doi: 10.1085/jgp.103.2.249

Hull, C. M., Sokolov, S., Van Slyke, A. C., and Claydon, T. W. (2014). Regional flexibility in the S4–S5 linker regulates hERG channel closed-state stabilization. *Pflugers Arch. Eur. J. Physiol.* 466, 1911–1919. doi: 10.1007/s00424-013-1431-9

Jiang, M., Dun, W., and Tseng, G. N. (1999). Mechanism for the effects of extracellular acidification on HERG-channel function. *Am. J. Physiol.* 277, H1283–H1292. doi: 10.1152/ajpheart.1999.277.4.H1283

Jo, S. H., Youm, J. B., Kim, I., Lee, C. O., Earm, Y. E., and Ho, W. K. (1999). Blockade of HERG channels expressed in Xenopus oocytes by external H^+. *Pflugers Arch. Eur. J. Physiol.* 438, 23–29. doi: 10.1007/s004240050875

Kang, J., Chen, X., Wang, H., Ji, J., Cheng, H., Incardona, J., et al. (2005). Discovery of a small molecule activator of the human. *Mol. Pharmacol.* 67, 827–836. doi: 10.1124/mol.104.006577

Kazmierczak, M., Zhang, X., Chen, B., Mulkey, D. K., Shi, Y., Wagner, P. G., et al. (2013). External pH modulates EAG superfamily K^+ channels through EAG-specific acidic residues in the voltage sensor. *J. Gen. Physiol.* 141, 721–735. doi: 10.1085/jgp.201210938

Kuzmenkin, A., Bezanilla, F., and Correa, A. M. (2004). Gating of the bacterial sodium channel, NaChBac. *J. Gen. Physiol.* 124, 349–356. doi: 10.1085/jgp.200409139

Lörinczi, É, Gómez-Posada, J. C., De La Peña, P., Tomczak, A. P., Fernández-Trillo, J., Leipscher, U., et al. (2015). Voltage-dependent gating of KCNH potassium channels lacking a covalent link between voltage-sensing and pore domains. *Nat. Commun.* 6, 6672. doi: 10.1038/ncomms7672

Labro, A. J., Lacroix, J. J., Villalba-Galea, C. A., Snyders, D. J., and Bezanilla, F. (2012). Molecular mechanism for depolarization-induced modulation of Kv channel closure. *J. Gen. Physiol.* 140, 481–493. doi: 10.1085/jgp.201210817

Labro, A. J., Priest, M. F., Lacroix, J. J., Snyders, D. J., and Bezanilla, F. (2015). Kv 3.1 uses a timely resurgent K^+ current to secure action potential repolarization. *Nat. Commun.* 6, 1–12. doi: 10.1038/ncomms10173

Lacroix, J. J., Labro, A. J., and Bezanilla, F. (2011). Properties of deactivation gating currents in Shaker channels. *Biophys. J.* 100, L28–L30. doi: 10.1016/j.bpj.2011.01.043

Li, Q., Gayen, S., Chen, A. S., Huang, Q., Raida, M., and Kang, C. (2010). NMR solution structure of the N-terminal domain of hERG and its interaction with the S4-S5 linker. *Biochem. Biophys. Res. Commun.* 403, 126–132. doi: 10.1016/j.bbrc.2010.10.132

Lin, M. C. A., and Papazian, D. M. (2007). Differences between ion binding to eag and herg voltage sensors contribute to differential regulation of activation and deactivation gating. *Channels* 1, 429–437. doi: 10.4161/chan.1.6.5760

Liu, B., and Qin, F. (2015). The Xenopus tropicalis orthologue of TRPV3 is heat sensitive. *J. Gen. Physiol.* 146, 411–421. doi: 10.1085/jgp.201511454

Liu, J., Zhang, M., Jiang, M., and Tseng, G.-N. (2003). Negative charges in the transmembrane domains of the HERG K channel are involved in the activation- and deactivation-gating processes. *J. Gen. Physiol.* 121, 599–614. doi: 10.1085/jgp.200308788

Liu, B., Yao, J., Zhu, M. X., and Qin, F. (2011). Hysteresis of gating underlines sensitization of TRPV3 channels. *J. Gen. Physiol.* 138, 509–520. doi: 10.1085/jgp.201110689

Long, S. B. (2005). Voltage sensor of Kv1.2: structural basis of electromechanical coupling. *Sci. (80-)* 309, 903–908. doi: 10.1126/science.1116270

Lu, Z., Klem, A. M., and Ramu, Y. (2002). Coupling between voltage sensors and activation gate in voltage-gated K^+ channels. *J. Gen. Physiol.* 120, 663–676. doi: 10.1085/jgp.20028696

Männikkö, R., Pandey, S., Larsson, H. P., and Elinder, F. (2005). Hysteresis in the voltage dependence of HCN channels. *J. Gen. Physiol.* 125, 305–326. doi: 10.1085/jgp.200409130

Malak, O. A., Es-Salah-Lamoureux, Z., and Loussouarn, G. (2017). hERG S4-S5 linker acts as a voltage-dependent ligand that binds to the activation gate and locks it in a closed state. *Sci. Rep.* 7, 1–12. doi: 10.1038/s41598-017-00155-2

Malak, O. A., Gluhov, G. S., Grizel, A. V., Kudryashova, K. S., Sokolova, O. S., and Loussouarn, G. (2019). Voltage-dependent activation in EAG channels follows a ligand-receptor rather than a mechanical-lever mechanism. *J. Biol. Chem.* 294, 6506–6521. doi: 10.1074/jbc.RA119.007626

Marques-Carvalho, M. J., Sahoo, N., Muskett, F. W., Vieira-Pires, R. S., Gabant, G., Cadene, M., et al. (2012). Structural, biochemical, and functional characterization of the cyclic nucleotide binding homology domain from the mouse EAG1 potassium channel. *J. Mol. Biol.* 423, 34–46. doi: 10.1016/j.jmb.2012.06.025

Mazhari, R., Greenstein, J. L., Winslow, R. L., Marbán, E., and Nuss, H. B. (2001). Gene Products, HERG and KCNE2, Rationalized by *In Vitro*. *Circ. Res.* 89, 33–38. doi: 10.1161/hh1301.093633

Muskett, F. W., Thouta, S., Thomson, S. J., Bowen, A., Stansfeld, P. J., and Mitcheson, J. S. (2011). Mechanistic insight into human ether-à-go-go-related gene (hERG) K^+ channel deactivation gating from the solution structure of the EAG domain. *J. Biol. Chem.* 286, 6184–6191. doi: 10.1074/jbc.M110.199364

Ng, C. A., Hunter, M. J., Perry, M. D., Mobli, M., Ke, Y., Kuchel, P. W., et al. (2011). The N-terminal tail of hERG contains an amphipathic α-helix that regulates channel deactivation. *PloS One* 6, e16191. doi: 10.1371/journal.pone.0016191

Ng, C. A., Perry, M. D., Tan, P. S., Hill, A. P., Kuchel, P. W., and Vandenberg, J. I. (2012). The S4-S5 linker acts as a signal integrator for hERG K^+ channel activation and deactivation gating. *PloS One* 7, e31640. doi: 10.1371/journal.pone.0031640

Oehmen, C. S., Giles, W. R., and Demir, S. S. (2002). Mathematical model of the rapidly activating delayed rectifier potassium current IKr in rabbit sinoatrial node. *J. Cardiovasc. Electrophysiol.* 13, 1131–1140. doi: 10.1046/j.1540-8167.2002.01131.x

Olcese, R., Latorre, R., Toro, L., Bezanilla, F., and Stefani, E. (1997). Correlation between charge movement and ionic current during slow inactivation in Shaker K^+ channels. *J. Gen. Physiol.* 110, 579–589. doi: 10.1085/jgp.110.5.579

Perry, M., and Sanguinetti, M. C. (2008). A single amino acid difference between ether-à-go-go- related gene channel subtypes determines differential sensitivity to a small molecule activator. *Mol. Pharmacol.* 73, 1044–1051. doi: 10.1124/mol.107.043018

Perry, M., Sachse, F. B., and Sanguinetti, M. C. (2007). Structural basis of action for a human ether-à-go-go-related gene 1 potassium channel activator. *Proc. Natl. Acad. Sci.* 104, 13827–13832. doi: 10.1073/pnas.0703934104

Piper, D. R., Varghese, A., Sanguinetti, M. C., and Tristani-Firouzi, M. (2003). Gating currents associated with intramembrane charge displacement in HERG potassium channels. *Proc. Natl. Acad. Sci.* 100, 10534–10539. doi: 10.1073/pnas.1832721100

Piper, D. R., Hinz, W. A., Tallurri, C. K., Sanguinetti, M. C., and Tristani-Firouzi, M. (2005). Regional specificity of human ether-à-go-go-related gene channel activation and inactivation gating. *J. Biol. Chem.* 280, 7206–7217. doi: 10.1074/jbc.M411042200

Piper, D. R., Rupp, J., Sachse, F. B., Sanguinetti, M. C., and Tristani-Firouzi, M. (2008). Cooperative interactions between R531 and acidic residues in the voltage sensing module of hERG1 channels. *Cell Physiol. Biochem.* 21, 37–46. doi: 10.1159/000113745

Priest, M. F., Lacroix, J. J., Villalba-Galea, C. A., and Bezanilla, F. (2013). S3-S4 linker length modulates the relaxed state of a voltage-gated potassium channel. *Biophys. J.* 105, 2312–2322. doi: 10.1016/j.bpj.2013.09.053

Rasmusson, R. L., Morales, M. J., Wang, S., Liu, S., Campbell, D. L., Brahmajothi, M. V., et al. (1998). Inactivation of voltage-gated cardiac K^+ channels. *Circ. Res.* 82, 739–750. doi: 10.1161/01.RES.82.7.739

Sanguinetti, M. C., and Xu, Q. P. (1999). Mutations of the S4-S5 linker alter activation properties of HERG potassium channels expressed in Xenopus oocytes. *J. Physiol.* 514, 667–675. doi: 10.1111/j.1469-7793.1999.667ad.x

Sanguinetti, M. C., Jiang, C., Curran, M. E., and Keating, M. T. (1995). A mechanistic link between an inherited and an acquird cardiac arrthytmia: HERG encodes the IKr potassium channel. *Cell* 81, 299–307. doi: 10.1016/0092-8674(95)90340-2

Schönherr, R., and Heinemann, S. H. (1996). Molecular determinants for activation and inactivation of HERG, a human inward rectifier potassium channel. *J. Physiol.* 493, 635–642. doi: 10.1113/jphysiol.1996.sp021410

Seoh, S.-A., Sigg, D., Papazian, D. M., and Bezanilla, F. (1996). Voltage-sensing residues in the S2 and S4 segments of the shaker K^+ channel. *Neuron* 16, 1159–1167. doi: 10.1016/S0896-6273(00)80142-7

Shi, Y. P., Cheng, Y. M., Van Slyke, A. C., and Claydon, T. W. (2014). External protons destabilize the activated voltage sensor in hERG channels. *Eur. Biophys. J.* 43, 59–69. doi: 10.1007/s00249-013-0940-y

Shi, Y. P., Thouta, S., Cheng, Y. M., and Claydon, T. W. (2019). Extracellular protons accelerate hERG channel deactivation by destabilizing voltage sensor relaxation. *J. Gen. Physiol.* 151, 231–246. doi: 10.1085/jgp.201812137

Shirokov, R., Levis, R., Shirokova, N., and Ríos, E. (1992). Two classes of gating current from L-type Ca channels in guinea pig ventricular myocytes. *J. Gen. Physiol.* 99, 863–895. doi: 10.1085/jgp.99.6.863

Smith, P. L., and Yellen, G. (2002). Fast and slow voltage sensor movements in HERG potassium channels. *J. Gen. Physiol.* 119, 275–293. doi: 10.1085/jgp.20028534

Smith, P. L., Baukrowitz, T., and Yellen, G. (1996). The inward rectification mechanism of the HERG cardiac potassium channel. *Nature* 379, 833–836. doi: 10.1038/379833a0

Spector, P. S. (1996). Fast inactivation causes rectification of the IKr channel. *J. Gen. Physiol.* 107, 611–619. doi: 10.1085/jgp.107.5.611

Starace, D. M., and Bezanilla, F. (2004). A proton pore in a potassium channel voltage sensor reveals a focused electric field. *Nature* 427, 548–553. doi: 10.1038/nature02270

Subbiah, R. N., Clarke, C. E., Smith, D. J., Zhao, J., Campbell, T. J., and Vandenberg, J. I. (2004). Molecular basis of slow activation of the human *ether-á-go-go* related gene potassium channel. *J. Physiol.* 558, 417–431. doi: 10.1113/jphysiol.2004.062588

Tan, P. S., Perry, M. D., Ng, C. A., Vandenberg, J. I., and Hill, A. P. (2012). Voltage-sensing domain mode shift is coupled to the activation gate by the N-terminal tail of hERG channels. *J. Gen. Physiol.* 140, 293–306. doi: 10.1085/jgp.201110761

ten Tusscher, K. H. W. J. (2003). A model for human ventricular tissue. *AJP Hear Circ. Physiol.* 286, H1573–H1589. doi: 10.1152/ajpheart.00794.2003

Terai, T., Furukawa, T., Katayama, Y., and Hiraoka, M. (2000). Effects of external acidosis on HERG current expressed in Xenopus oocytes. *J. Mol. Cell Cardiol.* 32, 11–21. doi: 10.1006/jmcc.1999.1048

Thouta, S., Sokolov, S., Abe, Y., Clark, S. J., Cheng, Y. M., and Claydon, T. W. (2014). Proline scan of the hERG channel S6 helix reveals the location of the intracellular pore gate. *Biophys. J.* 106, 1057–1069. doi: 10.1016/j.bpj.2014.01.035

Thouta, S., Hull, C. M., Shi, Y. P., Sergeev, V., Young, J., Cheng, Y. M., et al. (2017). Stabilization of the activated hERG channel voltage sensor by depolarization involves the S4-S5 linker. *Biophys. J.* 112, 300–312. doi: 10.1016/j.bpj.2016.12.021

Tilegenova, C., Cortes, D. M., and Cuello, L. G. (2017). Hysteresis of KcsA potassium channel's activation- deactivation gating is caused by structural changes at the channel's selectivity filter. *Proc. Natl. Acad. Sci. U. S. A* 114, 3234–3239. doi: 10.1073/pnas.1618101114

Tristani-Firouzi, M., Chen, J., and Sanguinetti, M. C. (2002). Interactions between S4-S5 linker and S6 transmembrane domain modulate gating of HERG K^+ channels. *J. Biol. Chem.* 277, 18994–19000. doi: 10.1074/jbc.M200410200

Trudeau, M., Warmke, J., Ganetzky, B., and Robertson, G. (1995). HERG, a human inward rectifier in the voltage-gated potassium channel family. *Sci. (80-)* 269, 92–95. doi: 10.1126/science.7604285

Van Slyke, A. C., Rezazadeh, S., Snopkowski, M., Shi, P., Allard, C. R., and Claydon, T. W. (2010). Mutations within the S4–S5 linker alter voltage sensor constraints in hERG K^+ channels. *Biophys. J.* 99, 2841–2852. doi: 10.1016/j.bpj.2010.08.030

Van Slyke, A. C., Cheng, Y. M., Mafi, P., Allard, C. R., Hull, C. M., Shi, Y. P., et al. (2012). Proton block of the pore underlies the inhibition of hERG cardiac K^+ channels during acidosis. *Am. J. Physiol. Physiol.* 302, C1797–C1806. doi: 10.1152/ajpcell.00324.2011

Vandenberg, J. I., Perry, M. D., Perrin, M. J., Mann, S. A., Ke, Y., and Hill, A. P. (2012). hERG K^+ channels: structure, function, and clinical significance. *Physiol. Rev.* 92, 1393–1478. doi: 10.1152/physrev.00036.2011

Villalba-Galea, C. A., Sandtner, W., Starace, D. M., and Bezanilla, F. (2008). S4-based voltage sensors have three major conformations. *Proc. Natl. Acad. Sci.* 105, 17600–17607. doi: 10.1073/pnas.0807387105

Villalba-Galea, C. A. (2014). Hv1 proton channel opening is preceded by a voltage-independent transition. *Biophys. J.* 107, 1564–1572. doi: 10.1016/j.bpj.2014.08.017

Villalba-Galea, C. A. (2017). Hysteresis in voltage-gated channels. *Channels* 11, 140–155. doi: 10.1080/19336950.2016.1243190

Wang, W., and MacKinnon, R. (2017). Cryo-EM structure of the open human ether-à-go-go-Related K^+ channel hERG. *Cell* 169, 422–430.e10. doi: 10.1016/j.cell.2017.03.048

Wang, S., Liu, S., Morales, M. J., Strauss, H. C., and Rasmusson, R. L. (1997). A quantitative analysis of the activation and inactivation kinetics of HERG expressed in Xenopus oocytes. *J. Physiol.* 502, 45–60. doi: 10.1111/j.1469-7793.1997.045bl.x

Wang, J., Trudeau, M. C., Zappia, A. M., and Robertson, G. A. (1998). Regulation of deactivation by an amino terminal domain in human ether-à-go-go-related gene potassium channels. *J. Gen. Physiol.* 112, 637–647. doi: 10.1085/jgp.112.5.637

Wang, J., Myers, C. D., and Robertson, G. A. (2000). Dynamic control of deactivation gating by a soluble amino-terminal domain in HERG K(+) channels. *J. Gen. Physiol.* 115, 749–758. doi: 10.1085/jgp.115.6.749

Wang, D. T., Hill, A. P., Mann, S. A., Tan, P. S., and Vandenberg, J. I. (2011). Mapping the sequence of conformational changes underlying selectivity filter gating in the Kv11.1 potassium channel. *Nat. Struct. Mol. Biol.* 18, 35–41. doi: 10.1038/nsmb.1966

Wang, Z., Dou, Y., Goodchild, S. J., Es-Salah-Lamoureux, Z., and Fedida, D. (2013). Components of gating charge movement and S4 voltage-sensor exposure during activation of hERG channels. *J. Gen. Physiol.* 141, 431–443. doi: 10.1085/jgp.201210942

Whicher, J. R., and MacKinnon, R. (2016). Structure of the voltage-gated K^+ channel Eag1 reveals an alternative voltage sensing mechanism. *Science* 353, 664–669. doi: 10.1126/science.aaf8070

Wu, W., Gardner, A., and Sanguinetti, M. C. (2015). Concatenated hERG1 tetramers reveal stoichiometry of altered channel gating by RPR-260243. *Mol. Pharmacol.* 87, 401–409. doi: 10.1124/mol.114.096693

Wu, W., Gardner, A., Sachse, F. B., and Sanguinetti, M. C. (2016). Ginsenoside Rg3, a gating modifier of EAG family K^+ channels. *Mol. Pharmacol.* 90, 469–482. doi: 10.1124/mol.116.104091

Zeng, J., Laurita, K. R., Rosenbaum, D. S., and Rudy, Y. (1995). Two components of the delayed rectifier K+ current in ventricular myocytes of the guinea pig type: theoretical formulation and their role in repolarization. *Circ. Res.* 77, 140–152. doi: 10.1161/01.RES.77.1.140

Zhang, M., Liu, J., and Tseng, G.-N. (2004). Gating charges in the activation and inactivation processes of the hERG channel. *J. Gen. Physiol.* 124, 703–718. doi: 10.1085/jgp.200409119

Zhang, M., Liu, J., Jiang, M., Wu, D. M., Sonawane, K., Guy, H. R., et al. (2005). Interactions between charged residues in the transmembrane segments of the voltage-sensing domain in the hERG channel. *J. Membr. Biol.* 207, 169–181. doi: 10.1007/s00232-005-0812-1

Zhao, J., and Blunck, R. (2016). The isolated voltage sensing domain of the shaker potassium channel forms a voltage-gated cation channel. *Elife* 5, 1–18. doi: 10.7554/eLife.18130

Zhao, Y., Goldschen-Ohm, M. P., Morais-Cabral, J. H., Chanda, B., and Robertson, G. A. (2017). The intrinsically liganded cyclic nucleotide-binding homology domain promotes KCNH channel activation. *J. Gen. Physiol.* 149, 249–260. doi: 10.1085/jgp.201611701

Zhou, Q., and Bett, G. C. L. (2010). Regulation of the voltage-insensitive step of HERG activation by extracellular pH. *Am. J. Physiol. Circ. Physiol.* 298, H1710–H1718. doi: 10.1152/ajpheart.01246.2009

Conflict of Interest: The authors declare that the research was conducted in the absence of any commercial or financial relationships that could be construed as a potential conflict of interest.

frontiers in Pharmacology

REVIEW
published: 15 April 2020
doi: 10.3389/fphar.2020.00411

The EAG Voltage-Dependent K^+ Channel Subfamily: Similarities and Differences in Structural Organization and Gating

Francisco Barros[1]*, *Pilar de la Peña*[1], *Pedro Domínguez*[1], *Luisa Maria Sierra*[2] and *Luis A. Pardo*[3]*

[1] Departamento de Bioquímica y Biología Molecular, Universidad de Oviedo, Edificio Santiago Gascón, Oviedo, Spain, [2] Departamento de Biología Funcional (Area de Genética), Instituto Universitario de Oncología del Principado de Asturias (IUOPA), Instituto de Investigación Sanitaria del Principado de Asturias (ISPA), Universidad de Oviedo, Oviedo, Spain, [3] Oncophysiology Group, Max Planck Institute of Experimental Medicine, Göttingen, Germany

OPEN ACCESS

Edited by:
Gildas Loussouarn,
Université de Nantes, France

Reviewed by:
Rikard Blunck,
Université de Montréal, Canada
Francesco Tombola,
University of California,
Irvine, United States

***Correspondence:**
Francisco Barros
fbarros@uniovi.es/fbarros@gmx.es
Luis A. Pardo
pardo@em.mpg.de

Specialty section:
This article was submitted to Pharmacology of Ion Channels and Channelopathies, a section of the journal Frontiers in Pharmacology

Received: 20 November 2019
Accepted: 18 March 2020
Published: 15 April 2020

Citation:
Barros F, de la Peña P, Domínguez P, Sierra LM and Pardo LA (2020) The EAG Voltage-Dependent K^+ Channel Subfamily: Similarities and Differences in Structural Organization and Gating. Front. Pharmacol. 11:411. doi: 10.3389/fphar.2020.00411

EAG (*ether-à-go-go* or *KCNH*) are a subfamily of the voltage-gated potassium (Kv) channels. Like for all potassium channels, opening of EAG channels drives the membrane potential toward its equilibrium value for potassium, thus setting the resting potential and repolarizing action potentials. As voltage-dependent channels, they switch between open and closed conformations (gating) when changes in membrane potential are sensed by a voltage sensing domain (VSD) which is functionally coupled to a pore domain (PD) containing the permeation pathway, the potassium selectivity filter, and the channel gate. All Kv channels are tetrameric, with four VSDs formed by the S1–S4 transmembrane segments of each subunit, surrounding a central PD with the four S5–S6 sections arranged in a square-shaped structure. Structural information, mutagenesis, and functional experiments, indicated that in "classical/*Shaker*-type" Kv channels voltage-triggered VSD reorganizations are transmitted to PD gating *via* the α-helical S4–S5 sequence that links both modules. Importantly, these *Shaker*-type channels share a domain-swapped VSD/PD organization, with each VSD contacting the PD of the adjacent subunit. In this case, the S4–S5 linker, acting as a rigid mechanical lever (electromechanical lever coupling), would lead to channel gate opening at the cytoplasmic S6 helices bundle. However, new functional data with EAG channels split between the VSD and PD modules indicate that, in some Kv channels, alternative VSD/PD coupling mechanisms do exist. Noticeably, recent elucidation of the architecture of some EAG channels, and other relatives, showed that their VSDs are non-domain swapped. Despite similarities in primary sequence and predicted structural organization for all EAG channels, they show marked kinetic differences whose molecular basis is not completely understood. Thus, while a common general architecture may establish the gating system used by the EAG channels and the physicochemical coupling of voltage sensing to gating, subtle changes in that common structure, and/or allosteric influences of protein domains relatively distant from the central gating machinery, can crucially influence the gating

process. We consider here the latest advances on these issues provided by the elucidation of eag1 and erg1 three-dimensional structures, and by both classical and more recent functional studies with different members of the EAG subfamily.

Keywords: potassium channel, EAG family, voltage-dependent gating, cytoplasmic domains, allosteric gating, structure-function relationships

OVERVIEW

KCNH (EAG or *ether-á-go-go*) channels constitute a subfamily of the voltage-gated family of potassium (Kv) channels (Gutman et al., 2005). Three subtypes (Kv10 to Kv12) are included in this group: (i) eag (Kv10) with two mammalian members, Kv10.1 or eag1 and Kv10.2 or eag2, encoded by the *KCNH1* and *KCNH5* genes, respectively; (ii) erg (eag-related gene or Kv11) comprising three channels, Kv11.1 or erg1, Kv11.2 or erg2, and Kv11.3 or erg3, encoded by *KCNH2*, *KCHN6*, and *KCNH7*; and (iii) elk (eag-like K^+ channel or Kv12) including Kv12.1 or elk1, Kv12.2 or elk2, and Kv12.3 or elk3, corresponding to genes *KCNH8*, *KCNH3*, and *KCNH4*. All of them present substantial sequence homology with the other Kv channel subfamilies (Kv1 to Kv9), and share a common primary structure organization (**Figure 1**). In addtion, they show a tetrameric assembly in which each subunit contributes its six transmembrane segments (S1-S6) to form a transmembrane core. **Figure 2** depicts a schematic representation of the general topology of these channels, exemplified by that of erg1 (Kv11.1/hERG). The schemes try to provide a better visual guidance through the structural and functional regions recognized in the channel, but do not recapitulate the whole set of interactions between them or their possible dynamic reorganizations during the gating process, as discussed below. Segments S1 to S4 form the voltage-sensing domain (VSD) of each subunit; S4 contains several positively charged residues and provides the main transmembrane voltage-sensing component. The two additional transmembrane helices (S5 and S6), plus the intervening pore loops of the four subunits, associate to form the tetrameric structure that surrounds a central conduction pathway, and constitutes the ion permeation pore-gate domain (PD) (Yellen, 1998; Yellen, 2002; Swartz, 2004; Yu et al., 2005; Ashcroft, 2006; Swartz, 2008; Bezanilla, 2008). To this common protein core different cytoplasmic modules (and accessory subunits), able to strongly influence the gating and other functional properties, have been added through evolution, (reviewed in Barros et al., 2012). A characteristic feature of EAG channels is the presence of long cytoplasmic N- and C-terminal ends, that include some structures not found in any other Kv channel type. Thus, in the amino terminus they contain an initial section conserved among all members of the group (**Figure 1**), named for this reason "eag domain" and that, due to the presence of a PAS (*P*er-*A*rnt-*S*im) region typical of the large family of the "PAS domain proteins", is also frequently called the "eag/PAS domain". Importantly, upstream this PAS region, there is a stretch of around 25 amino acids that appeared disordered and therefore unresolved in the initial high-resolution crystal structures of the erg1, eag1, and *Drosophila* elk eag/PAS domains (Morais-Cabral et al., 1998; Adaixo et al., 2013). This initial section of the protein has been named N-terminal tail or N-tail (Ng et al., 2011; De la Peña et al., 2011; Vandenberg et al., 2012; De la Peña et al., 2013; Barros et al., 2018), N-CAP (Gustina and Trudeau, 2012; Morais-Cabral and Robertson, 2015) or PAS-loop (Whicher and MacKinnon, 2019), and is composed of an initial short flexible segment, followed by an amphipatic alpha-helix (Gustina and Trudeau, 2012; Barros et al., 2012; Vandenberg et al., 2012; Morais-Cabral and Robertson, 2015; Whicher and MacKinnon, 2016; Wang and MacKinnon, 2017). Remarkably, the flexible N-tail could play specific role(s) on channel gating, independent from those of the PAS domain itself (Barros et al., 2012; Vandenberg et al., 2012; Gustina and Trudeau, 2012; Morais-Cabral and Robertson, 2015. See below). Interestingly, some of the cytoplasmic EAG channels sections display a high degree of homology with other domains from channels outside the Kv family [e.g., the cyclic nucleotide-gated (CNG), the hyperpolarization-activated and cyclic nucleotide-gated (HCN) and some inwardly rectifying plant K^+ channels], all of them pertaining to the named "S4" or "6TM1P" group of the pore-loop channel family, but having different selectivity, or no or even inverted voltage dependence (Gutman et al., 2005; Yu et al., 2005; Ashcroft, 2006; Lau et al., 2018). Indeed, the presence of intracellular domains either able to bind cyclic nucleotides (cyclic nucleotide-binding domain, CNBD), or sharing high structural homologies with those domains but unable to bind nucleotides (cyclic nucleotide-binding homology domain, CNBHD), has allowed classifying the EAG, CNG, and HCN channels under the named CNBD channel family (James and Zagotta, 2018), even though the voltage-dependence, selectivity, and cyclic nucleotide regulation of the EAG channels are different from those of the CNG and HCN channels (James and Zagotta, 2018; Barros et al., 2019).

We will consider here the differential properties exhibited by some of the EAG channels at the functional level, in order to establish possible structure-function correlations centered in their perhaps more conspicuous property, the voltage-dependent gating. Furthermore, we will summarize some of the most recent contributions to our knowledge of the molecular basis of EAG channel gating, mainly fueled by functional data from channel variants (S4–S5 split channels) lacking a covalent link between the VSD and the PD at the level of the S4–S5 linker, as well as by the recent cryo-electron microscopy (cryo-EM) elucidation of the three-dimensional structure of some EAG channels. Finally, we will consider some possible limitations of these studies and future directions to further advance this topic.

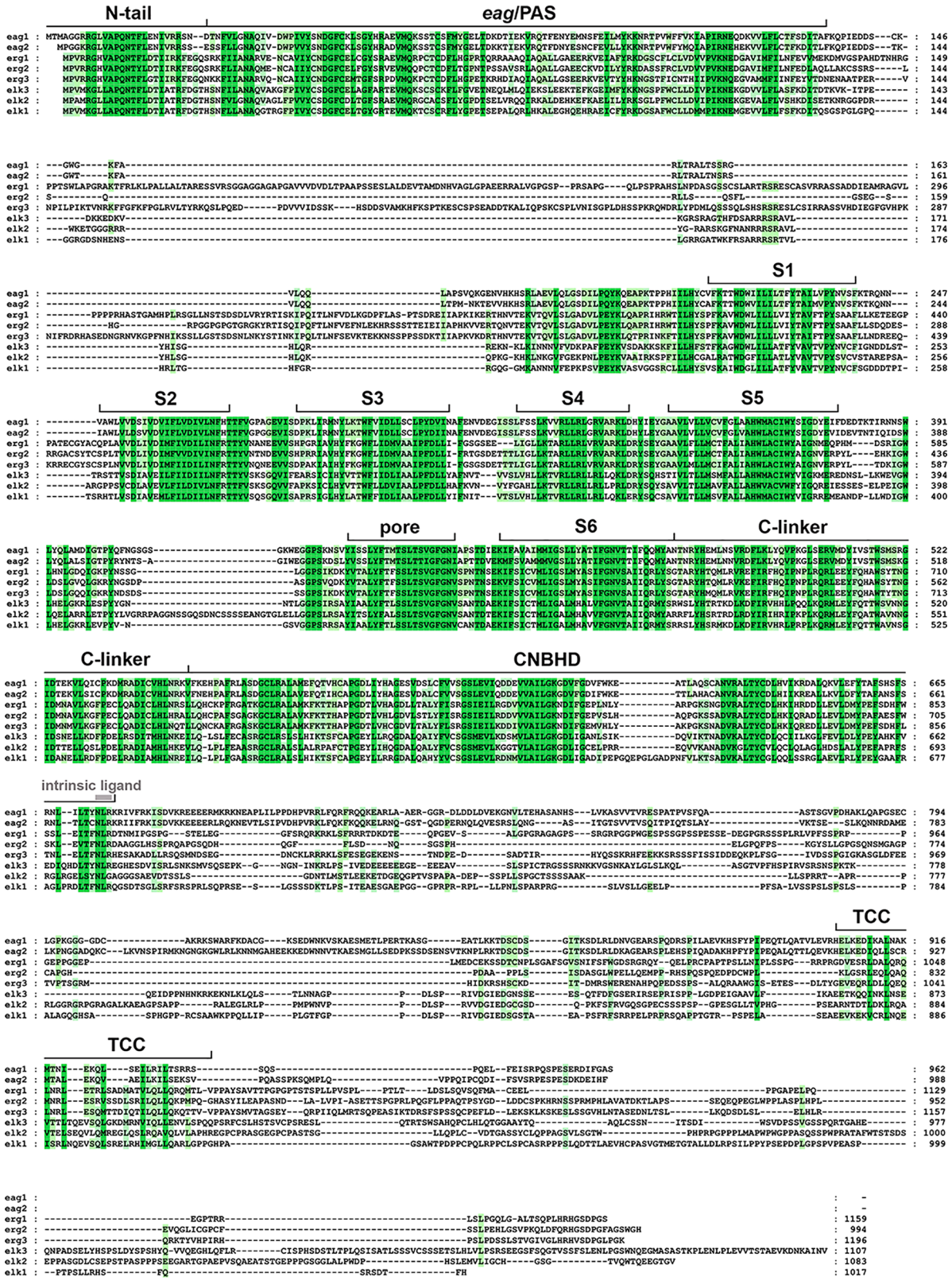

FIGURE 1 | Continued

FIGURE 1 | Amino acid sequence alignment of the human *ether-á-go-go* (EAG) channels polypeptides. The alignment was generated using Clustal Omega (https://www.ebi.ac.uk/Tools/msa/clustalo/) and analyzed and edited using GeneDoc software. Gaps required to optimize the alignment are shown as *dashes*. Identical or highly similar residues in *all* the EAG sequences are shadowed *dark green*, and residues conserved in *most* sequences are shadowed in *light green*. The boundaries of the transmembrane helices S1–S6, pore helix (pore), and intracellular domains [*P*er-*A*rnt-*S*im (PAS) domain preceded by the initial N-tail, C-linker, cyclic nucleotide-binding homology domain (CNBHD), and a carboxy terminal proposed tetramerization coiled-coil/TCC] are indicated above the sequence. The position of the residues corresponding to the intrinsic ligand of the CNBHD is also indicated using grey letters. The accession numbers for the polypeptide sequences are: eag1, NP_002229.1; eag2, NP_647479.2; erg1, NP_000229.1; erg2, 110406.1; erg3, NP_150375.2; elk3, NP_653234.2; elk2, NP_036416.1; elk1, NP_036417.1.

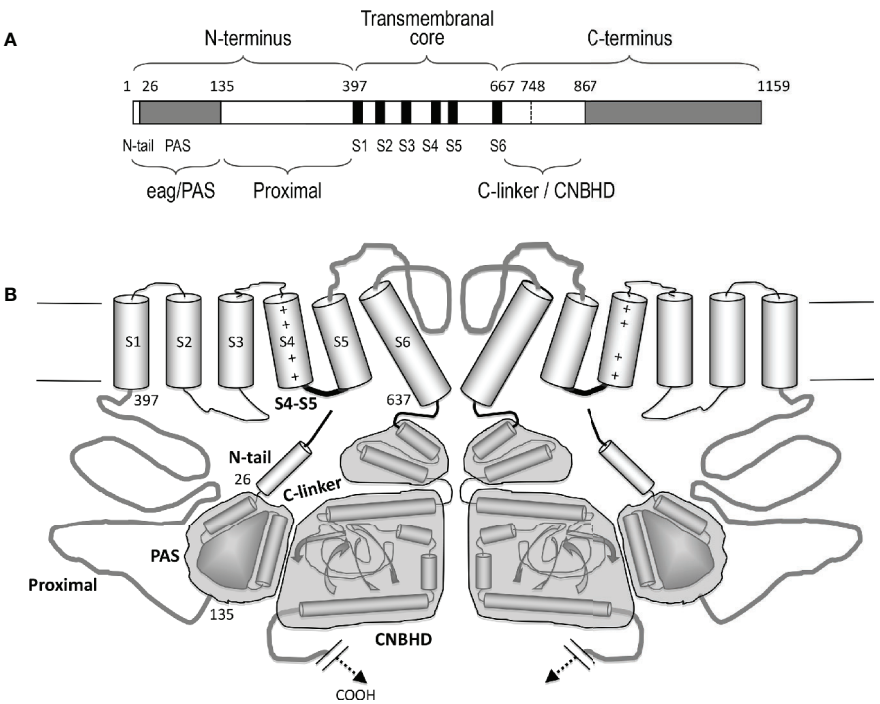

FIGURE 2 | Schematic representation of the structural organization of the erg1 (Kv11.1/hERG) channel. **(A)** Schematic linear diagram of an erg1 channel subunit. The six transmembrane helices (S1 to S6) are represented as black boxes. The position of the boundaries between the different channel domains denoted above and below the bar is indicated with numbers. The size of each region is represented approximately proportional to scale. **(B)** Schematic cartoon representing two α-subunits of a four-subunit erg1 channel tetramer. The S1–S4 transmembrane helical segments that make up the voltage sensor domain are linked *via* an S4–S5 linker (thick black line) to the pore-forming domains (segments S5 and S6 and intervening pore loop, thick grey line). Note the short length of the S4–S5 linker associated to the non-domain-swapped organization of the transmembranal core. Both the N- and the C-terminal regions are intracellular. At the N-terminus, the amphipatic helix (residues 10–23) that follows the initial flexible segment in the N-tail, and the PAS homologous domain (residues 26–134), are depicted as a small cylinder and a globular grey structure, respectively. The erg1 exclusive proximal domain of the N-terminus (residues 135–397) is represented as a grey line connected to the S1 helix. At the C-terminus, the C-linker and cyclic nucleotide-binding homology domain (CNBHD) domains are schematized, encompassed in grey blocks, as a pair of cylinders and as cylinders and sheets, respectively. The long distal region of the carboxy terminus that remains structurally uncharacterized and with no recognized direct influence in channel gating, has been omitted for clarity.

EAG CHANNELS: PROTOTYPIC EXAMPLES OF NON-DOMAIN-SWAPPED CHANNEL CORE ARCHITECTURE

The three-dimensional protein structures of many ion channels, including some EAG subfamily channels and other members of the structurally-related CNBD family have been elucidated, initially using X-ray crystallography and NMR spectroscopy, and currently, by the spectacular improvements in single particle cryo-EM (reviewed in Vandenberg et al., 2017; Lau et al., 2018; James and Zagotta, 2018; Okamura and Okochi, 2019; Barros et al., 2019). The discovery that, despite their shared common primary organization, the EAG channels and other members of the Kv family can adopt two main architectural patterns in their transmembrane core (**Figure 3**), caused an essential breakthrough in our view of the structural basis of the molecular mechanism(s) involved in the voltage-triggered gating of these entities.

In many Kv channels, the peripheral VSDs contact the PD of a neighboring subunit, leading to a domain-swapped architecture (**Figure 3**). In this case, a long α-helical linker (called the S4–S5 linker) covalently connects the last residue of the S4 helix of the

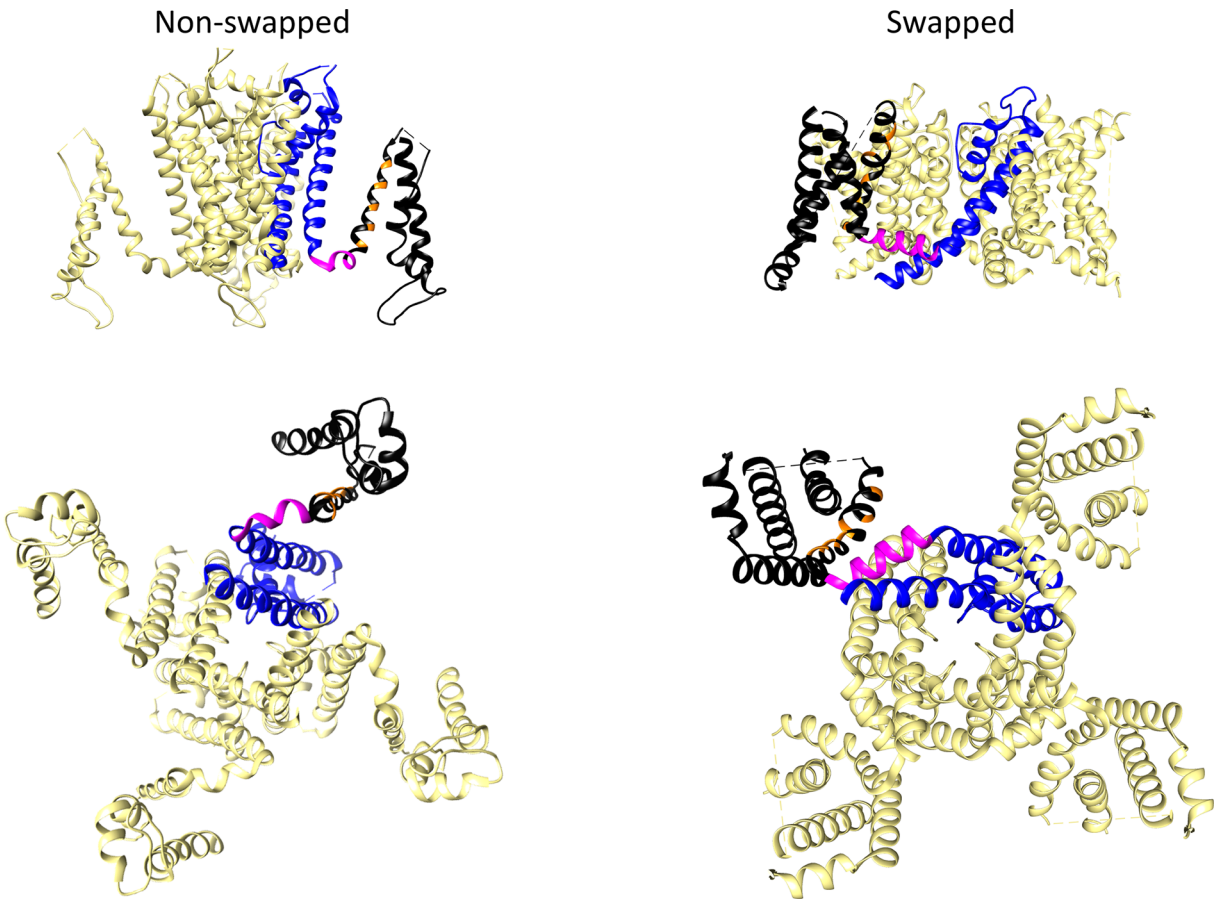

FIGURE 3 | Comparison of non-domain-swapped and domain-swapped architectures of Kv channels. Left, erg1 (Kv11.1/hERG, PDB: 5VA2) non-domain swapped structure. Right, Kv1.2 (PDB: 2A79) domain-swapped structure. Only the transmembrane core domains are depicted viewed from the membrane plane (top) and from the cytoplasmic side (bottom). One of the subunits is shown coloured with the pore domain (PD) structures in blue, the S4–S5 linker in magenta, and the voltage sensing domain (VSD) in black. Orange is used to mark the position of positively charged residues in the S4 transmembrane helix of the VSD.

VSD with the first one in the S5 helix of the PD, and cuffs around the helical bundle formed by the S6 helices that usually constitutes the cytoplasmic channel gate (Holmgren et al., 1998; Del Camino et al., 2000; Mitcheson et al., 2000; Del Camino and Yellen, 2001; Witchel, 2004; Webster et al., 2004; Del Camino et al., 2005; Swartz, 2005; Boulet et al., 2007; Wynia-Smith et al., 2008; Thouta et al., 2014). This is typical of the Kv1 to Kv9 (*Shaker*-type) subfamilies, but also occurs in the Nav and Cav voltage-gated sodium and calcium channels (Wisedchaisri et al., 2019), and in the channels from the transient receptor (TRP) family, which are structurally related to Kv channels but are generally non-selective among cations and in most cases voltage-independent (reviewed in Barros et al., 2019). There are indications that in the domain-swapped and voltage-dependent type of channels, an electromechanical coupling between the VSD and the gate exists, in which the S4–S5 linker, acting as a mechanical lever, transmits to the cytoplasmic gate the force generated by the VSD conformational rearrangements, leading to channel activation and/or deactivation (Long et al., 2005; Labro et al., 2008; Vardanyan and Pongs, 2012; Blunck and Batulan, 2012; Jensen et al., 2012; Chowdury et al., 2014; Kalstrup and Blunck, 2018).

In contrast to this architecture, in channels that display a very short and non α-helical S4–S5 linker, the VSD contacts the PD of the same subunit, inducing a non-domain-swapped organization of the transmembrane core (**Figure 3**). This structural characteristic was first demonstrated in the Kv10.1 (eag1) channel (Whicher and MacKinnon, 2016) and subsequently confirmed for Kv11.1 (erg1), Slo1 and SK Ca^{2+}-activated K^+ channels, the Na^+-dependent K^+ channel Slo2.2, the HCN1 hyperpolarization-activated and cyclic nucleotide-gated cation channel, and the prokaryotic and eukaryotic cyclic-nucleotide-gated (CNG) channels (Hite et al., 2015; Wang and MacKinnon, 2017; Hite et al., 2017; Tao et al., 2017; Lee and MacKinnon, 2017; James et al., 2017; Li et al., 2017; Lee and MacKinnon, 2018). Note, however, that although a short S4–S5 linker may determine

a non-swapped organization, such architecture is also present in the SK channels even though they contain a quite long S4–S5 with two α-helices (Lee and MacKinnon, 2018), and that a domain-swapped organization has been observed in TRPM8 channels showing no obvious or only a short S4–S5 linker (Yin et al., 2018). Strikingly, recent cryo-EM data indicate that in this case the transition between the closed conformation (lacking a canonical S4–S5 linker) and a desensitized conformation through binding of calcium induces a rearrangement of the S4–S5 into a typical α-helical S4–S5 linker architecture. However, in both cases a similar domain-swapped organization of the transmembrane channel core is maintained (Diver et al., 2019). Also, it has been reported that introducing a single point mutation in the S5 transmembrane helix of the TRPV6 channel converts the domain swapped organization to a non-domain swapped yet still functional one (Singh et al., 2017). Noticeably, the domain-swapped variant can be also converted to a non-domain-swapped conformation by shortening the S4–S5 linker, although in this case a non-functional channel is generated. This fact indicates that whereas a short length of the S4–S5 linker is indeed a critical determinant of a non-swapped architecture, other structural variations can also trigger alterations of swapping, associated or not to perturbations in gating function. This finding has been interpreted as an indication that, apart from differences in S4–S5 length, transmembrane domain arrangement can be altered under a variety of conditions, including functional and/or dynamic reorganizations of channel structure (Singh et al., 2017). This interpretation also opens the possibility that other channel regions relatively distant from the central gating machinery, may contribute to the structural organization of the protein. Note also that in many of the non-domain swapped channels gating is controlled by the binding of diverse ligands to intracellular regions that show an extensive domain swapping between the tetramer subunits (Stevens et al., 2009; Gustina and Trudeau, 2011; Gianulis et al., 2013; Haitin et al., 2013; Ng et al., 2014; Whicher and MacKinnon, 2016; Wang and MacKinnon, 2017; Zhao et al., 2017; Barros et al., 2019). In any case, it is clear that in non-domain-swapped, but genuinely voltage-dependent Kv channels, such as Kv10.1 and Kv11.1, the short length and organization of the S4–S5 linker would not allow it to act as a rigid mechanical lever able to pull apart the N-terminal portion of S5 and the C-terminal end of S6 to open the cytoplasmic channel gate, as it seems to happen in the canonical voltage-gated K^+ channels (Long et al., 2005; Labro et al., 2008; Vardanyan and Pongs, 2012; Blunck and Batulan, 2012; Jensen et al., 2012; Chowdury et al., 2014; Kalstrup and Blunck, 2018). Indeed, pioneer studies with Kv10.1 and Kv11.1 channels in which the separate N- and C-terminal halves of the protein were expressed after breaking the covalent continuity of the S4–S5 linker (S4–S5 split channels), demonstrated the production of voltage-gated channels exhibiting voltage-sensing and permeation properties similar to those of the complete protein (Lorinczi et al., 2015). Thus, both structural and functional evidences point to the existence of a new mechanism in this type of Kv channels, different to the classical lever one proposed for the *Shaker*-like Kv channels (Whicher and MacKinnon, 2016; Wang and MacKinnon, 2017; Tao et al., 2017; Flynn and Zagotta, 2018; Zhao et al., 2017; Lee and MacKinnon, 2018; James and Zagotta, 2018).

It is interesting to note that although the EAG subfamily channels and other members of the so-called CNBD channel group share some common structural features, such as the presence of a VSD and PD arrangement and a non-swapped architecture, this group includes entities exhibiting quite divergent functional and/or gating properties (reviewed in James and Zagotta, 2018; Barros et al., 2019). These divergences are even more evident when other non-domain-swapped channels are considered. Thus, this structural architecture is encountered in channels showing:

a. a pure ligand-mediated mechanism of gating with very little or no voltage dependence. In the case of the SK channels, Ca^{2+}-bound to calmodulin (Ca^{2+}-CaM), associated to a cytoplasmic CaM binding domain (CaMBD), opens the permeation pathway. In the case of Slo2.2, opening is the result of a Na^+-mediated allosteric regulation of a cytoplasmic gating ring. In the CNG channels, gating depends on the binding of cyclic nucleotides to intracellular CNBDs, that expand the S6 helices bundle and open the cytoplasmic channel gate (Hite et al., 2015; Hite and MacKinnon, 2017; James et al., 2017; Li et al., 2017; Lee and MacKinnon, 2018).
b. a dual ligand-voltage regulation of gating, as in BK/Slo1 channels, whose opening is synergistically regulated by both membrane depolarization and intracellular Ca^{2+} increase acting on a cytoplasmic gating ring (Horrigan and Aldrich, 2002; Yang et al., 2015; Jia et al., 2018).
c. a voltage-dependent activation with so-called "inverted" gating polarity, as in the HCN channels, in which, unlike the typical depolarization-dependent activation exhibited by the Kv channels, membrane depolarization causes channel closing while activation is triggered by membrane hyperpolarization. In this case, an increased activity is also elicited upon binding of cyclic nucleotides to their intracellular CNBDs (Lee and MacKinnon, 2017; James and Zagotta, 2018).
d. a pure voltage- and depolarization-dependent activation gating, as in the genuine Kv channels of the EAG subfamily. Noticeably, even within this channel group, in which strong similarities in primary structure (**Figure 1**) and three-dimensional architecture (Whicher and MacKinnon, 2016; Wang and MacKinnon, 2017) exist, clear differences in gating behavior can also be encountered (Schwarz and Bauer, 2004; Bauer and Schwarz, 2018). These include (i) different ranges of activation and deactivation voltage dependence and diverse gating kinetics, sometimes determined by the potential level previous to the stimulus, (ii) quite different inactivation behavior, and (iii) in the case of the erg (Kv11) channel subtype, gating kinetics inverse to those of other Kv channels, that functionally make them behave as inward-rectifiers (Vandenberg et al., 2012; Bauer and Schwarz, 2018; see next). Altogether, these data suggest that subtle differences in molecular architecture and/or divergences in modulation of the primary gating machinery (allosteric

influences), by relatively distant protein domains (e.g., by some cytoplasmic regions showing structural divergence in different members of the same family), can crucially determine the functional output.

FUNCTIONAL HETEROGENEITY AND EXPRESSION PATTERNS INSIDE THE EAG CHANNEL SUBFAMILY

Expression of different members of the EAG channel subfamily has been observed in a variety of tissues (Ganetzky et al., 1999; Morais-Cabral and Robertson, 2015; Bauer and Schwarz, 2018). All of them are highly expressed in the nervous system, in which they may help to regulate excitability of neuronal cells, although lack of selective blockers of eag and elk channel subtypes mostly precluded proper isolation of native currents in this type of cells, and limited the knowledge of their specific impact on cell excitability (Bauer and Schwarz, 2018). Noticeably, eag1 limits activity-dependent Ca^{2+} entry in presynaptic terminals in the cerebellum, although its function seems to be exclusively exerted in situations with high levels of activity (Mortensen et al., 2015). Nevertheless, a wealth of information has been obtained about the erg1 (hERG) and eag1 physiological roles, due to their recognized expression in heart and tumor cells. Thus, expression of erg1 in cardiac cells is the basis of the fast delayed-rectifier current (I_{Kr}), that contributes to termination of cardiac action potentials and determines the appearance of type 2 long-QT (LQT2) syndrome and higher probability of sudden cardiac death, when inherited mutations or pharmacological block cause loss of channel function (Sanguinetti and Tristani-Firouzi, 2006; Vandenberg et al., 2012). In this case, the particular kinetic properties of the erg-mediated currents, and the availability of some pharmacological inhibitors, also allowed to recognize a role of these channels setting the electrical activity in several non-neuronal and non-cardiac cells, such as gastrointestinal smooth muscle fibers, glomus cells of the carotid body, adenohypophysial lactotrophs, epinephrine-releasing chromaffin cells, and pancreatic islet insulin-releasing β-cells and glucagon-releasing α cells (Schwarz and Bauer, 2004; Wanke and Restano-Cassulini, 2007; Vandenberg et al., 2012; Barros et al., 2012; Babcock and Li, 2013; Bauer and Schwarz, 2018). Additionally, both erg1 and eag1 channel expression is aberrantly increased in a variety of tumor cells, where they increased cell proliferation level and tumor malignancy (Arcangeli et al., 2009; Pardo and Stühmer, 2014; Lastraioli et al., 2015; Prevarskaya et al., 2018).

Apart from their presence and putative role in different native tissues, all EAG channel subtypes have been heterologously expressed and their functional properties subsequently characterized. Thus, it has been found that, despite the considerable homogeneity in their gross structural organization (**Figure 1**), substantial differences exist in their biophysical properties and gating behavior, sometimes even between members of the same channel subfamily. Thus, when submitted to constant depolarizing pulses to positive voltages from negative resting potentials, both eag1 and eag2 channels mediate outward-rectifying K^+ currents that do not apparently inactivate. Furthermore, they show a prominent delay and slowing down of the activation when depolarization steps are preceded by negative prepulses, an effect (often misidentified as Cole-Moore effect, but see Hoshi and Armstrong, 2015) strongly dependent on extracellular Mg^{2+} and that sets the basis for their action under high frequency stimulation, since the activation is extremely slow in response to the initial stimuli, but speeds up with subsequent ones and, eventually, reaches a fairly fast activation which results in the current "appearing" only after a number of stimuli (Mortensen et al., 2015). Furthermore, both eag1 and eag2 are inhibited by binding the Ca^{2+}-calmodulin (Ca^{2+}-CaM) complex to several intracellular channel sites at the amino and carboxy termini. Nevertheless, clear differences in voltage dependence of activation are also exhibited by eag1 and eag2, since a much more positively shifted $V_{1/2}$ value and a steeper slope of the activation curve are observed in eag1 as compared with eag2 channels (reviewed in Bauer and Schwarz, 2018).

Unlike the eag subtype channels, all erg channels inactivate and show unusual gating properties that allow them to act as crucial regulators of cell excitability (Bauer and Schwarz, 2018). Thus, erg channels show a slow activation overlapping with a rapid and voltage-dependent inactivation, leading to limited levels of outward current upon depolarization. Indeed, the steady-state erg current amplitude gets increasingly smaller at larger depolarizations due to more pronounced inactivation. At negative repolarization voltages, erg channels reopen due to their rapid recovery from inactivation before closing at a slow rate, leading to the appearance of prominent tail currents (Trudeau et al., 1995; Sanguinetti et al., 1995; Smith et al., 1996; Schönherr and Heinemann, 1996; Spector et al., 1996; Wang et al., 1997; Viloria et al., 2000). This peculiar kinetic combination, opposite to those of other voltage-dependent K^+ channels, makes erg channels operate as inward rectifiers, although they have the six membrane-spanning domains and the VSD plus PD architecture typical of the depolarization-activated channels. Nevertheless, differences in gating behavior are also observed between the different erg channels. Thus, erg2 channels activate even more slowly than erg1, and erg3 channels show faster activation and deactivation but less inactivation, making them the weakest inward rectifiers of the group. Additionally, the erg2 activation curve is shifted to the right and that of erg3 to the left as compared to that of erg1 (Bauer and Schwarz, 2018). The physiological relevance of a population of inactivating voltage-dependent channels is determined by the so-called "window-current", a bell-shaped curve resulting from the overlap of activation and inactivation curves that represents the steady-state fractional open probability as function of membrane potential, and defines the range of potentials at which the channels remain conductive (Becchetti et al., 2002; Bauer and Schwarz, 2018). Therefore, due to the aforementioned kinetic differences, a larger window-current covering a much broader voltage range is exhibited by erg3 channels as compared with erg1 (Bauer and Schwarz, 2018).

Differences in functional behavior are also found between members of the elk subtype channels. Thus, whereas no inactivation is present in elk1 and elk3, a clear inactivation is

observed in elk2, that appears to be shifted to much more depolarized values than those of the erg subtype channels. Also, both elk1 and elk3 activate at more negative voltages, deactivate much more slowly and lack the typical Cole-Moore-like effect encountered in the non-inactivating channels of the eag subtype (Bauer and Schwarz, 2018). In our knowledge, the specific structural determinants for these differences in functional behavior remain unknown.

In summary, in spite of the obvious similarities in primary sequence (**Figure 1**) and in putative structural organization predicted for all EAG channels, the molecular basis of their kinetic characteristics and of the differences between them are not completely understood. It seems probable that whereas a common general architecture may determine the gating scheme used by the EAG channels and the physicochemical model involved in coupling voltage sensing to opening and closing the pore, subtle changes in such common structure and/or allosteric influences of protein domains, relatively distant from the central gating machinery, may crucially influence the gating process. The latest advances about this issue provided by the cryo-EM elucidation of eag1 and erg1 three-dimensional structures, and by both classical and more recent functional studies with different members of the EAG subfamily, are presented below.

MECHANISM(S) OF VSD-PD COUPLING FOR GATING THE NON-DOMAIN-SWAPPED KV CHANNELS OF THE EAG FAMILY

As mentioned, the observation that Kv10.1 and Kv11.1 channels split at the S4–S5 linker maintain an almost unaltered voltage-dependent gating (Lorinczi et al., 2015), and the more recent demonstration of their non-domain-swapped architecture (Whicher and MacKinnon, 2016; Wang and MacKinnon, 2017), indicate that they must use a molecular mechanism for voltage-dependent activation different from the canonical S4–S5 linker lever-type of electromechanical VSD-PD coupling proposed for other voltage-dependent K^+ (e.g., *Shaker*-like Kv1-9) and Na^+ channels (Fernández-Mariño et al., 2018). It is important to note that, despite some subtle differences evidenced by the recently elucidated three-dimensional maps (Whicher and MacKinnon, 2016; Wang and MacKinnon, 2017), in the EAG channels the VSD structure, the location of the charge-carrying residues, the intra-VSD charge-charge interactions, and the extent of S4 translocation across the membrane, are similar to those of the classical *Shaker*-type Kv channels (Cheng and Claydon, 2012; Wang et al., 2013; Goodchild and Fedida, 2014). Also, whereas eag subtype channels typically activate (and deactivate) rapidly, some EAG channels (e.g., erg1/Kv11.1) exhibit a particularly slow activation (and deactivation) process (see above). In this sense, eag1 gating currents triggered by membrane depolarization and repolarization are rapid in onset and decay, but those from erg1 contain a major component an order of magnitude slower than the charge movements observed in eag1 (Piper et al., 2003; Bannister et al., 2005; Wang et al., 2013) and other Kv channels (Hesketh and Fedida, 1999; Bezanilla, 2000). Such a slow component could act, at least in part, as a rate-limiting step to explain erg1 slowness in pore opening and ionic current flow (Piper et al., 2003). However, even these slow reorganizations of erg1 VSD are not rate-limiting for pore gating, particularly over physiological voltages and timescales, since their voltage dependences and time constants for gating charge movement are still orders of magnitude separated from those of the activation of ionic currents (Wang et al., 2013; Goodchild and Fedida, 2014; Goodchild et al., 2015). Indeed, this has been interpreted as an indication that further transitions downstream of VSD rearrangements (e.g., some VSD-PD coupling steps and/or some allosteric interactions with distant structural elements that increase the time to pore opening, see below) are critically involved in the major erg1 pore opening delays (Goodchild and Fedida, 2014; Goodchild et al., 2015). Noticeably, some non-domain swapped ion channels are ligand-operated channels (e.g., SK, Slo2.2 and CNG channels, see above). It is obvious that in these cases binding of the regulator ligand to some specific domain(s) must allosterically control gating. However, participation of allosteric mechanisms on gating is not restricted to ligand-only operated channels, since they are also present in dual ligand-voltage regulated channels such as BK/Slo1 and HCN channels (see above). Thus, it is likely that these mechanisms may also influence gating in other non-domain-swapped, but genuinely Kv channels, such as eag1 (Kv10.1) and erg1 (Kv11.1). Indeed, binding of an intrinsic ligand to the eag1 CNBHD, is able to modulate activation in a way analog to cyclic nucleotide binding to other CNG family members (Zhao et al., 2017). Therefore, structural and functional evidences that the indicated allosteric interactions exist and their possible role in gating of non-domain-swapped eag1 and erg1 channels are considered next.

Early work with the EAG channels eag1, KAT1 and erg1, suggested that some of their amino terminal domains play an important role in setting the activation and deactivation gating characteristics, and pointed to a key role of interactions between them and the channels transmembrane core in this process, mainly with the carboxy end of the S4 segment or the S4–S5 linker. Thus, although structural alterations of the eag1 N-terminus impacted activation kinetics and abolished the Cole-Moore effect, these effects may be compensated by a single mutation of His343 (Terlau et al., 1997), which was initially suggested to be included in the S4 segment but more recently has been unequivocally located in the eag1 S4–S5 linker (Whicher and MacKinnon, 2016). In the same way, functional analysis of KAT-1 N-terminal deletion mutants, combined with S4 mutations, indicated that the N-terminus could also determine activation/deactivation kinetics, voltage dependence, and voltage sensitivity, probably by interacting with the voltage-sensing S4 segment (Marten and Hoshi, 1998). Initial studies with erg1 also indicated that regulation of deactivation involves the N-terminus and the S4–S5 loop, as if an interaction between these regions were essential for bringing the functional domains of the N-terminus into proximity with their targets in the hydrophobic core (Wang et al., 1998). In this case, missense mutations or

chemical modification of the S4–S5 linker, mimic the effects of amino terminal deletion or missense mutations in the amino terminus, markedly increasing the rate of channel deactivation, and suggesting that the N-terminus of erg1 might interact with the S4–S5 linker to affect these changes (Sanguinetti and Xu, 1999; Chen et al., 1999). On the other hand, microinjection of a peptide corresponding to the entire eag domain into *Xenopus* oocytes expressing erg1 channels lacking this domain, or application of a peptide corresponding to the first 16 amino acids of the channel to excised membrane macropatches from oocytes expressing the same deleted erg1 channels, partially restored the slow deactivation gating properties that had been significantly accelerated by eag domain removal (Morais-Cabral et al., 1998; Wang et al., 2000). Moreover, expression of a recombinant eag domain (residues 1-135) in oocytes (Gustina and Trudeau, 2009), or transfected mammalian cells (Fernández-Trillo et al., 2011), causes complete recovery of the normal (slow) deactivation properties of N-terminally truncated erg1, lacking either the whole amino terminus or the eag domain. In this case, biochemical, functional and fluorescence resonance energy transfer (FRET) data directly demonstrated that the recombinant fragment interacts with the N-terminally truncated transmembrane channel core (Gustina and Trudeau, 2009; Gustina and Trudeau, 2011; Fernández-Trillo et al., 2011; Gustina and Trudeau, 2012; Gianulis et al., 2013; Codding and Trudeau, 2019). In this sense, a "master-switch" was proposed that maintains the erg1 slow rate of deactivation, requiring the simultaneous presence of all five Asp residues in the VSD. Binding of the N-terminal eag/PAS domain to the cytoplasmic S4–S5 linker would serve as such "master-switch" (Liu et al., 2003). Initial FRET experiments also suggested a very close proximity of the erg1 amino terminus to the central channel core, in good agreement with the proposed interaction(s) of the initial eag domain with the transmembrane channel structure, possibly at the level of the S4–S5 linker (Miranda et al., 2008; De la Peña et al., 2011; Barros et al., 2018). Indeed, this molecular organization has lately been corroborated by the eag1 and erg1 three-dimensional structures (Whicher and MacKinnon, 2016; Wang and MacKinnon, 2017). Finally, functional data indicate that two different domains regulating erg1 gating seem to be present in the N-terminus: a distal eag domain mainly controlling current deactivation, and a proximal domain regulating activation (Viloria et al., 2000). Removal of the eag domain from channels already lacking the proximal domain, noticeably reverses the effect on activation caused by the deletion of the proximal domain. This indicates that the effects of proximal domain removal are at least partially dependent on the presence of the eag domain, suggesting that an interaction of this domain with the channel core may be involved in alterations of activation caused by elimination of the proximal domain (Viloria et al., 2000).

It is important to note that direct interactions between the amino terminus and the transmembrane channel are not the only determinants for setting the activation and deactivation gating characteristics of *KCNH* channels. Indeed, the sequence similarity at the initial region of the C-terminus of these channels (from the end of the S6 helix to the end of the CNBHD) is also extendable to the cyclic nucleotide-dependent CNG and HCN channels (reviewed in Gustina and Trudeau, 2012; Morais-Cabral and Robertson, 2015; James and Zagotta, 2018). FRET data also suggested that, as proposed for the CNG and HCN channels (Zagotta et al., 2003; Craven and Zagotta, 2004; Hua and Gordon, 2005; Johnson and Zagotta, 2005; Taraska and Zagotta, 2007), the C-linker/CNBHD region "hangs" centrally below the transmembrane erg1 core, with the eag/PAS domain around its top and side surfaces, probably directed towards the gating machinery of the channel (Miranda et al., 2008). The recent cryo-EM structural models of both eag1 and erg1 (Whicher and MacKinnon, 2016; Wang and MacKinnon, 2017) confirmed that this region forms a tetrameric ring below the channel pore, which is surrounded by the eag domains docked to the outer surfaces of the CNBHDs. Interestingly, the predictions from the X-ray crystal structures of the isolated eag1 PAS-CNBHD complex (Haitin et al., 2013), and those based on homology modelling and protein-protein docking of the eag domain and the C-linker/CNBHD (Muskett et al., 2011), placed the N-tail interacting with the surface of the PAS region and/or the intracellular facing surface of the CNBHD, quite far from the elements of the gating machinery (e.g., the VSD/S4–S5 linker/gate interface) located at the intracellular plasma membrane surface (Muskett et al., 2011; Gustina and Trudeau, 2012; Vandenberg et al., 2012). This hypothesis was at odds with the idea of a direct interaction of the EAG channels N-tail with the transmembrane core (e.g., with the S4–S5 linker, see above) for regulation of gating. However, in some EAG channels the S4–S5 linker has been repeatedly proposed to act as an integrator of signals coming from other cytoplasmic domains to influence channel gating (Alonso-Ron et al., 2008; Ng et al., 2012; Tan et al., 2012; Zhao et al., 2017). In addition, a purified S4–S5 linker peptide (containing also residues from both S4 and S5) combines in solution with an isolated erg1 eag domain and causes a shift in the position of several amino acids in the eag domain NMR structure, suggesting that the peptide interacted with some region of such domain (Li et al., 2010). This possibility is also supported by results showing that in eag1 gating changes induced by small deletions in the initial portion of the N-terminus are compensated by a H343R point mutation at the S4–S5 linker (Terlau et al., 1997; Whicher and MacKinnon, 2016, see above). Finally, the observation that a disulfide cross-linkage can be formed between pairs of cysteine residues introduced in the erg1 N-tail and the S4–S5 linker, provided a more direct demonstration of a close physical proximity between both regions (De la Peña et al., 2011). Further analysis by the cysteine mutagenesis and disulfide chemistry approach suggested that, at least in some conformational state(s) of erg1, the flexible N-tail gets close to both the S4–S5 linker and some surface(s) of the C-linker/CNBHD domain relatively distant in the primary structure (De la Peña et al., 2013; De la Peña et al., 2015). Noticeably, whereas the N-tail region was disordered in the crystal structures of the erg1 eag domain, the solution structure solved by NMR spectroscopy indicated that the N-tail is structurally independent from the PAS region and contains a flexible initial segment of around 12 amino acids that form a highly dynamic, extended structure, followed by a helical

element up to residue 25 (Li et al., 2010; Ng et al., 2011; Muskett et al., 2011). These data also provided a basis for the proposal that the flexible N-tail dynamically changes its position and/or orientation long enough to be able to interact with the VSD and the S4–S5 linker or the C-linker/CNBHD (De la Peña et al., 2013; Ng et al., 2014; De la Peña et al., 2015). Indeed, albeit indirectly, additional support for this idea was provided by docking the ensemble of the twenty erg1 eag-domain structures obtained by NMR (Li et al., 2010; Ng et al., 2011; Muskett et al., 2011; PDB codes 2L4R, 2L0W and 2L1M), against the C-linker/cNBD crystal structure of HCN2 (Zagotta et al., 2003; Haitin et al., 2013; PDB code 1Q5O), also docked below an erg1 transmembrane core structure homologous to that of Kv1.2 (Long et al., 2005; Long et al., 2007; PDB code 2A79). This opens the possibility that the flexibility of the N-terminal tail could allow it to adopt several positions from the bottom surface of the cNBD up to the S4–S5 linker (De la Peña et al., 2013; Morais-Cabral and Robertson, 2015). It also led us to propose the unifying hypothesis that a dynamic network of interactions may exist in EAG channels, involving the N-terminal tail, the S4–S5 linker and the C-terminal portion of S6, as well as other more distant cytoplasmic regions such as the PAS region and the C-linker/CNBHD (De la Peña et al., 2011; De la Peña et al., 2018a; Barros et al., 2018). If such a network constitutes an essential part of the gating machinery itself, only a regulator of the gating process(es) remains to be established. As also suggested by other authors (Morais-Cabral and Robertson, 2015), it is possible that the complex between the PAS and the C-linker/CNBHD domains could serve as an anchor to properly place and orientate the distal N-tail, that may constitute an important regulator of channel gating kinetics. This would also imply that changes in the conformation of either of these domains, or modifications of the interactions between them (Gustina and Trudeau, 2009; Gustina and Trudeau, 2011; Gianulis et al., 2013; Perissinotti et al., 2018; Codding and Trudeau, 2019), could result in gating changes due to alterations in the C-linker assembly, the relative orientation of the PAS and CNBHD domains, or the position of the N-tail (Morais-Cabral and Robertson, 2015; Perissinotti et al., 2018).

NEW STRUCTURAL AND FUNCTIONAL DATA REGARDING ALLOSTERIC INFLUENCES OF CYTOPLASMIC DOMAINS IN VSD-PD COUPLING AND REGULATION OF EAG CHANNELS GATING

As indicated above, and mainly derived from important improvements in single particle cryo-EM, the architectural organizations of multiple ion channels pertaining to the named "S4-pore-loop" or "six-transmembrane domain one-pore domain" (6TM1P) group (Yu et al., 2005; Gutman et al., 2005; Ashcroft, 2006; Lau et al., 2018; Barros et al., 2019) have been determined. These findings led to the realization that, as initially demonstrated for eag1 and later confirmed for erg1 (Whicher and MacKinnon, 2016; Wang and MacKinnon, 2017), the overall architecture of the EAG channels subfamily differs from that of other Kv channels. Thus, the transmembrane core of these channels exhibits a non-domain-swapped molecular organization, in which the VSD of every subunit of the tetramer contacts the PD of the same polypeptide (**Figure 3**). This seems to preclude the possibility that the very short S4–S5 linker that connects both protein modules could act as a mechanical lever, like in domain-swapped Kv channels, that transmits the voltage-triggered reorganizations in the VSD (e.g., the movements of the S4 helix), to pull the S6 helices of neighboring subunits and open the channel gate at the bottom of the PD (Lu et al., 2002; Long et al., 2005; Long et al., 2007; Blunck and Batulan, 2012; Chowdury et al., 2014). The finding of such structural features also helped to understand previous data demonstrating that co-expressing N-terminal and C-terminal halves of these proteins separated at the S4–S5 linker (S4–S5 split channels) generated an almost unperturbed voltage-dependent activation gating (Lorinczi et al., 2015), further suggesting that in this type of Kv channels an alternative mechanism of voltage-dependent gating should exist. On the other hand, this opened some questions concerning the alternative molecular mechanism (s) and/or specific variations involved in voltage-dependent gating of these entities, and requested the possible contribution of additional structural and functional data, for example using split channels as an experimental tool, to better understand such new molecular mechanism(s).

In the solved cryo-EM structures of eag1 and erg1 the VSDs are in the depolarized/activated conformation, since they were obtained at a nominal voltage of 0 mV. Indeed, the observed structures of both VSD domains are almost identical (Whicher and MacKinnon, 2016; Wang and MacKinnon, 2017). However, an important difference between them is that whereas the erg1 intracellular gate at the S6 helical bundle is open, the eag1 structure shows the pore closed due to the inhibitory effect of the Ca^{2+}/CaM complex bound to the cytoplasmic face of the channel (Whicher and MacKinnon, 2016; Wang and MacKinnon, 2017). The overlap of both pore structures indicates that they start to significantly deviate at a glycine gating hinge of the S6 helix located below the selectivity filter, corresponding to the residues G648 in hERG and G460 in eag1 (Thouta et al., 2014; Wang and MacKinnon, 2017). A similar gating hinge has been observed in an equivalent position in other classical domain-swapped "*Shaker*-type" Kv channels (Jiang et al., 2002). On the other hand, extensive anti-parallel contacts between the S5 and S6 pore helices, and interactions of the intracellular end of S4 with S5 and/or the intracellular portion of S6 and the C-linker, are observed in the EAG channels structures. Altogether, these facts led to propose that in these channels, the inward and centric displacement of S4 would close the S6 helical gate, allowing the VSDs to push and compress the S5 helices and transmit force through the S5-S6 interface (Whicher and MacKinnon, 2016; Wang and MacKinnon, 2017). The possibility that the movement of S4 could allow it to interact with the C-linker to bend the S6 helix and close the

channel, in a way similar to that imposed by binding of Ca^{2+}/CaM, has been also proposed (Whicher and MacKinnon, 2016; Wang and MacKinnon, 2017). Interestingly, in all cases an intact S4–S5 linker would not be necessary for VSD-PD coupling (Lorinczi et al., 2015; De la Peña et al., 2018a).

Unfortunately, until the structures can be determined with the VSDs in both the up and down conformations, it would remain unclear if the Ca^{2+}/CaM-induced closed conformation of the eag1 pore is also representative of the closed state of both channels in response to changes in the VSD conformation triggered by membrane depolarization. Thus, the need for the S6 glycine kink is contradictory with previous data showing that, since in erg1 the S6 helices are inherently flexible, the S6 glycine residues are only required for the tight packing of the channel helices, but not as gating hinges for voltage-dependent activation (Hardman et al., 2007). On the other hand, in the erg1 open structure (Wang and MacKinnon, 2017), the S4–S5 linker residue Tyr542 seems to be directed towards the channel core, far from the initial residues of the N-tail to which it can be disulfide cross-linked, preferentially in the closed conformation, when cysteine pairs are introduced in both places (De la Peña et al., 2011). Also, the spatial locations of some residues in the C-linker (e.g., Cys723) do not seem optimal to establish disulfide bridges with N-tail engineered cysteines, as previously observed (De la Peña et al., 2013; De la Peña et al., 2015). Although it is possible that some of these cross-link results may be biased due to the introduction of cysteines in the putatively interacting positions, bringing on some alterations in the positioning or relationship between them, it seems clear that further functional and structural data with the VSD in both depolarized and hyperpolarized conformations, would be necessary to ascertain if the mentioned Ca^{2+}/CaM-induced eag1 closed state corresponds to that achieved through voltage sensor reorganizations triggered by changes in membrane voltage.

During peer review of this manuscript, two seminal works were published concerning the mechanism of hyperpolarization-dependent opening of the non-domain-swapped HCN channels. Using a combination of long molecular dynamics (MD) simulations with the depolarized human HCN1 cryo-EM structure (Lee and MacKinnon, 2017) as template, as well as functional studies with HCN-eag chimeras, a hyperpolarization-induced break in the S4 helix of the VSD was observed. This break originated two sub-helices and placing the lower sub-helix in an orientation almost parallel to the membrane plane as a surrogate S4–S5 helix (Kasimova et al., 2019). The breaking transition seemed to be important for HCN1 hyperpolarization-dependent activation. Strikingly, the hydrophobicity of the amino acid following the breakpoint determined the gating polarity of some chimeric channels, changing it from a depolarization- to a hyperpolarization-dependent activation, opening the possibility that divergence of both types of channels could have occurred through a single point mutation in the S4 segment (Kasimova et al., 2019). The presence of the interfacial S4 sub-helix following the aforementioned S4 helix break, has been demonstrated in the recent cryo-EM structure of the HCN1 channel with the VSD chemically trapped in a hyperpolarized conformation by reversible, metal-mediated cross bridging (Lee and MacKinnon, 2019). Leaving apart the differences between their gating polarity, although both the HCN and eag channels share the same non-domain-swapped architecture, it is unclear if the two-helices break model also applies to members of the eag family because: (i) a S4 helix much shorter than that of HCN1 is observed in the structures of the eag1 and erg1 channels (Whicher and MacKinnon, 2016; Wang and MacKinnon, 2017), and (ii) quite small voltage sensor conformational changes seem to be induced in eag channels by changing the polarization of the membrane, as compared to those elicited in other Kv channels (Wang and MacKinnon, 2017). Further work would be necessary to ascertain if the two-helix break property is a common feature to other non-domain-swapped channels outside those of the HCN group.

One interesting feature in both the eag1 and the erg1 cryo-EM structures is that, despite the lack of domain swapping in their transmembrane core, the cytoplasmic regions do show a domain-swapped architecture. Thus, consistent with previous functional and structural studies (Stevens et al., 2009; Gustina and Trudeau, 2011; Gianulis et al., 2013; Haitin et al., 2013; Ng et al., 2014), the CNBHD of one subunit, which folds below the C-linker of the same subunit to which it is backbone connected, interacts at the same time with the N-terminal eag domain of the neighboring subunit (Whicher and MacKinnon, 2016; Wang and MacKinnon, 2017). Furthermore, in the case of eag1, binding of Ca^{2+}/CaM to the PAS and CNBHD domains swapped between subunits establishes bridges between their N- and C-termini, that had been proposed to act as a molecular clamp to pull the two domains together translating the CNBHD interacting with the CaM toward the neighboring PAS (Whicher and MacKinnon, 2016; Barros et al., 2019). According to this proposal, since the CNBHD is connected to S6 *via* the C-linker, its movement toward the PAS domain would cause a rotation of both the C-linker and S6 to induce a 55° bend in a direction that tightens the helical bundle that forms the intracellular gate, inducing pore closure independently of transmembrane voltage (Whicher and MacKinnon, 2016). Recent data with this channel also described some interactions between the VSD, CNBHD and eag domains, that serve to modulate voltage-dependent channel gating, participate in the Cole-Moore effect, and are essential for Ca^{2+}/CaM inhibition (Whicher and MacKinnon, 2019). It is interesting to note that some structural and/or functional elements participating in these interactions have been regarded as important modulators of gating in other EAG channels such as erg1, even though it does neither exhibit a Cole-Moore effect nor Ca^{2+}/CaM-dependent regulation. The question that now arises is: what specific and distinctive molecular mechanism(s) could be involved in the voltage-dependent gating process of these channels and/or its possible regulation by the cytoplasmic domains?

An essential breakthrough provided by the new eag1 and erg1 structures was the direct confirmation that, through interactions between the PAS, C-linker/CNBHD and some other linkers at the VSD intracellular surface, the N-tail is directed towards the lower surface of the transmembrane core (Whicher and MacKinnon, 2016; Wang and MacKinnon, 2017). In the case of erg1, whose structure includes almost the entire N-tail, this region is positioned in close contact with both the S4–S5 linker of

the same subunit and the C-linker of the adjacent subunit, respectively attached to the carboxy termini of the S4 and S6 helices (**Figure 4**). In addition, it also interacts with the intracellular S2-S3 linker and the S1 C-terminus of the same subunit (Whicher and MacKinnon, 2016; Wang and MacKinnon, 2017; Whicher and MacKinnon, 2019; Barros et al., 2019). The proximity of the N-tail to the S2–S3 linker and its possible implication in gating, would be also consistent with data showing that disruption of this linker causes alterations of erg1 gating, similar to those triggered by interrupting the S4 at its C-terminal end (De la Peña et al., 2018b). The S2-S3 linker of Drosophila eag has been proposed to play a role in the modulation of gating by Mg^{2+}, perhaps through an electrostatic interaction with other intracellular domains or its interface with the transmembrane domains (Liu et al., 2010). On the other hand, the erg1 N-tail contact with residues H402 and T403 at the pre-S1 region could explain the gating perturbations triggered by mutations in these residues, similar to those caused by mutations in the N-tail itself (Phan et al., 2017). Furthermore, interaction and functional coupling of the erg1 S1 residue D411 with K538 at the inner end of S4 has been proposed (Zhang et al., 2005). In addition, it has been shown that interactions of D411 with lower S4 residues stabilize early closed states of the channel, and disruption of these interactions results both in: (i) faster rates

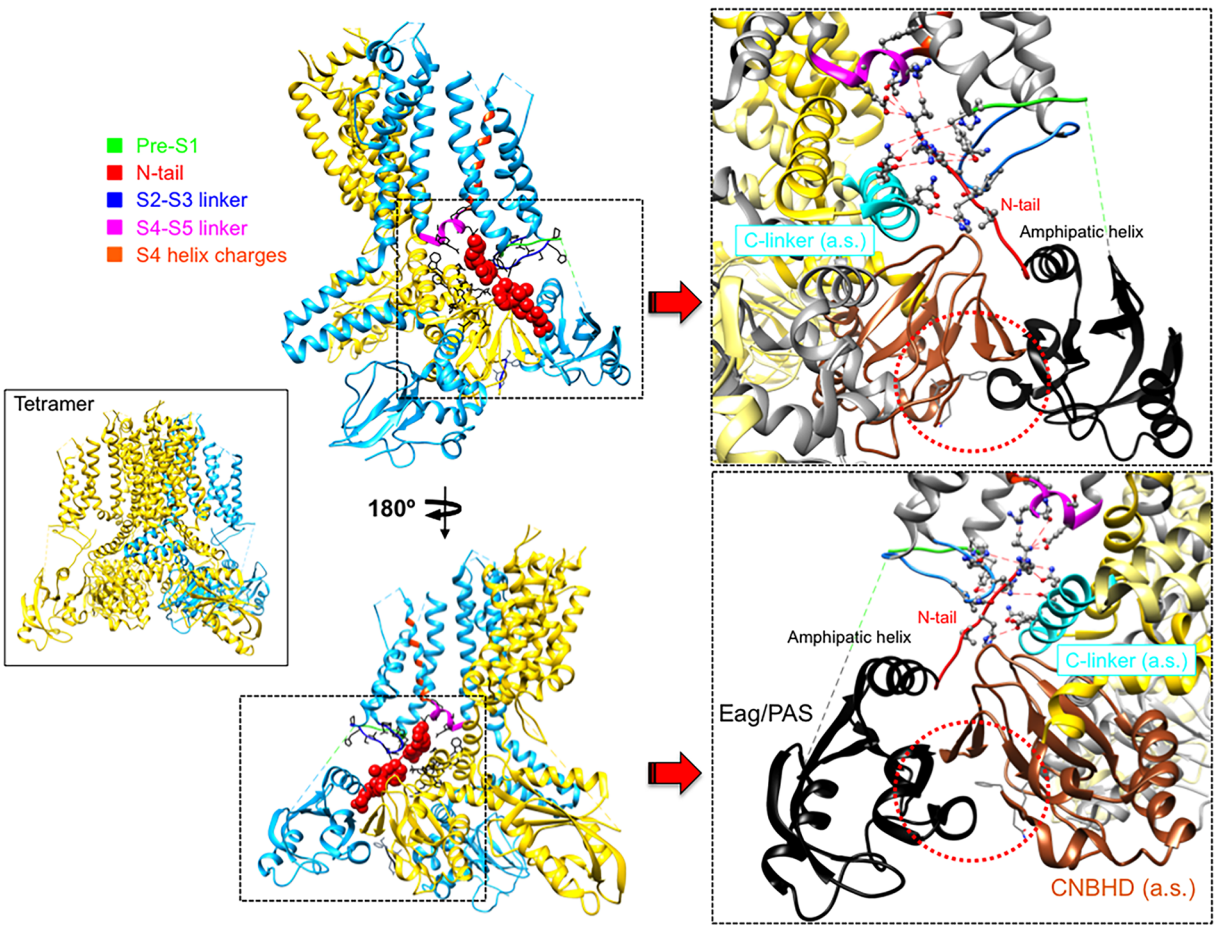

FIGURE 4 | Close apposition of the erg1 (Kv11.1) N-tail with other cytoplasmic linkers of the channel and possible network of interactions that may dynamically contribute to modulate channel gating. *Left.* Lateral view of the erg1 tetrameric structure (Wang and MacKinnon, 2017; PDB code 5VA2) shown with ribbons. A highlighted subunit is colored in blue. *Center.* View of only two adjacent subunits in which some domains of the blue subunit are colored as indicated at the left high corner. Atoms corresponding to the amino terminal N-tail (red) are shown as spheres. Lateral chains of selected residues surrounding the space(s) around the N-tail position, pertaining to the pre-S1, S2–S3 and S4–S5 linkers of the same subunit, and the C-linker of the adjacent subunit, are presented as black sticks. Grey sticks at the bottom correspond to the residues that constitute the intrinsic ligand of the cyclic nucleotide-binding homology domain (CNBHD), occupying the ligand-binding pocket analogous to where cyclic nucleotides bind to the cyclic nucleotide binding domains in other channels. *Right.* Enlarged views of the regions inside the squares delimited by black dotted lines are shown. Lateral chains of selected residues protruding from structure ribbons are shown as ball and stick with oxygen and nitrogen atoms as red and blue small spheres, respectively. Ribbon sections are colored red (N-tail), green (pre-S1), blue (S2-S3 linker), magenta (S4–S5 linker) and cyan (C-linker of the adjacent subunit). Red dashed lines indicate interatomic distances ranging between 3.0 and 6.0 Å. Black and brown colors are used for ribbons corresponding to the *P*er-*A*rnt-*S*im (PAS) domain, and the CNBHD of the adjacent subunit (*a.s.*), respectively. Red dotted circles are used to mark the close proximity of these domains and the location of the CNBHD intrinsic ligand (gray sticks) toward the PAS domain surface. Structures were processed with UCSF Chimera (Pettersen et al., 2004).

of activation gating, and (ii) elimination of the fast component of gating charge movement and fluorescence changes associated to fast movement of S4 (Dou et al., 2017).

As indicated above, even before the realization that the S4–S5 linker of EAG channels is very short and structurally divergent from those encountered in other voltage-dependent channels, it was proposed that this linker acts as an integrator of signals coming from other cytoplasmic regions, such as the eag domain and the C-linker/CNBHD (Ng et al., 2012; De la Peña et al., 2018a). Thus, the direct linkage of the CNBHD with the C-linker of the same subunit, and through it to the pore gate at the cytoplasmic S6 helices bundle, provides a conduit for the effect of the CNBHD on the gate, as depicted in **Figure 5**. At the same time, the interaction of the CNBHD with the PAS region of the neighboring subunit, and that of the eag domain with the S4–S5 linker and the VSD *via* the N-tail (**Figure 5**), would provide a second way to allosterically control not only the gate itself, but also the VSD. Such dual pathway has been proposed to contribute to the role of the CNBHD and its intrinsic ligand in both the gating and the VSD movements of eag1 (Zhao et al., 2017). This fact would be consistent with results indicating that destabilization of the intrinsic ligand could lead to widespread changes in the gating assembly located below the VSD/S4–S5 linker/gate interface, *via* alterations in position, orientation, or flexibility of not only the C-linker/CNBHD complex, but also the interfacing N-tail/PAS domain from the neighboring subunit (Zhao et al., 2017). Noticeably, through a combination of mutagenesis, electrophysiology, and structural modeling using eag1 as a representative template for the erg1 closed pore, a similar interplay between N-tail, eag/PAS and VSD domains, S4–S5 and C-linkers, and CNBHD has recently been envisioned as an important contributor to erg1 gating kinetics (Perissinotti et al., 2018). These data further support the view that interactions between soluble domains and the transmembrane part of these channels are critical determinants of gating characteristics (Vandenberg et al., 2004; De la Peña et al., 2011; Fernández-Trillo et al., 2011; Vandenberg et al., 2012; Barros et al., 2012; Cheng and Claydon, 2012; Gustina and Trudeau, 2012; De la Peña et al., 2013; Morais-Cabral and Robertson, 2015; Perry et al., 2015; Vandenberg et al., 2017; De la Peña et al., 2018a; De la Peña et al., 2018b; James and Zagotta, 2018; Perissinotti et al., 2018; Barros et al., 2019). Interestingly, recent experiments with elk channels also indicate that the absence of either just the N-tail region, or the entire eag domain, causes the loss of the typical

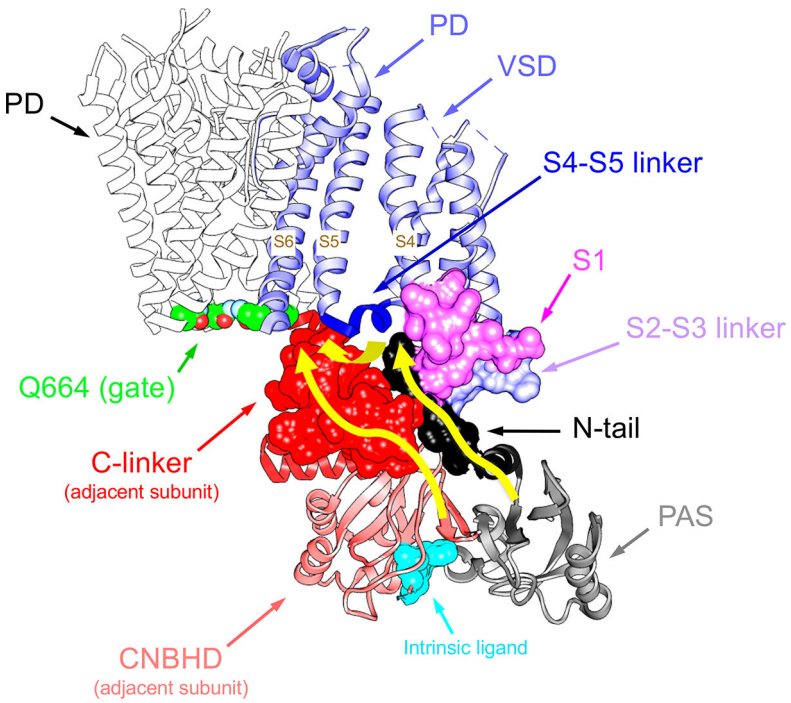

FIGURE 5 | Pathways linking cytoplasmic domains and their possible structural reorganizations to VSD-PD coupling and functional operation of the erg1 (Kv11.1/hERG) channel gate. For clarity, a single voltage sensor domain (VSD) is shown attached to the tetramer of the pore domain (PD). The four Q664 residues that mark the place of the cytoplasmic gate at the S6 helix bundle are highlighted. Atoms corresponding to the amino terminal N-tail (black), the S2-S3 linker (blue) and the S1 C-terminus of the same subunit (magenta), and the C-linker of the adjacent subunit (red), are shown in space-filling mode. The positions of the PAS domain (grey) and the S4–S5 linker (dark blue), as well as the cyclic nucleotide-binding homology domain (CNBHD), domain of the adjacent subunit (pink), are also depicted. Atoms corresponding to the intrinsic ligand that binds to the cyclic nucleotide binding site of the CNBHD in the *P*er-*A*rnt-*S*im (PAS)–CNBHD interface between two adjacent subunits are presented as cyan spheres at the bottom. Yellow arrows highlight pathways for: (i) direct propagation of CNBHD conformational reorganizations to the pore gate *via* the C-linker, and (ii) allosteric coupling of the CNBHD to the PAS domain of the neighbouring subunit, and subsequent interplay of the PAS/eag domain with the lower portion of the VSD and the gate *via* the N-tail and the S4–S5 linker.

mode-shift or hysteresis (also called prepulse facilitation and voltage-dependent potentiation or VDP). This is a phenomenon shared by elk and erg channels, in which, due to a slow depolarizing voltage-dependent transition to a state favoring channel opening, a shift in the voltage dependence of activation to more hyperpolarized voltage is induced. This has been envisioned as an indication that rearrangement of an interaction between the eag domain and the CNBHD leads to a transition of the CNBHD intrinsic ligand from antagonist to agonist, thus acting as an allosteric modulator of channel gating during mode-shift (Dai and Zagotta, 2017; Dai et al., 2018).

In addition to the new structural data, the ability of EAG channels to non-covalently assemble from independent VSD and PD modules, maintaining their voltage-dependent gating, could provide clues about new molecular gating mechanisms, as well as a new tool to better understand the nature of the interactions and the dynamics involved in the gating process. Indeed, data comparing gating characteristics of eag1 and erg1 channels split at different points along the S4–S5 linker have yielded some valuable information about these issues. Thus, covalent breaks either at the C-terminal end of S4, or at the N-terminus of the S4–S5 linker, prevent closing of eag1 and yield constitutively active channels, while disconnecting the linker at its carboxy terminus from S5 does not disrupt closing, only leading to alterations of channel kinetics (Lorinczi et al., 2015; Tomczak et al., 2017). Interestingly, interrupting the channel at the C-terminus of S4 (or at the S4–S5 linker N-terminus) has little or no influence on the voltage dependence of VSD motion, even in those channels that show a constitutively active phenotype, although the modulation of the channel resting state by prepulse voltage and Mg^{2+} can be significantly affected. On the other hand, the constitutive activity of the channels split at the end of S4 is reverted to a wild type-like closure either introducing a variety of point mutations in the first residue (D342) of the split C-terminal demi-channel, or when a structural alteration is introduced at the amino terminus of the N-terminal demi-channel (Tomczak et al., 2017). While these results suggest that the S4–S5 linker may interact with the most N-terminal region of the channel, the interaction partner of D342 and the reason by which the amino terminal alteration causes a similar effect still remain to be established.

Similar experiments with erg1, progressively displacing the split position from the carboxy to the amino end of the S4–S5 linker, revealed a gradual modification of the activation gating characteristics of the split channels (**Figure 6**). Although no constitutively open channels were observed, channels split at the base of the S4 helix (around residue D540) exhibit a strong shift to hyperpolarized values in the voltage dependence of activation, a reduced ability to reach more distal closed state(s) and a reduced voltage dependence of both activation and deactivation gating (De la Peña et al., 2018a). This would also be consistent with previous data indicating i) the existence of an interaction between the bottom of S6 and residue 540 at the beginning of the S4–S5 linker (Tristani-Firouzi et al., 2002; Ferrer et al., 2006), ii) the generation a more unstable closed channel by mutating D540 to cysteine (Alonso-Ron et al., 2008), and iii) the stabilization of a closed conformation of the activation gate by covalently bridging D540 and the C-terminal S6 residue L666 (Ferrer et al., 2006). However, in contrast with the results obtained with eag1, the gradual negative shifts in erg1 activation voltage dependence observed when the split point was moved along the S4–S5 linker were paralleled by similar shifts in S4 voltage dependent motion across the membrane, suggesting that VSD and PD disconnection could also modify the voltage-dependent conformational reorganizations of the erg1 VSD (De la Peña et al., 2018a). Despite these functional differences, it seems that both in eag1 and erg1 an intact C-terminal end of the S4 helix (and/or the initial section of the S4–S5 linker) is important to reach a stable closed state, and that the VSD acts as an inhibitory module to close the channel at negative potentials (Tomczak et al., 2017; De la Peña et al., 2018a; James and Zagotta, 2018).

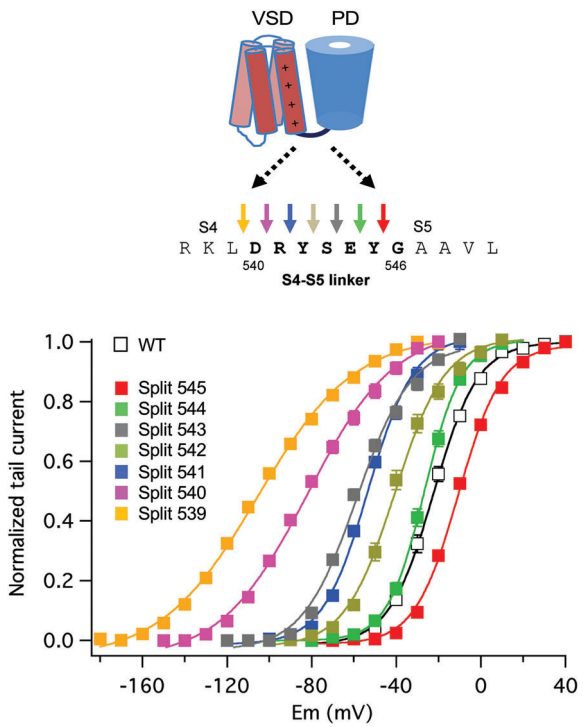

FIGURE 6 | Gradual modification of activation voltage dependence caused by breaking the covalent linkage at different points along the S4–S5 linker sequence in split erg1 (Kv11.1/hERG) channels. A schematic view of the transmembranal core of a channel subunit at the top is combined with the sequence of the S4–S5 linker region and a set of coloured arrows for each covalent break used to generate the split channels listed below. Plots of normalized conductance/voltage relationships for the different splits are shown in the graph. Plots were obtained from tail current measurements upon repolarization. Tail currents were recorded in oocytes expressing the indicated channel variants, submitted to 1-s depolarization pulses at different potentials in 10 mV intervals from a holding potential of -80/-100 mV, followed by a repolarization step at -50 (splits 545, 544, 543 and 542), -70 (wild type/WT and split 541), -120 (split 540), and -140 (split 539) mV. Different repolarization potentials were used to ensure closing of the different constructs and proper quantification of tail current magnitudes. Continuous lines are Boltzmann fits to the data. For details see De la Peña et al., 2018a, from which the Figure has been reproduced under Creative Commons Attribution 4.0 license.

It should be noted that the need of S4 reorganizations to hold the permeation gate closed seems contradictory with the fact that, in both channels, expression of an isolated PD that appears to be effectively transported to the membrane (Tomczak et al., 2017), yields no detectable currents. On first sight, these results with only PDs expressed could be taken as an indication against the existence of a stable open state. However, it has been shown that besides the contribution of the VSD to the switch between resting and conductive channel states, this domain is also necessary for the PD to reach a conducting conformation (Tomczak et al., 2017). Indeed, conductive pore modules are not even detected upon expression of either isolated eag1 or erg1 PDs carrying mutations that disrupt the cytoplasmic gate (e.g. Q477P in eag1 or Q664P in erg1; Thouta et al., 2014; Tomczak et al., 2017) and that yield full-length channels permanently open at all voltages. This indicates that the energy landscape of the isolated PD can be different from that of the complete VSD/PD assembly, which may favor a different, preferentially opened basal conformation of the PD (Zhao and Blunck, 2016; De la Peña et al., 2018a). Albeit still speculative, the existence of a network of non-covalent interactions between the VSD, the PD, and the intracellular domains, playing a relevant role for this purpose, remains as an interesting possibility.

Finally, it is important to note that the proposed existence of a network of interactions involving the N-terminus, the S4–S5 linker and the final portion of S6, and other C-terminal regions, is also compatible with the named ligand/receptor (allosteric) model of voltage-dependent gating (Malak et al., 2017; Malak et al., 2019), recently shown to be shared by both erg1 and eag2 channels, in which the VSD and PD are weakly coupled *via* a ligand constituted by the S4–S5 linker and a part of S5, and a receptor, the C-terminal part of the S6 segment (Malak et al., 2017; Malak et al., 2019). The reason why the presence of a substantial part of the S5 helix is necessary for the soluble peptides used as ligands to stabilize the closed channel state (Malak et al., 2017) remains to be established. Strikingly, this mechanism was first proposed (Choveau et al., 2011) for KCNQ1 (Kv7.1), which shows domain-swapped transmembrane topology. Kv7.1 has a long α-helical S4–S5 linker (Sun and MacKinnon, 2017), and electromechanical VSD-PD coupling was therefore assumed to be similar to that encountered in other *Shaker*-like Kv channels, and not to that of the non-domain swapped EAG channels. It is important to emphasize also that, both in non-domain-swapped and in those Kv channels with prototypical domain-swapped organization in which a long S4–S5 linker can act as a lever for electromechanical VSD-PD coupling, the helices bundle that forms the pore gate is located at the bottom of S6 (Holmgren et al., 1998; Del Camino et al., 2000; Mitcheson et al., 2000; Del Camino and Yellen, 2001; Witchel, 2004; Webster et al., 2004; Del Camino et al., 2005; Swartz, 2005; Boulet et al., 2007; Wynia-Smith et al., 2008; Thouta et al., 2014). Therefore, even in the typical domain-swapped channels the covalent connection of the VSD and PD modules *via* S4–S5 linker would only directly track the S5 helix, making necessary some additional non-covalent interactions to gate them. In this sense, a non-canonical coupling pathway, based in non-covalent specific interactions between residues of the S4 and S5 helices, has recently been shown to participate in voltage-dependent activation gating of the prototypical Drosophila *Shaker* channel (Fernández-Mariño et al., 2018). Moreover, the possibility that the amino terminal end of the eag2 channel modulates the S4–S5 linker interaction with S6 and, as a consequence, that a hypothetical ligand/receptor gating mechanism exists, has been considered. Unfortunately, as previously shown with erg1 channels split at the S4–S5 linker, deletions of amino terminal sequences of eag2 obliterated by themselves the functional expression of the channels, complicating the possible interpretation of the data (Malak et al., 2019). In any case, it is tempting to speculate that the existence of allosteric components for modulation of gating, documented in Kv10-12 (EAG) channels, but also in other Kv relatives (Barros et al., 2019), constitutes a way to provide evolutionary functional diversification to a common and particularly successful 6TM1P molecular channel design.

In summary, the evidences compiled here point to the existence of a global and (perhaps more importantly) dynamic network of interactions involving the N-tail and the PAS and proximal domains at the channel amino terminus, the carboxy end of S4 and the S4–S5 linker, the C-terminal portion of helix S6, and the carboxy terminal C-linker and CNBHD domains, that allosterically contribute to modulate EAG channels gating (De la Peña et al., 2011; Fernández-Trillo et al., 2011; De la Peña et al., 2013; De la Peña et al., 2015; De la Peña et al., 2018a; De la Peña et al., 2018b; Barros et al., 2019; Whicher and MacKinnon, 2019). Nevertheless, the functional consequences of these interactions on activation/deactivation gating, and even on channel inactivation, can vary according to the channel type, the relative positioning of the N- and C-terminal regions, and the presence of additional auxiliary subunits. Noticeably, despite recent advances provided by atomic models of many channels, including some members of the EAG group, obtaining mechanistic insights from these structures remains somehow challenging. Therefore, to gain a better understanding of these complex but thrilling issues, further work would be still necessary in which the more static structural view is complemented with additional dynamic information provided by mutagenesis, combined functional and/or fluorometric assays such as voltage-clamp fluorometry, kinetic modelling and *in silico* molecular dynamics simulations.

AUTHOR CONTRIBUTIONS

All authors contributed to literature collection, interpretation and integration, and to writing the manuscript.

ACKNOWLEDGMENTS

FB, PD, and PP work at the Hormone Receptors and Ion Channels group of the University of Oviedo was supported by Grant BFU2015-66429-P (MINECO/FEDER UE) from the Spanish Ministerio de Economía y Competitividad, co-financed

with European Fund for Economic and Regional Development (FEDER) funds. LP was supported by the Max Planck Society. LS pertains to the Mass Spectrometry & Biomedical Analysis group of the University of Oviedo and was supported by Grant MINECO CTQ2016-80069-C2-1-R from the Ministerio de Economía y Competitividad of Spain. Molecular graphics were performed with UCSF Chimera, developed by the Resource for Biocomputing, Visualization, and Informatics at the University of California, San Francisco, with support from NIH P41-GM103311 (Pettersen et al., 2004).

REFERENCES

Adaixo, R., Harley, C. A., Castro-Rodrigues, A. F., and Morais-Cabral, J. H. (2013). Structural Properties of PAS Domains from the KCNH Potassium Channels. *PloS One* 8, e59265. doi: 10.1371/journal.pone.0059265

Alonso-Ron, C., de la Peña, P., Miranda, P., Domínguez, P., and Barros, F. (2008). Thermodynamic and kinetic properties of amino-terminal and S4-S5 loop HERG channel mutants under steady-state conditions. *Biophys. J.* 94, 3893–3911. doi: 10.1529/biophysj.107.116731

Arcangeli, A., Crociani, O., Lastraioli, E., Masi, A., Pillozzi, S., and Becchetti, A. (2009). Targeting ion channels in cancer: a novel frontier in antineoplastic therapy. *Curr. Med. Chem.* 16, 66–93. doi: 10.2174/092986709787002835

Ashcroft, F. M. (2006). From molecule to malady. *Nature* 440, 440–447. doi: 10.1038/nature04707

Babcock, J. J., and Li, M. (2013). hERG channels function: beyond long QR. *Acta Pharmacol. Sin.* 34, 329–335. doi: 10.1038/aps.2013.6

Bannister, J. P. A., Chanda, B., Bezzanilla, F., and Papazian, D. M. (2005). Optical detection of rate-determining ion-modulated conformational changes of the ether-à-go-go K+ channel voltage sensor. *Proc. Nat. Acad. Sci. U. S. A.* 102, 18718–18723. doi: 10.1073/pnas.0505766102

Barros, F., Domínguez, P., and de la Peña, P. (2012). Cytoplasmic domains and voltage-dependent potassium channel gating. *Front. Pharmacol.* 3, 49. doi: 10.3389/fphar.2012.00049

Barros, F., Domínguez, P., and de la Peña, P. (2018). Relative positioning of Kv11.1 (hERG) K^+ channel cytoplasmic domain-located fluorescent tags toward the plasma membrane. *Sci. Rep.* 8, 15494. doi: 10.1038/s41598-018-33492-x

Barros, F., Pardo, L. A., Domínguez, P., Sierra, L. M., and de la Peña, P. (2019). New structures and gating of voltage-dependent poassium (Kv) channels and their relatives: A multi-domain and dynamic question. *Int. J. Mol. Sci.* 20, 248. doi: 10.3390/ijms20020248

Bauer, C. K., and Schwarz, J. R. (2018). Ether-à-go-go K^+ channels: effective modulators of neuronal excitability. *J. Physiol.* 596, 769–783. doi: 10.1113/JP275477

Becchetti, A., De Fusco, M., Crociani, O., Cherubini, A., Restano-Cassulini, R., Lecchi, M., et al. (2002). The functional properties of the human ether-á-go-go-like (HELK2) K^+ channel. *Eur. J. Neurosci.* 16, 415–428. doi: 10.1046/j.1460-9568.2002.02079.x

Bezanilla, F. (2000). The voltage sensor in voltage-dependent ion channels. *Physiol. Rev.* 80, 555–592. doi: 10.1152/physrev.2000.80.2.555

Bezanilla, F. (2008). How membrane proteins sense voltage. *Nat. Rev. Mol. Cell Biol.* 9, 323–332. doi: 10.1038/nrm2376

Blunck, R., and Batulan, Z. (2012). Mechanism of electromechanical coupling in voltage-gated potassium channels. *Front. Pharmacol.* 3, 166. doi: 10.3389/fphar.2012.00166

Boulet, I. R., Labro, A. J., Raes, A. L., and Snyders, D. J. (2007). Role of the S6 C-terminus in KCNQ1 channel gating. *J. Physiol.* 585, 325–337. doi: 10.1113/jphysiol.2007.145813

Chen, J., Zou, A., Splawski, I., Keating, M. T., and Sanguinetti, M. C. (1999). Long QT Syndrome-associated Mutations in the Per-Arnt-Sim (PAS) Domain of HERG Potassium Channels Accelerate Channel Deactivation. *J. Biol. Chem.* 274, 10113–10118. doi: 10.1074/jbc.274.15.10113

Cheng, Y. M., and Claydon, T. W. (2012). Voltage-dependent gating of hERG potassium channels. *Front. Pharmacol.* 3, 83. doi: 10.3389/fphar.2012.00083

Choveau, F. S., Rodriguez, N., Ali, F. A., Labro, A. J., Rose, T., Dahimene, S., et al. (2011). KCNQ1 channels voltage dependence through a voltage-dependent binding of the S4-S5 linker to the pore domain. *J. Biol. Chem.* 286, 707–716. doi: 10.1074/jbc.M110.146324

Chowdury, S., Haehnel, B. M., and Chanda, B. (2014). Interfacial gating triad is crucial for electromechanical transduction in voltage-activated potassium channels. *J. Gen. Physiol.* 144, 457–467. doi: 10.1085/jgp.201411185

Codding, S. J., and Trudeau, M. C. (2019). The hERG potassium channel intrinsic ligand regulates N- and C-terminal interactions and channel closure. *J. Gen. Physiol.* 151, 478–488. doi: 10.1085/jgp.201812129

Craven, K. B., and Zagotta, W. N. (2004). Salt bridges and gating in the COOH-terminal region of HCN2 and CNGA1 channels. *J. Gen. Physiol.* 124, 663–677. doi: 10.1085/jgp.200409178

Dai, G., and Zagotta, W. N. (2017). Molecular mechanism of voltage-dependent potentiation of KCNH potassium channels. *eLife* 6, e26355. doi: 10.7554/eLife.26355

Dai, G., James, Z. M., and Zagotta, W. N. (2018). Dynamic rearrangement of the intrinsic ligand regulates KCNH potassium channels. *J. Gen. Physiol.* 150, 625–635. doi: 10.1085/jgp.201711989

De la Peña, P., Alonso-Ron, C., Machín, A., Fernández-Trillo, J., Carretero, L., Domínguez, P., et al. (2011). Demonstration of physical proximity between the amino terminus and the S4-S5 linker of the hERG potassium channel. *J. Biol. Chem.* 286, 19065–19075. doi: 10.1074/jbc.M111.238899

De la Peña, P., Machín, A., Fernández-Trillo, J., Domínguez, P., and Barros, F. (2013). Mapping of interactions between the amino and carboxy termini and the channel core in hERG K^+ channels. *Biochem. J.* 451, 463–474. doi: 10.1042/BJ20121717

De la Peña, P., Machín, A., Fernández-Trillo, J., Domínguez, P., and Barros, F. (2015). Interactions between the N-terminal tail and the gating machinery of hERG K^+ channels both in closed and open/inactive states. *Pflügers Arch.* 467, 1747–1756. doi: 10.1007/s00424-014-1612-1

De la Peña, P., Dominguez, P., and Barros, F. (2018a). Gating mechanism of Kv11.1 (hERG) K^+ channels without covalent connection between voltage sensor and pore domains. *Pflügers Arch.* 470, 517–536. doi: 10.1007/s00424-017-2093-9

De la Peña, P., Dominguez, P., and Barros, F. (2018b). Functional characterization of Kv11.1 (hERG) potassium channels splits in the voltage-sensing domain. *Pflügers Arch.* 470, 1069–1085. doi: 10.1007/s00424-018-2135-y

Del Camino, D., and Yellen, G. (2001). Tight steric closure at the intracellular activation gate of a voltage-gated K^+ channel. *Neuron* 32, 649–656. doi: 10.1016/S0896-6273(01)00487-1

Del Camino, D., Holmgren, M., and Yellen, G. (2000). Blocker protection in the pore of a voltage-gated K^+ channel and its structural implications. *Nature* 403, 321–325. doi: 10.1038/35002099

Del Camino, D., Kanevsky, M., and Yellen, G. (2005). Status of the intracellular gate in the activated-not-open state of Shaker K^+ channels. *J. Gen. Physiol.* 126, 419–428. doi: 10.1085/jgp.200509385

Diver, M. M., Cheng, Y., and Julius, D. (2019). Structural insights into TRPM8 inhibition and desensitization. *Science* 365, 1434–1440. doi: 10.1126/science.aax6672

Dou, Y., Macdonald, L. C., Wu, Y., and Fedida, D. (2017). The fast component of hERG gating charge: An interaction between D411 in the S1 and S4 residues. *Biophys. J.* 113, 1979–1991. doi: 10.1016/j.bpj.2017.09.004

Fernández-Trillo, J., Barros, F., Machín, A., Carretero, L., Domínguez, P., and de la Peña, P. (2011). Molecular determinants of interactions between the N-terminal domain and the transmembrane core that modulate hERG K^+ channel gating. *PloS One* 6, e24674. doi: 10.1371/journal.pone.0024674

Fernández-Mariño, A. I., Harpole, T. J., Oelstrom, K., Delemotte, L., and Chanda, B. (2018). Gating interaction maps reveal a noncanonical electromechanical coupling mode in the Shaker K^+ channel. *Nat. Struct. Mol. Biol.* 25, 320–326. doi: 10.1038/s41594-018-0047-3

Ferrer, T., Rupp, J., Piper, D. R., and Tristani-Firouzi, M. (2006). The S4-S5 linker directly couples voltage sensor movement to the activation gate in the human ether-á-go-go-related gene (hERG) K^+ channel. *J. Biol. Chem.* 281, 12858–12864. doi: 10.1074/jbc.M513518200

Flynn, G. E., and Zagotta, W. N. (2018). Insights into the molecular mechanism for hyperpolarization-dependent activation of HCN channels. *Proc. Natl. Acad. Sci. U.S.A.* 115, E8086–E8095. doi: 10.1073/pnas.1805596115

Ganetzky, B., Robertson, G. A., Wilson, G. F., Trudeau, M. C., and Titus, S. A. (1999). The eag family of K^+ channels in Drosophila and mammals. *Ann. N.Y. Acad. Sci.* 868, 356–369. doi: 10.1111/j.1749-6632.1999.tb11297.x

Gianulis, E. C., Liu, Q., and Trudeau, M. C. (2013). Direct interaction of eag domains and cyclic nucleotide-binding homology domains regulate deactivation gating in hERG channels. *J. Gen. Physiol.* 142, 351–366. doi: 10.1085/jgp.201310995

Goodchild, S. J., and Fedida, D. (2014). Gating charge movement precedes ionic current activation in hERG channels. *Channels* 8, 84–89. doi: 10.4161/chan.26775

Goodchild, S. J., Macdonald, L. C., and Fedida, D. (2015). Sequence of gating charge movement and pore gating in hERG activation and deactivation pathways. *Biophys. J.* 108, 1435–1447. doi: 10.1016/j.bpj.2015.02.014

Gustina, A. S., and Trudeau, M. C. (2009). A recombinant N-terminal domain fully restores deactivation gating in N-truncated and long QT syndrome mutant hERG potassium channels. *Proc. Natl. Acad. Sci. U.S.A.* 106, 13082–13087. doi: 10.1073/pnas.0900180106

Gustina, A. S., and Trudeau, M. C. (2011). hERG potassium channel gating is mediated by N- and C-terminal region interactions. *J. Gen. Physiol.* 137, 315–325. doi: 10.1085/jgp.201010582

Gustina, A. S., and Trudeau, M. C. (2012). HERG potassium channel regulation by the N-terminal eag domain. *Cell. Signal.* 24, 1592–1598. doi: 10.1016/j.cellsig.2012.04.004

Gutman, G. A., Chandy, K. G., Grissmer, S., Lazdunski, M., McKinnon, D., Pardo, L. A., et al. (2005). International union of Pharmacology. LIII. Nomenclature and molecular relationships of voltage-gated potassium channels. *Pharmacol. Rev.* 57, 473–508. doi: 10.1124/pr.57.4.10

Haitin, Y., Carlson, A. E., and Zagotta, W. N. (2013). The structural mechanism of KCNH-channel regulation by the eag domain. *Nature* 501, 444–448. doi: 10.1038/nature12487

Hardman, R. M., Stansfeld, P. J., Dalibalta, S., Sutcliffe, M. J., and Mitcheson, J. S. (2007). Activation gating of hERG potassium channels: S6 glycines are not required as gating hinges. *J. Biol. Chem.* 282, 31972–31981. doi: 10.1074/jbc.M705835200

Hesketh, J. C., and Fedida, D. (1999). Sequential gating in the human heart K^+ channel Kv1.5 incorporates Q(1) and Q(2) charge components. *Am. J. Physiol.* 277, H1956–H1966. doi: 10.1152/ajpheart.1999.277.5.H1956

Hite, R. K., and MacKinnon, R. (2017). Structural titration of Slo2.2, a Na^+-dependent K^+ channel. *Cell* 168, 390–399. doi: 10.1016/j.cell.2016.12.030

Hite, R. K., Yuan, P., Li, Z., Hsuing, Y., Walz, T., and MacKinnon, R. (2015). Cryo-electron microscopy structure of the Slo2.2 Na^+-activated K^+ channel. *Nature* 527, 198–203. doi: 10.1038/nature14958

Hite, R. K., Tao, X., and MacKinnon, R. (2017). Structural basis for gating the high-conductance Ca^{2+}-activated K^+ channel. *Nature* 527, 198–203. doi: 10.1038/nature14958

Holmgren, M., Shin, K. S., and Yellen, G. (1998). The activation gate of voltage-gated K^+ channel can be trapped in the open state by an intersubunit metal bridge. *Neuron* 21, 617–621. doi: 10.1016/S0896-6273(00)80571-1

Horrigan, F. T., and Aldrich, R. W. (2002). Coupling between voltage sensor activation, Ca^{2+} binding and channel opening in large conductance (BK) potassium channels. *J. Gen. Physiol.* 120, 267–305. doi: 10.1085/jgp.20028605

Hoshi, T., and Armstrong, C. M. (2015). The Cole-Moore effect: still unexplained? *Biophys. J.* 109, 1312–1316. doi: 10.1016/j.bpj.2015.07.052

Hua, L., and Gordon, S. E. (2005). Functional interactions between A′ helices in the C-linker of open CNG channels. *J. Gen. Physiol.* 125, 335–344. doi: 10.1085/jgp.200409187

James, Z. M., and Zagotta, W. N. (2018). Structural insights into the mechanisms of CNBD channel function. *J. Gen. Physiol.* 150, 225–244. doi: 10.1085/jgp.201711898

James, Z. M., Borst, A. J., Haitin, Y., Frenz, B., DiMaio, F., Zagotta, W. N., et al. (2017). CryoEM structure of a prokaryotic cyclic nucleotide-gated ion channel. *Proc. Natl. Acad. Sci. U.S.A.* 114, 4430–4435. doi: 10.1073/pnas.1700248114

Jensen, M. O., Jogini, V., Borhani, D. W., Leffler, A. E., Dror, R. O., and Shaw, D. E. (2012). Mechanism of voltage gating in potassium channels. *Science* 336, 229–233. doi: 10.1126/science.1216533

Jia, Z., Yazdani, M., Zhang, G., Cui, J., and Chen, J. (2018). Hydrophobic gating in BK channels. *Nat. Commun.* 9, 3408. doi: 10.1038/s41467-018-05970-3

Jiang, Y., Lee, A., Chen, J., Cadene, M., Chait, B. T., and MacKinnon, R. (2002). The open pore conformation of potassium channels. *Nature* 417, 523–526. doi: 10.1038/417523a

Johnson, J. P., and Zagotta, W. N. (2005). The carboxyl-terminal region of cyclic nucleotide-modulated channels is a gating ring, not a permeation path. *Proc. Natl. Acad. Sci. U.S.A.* 102, 2742–2747. doi: 10.1073/pnas.0408323102

Kalstrup, T., and Blunck, R. (2018). S4–S5 linker movement during activation and inactivation in voltage-gated K^+ channels. *Proc. Natl. Acad. Sci. U.S.A.* 115, E6751–E6759. doi: 10.1073/pnas.1719105115

Kasimova, M. A., Tewari, D., Cowgill, J. B., Carrasquel Ursulaez, W., Lin, J. L., Delemotte, L., et al. (2019). Helix breaking transition in the S4 of HCN channel is critical for hyperpolarization-dependent gating. *eLife* 8, e53400. doi: 10.7554/eLife.53400

Labro, A. J., Raes, A. L., Grottesi, A., Van Hoorick, D., Sansom, M. S., and Snyders, D. J. (2008). Kv channel gating requires a compatible S4–S5 linker and bottom part of S6, constrained by non-interacting residues. *J. Gen. Physiol.* 132, 667–680. doi: 10.1085/jgp.200810048

Lastraioli, E., Perrone, G., Sette, A., Fiore, A., Crociani, O., Manoli, S., et al. (2015). hERG1 channels drive tumour malignancy and may serve as prognostic factor in pancreatic ductal adenocarcinoma. *Br. J. Cancer* 112, 1076–1087. doi: 10.1038/bjc.2015.28

Lau, C., Hunter, M. J., Stewart, A., Perozo, E., and Vandenberg, J. I. (2018). Never at rest: Insights into the conformational dynamics of ion channels from cryo-electron microscopy. *J. Physiol.* 596, 1107–1119. doi: 10.1113/JP274888

Lee, C.-H., and MacKinnon, R. (2017). Structures of the human HCN1 hyperpolarization-activated channel. *Cell* 168, 111–120. doi: 10.1016/j.cell.2016.12.023

Lee, C.-H., and MacKinnon, R. (2018). Activation mechanism of a human SK-calmodulin channel complex elucidated by cryo-EM structures. *Science* 360, 508–513. doi: 10.1126/science.aas9466

Lee, C.-H., and MacKinnon, R. (2019). Voltage sensor movements during hyperpolarization in the HCN channel. *Cell* 179, 1582–1589. doi: 10.1016/j.cell.2019.11.006

Li, Q., Gayen, S., Shuyi Chen, A. S., Huang, O., Raida, M., and Kang, C. (2010). NMR solution structure of the N-terminal domain of hERG and its interaction with the S4–S5 linker. *Biochem. Biophys. Res. Commun.* 403, 126–132. doi: 10.1016/j.bbrc.2010.10.132

Li, M., Zhou, X., Wang, S., Michailidisong, Y., Su, D., Li, H., et al. (2017). Structure of a eukaryotic cyclic-nucleotide-gated channel. *Nature* 542, 60–65. doi: 10.1038/nature20819

Liu, J., Zhang, M., Jiang, M., and Gea-Ny Tseng, G.-N. (2003). Negative Charges in the Transmembrane Domains of the HERG K Channel Are Involved in the Activation- and Deactivation-gating Processes. *J. Gen. Physiol.* 121, 599–614. doi: 10.1085/jgp.200308788

Liu, X., Wu, Y., and Zhou, Y. (2010). Intracellular linkers are involved in Mg^{2+}-dependent modulation of the Eag potassium channel. *Channels* 4, 311–318. doi: 10.4161/chan.4.4.12329

Long, S. B., Campbell, E. B., and MacKinnon, R. (2005). Voltage sensor of Kv1.2: Structural basis of electromechanical coupling. *Science* 309, 903–908. doi: 10.1126/science.1116270

Long, S. B., Tao, X., Campbell, E. B., and MacKinnon, R. (2007). Atomic structure of a voltage-dependent K^+ channel in a lipid membrane-like environment. *Nature* 450, 376–382. doi: 10.1038/nature06265

Lorinczi, E., Gomez-Posada, J. C., de la Peña, P., Tomczak, A. P., Fernandez-Trillo, J., Leipscher, U., et al. (2015). Voltage-dependent gating of KCNH potassium channels lacking a covalent link between voltage-sensing and pore domains. *Nat. Commun.* 6, 6672. doi: 10.1038/ncomms7672

Lu, Z., Klem, A. M., and Ramu, Y. (2002). Coupling between voltage sensors and activation gate in voltage-gated K^+ channels. *J. Gen. Physiol.* 120, 663–676. doi: 10.1085/jgp.20028696

Malak, O. A., Es-Salah-Lamoureux, Z., and Loussouarn, G. (2017). hERG S4-S5 linker acts as a voltage- dependent ligand that binds to the activation gate and locks it in a closed state. *Sci. Rep.* 7, 113. doi: 10.1038/s41598-017-00155-2

Malak, O. A., Gluhov, G. S., Grizel, A. V., Kudryashova, K. S., Sokolova, O. S., and Loussouarn, G. (2019). Voltage-dependent activation in EAG channels follows a ligand-receptor rather than a mechanical-lever mechanism. *J. Biol. Chem.* 294, 6506–6521. doi: 10.1074/jbc.RA119.007626

Marten, I., and Hoshi, T. (1998). The N-terminus of the K channel KAT1 controls its voltage-dependent gating by altering the membrane electric field. *Biophys. J.* 74, 2953–2962. doi: 10.1016/S0006-3495(98)78002-6

Miranda, P., Manso, D. G., Barros, F., Carretero, L., Hughes, T. E., Alonso-Ron, C., et al. (2008). FRET with multiply labeled HERG K^+ channels as a reporter of the in vivo coarse architecture of the cytoplasmic domains. *Biochim. Byophys. Acta* 1783, 1681–1699. doi: 10.1016/j.bbamcr.2008.06.009

Mitcheson, J. S., Chen, J., and Sanguinetti, M. C. (2000). Trapping of a methanesulfonanilide by closure of the HERG potassium channel activation gate. *J. Gen. Physiol.* 115, 229–240. doi: 10.1085/jgp.115.3.229

Morais-Cabral, J. H., and Robertson, G. A. (2015). The enigmatic cytoplasmic regions of KCNH channels. *J. Mol. Biol.* 427, 67–76. doi: 10.1016/j.jmb.2014.08.008

Morais-Cabral, J. H., Lee, A., Cohen, S. L., Chait, B. T., Li, M., and MacKinnon, R. (1998). Crystal structure and functional analysis of the HERG potassium channel N terminus: a eukaryotic PAS domain. *Cell* 95, 649–655. doi: 10.1016/S0092-8674(00)81635-9

Mortensen, L. S., Schmidt, H., Zohreh, Z., Barrantes-Freer, A., Rubio, M. E., Ufartes, R., et al. (2015). Kv10.1 opposes activity-dependent increase in Ca^{2+} influx into the presynaptic terminal of the parallel fibre–Purkinje cell synapse. *J. Physiol.* 593, 181–196. doi: 10.1113/jphysiol.2014.281600

Muskett, F. W., Thouta, S., Thomson, S. J., Bowen, A., Stansfeld, P. J., and Mitcheson, J. S. (2011). Mechanistic insight into human ether-á-go-go-related gene (hERG) K^+ channel deactivation gating from the solution structure of the EAG domain. *J. Biol. Chem.* 286, 6184–6191. doi: 10.1074/jbc.M110.199364

Ng, C. A., Hunter, M. J., Perry, M. D., Mobli, M., Ke, Y., Kuchel, P. W., et al. (2011). The N-terminal tail of hERG contains an amphipathic α-helix that regulates channel deactivation. *PloS One* 6, e16191. doi: 10.1371/journal.pone.0016191

Ng, C. A., Perry, M. D., Tan, P. S., Hill, A. P., and Vandenberg, J. I. (2012). The S4-S5 linker acts as a signal integrator for hERG K^+ channel activation and deactivation gating. *PloS One* 7, e31640. doi: 10.1371/journal.pone.0031640

Ng, C. A., Phan, K., Hill, A. P., Vandenberg, J. I., and Perry, M. D. (2014). Multiple interactions between iytoplasmic domains regulate slow deactivation of Kv11.1 channels. *J. Biol. Chem.* 289, 25822–25832. doi: 10.1074/jbc.M114.558379

Okamura, Y., and Okochi, Y. (2019). Molecular mechanisms of coupling to voltage sensors in voltage-evoked cellular signals. *Proc. Jpn. Acad. Ser. B.* 95, 111–135. doi: 10.2183/pjab.95.010

Pardo, L. A., and Stühmer, W. (2014). The roles of K^+ channels in cancer. *Nat. Rev. Cancer* 14, 39–48. doi: 10.1038/nrc3635

Perissinotti, L. L., De Biase, P. M., Guo, J., Yang, P.-C., Lee, M. C., Clancy, C. E., et al. (2018). Determinants of isoform-specific gating kinetics of hERG1 channel: Combined experimental and simulation study. *Front. Physiol.* 9, 207. doi: 10.3389/fphys.2018.00207

Perry, M. D., Ng, C.-A., Mann, S. A., Sadrieh, A., Imtiaz, M., Hill, A. P., et al. (2015). Getting to the heart of hERG K^+ channel gating. *J. Physiol.* 593, 2575–2585. doi: 10.1113/JP270095

Pettersen, E. F., Goddard, T. D., Huang, C. C., Couch, G. S., Greenblatt, D. M., Meng, E. C., et al. (2004). UCSF Chimera: A visualization system for exploratory research and análisis. *J. Comput. Chem.* 25, 1605–1612. doi: 10.1002/jcc.20084

Phan, K., Ng, C. A., David, E., Shishmarev, D., Kuchel, P. W., Vandenberg, J. I., et al. (2017). The S1 helix critically regulates the finely tuned gating of Kv11.1 channels. *J. Biol. Chem.* 292, 7688–7705. doi: 10.1074/jbc.M117.779298

Piper, D. R., Varghese, A., Sanguinetti, M. C., and Tristani-Firouzi, M. (2003). Gating currents associated with intramembrane charge displacement in HERG potassium channels. *Proc. Natl. Acad. Sci. U.S.A.* 100, 10534–10539. doi: 10.1073/pnas.1832721100

Prevarskaya, N., Skryma, R., and Shuba, Y. (2018). Ion Channels in Cancer: Are Cancer Hallmarks Oncochannelopathies? *Physiol. Rev.* 98, 559–621. doi: 10.1152/physrev.00044.2016

Sanguinetti, M. C., and Tristani-Firouzi, M. (2006). hERG potassium channels and cardiac arrhythmia. *Nature* 440, 463–469. doi: 10.1038/nature04710

Sanguinetti, M. C., and Xu, Q. P. (1999). Mutations of the S4-S5 linker alter activation properties of HERG potassium channels expressed in Xenopus oocytes. *J. Physiol.* 514, 667–675. doi: 10.1111/j.1469-7793.1999.667ad.x

Sanguinetti, M. C., Jiang, C., Curran, M. E., and Keating, M. T. (1995). A mechanistic link between an inherited and an acquired cardiac arrhythmia: HERG channel encodes the IKr potassium channel. *Cell* 81, 299–307. doi: 10.1016/0092-8674(95)90340-2

Schönherr, R., and Heinemann, S. H. (1996). Molecular determinants for activation and inactivation of HERG, a human inward rectifier potassium channel. *J. Physiol.* 493, 635–642. doi: 10.1113/jphysiol.1996.sp021410

Schwarz, J. R., and Bauer, C. K. (2004). Functions of erg K^+ channels in excitable cells. *J. Cell. Mol. Med.* 8, 22–30. doi: 10.1111/j.1582-4934.2004.tb00256.x

Singh, A. K., Saotome, K., and Sobolevsky, A. I. (2017). Swapping of transmembrane domains in the epithelial calcium channel TRPV6. *Sci. Rep.* 7, 10669. doi: 10.1038/s41598-017-10993-9

Smith, P. L., Baukrowitz, T., and Yellen, G. (1996). The inward rectification mechanism of the HERG cardiac potassium channel. *Nature* 379, 833–836. doi: 10.1038/379833a0

Spector, P. S., Curran, M. E., Zou, A., Keating, M. T., and Sanguinetti, M. C. (1996). Fast inactivation causes rectification of the IKr channel. *J. Gen. Physiol.* 107, 611–619. doi: 10.1085/jgp.107.5.611

Stevens, L., Ju, M., and Wray, D. (2009). Roles of surface residues of intracellular domains of heag potassium channels. *Eur. Biophys. J.* 38, 523–532. doi: 10.1007/s00249-009-0402-8

Sun, J., and MacKinnon, R. (2017). Cryo-EM structure of a KCNQ1/CaM complex reveals insights into congenital long QT syndrome. *Cell* 169, 1042–1050. doi: 10.1016/j.cell.2017.05.019

Swartz, K. J. (2004). Towards a structural view of gating in potassium channels. *Nat. Rev. Neurosci.* 5, 905–916. doi: 10.1038/nrn1559

Swartz, K. J. (2005). Structure and anticipatory movements of the S6 gate in Kv channels. *J. Gen. Physiol.* 126, 413–417. doi: 10.1085/jgp.200509430

Swartz, K. J. (2008). Sensing voltage across lipid membranes. *Nature* 456, 891–897. doi: 10.1038/nature07620

Tan, P. S., Perry, M. D., Ng, C. A., Vandenberg, J. I., and Hill, A. P. (2012). Voltage-sensing domain mode shift is coupled to the activation gate by the N-terminal tail of hERG channels. *J. Gen. Physiol.* 140, 293–306. doi: 10.1085/jgp.201110761

Tao, X., Hite, R. K., and MacKinnon, R. (2017). Cryo-EM structure of the open high-conductance Ca^{2+}-activated K^+ channel. *Nature* 541, 46–51. doi: 10.1038/nature20608

Taraska, J. W., and Zagotta, W. N. (2007). Cyclic nucleotide-regulated ion channels: spotlight on symmetry. *Structure* 15, 1023–1024. doi: 10.1016/j.str.2007.08.004

Terlau, H., Heinemann, S. H., Stühmer, W., Pongs, O., and Ludwig, J. (1997). Amino terminal-dependent gating of the potassium channel rat eag is compensated by a mutation in the S4 segment. *J. Physiol.* 502, 537–543. doi: 10.1111/j.1469-7793.1997.537bj.x

Thouta, S., Sokolov, S., Abe, Y., Clark, S. J., Cheng, Y. M., and Claydon, T. W. (2014). Proline scan of the HERG channel S6 helix reveals the location of the intracellular pore gate. *Biophys. J.* 106, 1057–1069. doi: 10.1016/j.bpj.2014.01.035

Tomczak, A. P., Fernández-Trillo, J., Bharill, S., Papp, F., Panyi, G., Stühmer, W., et al. (2017). A new mechanism of voltage-dependent gating exposed by Kv10.1 channels interrupted between voltage sensor and pore. *J. Gen. Physiol.* 149, 577–593. doi: 10.1085/jgp.201611742

Tristani-Firouzi, M., Chen, J., and Sanguinetti, M. C. (2002). Interactions between S4-S5 linker and S6 transmembrane domain modulate gating of HERG K^+ channels. *J. Biol. Chem.* 277, 18994–19000. doi: 10.1074/jbc.M200410200

Trudeau, M. C., Warmke, J. W., Ganetzky, B., and Robertson, G. A. (1995). HERG, a human inward rectifier in the voltage-gated potassium channel family. *Science* 269, 92–95. doi: 10.1126/science.7604285

Vandenberg, J. I., Torrres, A. M., Campbell, T. J., and Kuchel, P. W. (2004). The HERG K^+ channel: Progress in understanding the molecular basis of its unusual gating kinetics. *Eur. Biophys. J.* 33, 89–97. doi: 10.1007/s00249-003-0338-3

Vandenberg, J. I., Perry, M. D., Perrin, M. J., Mann, S. A., Ke, Y., and Hill, A. P. (2012). hERG K^+ channels: Structure, function, and clinical significance. *Physiol. Rev.* 92, 1393–1478. doi: 10.1152/physrev.00036.2011

Vandenberg, J. I., Perozo, E., and Allen, T. W. (2017). Towards a structural view of drug binding to hERG K^+ channels. *Trends Pharmacol. Sci.* 38, 899–907. doi: 10.1016/j.tips.2017.06.004

Vardanyan, V., and Pongs, O. (2012). Coupling of voltage sensors to the channel pore: A comparative view. *Front. Pharmacol.* 3, 145. doi: 10.3389/fphar.2012.00145

Viloria, C. G., Barros, F., Giráldez, T., Gómez-Varela, D., and de la Peña, P. (2000). Differential effects of amino-terminal distal and proximal domains in the regulation of human erg K^+ channel gating. *Biophys. J.* 79, 231–246. doi: 10.1016/S0006-3495(00)76286-2

Wang, W., and MacKinnon, R. (2017). Cryo-EM structure of the open human Ether-a-go-go-related K^+ channel hERG. *Cell* 169, 422–430. doi: 10.1016/j.cell.2017.03.048

Wang, S., Liu, S., Morales, M. J., H.C. Strauss, H. C., and Rasmusson, R. L. (1997). A quantitative analysis of the activation and inactivation kinetics of HERG expressed in Xenopus oocytes. *J. Physiol.* 502, 45–60. doi: 10.1111/j.1469-7793.1997.045bl.x

Wang, J., Trudeau, M. C., Zappia, A. M., and Robertson, G. A. (1998). Regulation of deactivation by an amino terminal domain in human ether-á-go-go-related gene potassium channels. *J. Gen. Physiol.* 112, 637–647. doi: 10.1085/jgp.112.5.637

Wang, J., Myers, C. D., and Robertson, G. A. (2000). Dynamic control of deactivation gating by a soluble amino-terminal domain in HERG K^+ channels. *J. Gen. Physiol.* 115, 749–758. doi: 10.1085/jgp.115.6.749

Wang, Z., Dou, Y., Goodchild, S. J., Es-Salah-Lamoureux, Z., and Fedida, D. (2013). Components of gating charge movement and S4 voltage-sensor exposure during activation of hERG channels. *J. Gen. Physiol.* 141, 431–443. doi: 10.1085/jgp.201210942

Wanke, E., and Restano-Cassulini, R. (2007). Toxins interacting with ether-à-go-go-related gene voltage-dependnet potassium channels. *Toxicon* 49 (2), 239–248. doi: 10.1016/j.toxicon.2006.09.025

Webster, S. M., del Camino, D., Dekker, J. P., and Yellen, G. (2004). Intracellular gate opening in Shaker K+ channels defined by high-affinity metal bridges. *Nature* 428, 864–868. doi: 10.1038/nature02468

Whicher, J. R., and MacKinnon, R. (2016). Structure of the voltage-gated K^+ channel eag1 reveals an alternative voltage sensing mechanism. *Science* 353, 664–669. doi: 10.1126/science.aaf8070

Whicher, J. R., and MacKinnon, R. (2019). Regulation of Eag1 gating by its intracellular domains. *eLife* 8, e49188. doi: 10.7554/eLife.49188

Wisedchaisri, G., Tonggu, L., McCord, E., Gamal El-Din, T. M., Wang, L., Zheng, N., et al. (2019). Resting-State Structure and Gating Mechanism of a Voltage-Gated Sodium Channel. *Cell* 178, 993–1003. doi: 10.1016/j.cell.2019.06.031

Witchel, H. J. (2004). The low-potency, voltage-dependent HERG blocker propafenone-molecular determinants and drug trapping. *Mol. Pharmacol.* 66, 1201–1212. doi: 10.1124/mol.104.001743

Wynia-Smith, S. L., Gillian-Daniel, A. L., Satyshur, K. A., and Robertson, G. A. (2008). hERG gating microdomains defined by S6 mutagenesis and molecular modeling. *J. Gen. Physiol.* 132, 507–520. doi: 10.1085/jgp.200810083

Yang, H., Zhang, G., and Cui, J. (2015). BK channels: Multiple sensors, one activation gate. *Front. Physiol.* 6, 29. doi: 10.3389/fphys.2015.00029

Yellen, G. (1998). The moving parts of voltage-gated ion channels. *Quart. Rev. Biophys.* 31, 239–295. doi: 10.1017/S0033583598003448

Yellen, G. (2002). The voltage-gated potassium channels and their relatives. *Nature* 419, 35–42. doi: 10.1038/nature00978

Yin, Y., Wu, M., Zubcevic, L., Borschel, W. F., Lander, G. C., and Lee, S.-Y. (2018). Structure of the cold- and mentol-sensing ion channel TRPM8. *Science* 359, 237–241. doi: 10.1126/science.aan4325

Yu, F. H., Yarov-Yarovoy, V., Gutman, G. A., and Catterall, W. A. (2005). Overview of molecular relationships in the voltage-gated ion channel superfamily. *Pharmacol. Rev.* 57, 387–395. doi: 10.1124/pr.57.4.13

Zagotta, W. N., Olivier, N. B., Black, K. D., Young, E. C., Olson, R., and Gouaux, E. (2003). Structural basis for modulation and agonist specificity of HCN pacemaker channels. *Nature* 425, 200–205. doi: 10.1038/nature01922

Zhang, M., Liu, J., Jiang, M., Wu, D.-M., Sonawane, K., Guy, H. R., et al. (2005). Interactions between charged residues in the transmembrane segments of the voltage-sensing domain in the hERG channel. *J. Membr. Biol.* 207, 169–181. doi: 10.1007/s00232-005-0812-1

Zhao, J., and Blunck, R. (2016). The isolated voltage sensing domain of the Shaker potassium channel forms a voltage-gated cation channel. *eLife* 5, e18130. doi: 10.7554/eLife.18130

Zhao, Y., Goldschen-Ohm, M. P., Morais-Cabral, J. H., Chanda, B., and Robertson, G. A. (2017). The intrinsically liganded cyclic nucleotide-binding homology domain promotes KCNH channel activation. *J. Gen. Physiol.* 149, 249–260. doi: 10.1085/jgp.201611701

Zhou, Y., Yang, H., Cui, J., and Lingle, C. J. (2017). Threading the biophysics of mammalian Slo1 channels onto structures of an invertebrate Slo1 channel. *J. Gen. Physiol.* 149, 985–1007. doi: 10.1085/jgp.201711845

Conflict of Interest: The authors declare that the research was conducted in the absence of any commercial or financial relationships that could be construed as a potential conflict of interest.

frontiers in Pharmacology

REVIEW
published: 04 May 2020
doi: 10.3389/fphar.2020.00550

Structures Illuminate Cardiac Ion Channel Functions in Health and in Long QT Syndrome

Kathryn R. Brewer[1,2†], *Georg Kuenze*[1,3†], *Carlos G. Vanoye*[4], *Alfred L. George Jr.*[4], *Jens Meiler*[1,3,5,6] *and Charles R. Sanders*[1,2*]

[1] Center for Structural Biology, Vanderbilt University School of Medicine Basic Sciences, Nashville, TN, United States, [2] Department of Biochemistry, Vanderbilt University, Nashville, TN, United States, [3] Department of Chemistry, Vanderbilt University, Nashville, TN, United States, [4] Department of Pharmacology, Feinberg School of Medicine, Northwestern University, Chicago, IL, United States, [5] Department of Pharmacology, Vanderbilt University School of Medicine Basic Sciences, Nashville, TN, United States, [6] Institute for Drug Discovery, Leipzig University Medical School, Leipzig, Germany

OPEN ACCESS

Edited by:
Mounir Tarek, Centre National de la Recherche Scientifique (CNRS), France

Reviewed by:
Sergei Noskov, University of Calgary, Canada
Clemens Möller, Hochschule Albstadt-Sigmaringen, Germany

***Correspondence:**
Charles R. Sanders
chuck.sanders@vanderbilt.edu

[†]*These authors have contributed equally to this work*

Specialty section:
This article was submitted to Pharmacology of Ion Channels and Channelopathies, a section of the journal Frontiers in Pharmacology

Received: *30 January 2020*
Accepted: *09 April 2020*
Published: *04 May 2020*

Citation:
Brewer KR, Kuenze G, Vanoye CG, George AL Jr., Meiler J and Sanders CR (2020) Structures Illuminate Cardiac Ion Channel Functions in Health and in Long QT Syndrome. Front. Pharmacol. 11:550. doi: 10.3389/fphar.2020.00550

The cardiac action potential is critical to the production of a synchronized heartbeat. This electrical impulse is governed by the intricate activity of cardiac ion channels, among them the cardiac voltage-gated potassium (K_v) channels KCNQ1 and hERG as well as the voltage-gated sodium (Na_v) channel encoded by *SCN5A*. Each channel performs a highly distinct function, despite sharing a common topology and structural components. These three channels are also the primary proteins mutated in congenital long QT syndrome (LQTS), a genetic condition that predisposes to cardiac arrhythmia and sudden cardiac death due to impaired repolarization of the action potential and has a particular proclivity for reentrant ventricular arrhythmias. Recent cryo-electron microscopy structures of human KCNQ1 and hERG, along with the rat homolog of SCN5A and other mammalian sodium channels, provide atomic-level insight into the structure and function of these proteins that advance our understanding of their distinct functions in the cardiac action potential, as well as the molecular basis of LQTS. In this review, the gating, regulation, LQTS mechanisms, and pharmacological properties of KCNQ1, hERG, and SCN5A are discussed in light of these recent structural findings.

Keywords: cardiac action potential, long QT syndrome, KCNQ1, hERG, SCN5A, structural biology

INTRODUCTION

The cardiac action potential is critical to proper heart function. Beginning with the activation of "pacemaker" cells, the action potential propagates through the atria and into the ventricles in a unidirectional waveform of excitation and relaxation, resulting in the coordinated expansion and contraction of heart tissue (Nerbonne and Kass, 2005). The action potential is governed by an intricate series of ion channel activities (Grant, 2009), including those of the KCNQ1 (K_VLQT1, K_V7.1) and hERG (KCNH2, K_V11.1) potassium channels and the SCN5A (Na_V1.5) sodium channel. Mutations in these three channels are the most frequent cause of congenital long QT syndrome (LQTS), a cardiac arrhythmia disorder that is one of the primary causes of sudden arrhythmic death syndrome (SADS) (Skinner et al., 2019).

KCNQ1, hERG, and SCN5A each play a distinct role in generating the cardiac action potential (**Figure 1**), consequently producing distinct LQTS forms when mutated (Skinner et al., 2019). The initial upstroke is governed primarily by SCN5A, producing the I_{Na} current that amplifies membrane depolarization and propagates the action potential (Moss and Kass, 2005; Skinner et al., 2019). Mutation in SCN5A causes LQTS type 3 (LQT3). hERG shapes both the plateau and the repolarization phases of the action potential, along with KCNQ1 in complex with the KCNE1 accessory protein (Moss and Kass, 2005; George, 2013). hERG and the KCNQ1–KCNE1 complex produce the rapid (I_{Kr}) and slow (I_{Ks}) delayed rectifier currents (**Figures 1B, C**), respectively. KCNQ1 mutation causes LQT1, and hERG, LQT2 (Skinner et al., 2019). Additional ion channels and transporters also shape the cardiac action potential (Skinner et al., 2019), among them $Ca_v1.2$, NCX1, and Kir2.1. The roles of these channels in the cardiac action potential and cardiac arrhythmias have been reviewed elsewhere (Bidaud and Lory, 2011; Hancox et al., 2018; Meza et al., 2018; Vaidyanathan et al., 2018; Li et al., 2019). These channels are not typically causative for LQTS and will not be discussed here.

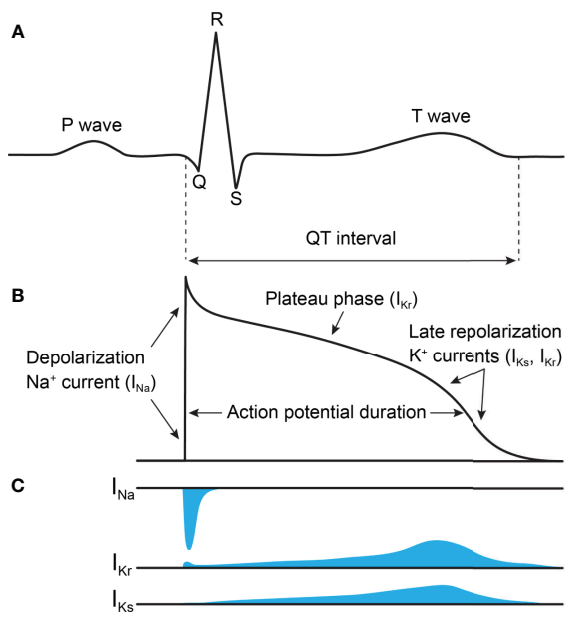

FIGURE 1 | Voltage-activated Na^+ and K^+ currents define the ventricular action potential and QT interval of the ECG. **(A)** ECG trace. The rapid upstroke of the ventricular action potential gives rise to the QRS complex. The duration of the QT interval is determined by the time of the ventricular repolarization. **(B)** Trace of the ventricular action potential. The rapidly activating and inactivating I_{Na} current drives membrane depolarization. Two K^+ currents, I_{Ks} and I_{Kr}, contribute most to the plateau phase and repolarization phase of the action potential, which reestablishes the membrane resting potential. **(C)** Time course of I_{Na}, I_{Kr}, and I_{Ks} currents (not drawn to scale). Currents of other ion channels contributing to the action potential (e.g. $I_{Ca,L}$, I_{Kur}, and I_{NCX}) are not shown for clarity. This figure is inspired by figures in Moss and Kass (2005) and George (2013).

Structurally, the KCNQ1, hERG, and SCN5A channels belong to the voltage-gated ion channel superfamily and share a general transmembrane topology (Bezanilla, 2005; Dehghani-Samani et al., 2019). The transmembrane channel domain is composed of six helices per subunit in hERG and KCNQ1 (**Figures 2A, B**) or a monomeric tetrad repeat of linked 6-helix domains for SCN5A, each repeat exhibiting varying sequences, lengths, and tertiary folds (**Figures 2C, D**). The assembled channel is tetrameric (pseudo-tetrameric for SCN5A), with each channel domain composed of four voltage sensing domains (VSDs) surrounding a central pore domain (PD) (**Figure 2D**). The VSD is comprised of the first four transmembrane helices (S1–S4) preceded by a small amphipathic helix—S0—in both KCNQ1 and SCN5A (Jiang et al., 2020; Sun and Mackinnon, 2020). The PD is formed by the tetramerization of S5 and S6 helices from each subunit/repeat (**Figure 2D**). A pore loop between S5 and S6 contains the selectivity filter (SF) that confers ion specificity. A linker helix between helices S4 and S5, termed the S4–S5 linker, connects the VSD to the PD (Bezanilla, 2005; Dehghani-Samani et al., 2019) (**Figures 2A–C**).

Given these similarities in channel topology and components, how is it that KCNQ1, hERG, and SCN5A perform such distinct functions, and produce phenotypically distinct forms of LQTS? To explore this question, a number of high-resolution ion channel structures, including cryo-electron microscopy (cryo-EM) structures of frog and human KCNQ1 (Sun and Mackinnon, 2020) and of human hERG (Wang and Mackinnon, 2017), as well as the structures of the rat homolog of SCN5A (Jiang et al., 2020) and human Na_v1 isoforms Nav1.4 and 1.7 (Pan et al., 2018; Shen et al., 2019; Xu et al., 2019), have been determined. Moreover, the frog KCNQ1 structure has been used to develop what is likely a reliable homology model for the human KCNQ1 channel in resting and fully active conformations (Kuenze et al., 2019). A homology model of human SCN5A in the resting state has also been devised (Kroncke et al., 2019). These structures and structural models reveal critical differences in the atomic details of KCNQ1, hERG, and SCN5A structures associated with their distinct functions and disease phenotypes. Notably, the subunits of KCNQ1 undergo domain swapping, with a similar arrangement observed in SCN5A but not in the hERG channel (**Figure 2D**). The monomeric sequence of SCN5A causes the channel to adopt an asymmetric three-dimensional fold, in contrast to the inherent symmetry of tetrameric hERG and KCNQ1 (**Figure 2D**). Additionally, the C-terminal domains contain distinct folds and mediate unique regulatory functions. These and other structural differences contribute to the varying properties of these three channels and to their distinct roles in the cardiac action potential.

The aim of this review is to compare and contrast the KCNQ1, hERG, and SCN5A channels using available structures and structural models as a guide. Through this lens, channel gating, regulation, LQTS mechanisms, and pharmacology will be discussed, in order to explore the molecular basis of these unique properties.

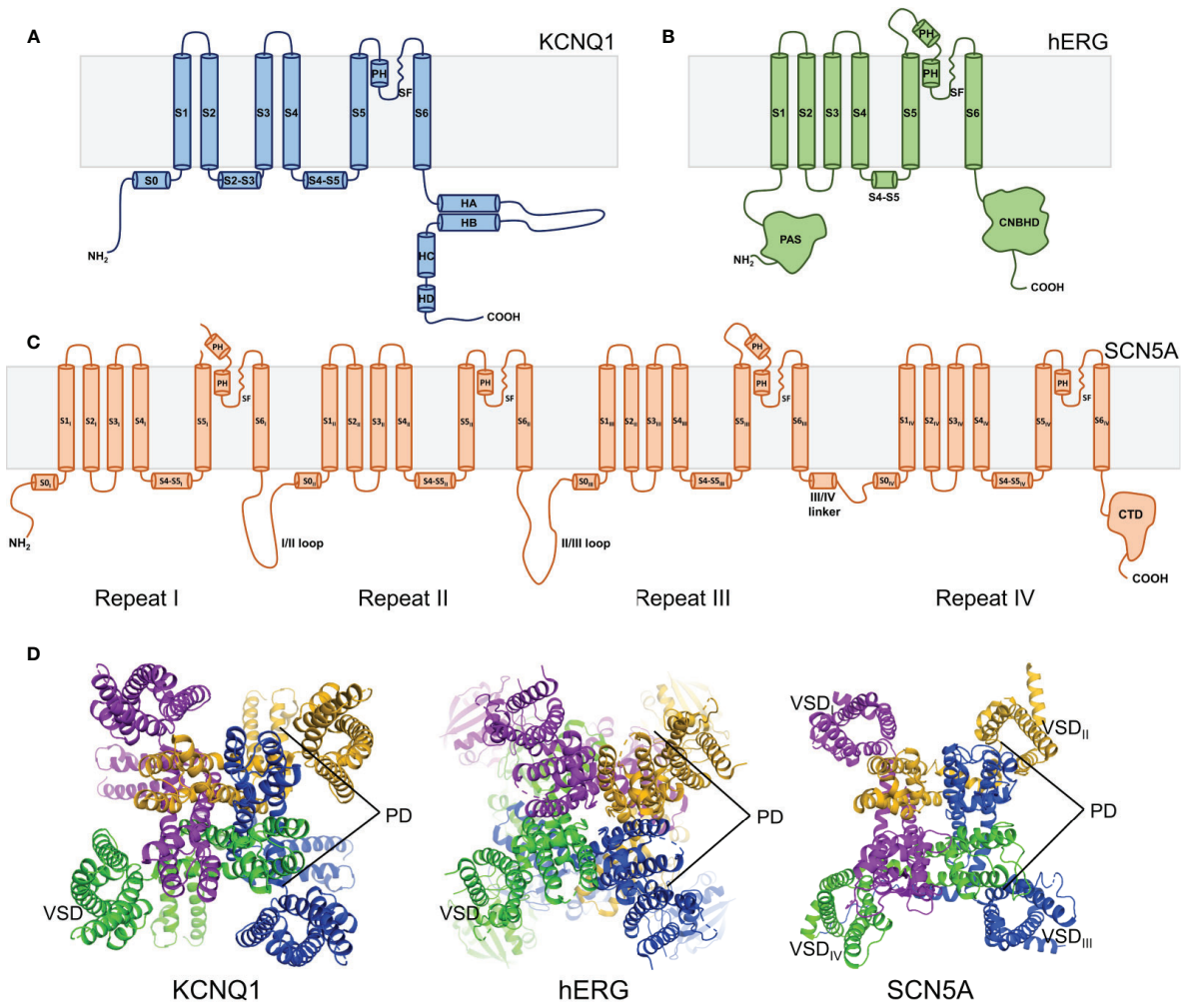

FIGURE 2 | Overall topology of KCNQ1, hERG, and SCN5A channels. **(A)** KCNQ1 topology. Transmembrane domain alpha helices are labeled S0–S6. PH indicates the pore helix. SF denotes the selectivity filter. S2–S3 indicates the S2–S3 linker. S4–S5 denotes the S4–S5 linker. Cytosolic alpha helices are labeled HA-HD. **(B)** hERG topology. PAS denotes the Per-ARNT-Sim domain. CNBHD indicates the C-terminal cyclic nucleotide-binding homology domain. **(C)** SCN5A topology. CTD indicates the C-terminal domain. **(D)** Top views of the human KCNQ1 (PDB ID: 6UZZ) (Sun and Mackinnon, 2020), human hERG (PDB ID: 5VA1) (Wang and Mackinnon, 2017), and rat SCN5A (PDB ID: 6UZ3) (Jiang et al., 2020) channels, respectively. Outer voltage-sensing domains (VSD) and the central pore domain (PD) are labeled.

STRUCTURAL MECHANISMS OF CHANNEL GATING

KCNQ1, hERG, and SCN5A undergo conformational changes in response to changes in membrane potential that result in channel opening or closing. These responses confer specific gating properties including activation, deactivation, inactivation, and recovery from inactivation (Hosseini, 2018; Zhang et al., 2018). In activation, protein conformational changes result in channel pore opening from a resting state, while deactivation entails a return to the resting state (Zhang et al., 2018). Inactivation confers a third channel state distinct from the activated and resting states which inhibits current flow prior to full deactivation (Zhang et al., 2018). While all three channels share common structural elements that are responsible for producing these states, there are also elements that give rise to specific gating properties in each channel, as discussed below.

Activation and Ion Conduction

KCNQ1

Voltage-gated channels contain up to six positively-charged basic residues in the S4 helix, called gating charges, which move in the electric field of the membrane in response to voltage (Jiang et al., 2003). Gating charges are numbered according to their position in the S4 helix, from the extracellular to the intracellular side. In KCNQ1, S4 contains four arginine (R) gating charges that are conserved in other K_V channels and confer voltage sensitivity. However, in KCNQ1 the canonical R3 is replaced by a neutral glutamine (Q234, Q3), and the fifth gating charge (K5 in Shaker) is replaced by histidine (H241, H5), which in the membrane

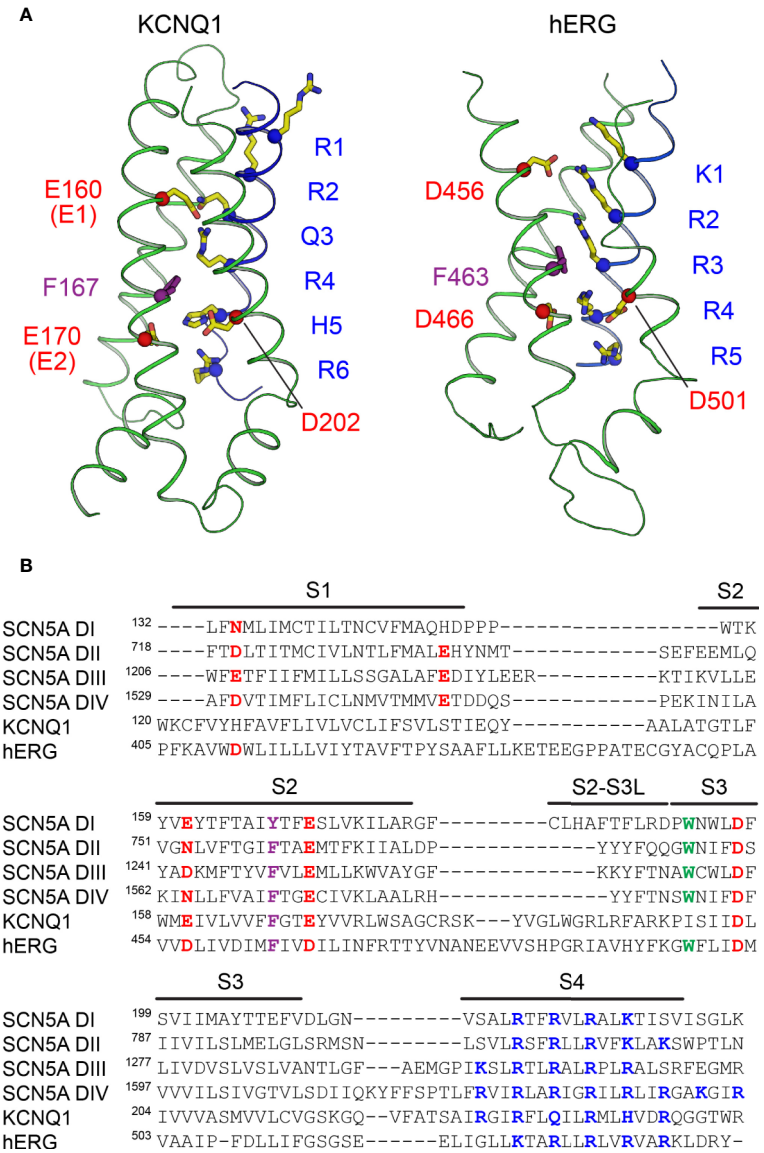

FIGURE 3 | The voltage sensors of KCNQ1, hERG, and SCN5A. **(A)** Structure of the VSD from human KCNQ1 (left) (PDB: 6UZZ) (Sun and Mackinnon, 2020) and hERG (right) (PDB: 5VA2) (Wang and Mackinnon, 2017) in putative activated conformations. Basic residues on S4 (labeled in blue), acidic residues on S2 and S3 (labeled in red), and the phenylalanine residue in the gating charge transfer center (purple) are shown as sticks. The first four basic residues on S4 (R1–R4) in KCNQ1 and the first three (K1–R3) in hERG are located above the charge transfer center. **(B)** Multiple sequence alignment of VSDs I-IV of SCN5A with the VSDs of human KCNQ1 and hERG. Basic residues in S4 implicated with voltage sensing are colored blue, and acidic or polar residues in S1–S3 suggested to interact with S4 gating charges are colored red. The conserved aromatic residue at the gating charge transfer center in S2 is colored purple. Another tryptophan residue in S3, conserved in the VSDs of Na_V channels and also present in hERG, is colored green.

environment is expected to be neutral at physiological pH (**Figures 3A, B**). Due to these substitutions at positions 3 and 5, the S4 helix of KCNQ1 has a lower net positive charge (+4) than Shaker-class K^+ channels, such as $K_V1.2$ (+6). The lower net positive charge may explain why KCNQ1 S4 mutations that result charge loss or reversal (Panaghie and Abbott, 2007; Wu et al., 2010b) result in constitutive channel activity.

Voltage-gated channels also feature a charge transfer center (CTC), formed by a bulky aromatic ring and two negatively charged residues, that facilitates S4 movement (Tao et al., 2010). The KCNQ1 CTC consists of E170 (E2) and F167 on S2, and D202 on S3, which work with E160 (E1) to define the S4 position. During activation, S4 moves towards the extracellular side of the membrane (Nakajo and Kubo, 2007; Rocheleau and Kobertz, 2008; Osteen et al., 2010; Ruscic et al., 2013; Barro-Soria et al., 2014; Nakajo and Kubo, 2014; Barro-Soria et al., 2017) through interactions between basic gating charges and E1 and E2 in the CTC (**Figure 3A**). These interactions change during the course

of activation, permitting S4 translocation. E1 interacts with R1 (R228) or R4 (R237) in the resting and activated states of the VSD, respectively (Wu et al., 2010a). S4 motion occurs in two distinct steps, transitioning through a stable intermediate before reaching the activated state (Wu et al., 2010a; Barro-Soria et al., 2014; Zaydman et al., 2014). The intermediate state features salt bridge interactions between E1 and R2, distinct from the resting and activated VSD states, according to the recently-determined structure of the intermediate state KCNQ1 VSD (Taylor et al., 2020). Interestingly, the pore of KCNQ1 opens in both the intermediate state (IO) and fully activated (AO) states (Zaydman et al., 2014). These two open states possess distinct channel properties with differing opening probabilities and pharmacology (Hou et al., 2017), and have distinct pore structures (Zaydman et al., 2014). Importantly, ion conductance when the VSD is in either the intermediate or activated state appears to be unique to KCNQ1. However, formation of the KCNQ1–KCNE1 complex eliminates the conductance associated with the VSD intermediate state (Zaydman et al., 2014), such that I_{Ks} reflects only the fully activated state.

The ion conduction pathway in KCNQ1 is lined by the four S6 helices, with the SF on the extracellular side of the pore. Mutations in S6 cause changes in current amplitude and voltage dependence of activation (Wang et al., 1999; Seebohm et al., 2005; Panaghie et al., 2006; Hoosien et al., 2013). Comparison of S6 in the closed pore structure of human KCNQ1 (Sun and Mackinnon, 2020) with that of the open channel demonstrates that channel opening results from bending of S6 so that the cytosolic ends of the four S6 segments swing away from the central axis, enlarging the diameter of the pore to allow diffusion of K^+ into the central cavity. The hinge responsible for this bending motion in S6 is the P343–A344–G345 (PAG) motif, which corresponds to PVP in Shaker K^+ channels (Labro and Snyders, 2012). Additionally, A336 may also be important in the motion of the activation gate, as mutations at this position alter the voltage dependence of activation (Seebohm et al., 2006).

Once the intracellular gate is opened, K^+ ions move through the pore along their electrochemical gradient. The backbone carbonyl oxygens of the TIGYG motif in the SF of KCNQ1 (TVGYG in K_V1.2 and KcsA) (**Figure 4A**) and the sidechain of T312 form four evenly spaced K^+ binding sites (**Figure 4B**) that facilitate K^+ movement (Zhou et al., 2001). The arrangement of these oxygens mimics the displaced hydration shell of K^+, which lowers the transfer energy from the aqueous cavity at the center of the channel to the SF, allowing conduction to occur at rates near the diffusion limit (Morais-Cabral et al., 2001; Zhou et al., 2001).

hERG

The cryo-EM structure of hERG shows an open pore and activated VSDs, with the first three gating charges (K1–R3) of S4 located on the extracellular side of the CTC (**Figure 3A**). This is a translocation of one charge fewer than in the activated VSD of KCNQ1 (Sun and Mackinnon, 2017) and Shaker-like K_V1.2–2.1 (Long et al., 2007) where four gating charges are located above the conserved phenylalanine in the CTC. This observation agrees with gating current measurements suggesting a total charge movement of only ~6 elementary charge units (movement of 1.5 positive charges per S4 helix) for hERG during activation (Zhang et al., 2004), compared to 8 to 9 (2 positive charges per helix) for KCNQ1 (Ruscic et al., 2013) and 12 to 16 (3–4 positive charges per helix) for Shaker-like K_V channels (Schoppa et al., 1992; Aggarwal and Mackinnon, 1996; Seoh et al., 1996). However, the ca. 50% lower total gating charge movement for hERG relative to Shaker-like channels is not explained by differences in the number of S4 gating charges, since hERG has a total of five positively-charged residues on S4

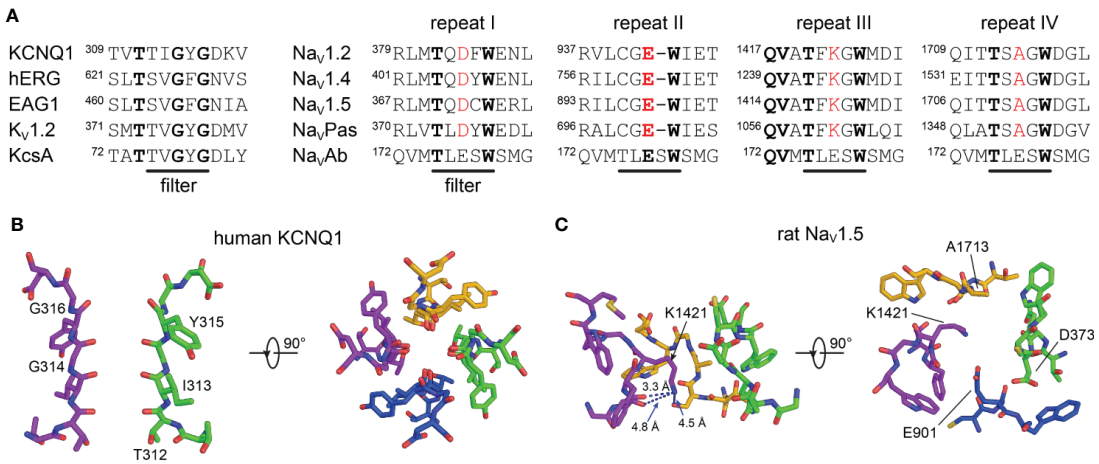

FIGURE 4 | The selectivity filters of K^+ and Na^+ channels. **(A)** Multiple sequence alignment of the SF region of selected K^+ (left) and Na^+ (right) channels. Conserved amino acids are highlighted in bold. Amino acids belonging to the DEKA signature motif in eukaryotic Na^+ channels are colored red. **(B)** Side and top view of the SF of human KCNQ1 (PDB: 6UZZ) (Sun and Mackinnon, 2020). Two subunits are omitted for clarity in the left plot. **(C)** Side and top view of the SF of SCN5A (PDB: 6UZ3) (Jiang et al., 2020). Repeat II is omitted for clarity in the left plot.

and Shaker has six (Pless et al., 2011b). These combined structural and functional data thus imply that S4 translocates less in hERG during activation, resulting in smaller overall VSD conformational changes.

However, the activated VSD of hERG may not be fully defined. While the position of K1–R3 above the CTC in the cryo-EM structure of hERG is consistent with a depolarized VSD, some salt bridge interactions in the VSD have suboptimal geometry, particularly with R4. This is likely due to the limited resolution of the VSD in the final map (approximately 4.5–5.5 Å) (Wang and Mackinnon, 2017), impeding unambiguous determination of sidechain conformations. While cryo-EM has proven to be a powerful structural tool, the resolution is often lower in the periphery of protein structures (Herzik et al., 2019). This can prevent accurate modeling of functional features and lead to discrepancies with experimental data. Molecular dynamics may be a be useful tool in refining cryo-EM structures to mitigate these discrepancies, as is currently being carried out for the hERG structure (Khan et al., 2020).

While a structure of hERG with a closed PD has not yet been determined, we can gain insight into the conformational changes that occur during pore opening using the closed-pore structure of the closely related rat potassium voltage-gated subfamily H member 1 channel (EAG1 or KCNH1) (Whicher and Mackinnon, 2016). In hERG, the intracellular gate is likely constricted by the Q664 side chains in S6, since the radius of the cavity at Q664 is almost 6 Å in the open state hERG structure (Wang and Mackinnon, 2017), while at the corresponding position (Q476) in the EAG1 closed state structure, the pore is at its narrowest (< 1 Å) (Whicher and Mackinnon, 2016). Bending and displacement of the S6 helices is suggested by a glycine residue, located at the same position in both channels, acting as a gating hinge (G648 in hERG, G460 in EAG1).

The SF in hERG is unique among K_v channels, containing a GFG motif (**Figure 4A**) in place of the typical GYG motif (Long et al., 2005). The position of the phenylalanine residue in this motif is different from the corresponding tyrosine in other K_v channels of known structure (Wang and Mackinnon, 2017). This structural variation may have important implications for fast inactivation in hERG, as discussed below.

SCN5A

The mechanism of voltage sensing in Na_V channels is thought to be similar to that of K_V channels. The S4 helix is the key sensor of transmembrane voltage. Pairing of the positively-charged residues in S4 with polar or negatively-charged residues catalyzes S4 movement from its inward resting-state position to the outward activated state upon membrane depolarization. Recent cryo-EM structures of Na_V channels with VSDs in activated (Yan et al., 2017b; Pan et al., 2018; Pan et al., 2019; Shen et al., 2019; Jiang et al., 2020) and resting (Clairfeuille et al., 2019; Wisedchaisri et al., 2019; Xu et al., 2019) conformations uncover a remarkable 10 to 15 Å translation of S4 across the membrane, fully consistent with the "sliding helix" model of VSD activation (Catterall, 1986). A conserved aromatic residue (tyrosine in repeat I, phenylalanine II, III, and IV) on S2 serves as the hydrophobic plug that constricts the S4 gating canal and prevents ion leak through the VSD (Jiang et al., 2020). This hydrophobic plug is mechanistically identical to the corresponding residues in the CTC of K_V channels (F167 in KCNQ1, F463 in hERG). However, in contrast to the VSD of KCNQ1 and hERG, the number of basic residues on S4 in SCN5A varies from four (repeat I) to six (repeat IV) (Jiang et al., 2020) (**Figure 3B**). The variation in the number of gating charges and the heterogenous distribution of acidic and polar residues on S1–S3 between KCNQ1, hERG, and SCN5A (**Figure 3B**) may be responsible for their distinct voltage sensitivities and kinetics of VSD activation. In Na_V channels, the VSDs of repeats I, II, and III are mainly responsible for channel activation and pore opening, while the VSD of repeat IV is responsible for initiating and maintaining fast inactivation (Chanda and Bezanilla, 2002; Capes et al., 2013; Clairfeuille et al., 2019). This activation process has been studied in detail for the human skeletal muscle channel $Na_V1.4$, giving rise to the "asynchronous gating model" (Chanda and Bezanilla, 2002; Capes et al., 2013; Goldschen-Ohm et al., 2013) wherein the S4 segments of repeats I, II, and III move quickly, permitting conductance before activation of VSD_{IV}, while S4 movement in repeat IV is slower and represents the rate-limiting step for development of and recovery from inactivation.

The structure and function of the selectivity filter in SCN5A and other Na_V channels differs fundamentally from that of K_V channels such as KCNQ1 and hERG (**Figure 4**). The SF gate in Na_V channels is wider to allow Na^+ ions to pass in a partially hydrated state (Hille, 1971; Naylor et al., 2016). The extracellular vestibule of Na_V channels is lined by negatively-charged residues that recruit Na^+ ions to the SF. Coordination by both sidechain and backbone carbonyls contribute to the Na^+ permeation mechanism (Chakrabarti et al., 2013; Ulmschneider et al., 2013; Naylor et al., 2016). Additionally, the SF of eukaryotic Na_V channels is formed in a pseudo-symmetric fashion by four short helix-connecting turn motifs from each subunit (**Figure 4A**). Four distinct residues–DEKA, one in each repeat-form the signature motif for Na^+ selectivity found in all human Na_V channel pore-forming repeats (**Figure 4C**). The lysine residue in the DEKA motif (K1419 in SCN5A) confers selectivity for Na^+ and prevents permeability of Ca^{2+} (Favre et al., 1996). The recent rat SCN5A structure suggests a mechanism by which K1419 contributes to this selectivity of Na^+ over Ca^{2+}, whrein lysine forms a charge delocalization network at a constriction point in the SF. Only Na^+ ions, which have a compatible size and electric field strength, are able to pass through (Jiang et al., 2020).

Electromechanical Coupling

KCNQ1

In the absence of accessory subunits, KCNQ1 exhibits a constitutive current reflecting close-to-open state transitions even at very negative (~−120 mV) voltages (Ma et al., 2011). Analysis of a large group of KCNQ1 mutants suggests that gating follows an allosteric model (Ma et al., 2011). According to this model, the pore can open independently of the state of the VSD, but VSD activation increases the probability of pore opening.

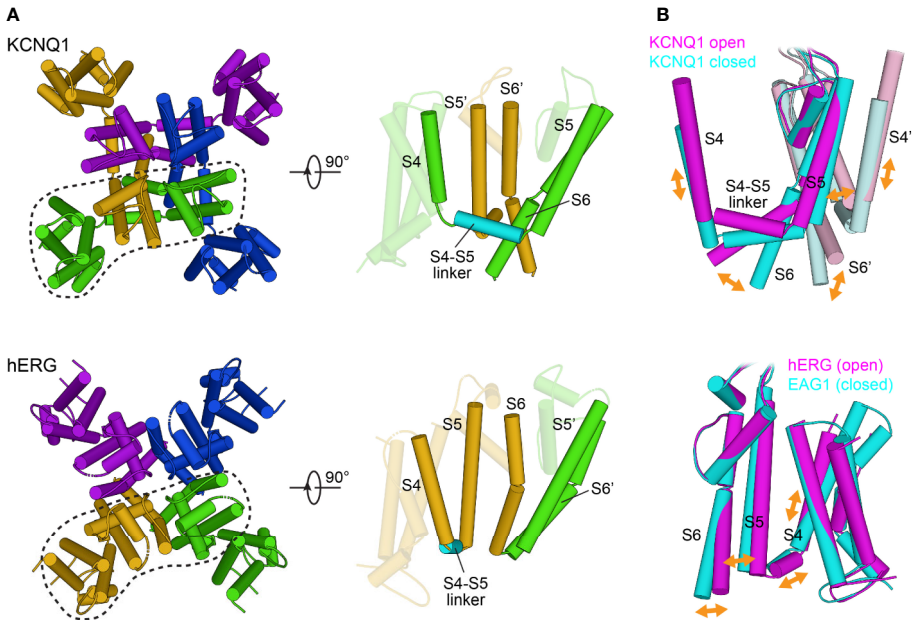

FIGURE 5 | Structural features of electromechanical coupling in the KCNQ1 and hERG channels. **(A)** Left: Extracellular view of KCNQ1 and hERG transmembrane segments S0 to S6. Individual subunits are drawn with different colors. KCNQ1 (PDB: 6UZZ) (Sun and Mackinnon, 2020) has a domain-swapped architecture whereas hERG (PDB: 5VA1) (Wang and Mackinnon, 2017) channels are non-domain-swapped. Right: Cartoon representation of a single subunit and its neighboring pore segments (S5 to S6). In KCNQ1, the VSD and PD are bridged by an extended α-helical S4–S5 linker, whereas in hERG, S4 and S5 are connected by only a short helix. **(B)** Implications for the direction of coupled motions between the VSD and PD based on molecular modeling of KCNQ1 in open and closed conformations (top) and comparison of the open state structure of hERG with the closed state structure of EAG1 (PDB: 5K7L) (Whicher and Mackinnon, 2016) (bottom). In the domain-swapped KCNQ1 channel, the S4 movement is transmitted to the gate through the S4–S5 linker. In hERG and EAG1, the S4 movement is proposed to exert a direct force on the S5–S6 interface to compress or open the channel gate.

Furthermore, KCNQ1 opening does not require concerted VSD movements (Osteen et al., 2012). Indeed, the VSDs appear to move independently, and pore opening can occur before all VSDs are activated (Osteen et al., 2012), consistent with an allosteric gating model.

Allosteric coupling for KCNQ1 is thought to be mediated by interactions between the VSD and the PD that translate S4 movement to channel opening and closing (**Figure 5**). Studies of KCNQ1 (Boulet et al., 2007; Labro et al., 2011) and of other K_V channels (Lu et al., 2001; Lu et al., 2002; Long et al., 2005) have pointed to the interface between the S4–S5 linker and the C-terminal end of S6 ($S6_C$) as one important mediator of electromechanical coupling (**Figure 5A**). Certain mutations in the S4–S5 linker (Labro et al., 2011) and $S6_C$ (Boulet et al., 2007) slow the opening rate and shift channel activation to more depolarized voltages, while other mutations, specifically at V254 in the S4–S5 linker and at L353 in $S6_C$, promote a constitutively open channel. Interestingly, a V254L/L353A double mutant rescued channel closing, suggesting that the S4–S5 linker interacts with $S6_C$ to stabilize the closed state. Relocation of the S4–S5 linker during gating abolishes this interaction, releasing tension on S6 and allowing it to kink at the PAG gating hinge in a cantilever-like fashion to promote channel opening (**Figure 5B**). This coupling mechanism is intrinsically weak for KCNQ1, requiring modulation by auxiliary molecules (see below). Recent work has further elucidated the molecular details of S4–S5 linker relocation, revealing a two-stage mechanism involving alternative binding modes of the S4–S5 linker to the PD (Hou et al., 2020). This two-stage mechanism may apply to the majority of domain-swapped K_V channels.

hERG

The relative positioning of the VSD and PD in hERG (Wang and Mackinnon, 2017) (**Figure 5A**) and the EAG1 channel (Whicher and Mackinnon, 2016) suggests that the mechanism by which movements in the VSD are transduced to pore opening is different from other K_V channels (Toombes and Swartz, 2016; Barros et al., 2019). This notion is supported by the finding that cutting the S4–S5 linker in hERG through separate expression of the VSD and PD fails to significantly perturb activation kinetics (Lorinczi et al., 2015). In contrast to the lever mechanism proposed for KCNQ1, lateral S4 movement in hERG toward the pore could both alter S4–S5 linker/S6 interactions and exert force through the S4–S5 linker directly onto S5. Displacement of S5 may be transmitted through the S5–S6 interface for opening or closing of the cytosolic gate (Wang and Mackinnon, 2017) (**Figure 5B**). A structure of hERG in the resting state may provide further insight into the molecular features of this distinct coupling mechanism.

SCN5A

Much of our knowledge about the coupling in SCN5A originates from studies of ancestral Na_V channels. Comparison of locked resting state structures of the bacterial sodium channel Na_VAb (Wisedchaisri et al., 2019) and of the chimeric human $Na_V1.7$–VSD_{II}–Na_VAb channel (Xu et al., 2019) with activated state structures (Yan et al., 2017b; Pan et al., 2018; Pan et al., 2019; Shen et al., 2019; Jiang et al., 2020) provide new insight into the mechanism of electromechanical coupling in Na_V channels. The S4–S5 linker appears to undergo movement similar to that of KCNQ1. The linker constrains the S5 and S6 helices in the resting/closed state, with looser interactions in the activated/open state. Coupling between the VSD and PD during pore opening must involve loosening of linker/PD interactions as S4 moves outward as in KCNQ1, albeit with tighter coupling of S4 and S4–S5 linker movement. The direct connection between S4 movement and pore opening may be crucial for rapid activation of sodium channels.

Comparison of the cockroach Na_VPaS channel structure (Shen et al., 2017), featuring a closed pore and VSDs in distinct activation states, to other eukaryotic Na_V channel structures suggests that additional structural shifts may be at work in eukaryotic Na_V channels to couple VSD to PD movement. Moreover, the distinct sequence of repeats I to IV (including that of the four S4–S5 linkers) and asynchronous voltage sensor movement in eukaryotic Na_V channels (Chanda and Bezanilla, 2002) suggest that distinct interactions couple the VSD of each repeat to the PD. Electromechanical coupling mechanisms may thus be more complex in SCN5A.

Inactivation

KCNQ1

Inactivation in KCNQ1 follows a mechanism distinct from canonical mechanisms (Hou et al., 2017). In the absence of KCNE1, KCNQ1 only partially inactivates, in a manner dependent on the IO and AO open states (Pusch et al., 1998). Differences in VSD-PD coupling between these two states appear to contribute to inactivation. The AO state has a lower coupling efficiency than IO, producing a lower open probability. Transition from IO to AO thus results in partial inactivation because the channel is open but less conductive (Hou et al., 2017). However, association with the KCNE1 accessory β subunit removes KCNQ1 inactivation (Pusch et al., 1998; Seebohm et al., 2003c), making inactivation irrelevant to cardiac KCNQ1 function.

hERG

Inactivation plays a critical role in hERG activity in the action potential. Entry into and out of inactivation is both fast and voltage-dependent, properties that maintain the plateau of the action potential (Perry et al., 2015). Additionally, the voltage dependence of inactivation appears to be independent of that of activation (Vandenberg et al., 2006; Cheng and Claydon, 2012), indicating that activation and inactivation may operate through distinct mechanisms. Inactivation in hERG is C-type (Smith et al., 1996), occurring through structural changes in the SF (Herzberg et al., 1998 14243; Hoshi and Armstrong, 2013). While the structural basis of C-type inactivation is not completely understood, work on hERG and other K^+ channels has provided useful insight. Several residues in the KcsA SF form stabilizing hydrogen bond networks that suppress inactivation (Doyle et al., 1998; Bhate et al., 2010; Cuello et al., 2010; Vandenberg et al., 2012). While these residues are conserved in many K_v channels (Whicher and Mackinnon, 2016), they are not present in hERG. This implies that the hERG SF is more liable to collapse, leading to inactivation (Fan et al., 1999; Vandenberg et al., 2012). Indeed, in molecular dynamics simulations, several residues in the hERG SF shift in and out of the pore axis, particularly F627 in the GFG motif (Stansfeld et al., 2008). In the hERG cryo-EM structure, the orientation of F627 is offset compared to other K_v channels (Whicher and Mackinnon, 2016), and a hERG S631A mutant, which has an F627 sidechain orientation similar to other structures, does not inactivate (Wang and Mackinnon, 2017). Additionally, mutation of T432 and A443 (corresponding to S620 and S631 in hERG) in non-inactivating EAG1 to serine was sufficient to impart inactivation behavior (Ficker et al., 2001), perhaps due to reorientation of the SF to match that of hERG. These results indicate that the unique positioning of F627 is critical for hERG fast inactivation behavior. C-type inactivation may involve other rearrangements (Loots and Isacoff, 1998), including coupling the SF to motions in S1, S5, and S6 (Ferrer et al., 2011; Wang et al., 2011; Perry et al., 2013a; Perry et al., 2013b).

SCN5A

Fast inactivation in SCN5A halts inward Na^+ current triggered by cardiac depolarization, permitting subsequent outward currents (e.g. I_{Ks}, I_{Kr}) to repolarize the cell in preparation for the next action potential (Ghovanloo et al., 2016) (**Figure 6A**). The S4 segment in VSD_{IV} ($S4_{IV}$) is critical for fast inactivation, along with the IFM motif in the III/IV linker (Ahern et al., 2016; Ghovanloo et al., 2016) (**Figures 6B, C**). Roles of individual basic sites of $S4_{IV}$ in Na_v inactivation have been elucidated, with mutations in R1 and R2 delaying inactivation onset and mutations in R3 and R4 delaying recovery from inactivation (Nakajima et al., 2019). Furthermore, structures of an engineered human $Na_V1.7$–Na_VPaS channel with VSD_{IV} trapped in a resting state (Clairfeuille et al., 2019) along with the structures of Na_vPaS (Shen et al., 2017), electric eel (Yan et al., 2017b) and human $Na_v1.4$ channels (Pan et al., 2018) have provided new structural insight into the mechanism of fast inactivation in Na_V channels (**Figure 6D**). In the resting state R5 on $S4_{IV}$ forms an electrostatic bridge with the α1 helix of the C-terminal cytoplasmic domain (CTD), together with K7 and R8 on the S4–S5 linker. The CTD in turn binds the III/IV linker, sequestering the IFM motif (**Figure 6D**, left plot). VSD_{IV} activation releases the connection between the CTD and the III/IV linker (middle and right plots in **Figure 6D**), permitting the IFM motif to bind to a hydrophobic pocket formed by the S4–S5 linkers and S6 helices of repeats III and IV, along with $S5_{IV}$ (**Figures 6C, E**). The insertion of the IFM motif into this pocket causes a twisting in the S6 helices that closes the gate (Yan et al., 2017b; Pan et al., 2018).

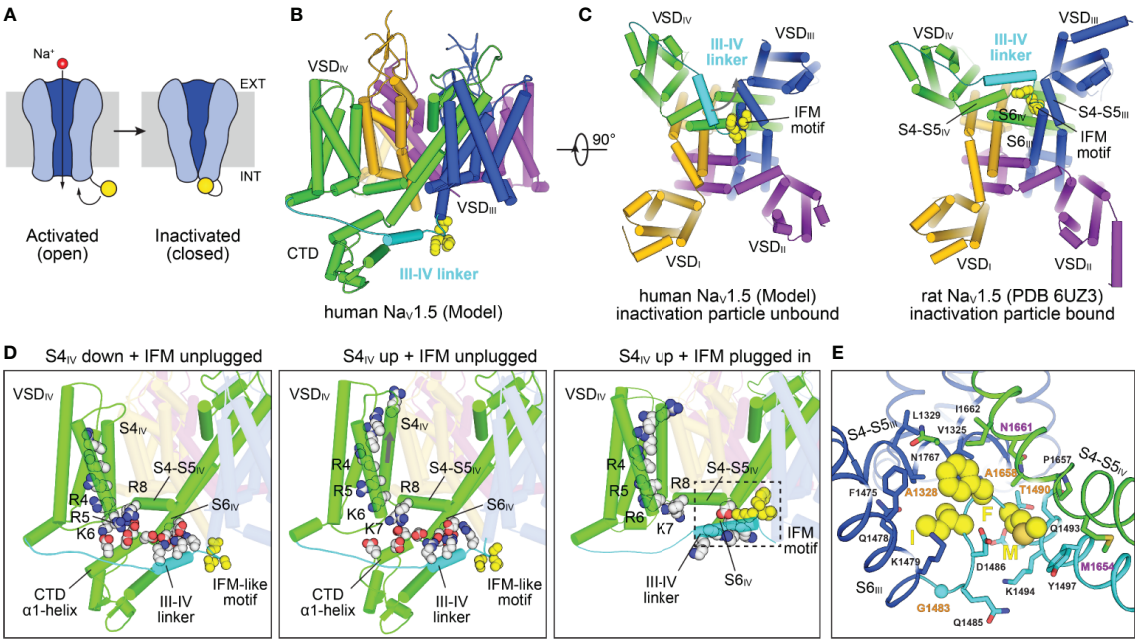

FIGURE 6 | Structural mechanisms of Na_V channel inactivation. **(A)** Na_V channels transition from an activated open state to a non-conducting inactivated state after depolarization. Inactivation is induced by binding of a C-terminal motif (yellow) to the cytosolic side of the channel leading to pore closure. The cell membrane is indicated with a gray rectangle, with the extracellular (EXT) and intracellular space (INT) labeled. **(B)** Closed state model of SCN5A (Kroncke et al., 2019) highlighting structural elements involved in fast inactivation. The III-IV linker (cyan) connecting $S6_{III}$ (blue) with VSD_{IV} (green) contains the IFM motif (yellow spheres) which is the key structural element responsible for inactivation. The position of the III-IV linker is constrained by the CTD following $S6_{IV}$. **(C)** Comparison of the SCN5A model in **(B)** with a cryo-EM structural model of rat SCN5A (PDB: 6UZ3)(Jiang et al., 2020) in a putative inactivated state viewed from the intracellular side. The III-IV linker undergoes a large shift in the SCN5A structure and the IFM motif is docked into a pocket surrounded by the S4–S5 linkers and S6 helices of repeats III and IV. **(D)** Structural states and transitions proposed to be involved in fast inactivation in Na_V channels. Left: Structure of a chimeric $Na_V1.7$–Na_VPaS channel (Clairfeuille et al., 2019) (PDB: 6NT3) with $S4_{IV}$ in a "down" position and an IFM-like motif unbound. Basic sites R5–R8 bridge to conserved acidic residues on the CTD which facilitates binding of the III-IV linker to $S6_{IV}$. Middle: Structure of a chimeric $Na_V1.7$–Na_VPaS channel (Clairfeuille et al., 2019) (PDB: 6NT4) with $S4_{IV}$ in a 'up' position and an IFM-like motif unbound. The electrostatic bridge between $S4_{IV}$ and the CTD is broken possibly increasing the positional dynamics of the CTD and III-IV linker. Right: Structure of SCN5A (PDB: 6UZ3) (Jiang et al., 2020) with $S4_{IV}$ in an 'up' position and the IFM motif plugged into the cytosolic cavity between repeats III and IV. Note, that the CTD is missing in the cryo-EM structure. **(E)** IFM binding pocket residues on $S4–S5_{III}$, $S4–S5_{IV}$, $S6_{III}$, and $S6_{IV}$ of SCN5A (PDB: 6UZ3) (Jiang et al., 2020). The $S6_{IV}$ helix backbone in the front is not shown for clarity. Residues that are important for fast inactivation and those found in various types of myotonia (Pan et al., 2018) are labeled magenta and orange, respectively.

REGULATION OF CHANNEL GATING BY INTRACELLULAR DOMAINS AND AUXILIARY MOLECULES

The function of these cardiac channels is tightly regulated to produce currents that faithfully give rise to the cardiac action potential under a host of physiological conditions and prevent early or delayed contractility. We focus here on regulation through the channel cytoplasmic domains as well as regulation by auxiliary (beta) subunits and lipids. Channels are regulated through other mechanisms such as phosphorylation, but are not covered in this review.

Regulation Involving Cytoplasmic Domains

KCNQ1

The C-terminal cytoplasmic domain (CTD) of KCNQ1 contains four alpha helices in lieu of the T1 tetramerization domain common to K_v channels outside the KCNQ family (Haitin and Attali, 2008). The proximal HA and HB helices form an antiparallel bundle with an IQ motif in HA and a 1-5-10 motif in HB that together enable calmodulin (CaM) binding (Yus-Najera et al., 2002). When bound, CaM prevents channel inactivation in KCNQ1, but inhibits the opening of other KCNQ family members (KCNQ2–KCNQ5) (Chang et al., 2018). While the N-lobe of CaM may be constitutively bound to both calcium and the proximal HA and HB helices (Ghosh et al., 2006; Bernardo-Seisdedos et al., 2018), the C-lobe of CaM binds calcium only at higher concentrations (Bernardo-Seisdedos et al., 2018). Calcium binding by the C-lobe induces a conformational change in CaM, facilitating KCNQ1 opening (Bernardo-Seisdedos et al., 2018; Chang et al., 2018). The C-lobe interacts with HA and with a loop in the S2–S3 linker (Sun and Mackinnon, 2017). This feature may contribute to the unique mode of CaM modulation of KCNQ1.

The distal helices HC and HD of KCNQ1 form a self-assembling intersubunit coiled-coil motif that promotes channel tetramerization (Yus-Najera et al., 2002; Howard et al., 2007; Sun and Mackinnon, 2017). The distal coiled-coil domain

is not only essential for channel tetramerization, but also for subunit specificity, permitting the exclusive formation of KCNQ1 homotetramers (Schwake et al., 2003; Haitin and Attali, 2008; Sachyani et al., 2014). In contrast, other KCNQ family proteins form heteromers (Schwake et al., 2003). Swapping the coiled-coil domain of KCNQ1 with that of KCNQ3 allows the resulting chimera to co-assemble with other KCNQ isoforms and generate channels with altered gating properties (Schwake et al., 2003; Schwake et al., 2006). Residues conferring specific KCNQ1 homotetramer formation have been identified in the HD helix (Schwake et al., 2006; Wiener et al., 2008). Key interactions involve both the hydrophobic core of the assembly and exterior electrostatic interactions, with a number of the residues involved subject to LQTS-associated mutations (Howard et al., 2007; Wiener et al., 2008).

hERG

hERG channels contain an N-terminal Per-ARNT-Sim (PAS) domain, which is also present in the N-terminus of many signaling proteins (Henry and Crosson, 2011). An additional C-terminal cyclic nucleotide-binding homology domain (CNBHD) similar to cytoplasmic domains in hyperpolarization-sensitive cyclic nucleotide-gated channels is present, but without ligand-binding properties (Codding and Trudeau, 2019). The PAS and the CNBHD appear to be critical for modulating the kinetics of slow deactivation in hERG (Gustina and Trudeau, 2011). Furthermore, slow deactivation is dependent on the direct interaction of these domains, particularly between R56 of the PAS and D803 of the CNBHD and between N12 of the N-terminal Cap (N-Cap) and E788 of the CNBHD (Ng et al., 2014; Kume et al., 2018). Interactions between the N-Cap and PAS domains with the C-linker also appear to be important for deactivation (Gustina and Trudeau, 2011; Ng et al., 2014), and the extreme N-terminus is likely essential, possibly interacting with the VSD through a patch of positively-charged residues in the N-Cap tail (Muskett et al., 2011). Indeed, the hERG cryo-EM structure corroborates the positioning of the N-Cap tail relative to the VSD (Wang and Mackinnon, 2017). The N-Cap tail may even be constitutively bound to the VSD (Morais Cabral et al., 1998; De La Pena et al., 2011), implying that slow deactivation could involve movement of the PAS toward the plasma membrane to alter this interaction (Barros et al., 2018).

SCN5A

Multiple structures of the SCN5A CTD in complex with regulatory factors (Wang et al., 2012; Gabelli et al., 2014; Gardill et al., 2019) have been determined, helping to elucidate how CaM (Johnson et al., 2018) and fibroblast growth factor-homologous factors (FHFs), specifically FGF13, modulate inactivation (Liu et al., 2003; Wang et al., 2012; Musa et al., 2015; Yang et al., 2016). CaM binds the CTD in a calcium-dependent manner (Kim et al., 2004; Hovey et al., 2017; Johnson et al., 2018; Urrutia et al., 2019), altering inactivation kinetics (Yan et al., 2017a; Johnson et al., 2018) and promoting recovery from inactivation (Johnson et al., 2018). In the absence of FHF, the C-lobe of apo-CaM binds to the IQ motif located in an extended helix on the CTD, while the N-lobe binds to the preceding EF hand-like domain (EFL) (Gabelli et al., 2014). With increasing intracellular calcium, holo-CaM has stronger affinity for the SCN5A III/IV linker (Johnson et al., 2018) and the N-lobe disassociates from the EFL (Gardill et al., 2019). These calcium-dependent interactions with the III/IV linker may facilitate CaM modulation of inactivation (Hovey et al., 2017; Johnson et al., 2018). FGF13 slows both inactivation onset and inactivation recovery in SCN5A (Yang et al., 2016), opposing CaM modulation. Importantly, binding of FGF13 to the SCN5A EFL (Wang et al., 2012) prevents binding of the apo-CaM N-lobe to the same domain (Wang et al., 2012). The EFL itself also adopts different orientations when bound to FGF13 (Wang et al., 2012) or CaM (Gabelli et al., 2014). Because the EFL also binds to the III/IV linker containing the IFM inactivation motif (Shen et al., 2017; Clairfeuille et al., 2019), EFL conformational changes upon binding of CaM or FGF13 may contribute to inactivation modulation by these proteins.

SCN5A also contains two cytoplasmic loops linking repeats I and II and repeats II and III, respectively. Unlike the III/IV linker, these loops are around 200 residues long (Pan et al., 2018) and likely disordered, based on the absence of these loops in cryo-EM structures. However, important regulatory events such as phosphorylation (Marionneau et al., 2012; Iqbal et al., 2018) and cofactor binding (Wu et al., 2008) that modulate channel properties have been identified in these loops.

Auxiliary Beta Subunits

KCNQ1

KCNQ1 co-assembles with a family of single span membrane proteins (KCNE1–5) (Abbott, 2014), and this interaction appears to be tissue–specific. In the heart, KCNQ1 is complexed with KCNE1, and the KCNQ1-KCNE1 channel exhibits greater single-channel conductance, opening at more positive potentials, and delayed activation compared to KCNQ1 alone (Barhanin et al., 1996; Sanguinetti et al., 1996). This heteromultimeric channel also exhibits altered Rb^+/K^+ selectivity (Pusch et al., 2000) and loss of inactivation (Pusch et al., 1998; Pusch et al., 2000). These properties are essential for the generation of the slow delayed rectifier current (I_{Ks}) in repolarizing cardiomyocytes. In gastric parietal cells, KCNQ1 co-assembles with KCNE2 to create constitutive K^+ currents essential for gastric acid secretion (Heitzmann et al., 2004; Roepke et al., 2006). In intestinal epithelial cells KCNQ1 complexes with KCNE3 to allow K^+ recycling for trans-epithelial chloride ion secretion (Preston et al., 2010). In contrast to KCNE1, KCNE2 and KCNE3 render KCNQ1 constitutively open (Schroeder et al., 2000; Tinel et al., 2000).

Due to the critical role of the KCNQ1-KCNE1 channel in the cardiac action potential, many research groups have probed the structural interaction between these proteins (Tapper and George, 2001; Xu et al., 2008; Chung et al., 2009; Strutz-Seebohm et al., 2011; Wang et al., 2011; Chan et al., 2012; Li et al., 2014). Combined results indicate that the transmembrane helix of KCNE1 binds in the cleft between neighboring KCNQ1

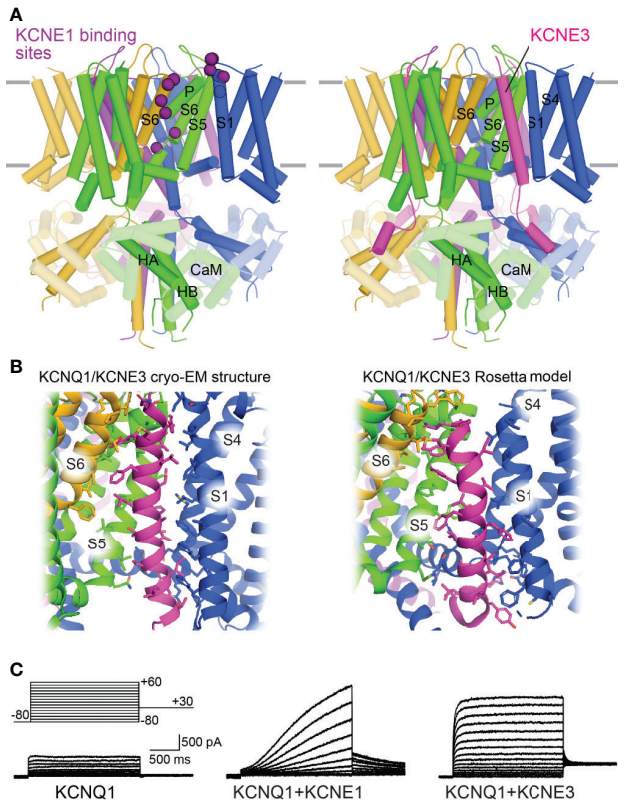

FIGURE 7 | Binding sites of KCNE proteins on the KCNQ1 channel. **(A)** Left: Mapping of putative KCNE binding sites onto the human KCNQ1 structure (PDB: 6V00) (Sun and Mackinnon, 2020). The position of residues identified to interact with KCNE1 (purple) are indicated by spheres. Right: Cryo-EM structure of human KCNQ1 with CaM and KCNE3 (PDB: 6v00)(Sun and Mackinnon, 2020). **(B)** KCNQ1/KCNE3 interaction sites. Left: 6V00. Right: KCNQ1/KCNE3 Rosetta model (Kroncke et al., 2016). Interactions sites were calculated with the InterResidues Python script in PYMOL (The PyMOL Molecular Graphics System, Version 2.2 Schrödinger, LLC.). Interaction positions indicated with sticks. **(C)** Example current traces of KCNQ1 alone or with KCNE proteins. Adapted with permission from (Van Horn et al., 2011).

subunits and interacts with both the VSD and PD. These binding sites overlap the binding cleft of KCNE3 (Sun and Mackinnon, 2020), indicating that KCNE1 may bind to the same site (**Figure 7A**). In the human KCNQ1-KCNE3 cryo-EM structure (Sun and Mackinnon, 2020) and an earlier Rosetta model of the complex (Kroncke et al., 2016), this cleft is formed by three KCNQ1 subunits (**Figure 7B**). KCNE3 contacts the cytoplasmic half of S5 in one subunit, the extracellular side of S6 in a second one, and along the entire length of S1 and the cytoplasmic side of S4 in a third subunit. Importantly, KCNE1 and KCNE3 produce KCNQ1 currents with different voltage dependencies and gating kinetics (**Figure 7C**). Given the possibility of a common binding cleft, differential modulation of KCNQ1 by KCNE1 and KCNE3 may involve different sidechain interactions within this cleft.

Mutations in the KCNE1 transmembrane helix, particularly at F57, T58, and L59 (Melman et al., 2001; Melman et al., 2002), alter the ability of this subunit to modulate the function of KCNQ1. The effect of this 'activation' triplet on KCNQ1 gating is altered by mutations at residues S338, F339, F340, and A341 in S6 (Melman et al., 2004; Panaghie et al., 2006; Strutz-Seebohm et al., 2011; Li et al., 2014), suggesting a functional link between these residues. However, modeling studies fail to indicate direct contact between the activation triplet on KCNE1 and these S6 sites (Kang et al., 2008; Gofman et al., 2012; Xu et al., 2013), suggesting that the functional coupling may be mediated allosterically. Interestingly, KCNE1 also affects S4 movement (Rocheleau and Kobertz, 2008; Wu et al., 2010a; Nakajo and Kubo, 2014) and shifts VSD voltage-dependence of activation to more negative voltages (Osteen et al., 2010; Ruscic et al., 2013; Barro-Soria et al., 2014). A model of KCNE1 regulation has recently been proposed, in which KCNE1 alters VSD-PD coupling interactions to suppress the IO state and modulate the AO state (Zaydman et al., 2014). This model accounts for many of the observed effects of KCNE1 on KCNQ1, including KCNE1-induced inhibition of inactivation. However, this model is not structurally elaborated.

hERG

Previous studies indicate that KCNE1 (Mcdonald et al., 1997) and KCNE2 (Abbott et al., 1999) can interact with and modulate hERG function. However, whether this interaction occurs under physiological conditions is debated (Weerapura et al., 2002; Anantharam and Abbott, 2005; Abbott et al., 2007). Although KCNE1 and KCNE2 alter hERG gating kinetics *in vivo* (Mcdonald et al., 1997; Mazhari et al., 2001), co-expression of KCNE2 with hERG *in vitro* does not reproduce the native I_{Kr} current (Weerapura et al., 2002). This suggests that KCNE1 and KCNE2 may not be essential for hERG channel function or that additional factors are required for KCNE-hERG interaction in cardiac cells. The latter possibility is supported by the observation that mutations in KCNE2 may predispose patients to drug-induced LQTS (Abbott et al., 1999; Sesti et al., 2000). As hERG is particularly drug-sensitive, this finding suggests that hERG may, in fact, be modulated by KCNEs in native tissue. Additionally, a T10M mutation in KCNE2 causes arrhythmia induced by auditory stimulation, a known trigger of LQT2, (Gordon et al., 2008). Further studies are needed to resolve these conflicting results and clarify the role of KCNE proteins in regulation of hERG function.

SCN5A

In humans there are five Na_V-β-subunit protein isoforms encoded by four genes, SCN1B-SCN4B (β1 to β4) (Detta et al., 2015; O'malley and Isom, 2015). All are expressed in the heart and have been shown to associate with SCN5A in heterologous conditions (Makita et al., 1996; Dhar Malhotra et al., 2001; Malhotra et al., 2004; Medeiros-Domingo et al., 2007; Watanabe et al., 2009; Valdivia et al., 2010). β1 to β4 are single-span transmembrane proteins containing an extracellular N-terminal immunoglobulin (Ig) domain, while β1B, a splice variant of SCN1B, lacks the transmembrane domain (Brackenbury and Isom, 2011). Generally, β-subunits modulate the biophysical properties and cell surface expression

of Na_V channels in heterologous cells (Calhoun and Isom, 2014). β1 and β3 interact non-covalently with Na_V channels (Meadows et al., 2001), while β2 and β4 are covalently bound through cysteine bonds between the extracellular Ig domain and channel pore loops. However, modulation of SCN5A by β-subunits has been difficult to assess. Varying effects of β1 (Qu et al., 1995; Dhar Malhotra et al., 2001; Baroni et al., 2014; Zhu et al., 2017) as well as β3 (Hu et al., 2009; Valdivia et al., 2010; Wang et al., 2010) on SCN5A have been reported. The rat SCN5A structure provides a potential explanation for this difficulty, as SCN5A is missing a cysteine residue critical for covalent interaction with β2, and contains a glycosylation site that may sterically occlude β1 interaction (Jiang et al., 2020). SCN5A may not bind tightly with any β-subunit. Nevertheless, the potential importance of β-subunits in SCN5A modulation has been suggested by arrhythmia-associated mutations in all four β-subunit genes, including mutations causing Brugada syndrome (Watanabe et al., 2008; Hu et al., 2009; Hu et al., 2012), LQT3 (Medeiros-Domingo et al., 2007; Riuro et al., 2014), and atrial fibrillation (Watanabe et al., 2009; Olesen et al., 2011). However, a recent review of genetic evidence supporting these associations has disputed the clinical validity of β subunits as monogenic causes of arrhythmia syndromes (Hosseini et al., 2018; Adler et al., 2020).

SCN5A subcellular localization also contributes importantly to channel regulation. SCN5A channels in cardiac tissue are localized at the lateral membranes and at the anchoring junction between cardiomyocytes (the intercalated disc). These expression patterns give rise to distinct sets of protein-protein interactions and biophysical properties (Lin et al., 2011; Shy et al., 2013). At the lateral membrane SCN5A interacts with the dystrophin/syntrophin multicomplex, but at the intercalated disc SCN5A interacts with ankyrin-G (Lemaillet et al., 2003; Mohler et al., 2004), which links the channel to cytoskeletal proteins such as actin and the desmosomal protein plakophilin-2 (Makara et al., 2014). Intriguingly, the functional properties of SCN5A channels between these two pools also differ: SCN5A at the lateral membrane has smaller current amplitude, distinct voltage-dependence, and slower recovery from inactivation as compared to channels in the intercalated disc (Lin et al., 2011). The functional implications of these differences are not yet clear and remain an active area of study.

Lipid Molecules

KCNQ1

KCNQ1 and other KCNQ channels are dependent on phosphatidyl-4,5-bisphosphate (PIP_2) for function (Loussouarn et al., 2003; Zaydman et al., 2013; Taylor and Sanders, 2017), and are inhibited upon stimulation of G_q- and G_{11}-protein coupled receptors, which trigger phospholipase C-catalyzed PIP_2 hydrolysis (Selyanko et al., 2000; Loussouarn et al., 2003; Zhang et al., 2003) (**Figure 8B**). Growing evidence suggests that PIP_2 acts as a coupling element for KCNQ1, enhancing weak allosteric interactions between the VSD and PD (Vardanyan and Pongs, 2012; Zaydman et al., 2013; Kasimova et al., 2015; Cui, 2016). Structure-function studies, confirmed by the human KCNQ1/PIP_2 structure, localize PIP_2 binding to the cleft between neighboring channel subunits, with interactions involving mostly positively-charged residues in the S2–S3 linker, S4–S5 linker, and $S6_C$ (**Figure 8A**) (Thomas et al., 2011; Zaydman et al., 2013; Eckey et al., 2014; Chen et al., 2015; Sun and Mackinnon, 2020). This binding site seems well-suited to modulate coupling of VSD movement to the activation gate. Questions remain regarding the mechanism of PIP_2 regulation of VSD-PD coupling, PIP_2:KCNQ1 stoichiometry, and binding site differences between the activated and resting states.

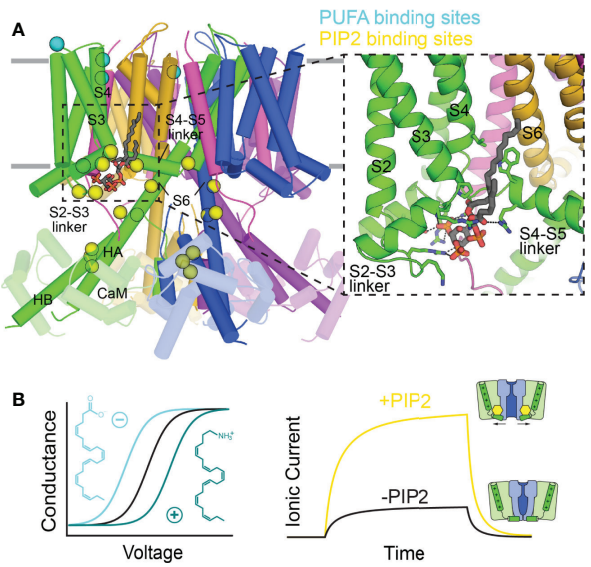

FIGURE 8 | Binding sites of lipids on the KCNQ1 channel. **(A)** Mapping of positions that have been implicated in the regulation of KCNQ1 by PUFAs (cyan) and PIP_2 (yellow) onto the PIP_2-bound KCNQ1 structure (6V01) (Sun and Mackinnon, 2020). Inset: the PIP_2 cryo-EM binding site. **(B)** Left: Effect of the PUFA head group charge on the voltage dependence of KCNQ1 conductance (inspired from results in Liin et al., 2015). Right: PIP_2 depletion reduces KCNQ1 ionic currents due to decreased VSD-PD coupling.

PIP_2 also binds to the CTD at a site shared with CaM (Tobelaim et al., 2017b). These two regulators may competitively regulate KCNQ1 at this site (Tobelaim et al., 2017a). Indeed, in the human KCNQ1 cryo-EM structure, CaM exhibits a nearly 180° rotation when PIP_2 is bound, losing contact with the S2–S3 linker (Sun and Mackinnon, 2020). Additionally, S6 and HA in KCNQ1 form a single helix in the open channel. These structural shifts point to an interplay between PIP_2 and CaM, but does not clarify the nature of this interaction, as no PIP_2 density was seen at the CTD binding site in the cryo-EM structure. The details of the coordination between CaM and PIP_2, and its role in channel function, remain to be elucidated.

Polyunsaturated fatty acids (PUFAs) also modulate KCNQ1 function (Taylor and Sanders, 2017). While PUFAs generally inhibit ion channel current (Boland and Drzewiecki, 2008), the KCNQ1-KCNE1 channel is a notable exception. The I_{Ks} current is enhanced by docosahexaenoic acid (DHA) and, to a lesser

extent, oleic acid (Doolan et al., 2002) by shifting the conductance-vs-voltage curve (GV) to more negative voltages. Interestingly, the charge of the head group determines the direction of the (GV) shift (**Figure 8B**): negatively-charged DHA causes a negative shift, a neutral head group has no effect, and a positively-charged one shifts the (GV) curve to positive potentials, reducing channel function (Liin et al., 2015). Negative head group charge and a polyunsaturated acyl chain appear to be required for channel activation. The PUFA binding site in KCNQ1 appears to involve residues in the extracellular S3–S4 loop, R1 and R2 on S4, and the PD (**Figure 8A**), as mutations in these regions either reduce the PUFA effect or completely abolish the (GV) shift (Liin et al., 2015; Liin et al., 2018).

hERG

As with KCNQ1, the function of hERG is upregulated by PIP_2 by means of increased current amplitude, a hyperpolarizing shift in voltage-dependence of activation, as well as faster activation and slower inactivation rates (Bian et al., 2001). Stimulation of $G_{\alpha q}$-protein coupled receptors also suppresses the I_{Kr} current through PIP_2 depletion (Bian et al., 2001; Bian et al., 2004). Binding of PIP_2 to hERG likely localizes to a cluster of basic residues (R883–Q900) C-terminal to the CNBHD, as substitution of these residues to neutral or negatively-charged amino acids prevented PIP_2 effects on hERG function and abolished PIP_2 binding (Bian et al., 2004). Unfortunately, these residues are not resolved in the available hERG structure (Wang and Mackinnon, 2017).

SCN5A

In contrast to KCNQ1, PUFAs such as eicosapentaenoic acid (EPA), docosahexaenoic acid (DHA), linoleic acid (LA), and α-linolenic acid (ALA) suppress I_{Na} current in a concentration-dependent manner by shifting the voltage dependence of I_{Na} inactivation to more hyperpolarized potentials (Kang et al., 1995; Kang et al., 1997; Leifert et al., 1999). EPA also accelerates the transition from the resting state to the inactivated state and slows recovery from inactivation (Xiao et al., 1998; Isbilen et al., 2006). However, the effect was reduced by β1 subunit expression (Xiao et al, 2000). Furthermore, N406K renders SCN5A less sensitive to inhibition by EPA, an effect strengthened by β1 subunit expression (Xiao et al., 2001). The structural basis for PUFA binding and modulation is not well understood.

CHANNEL DYSFUNCTION IN CONGENITAL LONG QT SYNDROME

Alterations in the action potential disturb impulse propagation and cause reentry (Kleber Ag, 2004), whereby the impulse re-stimulates the heart tissue that generated it. Reentry promotes cardiac arrhythmias and predisposes to sudden unexplained death (Skinner et al., 2019). LQTS is a prevalent cause of such events, with an estimated population prevalence of approximately 1:2500 (Schwartz et al., 2009).

LQTS is characterized by a prolonged rate-corrected QT interval in patient electrocardiograms (ECGs), indicative of impaired repolarization (Schwartz et al., 2012). In a large proportion of cases, QT interval prolongation is the result of either a loss-of-function in KCNQ1 or hERG, or a gain-of-function in the SCN5A channel (Moss and Kass, 2005; Schwartz et al., 2012; Earle et al., 2013; Skinner et al., 2019). Mutations in these genes confer distinct subtypes of LQTS (denoted LQT1–3, respectively), each with unique ECG features, risk factors, arrhythmia triggers, and responsiveness to β-adrenergic receptor blockers, the most common LQTS treatment (Ackerman, 2005; Moss and Kass, 2005; Skinner et al., 2019; Wallace et al., 2019). Below, the function of each ion channel in the cardiac action potential is discussed, along with how each can cause action potential dysfunction in LQTS.

Channel Function in the Cardiac Action Potential and Dysfunction in LQTS

KCNQ1

In complex with KCNE1, KCNQ1 conducts I_{Ks}, which helps shape the plateau and repolarization phases of the action potential, in part by counteracting calcium influx (Skinner et al., 2019). Due to slow activation, the KCNQ1-KCNE1 channel is only slightly open during the plateau phase, with I_{Ks} increasing slowly in a nearly linear fashion (**Figure 7C**) until the repolarization phase is reached and the channel becomes fully activated (**Figures 1B, C**) (Moss and Kass, 2005). KCNQ1-KCNE1 channels do not inactivate (Pusch et al., 1998), conducting current throughout activation and deactivation. The channel slowly deactivates, shaping the tail of the repolarization phase and mediating return to the resting potential (Moss and Kass, 2005; George, 2013; Skinner et al., 2019). Thus, loss-of-function in KCNQ1 prolongs repolarization primarily by preventing completion of the repolarization phase, broadening the tail of the T-wave (**Figure 1A**) and causing type 1 LQTS (LQT1). (Ackerman, 2005; Tester and Ackerman, 2014; Skinner et al., 2019; Wallace et al., 2019). The effects of a KCNQ1 mutation are exacerbated upon sympathetic activation of β-adrenergic receptors due to I_{Ks} potentiation, while resting heart rates show few perturbations (Shimizu and Antzelevitch, 1998). The QT interval is unable to shorten in response to this stimulation, making physical exertion accompanied by heightened sympathetic nervous system activity a prevalent LQT1 trigger (Schwartz et al., 2012; Bohnen et al., 2017).

hERG

hERG makes up the other primary inward rectifier current I_{Kr}, which acts in both the plateau and the repolarization phase (**Figures 1B, C**) (Moss and Kass, 2005; Skinner et al., 2019). As the channel activates, rapid entry into and out of inactivation (due to SF fluctuations) creates a persistent current through the plateau phase until slow deactivation, regulated by the PAS and CNBHD domains, closes the channel during the repolarization phase. While both hERG and KCNQ1 are conductive during the plateau and repolarization phases, hERG has a higher unitary conductance than KCNQ1 in both phases (Moss and Kass, 2005;

George, 2013). The resulting I_{Kr} current thus supplies a greater proportion of the overall I_K current (Cheng and Kodama, 2004), with loss-of-function in hERG (LQT2) correlating with a lower T-wave amplitude in contrast to the normal T-wave amplitude associated with LQT1. Additionally, LQT2 is often triggered at rest (Skinner et al., 2019), consistent with the greater hERG contribution to I_K. However, while I_{Kr} is usually more prominent (Cheng and Kodama, 2004), the relative density of I_{Kr} and I_{Ks} vary by ventricular cell type (Liu and Antzelevitch, 1995; Viswanathan et al., 1999).

SCN5A

SCN5A produces the I_{Na} current that shapes the initial upstroke of the cardiac action potential (Skinner et al., 2019), initiating depolarization. SCN5A is rapidly activated through asynchronous motion of the VSD's in repeats I-III coupled to pore opening, then quickly inactivates through interaction of the IFM motif with the channel, resulting in a brief inward spike of sodium current that depolarizes the cell (Ghovanloo et al., 2016) (**Figures 1B, C**). Unlike KCNQ1 and hERG, LQT3 is conferred by SCN5A gain-of-function mutations that cause a "leaky" inward sodium current (Wilde and Amin, 2018; Skinner et al., 2019). The functional I_{Kr} and I_{Ks} outward currents are unable to compensate for the persistent inward I_{Na} current, prolonging entry into and completion of the repolarization phase and giving rise to LQT3. As in LQT2, LQT3-related arrhythmias occur most often at rest, rather than in response to stress or exercise (Schwartz et al., 2012). It should be noted that while loss-of-function mutations for SCN5A are not relevant to LQTS, they are prevalent in other channelopathies, particularly Brugada syndrome (Wilde and Amin, 2018; Skinner et al., 2019).

Molecular Mechanisms of LQTS

Mutations in KCNQ1, hERG, and SCN5A can lead to LQTS by perturbing channel function through distinct molecular mechanisms. Structural studies of these channels can help tease apart these molecular mechanisms for a more detailed understanding of LQTS. We have mapped LQTS mutations identified as pathogenic according to ClinVar (Harrison et al., 2016) and HGMD (Stenson et al., 2012) databases onto the human KCNQ1 (Sun and Mackinnon, 2020) and hERG structures (Wang and Mackinnon, 2017), as well as a recent model of SCN5A (Kroncke et al., 2019) and the rat SCN5A homolog (Jiang et al., 2020) (**Figures 9**–**11**). The list of curated mutations is found in **Table 1**: 261 mutations in KCNQ1, 320 mutations in hERG, and 122 mutations in SCN5A. Examination of these mutation sites provides some insight into the channel mechanisms that may be commonly disrupted in LQT1–3.

KCNQ1

KCNQ1 mutations studied to date are highly varied in molecular effects, with the potential to induce defects in channel stability, trafficking, electrophysiology, or all three (Chen et al., 2011; Heijman et al., 2012; Wu et al., 2016; Bohnen et al., 2017). So far, a strong disposition for either expression or functional defects has not been elucidated. However, analysis of mutation sites points to regions of increased pathological risk and provides hints regarding prevalent mechanisms.

LQT1-associated mutations are found in every domain of the protein (**Figure 9A**), particularly in the transmembrane channel domain (Shimizu et al., 2004; Moss et al., 2007; Kapa et al., 2009). Mutations in the SF, (**Figure 9A**, inset), VSD (**Figure 9B**), and the S4–S5 linker (**Figure 9C**) are especially prominent.

Mutations in and around the SF (**Figure 9A**, inset) point to a potential ion permeation defect, as conformational changes may prevent potassium ion permeation and thus decrease the effective I_{Ks} current (Choveau and Shapiro, 2012), as noted in several SF mutations (Ikrar et al., 2008; Thomas et al., 2010; Burgess et al., 2012; Chen et al., 2019). Molecular dynamics simulations of analogous mutations in KcsA indicated that mutations in the SF-interacting residues (including T322M, T322A, or G325R) may disrupt the organization of backbone atoms in the SF, abolishing K^+ ion coordination and producing a dominant-negative effect on channel current (Burgess et al., 2012).

VSD mutations are more common in KCNQ1 compared to hERG and SCN5A (see **Figures 9B**, **10B**, and **11A**), indicating that the VSD is more important in LQT1. Analysis of LQTS mutations located in the VSD (Huang et al., 2018; Vanoye et al., 2018) indicate that loss of channel function was most commonly a consequence of mutation-induced destabilization of the channel, resulting in mistrafficking and lower surface expression. These results strongly correlated with Rosetta energy calculations of VSD mutants (Kuenze et al., 2019), supporting the importance of VSD destabilization as a LQT1 mechanism. A number of the deleterious mutations were found in the S0 helix and S0-contacting regions of the VSD. Among the 50 VSD mutations studied, the S0 mutations had the largest energetic destabilizations consistent with the large number of contacts formed between S0 and other regions of the VSD. (Huang et al., 2018; Kuenze et al., 2019). However, these studies also identified variants that did not exhibit folding and trafficking defects, but were either non-functional (low conductance) or dysfunctional, with modified gating, again pointing to a complex spectrum of LQT1 disease mechanisms.

Mutations in the KCNQ1 S4–S5 linker and its contacting regions (**Figure 9C**) have the potential to perturb VSD-PD coupling and channel gating. Such effects have been demonstrated for a number of LQTS-associated mutations in the S4–S5 linker and the cytoplasmic end of S6, particularly for R243C, W248F/R, and Q357R, producing positive shifts in the voltage dependence of activation or inactivation and and/or decreased current amplitude (Franqueza et al., 1999; Boulet et al., 2006; Mousavi Nik et al., 2015). Because the S4–S5 linker is involved in both VSD/PD interactions and in binding of PIP_2 (Eckey et al., 2014; Sun and Mackinnon, 2017) and KCNE1 (Kang et al., 2008; Xu et al., 2013; Cui, 2016), mutations in this region may affect gating either by weakening VSD-PD coupling or by hindering modulation by auxiliary molecules. Some LQT1 variant-induced changes in PIP_2 binding at the S4–S5 linker have been noted (including R243H, R539W, and R555C) (Park et al., 2005). Due to the complex nature of electromechanical coupling

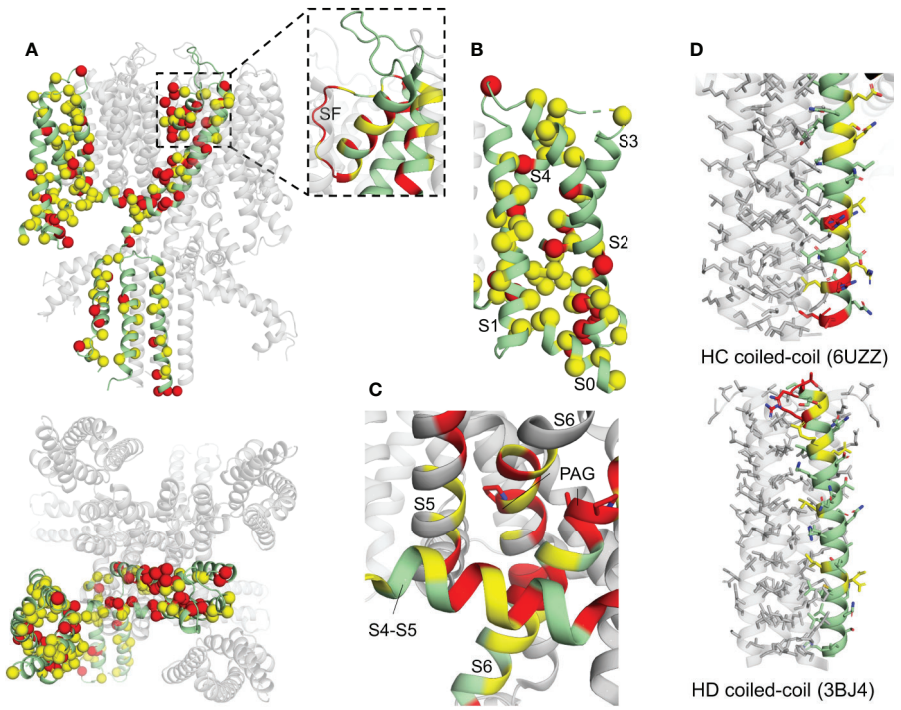

FIGURE 9 | Human KCNQ1 structure with deleterious mutation sites indicated. **(A)** Full KCNQ1 structure (PDB: 6UZZ) (Sun and Mackinnon, 2020). Yellow sites denote locations of a single deleterious mutation, while red indicates sites with multiple mutations identified. Spheres indicate C-alpha positions of mutation sites. Subunit with LQT1 mutations sites mapped is colored green. Inset: of SF and pore helix. **(B)** KCNQ1 VSD. **(C)** S4–S5 linker (S4–S5) interaction site close-up. One subunit is colored green and the others in gray, for clarity. The PAG motif (PAG) is indicated with sticks. **(D)** Top: HC coiled-coil domain. Bottom: HD coiled-coil domain (PDB: 3BJ4) (Wiener et al., 2008). Residue side chains are indicated with sticks.

in KCNQ1 and the requirement for auxiliary subunits, a detailed structural understanding of mutation effects in this region is particularly challenging. However, the human KCNQ1, KCNQ1-KCNE3, and KCNQ1-KCNE3/PIP_2 channel structures (Sun and Mackinnon, 2020) may provide guidance in experimental design to elucidate LQT1-associated coupling defects in this region.

While the majority of LQT1 mutations map to the transmembrane domain, mutations are also found in the CTD, both in the HA/HB helix bundle, where CaM binds, and in the HC and HD coiled-coil domains (**Figure 9A**). Mutations in HC and HD are particularly prevalent in sites of hydrophobic and electrostatic interactions that stabilize the coil, hinting at channel assembly defects (**Figure 9D**). Defects in CaM binding and tetramerization cause some forms of LQT1, as demonstrated for several mutations (Kanki et al., 2004; Ghosh S, 2006; Schwake et al., 2006; Wiener et al., 2008).

hERG

Loss-of-function mutations in hERG may lead to folding/trafficking defects, gating defects, or both (Anderson et al., 2014; Smith et al., 2016; Bohnen et al., 2017). However, as many as 90% of hERG loss-of-function mutations appear to cause trafficking defects, independent of which domain is mutated (Smith et al., 2016). As in KCNQ1, pore domain mutations in hERG demonstrated stronger dominant-negative effects in hERG than other regions, hinting that mutations in this region are more severe (Anderson et al., 2014).

Although hERG mutations span the entire protein, they are prominent in the SF (**Figure 10A**, inset), the extracellular VSD/PD interface between S1 and S5 (**Figure 10C**), and in the PAS and CNBHD cytoplasmic domains (**Figure 10D**). Given the inherent instability of the hERG SF (Fan et al., 1999; Stansfeld et al., 2008; Vandenberg et al., 2012) and the functional necessity of the SF for fast inactivation (Herzberg et al., 1998; Hoshi and Armstrong, 2013), mutations may act by both affecting channel stability and inactivation. Inactivation defects due to LQT2-associated pore helix mutations have been identified (Zhao et al., 2009; Poulsen et al., 2015). However, mutations in LQT2 more commonly cause misfolding and/or trafficking defects. Potassium ions appear to stabilize the mature hERG channel (possibly by interacting with the SF) to promote trafficking (Wang et al., 2009; Apaja et al., 2013), with intracellular K^+ depletion resulting in ER retention. G601S mimicked this phenotype (Apaja et al., 2013). G601S, a mutation in the pore loop near the SF, mimicked also impedes trafficking through enhanced chaperone association in the ER (Ficker et al., 2003), supporting the idea of SF destabilization as a cause for channel mistrafficking. A detailed understanding of mutations in the SF region requires both intensive structural and cellular analysis to uncover not only protein conformational changes upon

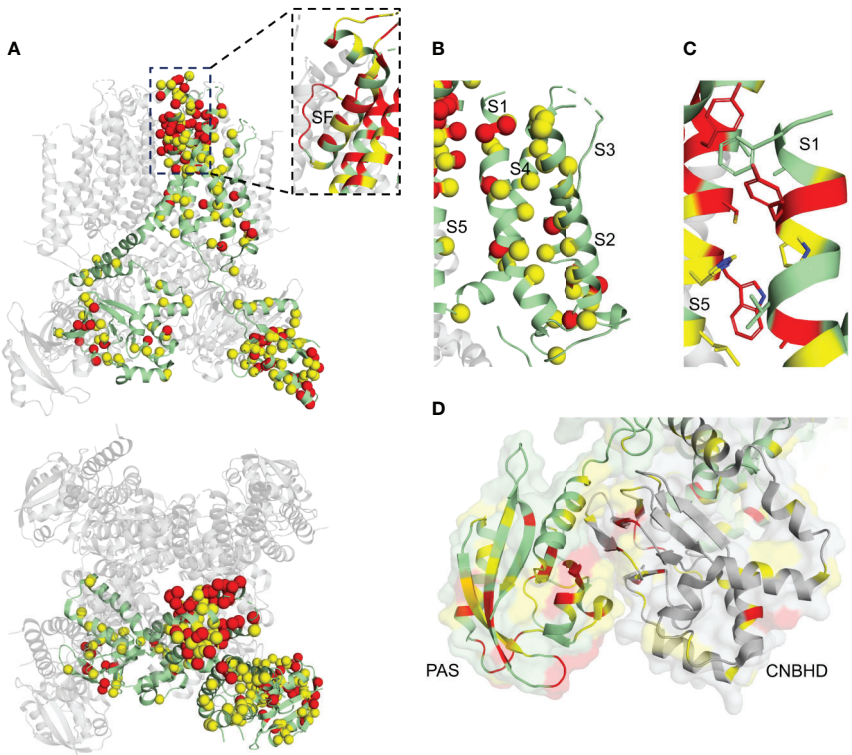

FIGURE 10 | hERG structure with deleterious mutation sites indicated. **(A)** Full hERG structure (PDB: 5VA1) (Wang and Mackinnon, 2017). Yellow sites denote locations of a single deleterious mutation, while red indicates sites with multiple mutations identified. Spheres indicate C-alpha positions of mutation sites. Subunit with LQT2 mutations sites mapped is colored green. Inset: close-up of SF and pore helix. **(B)** hERG VSD. **(C)**. Close-up of the S1/S5 interface. Residues at the interface are indicated with sticks **(D)** N-terminal PAS (dark gray) and C-terminal CNBHD (light gray) domain interface, cartoon representation with surface representation overlay. One subunit is green and the other gray, for clarity.

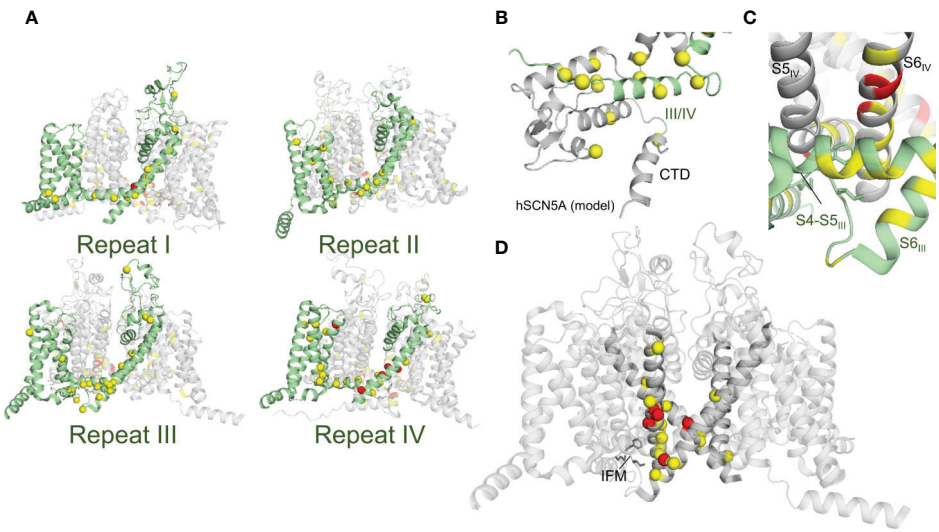

FIGURE 11 | Rat SCN5A structure with deleterious mutation sites indicated. **(A)** Full SCN5A structure (PDB: 6UZ3) (Jiang et al., 2020). Yellow sites denote locations of a single deleterious mutation, while red indicates sites with multiple mutations identified. Spheres indicate C-alpha positions of mutation sites. Side views of individual repeats are shown with 90° rotations between panels. In each panel, one repeat is colored green and LQT3 mutation sites for that repeat are mapped. **(B)** C-terminal domain with bound III/IV linker (human SCN5A model: [(Kroncke Bm, 2019)]. **(C)** Putative inactivation gate. IFM motif is indicated with sticks. **(D)** SCN5A constriction site. S6 helices are shown at full opacity, with the IFM motif indicated with sticks.

TABLE 1 | LQTS mutations in KCNQ1, hERG, and SCN5A.

KCNQ1				hERG				SCN5A			
Mutant	**Database**	**Mutant**	**Database**	**Mutant**	**Database**	**Mutant**	**Database**	**Mutant**	**Database**	**Mutant**	**Database**
A58P*	HGMD	T311I	HGMD	G6R	HGMD	G572R	ClinVar, HGMD	G9V*	HGMD	G1329S	HGMD
S66F*	HGMD	T312S	HGMD	G6V	HGMD	G572S	HGMD	R18W*	HGMD	A1330P	HGMD
T96R*	HGMD	T312I	ClinVar, HGMD	T13N	HGMD	G572V	HGMD	A29V*	HGMD	A1330T	HGMD
T104I	HGMD	I313M	HGMD	D16A	HGMD	M574V	HGMD	E30G*	HGMD	P1332L	HGMD
Q107H	HGMD	G314A	HGMD	R20G	HGMD	E575G	HGMD	P52S*	HGMD	S1333Y	HGMD
R109L	HGMD	G314D	HGMD	F22S	HGMD	E575K	HGMD	R53Q*	HGMD	L1338V	HGMD
Y111C	ClinVar, HGMD	G314C	HGMD	F22Y	HGMD	R582C*	ClinVar	R104G*	HGMD	A1357V	HGMD
L114P	HGMD	G314R	ClinVar, HGMD	S26I	HGMD	G584S	HGMD	A110T*	HGMD	G1391R	HGMD
E115G	HGMD	G314S	ClinVar, HGMD	R27P	HGMD	G584V	HGMD	V113I*	HGMD	A1428S	HGMD
P117L	ClinVar, HGMD	Y315N	HGMD	K28E	HGMD	W585C	HGMD	S115G*	HGMD	S1458Y	ClinVar, HGMD
C122Y	ClinVar, HGMD	Y315C	HGMD	F29L	HGMD	L586M	HGMD	I176M	HGMD	N1472S	HGMD
Y125D	HGMD	Y315H	HGMD	F29S	HGMD	N588D	HGMD	A185T	HGMD	F1473C	HGMD
F127L	HGMD	Y315F	HGMD	I31S	HGMD	G590V	HGMD	I239V	HGMD	F1473S	HGMD
L131P	HGMD	Y315S	HGMD	I31T	ClinVar, HGMD	I593T	ClinVar	V240M	HGMD	Q1476R	HGMD
I132L	HGMD	G316E	HGMD	A32T	HGMD	I593K	ClinVar, HGMD	Q245K	HGMD	G1481E	HGMD
V133I	HGMD	G316V	HGMD	N33T	HGMD	I593R	ClinVar, HGMD	V258A	HGMD	T1488R	HGMD
L134P	ClinVar, HGMD	G316R	ClinVar, HGMD	R35W	HGMD	I593V	HGMD	R340Q	HGMD	Y1495S	HGMD
C136F	HGMD	D317N	ClinVar, HGMD	V41F	HGMD	G594D	HGMD	A385T	HGMD	K1505N	HGMD
L137F	ClinVar, HGMD	D317G	HGMD	V41A	HGMD	K595N	HGMD	I397T	HGMD	T1544P	HGMD
S140R	HGMD	D317Y	HGMD	I42N	HGMD	K595E	HGMD	L404Q	HGMD	L1560F	HGMD
E146G	HGMD	K318N	ClinVar, HGMD	Y43C	HGMD	P596H	ClinVar, HGMD	N406K	HGMD	I1593M	HGMD
E146K	HGMD	P320A	HGMD	Y43D	HGMD	P596A	ClinVar, HGMD	L409P	HGMD	F1594S	HGMD
A150G	HGMD	T322K	HGMD	C44F	HGMD	P596R	HGMD	L409V	HGMD	V1597M	HGMD
T153M	HGMD	T322A	ClinVar, HGMD	C44W	HGMD	P596L	HGMD	V411M	ClinVar, HGMD	S1609W	HGMD
F157C	HGMD	T322M	ClinVar, HGMD	C44Y	HGMD	P596S	HGMD	A413E	HGMD	R1623Q	ClinVar, HGMD
E160K	HGMD	G325R	ClinVar, HGMD	N45D	HGMD	P596T	HGMD	R504T*	HGMD	R1623L	HGMD
E160V	HGMD	G325E	HGMD	N45S	HGMD	Y597C	HGMD	M506K*	HGMD	R1626P	HGMD
G168R	ClinVar, HGMD	G325W	HGMD	N45Y	HGMD	G604D	HGMD	F530V*	HGMD	R1644H	ClinVar, HGMD
T169R	HGMD	S338F	HGMD	D46Y	HGMD	G604S	ClinVar, HGMD	D536H*	HGMD	L1646R	HGMD
T169K	HGMD	F339S	HGMD	G47D	HGMD	P605S	HGMD	R569W*	HGMD	L1650F	HGMD
E170G	HGMD	F339V	HGMD	G47V	HGMD	S606F	HGMD	Q573E*	HGMD	M1652R	HGMD
V173D	HGMD	F340L	HGMD	C49Y	HGMD	S606P	HGMD	G579R*	HGMD	M1652T	HGMD
R174C	ClinVar, HGMD	A341G	HGMD	G53R	HGMD	D609G	HGMD	P637L*	HGMD	P1725L	HGMD
R174H	ClinVar, HGMD	A341V	ClinVar, HGMD	G53D	HGMD	D609H	HGMD	E654K*	HGMD	A1746T	HGMD
W176R	HGMD	A341E	ClinVar, HGMD	G53S	HGMD	D609N	ClinVar, HGMD	A665S*	HGMD	I1758V	HGMD
A178T	HGMD	L342F	HGMD	G53V	HGMD	D609Y	HGMD	R689C*	HGMD	L1761H	HGMD
A178P	ClinVar, HGMD	P343R	HGMD	Y54H	HGMD	K610N	HGMD	G709V*	HGMD	L1761F	HGMD
K183R	HGMD	P343L	HGMD	S55L	ClinVar, HGMD	Y611D	HGMD	T731I	HGMD	V1763L	HGMD
K183M	HGMD	P343S	HGMD	R56Q	HGMD	Y611H	ClinVar, HGMD	Q750R	HGMD	V1763M	ClinVar, HGMD
Y184C	HGMD	A344E	HGMD	A57P	HGMD	V612L	HGMD	Q779K	HGMD	M1766L	ClinVar, HGMD
Y184H	HGMD	A344V	ClinVar, HGMD	E58A	HGMD	V612M	HGMD	R800L*	HGMD	M1766V	HGMD
Y184S	HGMD	G345R	ClinVar, HGMD	E58D	HGMD	T613A	HGMD	R808P	HGMD	Y1767C	HGMD
G186R	HGMD	G345E	ClinVar, HGMD	E58G	ClinVar, HGMD	T613K	HGMD	F816Y	HGMD	I1768V	ClinVar, HGMD
G189A	HGMD	G345A	HGMD	E58K	HGMD	T613M	ClinVar, HGMD	L828V	HGMD	L1772V	HGMD
G189E	HGMD	G345V	HGMD	Q61R	HGMD	A614V	ClinVar, HGMD	N834D	HGMD	N1774D	HGMD
G189R	ClinVar, HGMD	L347P	HGMD	R62Q	HGMD	L615F	HGMD	G840R	HGMD	E1781G	HGMD
R190Q	ClinVar, HGMD	S349W	ClinVar, HGMD	C64W	HGMD	Y616C	HGMD	T843A	ClinVar, HGMD	E1784K	HGMD
R190L	HGMD	S349P	HGMD	C64Y	HGMD	F617L	HGMD	Q912R	HGMD	D1790G	HGMD
R190W	HGMD	G350R	HGMD	T65P	ClinVar, HGMD	F617V	HGMD	S941N	ClinVar	Y1795C	ClinVar, HGMD
L191P	HGMD	G350V	HGMD	C66G	HGMD	T618S	HGMD	Q960K*	HGMD	P1824A	HGMD
R192P	HGMD	F351L	ClinVar	F68L	HGMD	S620N	HGMD	R975W*	HGMD	D1839G	HGMD
F193L	HGMD	F351S	HGMD	L69P	HGMD	S620G	HGMD	C981F*	HGMD	R1860S	HGMD
R195P	HGMD	L353P	ClinVar, HGMD	H70R	HGMD	S621R	HGMD	P1021S*	HGMD	A1870T	HGMD
K196T	HGMD	K354R	HGMD	H70N	HGMD	S621N	HGMD	D1166N*	HGMD	R1897W*	HGMD
P197S	HGMD	Q357R	HGMD	G71E	HGMD	T623I	HGMD	R1175C*	HGMD	E1901Q*	HGMD
I198V	ClinVar, HGMD	R360M	HGMD	G71R	ClinVar, HGMD	V625A	HGMD	P1177L*	HGMD	A1949S*	HGMD
S199A	HGMD	R360T	HGMD	G71W	HGMD	V625E	HGMD	Y1199S*	HGMD	E1954K*	HGMD
I200N	HGMD	K362R	HGMD	P72L	ClinVar, HGMD	G626A	HGMD	Y1241S	HGMD	Y1977N*	HGMD
D202G	ClinVar	H363N	ClinVar, HGMD	P72T	HGMD	G626D	HGMD	I1278N	HGMD	L1988R*	HGMD
D202H	HGMD	N365H	HGMD	T74P	HGMD	G626S	HGMD	N1325S	ClinVar, HGMD	R1991Q*	HGMD
L203P	HGMD	R366Q	ClinVar	T74R	ClinVar, HGMD	G626V	HGMD	A1326S	ClinVar, HGMD	F2004V*	HGMD

(Continued)

TABLE 1 | Continued

KCNQ1				hERG				SCN5A			
Mutant	**Database**	**Mutant**	**Database**	**Mutant**	**Database**	**Mutant**	**Database**	**Mutant**	**Database**	**Mutant**	**Database**
I204M	HGMD	R366P	HGMD	A78V	HGMD	F627I	HGMD				
I204F	HGMD	R366W	HGMD	A78T	HGMD	F627L	HGMD				
V205M	ClinVar, HGMD	Q367H	HGMD	A80P	HGMD	G628R	HGMD				
S209F	HGMD	A371T	HGMD	A85P	HGMD	G628D	HGMD				
K218E	HGMD	A372D	HGMD	A85V	HGMD	G628S	ClinVar, HGMD				
T224M	HGMD	S373P	HGMD	L86R	HGMD	G628V	HGMD				
S225L	HGMD	W379G	HGMD	L86P	HGMD	G628A	HGMD				
A226V	HGMD	W379S	HGMD	A89V	HGMD	N629D	ClinVar, HGMD				
I227L	HGMD	R380G	HGMD	E90K	HGMD	N629I	HGMD				
G229D	HGMD	R380S	HGMD	V94M	HGMD	N629K	HGMD				
R231C	HGMD	E385K	HGMD	E95G	HGMD	N629S	ClinVar, HGMD				
R231H	ClinVar, HGMD	S389P	HGMD	I96T	HGMD	N629T	HGMD				
I235N	ClinVar, HGMD	S389Y	HGMD	F98S	HGMD	V630A	HGMD				
L236R	HGMD	T391I	HGMD	Y99S	HGMD	V630L	HGMD				
L236P	HGMD	W392R	HGMD	R100Q	ClinVar, HGMD	S631A	HGMD				
L239P	HGMD	Y395S	ClinVar	R100W	HGMD	P632A	HGMD				
V241G	HGMD	K422T*	HGMD	K101E	HGMD	P632S	HGMD				
D242N	HGMD	T444M*	HGMD	D102A	HGMD	N633D	HGMD				
D242Y	HGMD	D446E*	HGMD	D102H	HGMD	N633I	HGMD				
R243C	ClinVar, HGMD	H455Y*	HGMD	D102V	HGMD	N633K	HGMD				
R243P	ClinVar, HGMD	R511W	HGMD	F106L	HGMD	N633S	HGMD				
G245V	HGMD	T513S	HGMD	F106Y	HGMD	T634A	HGMD				
W248C	HGMD	I517T	HGMD	C108R	HGMD	T634I	HGMD				
L250H	HGMD	M520R	HGMD	C108Y	HGMD	N635D	HGMD				
L250P	HGMD	Y522S	HGMD	L109R	HGMD	N635I	HGMD				
L251Q	HGMD	V524G	HGMD	L109P	HGMD	N635K	HGMD				
L251P	ClinVar, HGMD	A525T	HGMD	D111V	HGMD	E637D	HGMD				
G252D	HGMD	A525V	HGMD	P114S	HGMD	E637G	HGMD				
S253C	ClinVar	R539W	ClinVar, HGMD	M124R	HGMD	E637K	ClinVar, HGMD				
V254M	ClinVar, HGMD	E543K	HGMD	M124T	HGMD	K638N	HGMD				
V254L	HGMD	S546L	HGMD	F129I	HGMD	K638E	HGMD				
H258N	HGMD	Q547R	HGMD	D219V*	ClinVar	F640L	ClinVar, HGMD				
H258P	HGMD	G548D	HGMD	P334L*	ClinVar	F640V	HGMD				
H258R	ClinVar, HGMD	V554A	HGMD	I400N	HGMD	V644L	HGMD				
R259C	ClinVar, HGMD	R555C	ClinVar, HGMD	W410S	HGMD	V644F	HGMD				
R259L	ClinVar, HGMD	R555H	HGMD	L413P	HGMD	M645L	HGMD				
R259H	HGMD	R555S	HGMD	Y420C	HGMD	M645V	ClinVar, HGMD				
E261Q	HGMD	K557E	HGMD	A422D	HGMD	G648S	HGMD				
E261K	HGMD	R561G	HGMD	A422T	HGMD	S649P	HGMD				
E261V	HGMD	R562M	HGMD	P426H	HGMD	M651R	HGMD				
L262V	HGMD	R562S	HGMD	Y427C	HGMD	S654G	HGMD				
T265I	ClinVar, HGMD	L563P	HGMD	Y427H	HGMD	F656C	HGMD				
L266P	HGMD	S566F	HGMD	Y427S	HGMD	F656L	HGMD				
G269S	ClinVar, HGMD	S566P	HGMD	S428L	HGMD	G657R	HGMD				
G269D	ClinVar, HGMD	I567F	HGMD	S428P	HGMD	G657C	HGMD				
G272D	ClinVar	I567S	HGMD	A429P	HGMD	G657S	ClinVar, HGMD				
G272V	HGMD	I567T	HGMD	P451L	HGMD	I662T	HGMD				
L273F	ClinVar, HGMD	G568A	ClinVar, HGMD	D456Y	HGMD	R685H	HGMD				
L273R	HGMD	G568R	HGMD	L457P	HGMD	H687Y	HGMD				
F275S	HGMD	K569E*	HGMD	D460Y	HGMD	R694H	HGMD				
S277L	ClinVar, HGMD	S571L*	HGMD	F463L	HGMD	R696P	HGMD				
S277P	HGMD	F573L*	HGMD	D466Y	HGMD	S706C	HGMD				
S277W	HGMD	R583C*	HGMD	N470D	ClinVar, HGMD	A715V	HGMD				
Y278H	HGMD	R583G*	HGMD	T473N	HGMD	P721L	HGMD				
Y281C	HGMD	N586D	HGMD	T473P	HGMD	I728F	HGMD				
L282P	HGMD	N586S	HGMD	T474I	ClinVar, HGMD	R744P	HGMD				
A283T	HGMD	T587M	ClinVar, HGMD	Y475C	HGMD	R752Q	HGMD				
A302T	HGMD	G589D	ClinVar, HGMD	E480V	HGMD	R752W	HGMD				
A302V	HGMD	T587R	HGMD	I489F	HGMD	A753S	HGMD				
L303P	HGMD	A590T	HGMD	A490P	HGMD	K757N	HGMD				
W304R	HGMD	R591C	HGMD	A490T	ClinVar, HGMD	D767Y	HGMD				

(Continued)

TABLE 1 | Continued

KCNQ1				hERG				SCN5A			
Mutant	**Database**	**Mutant**	**Database**	**Mutant**	**Database**	**Mutant**	**Database**	**Mutant**	**Database**	**Mutant**	**Database**
W305R	HGMD	R591H	ClinVar, HGMD	H492Y	HGMD	V770A	HGMD				
W305L	ClinVar, HGMD	R591L	HGMD	Y493C	HGMD	D774Y	HGMD				
G306R	ClinVar, HGMD	R594Q	HGMD	Y493F	HGMD	G785A	HGMD				
G306V	HGMD	E596K	HGMD	Y493S	HGMD	G785V	HGMD				
V308D	HGMD	L602P	HGMD	W497L	HGMD	G785D	HGMD				
T309R	HGMD	I609N	HGMD	D501N	HGMD	E788D	HGMD				
T309I	HGMD	D611Y	HGMD	D501G	ClinVar, HGMD	E788K	HGMD				
V310I	HGMD	G635R*	HGMD	D501H	HGMD	V795I	HGMD				
T311A	HGMD			G522R	HGMD	G800A	ClinVar				
				K525N	HGMD	G800E	HGMD				
				R528P	HGMD	G800W	HGMD				
				R531Q	HGMD	M801I	ClinVar				
				R534C	ClinVar, HGMD	D803Y	HGMD				
				R534L	HGMD	F805C	HGMD				
				R537W	HGMD	F805S	ClinVar, HGMD				
				L552S	ClinVar, HGMD	G806E	ClinVar, HGMD				
				E544A	HGMD	P815L	HGMD				
				A558E	HGMD	G816V	HGMD				
				A558P	ClinVar, HGMD	S818L	HGMD				
				L559H	HGMD	S818P	HGMD				
				A561P	ClinVar, HGMD	S818W	HGMD				
				A561T	ClinVar, HGMD	G820E	HGMD				
				A561V	HGMD	G820R	ClinVar, HGMD				
				H562R	HGMD	V822I	ClinVar				
				W563C	HGMD	V822L	HGMD				
				W563G	HGMD	V822M	HGMD				
				L564P	HGMD	R823W	HGMD				
				A565T	HGMD	T826I	ClinVar, HGMD				
				C566F	HGMD	R835W	HGMD				
				C566S	HGMD	D837N	HGMD				
				W568R	HGMD	D837G	HGMD				
				W568C	HGMD	D837H	HGMD				
				Y569C	HGMD	D837Y	HGMD				
				Y569H	HGMD	V841L	HGMD				
				I571L	HGMD	P846T	HGMD				
				I571M	HGMD	I858T	HGMD				
				G572D	HGMD	N861H	HGMD				
				G572C	HGMD	N861I	ClinVar, HGMD				

*Curated mutations classified as pathogenic in the ClinVar (Harrison et al., 2016) and HGMD (Stenson et al., 2012) databases. Mutations were cross-referenced to remove any mutations with conflicting classifications. Asterisked mutations are not mapped onto the channel structures presented in **Figures 9–11** because those positions are not resolved in the final models. The Excel file for this table can be found as "**Table 1**" in the **Supplementary Material**.*

mutation, but also cellular quality control responses to these changes.

The VSD of hERG has fewer pathogenic mutations than that of KCNQ1 (**Figure 10B**), perhaps an indication that the hERG VSD has a higher folding stability. Indeed, when a set of hERG VSD mutations were assessed for membrane insertion efficiency, the majority of mutations were predicted to have no change in the free energy of insertion (Anderson et al., 2014). However, there are a surprising number of disease mutations at the extracellular interface between S1 and S5, specifically at the A422, P426, Y427, S428, H562, W563, C566, and Y569 positions (**Figures 10B, C**). This interface has not been studied extensively. However, we speculate that it may be important to channel stability by providing an additional contact surface between the VSD and the PD distinct from the S4–S5 linker. Destabilization of this interface may therefore lead to mistrafficking. Mutation Indeed, A422T results in ER retention but was rescued with a pharmacological chaperone (Guo et al., 2012). Other mutations in S1 alter gating properties in addition to trafficking (Anderson et al., 2014; Phan et al., 2017), indicating that gating properties may also be affected. Further studies are needed to determine the impact of mutations in this interface on folding, trafficking, and gating properties of hERG.

A number of mutations are found in the PAS and CNBHD, particularly in the PAS and at the interface between the two domains (**Figures 10A, D**). The structural stability of both domains impacts trafficking (Akhavan et al., 2005; Harley et al., 2012; Ke et al., 2013; Ke et al., 2014), and several trafficking-defective mutants have been characterized at the PAS/CNBHD interface (F29L, I31S, I42N, Y43C, R56Q, M124R), suggesting that occlusion of a PAS hydrophobic patch from the cytoplasm through interaction with the CNBHD is critical for proper trafficking (Ke et al., 2013). Trafficking defects due to destabilization of the PAS, the CNBHD, or their interaction may thus be a prominent mechanism

in LQT2. The direct interaction of these two domains has also been implicated in slow deactivation of the channel (Ng et al., 2014; Kume et al., 2018), as deactivation defects have been noted in channels with mutations at this interface (Anderson et al., 2014). Deactivation defects may be a secondary source of LQT2. Detailed structural analysis of mutation-induced destabilization of the PAS and the CNBHD as well as studies of cellular responses to PAS/CNBHD destabilization would be highly informative to our understanding of LQT2. Indeed, similar studies have already revealed differential cellular responses to LQT2 PAS mutations, depending on the severity of PAS destabilization (Foo et al., 2019).

SCN5A

LQT3 mutations induce channel gain-of-function in SCN5A (Wilde and Amin, 2018; Skinner et al., 2019). Accordingly, mutations that interfere with SCN5A folding and trafficking do not cause LQT3 (Bohnen et al., 2017; Wilde and Amin, 2018). The primary mechanism leading to LQT3 is rather impairment of fast inactivation (Bohnen et al., 2017; Wilde and Amin, 2018). The results of our analysis are consistent with this notion. The site where the S5 and S6 helices of repeats III and IV cross, in the binding pocket for the IFM motif, contains the majority of the mutations curated in this study (**Figures 11A, C**). These mutations may impact interaction of the IFM motif with other channel structures, hindering fast inactivation and generating a persistent sodium current. For instance, A1326 (A1328 in rSCN5A) and G1329 (G1331 in rSCN5A) make critical backbone interactions to help form a tight hydrophobic pocket for IFM interactions (Jiang et al., 2020). Mutations A1326P and G1329S (**Table 1**) may thus compromise the stability of this pocket, hindering inactivation. Additionally, S6 mutations surrounding this putative inactivation gate also map to the constriction site of the channel pore, with additional mutations in $S6_I$ and $S6_{II}$ (**Figure 11D**). It has been proposed that binding of the IFM motif causes a rotation in the S6 helices that closes the pore (Yan et al., 2017b). Therefore mutations in S6 may also alter inactivation by preventing helix rotation. Indeed, residues important to defining the constriction site of the $Na_v1.7$ pore cause LQTS upon mutation in SCN5A (L398 and Y1755) (Shen et al., 2019). A few mutations also map to the CTD of SCN5A (**Figure 11B**), which could alter interactions with the III/IV linker and hinder fast inactivation.

The recent structure of the rat homolog of SCN5A (Jiang et al., 2020) suggests another gain-of-function mechanism, namely that VSD mutant R225P could promote current leak through the VSD (gating pore current). Experimental evidence supporting this mechanism exists for other SCN5A (Moreau et al., 2015) and $Na_V1.4$ (Sokolov et al., 2007) VSD mutations.

STRUCTURAL BASIS FOR CHANNEL PHARMACOLOGY

Pharmacological management of LQTS aims to minimize symptomatic arrhythmia and prevent life-threatening cardiac events. According to consensus guidelines (Zipes et al., 2006; Priori et al., 2013), treatment with β-blockers is beneficial and effective in the case of LQTS diagnosis, but should be considered only after additional diagnostics for carriers of LQTS mutations. β-blockers work by inhibiting β-adrenergic receptors, consequently slowing heart rate and preventing arrhythmias triggered by activation of the sympathetic nervous system (Bohnen et al., 2017). However, the efficacy of β-blockers is strongly genotype- and trigger-specific (Moss et al., 2000; Schwartz et al., 2001; Bohnen et al., 2017). β-blockers reduce the risk of exercise-induced arrhythmia by 78% and 71% in patients with LQT1 and LQT2, respectively, but neither are protective against cardiac events triggered by emotional arousal or during rest (Kim et al., 2010; Goldenberg et al., 2012). Patients with LQT3 tend to experience the highest breakthrough rate for cardiac events (10–15%) with β-blocker treatment (Giudicessi and Ackerman, 2013). Use of local anesthetic-type anti-arrhythmic agents (e.g. mexiletine) for clinical treatment of LQT3, however, can be accompanied by undesirable side effects (Moreno et al., 2011). The need for improved LQTS pharmacotherapy is further supported by the difficulties surrounding hERG modulation, as several clinically-used drugs can cause drug-induced LQTS by blocking hERG and suppressing I_{Kr} (Vandenberg et al., 2012; Kalyaanamoorthy and Barakat, 2018). This section summarizes some known pharmacological agents and the modes of interaction with KCNQ1, hERG, and SCN5A. Special focus is dedicated toward unique structural features of hERG that have been implicated in the promiscuity of this channel for pro-arrhythmic drugs.

KCNQ1

KCNQ1 channels are targeted by several non-selective anti-arrhythmic drugs such as quinidine (Balser et al., 1991), amiodarone (Balser et al., 1991; Kamiya et al., 2001), azimilide (Busch et al., 1997), and clofilium (Yang et al., 1997). More specific KCNQ1 blockers include chromanol 293B (Bosch et al., 1998), and the benzodiazepine L-735821 (Lengyel et al., 2001). The binding site of L-735821 has been located to the SF and S6 (Seebohm et al., 2003a).

Benzodiazepine R-L3 was the first KCNQ1 activator to be described. The compound acts to slow the deactivation rate and causes a hyperpolarizing shift in the voltage-dependence of channel activation (Salata et al., 1998). R-L3 appears to bind residues on S5 and S6 lining the membrane-exposed surface of the PD (Seebohm et al., 2003b) rather than to the inner channel cavity. Drug binding outside of the PD cavity was also reported for quinidine (Yang et al., 2013), which occupies a pocket between S6 and the S4–S5 linker and is postulated to elicit an allosteric channel blocking mechanism. More recently, ML277 was identified as a potent KCNQ1 agonist (Mattmann et al., 2012). ML277 has been proposed to bind to a side pocket surrounded by the S2–S3 and S4–S5 linkers on the intracellular side and helices S4 and S6 on the intramembrane lateral side (Xu et al., 2015). Binding of ML277 may selectively alter VSD/PD coupling to stabilize the AO state relative to the IO state (Hou et al., 2019).

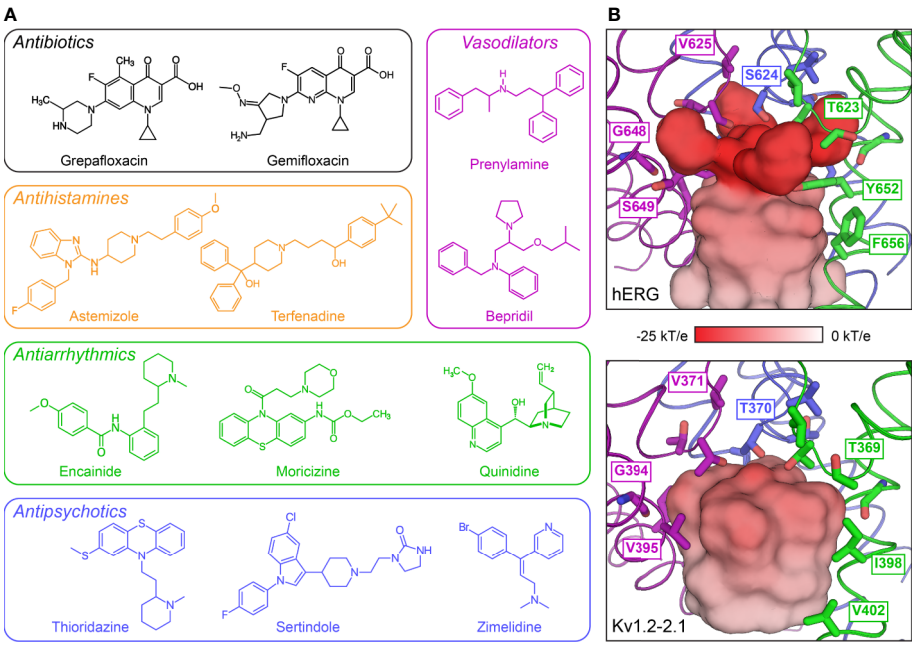

FIGURE 12 | Structural features of the drug-binding cavity of the hERG channel pore. **(A)** Examples of drugs discontinued by the US FDA because of side effects related to hERG inhibition (adapted from **Table 1** in (Kalyaanamoorthy and Barakat, 2018)). **(B)** Internal molecular surface of the central cavity below the SF in hERG (PDB: 5VA1)(Wang and Mackinnon, 2017) (top) and the $K_V1.2$–2.1 chimeric channel (PDB: 2R9R)(Long et al., 2007) (bottom). The surface is colored by the electrostatic potential calculated with the APBS tool in PyMOL (The PyMOL Molecular Graphics System, Version 2.2 Schrödinger, LLC.). Residues related to drug binding by hERG and the corresponding residues in the $K_V1.2$–2.1 structure are shown as sticks. This panel is inspired by **Figure 5** in (Wang and Mackinnon, 2017).

hERG

hERG channels can be blocked by a wide spectrum of compounds, leading to drug-induced LQTS (Cubeddu, 2016). The list of drugs that inhibit hERG includes, among others, antibiotics (grepafloxacin (Bischoff et al., 2000)), antihistamines (astemizole (Zhou et al., 1999)), anti-arrhythmics (quinidine (Roden et al., 1986), dofetilide (Jurkiewicz and Sanguinetti, 1993)), antipsychotics (sertindole (Rampe et al., 1998)), and gastroprokinetic agents (cisapride (Vitola et al., 1998)) (**Figure 12A**). Several prescription drugs have been withdrawn from the market because of cardiotoxic side effects triggered by off-target interaction with hERG (Kalyaanamoorthy and Barakat, 2018). In fact, an estimated 15% of drugs still on the market may cause QT phase prolongation, and 60% of drugs in development show hERG liability (Vandenberg et al., 2017). It is now required by the US FDA that all compounds considered for advancement to clinical trials be tested for their impact on hERG channel function as part of preclinical toxicity assessments (Center for Drug Evaluation and Research, 2005a; Center for Drug Evaluation and Research, I.C.O.H., 2005b).

Considerable progress has been made in understanding the basic features of drug binding to hERG, and a plausible mechanism for promiscuity of drug binding has emerged. Pro-arrhythmic drugs commonly bind to the central inner cavity of the PD in hERG. Two pore-lining aromatic residues in S6 (Y652 and F656) are the most crucial for drug binding (Mitcheson et al., 2000), although additional residues at the end of the pore helix (T623, S624, and V625) contribute to binding for some drugs (Mitcheson et al., 2000), and mutations at F557 in the S5 helix can also affect binding (Saxena et al., 2016). The side chains of the S6 and pore helix residues point towards a putative drug binding site located in the central cavity below the SF. This cavity is slightly narrower in hERG than in the Shaker family $K_V1.2$–2.1 chimeric channel (Long et al., 2007). As a consequence, there is a greater negative electrostatic potential in this region (Wang and Mackinnon, 2017), which could enhance drug binding capabilities (**Figure 12B**). In addition, four lateral hydrophobic pockets, which are not observed in the $K_V1.2$–2.1 structure, extend outwards from that central constriction site, generating additional space to trap chemical moieties (Wang and Mackinnon, 2017).

Quantitative structure-activity relationship studies have identified a pharmacophore for drugs that bind to hERG (Cavalli et al., 2002). The pharmacophore consists of three centers of mass (usually aromatic rings) and an amino group that together form a flattened tetrahedron. It has been suggested that the aromatic rings could fit into one or more lateral hydrophobic pockets in hERG and/or bind by pi-pi stacking or hydrophobic interactions with Y652 and F656 (Chen et al., 2002). Likewise, the greater negative electrostatic potential in the central cavity could explain why many drugs that bind hERG, including off-targets, contain a positive charge (Fernandez et al., 2004). Additionally, a number of docking models for drug-

bound hERG, with and without this pharmacophore, are being generated (Wacker et al., 2017; Helliwell et al., 2018; Negami et al., 2019), making possible further delineation of drug binding modes within this pocket and the structural basis of their affinity for hERG.

The majority of high-affinity drugs that bind hERG off-target preferentially bind to the inactivated state rather the open state, with affinity differences ranging from 2- to 100-fold (Perrin et al., 2008). Interestingly, the related EAG1 channel (Whicher and Mackinnon, 2016) is less sensitive to inhibition by most of hERG-blocking drugs even though they share the same pore-lining aromatic residues. One major difference between hERG and EAG1 is that EAG1 channels undergo minimal inactivation (Garg et al., 2012) whereas hERG channels undergo rapid and complete inactivation (Vandenberg et al., 2012). The contribution of inactivation to high-affinity binding is further substantiated by the observation that inactivating EAG1–hERG chimeras, containing the upper half of the hERG PD, can bind drugs with almost hERG-like affinity (Herzberg et al., 1998). While cryo-EM structures have been determined for both hERG and EAG1 (Whicher and Mackinnon, 2016; Wang and Mackinnon, 2017), the structural basis of the functional and pharmacological differences requires higher resolution (Wang and Mackinnon, 2017).

SCN5A

Limited progress has been made in the development of SCN5A-targeted treatment strategies. Classical non-selective sodium channel blockers like the Vaughan-Williams class I anti-arrhythmic drugs quinidine, lidocaine, and propafenone have only limited clinical applicability. Ranolazine is a more selective SCN5A blocker (Belardinelli et al., 2006; Zaza et al., 2008) and has been shown to attenuate action potential duration and reduce or prevent intracellular calcium overload in LQT3 models (Wu et al., 2004; Lindegger et al., 2009). Mexiletine is a potent inhibitor of SCN5A and may be beneficial for treatment of LQT3 (Mazzanti et al., 2016), but effectiveness may depend on the baseline QT prolongation of the mutant channel (Li and Zhang, 2018).

Despite the clinical relevance of SCN5A-targeting drugs, the molecular mechanisms of promising and potentially problematic drugs are not well understood at a structural level, hindering drug design. However, key residues for apparent drug binding have been suggested within the sodium channel pore domain. Specifically, mutations of two conserved aromatic residues in $S6_{IV}$, F1760 and Y1767, (Ragsdale et al., 1994; Ragsdale et al., 1996) or other S6 residues in repeats I and III (Yarov-Yarovoy et al., 2001; Yarov-Yarovoy et al., 2002) may affect drug binding. Using fluorinated phenylalanine derivatives incorporated at F1760 (Pless et al., 2011a), a strong cation-pi interaction between F1760 and the protonated amine group in class Ib anti-arrhythmic drugs was observed, defining the molecular basis for inhibition of SCN5A by this group of drugs. Additionally, mutations within the SF region can affect apparent drug binding either by enhancing slow inactivation or forming an alternative access pathway (Sunami et al., 1997; Lee et al., 2001; Tsang et al., 2005). Interactions of anti-arrhythmic and local anesthetic drugs (lidocaine, QX-314, etidocaine, flecainide, and ranolazine) docked into an inactivated state model of SCN5A (Nguyen et al., 2019) revealed several key drug binding sites in the inner pore lumen that can simultaneously accommodate up to two drug molecules. Subsequent MD simulations suggested alternative access mechanisms for drugs into the SCN5A lumen – a hydrophilic pathway through the intracellular gate and a hydrophobic pathway through a membrane-exposed fenestration between repeats III and IV.

The recent structure of rat $Na_v1.5$ (Jiang et al., 2020) has provided insight into the binding mode of the class Ic anti-arrhythmic drug flecainide, which has higher affinity for the open conformation of SCN5A (Ramos and O'leary M, 2004). Flecainide binds in the central cavity on the intracellular side of the SF. The piperidine ring of flecainide lies across the top of the central cavity with the positively-charged nitrogen pointing towards the exit of the SF and its hydrophobic edge extending towards the phenyl ring of F1762 (F1760 in human $Na_v1.5$). The trifluoroethoxy tails of flecainide extend into fenestrations formed between the pore helices of repeats I and II as well as repeats II and III, through which the central cavity is accessible from the lipid bilayer. These fenestrations represent possible entry points for flecainide and similar class Ic drugs.

FUTURE DIRECTIONS

The growing number of structural and functional studies of KCNQ1, hERG, and SCN5A have provided new insight into channel molecular physiology and channel dysfunction in congenital LQTS. This further motivates the study of fundamental biophysical mechanisms in ion channels. One of these mechanisms, electromechanical coupling, remains enigmatic due to a dearth of experimental resting state structures and robust methods to identify allosteric pathways, which cannot easily be discerned from ion channel structures resolved in a single conformation. However, interaction energy and MD dynamical network analysis in the Shaker K^+ channel (Fernandez-Marino et al., 2018) has suggested that movements in the VSD and PD are linked by two distinct pathways – a canonical pathway through the S4–S5 linker and a hitherto unknown non-canonical pathway involving contacts at the interface between S4 and S5. Such work may provide a useful alternative approach to explore electromechanical coupling in detail.

Another major effort involves the experimental characterization of hundreds of previously uncharacterized variants of unknown significance (VUS) and LQTS mutations in KCNQ1, hERG, and SCN5A. Widespread use of whole genome and exome sequencing has provided a nearly complete catalog of common sequence variations in protein-coding genes (Lek et al., 2016), although rare sequence variants continue to be discovered. For many LQTS mutations, the molecular mechanisms responsible for impaired channel function remain poorly understood. Such mutations may cause potassium channel loss-of-function or dysfunction by promoting misfolding, mistrafficking, aggregation, or improper gating of the channel protein, as discussed above. Continued experimental testing will be required to complete functional annotation of KCNQ1, hERG, and SCN5A variants

and to elucidate how these mutations lead to channel dysfunction. In this regard, new techniques such as high-throughput patch clamp recording (Vanoye et al., 2018; Toh et al., 2020), which allows rapid screening of ion channel variants found in patients, and the use of induced-pluripotent stem cell-derived cardiomyocytes (Moretti et al., 2010; Ma et al., 2013; Terrenoire et al., 2013; Jouni et al., 2015) developed from cells of healthy or mutation-carrying patients, represent helpful tools for large-scale examination of ion channel variants.

Finally, experimentally-informed bioinformatics and modeling approaches are being developed to predict variant pathogenicity (Kroncke et al., 2015; Li et al., 2017; Kroncke et al., 2019). These computational algorithms can help to decrypt newly discovered VUS for which there is not enough data to determine pathogenicity. Decrypting VUS can inform medical practice and has the potential to improve LQTS therapy, both for the prevention of cardiac events in susceptible patients and as a basis for avoiding unneeded treatment in healthy patients. With improved understanding of the molecular pathophysiology and the role of mutations associated with distinct LQTS subtypes, the ultimate hope is that identifying a patient's genotype will lead to more specific treatment considerations and the delivery of optimal care.

AUTHOR CONTRIBUTIONS

KB and GK wrote the primary draft of this article, with edits by KB, GK, JM, CV, AG, and CS. KB and GK contributed equally to this manuscript.

FUNDING

This work was supported by US NIH grant RO1 HL122010. GK was supported by a postdoctoral fellowship from the American Heart Association (18POST34080422) and KB was supported by NIH training grant T32 GM008320.

SUPPLEMENTARY MATERIAL

The Supplementary Material for this article can be found online at: https://www.frontiersin.org/articles/10.3389/fphar.2020.00550/full#supplementary-material

TABLE 1 | LQTS mutations in KCNQ1, hERG, and SCN5A.

REFERENCES

Abbott, G. W., Sesti, F., Splawski, I., Buck, M. E., Lehmann, M. H., Timothy, K. W., et al. (1999). MiRP1 forms IKr potassium channels with HERG and is associated with cardiac arrhythmia. *Cell* 97, 175–187. doi: 10.1016/S0092-8674(00)80728-X

Abbott, G. W., Xu, X., and Roepke, T. K. (2007). Impact of ancillary subunits on ventricular repolarization. *J. Electrocardiol.* 40, S42–S46. doi: 10.1016/j.jelectrocard.2007.05.021

Abbott, G. W. (2014). Biology of the KCNQ1 Potassium Channel. *New J. Sci.* 2014, 26. doi: 10.1155/2014/237431

Ackerman, M. J. (2005). Genotype-phenotype relationships in congenital long QT syndrome. *J. Electrocardiol.* 38, 64–68. doi: 10.1016/j.jelectrocard.2005.06.018

Adler, A., Novelli, V., Amin, A. S., Abiusi, E., Care, M., Nannenberg, E. A., et al. (2020). An International, Multicentered, Evidence-Based Reappraisal of Genes Reported to Cause Congenital Long QT Syndrome. *Circulation* 141, 418–428. doi: 10.1161/CIRCULATIONAHA.119.043132

Aggarwal, S. K., and Mackinnon, R. (1996). Contribution of the S4 segment to gating charge in the Shaker K+ channel. *Neuron* 16, 1169–1177. doi: 10.1016/S0896-6273(00)80143-9

Ahern, C. A., Payandeh, J., Bosmans, F., and Chanda, B. (2016). The hitchhiker's guide to the voltage-gated sodium channel galaxy. *J. Gen. Physiol.* 147, 1–24. doi: 10.1085/jgp.201511492

Akhavan, A., Atanasiu, R., Noguchi, T., Han, W., Holder, N., and Shrier, A. (2005). Identification of the cyclic-nucleotide-binding domain as a conserved determinant of ion-channel cell-surface localization. *J. Cell Sci.* 118, 2803–2812. doi: 10.1242/jcs.02423

Anantharam, A., and Abbott, G. W. (2005). Does hERG coassemble with a beta subunit? Evidence for roles of MinK and MiRP1. *Novartis Found Symp* 266, 100–112discussion 112–107, 155-108. doi: 10.1002/047002142X.ch9

Anderson, C. L., Kuzmicki, C. E., Childs, R. R., Hintz, C. J., Delisle, B. P., and January, C. T. (2014). Large-scale mutational analysis of Kv11.1 reveals molecular insights into type 2 long QT syndrome. *Nat. Commun.* 5, 5535. doi: 10.1038/ncomms6535

Apaja, P. M., Foo, B., Okiyoneda, T., Valinsky, W. C., Barriere, H., Atanasiu, R., et al. (2013). Ubiquitination-dependent quality control of hERG K+ channel with acquired and inherited conformational defect at the plasma membrane. *Mol. Biol. Cell* 24, 3787–3804. doi: 10.1091/mbc.e13-07-0417

Balser, J. R., Bennett, P. B., Hondeghem, L. M., and Roden, D. M. (1991). Suppression of Time-Dependent Outward Current in Guinea-Pig Ventricular Myocytes - Actions of Quinidine and Amiodarone. *Circ. Res.* 69, 519–529. doi: 10.1161/01.RES.69.2.519

Barhanin, J., Lesage, F., Guillemare, E., Fink, M., Lazdunski, M., and Romey, G. (1996). K(v)LQT1 and IsK (minK) proteins associate to form the I-Ks cardiac potassium current. *Nature* 384, 78–80. doi: 10.1038/384078a0

Baroni, D., Picco, C., Barbieri, R., and Moran, O. (2014). Antisense-mediated post-transcriptional silencing of SCN1B gene modulates sodium channel functional expression. *Biol. Cell* 106, 13–29. doi: 10.1111/boc.201300040

Barros, F., Dominguez, P., and De La Pena, P. (2018). Relative positioning of Kv11.1 (hERG) K(+) channel cytoplasmic domain-located fluorescent tags toward the plasma membrane. *Sci. Rep.* 8, 15494. doi: 10.1038/s41598-018-33492-x

Barros, F., Pardo, L. A., Dominguez, P., Sierra, L. M., and De La Pena, P. (2019). New Structures and Gating of Voltage-Dependent Potassium (Kv) Channels and Their Relatives: A Multi-Domain and Dynamic Question. *Int. J. Mol. Sci.* 20, pii: E248. doi: 10.3390/ijms20020248

Barro-Soria, R., Rebolledo, S., Liin, S. I., Perez, M. E., Sampson, K. J., Kass, R. S., et al. (2014). KCNE1 divides the voltage sensor movement in KCNQ1/KCNE1 channels into two steps. *Nat. Commun.* 5, 3750. doi: 10.1038/ncomms4750

Barro-Soria, R., Ramentol, R., Liin, S. I., Perez, M. E., Kass, R. S., and Larsson, H. P. (2017). KCNE1 and KCNE3 modulate KCNQ1 channels by affecting different gating transitions. *Proc. Natl. Acad. Sci. U. S. A* 114, E7367–E7376. doi: 10.1073/pnas.1710335114

Belardinelli, L., Shryock, J. C., and Fraser, H. (2006). Inhibition of the late sodium current as a potential cardioprotective principle: effects of the late sodium current inhibitor ranolazine. *Heart* 92 Suppl 4, iv6–iv14. doi: 10.1136/hrt.2005.078790

Bernardo-Seisdedos, G., Nunez, E., Gomis-Perez, C., Malo, C., Villarroel, A., and Millet, O. (2018). Structural basis and energy landscape for the Ca(2+) gating and calmodulation of the Kv7.2 K(+) channel. *Proc. Natl. Acad. Sci. U. S. A* 115, 2395–2400. doi: 10.1073/pnas.1800235115

Bezanilla, F. (2005). Voltage-gated ion channels. *IEEE Trans. Nanobiosci.* 4, 34–48. doi: 10.1109/TNB.2004.842463

Bhate, M. P., Wylie, B. J., Tian, L., and Mcdermott, A. E. (2010). Conformational dynamics in the selectivity filter of KcsA in response to potassium ion concentration. *J. Mol. Biol.* 401, 155–166. doi: 10.1016/j.jmb.2010.06.031

Bian, J., Cui, J., and Mcdonald, T. V. (2001). HERG K(+) channel activity is regulated by changes in phosphatidyl inositol 4,5-bisphosphate. *Circ. Res.* 89, 1168–1176. doi: 10.1161/hh2401.101375

Bian, J. S., Kagan, A., and Mcdonald, T. V. (2004). Molecular analysis of PIP2 regulation of HERG and IKr. *Am. J. Physiol. Heart Circ. Physiol.* 287, H2154–H2163. doi: 10.1152/ajpheart.00120.2004

Bidaud, I., and Lory, P. (2011). Hallmarks of the channelopathies associated with L-type calcium channels: a focus on the Timothy mutations in Ca(v)1.2 channels. *Biochimie* 93, 2080–2086. doi: 10.1016/j.biochi.2011.05.015

Bischoff, U., Schmidt, C., Netzer, R., and Pongs, O. (2000). Effects of fluoroquinolones on HERG currents. *Eur. J. Pharmacol.* 406, 341–343. doi: 10.1016/S0014-2999(00)00693-2

Bohnen, M. S., Peng, G., Robey, S. H., Terrenoire, C., Iyer, V., Sampson, K. J., et al. (2017). Molecular Pathophysiology of Congenital Long QT Syndrome. *Physiol. Rev.* 97, 89–134. doi: 10.1152/physrev.00008.2016

Boland, L. M., and Drzewiecki, M. M. (2008). Polyunsaturated fatty acid modulation of voltage-gated ion channels. *Cell Biochem. Biophys.* 52, 59–84. doi: 10.1007/s12013-008-9027-2

Bosch, R. F., Gaspo, R., Busch, A. E., Lang, H. J., Li, G. R., and Nattel, S. (1998). Effects of the chromanol 293B, a selective blocker of the slow, component of the delayed rectifier K+ current, on repolarization in human and guinea pig ventricular myocytes. *Cardiovasc. Res.* 38, 441–450. doi: 10.1016/S0008-6363(98)00021-2

Boulet, I. R., Raes, A. L., Ottschytsch, N., and Snyders, D. J. (2006). Functional effects of a KCNQ1 mutation associated with the long QT syndrome. *Cardiovasc. Res.* 70, 466–474. doi: 10.1016/j.cardiores.2006.02.006

Boulet, I. R., Labro, A. J., Raes, A. L., and Snyders, D. J. (2007). Role of the S6 C-terminus in KCNQ1 channel gating. *J. Physiol.* 585, 325–337. doi: 10.1113/jphysiol.2007.145813

Brackenbury, W. J., and Isom, L. L. (2011). Na Channel beta Subunits: Overachievers of the Ion Channel Family. *Front. Pharmacol.* 2, 53. doi: 10.3389/fphar.2011.00053

Burgess, D. E., Bartos, D. C., Reloj, A. R., Campbell, K. S., Johnson, J. N., Tester, D. J., et al. (2012). High-risk long QT syndrome mutations in the Kv7.1 (KCNQ1) pore disrupt the molecular basis for rapid K(+) permeation. *Biochemistry* 51, 9076–9085. doi: 10.1021/bi3009449

Busch, A. E., Busch, G. L., Ford, E., Suessbrich, H., Lang, H. J., Greger, R., et al. (1997). The role of the IsK protein in the specific pharmacological properties of the IKs channel complex. *Br. J. Pharmacol.* 122, 187–189. doi: 10.1038/sj.bjp.0701434

Calhoun, J. D., and Isom, L. L. (2014). The role of non-pore-forming beta subunits in physiology and pathophysiology of voltage-gated sodium channels. *Handb. Exp. Pharmacol.* 221, 51–89. doi: 10.1007/978-3-642-41588-3_4

Capes, D. L., Goldschen-Ohm, M. P., Arcisio-Miranda, M., Bezanilla, F., and Chanda, B. (2013). Domain IV voltage-sensor movement is both sufficient and rate limiting for fast inactivation in sodium channels. *J. Gen. Physiol.* 142, 101–112. doi: 10.1085/jgp.201310998

Catterall, W. A. (1986). Molecular properties of voltage-sensitive sodium channels. *Annu. Rev. Biochem.* 55, 953–985. doi: 10.1146/annurev.bi.55.070186.004513

Cavalli, A., Poluzzi, E., De Ponti, F., and Recanatini, M. (2002). Toward a pharmacophore for drugs inducing the long QT syndrome: insights from a CoMFA study of HERG K(+) channel blockers. *J. Med. Chem.* 45, 3844–3853. doi: 10.1021/jm0208875

Chakrabarti, N., Ing, C., Payandeh, J., Zheng, N., Catterall, W. A., and Pomes, R. (2013). Catalysis of Na+ permeation in the bacterial sodium channel Na(V)Ab. *Proc. Natl. Acad. Sci. U. S. A* 110, 11331–11336. doi: 10.1073/pnas.1309452110

Chan, P. J., Osteen, J. D., Xiong, D., Bohnen, M. S., Doshi, D., Sampson, K. J., et al. (2012). Characterization of KCNQ1 atrial fibrillation mutations reveals distinct dependence on KCNE1. *J. Gen. Physiol.* 139, 135–144. doi: 10.1085/jgp.201110672

Chanda, B., and Bezanilla, F. (2002). Tracking voltage-dependent conformational changes in skeletal muscle sodium channel during activation. *J. Gen. Physiol.* 120, 629–645. doi: 10.1085/jgp.20028679

Chang, A., Abderemane-Ali, F., Hura, G. L., Rossen, N. D., Gate, R. E., and Minor, D. L.Jr. (2018). A Calmodulin C-Lobe Ca(2+)-Dependent Switch Governs Kv7 Channel Function. *Neuron* 97, 836–852 e836. doi: 10.1016/j.neuron.2018.01.035

Chen, J., Seebohm, G., and Sanguinetti, M. C. (2002). Position of aromatic residues in the S6 domain, not inactivation, dictates cisapride sensitivity of HERG and eag potassium channels. *Proc. Natl. Acad. Sci. U. S. A* 99, 12461–12466. doi: 10.1073/pnas.192367299

Chen, J., Weber, M., Um, S. Y., Walsh, C. A., Tang, Y., and Mcdonald, T. V. (2011). A dual mechanism for I(Ks) current reduction by the pathogenic mutation KCNQ1-S277L. *Pacing Clin. Electrophysiol.* 34, 1652–1664. doi: 10.1111/j.1540-8159.2011.03190.x

Chen, L., Zhang, Q., Qiu, Y., Li, Z., Chen, Z., Jiang, H., et al. (2015). Migration of PIP2 lipids on voltage-gated potassium channel surface influences channel deactivation. *Sci. Rep.* 5, 15079. doi: 10.1038/srep15079

Chen, X. M., Guo, K., Li, H., Lu, Q. F., Yang, C., Yu, Y., et al. (2019). A novel mutation KCNQ1p.Thr312del is responsible for long QT syndrome type 1. *Heart Vessels* 34, 177–188. doi: 10.1007/s00380-018-1223-4

Cheng, Y. M., and Claydon, T. W. (2012). Voltage-dependent gating of HERG potassium channels. *Front. Pharmacol.* 3, 83. doi: 10.3389/fphar.2012.00083

Cheng, J. H., and Kodama, I. (2004). Two components of delayed rectifier K+ current in heart: molecular basis, functional diversity, and contribution to repolarization. *Acta Pharmacol. Sin.* 25, 137–145.

Choveau, F. S., and Shapiro, M. S. (2012). Regions of KCNQ K(+) channels controlling functional expression. *Front. Physiol.* 3, 397. doi: 10.3389/fphys.2012.00397

Chung, D. Y., Chan, P. J., Bankston, J. R., Yang, L., Liu, G., Marx, S. O., et al. (2009). Location of KCNE1 relative to KCNQ1 in the I(KS) potassium channel by disulfide cross-linking of substituted cysteines. *Proc. Natl. Acad. Sci. U. S. A* 106, 743–748. doi: 10.1073/pnas.0811897106

Clairfeuille, T., Cloake, A., Infield, D. T., Llongueras, J. P., Arthur, C. P., Li, Z. R., et al. (2019). Structural basis of alpha-scorpion toxin action on Nav channels. *Science* 363, pii: eaav8573. doi: 10.1126/science.aav8573

Codding, S. J., and Trudeau, M. C. (2019). The hERG potassium channel intrinsic ligand regulates N- and C-terminal interactions and channel closure. *J. Gen. Physiol.* 151, 478–488. doi: 10.1085/jgp.201812129

Cubeddu, L. X. (2016). Drug-induced Inhibition and Trafficking Disruption of ion Channels: Pathogenesis of QT Abnormalities and Drug-induced Fatal Arrhythmias. *Curr. Cardiol. Rev.* 12, 141–154. doi: 10.2174/1573403X12666160301120217

Cuello, L. G., Jogini, V., Cortes, D. M., and Perozo, E. (2010). Structural mechanism of C-type inactivation in K(+) channels. *Nature* 466, 203–208. doi: 10.1038/nature09153

Cui, J. (2016). Voltage-Dependent Gating: Novel Insights from KCNQ1 Channels. *Biophys. J.* 110, 14–25. doi: 10.1016/j.bpj.2015.11.023

De La Pena, P., Alonso-Ron, C., Machin, A., Fernandez-Trillo, J., Carretero, L., Dominguez, P., et al. (2011). Demonstration of physical proximity between the N terminus and the S4-S5 linker of the human ether-a-go-go-related gene (hERG) potassium channel. *J. Biol. Chem.* 286, 19065–19075. doi: 10.1074/jbc.M111.238899

Dehghani-Samani, A., Madreseh-Ghahfarokhi, S., and Dehghani-Samani, A. (2019). Mutations of Voltage-Gated Ionic Channels and Risk of Severe Cardiac Arrhythmias. *Acta Cardiol. Sin.* 35, 99–110. doi: 10.6515/ACS.201903_35(2).20181028A

Detta, N., Frisso, G., and Salvatore, F. (2015). The multi-faceted aspects of the complex cardiac Nav1.5 protein in membrane function and pathophysiology. *Biochim. Biophys. Acta* 1854, 1502–1509. doi: 10.1016/j.bbapap.2015.07.009

Dhar Malhotra, J., Chen, C., Rivolta, I., Abriel, H., Malhotra, R., Mattei, L. N., et al. (2001). Characterization of sodium channel alpha- and beta-subunits in rat and mouse cardiac myocytes. *Circulation* 103, 1303–1310. doi: 10.1161/01.CIR.103.9.1303

Doolan, G. K., Panchal, R. G., Fonnes, E. L., Clarke, A. L., Williams, D. A., and Petrou, S. (2002). Fatty acid augmentation of the cardiac slowly activating delayed rectifier current (IKs) is conferred by hminK. *FASEB J.* 16, 1662–1664. doi: 10.1096/fj.02-0084fje

Doyle, D. A., Morais Cabral, J., Pfuetzner, R. A., Kuo, A., Gulbis, J. M., Cohen, S. L., et al. (1998). The structure of the potassium channel: molecular basis of K+ conduction and selectivity. *Science* 280, 69–77. doi: 10.1126/science.280.5360.6923

Earle, N., Crawford, J., Smith, W., Hayes, I., Shelling, A., Hood, M., et al. (2013). Community detection of long QT syndrome with a clinical registry: an alternative to ECG screening programs? *Heart Rhythm.* 10, 233–238. doi: 10.1016/j.hrthm.2012.10.043

Eckey, K., Wrobel, E., Strutz-Seebohm, N., Pott, L., Schmitt, N., and Seebohm, G. (2014). Novel Kv7.1-phosphatidylinositol 4,5-bisphosphate interaction sites uncovered by charge neutralization scanning. *J. Biol. Chem.* 289, 22749–22758. doi: 10.1074/jbc.M114.589796

Fan, J. S., Jiang, M., Dun, W., Mcdonald, T. V., and Tseng, G. N. (1999). Effects of outer mouth mutations on hERG channel function: a comparison with similar mutations in the Shaker channel. *Biophys. J.* 76, 3128–3140. doi: 10.1016/S0006-3495(99)77464-3

Favre, I., Moczydlowski, E., and Schild, L. (1996). On the structural basis for ionic selectivity among Na+, K+, and Ca2+ in the voltage-gated sodium channel. *Biophys. J.* 71, 3110–3125. doi: 10.1016/S0006-3495(96)79505-X

Ferrer, T., Cordero-Morales, J. F., Arias, M., Ficker, E., Medovoy, D., Perozo, E., et al (2011). Molecular coupling in the human ether-a-go-go-related gene-1 (hERG1) K+ channel inactivation pathway. *J. Biol. Chem.* 286 (45), 39091–39099. doi: 10.1074/jbc.M111.292060

Fernandez, D., Ghanta, A., Kauffman, G. W., and Sanguinetti, M. C. (2004). Physicochemical features of the HERG channel drug binding site. *J. Biol. Chem.* 279, 10120–10127. doi: 10.1074/jbc.M310683200

Fernandez-Marino, A. I., Harpole, T. J., Oelstrom, K., Delemotte, L., and Chanda, B. (2018). Gating interaction maps reveal a noncanonical electromechanical coupling mode in the Shaker K(+) channel. *Nat. Struct. Mol. Biol.* 25, 320–326. doi: 10.1038/s41594-018-0047-3

Ficker, E., Jarolimek, W., and Brown, A. M. (2001). Molecular determinants of inactivation and dofetilide block in ether a-go-go (EAG) channels and EAG-related K(+) channels. *Mol. Pharmacol.* 60, 1343–1348. doi: 10.1124/mol.60.6.1343

Ficker, E., Dennis, A. T., Wang, L., and Brown, A. M. (2003). Role of the cytosolic chaperones Hsp70 and Hsp90 in maturation of the cardiac potassium channel HERG. *Circ. Res.* 92, e87–100. doi: 10.1161/01.RES.0000079028.31393.15

Foo, B., Barbier, C., Guo, K., Vasantharuban, J., Lukacs, G. L., and Shrier, A. (2019). Mutation-specific peripheral and ER quality control of hERG channel cell-surface expression. *Sci. Rep.* 9, 6066. doi: 10.1038/s41598-019-42331-6

Franqueza, L., Lin, M., Shen, J., Splawski, I., Keating, M. T., and Sanguinetti, M. C. (1999). Long QT syndrome-associated mutations in the S4-S5 linker of KvLQT1 potassium channels modify gating and interaction with minK subunits. *J. Biol. Chem.* 274, 21063–21070. doi: 10.1074/jbc.274.30.21063

Gabelli, S. B., Boto, A., Kuhns, V. H., Bianchet, M. A., Farinelli, F., Aripirala, S., et al. (2014). Regulation of the NaV1.5 cytoplasmic domain by calmodulin. *Nat. Commun.* 5, 5126. doi: 10.1038/ncomms6126

Gardill, B. R., Rivera-Acevedo, R. E., Tung, C. C., and Van Petegem, F. (2019). Crystal structures of Ca(2+)-calmodulin bound to NaV C-terminal regions suggest role for EF-hand domain in binding and inactivation. *Proc. Natl. Acad. Sci. U. S. A* 116, 10763–10772. doi: 10.1073/pnas.1818618116

Garg, V., Sachse, F. B., and Sanguinetti, M. C. (2012). Tuning of EAG K(+) channel inactivation: molecular determinants of amplification by mutations and a small molecule. *J. Gen. Physiol.* 140, 307–324. doi: 10.1085/jgp.201210826

George, A. L. Jr. (2013). Molecular and genetic basis of sudden cardiac death. *J. Clin. Invest.* 123, 75–83. doi: 10.1172/JCI62928

Ghosh, S., Nunziato, D. A., and Pitt, G. S. (2006). KCNQ1 assembly and function is blocked by long-QT syndrome mutations that disrupt interaction with calmodulin. *Circ. Res.* 98, 1048–1054. doi: 10.1161/01.RES.0000218863.44140.f2

Ghovanloo, M. R., Aimar, K., Ghadiry-Tavi, R., Yu, A., and Ruben, P. C. (2016). Physiology and Pathophysiology of Sodium Channel Inactivation. *Curr. Top. Membr.* 78, 479–509. doi: 10.1016/bs.ctm.2016.04.001

Giudicessi, J. R., and Ackerman, M. J. (2013). Genotype- and phenotype-guided management of congenital long QT syndrome. *Curr. Probl. Cardiol.* 38, 417–455. doi: 10.1016/j.cpcardiol.2013.08.001

Gofman, Y., Shats, S., Attali, B., Haliloglu, T., and Ben-Tal, N. (2012). How does KCNE1 regulate the Kv7.1 potassium channel? Model-structure, mutations, and dynamics of the Kv7.1-KCNE1 complex. *Structure* 20, 1343–1352. doi: 10.1016/j.str.2012.05.016

Goldenberg, I., Thottathil, P., Lopes, C. M., Moss, A. J., Mcnitt, S., O-Uchi, J., et al. (2012). Trigger-specific ion-channel mechanisms, risk factors, and response to therapy in type 1 long QT syndrome. *Heart Rhythm.* 9, 49–56. doi: 10.1016/j.hrthm.2011.08.020

Goldschen-Ohm, M. P., Capes, D. L., Oelstrom, K. M., and Chanda, B. (2013). Multiple pore conformations driven by asynchronous movements of voltage sensors in a eukaryotic sodium channel. *Nat. Commun.* 4, 1350. doi: 10.1038/ncomms2356

Gordon, E., Panaghie, G., Deng, L., Bee, K. J., Roepke, T. K., Krogh-Madsen, T., et al. (2008). A KCNE2 mutation in a patient with cardiac arrhythmia induced by auditory stimuli and serum electrolyte imbalance. *Cardiovasc. Res.* 77, 98–106. doi: 10.1093/cvr/cvm030

Grant, A. O. (2009). Cardiac ion channels. *Circ. Arrhythm Electrophysiol.* 2, 185–194. doi: 10.1161/CIRCEP.108.789081

Guo, J., Zhang, X., Hu, Z., Zhuang, Z., Zhu, Z., Chen, Z., et al. (2012). A422T mutation in HERG potassium channel retained in ER is rescurable by pharmacologic or molecular chaperones. *Biochem. Biophys. Res. Commun.* 422, 305–310. doi: 10.1016/j.bbrc.2012.04.153

Gustina, A. S., and Trudeau, M. C. (2011). hERG potassium channel gating is mediated by N- and C-terminal region interactions. *J. Gen. Physiol.* 137, 315–325. doi: 10.1085/jgp.201010582

Haitin, Y., and Attali, B. (2008). The C-terminus of Kv7 channels: a multifunctional module. *J. Physiol.* 586, 1803–1810. doi: 10.1113/jphysiol.2007.149187

Hancox, J. C., Whittaker, D. G., Du, C., Stuart, A. G., and Zhang, H. (2018). Emerging therapeutic targets in the short QT syndrome. *Expert Opin. Ther. Targets* 22, 439–451. doi: 10.1080/14728222.2018.1470621

Harley, C. A., Jesus, C. S., Carvalho, R., Brito, R. M., and Morais-Cabral, J. H. (2012). Changes in channel trafficking and protein stability caused by LQT2 mutations in the PAS domain of the HERG channel. *PloS One* 7, e32654. doi: 10.1371/journal.pone.0032654

Harrison, S. M., Riggs, E. R., Maglott, D. R., Lee, J. M., Azzariti, D. R., Niehaus, A., et al. (2016). Using ClinVar as a Resource to Support Variant Interpretation. *Curr. Protoc. Hum. Genet.* 898 16, 11–18 16 23. doi: 10.1002/0471142905.hg0816s89

Heijman, J., Spatjens, R. L., Seyen, S. R., Lentink, V., Kuijpers, H. J., Boulet, I. R., et al. (2012). Dominant-negative control of cAMP-dependent IKs upregulation in human long-QT syndrome type 1. *Circ. Res.* 110, 211–219. doi: 10.1161/CIRCRESAHA.111.249482

Heitzmann, D., Grahammer, F., Von Hahn, T., Schmitt-Graff, A., Romeo, E., Nitschke, R., et al. (2004). Heteromeric KCNE2/KCNQ1 potassium channels in the luminal membrane of gastric parietal cells. *J. Physiol.* 561, 547–557. doi: 10.1113/jphysiol.2004.075168

Helliwell, M. V., Zhang, Y., El Harchi, A., Du, C., Hancox, J. C., and Dempsey, C. E. (2018). Structural implications of hERG K(+) channel block by a high-affinity minimally structured blocker. *J. Biol. Chem.* 293, 7040–7057. doi: 10.1074/jbc.RA117.000363

Henry, J. T., and Crosson, S. (2011). Ligand-binding PAS domains in a genomic, cellular, and structural context. *Annu. Rev. Microbiol.* 65, 261–286. doi: 10.1146/annurev-micro-121809-151631

Herzberg, I. M., Trudeau, M. C., and Robertson, G. A. (1998). Transfer of rapid inactivation and sensitivity to the class III antiarrhythmic drug E-4031 from HERG to M-eag channels. *J. Physiol.* 511 (Pt 1), 3–14. doi: 10.1111/j.1469-7793.1998.003bi.x

Herzik, M. A.Jr., Fraser, J. S., and Lander, G. C. (2019). A Multi-model Approach to Assessing Local and Global Cryo-EM Map Quality. *Structure* 27344-358, e343. doi: 10.1016/j.str.2018.10.003

Hille, B. (1971). The hydration of sodium ions crossing the nerve membrane. *Proc. Natl. Acad. Sci. U. S. A* 68, 280–282. doi: 10.1073/pnas.68.2.280

Hoosien, M., Ahearn, M. E., Myerburg, R. J., Pham, T. V., Miller, T. E., Smets, M. J., et al. (2013). Dysfunctional potassium channel subunit interaction as a novel mechanism of long QT syndrome. *Heart Rhythm.* 10, 728–737. doi: 10.1016/j.hrthm.2012.12.033

Hoshi, T., and Armstrong, C. M. (2013). C-type inactivation of voltage-gated K+ channels: pore constriction or dilation? *J. Gen. Physiol.* 141, 151–160. doi: 10.1085/jgp.201210888

Hosseini, S. M., Kim, R., Udupa, S., Costain, G., Jobling, R., Liston, E., et al. (2018). Reappraisal of Reported Genes for Sudden Arrhythmic Death: Evidence-Based Evaluation of Gene Validity for Brugada Syndrome. *Circulation* 138, 1195–1205. doi: 10.1161/CIRCULATIONAHA.118.035070

Hosseini, S. M. (2018). A useful hand mnemonic to demonstrate ion channel gating. *Adv. Physiol. Educ.* 42, 321–323. doi: 10.1152/advan.00080.2017

Hou, P., Eldstrom, J., Shi, J., Zhong, L., Mcfarland, K., Gao, Y., et al. (2017). Inactivation of KCNQ1 potassium channels reveals dynamic coupling between

voltage sensing and pore opening. *Nat. Commun.* 8, 1730. doi: 10.1038/s41467-017-01911-8

Hou, P., Shi, J., White, K. M., Gao, Y., and Cui, J. (2019). ML277 specifically enhances the fully activated open state of KCNQ1 by modulating VSD-pore coupling. *Elife* 8, e48576. doi: 10.7554/eLife.48576

Hou, P., Kang, P. W., Kongmeneck, A. D., Yang, N. D., Liu, Y., Shi, J., et al. (2020). Two-stage electro-mechanical coupling of a KV channel in voltage-dependent activation. *Nat. Commun.* 11, 676. doi: 10.1038/s41467-020-14406-w

Hovey, L., Fowler, C. A., Mahling, R., Lin, Z., Miller, M. S., Marx, D. C., et al. (2017). Calcium triggers reversal of calmodulin on nested anti-parallel sites in the IQ motif of the neuronal voltage-dependent sodium channel NaV1.2. *Biophys. Chem.* 224, 1–19. doi: 10.1016/j.bpc.2017.02.006

Howard, R. J., Clark, K. A., Holton, J. M., and Minor, D. L.Jr. (2007). Structural insight into KCNQ (Kv7) channel assembly and channelopathy. *Neuron* 53, 663–675. doi: 10.1016/j.neuron.2007.02.010

Hu, D., Barajas-Martinez, H., Burashnikov, E., Springer, M., Wu, Y., Varro, A., et al. (2009). A mutation in the beta 3 subunit of the cardiac sodium channel associated with Brugada ECG phenotype. *Circ. Cardiovasc. Genet.* 2, 270–278. doi: 10.1161/CIRCGENETICS.108.829192

Hu, D., Barajas-Martinez, H., Medeiros-Domingo, A., Crotti, L., Veltmann, C., Schimpf, R., et al. (2012). A novel rare variant in SCN1Bb linked to Brugada syndrome and SIDS by combined modulation of Na(v)1.5 and K(v)4.3 channel currents. *Heart Rhythm.* 9, 760–769. doi: 10.1016/j.hrthm.2011.12.006

Huang, H., Kuenze, G., Smith, J. A., Taylor, K. C., Duran, A. M., Hadziselimovic, A., et al. (2018). Mechanisms of KCNQ1 channel dysfunction in long QT syndrome involving voltage sensor domain mutations. *Sci. Adv.* 4, eaar2631. doi: 10.1126/sciadv.aar2631

Center for Drug Evaluation and Research. (2005a). "E14: clinical evaluation of QT/QTc interval prolongation and proarrhythmic potential for non-arrhythmic drugs", (ed.) U.S.F.a.D. Administration.).

Center for Drug Evaluation and Research. (2005b). "S7B: The non-clinical evaluation of the potential for delayed ventricular depolarization (QT interval prolongation) by human pharmaceruticals", (ed.) U.S.F.a.D. Administration.)

Ikrar, T., Hanawa, H., Watanabe, H., Okada, S., Aizawa, Y., Ramadan, M. M., et al. (2008). A double-point mutation in the selectivity filter site of the KCNQ1 potassium channel results in a severe phenotype, LQT1, of long QT syndrome. *J. Cardiovasc. Electrophysiol.* 19, 541–549. doi: 10.1111/j.1540-8167.2007.01076.x

Iqbal, S. M., Aufy, M., Shabbir, W., and Lemmens-Gruber, R. (2018). Identification of phosphorylation sites and binding pockets for modulation of NaV 1.5 channel by Fyn tyrosine kinase. *FEBS J.* 285, 2520–2530. doi: 10.1111/febs.14496

Isbilen, B., Fraser, S. P., and Djamgoz, M. B. (2006). Docosahexaenoic acid (omega-3) blocks voltage-gated sodium channel activity and migration of MDA-MB-231 human breast cancer cells. *Int. J. Biochem. Cell Biol.* 38, 2173–2182. doi: 10.1016/j.biocel.2006.06.014

Jiang, Y., Ruta, V., Chen, J., Lee, A., and Mackinnon, R. (2003). The principle of gating charge movement in a voltage-dependent K+ channel. *Nature* 423, 42–48. doi: 10.1038/nature01581

Jiang, D., Shi, H., Tonggu, L., Gamal El-Din, T. M., Lenaeus, M. J., Zhao, Y., et al. (2020). Structure of the Cardiac Sodium Channel. *Cell* 180, 122–134 e110. doi: 10.1016/j.cell.2019.11.041

Johnson, C. N., Potet, F., Thompson, M. K., Kroncke, B. M., Glazer, A. M., Voehler, M. W., et al. (2018). A Mechanism of Calmodulin Modulation of the Human Cardiac Sodium Channel. *Structure* 26, 683–694 e683. doi: 10.1016/j.str.2018.03.005

Jouni, M., Si-Tayeb, K., Es-Salah-Lamoureux, Z., Latypova, X., Champon, B., Caillaud, A., et al. (2015). Toward Personalized Medicine: Using Cardiomyocytes Differentiated From Urine-Derived Pluripotent Stem Cells to Recapitulate Electrophysiological Characteristics of Type 2 Long QT Syndrome. *J. Am. Heart Assoc.* 4, e002159. doi: 10.1161/JAHA.115.002159

Jurkiewicz, N. K., and Sanguinetti, M. C. (1993). Rate-dependent prolongation of cardiac action potentials by a methanesulfonanilide class III antiarrhythmic agent. Specific block of rapidly activating delayed rectifier K+ current by dofetilide. *Circ. Res.* 72, 75–83. doi: 10.1161/01.RES.72.1.75

Kalyaanamoorthy, S., and Barakat, K. H. (2018). Development of Safe Drugs: The hERG Challenge. *Med. Res. Rev.* 38, 525–555. doi: 10.1002/med.21445

Kamiya, K., Nishiyama, A., Yasui, K., Hojo, M., Sanguinetti, M. C., and Kodama, I. (2001). Short- and long-term effects of amiodarone on the two components of cardiac delayed rectifier K(+) current. *Circulation* 103, 1317–1324. doi: 10.1161/01.CIR.103.9.1317

Kang, J. X., Xiao, Y. F., and Leaf, A. (1995).). Free, long-chain, polyunsaturated fatty acids reduce membrane electrical excitability in neonatal rat cardiac myocytes. *Proc. Natl. Acad. Sci. U. S. A* 92, 3997–4001. doi: 10.1073/pnas.92.9.3997

Kang, J. X., Li, Y., and Leaf, A. (1997). Regulation of sodium channel gene expression by class I antiarrhythmic drugs and n - 3 polyunsaturated fatty acids in cultured neonatal rat cardiac myocytes. *Proc. Natl. Acad. Sci. U. S. A* 94, 2724–2728. doi: 10.1073/pnas.94.6.2724

Kang, C., Tian, C., Sonnichsen, F. D., Smith, J. A., Meiler, J., George, A. L.Jr., et al. (2008). Structure of KCNE1 and implications for how it modulates the KCNQ1 potassium channel. *Biochemistry* 47, 7999–8006. doi: 10.1021/bi800875q

Kanki, H., Kupershmidt, S., Yang, T., Wells, S., and Roden, D. M. (2004). A structural requirement for processing the cardiac K+ channel KCNQ1. *J. Biol. Chem.* 279, 33976–33983. doi: 10.1074/jbc.M404539200

Kapa, S., Tester, D. J., Salisbury, B. A., Harris-Kerr, C., Pungliya, M. S., Alders, M., et al. (2009). Genetic testing for long-QT syndrome: distinguishing pathogenic mutations from benign variants. *Circulation* 120, 1752–1760. doi: 10.1161/CIRCULATIONAHA.109.863076

Kasimova, M. A., Zaydman, M. A., Cui, J., and Tarek, M. (2015). PIP2-dependent coupling is prominent in Kv7.1 due to weakened interactions between S4-S5 and S6. *Sci. Rep.* 5, 7474–7474. doi: 10.1038/srep07474

Ke, Y., Ng, C. A., Hunter, M. J., Mann, S. A., Heide, J., Hill, A. P., et al. (2013). Trafficking defects in PAS domain mutant Kv11.1 channels: roles of reduced domain stability and altered domain-domain interactions. *Biochem. J.* 454, 69–77. doi: 10.1042/BJ20130328

Ke, Y., Hunter, M. J., Ng, C. A., Perry, M. D., and Vandenberg, J. I. (2014). Role of the cytoplasmic N-terminal Cap and Per-Arnt-Sim (PAS) domain in trafficking and stabilization of Kv11.1 channels. *J. Biol. Chem.* 289, 13782–13791. doi: 10.1074/jbc.M113.531277

Khan, H. M., Tieleman, P. D., and Noskov, S. Y. (2020). "Refinement of High-resolution Cryo-EM Structure of hERG: What Can We Expect?", in *The Biophysical Society 64th Annual Meeting* (San Diego: Cell Press).

Kim, J., Ghosh, S., Liu, H., Tateyama, M., Kass, R. S., and Pitt, G. S. (2004). Calmodulin mediates Ca2+ sensitivity of sodium channels. *J. Biol. Chem.* 279, 45004–45012. doi: 10.1074/jbc.M407286200

Kim, J. A., Lopes, C. M., Moss, A. J., Mcnitt, S., Barsheshet, A., Robinson, J. L., et al. (2010). Trigger-specific risk factors and response to therapy in long QT syndrome type 2. *Heart Rhythm.* 7, 1797–1805. doi: 10.1016/j.hrthm.2010.09.011

Kleber Ag, R. Y. (2004). Basic mechanisms of cardiac impulse propagation and associated arrhythmias. *Physiol. Rev.* 84, 431–488. doi: 10.1152/physrev.00025.2003

Kroncke Bm, E. A. (2019). Protein structure aids in predicting functional perturbation of missense variants of SCN5A and KCNQ1. *Comput. Struct. Biotechnol. J.* 17,206–214. doi: 10.1016/j.csbj.2019.01.008

Kroncke, B. M., Vanoye, C. G., Meiler, J., George, A. L. Jr., and Sanders, C. R. (2015). Personalized biochemistry and biophysics. *Biochemistry* 54, 2551–2559. doi: 10.1021/acs.biochem.5b00189

Kroncke, B. M., Van Horn, W. D., Smith, J., Kang, C., Welch, R. C., Song, Y., et al. (2016). Structural basis for KCNE3 modulation of potassium recycling in epithelia. *Sci. Adv.* 2, e1501228. doi: 10.1126/sciadv.1501228

Kroncke, B. M., Mendenhall, J., Smith, D. K., Sanders, C. R., Capra, J. A., George, A. L., et al. (2019). Protein structure aids predicting functional perturbation of missense variants in SCN5A and KCNQ1. *Comput. Struct. Biotechnol. J.* 17, 206–214. doi: 10.1016/j.csbj.2019.01.008

Kuenze, G., Duran, A. M., Woods, H., Brewer, K. R., Mcdonald, E. F., Vanoye, C. G., et al. (2019). Upgraded molecular models of the human KCNQ1 potassium channel. *PloS One* 14, e0220415. doi: 10.1371/journal.pone.0220415

Kume, S., Shimomura, T., Tateyama, M., and Kubo, Y. (2018). Two mutations at different positions in the CNBH domain of the hERG channel accelerate deactivation and impair the interaction with the EAG domain. *J. Physiol.* 596, 4629–4650. doi: 10.1113/JP276208

Labro, A. J., and Snyders, D. J. (2012). Being flexible: the voltage-controllable activation gate of kv channels. *Front. Pharmacol.* 3, 168. doi: 10.3389/fphar.2012.00168

Labro, A. J., Boulet, I. R., Choveau, F. S., Mayeur, E., Bruyns, T., Loussouarn, G., et al. (2011). The S4-S5 linker of KCNQ1 channels forms a structural scaffold with the S6 segment controlling gate closure. *J. Biol. Chem.* 286, 717–725. doi: 10.1074/jbc.M110.146977

Lee, P. J., Sunami, A., and Fozzard, H. A. (2001). Cardiac-specific external paths for lidocaine, defined by isoform-specific residues, accelerate recovery from use-dependent block. *Circ. Res.* 89, 1014–1021. doi: 10.1161/hh2301.100002

Leifert, W. R., Mcmurchie, E. J., and Saint, D. A. (1999). Inhibition of cardiac sodium currents in adult rat myocytes by n-3 polyunsaturated fatty acids. *J. Physiol.* 520 (Pt 3), 671–679. doi: 10.1111/j.1469-7793.1999.00671.x

Lek, M., Karczewski, K. J., Minikel, E. V., Samocha, K. E., Banks, E., Fennell, T., et al. (2016). Analysis of protein-coding genetic variation in 60,706 humans. *Nature* 536, 285–291. doi: 10.1038/nature19057

Lemaillet, G., Walker, B., and Lambert, S. (2003). Identification of a conserved ankyrin-binding motif in the family of sodium channel alpha subunits. *J. Biol. Chem.* 278, 27333–27339. doi: 10.1074/jbc.M303327200

Lengyel, C., Iost, N., Virag, L., Varro, A., Lathrop, D. A., and Papp, J. G. (2001). Pharmacological block of the slow component of the outward delayed rectifier current (I(Ks)) fails to lengthen rabbit ventricular muscle QT(c) and action potential duration. *Br. J. Pharmacol.* 132, 101–110. doi: 10.1038/sj.bjp.0703777

Li, G., and Zhang, L. (2018). The role of mexiletine in the management of long QT syndrome. *J. Electrocardiol.* 51, 1061–1065. doi: 10.1016/j.jelectrocard.2018.08.035

Li, P., Liu, H., Lai, C., Sun, P., Zeng, W., Wu, F., et al. (2014). Differential modulations of KCNQ1 by auxiliary proteins KCNE1 and KCNE2. *Sci. Rep.* 4, 4973. doi: 10.1038/srep04973

Li, B., Mendenhall, J. L., Kroncke, B. M., Taylor, K. C., Huang, H., Smith, D. K., et al. (2017). Predicting the Functional Impact of KCNQ1 Variants of Unknown Significance. *Circ. Cardiovasc. Genet.* 10, pii: e001754. doi: 10.1161/CIRCGENETICS.117.001754

Li, M. C. H., O'brien, T. J., Todaro, M., and Powell, K. L. (2019). Acquired cardiac channelopathies in epilepsy: Evidence, mechanisms, and clinical significance. *Epilepsia* 60, 1753–1767. doi: 10.1111/epi.16301

Liin, S. I., Silvera Ejneby, M., Barro-Soria, R., Skarsfeldt, M. A., Larsson, J. E., Starck Harlin, F., et al. (2015). Polyunsaturated fatty acid analogs act antiarrhythmically on the cardiac IKs channel. *Proc. Natl. Acad. Sci. U. S. A* 112, 5714–5719. doi: 10.1073/pnas.1503488112

Liin, S. I., Yazdi, S., Ramentol, R., Barro-Soria, R., and Larsson, H. P. (2018). Mechanisms Underlying the Dual Effect of Polyunsaturated Fatty Acid Analogs on Kv7.1. *Cell Rep.* 24, 2908–2918. doi: 10.1016/j.celrep.2018.08.031

Lin, X., Liu, N., Lu, J., Zhang, J., Anumonwo, J. M., Isom, L. L., et al. (2011). Subcellular heterogeneity of sodium current properties in adult cardiac ventricular myocytes. *Heart Rhythm.* 8, 1923–1930. doi: 10.1016/j.hrthm.2011.07.016

Lindegger, N., Hagen, B. M., Marks, A. R., Lederer, W. J., and Kass, R. S. (2009). Diastolic transient inward current in long QT syndrome type 3 is caused by Ca2+ overload and inhibited by ranolazine. *J. Mol. Cell Cardiol.* 47, 326–334. doi: 10.1016/j.yjmcc.2009.04.003

Liu, D. W., and Antzelevitch, C. (1995). Characteristics of the delayed rectifier current (IKr and IKs) in canine ventricular epicardial, midmyocardial, and endocardial myocytes. A weaker IKs contributes to the longer action potential of the M cell. *Circ. Res.* 76, 351–365. doi: 10.1161/01.RES.76.3.351

Liu, C. J., Dib-Hajj, S. D., Renganathan, M., Cummins, T. R., and Waxman, S. G. (2003). Modulation of the cardiac sodium channel Nav1.5 by fibroblast growth factor homologous factor 1B. *J. Biol. Chem.* 278, 1029–1036. doi: 10.1074/jbc.M207074200

Long, S. B., Campbell, E. B., and Mackinnon, R. (2005). Crystal structure of a mammalian voltage-dependent Shaker family K+ channel. *Science* 309, 897–903. doi: 10.1126/science.1116269

Long, S. B., Tao, X., Campbell, E. B., and Mackinnon, R. (2007). Atomic structure of a voltage-dependent K+ channel in a lipid membrane-like environment. *Nature* 450, 376–382. doi: 10.1038/nature06265

Loots, E., and Isacoff, E. Y. (1998). Protein rearrangements underlying slow inactivation of the Shaker K+ channel. *J. Gen. Physiol.* 112, 377–389. doi: 10.1085/jgp.112.4.377

Lorinczi, E., Gomez-Posada, J. C., De La Pena, P., Tomczak, A. P., Fernandez-Trillo, J., Leipscher, U., et al. (2015). Voltage-dependent gating of KCNH potassium channels lacking a covalent link between voltage-sensing and pore domains. *Nat. Commun.* 6, 6672. doi: 10.1038/ncomms7672

Loussouarn, G., Park, K. H., Bellocq, C., Baro, I., Charpentier, F., and Escande, D. (2003). Phosphatidylinositol-4,5-bisphosphate, PIP2, controls KCNQ1/KCNE1 voltage-gated potassium channels: a functional homology between voltage-gated and inward rectifier K+ channels. *EMBO J.* 22, 5412–5421. doi: 10.1093/emboj/cdg526

Lu, Z., Klem, A. M., and Ramu, Y. (2001). Ion conduction pore is conserved among potassium channels. *Nature* 413 (6858), 809–813. doi: 10.1038/35101535

Lu, Z., Klem, A. M., and Ramu,, Y. (2002). Coupling between voltage sensors and activation gate in voltage-gated K+ channels. *J. Gen. Physiol.* 120 (5), 663–676. doi: 10.1085/jgp.20028696

Ma, L. J., Ohmert, I., and Vardanyan, V. (2011). Allosteric features of KCNQ1 gating revealed by alanine scanning mutagenesis. *Biophys. J.* 100, 885–894. doi: 10.1016/j.bpj.2010.12.3726

Ma, D., Wei, H., Zhao, Y., Lu, J., Li, G., Sahib, N. B., et al. (2013). Modeling type 3 long QT syndrome with cardiomyocytes derived from patient-specific induced pluripotent stem cells. *Int. J. Cardiol.* 168, 5277–5286. doi: 10.1016/j.ijcard.2013.08.015

Makara, M. A., Curran, J., Little, S. C., Musa, H., Polina, I., Smith, S. A., et al. (2014). Ankyrin-G coordinates intercalated disc signaling platform to regulate cardiac excitability in vivo. *Circ. Res.* 115, 929–938. doi: 10.1161/CIRCRESAHA.115.305154

Makita, N., Bennett, P. B., and George, A. L.Jr. (1996). Molecular determinants of beta 1 subunit-induced gating modulation in voltage-dependent Na+ channels. *J. Neurosci.* 16, 7117–7127. doi: 10.1523/JNEUROSCI.16-22-07117.1996

Malhotra, J. D., Thyagarajan, V., Chen, C., and Isom, L. L. (2004). Tyrosine-phosphorylated and nonphosphorylated sodium channel beta1 subunits are differentially localized in cardiac myocytes. *J. Biol. Chem.* 279, 40748–40754. doi: 10.1074/jbc.M407243200

Marionneau, C., Lichti, C. F., Lindenbaum, P., Charpentier, F., Nerbonne, J. M., Townsend, R. R., et al. (2012). Mass spectrometry-based identification of native cardiac Nav1.5 channel alpha subunit phosphorylation sites. *J. Proteome Res.* 11, 5994–6007. doi: 10.1021/pr300702c

Mattmann, M. E., Yu, H., Lin, Z., Xu, K., Huang, X., Long, S., et al. (2012). Identification of (R)-N-(4-(4-methoxyphenyl)thiazol-2-yl)-1-tosylpiperidine-2-carboxamide, ML277, as a novel, potent and selective K(v)7.1 (KCNQ1) potassium channel activator. *Bioorg. Med. Chem. Lett.* 22, 5936–5941. doi: 10.1016/j.bmcl.2012.07.060

Mazhari, R., Greenstein, J. L., Winslow, R. L., Marban, E., and Nuss, H. B. (2001). Molecular interactions between two long-QT syndrome gene products, HERG and KCNE2, rationalized by in vitro and in silico analysis. *Circ. Res.* 89, 33–38. doi: 10.1161/hh1301.093633

Mazzanti, A., Maragna, R., Faragli, A., Monteforte, N., Bloise, R., Memmi, M., et al. (2016). Gene-Specific Therapy With Mexiletine Reduces Arrhythmic Events in Patients With Long QT Syndrome Type 3. *J. Am. Coll. Cardiol.* 67, 1053–1058. doi: 10.1016/j.jacc.2015.12.033

Mcdonald, T. V., Yu, Z., Ming, Z., Palma, E., Meyers, M. B., Wang, K. W., et al. (1997). A minK-HERG complex regulates the cardiac potassium current I(Kr). *Nature* 388, 289–292. doi: 10.1038/40882

Meadows, L., Malhotra, J. D., Stetzer, A., Isom, L. L., and Ragsdale, D. S. (2001). The intracellular segment of the sodium channel beta 1 subunit is required for its efficient association with the channel alpha subunit. *J. Neurochem.* 76, 1871–1878. doi: 10.1046/j.1471-4159.2001.00192.x

Medeiros-Domingo, A., Kaku, T., Tester, D. J., Iturralde-Torres, P., Itty, A., Ye, B., et al. (2007). SCN4B-encoded sodium channel beta4 subunit in congenital long-QT syndrome. *Circulation* 116, 134–142. doi: 10.1161/CIRCULATIONAHA.106.659086

Melman, Y. F., Domenech, A., De La Luna, S., and Mcdonald, T. V. (2001). Structural determinants of KvLQT1 control by the KCNE family of proteins. *J. Biol. Chem.* 276, 6439–6444. doi: 10.1074/jbc.M010713200

Melman, Y. F., Krumerman, A., and Mcdonald, T. V. (2002). A single transmembrane site in the KCNE-encoded proteins controls the specificity of KvLQT1 channel gating. *J. Biol. Chem.* 277, 25187–25194. doi: 10.1074/jbc.M200564200

Melman, Y. F., Um, S. Y., Krumerman, A., Kagan, A., and Mcdonald, T. V. (2004). KCNE1 binds to the KCNQ1 pore to regulate potassium channel activity. *Neuron* 42, 927–937. doi: 10.1016/j.neuron.2004.06.001

Meza, U., Beqollari, D., and Bannister, R. A. (2018). Molecular mechanisms and physiological relevance of RGK proteins in the heart. *Acta Physiol. (Oxf)* 222, e13016. doi: 10.1111/apha.13016

Mitcheson, J. S., Chen, J., Lin, M., Culberson, C., and Sanguinetti, M. C. (2000). A structural basis for drug-induced long QT syndrome. *Proc. Natl. Acad. Sci. U. S. A* 97, 12329–12333. doi: 10.1073/pnas.210244497

Mohler, P. J., Rivolta, I., Napolitano, C., Lemaillet, G., Lambert, S., Priori, S. G., et al. (2004). Nav1.5 E1053K mutation causing Brugada syndrome blocks binding to ankyrin-G and expression of Nav1.5 on the surface of cardiomyocytes. *Proc. Natl. Acad. Sci. U. S. A* 101, 17533–17538. doi: 10.1073/pnas.0403711101

Morais Cabral, J. H., Lee, A., Cohen, S. L., Chait, B. T., Li, M., and Mackinnon, R. (1998). Crystal structure and functional analysis of the HERG potassium channel N terminus: a eukaryotic PAS domain. *Cell* 95, 649–655. doi: 10.1016/S0092-8674(00)81635-9

Morais-Cabral, J. H., Zhou, Y., and Mackinnon, R. (2001). Energetic optimization of ion conduction rate by the K+ selectivity filter. *Nature* 414, 37–42. doi: 10.1038/35102000

Moreau, A., Gosselin-Badaroudine, P., Delemotte, L., Klein, M. L., and Chahine, M. (2015). Gating pore currents are defects in common with two Nav1.5 mutations in patients with mixed arrhythmias and dilated cardiomyopathy. *J. Gen. Physiol.* 145, 93–106. doi: 10.1085/jgp.201411304

Moreno, J. D., Zhu, Z. I., Yang, P. C., Bankston, J. R., Jeng, M. T., Kang, C., et al. (2011). A computational model to predict the effects of class I anti-arrhythmic drugs on ventricular rhythms. *Sci. Transl. Med.* 3, 98ra83. doi: 10.1126/scitranslmed.3002588

Moretti, A., Bellin, M., Welling, A., Jung, C. B., Lam, J. T., Bott-Flugel, L., et al. (2010). Patient-specific induced pluripotent stem-cell models for long-QT syndrome. *N. Engl. J. Med.* 363, 1397–1409. doi: 10.1056/NEJMoa0908679

Moss, A. J., and Kass, R. S. (2005). Long QT syndrome: from channels to cardiac arrhythmias. *J. Clin. Invest.* 115, 2018–2024. doi: 10.1172/JCI25537

Moss, A. J., Zareba, W., Hall, W. J., Schwartz, P. J., Crampton, R. S., Benhorin, J., et al. (2000). Effectiveness and limitations of beta-blocker therapy in congenital long-QT syndrome. *Circulation* 101, 616–623. doi: 10.1161/01.CIR.101.6.616

Moss, A. J., Shimizu, W., Wilde, A. A., Towbin, J. A., Zareba, W., Robinson, J. L., et al. (2007). Clinical aspects of type-1 long-QT syndrome by location, coding type, and biophysical function of mutations involving the KCNQ1 gene. *Circulation* 115, 2481–2489. doi: 10.1161/CIRCULATIONAHA.106.665406

Mousavi Nik, A., Gharaie, S., and Jeong Kim, H. (2015). Cellular mechanisms of mutations in Kv7.1: auditory functions in Jervell and Lange-Nielsen syndrome vs. Romano-Ward syndrome. *Front. Cell Neurosci.* 9, 32. doi: 10.3389/fncel.2015.00032

Musa, H., Kline, C. F., Sturm, A. C., Murphy, N., Adelman, S., Wang, C., et al. (2015). SCN5A variant that blocks fibroblast growth factor homologous factor regulation causes human arrhythmia. *Proc. Natl. Acad. Sci. U. S. A.* 112, 12528–12533. doi: 10.1073/pnas.1516430112

Muskett, F. W., Thouta, S., Thomson, S. J., Bowen, A., Stansfeld, P. J., and Mitcheson, J. S. (2011). Mechanistic insight into human ether-a-go-go-related gene (hERG) K+ channel deactivation gating from the solution structure of the EAG domain. *J. Biol. Chem.* 286, 6184–6191. doi: 10.1074/jbc.M110.199364

Nakajima, T., Kaneko, Y., Dharmawan, T., and Kurabayashi, M. (2019). Role of the voltage sensor module in Nav domain IV on fast inactivation in sodium channelopathies: The implication of closed-state inactivation. *Channels (Austin)* 13, 331–343. doi: 10.1080/19336950.2019.1649521

Nakajo, K., and Kubo, Y. (2007). KCNE1 and KCNE3 stabilize and/or slow voltage sensing S4 segment of KCNQ1 channel. *J. Gen. Physiol.* 130, 269–281. doi: 10.1085/jgp.200709805

Nakajo, K., and Kubo, Y. (2014). Steric hindrance between S4 and S5 of the KCNQ1/KCNE1 channel hampers pore opening. *Nat. Commun.* 5, 4100–4100. doi: 10.1038/ncomms5100

Naylor, C. E., Bagneris, C., Decaen, P. G., Sula, A., Scaglione, A., Clapham, D. E., et al. (2016). Molecular basis of ion permeability in a voltage-gated sodium channel. *EMBO J.* 35, 820–830. doi: 10.15252/embj.201593285

Negami, T., Araki, M., Okuno, Y., and Terada, T. (2019). Calculation of absolute binding free energies between the hERG channel and structurally diverse drugs. *Sci. Rep.* 9, 16586. doi: 10.1038/s41598-019-53120-6

Nerbonne, J. M., and Kass, R. S. (2005). Molecular physiology of cardiac repolarization. *Physiol. Rev.* 85, 1205–1253. doi: 10.1152/physrev.00002.2005

Ng, C. A., Phan, K., Hill, A. P., Vandenberg, J. I., and Perry, M. D. (2014). Multiple interactions between cytoplasmic domains regulate slow deactivation of Kv11.1 channels. *J. Biol. Chem.* 289, 25822–25832. doi: 10.1074/jbc.M114.558379

Nguyen, P. T., Demarco, K. R., Vorobyov, I., Clancy, C. E., and Yarov-Yarovoy, V. (2019). Structural basis for antiarrhythmic drug interactions with the human cardiac sodium channel. *Proc. Natl. Acad. Sci. U. S. A* 116, 2945–2954. doi: 10.1073/pnas.1817446116

O'malley, H. A., and Isom, L. L. (2015). Sodium channel beta subunits: emerging targets in channelopathies. *Annu. Rev. Physiol.* 77, 481–504. doi: 10.1146/annurev-physiol-021014-071846

Olesen, M. S., Jespersen, T., Nielsen, J. B., Liang, B., Moller, D. V., Hedley, P., et al. (2011). Mutations in sodium channel beta-subunit SCN3B are associated with early-onset lone atrial fibrillation. *Cardiovasc. Res.* 89, 786–793. doi: 10.1093/cvr/cvq348

Osteen, J. D., Gonzalez, C., Sampson, K. J., Iyer, V., Rebolledo, S., Larsson, H. P., et al. (2010). KCNE1 alters the voltage sensor movements necessary to open the KCNQ1 channel gate. *Proc. Natl. Acad. Sci. U. S. A* 107, 22710–22715. doi: 10.1073/pnas.1016300108

Osteen, J. D., Barro-Soria, R., Robey, S., Sampson, K. J., Kass, R. S., and Larsson, H. P. (2012). Allosteric gating mechanism underlies the flexible gating of KCNQ1 potassium channels. *Proc. Natl. Acad. Sci. U. S. A* 109, 7103–7108. doi: 10.1073/pnas.1201582109

Pan, X., Li, Z., Zhou, Q., Shen, H., Wu, K., Huang, X., et al. (2018). Structure of the human voltage-gated sodium channel Nav1.4 in complex with beta1. *Science* 362, pii: eaau2486. doi: 10.1126/science.aau2486.

Pan, X., Li, Z., Huang, X., Huang, G., Gao, S., Shen, H., et al. (2019). Molecular basis for pore blockade of human Na(+) channel Nav1.2 by the mu-conotoxin KIIIA. *Science* 363, 1309–1313. doi: 10.1126/science.aaw2999

Panaghie, G., and Abbott, G. W. (2007). The role of S4 charges in voltage-dependent and voltage-independent KCNQ1 potassium channel complexes. *J. Gen. Physiol.* 129, 121–133. doi: 10.1085/jgp.200609612

Panaghie, G., Tai, K.-K., and Abbott, G. W. (2006). Interaction of KCNE subunits with the KCNQ1 K+ channel pore. *J. Physiol.* 570, 455–467. doi: 10.1113/jphysiol.2005.100644

Park, K. H., Piron, J., Dahimene, S., Merot, J., Baro, I., Escande, D., et al. (2005). Impaired KCNQ1-KCNE1 and phosphatidylinositol-4,5-bisphosphate interaction underlies the long QT syndrome. *Circ. Res.* 96, 730–739. doi: 10.1161/01.RES.0000161451.04649.a8

Perrin, M. J., Kuchel, P. W., Campbell, T. J., and Vandenberg, J. I. (2008). Drug binding to the inactivated state is necessary but not sufficient for high-affinity binding to human ether-a-go-go-related gene channels. *Mol. Pharmacol.* 74, 1443–1452. doi: 10.1124/mol.108.049056

Perry, M. D., Wong, S., Ng, C. A., and Vandenberg, J. I. (2013a). Hydrophobic interactions between the voltage sensor and pore mediate inactivation in Kv11.1 channels. *J. Gen. Physiol.* 142 (3), 275–288. doi: 10.1085/jgp.201310975

Perry, M. D., Wong, S., Ng, C. A., and Vandenberg, J. I. (2013b). Pore helices play a dynamic role as integrators of domain motion during Kv11.1 channel inactivation gating. *J. Biol. Chem.* 288 (16), 11482–11491. doi: 10.1074/jbc.M113.461442

Perry, M. D., Ng, C. A., Mann, S. A., Sadrieh, A., Imtiaz, M., Hill, A. P., et al. (2015). Getting to the heart of hERG K(+) channel gating. *J. Physiol.* 593, 2575–2585. doi: 10.1113/JP270095

Phan, K., Ng, C. A., David, E., Shishmarev, D., Kuchel, P. W., Vandenberg, J. I., et al. (2017). The S1 helix critically regulates the finely tuned gating of Kv11.1 channels. *J. Biol. Chem.* 292, 7688–7705. doi: 10.1074/jbc.M117.779298

Pless, S. A., Galpin, J. D., Frankel, A., and Ahern, C. A. (2011a). Molecular basis for class Ib anti-arrhythmic inhibition of cardiac sodium channels. *Nat. Commun.* 2, 351. doi: 10.1038/ncomms1351

Pless, S. A., Galpin, J. D., Niciforovic, A. P., and Ahern, C. A. (2011b). Contributions of counter-charge in a potassium channel voltage-sensor domain. *Nat. Chem. Biol.* 7, 617–623. doi: 10.1038/nchembio.622

Poulsen, K. L., Hotait, M., Calloe, K., Klaerke, D. A., Rebeiz, A., Nemer, G., et al. (2015). The Mutation P.T613a in the Pore Helix of the Kv 11.1 Potassium Channel is Associated with Long QT Syndrome. *Pacing Clin. Electrophysiol.* 38, 1304–1309. doi: 10.1111/pace.12693

Preston, P., Wartosch, L., Gunzel, D., Fromm, M., Kongsuphol, P., Ousingsawat, J., et al. (2010). Disruption of the K+ channel beta-subunit KCNE3 reveals an important role in intestinal and tracheal Cl- transport. *J. Biol. Chem.* 285, 7165–7175. doi: 10.1074/jbc.M109.047829

Priori, S. G., Wilde, A. A., Horie, M., Cho, Y., Behr, E. R., Berul, C., et al. (2013). HRS/EHRA/APHRS expert consensus statement on the diagnosis and management of patients with inherited primary arrhythmia syndromes: document endorsed by HRS, EHRA, and APHRS in May 2013 and by ACCF, AHA, PACES, and AEPC in June 2013. *Heart Rhythm.* 10, 1932–1963. doi: 10.1016/j.hrthm.2013.05.014

Pusch, M., Magrassi, R., Wollnik, B., and Conti, F. (1998). Activation and inactivation of homomeric KvLQT1 potassium channels. *Biophys. J.* 75, 785–792. doi: 10.1016/S0006-3495(98)77568-X

Pusch, M., Bertorello, L., and Conti, F. (2000). Gating and flickery block differentially affected by rubidium in homomeric KCNQ1 and heteromeric KCNQ1/KCNE1 potassium channels. *Biophys. J.* 78, 211–226. doi: 10.1016/S0006-3495(00)76586-6

Qu, Y., Isom, L. L., Westenbroek, R. E., Rogers, J. C., Tanada, T. N., Mccormick, K. A., et al. (1995). Modulation of cardiac Na+ channel expression in Xenopus oocytes by beta 1 subunits. *J. Biol. Chem.* 270, 25696–25701. doi: 10.1074/jbc.270.43.25696

Ragsdale, D. S., Mcphee, J. C., Scheuer, T., and Catterall, W. A. (1994). Molecular determinants of state-dependent block of Na+ channels by local anesthetics. *Science* 265, 1724–1728. doi: 10.1126/science.8085162

Ragsdale, D. S., Mcphee, J. C., Scheuer, T., and Catterall, W. A. (1996). Common molecular determinants of local anesthetic, antiarrhythmic, and anticonvulsant block of voltage-gated Na+ channels. *Proc. Natl. Acad. Sci. U. S. A* 93, 9270–9275. doi: 10.1073/pnas.93.17.9270

Ramos, E., and O'leary M, E. (2004). State-dependent trapping of flecainide in the cardiac sodium channel. *J. Physiol.* 560, 37–49. doi: 10.1113/jphysiol.2004.065003

Rampe, D., Murawsky, M. K., Grau, J., and Lewis, E. W. (1998). The antipsychotic agent sertindole is a high affinity antagonist of the human cardiac potassium channel HERG. *J. Pharmacol. Exp. Ther.* 286, 788–793.

Riuro, H., Campuzano, O., Arbelo, E., Iglesias, A., Batlle, M., Perez-Villa, F., et al. (2014). A missense mutation in the sodium channel beta1b subunit reveals SCN1B as a susceptibility gene underlying long QT syndrome. *Heart Rhythm.* 11, 1202–1209. doi: 10.1016/j.hrthm.2014.03.044

Rocheleau, J. M., and Kobertz, W. R. (2008). KCNE peptides differently affect voltage sensor equilibrium and equilibration rates in KCNQ1 K+ channels. *J. Gen. Physiol.* 131, 59–68. doi: 10.1085/jgp.200709816

Roden, D. M., Woosley, R. L., and Primm, R. K. (1986). Incidence and clinical features of the quinidine-associated long QT syndrome: implications for patient care. *Am. Heart J.* 111, 1088–1093. doi: 10.1016/0002-8703(86)90010-4

Roepke, T. K., Anantharam, A., Kirchhoff, P., Busque, S. M., Young, J. B., Geibel, J. P., et al. (2006). The KCNE2 potassium channel ancillary subunit is essential for gastric acid secretion. *J. Biol. Chem.* 281, 23740–23747. doi: 10.1074/jbc.M604155200

Ruscic, K. J., Miceli, F., Villalba-Galea, C. A., Dai, H., Mishina, Y., Bezanilla, F., et al. (2013). IKs channels open slowly because KCNE1 accessory subunits slow the movement of S4 voltage sensors in KCNQ1 pore-forming subunits. *Proc. Natl. Acad. Sci. U. S. A* 110, E559–E566. doi: 10.1073/pnas.1222616110

Sachyani, D., Dvir, M., Strulovich, R., Tria, G., Tobelaim, W., Peretz, A., et al. (2014). Structural basis of a Kv7.1 potassium channel gating module: studies of the intracellular c-terminal domain in complex with calmodulin. *Structure* 22, 1582–1594. doi: 10.1016/j.str.2014.07.016

Salata, J. J., Jurkiewicz, N. K., Wang, J., Evans, B. E., Orme, H. T., and Sanguinetti, M. C. (1998). A novel benzodiazepine that activates cardiac slow delayed rectifier K+ currents. *Mol. Pharmacol.* 54, 220–230. doi: 10.1124/mol.54.1.220

Sanguinetti, M. C., Curran, M. E., Zou, A., Shen, J., Spector, P. S., Atkinson, D. L., et al. (1996). Coassembly of K(v)LQT1 and minK (IsK) proteins to form cardiac I-Ks potassium channel. *Nature* 384, 80–83. doi: 10.1038/384080a0

Saxena, P., Zangerl-Plessl, E. M., Linder, T., Windisch, A., Hohaus, A., Timin, E., et al. (2016). New potential binding determinant for hERG channel inhibitors. *Sci. Rep.* 6, 24182. doi: 10.1038/srep24182

Schoppa, N. E., Mccormack, K., Tanouye, M. A., and Sigworth, F. J. (1992). The size of gating charge in wild-type and mutant Shaker potassium channels. *Science* 255, 1712–1715. doi: 10.1126/science.1553560

Schroeder, B. C., Waldegger, S., Fehr, S., Bleich, M., Warth, R., Greger, R., et al. (2000). A constitutively open potassium channel formed by KCNQ1 and KCNE3. *Nature* 403, 196–199. doi: 10.1038/35003200

Schwake, M., Jentsch, T. J., and Friedrich, T. (2003). A carboxy-terminal domain determines the subunit specificity of KCNQ K+ channel assembly. *EMBO Rep.* 4, 76–81. doi: 10.1038/sj.embor.embor715

Schwake, M., Athanasiadu, D., Beimgraben, C., Blanz, J., Beck, C., Jentsch, T. J., et al. (2006). Structural determinants of M-type KCNQ (Kv7) K+ channel assembly. *J. Neurosci.* 26, 3757–3766. doi: 10.1523/JNEUROSCI.5017-05.2006

Schwartz, P. J., Priori, S. G., Spazzolini, C., Moss, A. J., Vincent, G. M., Napolitano, C., et al. (2001). Genotype-phenotype correlation in the long-QT syndrome: gene-specific triggers for life-threatening arrhythmias. *Circulation* 103, 89–95. doi: 10.1161/01.CIR.103.1.89

Schwartz, P. J., Stramba-Badiale, M., Crotti, L., Pedrazzini, M., Besana, A., Bosi, G., et al. (2009). Prevalence of the congenital long-QT syndrome. *Circulation* 120, 1761–1767. doi: 10.1161/CIRCULATIONAHA.109.863209

Schwartz, P. J., Crotti, L., and Insolia, R. (2012). Long-QT syndrome: from genetics to management. *Circ. Arrhythm Electrophysiol.* 5, 868–877. doi: 10.1161/CIRCEP.111.962019

Seebohm, G., Chen, J., Strutz, N., Culberson, C., Lerche, C., and Sanguinetti, M. C. (2003a). Molecular determinants of KCNQ1 channel block by a benzodiazepine. *Mol. Pharmacol.* 64, 70–77. doi: 10.1124/mol.64.1.70

Seebohm, G., Pusch, M., Chen, J., and Sanguinetti, M. C. (2003b). Pharmacological activation of normal and arrhythmia-associated mutant KCNQ1 potassium channels. *Circ. Res.* 93, 941–947. doi: 10.1161/01.RES.0000102866.67863.2B

Seebohm, G., Sanguinetti, M. C., and Pusch, M. (2003c). Tight coupling of rubidium conductance and inactivation in human KCNQ1 potassium channels. *J. Physiol. London* 552, 369–378. doi: 10.1113/jphysiol.2003.046490

Seebohm, G., Westenskow, P., Lang, F., and Sanguinetti, M. C. (2005). Mutation of colocalized residues of the pore helix and transmembrane segments S5 and S6 disrupt deactivation and modify inactivation of KCNQ1 K+ channels. *J. Physiol.* 563, 359–368. doi: 10.1113/jphysiol.2004.080887

Seebohm, G., Strutz-Seebohm, N., Ureche, O. N., Baltaev, R., Lampert, A., Kornichuk, G., et al. (2006). Differential roles of S6 domain hinges in the gating of KCNQ potassium channels. *Biophys. J.* 90, 2235–2244. doi: 10.1529/biophysj.105.067165

Selyanko, A. A., Hadley, J. K., Wood, I. C., Abogadie, F. C., Jentsch, T. J., and Brown, D. A. (2000). Inhibition of KCNQ1-4 potassium channels expressed in mammalian cells via M1 muscarinic acetylcholine receptors. *J. Physiol.* 522 (Pt 3), 349–355. doi: 10.1111/j.1469-7793.2000.t01-2-00349.x

Seoh, S. A., Sigg, D., Papazian, D. M., and Bezanilla, F. (1996). Voltage-sensing residues in the S2 and S4 segments of the Shaker K+ channel. *Neuron* 16, 1159–1167. doi: 10.1016/S0896-6273(00)80142-7

Sesti, F., Abbott, G. W., Wei, J., Murray, K. T., Saksena, S., Schwartz, P. J., et al. (2000). A common polymorphism associated with antibiotic-induced cardiac arrhythmia. *Proc. Natl. Acad. Sci. U. States America* 97, 10613–10618. doi: 10.1073/pnas.180223197

Shen, H., Zhou, Q., Pan, X., Li, Z., Wu, J., and Yan, N. (2017). Structure of a eukaryotic voltage-gated sodium channel at near-atomic resolution. *Science* 355, pii: eaal4326. doi: 10.1126/science.aal4326

Shen, H., Liu, D., Wu, K., Lei, J., and Yan, N. (2019). Structures of human Nav1.7 channel in complex with auxiliary subunits and animal toxins. *Science* 363, 1303–1308. doi: 10.1126/science.aaw2493

Shimizu, W., and Antzelevitch, C. (1998). Cellular basis for the ECG features of the LQT1 form of the long-QT syndrome: effects of beta-adrenergic agonists and antagonists and sodium channel blockers on transmural dispersion of repolarization and torsade de pointes. *Circulation* 98, 2314–2322. doi: 10.1161/01.CIR.98.21.2314

Shimizu, W., Horie, M., Ohno, S., Takenaka, K., Yamaguchi, M., Shimizu, M., et al. (2004). Mutation site-specific differences in arrhythmic risk and sensitivity to sympathetic stimulation in the LQT1 form of congenital long QT syndrome: multicenter study in Japan. *J. Am. Coll. Cardiol.* 44, 117–125. doi: 10.1016/j.jacc.2004.03.043

Shy, D., Gillet, L., and Abriel, H. (2013). Cardiac sodium channel NaV1.5 distribution in myocytes via interacting proteins: the multiple pool model. *Biochim. Biophys. Acta* 1833, 886–894. doi: 10.1016/j.bbamcr.2012.10.026

Skinner, J. R., Winbo, A., Abrams, D., Vohra, J., and Wilde, A. A. (2019). Channelopathies That Lead to Sudden Cardiac Death: Clinical and Genetic Aspects. *Heart Lung Circ.* 28, 22–30. doi: 10.1016/j.hlc.2018.09.007

Smith, P. L., Baukrowitz, T., and Yellen, G. (1996). The inward rectification mechanism of the HERG cardiac potassium channel. *Nature* 379, 833–836. doi: 10.1038/379833a0

Smith, J. L., Anderson, C. L., Burgess, D. E., Elayi, C. S., January, C. T., and Delisle, B. P. (2016). Molecular pathogenesis of long QT syndrome type 2. *J. Arrhythm* 32, 373–380. doi: 10.1016/j.joa.2015.11.009

Sokolov, S., Scheuer, T., and Catterall, W. A. (2007). Gating pore current in an inherited ion channelopathy. *Nature* 446, 76–78. doi: 10.1038/nature05598

Stansfeld, P. J., Grottesi, A., Sands, Z. A., Sansom, M. S., Gedeck, P., Gosling, M., et al. (2008). Insight into the mechanism of inactivation and pH sensitivity in potassium channels from molecular dynamics simulations. *Biochemistry* 47, 7414–7422. doi: 10.1021/bi800475j

Stenson, P. D., Ball, E. V., Mort, M., Phillips, A. D., Shaw, K., and Cooper, D. N. (2012). The Human Gene Mutation Database (HGMD) and its exploitation in the fields of personalized genomics and molecular evolution. *Curr. Protoc. Bioinf.* Chapter 1, Unit1 13. 1.13.1–1.13.20 doi: 10.1002/0471250953.bi0113s39

Strutz-Seebohm, N., Pusch, M., Wolf, S., Stoll, R., Tapken, D., Gerwert, K., et al. (2011). Structural basis of slow activation gating in the cardiac I Ks channel complex. *Cell Physiol. Biochem.* 27, 443–452. doi: 10.1159/000329965

Sun, J., and Mackinnon, R. (2017). Cryo-EM Structure of a KCNQ1/CaM Complex Reveals Insights into Congenital Long QT Syndrome. *Cell* 169, 1042–1050.e1049. doi: 10.1016/j.cell.2017.05.019

Sun, J., and Mackinnon, R. (2020). Structural Basis of Human KCNQ1 Modulation and Gating. *Cell* 180, 340–347 e349. doi: 10.1016/j.cell.2019.12.003

Sunami, A., Dudley, S. C.Jr., and Fozzard, H. A. (1997). Sodium channel selectivity filter regulates antiarrhythmic drug binding. *Proc. Natl. Acad. Sci. U. S. A* 94, 14126–14131. doi: 10.1073/pnas.94.25.14126

Tao, X., Lee, A., Limapichat, W., Dougherty, D. A., and Mackinnon, R. (2010). A gating charge transfer center in voltage sensors. *Science* 328, 67–73. doi: 10.1126/science.1185954

Tapper, A. R., and George, A. L. (2001). Location and orientation of minK within the I-Ks potassium channel complex. *J. Biol. Chem.* 276, 38249–38254. doi: 10.1074/jbc.M103956200

Taylor, K. C., and Sanders, C. R. (2017). Regulation of KCNQ/Kv7 family voltage-gated K(+) channels by lipids. *Biochim. Biophys. Acta Biomembr* 1859, 586–597. doi: 10.1016/j.bbamem.2016.10.023

Taylor, K. C., Kang, P. W., Hou, P., Yang, N.-D., Kuenze, G., Smith, J. A., et al. (2020). Structure and Physiological Function of the Human KCNQ1 Channel Voltage Sensor Intermediate State. *eLife* 9, e53901. doi: 10.7554/eLife.53901

Terrenoire, C., Wang, K., Tung, K. W., Chung, W. K., Pass, R. H., Lu, J. T., et al. (2013). Induced pluripotent stem cells used to reveal drug actions in a long QT syndrome family with complex genetics. *J. Gen. Physiol.* 141, 61–72. doi: 10.1085/jgp.201210899

Tester, D. J., and Ackerman, M. J. (2014). Genetics of long QT syndrome. *Methodist Debakey Cardiovasc. J.* 10, 29–33. doi: 10.14797/mdcj-10-1-29

Thomas, D., Khalil, M., Alter, M., Schweizer, P. A., Karle, C. A., Wimmer, A. B., et al. (2010). Biophysical characterization of KCNQ1 P320 mutations linked to long QT syndrome 1. *J. Mol. Cell Cardiol.* 48, 230–237. doi: 10.1016/j.yjmcc.2009.06.009

Thomas, A. M., Harmer, S. C., Khambra, T., and Tinker, A. (2011). Characterization of a binding site for anionic phospholipids on KCNQ1. *J. Biol. Chem.* 286, 2088–2100. doi: 10.1074/jbc.M110.153551

Tinel, N., Diochot, S., Borsotto, M., Lazdunski, M., and Barhanin, J. (2000). KCNE2 confers background current characteristics to the cardiac KCNQ1 potassium channel. *EMBO J.* 19, 6326–6330. doi: 10.1093/emboj/19.23.6326

Tobelaim, W. S., Dvir, M., Lebel, G., Cui, M., Buki, T., Peretz, A., et al. (2017a). Ca(2+)-Calmodulin and PIP2 interactions at the proximal C-terminus of Kv7 channels. *Channels (Austin)* 11, 686–695. doi: 10.1080/19336950.2017.1388478

Tobelaim, W. S., Dvir, M., Lebel, G., Cui, M., Buki, T., Peretz, A., et al. (2017b). Competition of calcified calmodulin N lobe and PIP2 to an LQT mutation site in Kv7.1 channel. *Proc. Natl. Acad. Sci. U. S. A* 114, E869–E878. doi: 10.1073/pnas.1612622114

Toh, M. F., Brooks, J. M., Strassmaier, T., Haedo, R. J., Puryear, C. B., Roth, B. L., et al. (2020). Application of High-Throughput Automated Patch-Clamp Electrophysiology to Study Voltage-Gated Ion Channel Function in Primary Cortical Cultures. *SLAS Discovery*, 2472555220902388. doi: 10.1177/2472555220902388

Toombes, G. E., and Swartz, K. J. (2016). STRUCTURAL BIOLOGY. Twists and turns in gating ion channels with voltage. *Science* 353, 646–647. doi: 10.1126/science.aah4194

Tsang, S. Y., Tsushima, R. G., Tomaselli, G. F., Li, R. A., and Backx, P. H. (2005). A multifunctional aromatic residue in the external pore vestibule of Na+ channels contributes to the local anesthetic receptor. *Mol. Pharmacol.* 67, 424–434. doi: 10.1124/mol.67.2.424

Ulmschneider, M. B., Bagneris, C., Mccusker, E. C., Decaen, P. G., Delling, M., Clapham, D. E., et al. (2013). Molecular dynamics of ion transport through the open conformation of a bacterial voltage-gated sodium channel. *Proc. Natl. Acad. Sci. U. S. A* 110, 6364–6369. doi: 10.1073/pnas.1214667110

Urrutia, J., Aguado, A., Muguruza-Montero, A., Nunez, E., Malo, C., Casis, O., et al. (2019). The Crossroad of Ion Channels and Calmodulin in Disease. *Int. J. Mol. Sci.* 20, pii: E400. doi: 10.3390/ijms20020400

Vaidyanathan, R., Reilly, L., and Eckhardt, L. L. (2018). Caveolin-3 Microdomain: Arrhythmia Implications for Potassium Inward Rectifier and Cardiac Sodium Channel. *Front. Physiol.* 9, 1548. doi: 10.3389/fphys.2018.01548

Valdivia, C. R., Medeiros-Domingo, A., Ye, B., Shen, W. K., Algiers, T. J., Ackerman, M. J., et al. (2010). Loss-of-function mutation of the SCN3B-encoded sodium channel {beta}3 subunit associated with a case of idiopathic ventricular fibrillation. *Cardiovasc. Res.* 86, 392–400. doi: 10.1093/cvr/cvp417

Van Horn, W. D., Vanoye, C. G., and Sanders, C. R. (2011). Working model for the structural basis for KCNE1 modulation of the KCNQ1 potassium channel. *Curr. Opin. Struct. Biol.* 21, 283–291. doi: 10.1016/j.sbi.2011.01.001

Vandenberg, J. I., Varghese, A., Lu, Y., Bursill, J. A., Mahaut-Smith, M. P., and Huang, C. L. (2006). Temperature dependence of human ether-a-go-go-related gene K+ currents. *Am. J. Physiol. Cell Physiol.* 291, C165–C175. doi: 10.1152/ajpcell.00596.2005

Vandenberg, J. I., Perry, M. D., Perrin, M. J., Mann, S. A., Ke, Y., and Hill, A. P. (2012). hERG K(+) channels: structure, function, and clinical significance. *Physiol. Rev.* 92, 1393–1478. doi: 10.1152/physrev.00036.2011

Vandenberg, J. I., Perozo, E., and Allen, T. W. (2017). Towards a Structural View of Drug Binding to hERG K(+) Channels. *Trends Pharmacol. Sci.* 38, 899–907. doi: 10.1016/j.tips.2017.06.004

Vanoye, C. G., Desai, R. R., Fabre, K. L., Gallagher, S. L., Potet, F., Dekeyser, J. M., et al. (2018). High-Throughput Functional Evaluation of KCNQ1 Decrypts Variants of Unknown Significance. *Circ. Genom. Precis Med.* 11, e002345. doi: 10.1161/CIRCGEN.118.002345

Vardanyan, V., and Pongs, O. (2012). Coupling of voltage-sensors to the channel pore: a comparative view. *Front. Pharmacol.* 3, 145. doi: 10.3389/fphar.2012.00145

Viswanathan, P. C., Shaw, R. M., and Rudy, Y. (1999). Effects of IKr and IKs heterogeneity on action potential duration and its rate dependence: a simulation study. *Circulation* 99, 2466–2474. doi: 10.1161/01.CIR.99.18.2466

Vitola, J., Vukanovic, J., and Roden, D. M. (1998). Cisapride-induced torsades de pointes. *J. Cardiovasc. Electrophysiol.* 9, 1109–1113. doi: 10.1111/j.1540-8167.1998.tb00888.x

Wacker, S., Noskov, S. Y., and Perissinotti, L. L. (2017). Computational Models for Understanding of Structure, Function and Pharmacology of the Cardiac Potassium Channel Kv11.1 (hERG). *Curr. Top. Med. Chem.* 17, 2681–2702. doi: 10.2174/1568026617666170414143430

Wallace, E., Howard, L., Liu, M., O'brien, T., Ward, D., Shen, S., et al. (2019). Long QT Syndrome: Genetics and Future Perspective. *Pediatr. Cardiol.* 40, 1419–1430. doi: 10.1007/s00246-019-02151-x

Wang, W., and Mackinnon, R. (2017). Cryo-EM Structure of the Open Human Ether-a-go-go-Related K(+) Channel hERG. *Cell* 169, 422–430 e410. doi: 10.1016/j.cell.2017.03.048

Wang, Z., Tristani-Firouzi, M., Xu, Q., Lin, M., Keating, M. T., and Sanguinetti, M. C. (1999). Functional effects of mutations in KvLQT1 that cause long QT syndrome. *J. Cardiovasc. Electrophysiol.* 10, 817–826. doi: 10.1111/j.1540-8167.1999.tb00262.x

Wang, L., Dennis, A. T., Trieu, P., Charron, F., Ethier, N., Hebert, T. E., et al. (2009). Intracellular potassium stabilizes human ether-a-go-go-related gene channels for export from endoplasmic reticulum. *Mol. Pharmacol.* 75, 927–937. doi: 10.1124/mol.108.053793

Wang, P., Yang, Q., Wu, X., Yang, Y., Shi, L., Wang, C., et al. (2010). Functional dominant-negative mutation of sodium channel subunit gene SCN3B associated with atrial fibrillation in a Chinese GeneID population. *Biochem. Biophys. Res. Commun.* 398, 98–104. doi: 10.1016/j.bbrc.2010.06.042

Wang, Y. H., Jiang, M., Xu, X. L., Hsu, K.-L., Zhang, M., and Tseng, G.-N. (2011). Gating-related molecular motions in the extracellular domain of the IKs channel: implications for IKs channelopathy. *J. Membr. Biol.* 239, 137–156. doi: 10.1007/s00232-010-9333-7

Wang, C., Chung, B. C., Yan, H., Lee, S. Y., and Pitt, G. S. (2012). Crystal structure of the ternary complex of a NaV C-terminal domain, a fibroblast growth factor homologous factor, and calmodulin. *Structure* 20, 1167–1176. doi: 10.1016/j.str.2012.05.001

Watanabe, H., Koopmann, T. T., Le Scouarnec, S., Yang, T., Ingram, C. R., Schott, J. J., et al. (2008). Sodium channel beta1 subunit mutations associated with Brugada syndrome and cardiac conduction disease in humans. *J. Clin. Invest.* 118, 2260–2268. doi: 10.1172/JCI33891

Watanabe, H., Darbar, D., Kaiser, D. W., Jiramongkolchai, K., Chopra, S., Donahue, B. S., et al. (2009). Mutations in sodium channel beta1- and beta2-subunits associated with atrial fibrillation. *Circ. Arrhythm Electrophysiol.* 2, 268–275. doi: 10.1161/CIRCEP.108.779181

Weerapura, M., Nattel, S., Chartier, D., Caballero, R., and Hebert, T. E. (2002). A comparison of currents carried by HERG, with and without coexpression of MiRP1, and the native rapid delayed rectifier current. Is MiRP1 the missing link? *J. Physiol.* 540, 15–27. doi: 10.1113/jphysiol.2001.013296

Whicher, J. R., and Mackinnon, R. (2016). Structure of the voltage-gated K(+) channel Eag1 reveals an alternative voltage sensing mechanism. *Science* 353, 664–669. doi: 10.1126/science.aaf8070

Wiener, R., Haitin, Y., Shamgar, L., Fernandez-Alonso, M. C., Martos, A., Chomsky-Hecht, O., et al. (2008). The KCNQ1 (Kv7.1) COOH terminus, a multitiered scaffold for subunit assembly and protein interaction. *J. Biol. Chem.* 283, 5815–5830. doi: 10.1074/jbc.M707541200

Wilde, A., and Amin, A. S. (2018). Clinical Spectrum of SCN5A Mutations: Long QT Syndrome, Brugada Syndrome, and Cardiomyopathy. *JACC Clin. Electrophysiol.* 4, 569–579. doi: 10.1016/j.jacep.2018.03.006

Wisedchaisri, G., Tonggu, L., Mccord, E., Gamal El-Din, T. M., Wang, L., Zheng, N., et al. (2019). Resting-State Structure and Gating Mechanism of a Voltage-Gated Sodium Channel. *Cell* 178, 993–1003 e1012. doi: 10.1016/j.cell.2019.06.031

Wu, L., Shryock, J. C., Song, Y., Li, Y., Antzelevitch, C., and Belardinelli, L. (2004). Antiarrhythmic effects of ranolazine in a guinea pig in vitro model of long-QT syndrome. *J. Pharmacol. Exp. Ther.* 310, 599–605. doi: 10.1124/jpet.104.066100

Wu, L., Yong, S. L., Fan, C., Ni, Y., Yoo, S., Zhang, T., et al. (2008). Identification of a new co-factor, MOG1, required for the full function of cardiac sodium channel Nav 1.5. *J. Biol. Chem.* 283, 6968–6978. doi: 10.1074/jbc.M709721200

Wu, D., Delaloye, K., Zaydman, M. A., Nekouzadeh, A., Rudy, Y., and Cui, J. (2010a). State-dependent electrostatic interactions of S4 arginines with E1 in S2 during Kv7.1 activation. *J. Gen. Physiol.* 135, 595–606. doi: 10.1085/jgp.201010408

Wu, D., Pan, H., Delaloye, K., and Cui, J. (2010b). KCNE1 remodels the voltage sensor of Kv7.1 to modulate channel function. *Biophys. J.* 99, 3599–3608. doi: 10.1016/j.bpj.2010.10.018

Wu, J., Ding, W. G., and Horie, M. (2016). Molecular pathogenesis of long QT syndrome type 1. *J. Arrhythm* 32, 381–388. doi: 10.1016/j.joa.2015.12.006

Xiao, Y. F., Wright, S. N., Wang, G. K., Morgan, J. P., and Leaf, A. (1998). Fatty acids suppress voltage-gated Na+ currents in HEK293t cells transfected with the alpha-subunit of the human cardiac Na+ channel. *Proc. Natl. Acad. Sci. U. S. A* 95, 2680–2685. doi: 10.1073/pnas.95.5.2680

Xiao, Y. F., Ke, Q., Wang, S. Y., Auktor, K., Yang, Y., Wang, G. K., et al. (2001). Single point mutations affect fatty acid block of human myocardial sodium channel alpha subunit Na+ channels. *Proc. Natl. Acad. Sci. U. S. A* 98, 3606–3611. doi: 10.1073/pnas.061003798

Xu, X., Jiang, M., Hsu, K.-L., Zhang, M., and Tseng, G.-N. (2008). KCNQ1 and KCNE1 in the IKs channel complex make state-dependent contacts in their extracellular domains. *J. Gen. Physiol.* 131, 589–603. doi: 10.1085/jgp.200809976

Xu, Y., Wang, Y., Meng, X.-Y., Zhang, M., Jiang, M., Cui, M., et al. (2013). Building KCNQ1/KCNE1 channel models and probing their interactions by molecular-dynamics simulations. *Biophys. J.* 105, 2461–2473. doi: 10.1016/j.bpj.2013.09.058

Xu, Y., Wang, Y., Zhang, M., Jiang, M., Rosenhouse-Dantsker, A., Wassenaar, T., et al. (2015). Probing binding sites and mechanisms of action of an I(Ks) activator by computations and experiments. *Biophys. J.* 108, 62–75. doi: 10.1016/j.bpj.2014.10.059

Xu, H., Li, T., Rohou, A., Arthur, C. P., Tzakoniati, F., Wong, E., et al. (2019). Structural Basis of Nav1.7 Inhibition by a Gating-Modifier Spider Toxin. *Cell* 176702-715, e714. doi: 10.1016/j.cell.2018.12.018

Yan, H., Wang, C., Marx, S. O., and Pitt, G. S. (2017a). Calmodulin limits pathogenic Na+ channel persistent current. *J. Gen. Physiol.* 149, 277–293. doi: 10.1085/jgp.201611721

Yan, Z., Zhou, Q., Wang, L., Wu, J., Zhao, Y., Huang, G., et al. (2017b). Structure of the Nav1.4-beta1 Complex from Electric Eel. *Cell* 170, 470–482 e411. doi: 10.1016/j.cell.2017.06.039

Yang, W. P., Levesque, P. C., Little, W. A., Conder, M. L., Shalaby, F. Y., and Blanar, M. A. (1997). KvLQT1, a voltage-gated potassium channel responsible for human cardiac arrhythmias. *Proc. Natl. Acad. Sci. U. S. A* 94, 4017–4021. doi: 10.1073/pnas.94.8.4017

Yang, T., Smith, J. A., Leake, B. F., Sanders, C. R., Meiler, J., and Roden, D. M. (2013). An allosteric mechanism for drug block of the human cardiac potassium channel KCNQ1. *Mol. Pharmacol.* 83, 481–489. doi: 10.1124/mol.112.081513

Yang, J., Wang, Z., Sinden, D. S., Wang, X., Shan, B., Yu, X., et al. (2016). FGF13 modulates the gating properties of the cardiac sodium channel Nav1.5 in an isoform-specific manner. *Channels (Austin)* 10, 410–420. doi: 10.1080/19336950.2016.1190055

Yarov-Yarovoy, V., Brown, J., Sharp, E. M., Clare, J. J., Scheuer, T., and Catterall, W. A. (2001). Molecular determinants of voltage-dependent gating and binding of pore-blocking drugs in transmembrane segment IIIS6 of the Na(+) channel alpha subunit. *J. Biol. Chem.* 276, 20–27. doi: 10.1074/jbc.M006992200

Yarov-Yarovoy, V., Mcphee, J. C., Idsvoog, D., Pate, C., Scheuer, T., and Catterall, W. A. (2002). Role of amino acid residues in transmembrane segments IS6 and IIS6 of the Na+ channel alpha subunit in voltage-dependent gating and drug block. *J. Biol. Chem.* 277, 35393–35401. doi: 10.1074/jbc.M206126200

Yus-Najera, E., Santana-Castro, I., and Villarroel, A. (2002). The identification and characterization of a noncontinuous calmodulin-binding site in noninactivating voltage-dependent KCNQ potassium channels. *J. Biol. Chem.* 277, 28545–28553. doi: 10.1074/jbc.M204130200

Zaydman, M. A., Silva, J. R., Delaloye, K., Li, Y., Liang, H., Larsson, H. P., et al. (2013). Kv7.1 ion channels require a lipid to couple voltage sensing to pore opening. *Proc. Natl. Acad. Sci. U. S. A* 110, 13180–13185. doi: 10.1073/pnas.1305167110

Zaydman, M. A., Kasimova, M. A., Mcfarland, K., Beller, Z., Hou, P., Kinser, H. E., et al. (2014). Domain-domain interactions determine the gating, permeation, pharmacology, and subunit modulation of the IKs ion channel. *eLife* 3, e03606. doi: 10.7554/eLife.03606

Zaza, A., Belardinelli, L., and Shryock, J. C. (2008). Pathophysiology and pharmacology of the cardiac "late sodium current". *Pharmacol. Ther.* 119, 326–339. doi: 10.1016/j.pharmthera.2008.06.001

Zhang, H., Craciun, L. C., Mirshahi, T., Rohacs, T., Lopes, C. M., Jin, T., et al. (2003). PIP(2) activates KCNQ channels, and its hydrolysis underlies receptor-mediated inhibition of M currents. *Neuron* 37, 963–975. doi: 10.1016/S0896-6273(03)00125-9

Zhang, M., Liu, J., and Tseng, G. N. (2004). Gating charges in the activation and inactivation processes of the HERG channel. *J. Gen. Physiol.* 124, 703–718. doi: 10.1085/jgp.200409119

Zhang, X. C., Yang, H., Liu, Z., and Sun, F. (2018). Thermodynamics of voltage-gated ion channels. *Biophys. Rep.* 4, 300–319. doi: 10.1007/s41048-018-0074-y

Zhao, J. T., Hill, A. P., Varghese, A., Cooper, A. A., Swan, H., Laitinen-Forsblom, P. J., et al. (2009). Not all hERG pore domain mutations have a severe phenotype: G584S has an inactivation gating defect with mild phenotype compared to G572S, which has a dominant negative trafficking defect and a severe phenotype. *J. Cardiovasc. Electrophysiol.* 20, 923–930. doi: 10.1111/j.1540-8167.2009.01468.x

Zhou, Z., Vorperian, V. R., Gong, Q., Zhang, S., and January, C. T. (1999). Block of HERG potassium channels by the antihistamine astemizole and its metabolites desmethylastemizole and norastemizole. *J. Cardiovasc. Electrophysiol.* 10, 836–843. doi: 10.1111/j.1540-8167.1999.tb00264.x

Zhou, Y., Morais-Cabral, J. H., Kaufman, A., and Mackinnon, R. (2001). Chemistry of ion coordination and hydration revealed by a K+ channel-Fab complex at 2.0 A resolution. *Nature* 414, 43–48. doi: 10.1038/35102009

Zhu, W., Voelker, T. L., Varga, Z., Schubert, A. R., Nerbonne, J. M., and Silva, J. R. (2017). Mechanisms of noncovalent beta subunit regulation of NaV channel gating. *J. Gen. Physiol.* 149 (8), 813–831. doi: 10.1085/jgp.201711802

Zipes, D. P., Camm, A. J., Borggrefe, M., Buxton, A. E., Chaitman, B., Fromer, M., et al. (2006). ACC/AHA/ESC 2006 Guidelines for Management of Patients With Ventricular Arrhythmias and the Prevention of Sudden Cardiac Death: a report of the American College of Cardiology/American Heart Association Task Force and the European Society of Cardiology Committee for Practice Guidelines (writing committee to develop Guidelines for Management of Patients With Ventricular Arrhythmias and the Prevention of Sudden Cardiac Death): developed in collaboration with the European Heart Rhythm Association and the Heart Rhythm Society. *Circulation* 114, e385–e484. doi: 10.1161/CIRCULATIONAHA.106.178233

Conflict of Interest: The authors declare that the research was conducted in the absence of any commercial or financial relationships that could be construed as a potential conflict of interest.

frontiers in Pharmacology

REVIEW
published: 15 May 2020
doi: 10.3389/fphar.2020.00735

Hydrophobic Drug/Toxin Binding Sites in Voltage-Dependent K^+ and Na^+ Channels

Kenny M. Van Theemsche†, *Dieter V. Van de Sande*†, *Dirk J. Snyders and Alain J. Labro**

Laboratory of Molecular, Cellular, and Network Excitability, University of Antwerp, Antwerp, Belgium

In the Na_v channel family the lipophilic drugs/toxins binding sites and the presence of fenestrations in the channel pore wall are well defined and categorized. No such classification exists in the much larger K_v channel family, although certain lipophilic compounds seem to deviate from binding to well-known hydrophilic binding sites. By mapping different compound binding sites onto 3D structures of Kv channels, there appear to be three distinct lipid-exposed binding sites preserved in K_v channels: the front and back side of the pore domain, and S2-S3/S3-S4 clefts. One or a combination of these sites is most likely the orthologous equivalent of neurotoxin site 5 in Na_v channels. This review describes the different lipophilic binding sites and location of pore wall fenestrations within the K_v channel family and compares it to the knowledge of Na_v channels.

Keywords: hydrophobic binding sites, voltage-gated potassium channels, voltage-gated sodium channels, channel fenestrations, lipophilic compounds

OPEN ACCESS

Edited by:
Mounir Tarek,
Centre National de la Recherche Scientifique (CNRS), France

Reviewed by:
Michael E. O'Leary,
Cooper Medical School of Rowan University, United States
Roope Mannikko,
University College London, United Kingdom

***Correspondence:**
Alain J. Labro
alain.labro@uantwerpen.be

†*These authors share first authorship*

Specialty section:
This article was submitted to Pharmacology of Ion Channels and Channelopathies, a section of the journal Frontiers in Pharmacology

Received: *31 January 2020*
Accepted: *04 May 2020*
Published: *15 May 2020*

Citation:
Van Theemsche KM, Van de Sande DV, Snyders DJ and Labro AJ (2020) Hydrophobic Drug/Toxin Binding Sites in Voltage-Dependent K^+ and Na^+ Channels. Front. Pharmacol. 11:735. doi: 10.3389/fphar.2020.00735

INTRODUCTION

Voltage-gated ion channels are transmembrane proteins that are selectively permeable to physiological important ions such as Na^+, K^+, Ca^{2+}, and Cl^-. Under influence of the membrane potential (Vm) these channels change their conductance. In the conductive open (or activated) state, ions flow down their electrochemical gradient through the channel pore. The flux of these ions elicits an electrical current that directly influences the Vm. For voltage-gated sodium and potassium channels (Na_v and K_v), the main focus of this review, the Vm will shift towards the ion's equilibrium potential, which under normal conditions is depolarizing and repolarizing, respectively (Hille, 2001). Although Na_v and K_v channels differ in selectivity from one another, their structure is quite similar. However, a main difference is that Na_v channels are characterized by one large α-subunit containing four recognizable domains (DI–IV), whereas K_v channels are formed by tetramerization of four individual α-subunits. In both cases, these four entities comprise six transmembrane segments (S1–S6), which are divided into a voltage sensing domain (VSD, S1–S4) and a pore-forming domain (PD, S5–S6) that are connected by the S4–S5 linker. The four PDs assemble into the ion permeation pathway (or pore) that is surrounded by four VSDs. In the non-conductive closed (or deactivated) state, ion permeation is prevented by the intracellular activation gate, located at the point where the four S6 helices cross. The aperture-like opening and closure of this gate is controlled by the VSD (Doyle et al., 1998; Bavro et al., 2012; Labro and Snyders, 2012; Lenaeus et al., 2017). The main component of the VSD is the S4 segment that physically moves in response to a change in Vm, due to the presence of positively charged residues (arginine and lysine) that detect

changes in the membrane electric field (Bezanilla, 2008). The S4–S5 linker is a component of the electro-mechanical coupling that translates S4 movements into opening or closing of the activation gate (Bezanilla, 2008; Blunck and Batulan, 2012). After opening, fast inactivation occurs in Na_v and in some K_v channels, which is caused by the physical occlusion of the pore by an inactivation particle. For Na_v channels this inactivation particle is the linker between DIII and DIV, while in K_v channels it is located at the N-terminus of each subunit, hence termed N-type inactivation (Hoshi et al., 1990; West et al., 1992; Armstrong and Hollingworth, 2018). Alternatively, K_v channel inactivation can occur *via* the slower C- or U-type inactivation mechanism that makes the channels non or less conductive (Hoshi et al., 1991; Klemic et al., 1998; Cuello et al., 2010).

Binding of drugs/toxins to Na_v and K_v channels may alter the activation, deactivation, and/or inactivation process(es), which may cause or alleviate aberrant electrical excitability. Therefore, knowledge about the different binding sites is key for drug development and pharmacovigilance. The binding sites for these drugs/toxins are well defined and categorized within the Na_v channel family, as opposed to the much larger K_v channel family. Most binding sites are enveloped by water, locating either inside or outside the channel's pore. However, some compounds bind to a site(s) that does not fit any of the hydrophilic binding sites. For instance, brevetoxins and ciguatoxins bind to a conserved hydrophobic site within the Na_v channel family, termed neurotoxin site 5 (Catterall and Risk, 1981; Cestele and Catterall, 2000). For the K_v channel family no such site has been described, but certain compounds have been shown to deviate from binding to hydrophilic binding sites like; retigabine, gambierol, psora-4, polyunsaturated fatty acids (PUFAs), ICA-compounds (Vennekamp et al., 2004; Kopljar et al., 2009; Lange et al., 2009; Borjesson and Elinder, 2011). It is notable that these are rather lipophilic compounds and there has been, and still is, a growing interest in such compounds for their use in treating neurological disorders (e.g., as anti-convulsant).

So, is there a unifying picture of the lipid exposed/accessible drug/toxin binding sites within the large K_v channel family and even between K_v and Na_v channels? Several lipophilic binding sites have been described in different K_v channels, while in fact some may converge to just one binding region preserved between Kv channel (sub)families. In this review, the well-documented Na_v lipophilic binding sites, neurotoxin site 2, site 5, and the access to the local anaesthetic (LA) binding site within the pore through fenestrations is compared to what has been reported for K_v channels.

VOLTAGE-GATED SODIUM CHANNELS

The Na_v channel family contains nine isoforms ($Na_v1.1$ to $Na_v1.9$) that display a high sequence homology, especially within the transmembrane segments (Marban et al., 1998; Ahern et al., 2016). This facilitated the categorization of drug/toxin binding sites within the Na_v channel family. Over the past decades a detailed picture emerged on where compounds bind within these channels and resulted in a well-documented classification of seven different sites (site 1 to 7) and a LA binding site (Stevens et al., 2011; De Lera Ruiz and Kraus, 2015). As the focus of this review is on the binding sites that involve lipid soluble and/or transmembrane binding compounds only binding site 5 and site 2 will be briefly discussed. The LA binding site is also mentioned as some compounds can reach their binding site *via* hydrophobic fenestrations in the pore wall of the channel protein. To maintain an orderly overview, all Na_v residues are numbered according to the $Na_v1.4$ channel when possible. In case the sequence could not be aligned, as for bacterial Na_v structures, it will be noted and the original numbering is maintained.

The Closed State Accessible LA Binding Site: Pore-Accessibility Through Channel Fenestrations

LA compounds and anti-arrhythmic drugs inhibit Na_v channels by occlusion of the pore. Most LA compounds have a similar structure consisting of a tertiary hydrophilic amine domain (head) linked with an aromatic hydrophobic ring domain, with a total length of 10–15Å (Courtney, 1988). Three types of block can be observed. First type is the use dependent open state block, or high affinity block, which occurs after channel opening and LA compounds enter the pore *via* the intracellular side (Grant et al., 1989; Benz and Kohlhardt, 1991; Gingrich et al., 1993). The second type is flicker block, or fast block, which is only observed when the channel's inactivation process is modulated. For example, by other compounds such as batrachotoxin (BTX) (CAS No.:23509-16-2) that binds at site 2 (Cahalan, 1978; Uehara and Moczydlowski, 1986; Zamponi et al., 1993). The third and least common type is the resting or hydrophilic block that establishes when the channel is closed. LA compounds are thought to enter the ion conductive pore and find their binding site trough fenestrations in the lipid exposed part of the PD (Gamal El-Din et al., 2018). LA compounds are protonated but for crossing the cell membrane they need to be deprotonated. This is possible when their pKA value is close to the physiological pH values in the extracellular environment. After traversing the cell membrane the compounds are protonated again to exert their pharmacological effect (Hille, 1977). As the binding site is located within the pore, block occurs with the highest affinity when the channel is opened or used, while applying frequent channel activating stimuli. Two residues within the S6 of domain four (DIV-S6) have been identified to be important for LA binding/modulation, namely, F1586 and Y1593, ($Na_v1.4$ numbering). F1586 probably binds to the alkylamino head, while Y1593 interacts with the aromatic ring structure (Ragsdale et al., 1994; Yarov-Yarovoy et al., 2002) (**Figures 1A, B**). As these residues reside within the pore and certain compounds display closed state block, this requires a hydrophobic pathway to the binding site when the channel gate is closed (Hille, 1977).

These pathways, or fenestrations, in the lipid exposed part of the PD were first observed in the crystal structure of bacterial Na_v channels such as Na_vAb (Payandeh et al., 2011;

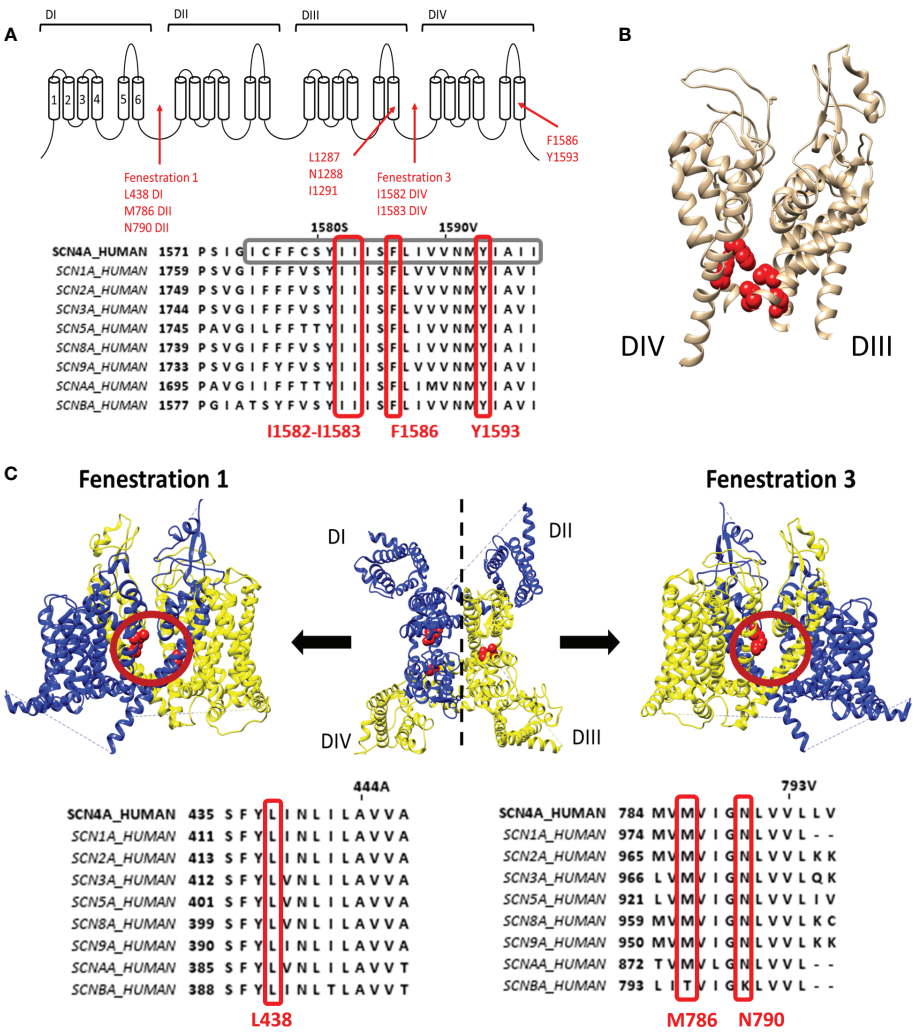

FIGURE 1 | Representation of the local anaesthetic (LA) binding site and the hydrophobic access paths or fenestrations. **(A)** Schematic representation of the Na_v channel topology which contains four domains (DI to DIV) each consisting out of six transmembrane segments (S1–S6). Regions and location of residues important for LA binding are indicated with red arrows. Fenestrations that are sufficiently large to allow passage of LA compound are between DI–DII (fenestration 1) and DIII–DIV (fenestration 3) with the bottleneck residues listed below. This schematic representation is then followed by an alignment of $Na_v1.4$ DIV with the other human isoforms, with marked in grey S6 and marked in red well conserved residues for LA binding and the fenestration bottleneck (I1582–I1583). Mutation of I1582 can also create a pathway connecting the inner pore with the extracellular environment. **(B)** 3D structure of the $Na_v1.4$ channel representing the S5–S6 segments of DIII and DIV. In red are the residues, forming the LA binding site, visualized which are listed in panel A, clearly marking the inner pore LA binding site. **(C)** In the middle a top view of the 3D structure of the $Na_v1.4$ channel is shown with in blue the DI–DII domains and in yellow the DIII-DIV domains. Fenestration 1 locates between DI and DII a side view of it shown on the left. A side view of fenestration 3 is shown on the right. Both fenestrations are highlighted by a red circle and the residues responsible for creating the bottleneck of the fenestration are represented in red. Below are the alignments of $Na_v1.4$ with the other isoforms. On the left the bottleneck residue of DI is marked in red, on the right the bottleneck residues of DII. Amino acid sequence alignment and 3D structures are visualized using Jalview and chimera software, respectively (Pettersen et al., 2004; Waterhouse et al., 2009).

Payandeh et al., 2012), Na_vMs (Mccusker et al., 2012) and Na_vRh (Zhang et al., 2012). It should be noted that bacterial Na_v channels are constructed out of four separate α-subunits instead of one large subunit. For the bacterial Na_v channels, four fenestrations are observed between the different domains where the radius of the fenestration varies from 0.8Å minimally to 2.59-2.83Å (Kaczmarski and Corry, 2014). Nonetheless, these fenestrations are wide enough for small LA compounds and anti-arrhythmic drugs to pass. The narrowest point in the fenestration, termed "bottleneck", is created by the amino acid residues M174, T175, F203, T206, and M209 (Na_vAb numbering), with F203 being the most important residue (**Figure 1C**). These amino acids will sterically hinder the passage of compounds through the fenestration. Mutation of F203 to an alanine increased the size of the fenestration allowing easier access of flecainide (CAS No.:54143-55-4, polar surface area=59.6Å) to its binding site within the pore, with as result an increased tonic, closed state, block (Gamal El-Din et al., 2018).

The mutation did not affect lidocaine block as this compound is smaller (polar surface area=32.3Å) and can easily traverse the wild type fenestration (Courtney, 1988). The F203W mutation on the other hand reduces fenestration size and consequently the access of both lidocaine and flecainide is reduced, decreasing tonic block (Gamal El-Din et al., 2018). Computational modelling using the $Na_v1.4$ 3D structure resulted in the observation of four fenestrations just as in bacterial Na_v channels, with the exception that the size of two out of the four fenestrations seemed inadequate for compound access, namely the fenestration constructed by DII–DIII and DIV–DI (Kaczmarski and Corry, 2014). Fenestrations in between DI-DII and DIII-DIV seemed sufficiently wide for compounds to cross (**Figure 1C**). The bottleneck of these fenestrations is formed by residues N790, L438, and M786 for the fenestration between DI-DII and by I1582, I1583, and F1586 (if rotated) for the fenestration between DIII-DIV. These fenestrations lining residues, are well conserved in the different Na_v channel isoforms. Mutating DIV-S6 residue I1582 appeared to create an extra pore access pathway (Ragsdale et al., 1994) and allowed the external blocker QX314 (CAS No.:24003-58-5, polar surface area: 29.1Å), which is a charged LA compound at physiological pH and therefore not able to traverse the membrane, to access the LA binding site when added in the extracellular environment (Sunami et al., 2001).

Apart from LAs that have a distinct binding site, sevoflurane (CAS No.: 28523-86-6), an inhalational anaesthetic, has a more complex binding profile. Sevoflurane binding results in a decrease of the peak sodium current, a hyperpolarised shift in the voltage dependence of inactivation and a slowing of the recovery from inactivation (Horishita et al., 2008; Ouyang et al., 2009). Within the bacterial sodium channel NaChBac, binding regions have been located at the pore region, selectivity filter, and the S4–S5 linker/S6 interface (Ouyang et al., 2007; Raju et al., 2013). MD simulations suggested that the binding of sevoflurane to the selectivity filter and the S4–S5 linker occurs mainly when the channel is in the activated/open state, while in the closed state the channel gate and the VSD are targeted (Barber et al., 2014). A state independent binding site is possibly the central cavity that is accessed by the fenestrations. Residues T220 and F227 (NavChBac numbering) are proposed to be responsible for sevoflurane binding in the central cavity, which are the homologue residues for LA binding in Nav1.4 (F1764, Y1771).

Binding Site 2 Compounds, Though Being Lipophilic, Bind to the Inner Pore

Compounds binding at site 2 of the Na_v channel include batrachotoxin (Daly et al., 1965; Huang et al., 1982), grayanotoxin (Yuki et al., 2001; Jansen et al., 2012), CAS No.: 54781-61-2), and alkaloids from plant such as veratridine (Ulbricht, 1969; Sutro, 1986), CAS No.:71-62-5), aconitine and mesaconitine (Herzog et al., 1964; Friese et al., 1997) (CAS No.: 302-27-2). All these compounds are lipid soluble and need to traverse the cell membrane before influencing the channel in a use-dependent manner, comparable to the action of LA compounds (Herzog et al., 1964; Catterall, 1980; Huang et al., 1982; Dubois et al., 1983; Sutro, 1986; Barnes and Hille, 1988; Ameri et al., 1996; Yuki et al., 2001; Wang and Wang, 2003). Their effects can be a combination of: (1) a hyperpolarised shift of the voltage dependence of activation, (2) inhibition of the fast inactivation process, leading to persistent sodium currents, (3) decrease in ion conductance, and/or (4) decrease of the Na^+ selectivity. The location of binding site 2 is thought to be at the S6 of all four domains and to overlap with the LA binding site or at least allosterically hinder LA binding.

To describe neurotoxin site 2 in more detail, we focus on the most potent site 2 toxin reported to date, batrachotoxin (BTX) a steroidal alkaloid indirectly produced by the South-American poison dart frogs of the genus *Phyllobates* (Daly et al., 1965). Binding of BTX is highly irreversible and only possible when the channel is in its activated open state (Huang et al., 1982; Dubois et al., 1983). BTX shifts the voltage dependence of channel activation by approximately −40 mV toward more hyperpolarized potentials (Linford et al., 1998), reducing the channel's ion conductance and selectivity. BTX also reduces the affinity for LA, which is thought to be caused by non-competitive antagonism (i.e., allosteric effect) because of overlapping binding sites as BTX and LA share the binding residue F1586 (Linford et al., 1998). Residue mutations affecting BTX in $Na_v1.4$ were first described in DI-S6 and DIV-S6: I439K, N440K, L443K, F1586K, and N1591K, respectively (Wang and Wang, 1998; Wang and Wang, 1999). Afterwards the DIII-S6 residues Ser1283 and leu1287 were identified (Wang et al., 2000) and finally DII-S6 residues N790 and L794 (Wang et al., 2001). All these residues line the inside of the pore (**Figure 2**). Non-pore lining residues involved in BTX sensitivity locate at the putative hinge region of the channel gate, Gly1282 and Phe1284, respectively (Du et al., 2011). While Phe1284 is important for the stabilisation of the ammonium group of BTX, Gly1282 is not a direct binding receptor for BTX and mutations of this residue affect binding allosterically by changing the channels gating properties. Modeling studies suggest that BTX binds to the pore but does not completely prevent ion conduction because of its "horseshoe-like" structure (Du et al., 2011). Only upon mutation of DII-S6 N790 BTX becomes a full blocker (Wang et al., 2007).

Binding Site 5 Locates Between DIS6 and DIVS5

Some of the toxins that bind to site 5 of Na_v channels are brevetoxins (Catterall and Gainer, 1985; Poli et al., 1986) and ciguatoxins (Murata et al., 1990; Lewis et al., 1998), both originate from marine dinoflagellates (*Gambierdiscus toxicus*) and are structurally comparable. Brevetoxins are produced by unarmoured marine dinoflagellates (e.g., Karenia brevis, Gymnodinium breve, or Ptychodiscus brevis). Ingestion of these toxins can lead to poisoning and death of marine animals and cause the disease neurotoxic shellfish poisoning in humans (Baden, 1983; Flewelling et al., 2005). Eleven different brevetoxins have been discovered today with brevetoxin A (PbTX1, CAS No.:98112-41-5) and brevetoxin B (PbTX2 and 3, CAS No.:79580-28-2 and 85079-48-7) being the most

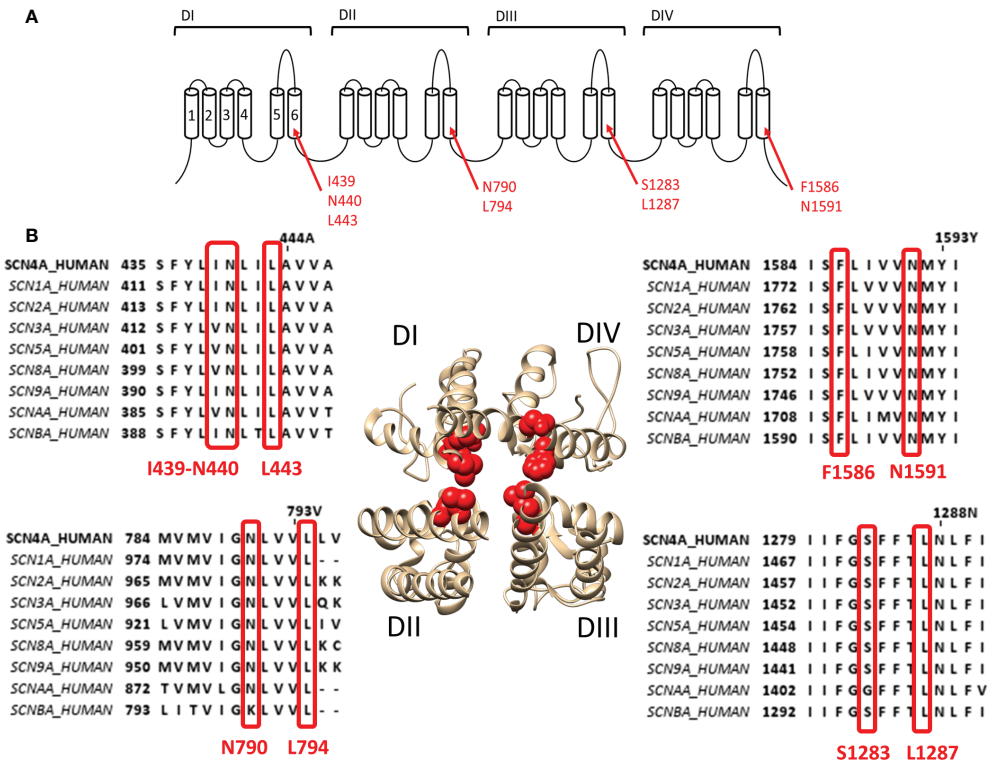

FIGURE 2 | Location of binding site 2 within the $Na_v1.4$ channel. **(A)** Schematic visualisation of the Na_v ion channel structure which is constructed out of four domains (DI to DIV) each consisting out of six transmembrane segments (S1–S6). The red arrows indicate the probable residues responsible for constructing the site 2 receptor, residues are noted in their $Na_v1.4$ annotation. **(B)** The bottom view of a 3D structure of the $Na_v1.4$ channel with in red marking the residues constructing the binding site 2. Only the S5–S6 segments of each domain is shown for a clear view on the inner pore binding site. Around the 3D structure are the alignments of the known human sodium channels with the Nav1.4 channel (SCN4A) as reference, all positioned at the corresponding domain of the 3D structure. Marked in red are the residues which are necessary for site 2 toxin binding. While some variability is observed between some isoform, most of the residues are well conserved. Amino acid sequence alignment and 3D structure are visualized using Jalview and chimera software, respectively (Pettersen et al., 2004; Waterhouse et al., 2009).

investigated ones. These toxins are about 30Å in length, 6Å in width, and 6Å high. They are composed of four recognizable parts: a lactone ring (the head) linked with a linker to a multiple carbon ring (the tail) ending in a rest-group (Lin et al., 1981). While the head is responsible for the effect, without the linker and the tail the toxin cannot modulate the channel as it allows the head region to reach its binding site (Rein et al., 1994). PbTX binds to the Na_v channel at the DI-S6, DIV-S5, and DIV-S6 segments (Trainer et al., 1991; Trainer et al., 1994; Konoki et al., 2019). The region spans within DI-S6 from Ala418/Thr422 to Lys465/Lys477 and within DIV-S5 from Glu1510 to lys1557 with possible extension to Lys1565 (**Figure 3**). The tail of the molecule will be situated at the S5–S6 extracellular loop while the head is able to reach, due to the long linker and tail region, the inactivation gate at the intracellular side of the channel (Trainer et al., 1991; Trainer et al., 1994). Interaction of the head with the inactivation gate reduces channel inactivation, leading to a persistent sodium current (Sheridan and Adler, 1989; Schreibmayer and Jeglitsch, 1992).

Like brevetoxins, ciguatoxins (CTX) bind at site 5 and their effects are consequently similar. Ciguatoxins are classified based on their geographic origin, with P-CTX (Murata et al., 1990) and C-CTX (Lewis et al., 1998) standing for Pacific and Caribbean, respectively. In all Na_v channel isoforms P-CTX1 (CAS No.:11050 21 8), the most potent CTX discovered to date, induces a hyperpolarizing shift in the voltage dependence of channel activation (Bidard et al., 1984; Benoit et al., 1986; Strachan et al., 1999) concomitantly with a shift in the voltage dependence of inactivation in some (Inserra et al., 2017). As CTX and brevetoxin share the same binding site, they are logically going into competition with each other (Lombet et al., 1987). Gambierol (CAS No.: 146763-62-4, origin *Gambierdiscus Toxicus*) has a similar structure as brevetoxins and CTXs, being a lipophilic multi-ring polyether toxin, but has no effect on the sodium currents (Lepage et al., 2007). However, when administered simultaneously it decreases the effect of CTX and brevetoxin, suggesting that gambierol acts as a competitive antagonist that binds to site 5 or at least exerts a negative allosteric effect.

VOLTAGE-GATED POTASSIUM CHANNELS

The K_v channel family is impressively large compared to this of Na_v channels, due to an extensive library of genes encoding

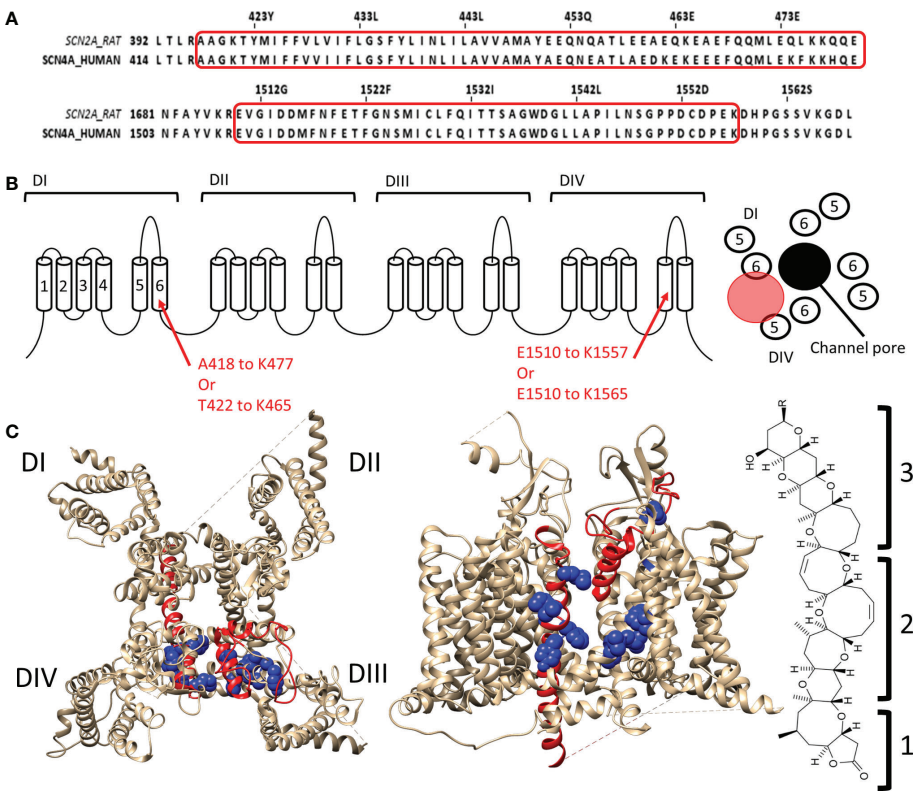

FIGURE 3 | Location of binding site 5 in $Na_v1.4$. **(A)** Alignment of the rat brain IIa sodium channel (SCN2A) with the human $Na_v1.4$ (SCN4A) as reference. Marked in red are the regions where brevetoxin could bind. **(B)** Schematic topology of the $Na_v1.4$ channel with the residues of DIS6 and DIVS5 that form the binding site listed below. On the right a schematic representation of the PD (top view) with the ion permeation pore represented in black and the location of binding site 5 indicated by the red circle. **(C)** 3D structures of the $Na_v1.4$ channel seen from the top (left) and side (center, between DIII and DIV) are represented with in red the regions which are, using radioactive labelling studies, probably the location for brevetoxin binding. In blue residues are shown which had an effect on brevetoxin binding. With for DI M424, V429, I430, G434 decreasing affinity and F436, Y437 increasing affinity when mutated to alanine. In case of DIV mutation of I1485, G1486, L1488, L1489 lead to decrease and L1491, V1492, G1500, Y1506 to increase of affinity when mutated (Nav1.4 numbering) (Konoki et al., 2019). A cleft can be observed in between DIS6 and DIVS5, at the side view, where the toxin could bind. This cleft is also located around fenestration four of the ion channel. At the left the structure of brevetoxin with the head region (1) attached with a linker (2) to the tail structure (3). The structure is orientated as it would bind at the channel compared to the side view. Amino acid sequence alignment and 3D structures are visualized using Jalview and chimera software, respectively (Pettersen et al., 2004; Waterhouse et al., 2009).

different α-subunits that in some subfamilies can "mix-and-match" to form functional K_v channels. Additionally, alternative splicing, RNA editing, and post-translational modification further expand on the K_v channel family (Jan and Jan, 2012). This explains why the binding sites of the much larger K_v channel family are less well categorized than those of the Na_v channel family. The next part will highlight different binding sites and pore wall fenestrations within several, but not all, members of the K_v channel family. After a short overview of the well-documented extracellular and intracellular exposed "hydrophilic" binding sites, we will discuss in detail the lesser-known lipid embedded "hydrophobic" binding site(s) in different K_v channels.

Extracellular and Intracellular Exposed "Hydrophilic" Binding Sites

The well-documented K_v channel binding sites can be topologically located on the intracellular or extracellular side of the channels. Extracellularly the most well-known conserved binding sites are those of the pore blockers and VSD targeting gating modifiers, while intracellularly the inner pore block is the most notable one (Wulff et al., 2009). Certain toxins from a variety of venomous animals target the extracellular binding sites. For example, scorpion toxins like charybdotoxin (CTX, CAS No.: 95751-30-7) and agitoxin (AgTx, CAS No.: 168147-41-9) target the water enveloped extracellular mouth of K_v channels, thereby physically occluding the permeation pore (Eriksson and Roux, 2002; Banerjee et al., 2013). Other scorpion toxins, like ergotoxin (ErgTx1, CAS No.: 8006-25-5) and BeKm-1 (CAS No.: 524962-01-4), cause an incomplete block of K_v current. This is because they only partially occlude the permeation pathway, which is known as "turret-block" (Xu et al., 2003; Zhang et al., 2003; Hill et al., 2007). Gating modifier toxins, like tarantula toxins (Hanatoxin, SGTx1, and VSTx1), bind to the paddle motif (S3b helices, S3–S4 linkers, and S4 helices) at the extracellular protein-lipid interface of the VSD. This binding site cannot be

characterized as strictly hydrophilic as the hydrophobic residues of these amphipathic peptide toxins allow it to partially partition into the membrane, and interact with the VSD (Lee et al., 2004; Jung et al., 2005; Alabi et al., 2007; Swartz, 2007; Jung et al., 2010; Mihailescu et al., 2014). Intracellularly, compounds can bind in the inner cavity, either physically blocking ion permeation (e.g., quaternary ammonium ions) or allosterically modulating the gating machinery of K_v channels (e.g., 4-aminopyridine, CAS No.: 504-24-5) (Armstrong, 1971; Armstrong and Loboda, 2001; Del Camino et al., 2005). Also, the quaternary ammonium ion TEA can occlude the external K_v pore, similar to the scorpion toxins mentioned above (Luzhkov and Aqvist, 2001). Apart from the gating modifier binding site, which is partially enveloped by water, the binding sites mentioned here are exposed to an aqueous environment. Hence, referring them here as "hydrophilic" binding sites.

Lipid Embedded "Hydrophobic" Binding Site(s) and Pore Wall Fenestrations in the *Shaker*-Type K_v Family, K_v7 Family, and K_v10.1/K_v11.1 Channel

The next part reviews the potential lipophilic binding sites and pore wall fenestrations in different K_v channel types. To define the binding site(s) of certain compounds, the PD is divided into a "front side" and "back side". Residues of the front side point towards the VSD of the same α-subunit, while residues of the "back side" point in the opposite direction, thus towards the VSD of a neighboring α-subunit (**Figures 4D**, **5D** and **6C**).

The *Shaker*-Type K_v Channel Family

Whereas gambierol does not modulate Nav channels, it is capable of inhibiting K_v1 and K_v3 channels (Nicholson and Lewis, 2006; Cuypers et al., 2008; Kopljar et al., 2009). Gambierol's inhibitory mechanism has been extensively studied, whereby a threonine on S6, T427 in K_v3.1, is an important determinant (Kopljar et al., 2009). Substitution of the polar threonine by a hydrophobic valine abolishes the high gambierol affinity (Kopljar et al., 2009). Additional determinants are a leucine and phenylalanine on S5: L348 and F351 in K_v3.1, respectively. K_v1 channels possess a threonine residue equivalent to T427 (T401 in K_v1.2), explaining their similar gambierol sensitivity (Cuypers et al., 2008; Kopljar et al., 2009; Martinez-Morales et al., 2016). These residues are mostly positioned on the front side of the PD (**Figure 4**).

On the other hand, psora-4 (CAS No.: 724709-68-6), a potent inhibitor of K_v1.3, has been shown to predominantly bind to the back side of the PD (**Figure 4**) (Vennekamp et al., 2004; Marzian et al., 2013). A single psora-4 molecule acts as a central pore blocker of K_v1 channels (K_v1.1-K_v1.5, and K_v1.7), thereby preventing ions from permeating. However, four additional drug molecules can bind the lipid-exposed pocket on the back side of the PD, thereby causing the selectivity filter to narrow. Thus, the binding of five psora-4 molecules leads to a stable non-conducting state. The residues identified in K_v1.5 as playing a key role in psora-4 action map on the back side of S5–S6 (**Figure 4**). Additionally, some residues in S4 and the S4–S5 linker also seem involved (Marzian et al., 2013).

The inhalation anaesthetic, sevoflurane, seems to bind within the central cavity and to a similar hydrophobic pocket as psora-4 (Stock et al., 2018). Apart from these binding regions, the polar lipophilic molecule has been shown to interact with the S4–S5 linker, pore helix, segment S6, and even the VSD, likewise to the many binding regions of sevoflurane on the Na_v channel (Barber et al., 2011; Barber et al., 2014). These sites are primarily dehydrated and lipid accessible, which is highly favourable for the polar lipophilic sevoflurane molecule (Stock et al., 2018). The specific residues involved in sevoflurane binding are not known, but one residue within the S4–S5 linker (G329 according to K_v1.2 numbering) has been identified to play an important role (Liang et al., 2015).

PUFAs are charged lipophilic compounds that position at the lipid membrane interface, although in small quantities (Yazdi et al., 2016). Nonetheless, PUFAs may play an important role in the treatment of arrhythmias and epilepsy, due to their modulating effect on, but not limited to, voltage-gated ion channels (Lefevre and Aronson, 2000; Leaf, 2007; Boland and Drzewiecki, 2008; Borjesson and Elinder, 2011). The *Shaker* K_v channel has been extensively studied as one of the targets of PUFAs. They interact with the channel at several sites, but the major one seems located within the lipid-facing cleft between S3 and S4 (S3–S4 cleft) of the VSD (Borjesson and Elinder, 2011). This hydrophobic cleft is perfectly shaped to accommodate the lipophilic carbon tail of the PUFAs, causing the negatively charged carboxyl head group to be positioned close to the S4 segment. In this way, PUFAs electrostatically affect the VSD by trapping S4 toward the extracellular position, stabilizing the open state of *Shaker* K_v channels (Borjesson et al., 2008; Yazdi et al., 2016). Accordingly, a series of point mutations on the lipid facing side of S3-S4 (I325C, T329C, A359C, and I360C, *Shaker* numbering) had a significant impact on the PUFA-induced hyperpolarizing shift in the channel's voltage dependence of activation (**Figure 4**) (Borjesson and Elinder, 2011). Although the binding site for gating modifier toxins is in close proximity to that of PUFAs, the action sites do most likely not overlap as the residues important for PUFA action are more deeply embedded into the lipid bilayer (Borjesson and Elinder, 2011). Interestingly, dehydroabietic acid (DHAA) and some of its derivatives, the most potent being Wu32and Wu122, have a similar effect on *Shaker* K_v channels. The carboxyl group of DHAA is positioned at roughly the same site, namely the S3–S4 cleft (Ottosson et al., 2017). Wu32 possibly interacts with residues between the S2–S3 and/or S3–S4 cleft as five cysteine mutations in S3, which have been shown to alter its affinity and/or efficacy, point towards S2 (I320C and F324C, *shaker* numbering) and S4 (I318C, P322C, and T326C), respectively (Ottosson et al., 2017).

The K_v7 Family

The well characterized retigabine (RTG, CAS No.: 150812-12-7) binding site is localized between the front side of one PD and the back side of an adjacent PD of K_v7.2–K_v7.5 (KCNQ2-5) channels (**Figure 5**) (Schenzer et al., 2005; Lange et al., 2009). These channels are predominantly expressed in neurons where they underlie the native M-current that plays a major role in regulating neuronal excitability (Wang et al., 1998; Kubisch

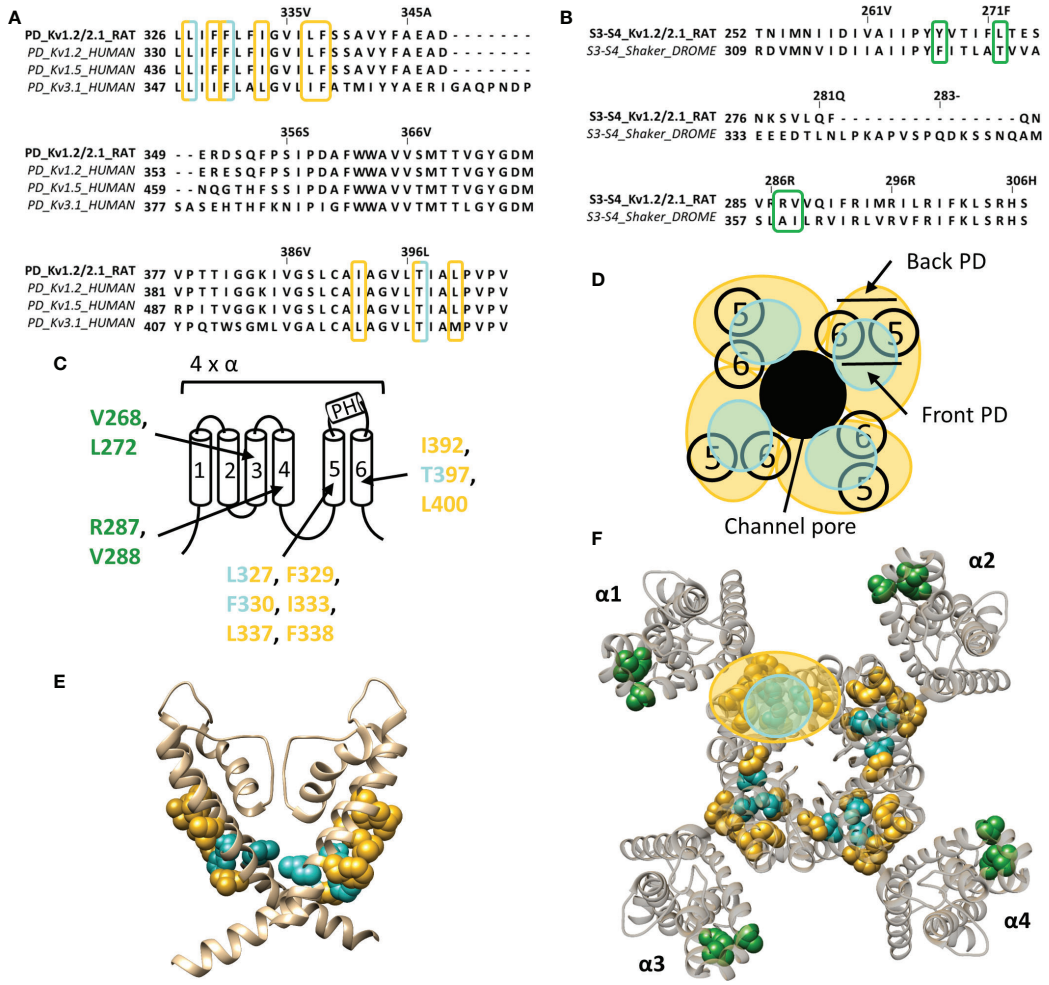

FIGURE 4 | Lipid-exposed binding sites within the crystal structure of a $K_v1.2$–$K_v2.1$ paddle chimera channel (PDB: 2R9R). **(A)** Sequence alignment of part of the PD (S5-S6 segment) of $K_v1.2$-2.1, $K_v1.2$, $K_v1.5$, and $K_v3.1$, with $K_v1.2$-2.1 as reference. Residues important for gambierol and psora-4 action are highlighted in blue and yellow respectively. **(B)** Sequence alignment of the S3–S4 segments of $K_v1.2$–2.1 and *shaker*, with $K_v1.2$–2.1 as reference. Highlighted in green are the residues important for PUFA action. **(C)** Schematic visualization of one K_v channel α-subunit consisting out of six transmembrane segments (1–6) and a pore helix (PH). In blue the residues important for gambierol binding (L327, F330, and T397 according to Kv1.2–2.1 numbering) and in yellow those for psora-4 binding (L327, F329, F330, I333, L337, F338, I392, T397, and L400). Residues important for PUFA interaction are shown in green (V268, R287, V288, and L272). **(D)** Schematic visualization of the pore domain of the $K_v1.2$–$K_v2.1$ channel. Four pore-forming domains tetramerize to form the channel pore. The blue and yellow circle highlights the proposed gambierol/psora-4 binding site regions on the front- and/or backside of the pore-forming domain, respectively. **(E)** Side view of the $K_v1.2$–$K_v2.1$ channel with the front and back subunit omitted for clarity. Residues involved in gambierol and psora-4 interaction are shown in blue (L327, F330, and T397) and yellow (I392, T397, and L400), respectively. The PUFA action site is visualized in green (V268, R287, V288, and L272). **(F)** Top view of the $K_v1.2$–$K_v2.1$ channel, with each α subunit named α1–α4. Residues involved in gambierol and psora-4 interaction are shown in blue (L327, F330, and T397) and yellow (I392, T397, and L400), respectively. In green the PUFA action site comprising residuesV268, R287, V288, and L272. $K_v1.2$–$K_v2.1$ crystal structure (PDB: 2R9R) (Long et al., 2007) was visualized with chimera software (Pettersen et al., 2004) and amino acid sequence alignment with Jalview (Waterhouse et al., 2009).

et al., 1999; Schroeder et al., 2000). RTG amplifies the $K_v7.2$–$K_v7.5$ currents by stabilizing the open-channel conformation, by which it acts as a brake on neuronal excitability *in vivo* (Lange et al., 2009). Hence, the potential use of RTG and RTG-derived compounds as anticonvulsants (Rundfeldt, 1997; Wang et al., 2018). RTG binding has been attributed to several conserved residues on S5–S6, lining a hydrophobic pocket near the channel gate of $K_v7.2$–$K_v7.5$. According to $K_v7.2$ numbering these residues are: W236, L243, L275, L299, and G301 (**Figure 5**). $K_v7.1$ channels lack these amino acids (apart from L243), explaining their RTG-insensitivity (Schenzer et al., 2005; Lange et al., 2009). Because of the role of K_v7 in diseases of neuronal hyperexcitability, the search for positive allosteric modulators such as RTG, for which the clinical use is currently discontinued (Wang et al., 2018), is pursued. For example, BMS-204352, ML-213, and the acrylamide compound (S)-1 act on the canonical

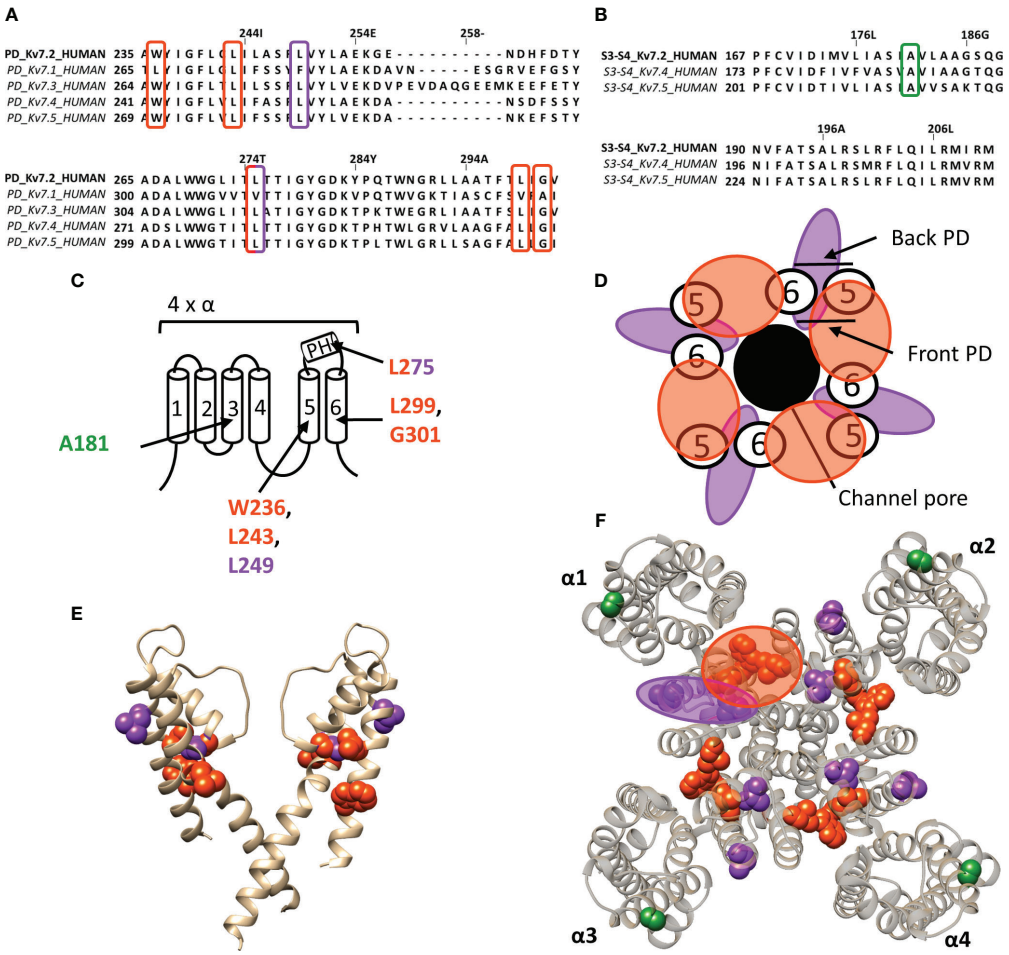

FIGURE 5 | Lipid-exposed binding sites within a homology model of the $K_v7.2$ channel based on the 3D structure of $K_v7.1$ (PDB: 5VMS). **(A)** Sequence alignment of part of the PD of $K_v7.1$–$K_v7.5$, with $K_v7.2$ residue numbering. Highlighted in red and purple are the residues important for RTG and zinc pyrithione action, respectively. **(B)** Sequence alignment of the S3-S4 segment of $K_v7.2$, $K_v7.4$, and $K_v7.5$, with $K_v7.2$ as reference. Highlighted in green is the residue important for ICA73 action. **(C)** Schematic visualization of one K_v7 channel α-subunit consisting out of 6 transmembrane segments (1–6) and a pore helix (PH). Location of the residues involved in the interaction of $K_v7.2$ with retigabine are represented in red. Represented in purple are residues important for zinc pyrithione action). The residue important for ICA73 interaction is shown in green. **(D)** Schematic visualization of the PD of $K_v7.2$. The red and purple circle highlight the proposed retigabine/zinc pyrithione binding site on either the front- or back-side of the PD pore-forming domain, respectively. **(E)** Side view of $K_v7.2$ with the front and back subunit omitted for clarity. Residues involved in retigabine and zinc pyrithione interaction are shown in red (W236, L243, L299, and G301) and purple (L249 and L275), respectively. In green the ICA73 action site is visualized (A181). **(F)** Top view of $K_v7.2$, with each α subunit named α1–α4. Residues important for retigabine, zinc pyrithione, and ICA73 action are shown in red (W236, L243, L299, and G301), purple (L249 and L275), and green (A181), respectively. Shown $K_v7.2$ structure is a homology model of the 3D structure of $K_v7.1$ (PDB: 5VMS) (Sun and Mackinnon, 2017), generated with SWISS-MODEL (Waterhouse et al., 2018) and visualized using chimera software (Pettersen et al., 2004). The amino acid sequences are aligned using Jalview (Waterhouse et al., 2009).

RTG binding site (Bentzen et al., 2006; Kim et al., 2015; Wang et al., 2018).

The hydrophobic pocket of the RTG binding site also seems to be able to accommodate endogenous hydrophilic neurotransmitters like γ-aminobutyric acid (GABA), which directly activates $K_v7.3$ and $K_v7.5$ *via* W236. In contrast to RTG, GABA does not readily cross the plasma membrane to reach its site of action. Based on the $K_v1.2$–$K_v2.1$ paddle chimera structure the tryptophan also seems to be accessible from the extracellular side (Manville et al., 2018). It is possible that this accessibility is dependent of the state of the channel, such that in certain conformations the mostly hydrophobic binding pocket can be reached by hydrophilic compounds like GABA. Additionally, not all K_v7 channel openers interact with residue W236. Zinc pyrithione for instance interacts with two residues at the back side of S5 and the pore helix (L249 and L275) (**Figure 5**) (Schenzer et al., 2005; Xiong et al., 2007; Lange et al., 2009).

ICA-compounds (ICAgen, Durham, NC, US), which are benzanilide K_v7 channel openers, were developed as RTG alternatives (Mcnaughton-Smith et al., 2002). Of these, the most well-documented is ICA-27243 (ICA43), which has been shown to be more selective than RTG (Wickenden et al., 2008).

The individual residues that determine ICA43 binding have not been identified, but the C-terminal end of S2 and the N-terminal part of S3 (S2–S3 cleft) are proposed to be involved (Padilla et al., 2009). Later, Wang AW, et al. continued the investigation of the mechanism of action of ICA-compounds on K_v7 channels, but focussed on ICA-069673 (ICA73) (Wang et al., 2017). They identified two key residues in S3 of $K_v7.2$: A181 and F168, respectively. Mutation of these residues did not affect RTG-mediated gating, but did alter the action of ICA73 (Wang et al., 2017). Furthermore, it has been shown that ICA43 and ICA73 are resistant to mutation of the RTG binding site, supporting that not all K_v7 channel openers bind to the PD, but also can interact with a VSD site (Padilla et al., 2009; Wang et al., 2017). However, it remains debated whether residues A181 and F168 are involved in ICA binding directly or allosterically (Wang et al., 2018). In case these residues are binding ICA73, the position of residue A181 toward the lipid-exposed surface of the VSD suggests the presence of a drug binding site at the lipid-exposed cleft of S2–S3 and/or S3–S4 in K_v7 channels, similar to the interaction of Wu32 with *Shaker* K_v channels (**Figure 5**).

PUFAs have also been described to electrostatically affect $K_v7.1$ channels, resulting in a negative shift of the conductance-voltage curve. This modulation of $K_v7.1$ channels by PUFAs is similar to what has been described for *shaker* K_v channels (Borjesson et al., 2008; Borjesson and Elinder, 2011). Hence, the binding site and mechanism of action of PUFAs are most likely similar for both channels (Liin et al., 2015).

The hERG ($K_v11.1$) and EAG ($K_v10.1$) Channel

The human *ether-a-go-go* related gene (hERG) type 1 encodes for the $K_v11.1$ channel, which functions as the rapid component of the delayed rectifier K^+ current contributing to the repolarization of cardiac action potentials (Vandenberg et al., 2012). Alteration of the native functioning of $K_v11.1$ channels, either genetically or pharmacologically, can disrupt this repolarization, leading to various cardiac rhythm disorders (Thomas et al., 2006). Furthermore, the role of $K_v11.1$ is not limited to the heart, as it also seems to play a role in the central nervous system, digestive, secretory, and reproductive system, and even cancer (Babcock and Li, 2013). Hence, it has become common practice to screen compounds on hERG channel activity during the early stages of drug development, as unintentional side-effects may lead to disease and sudden-death (Mitcheson et al., 2000; Thomas et al., 2006; Babcock and Li, 2013). Most hERG inhibitors interact with residues inside the channel's permeation pathway, either located on the pore helix (T623,S624, and V625, according to hERG numbering) or on segment S6 (G648, Y652, and F656) (Lees-Miller et al., 2000; Mitcheson et al., 2000; Kamiya et al., 2001; Sanchez-Chapula et al., 2002; Sanchez-Chapula et al., 2003; Fernandez et al., 2004; Kamiya et al., 2008). On the other hand, some small molecule hERG activators have been discovered who deviate from this binding site, like ICA-105574 (ICA74) and PD-118057 (PD57). The most critical binding determinants for ICA74 are F557 and L622 (Garg et al., 2011), which topologically would situate the binding site at the front side of the PD (**Figure 6**). Apart from these critical binding determinants several other residues have been proposed to line the hydrophobic ICA binding pocket of $K_v11.1$ (F619, T623, M645, L646, M651, Y652, and F656), situating the ICA74 binding site between the front side of one α-subunit and the back side of an adjacent α-subunit (Garg et al., 2013). PD57 seems to bind the same hydrophobic pocket, with key residues being L646 on segment S6 and F619 on the pore helix of an adjacent subunit (**Figure 6**) (Perry et al., 2009).

Interestingly, ICA74 binds to a similar hydrophobic pocket in the related ether-a-go-go (EAG) type 1 channel ($K_v10.1$), although eliciting an opposite effect as in $K_v11.1$. ICA74 inhibits $K_v10.1$ currents by enhancing channel inactivation (Garg et al., 2012). The key residues for ICA74 binding in $K_v11.1$ (F557 and L622) are indeed conserved in $K_v10.1$ (F359 and L434). Furthermore, only three residues (F619, L646, and M651) of the proposed ICA binding pocket in $K_v11.1$ appeared not to be conserved in the $K_v10.1$ channel. This strongly suggests that ICA74 binds to the same hydrophobic site in $K_v10.1$ and $K_v11.1$ channels (Garg et al., 2013).

Lateral Pore Wall Fenestrations

The reports of compounds that can access the inner cavity from lipid exposed side-pocket through lateral pore wall fenestrations in Kv channels is still very limited. In $K_v7.1$ a pore wall fenestration is formed upon interaction with the β-subunit KCNE1 such that adamantane compounds, AC-1 (CAS No.: 878489-28-2) and its analogs (ACs), can reach their binding site (Jaraskova et al., 2005; Wrobel et al., 2016). Interestingly, AC-1 does not affect currents generated by homomeric $K_v7.1$, channels, nor $K_v7.1$ co-expressed with other KCNE isoforms (KCNE2-5). Thus, the "β-subunit-induced fenestrations" seem to be required for AC binding. Within these fenestrations many residues have been identified as important for AC-1 activity (V334, F335, I337, F340, and A344, according $K_v7.1$ numbering), but its position relative to the central cavity and lipophilic side-pocket could not be elucidated (Wrobel et al., 2016).

In $K_v11.1$, a lateral pore wall fenestration is possibly formed upon mutation of residue F557 to leucine (F557L), explaining the decrease in current inhibition of six known hERG blockers (dofetilide, haloperidol, terfenadine, astemizole, cisapride, and amiodarone) (Saxena et al., 2016). For $K_v1.5$ it has been proposed that psora-4 molecules can move in the I502A mutant between the central cavity and the lipophilic side-pockets through fenestration between segments S5–S6 (Marzian et al., 2013).Hence, the presence of pore wall fenestrations has thus far only been observed upon β-subunit interaction with $K_v7.1$ and to be induced by mutations in $K_v1.5$ and $K_v11.1$ (Marzian et al., 2013; Saxena et al., 2016; Wrobel et al., 2016). Although the presence of fenestrations has not been reported yet for wild-type channels, the likelihood that some K_v channel types express lateral pore wall fenestrations increases. If present, these fenestrations may be similar to those characterized in Na_v channels, which allow LA's to pass between the central cavity and lipophilic side-pockets (Payandeh et al., 2011; Mccusker et al., 2012; Payandeh et al., 2012; Zhang et al., 2012; Kaczmarski and Corry, 2014; Wrobel et al., 2016).

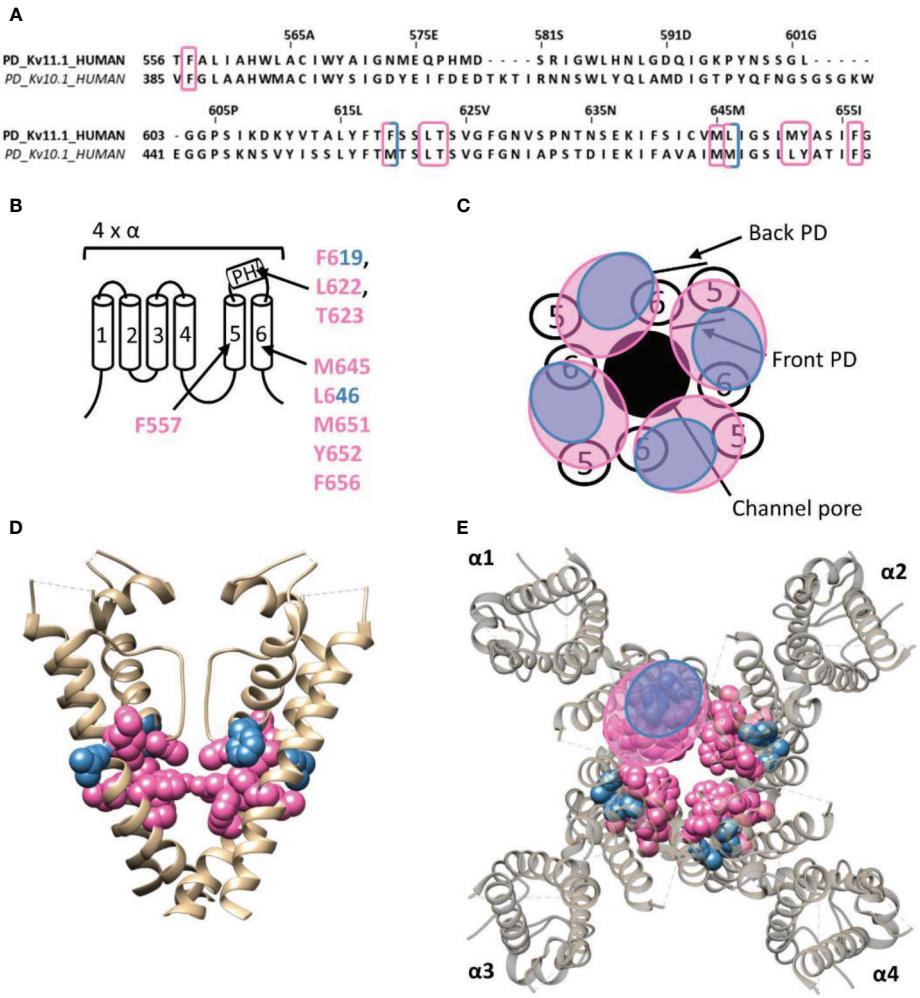

FIGURE 6 | Lipid-exposed binding site(s) within the cryo-EM structure of the K_v11.1 (hERG) channel (PDB: 5VA1). **(A)** Sequence alignment of part of the PD of K_v11.1 and K_v10.1, with K_v11.1 residue numbering. Highlighted in pink and blue are the residues important for ICA74 and PD57 action, respectively. **(B)** Schematic visualization of one K_v channel α-subunit consisting out of six transmembrane segments (1–6) and a pore helix (PH). In blue the critical residues of PD57 (F619 and L646 according to Kv11.1 numbering) and in pink the residues lining the proposed hydrophobic ICA74 binding pocket (F619, F557, L622, T623, M645, L646, M651, Y652, and F656). **(C)** Schematic visualization of the pore domain of the K_v11.1 channel. Four pore-forming domains tetramerize to form the channel pore. The blue and pink circle highlights the proposed PD57 and ICA74 binding site regions on the front- and/or backside of the pore-forming domain. **(D)** Side view of the K_v11.1 channel with the front and back subunit omitted for clarity. Residues involved in PD57 and ICA74 interaction are shown in blue (F619 and L646) and pink (F619, F557, L622, T623, M645, L646, M651, Y652, and F656), respectively. The residues F619 and L646 are both critical residues for PD57 and ICA74, but are shown in blue. **(E)** Top view of the K_v11.1 channel, with each α subunit named α1–α4. Residues involved in PD57 and ICA74 interaction are shown in blue (F619 and L646) and pink (F619, F557, L622, T623, M645, L646 M651, Y652, and F656), respectively. K_v11.1 cryo-EM structure (PDB: 5VA1) (Wang and Mackinnon, 2017) was visualized with chimera software (Pettersen et al., 2004) and amino acid sequence alignment with Jalview (Waterhouse et al., 2009).

UNIFYING THE LIPID EXPOSED/ ACCESSIBLE DRUG/TOXIN BINDING SITES OF K_V AND NA_V CHANNELS

Whereas a classification exists for the different drug/toxin binding sites in Na_v channels, such a categorization is currently lacking for the Kv channel family. In this review we take a first step and describe the hydrophobic binding sites reported in different K_v channel families. A compound like gambierol (**Figures 4** and **7**) has been shown to mostly bind to the front side of the PD, while RTG (**Figures 5** and **7**) PD57, and ICA74 (**Figure 6**) also interact with the back side of the PD of an adjacent α-subunit. When mapping all the sites it appears that gambierol, ICA74, RTG, and PD57 bind to an analogues binding site present in different K_v channel types (**Figure 7**) (Schenzer et al., 2005; Kopljar et al., 2009; Lange et al., 2009; Perry et al., 2009; Garg et al., 2011; Martinez-Morales et al., 2016). This indicates that an analogues lipophilic binding site is conserved between the different K_v channel types.

Zinc pyrithione, on the other hand, seems to solely bind to the back side of the PD, implying that the front and back side of the PD could serve as distinct binding sites (**Figures 5** and **7**) (Xiong et al., 2007). Psora-4 and sevoflurane are less specific regarding their binding site, as they both bind to the front and back side of the PD, among others (Marzian et al., 2013; Liang et al., 2015; Stock et al., 2018). Although certain compounds solely bind to the front or back side of the PD it seems that all residues point toward a similar lipophilic region, leading to the speculation that these seemingly distinct binding sites may converge to just one conserved lipophilic binding region in K_v channels. This binding site is then most likely similar to neurotoxin site 5 in Na_v channels (**Figure 3**) (Catterall and Risk, 1981; Cestele and Catterall, 2000), located between DIS6-DIVS5 (**Figures 3**, **4**, **5**) (Konoki et al., 2019). The idea that these binding sites are orthologous equivalents is because gambierol presumably binds to site 5 in Na_v channels (Lepage et al., 2007). In the case of K_v channels four such binding sites are present due to its tetrameric nature, as opposed to Na_v channels who only have one neurotoxin site 5 (Schenzer et al., 2005; Kopljar et al., 2009; Lange et al., 2009; Marzian et al., 2013; Stock et al., 2018).

Another lipid facing binding site is located on the VSD, in particular the cleft between segments S2–S3 and S3–S4. PUFAs, DHAA and its derivatives, and ICA-compounds allegedly bind to these clefts in *Shaker* and K_v7 channels, respectively (**Figures 4D**, **5D**, and **7**) (Padilla et al., 2009; Borjesson and Elinder, 2011; Ottosson et al., 2017; Wang et al., 2017). This leads to the assumption that also this lipophilic binding site is conserved between different K_v channel types. Additionally, certain compounds of Na_v (LAs and sevoflurane) and K_v (AC-1, psora-4, and several hERG blockers) channels have been proposed to use hydrophobic lateral pore wall fenestrations to reach their binding sites. The location of these fenestrations in Na_v channels are situated between DI–DII and DIII–DIV (**Figure 1**), while in K_v channels they are most likely present between segments S5–S6, allowing lipid soluble compounds to reach their binding site even when the channel is in its closed state (Payandeh et al., 2011; Mccusker et al., 2012; Payandeh et al., 2012; Zhang et al., 2012; Marzian et al., 2013; Barber et al., 2014; Kaczmarski and Corry, 2014; Saxena et al., 2016; Wrobel et al., 2016).

Of note, the residues reported to affect drug/toxin affinity were in this review mapped on available 3D structures that are

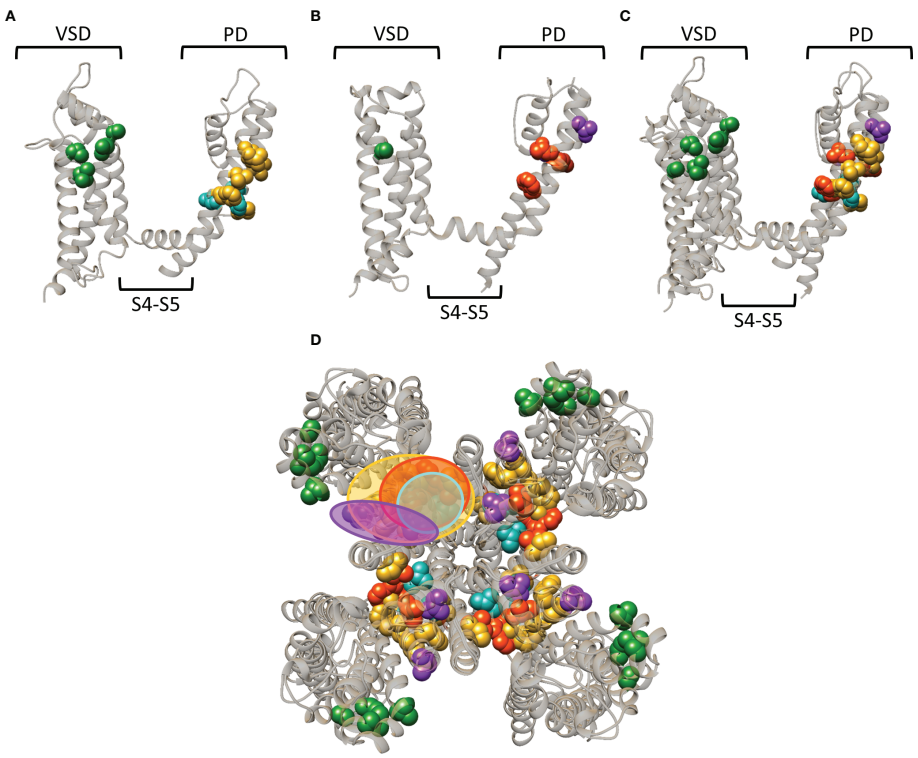

FIGURE 7 | Superposition of the lipid-exposed binding sites within the $K_v1.2$–2.1 paddle chimera channel (PDB: 2R9R) and $K_v7.2$. **(A)** Side view of one α-subunit of the $K_v1.2$–2.1 channel with the residues important for gambierol, psora-4, and PUFA action represented by spheres and highlighted in blue, yellow, and green, respectively. The VSD, PD, and S4–S5 linker are also indicated. **(B)** Side view of one $K_v7.2$ α-subunit with the residues important for retigabine, zinc pyrithione, and ICA73 action represented by red, purple, and green spheres, respectively. **(C)** Superposition of the structures shown in panel **(A, B)**. **(D)** Superposition of the $K_v1.2$–2.1 and $K_v7.2$ channel structure shown as top view. The red and blue circle highlight the proposed retigabine/gambierol binding site on the "front side" of the PD, while the binding sites for zinc pyrithione and psora-4 on the "back side" of the PD are highlighted with the purple and yellow circles, respectively. Structures are visualized using chimera software (Pettersen et al., 2004).

snapshots of the channel in a certain state, which should not be the high affinity state for the respective drug/toxin. As mentioned, several drugs/toxins are state dependent and bind with highest affinity to a certain conformation of the channel (e.g., the closed or open channel configuration). Consequently, the residues reported to be important for drug/toxin effect might orient differently when the conformation of the channel changes. Thus, when the channel is in its high affinity drug/toxin state, the orientation of the residues might be slightly different resulting in possibly broader binding regions than highlighted in the figures. Furthermore, several of the residues reported to be important for drug/toxin effect are likely not the binding partners of the drugs/toxins but alter affinity in an allosteric way. Nonetheless, there seem to be three distinct lipid-exposed binding sites preserved in K_v channels: the front and back side of the PD, and S2–S3/S3–S4 clefts. Future experiments will determine if the front and back PD binding sites are two distinct entities or if they converge to just one larger lipophilic binding site region.

AUTHOR CONTRIBUTIONS

All authors contributed in writing this review.

FUNDING

This review was supported by a grant of the FWO (Fonds voor Wetenschappelijk onderzoek) G0C6220N (DJS) and by a GOA grant of the University of Antwerp.

REFERENCES

Ahern, C. A., Payandeh, J., Bosmans, F., and Chanda, B. (2016). The hitchhiker's guide to the voltage-gated sodium channel galaxy. *J. Gen. Physiol.* 147, 1–24. doi: 10.1085/jgp.201511492

Alabi, A. A., Bahamonde, M. I., Jung, H. J., Kim, J. I., and Swartz, K. J. (2007). Portability of paddle motif function and pharmacology in voltage sensors. *Nature* 450, 370–375. doi: 10.1038/nature06266

Ameri, A., Shi, Q., Aschoff, J., and Peters, T. (1996). Electrophysiological effects of aconitine in rat hippocampal slices. *Neuropharmacology* 35, 13–22. doi: 10.1016/0028-3908(95)00153-0

Armstrong, C. M., and Hollingworth, S. (2018). A perspective on Na and K channel inactivation. *J. Gen. Physiol.* 150, 7–18. doi: 10.1085/jgp.201711835

Armstrong, C. M., and Loboda, A. (2001). A model for 4-aminopyridine action on K channels: similarities to tetraethylammonium ion action. *Biophys. J.* 81, 895–904. doi: 10.1016/S0006-3495(01)75749-9

Armstrong, C. M. (1971). Interaction of tetraethylammonium ion derivatives with the potassium channels of giant axons. *J. Gen. Physiol.* 58, 413–437. doi: 10.1085/jgp.58.4.413

Babcock, J. J., and Li, M. (2013). hERG channel function: beyond long QT. *Acta Pharmacol. Sin.* 34, 329–335. doi: 10.1038/aps.2013.6

Baden, D. G. (1983). Marine food-borne dinoflagellate toxins. *Int. Rev. Cytol.* 82, 99–150. doi: 10.1016/S0074-7696(08)60824-4

Banerjee, A., Lee, A., Campbell, E., and Mackinnon, R. (2013). Structure of a pore-blocking toxin in complex with a eukaryotic voltage-dependent K(+) channel. *Elife* 2, e00594. doi: 10.7554/eLife.00594

Barber, A. F., Liang, Q., Amaral, C., Treptow, W., and Covarrubias, M. (2011). Molecular mapping of general anesthetic sites in a voltage-gated ion channel. *Biophys. J.* 101, 1613–1622. doi: 10.1016/j.bpj.2011.08.026

Barber, A. F., Carnevale, V., Klein, M. L., Eckenhoff, R. G., and Covarrubias, M. (2014). Modulation of a voltage-gated Na+ channel by sevoflurane involves multiple sites and distinct mechanisms. *Proc. Natl. Acad. Sci. United States America* 111, 6726–6731. doi: 10.1073/pnas.1405768111

Barnes, S., and Hille, B. (1988). Veratridine modifies open sodium channels. *J. Gen. Physiol.* 91, 421–443. doi: 10.1085/jgp.91.3.421

Bavro, V. N., De Zorzi, R., Schmidt, M. R., Muniz, J. R., Zubcevic, L., Sansom, M. S., et al. (2012). Structure of a KirBac potassium channel with an open bundle crossing indicates a mechanism of channel gating. *Nat. Struct. Mol. Biol.* 19, 158–163. doi: 10.1038/nsmb.2208

Benoit, E., Legrand, A. M., and Dubois, J. M. (1986). Effects of ciguatoxin on current and voltage clamped frog myelinated nerve fibre. *Toxicon* 24, 357–364. doi: 10.1016/0041-0101(86)90195-9

Bentzen, B. H., Schmitt, N., Calloe, K., Dalby Brown, W., Grunnet, M., and Olesen, S. P. (2006). The acrylamide (S)-1 differentially affects Kv7 (KCNQ) potassium channels. *Neuropharmacology* 51, 1068–1077. doi: 10.1016/j.neuropharm.2006.07.001

Benz, I., and Kohlhardt, M. (1991). Responsiveness of cardiac Na+ channels to antiarrhythmic drugs: the role of inactivation. *J. Membr. Biol.* 122, 267–278. doi: 10.1007/BF01871427

Bezanilla, F. (2008). How membrane proteins sense voltage. *Nat. Rev. Mol. Cell Biol.* 9, 323–332. doi: 10.1038/nrm2376

Bidard, J. N., Vijverberg, H. P., Frelin, C., Chungue, E., Legrand, A. M., Bagnis, R., et al. (1984). Ciguatoxin is a novel type of Na+ channel toxin. *J. Biol. Chem.* 259, 8353–8357.

Blunck, R., and Batulan, Z. (2012). Mechanism of electromechanical coupling in voltage-gated potassium channels. *Front. Pharmacol.* 3, 166. doi: 10.3389/fphar.2012.00166

Boland, L. M., and Drzewiecki, M. M. (2008). Polyunsaturated fatty acid modulation of voltage-gated ion channels. *Cell Biochem. Biophys.* 52, 59–84. doi: 10.1007/s12013-008-9027-2

Borjesson, S. I., and Elinder, F. (2011). An electrostatic potassium channel opener targeting the final voltage sensor transition. *J. Gen. Physiol.* 137, 563–577. doi: 10.1085/jgp.201110599

Borjesson, S. I., Hammarstrom, S., and Elinder, F. (2008). Lipoelectric modification of ion channel voltage gating by polyunsaturated fatty acids. *Biophys. J.* 95, 2242–2253. doi: 10.1529/biophysj.108.130757

Cahalan, M. D. (1978). Local anesthetic block of sodium channels in normal and pronase-treated squid giant axons. *Biophys. J.* 23, 285–311. doi: 10.1016/S0006-3495(78)85449-6

Catterall, W. A., and Gainer, M. (1985). Interaction of brevetoxin A with a new receptor site on the sodium channel. *Toxicon* 23, 497–504. doi: 10.1016/0041-0101(85)90034-0

Catterall, W. A., and Risk, M. (1981). Toxin T4(6) from Ptychodiscus brevis (formerly Gymnodinium breve) enhances activation of voltage-sensitive sodium channels by veratridine. *Mol. Pharmacol.* 19, 345–348.

Catterall, W. A. (1980). Neurotoxins that act on voltage-sensitive sodium channels in excitable membranes. *Annu. Rev. Pharmacol. Toxicol.* 20, 15–43. doi: 10.1146/annurev.pa.20.040180.000311

Cestele, S., and Catterall, W. A. (2000). Molecular mechanisms of neurotoxin action on voltage-gated sodium channels. *Biochimie* 82, 883–892. doi: 10.1016/S0300-9084(00)01174-3

Courtney, K. R. (1988). Why do some drugs preferentially block open sodium channels? *J. Mol. Cell Cardiol.* 20, 461–464. doi: 10.1016/S0022-2828(88)80073-7

Cuello, L. G., Jogini, V., Cortes, D. M., and Perozo, E. (2010). Structural mechanism of C-type inactivation in K(+) channels. *Nature* 466, 203–208. doi: 10.1038/nature09153

Cuypers, E., Abdel-Mottaleb, Y., Kopljar, I., Rainier, J. D., Raes, A. L., Snyders, D. J., et al. (2008). Gambierol, a toxin produced by the dinoflagellate Gambierdiscus

toxicus, is a potent blocker of voltage-gated potassium channels. *Toxicon : Off. J. Int. Soc. Toxinol.* 51, 974–983. doi: 10.1016/j.toxicon.2008.01.004

Daly, J. W., Witkop, B., Bommer, P., and Biemann, K. (1965). Batrachotoxin. The active principle of the Colombian arrow poison frog, Phyllobates bicolor. *J. Am. Chem. Soc.* 87, 124–126. doi: 10.1021/ja01079a026

De Lera Ruiz, M., and Kraus, R. L. (2015). Voltage-Gated Sodium Channels: Structure, Function, Pharmacology, and Clinical Indications. *J. Med. Chem.* 58, 7093–7118. doi: 10.1021/jm501981g

Del Camino, D., Kanevsky, M., and Yellen, G. (2005). Status of the intracellular gate in the activated-not-open state of shaker K+ channels. *J. Gen. Physiol.* 126, 419–428. doi: 10.1085/jgp.200509385

Doyle, D. A., Morais Cabral, J., Pfuetzner, R. A., Kuo, A., Gulbis, J. M., Cohen, S. L., et al. (1998). The structure of the potassium channel: molecular basis of K+ conduction and selectivity. *Science* 280, 69–77. doi: 10.1126/science.280.5360.69

Du, Y., Garden, D. P., Wang, L., Zhorov, B. S., and Dong, K. (2011). Identification of new batrachotoxin-sensing residues in segment IIIS6 of the sodium channel. *J. Biol. Chem.* 286, 13151–13160. doi: 10.1074/jbc.M110.208496

Dubois, J. M., Schneider, M. F., and Khodorov, B. I. (1983). Voltage dependence of intramembrane charge movement and conductance activation of batrachotoxin-modified sodium channels in frog node of Ranvier. *J. Gen. Physiol.* 81, 829–844. doi: 10.1085/jgp.81.6.829

Eriksson, M. A., and Roux, B. (2002). Modeling the structure of agitoxin in complex with the Shaker K+ channel: a computational approach based on experimental distance restraints extracted from thermodynamic mutant cycles. *Biophys. J.* 83, 2595–2609. doi: 10.1016/S0006-3495(02)75270-3

Fernandez, D., Ghanta, A., Kauffman, G. W., and Sanguinetti, M. C. (2004). Physicochemical features of the HERG channel drug binding site. *J. Biol. Chem.* 279, 10120–10127. doi: 10.1074/jbc.M310683200

Flewelling, L. J., Naar, J. P., Abbott, J. P., Baden, D. G., Barros, N. B., Bossart, G. D., et al. (2005). Brevetoxicosis: red tides and marine mammal mortalities. *Nature* 435, 755–756. doi: 10.1038/nature435755a

Friese, J., Gleitz, J., Gutser, U. T., Heubach, J. F., Matthiesen, T., Wilffert, B., et al. (1997). Aconitum sp. alkaloids: the modulation of voltage-dependent Na+ channels, toxicity and antinociceptive properties. *Eur. J. Pharmacol.* 337, 165–174. doi: 10.1016/S0014-2999(97)01268-5

Gamal El-Din, T. M., Lenaeus, M. J., Zheng, N., and Catterall, W. A. (2018). Fenestrations control resting-state block of a voltage-gated sodium channel. *Proc. Natl. Acad. Sci. U. S. A* 115, 13111–13116. doi: 10.1073/pnas.1814928115

Garg, V., Stary-Weinzinger, A., Sachse, F., and Sanguinetti, M. C. (2011). Molecular determinants for activation of human ether-a-go-go-related gene 1 potassium channels by 3-nitro-n-(4-phenoxyphenyl) benzamide. *Mol. Pharmacol.* 80, 630–637. doi: 10.1124/mol.111.073809

Garg, V., Sachse, F. B., and Sanguinetti, M. C. (2012). Tuning of EAG K(+) channel inactivation: molecular determinants of amplification by mutations and a small molecule. *J. Gen. Physiol.* 140, 307–324. doi: 10.1085/jgp.201210826

Garg, V., Stary-Weinzinger, A., and Sanguinetti, M. C. (2013). ICA-105574 interacts with a common binding site to elicit opposite effects on inactivation gating of EAG and ERG potassium channels. *Mol. Pharmacol.* 83, 805–813. doi: 10.1124/mol.112.084384

Gingrich, K. J., Beardsley, D., and Yue, D. T. (1993). Ultra-deep blockade of Na+ channels by a quaternary ammonium ion: catalysis by a transition-intermediate state? *J. Physiol.* 471, 319–341. doi: 10.1113/jphysiol.1993.sp019903

Grant, A. O., Dietz, M. A., Gilliam, F. R., and Starmer, C. F. (1989). Blockade of cardiac sodium channels by lidocaine. Single-channel analysis. *Circ. Res.* 65, 1247–1262. doi: 10.1161/01.res.65.5.1247

Herzog, W. H., Feibel, R. M., and Bryant, S. H. (1964). The Effect of Aconitine on the Giant Axon of the Squid. *J. Gen. Physiol.* 47, 719–733. doi: 10.1085/jgp.47.4.719

Hill, A. P., Sunde, M., Campbell, T. J., and Vandenberg, J. I. (2007). Mechanism of block of the hERG K+ channel by the scorpion toxin CnErg1. *Biophys. J.* 92, 3915–3929. doi: 10.1529/biophysj.106.101956

Hille, B. (1977). Local anesthetics: hydrophilic and hydrophobic pathways for the drug-receptor reaction. *J. Gen. Physiol.* 69, 497–515. doi: 10.1085/jgp.69.4.497

Hille, B. (2001). *Ion Channels of Excitable Membranes*.

Horishita, T., Eger, E. I.2nd, and Harris, R. A. (2008). The effects of volatile aromatic anesthetics on voltage-gated Na+ channels expressed in Xenopus oocytes. *Anesth Analg.* 107, 1579–1586. doi: 10.1213/ane.0b013e318184b966

Hoshi, T., Zagotta, W. N., and Aldrich, R. W. (1990). Biophysical and molecular mechanisms of Shaker potassium channel inactivation. *Science* 250, 533–538. doi: 10.1126/science.2122519

Hoshi, T., Zagotta, W. N., and Aldrich, R. W. (1991). Two types of inactivation in Shaker K+ channels: effects of alterations in the carboxy-terminal region. *Neuron* 7, 547–556. doi: 10.1016/0896-6273(91)90367-9

Huang, L. Y., Moran, N., and Ehrenstein, G. (1982). Batrachotoxin modifies the gating kinetics of sodium channels in internally perfused neuroblastoma cells. *Proc. Natl. Acad. Sci. U. S. A.*. 79, 2082–2085. doi: 10.1073/pnas.79.6.2082

Inserra, M. C., Israel, M. R., Caldwell, A., Castro, J., Deuis, J. R., Harrington, A. M., et al. (2017). Multiple sodium channel isoforms mediate the pathological effects of Pacific ciguatoxin-1. *Sci. Rep.* 7, 42810. doi: 10.1038/srep42810

Jan, L. Y., and Jan, Y. N. (2012). Voltage-gated potassium channels and the diversity of electrical signalling. *J. Physiol.* 590, 2591–2599. doi: 10.1113/jphysiol.2011.224212

Jansen, S. A., Kleerekooper, I., Hofman, Z. L., Kappen, I. F., Stary-Weinzinger, A., and Van Der Heyden, M. A. (2012). Grayanotoxin poisoning: 'mad honey disease' and beyond. *Cardiovasc. Toxicol.* 12, 208–215. doi: 10.1007/s12012-012-9162-2

Jaraskova, L., Linders, J. T. M., Van Der Veken, L. J. E., Willemsens, G. H. M., and Bischoff, F. P. (2005). *N-2 Adamantanyl-2-Phenoxy-Acetamide Derivatives as 11-Beta Hydroxysteroid Dehydrogenase Inhibitors*.

Jung, H. J., Lee, J. Y., Kim, S. H., Eu, Y. J., Shin, S. Y., Milescu, M., et al. (2005). Solution structure and lipid membrane partitioning of VSTx1, an inhibitor of the KvAP potassium channel. *Biochemistry* 44, 6015–6023. doi: 10.1021/bi0477034

Jung, H. H., Jung, H. J., Milescu, M., Lee, C. W., Lee, S., Lee, J. Y., et al. (2010). Structure and orientation of a voltage-sensor toxin in lipid membranes. *Biophys. J.* 99, 638–646. doi: 10.1016/j.bpj.2010.04.061

Kaczmarski, J. A., and Corry, B. (2014). Investigating the size and dynamics of voltage-gated sodium channel fenestrations. *Channels (Austin)* 8, 264–277. doi: 10.4161/chan.28136

Kamiya, K., Mitcheson, J. S., Yasui, K., Kodama, I., and Sanguinetti, M. C. (2001). Open channel block of HERG K(+) channels by vesnarinone. *Mol. Pharmacol.* 60, 244–253. doi: 10.1124/mol.60.2.244

Kamiya, K., Niwa, R., Morishima, M., Honjo, H., and Sanguinetti, M. C. (2008). Molecular determinants of hERG channel block by terfenadine and cisapride. *J. Pharmacol. Sci.* 108, 301–307. doi: 10.1254/jphs.08102FP

Kim, R. Y., Yau, M. C., Galpin, J. D., Seebohm, G., Ahern, C. A., Pless, S. A., et al. (2015). Atomic basis for therapeutic activation of neuronal potassium channels. *Nat. Commun.* 6, 8116. doi: 10.1038/ncomms9116

Klemic, K. G., Shieh, C. C., Kirsch, G. E., and Jones, S. W. (1998). Inactivation of Kv2.1 potassium channels. *Biophys. J.* 74, 1779–1789. doi: 10.1016/S0006-3495(98)77888-9

Konoki, K., Baden, D. G., Scheuer, T., and Catterall, W. A. (2019). Molecular Determinants of Brevetoxin Binding to Voltage-Gated Sodium Channels. *Toxins* 11, 513. doi: 10.3390/toxins11090513

Kopljar, I., Labro, A. J., Cuypers, E., Johnson, H. W., Rainier, J. D., Tytgat, J., et al. (2009). A polyether biotoxin binding site on the lipid-exposed face of the pore domain of Kv channels revealed by the marine toxin gambierol. *Proc. Natl. Acad. Sci. U. S. A.* 106, 9896–9901. doi: 10.1073/pnas.0812471106

Kubisch, C., Schroeder, B. C., Friedrich, T., Lutjohann, B., El-Amraoui, A., Marlin, S., et al. (1999). KCNQ4, a novel potassium channel expressed in sensory outer hair cells, is mutated in dominant deafness. *Cell* 96, 437–446. doi: 10.1016/S0092-8674(00)80556-5

Labro, A. J., and Snyders, D. J. (2012). Being flexible: the voltage-controllable activation gate of kv channels. *Front. Pharmacol.* 3, 168. doi: 10.3389/fphar.2012.00168

Lange, W., Geissendorfer, J., Schenzer, A., Grotzinger, J., Seebohm, G., Friedrich, T., et al. (2009). Refinement of the binding site and mode of action of the anticonvulsant Retigabine on KCNQ K+ channels. *Mol. Pharmacol.* 75, 272–280. doi: 10.1124/mol.108.052282

Leaf, A. (2007). Prevention of sudden cardiac death by n-3 polyunsaturated fatty acids. *J. Cardiovasc. Med. (Hagerstown)* 8 Suppl 1, S27–S29. doi: 10.2459/01.JCM.0000289270.98105.b3

Lee, C. W., Kim, S., Roh, S. H., Endoh, H., Kodera, Y., Maeda, T., et al. (2004). Solution structure and functional characterization of SGTx1, a modifier of Kv2.1 channel gating. *Biochemistry* 43, 890–897. doi: 10.1021/bi0353373

Lees-Miller, J. P., Duan, Y., Teng, G. Q., and Duff, H. J. (2000). Molecular determinant of high-affinity dofetilide binding to HERG1 expressed in Xenopus oocytes: involvement of S6 sites. *Mol. Pharmacol.* 57, 367–374.

Lefevre, F., and Aronson, N. (2000). Ketogenic diet for the treatment of refractory epilepsy in children: A systematic review of efficacy. *Pediatrics* 105, E46. doi: 10.1542/peds.105.4.e46

Lenaeus, M. J., Gamal El-Din, T. M., Ing, C., Ramanadane, K., Pomes, R., Zheng, N., et al. (2017). Structures of closed and open states of a voltage-gated sodium channel. *Proc. Natl. Acad. Sci. U. S. A* 114, E3051–E3060. doi: 10.1073/pnas.1700761114

Lepage, K., Rainier, J., Johnson, H., Baden, D., and Murray, T. (2007). Gambierol Acts as a Functional Antagonist of Neurotoxin Site 5 on Voltage-Gated Sodium Channels in Cerebellar Granule Neurons. *J. Pharmacol. Exp. Ther.* 323, 174–179. doi: 10.1124/jpet.107.124271

Lewis, R. J., Vernoux, J.-P., and Brereton, I. M. (1998). Structure of Caribbean Ciguatoxin Isolated from Caranx latus. *J. Am. Chem. Soc.* 120, 5914–5920. doi: 10.1021/ja980389e

Liang, Q., Anderson, W. D., Jones, S. T., Souza, C. S., Hosoume, J. M., Treptow, W., et al. (2015). Positive Allosteric Modulation of Kv Channels by Sevoflurane: Insights into the Structural Basis of Inhaled Anesthetic Action. *PloS One* 10, e0143363. doi: 10.1371/journal.pone.0143363

Liin, S. I., Silvera Ejneby, M., Barro-Soria, R., Skarsfeldt, M. A., Larsson, J. E., Starck Harlin, F., et al. (2015). Polyunsaturated fatty acid analogs act antiarrhythmically on the cardiac IKs channel. *Proc. Natl. Acad. Sci. U. S. A.* 112, 5714–5719. doi: 10.1073/pnas.1503488112

Lin, Y.-Y., Risk, M., Ray, S. M., Van Engen, D., Clardy, J., Golik, J., et al. (1981). Isolation and structure of brevetoxin B from the "red tide" dinoflagellate Ptychodiscus brevis (Gymnodinium breve). *J. Am. Chem. Soc.* 103, 6773–6775. doi: 10.1021/ja00412a053

Linford, N. J., Cantrell, A. R., Qu, Y., Scheuer, T., and Catterall, W. A. (1998). Interaction of batrachotoxin with the local anesthetic receptor site in transmembrane segment IVS6 of the voltage-gated sodium channel. *Proc. Natl. Acad. Sci. U. S. A.* 95, 13947–13952. doi: 10.1073/pnas.95.23.13947

Lombet, A., Bidard, J. N., and Lazdunski, M. (1987). Ciguatoxin and brevetoxins share a common receptor site on the neuronal voltage-dependent Na+ channel. *FEBS Lett.* 219, 355–359. doi: 10.1016/0014-5793(87)80252-1

Long, S. B., Tao, X., Campbell, E. B., and Mackinnon, R. (2007). Atomic structure of a voltage-dependent K+ channel in a lipid membrane-like environment. *Nature* 450, 376–382. doi: 10.1038/nature06265

Luzhkov, V. B., and Aqvist, J. (2001). Mechanisms of tetraethylammonium ion block in the KcsA potassium channel. *FEBS Lett.* 495, 191–196. doi: 10.1016/S0014-5793(01)02381-X

Manville, R. W., Papanikolaou, M., and Abbott, G. W. (2018). Direct neurotransmitter activation of voltage-gated potassium channels. *Nat. Commun.* 9, 1847. doi: 10.1038/s41467-018-04266-w

Marban, E., Yamagishi, T., and Tomaselli, G. F. (1998). Structure and function of voltage-gated sodium channels. *J. Physiol.* 508 (Pt 3), 647–657. doi: 10.1111/j.1469-7793.1998.647bp.x

Martinez-Morales, E., Kopljar, I., Rainier, J. D., Tytgat, J., Snyders, D. J., and Labro, A. J. (2016). Gambierol and n-alkanols inhibit Shaker Kv channel via distinct binding sites outside the K(+) pore. *Toxicon* 120, 57–60. doi: 10.1016/j.toxicon.2016.07.017

Marzian, S., Stansfeld, P. J., Rapedius, M., Rinne, S., Nematian-Ardestani, E., Abbruzzese, J. L., et al. (2013). Side pockets provide the basis for a new mechanism of Kv channel-specific inhibition. *Nat. Chem. Biol.* 9, 507–513. doi: 10.1038/nchembio.1271

Mccusker, E. C., Bagneris, C., Naylor, C. E., Cole, A. R., D'avanzo, N., Nichols, C. G., et al. (2012). Structure of a bacterial voltage-gated sodium channel pore reveals mechanisms of opening and closing. *Nat. Commun.* 3, 1102. doi: 10.1038/ncomms2077

Mcnaughton-Smith, G. A., Gross, M. F., and Wickenden, A. D. (2002). *Benzanilides as potassium channel openers*, United States patent application 6372767.

Mihailescu, M., Krepkiy, D., Milescu, M., Gawrisch, K., Swartz, K. J., and White, S. (2014). Structural interactions of a voltage sensor toxin with lipid membranes. *Proc. Natl. Acad. Sci. U. S. A* 111, E5463–E5470. doi: 10.1073/pnas.1415324111

Mitcheson, J. S., Chen, J., Lin, M., Culberson, C., and Sanguinetti, M. C. (2000). A structural basis for drug-induced long QT syndrome. *Proc. Natl. Acad. Sci. U. S. A.* 97, 12329–12333. doi: 10.1073/pnas.210244497

Murata, M., Legrand, A. M., Ishibashi, Y., Fukui, M., and Yasumoto, T. (1990). Structures and configurations of ciguatoxin from the moray eel Gymnothorax javanicus and its likely precursor from the dinoflagellate Gambierdiscus toxicus. *J. Am. Chem. Soc.* 112, 4380–4386. doi: 10.1021/ja00167a040

Nicholson, G., and Lewis, R. (2006). Ciguatoxins: Cyclic Polyether Modulators of Voltage-gated Ion Channel Function. *Marine Drugs* 4, 82–118. doi: 10.3390/md403082

Ottosson, N. E., Silvera Ejneby, M., Wu, X., Yazdi, S., Konradsson, P., Lindahl, E., et al. (2017). A drug pocket at the lipid bilayer-potassium channel interface. *Sci. Adv.* 3, e1701099. doi: 10.1126/sciadv.1701099

Ouyang, W., Jih, T. Y., Zhang, T. T., Correa, A. M., and Hemmings, H. C. Jr. (2007). Isoflurane inhibits NaChBac, a prokaryotic voltage-gated sodium channel. *J. Pharmacol. Exp. Ther.* 322, 1076–1083. doi: 10.1124/jpet.107.122929

Ouyang, W., Herold, K. F., and Hemmings, H. C. Jr. (2009). Comparative effects of halogenated inhaled anesthetics on voltage-gated Na+ channel function. *Anesthesiology* 110, 582–590. doi: 10.1097/ALN.0b013e318197941e

Padilla, K., Wickenden, A. D., Gerlach, A. C., and Mccormack, K. (2009). The KCNQ2/3 selective channel opener ICA-27243 binds to a novel voltage-sensor domain site. *Neurosci. Lett.* 465, 138–142. doi: 10.1016/j.neulet.2009.08.071

Payandeh, J., Scheuer, T., Zheng, N., and Catterall, W. A. (2011). The crystal structure of a voltage-gated sodium channel. *Nature* 475, 353–358. doi: 10.1038/nature10238

Payandeh, J., Gamal El-Din, T. M., Scheuer, T., Zheng, N., and Catterall, W. A. (2012). Crystal structure of a voltage-gated sodium channel in two potentially inactivated states. *Nature* 486, 135–139. doi: 10.1038/nature11077

Perry, M., Sachse, F. B., Abbruzzese, J., and Sanguinetti, M. C. (2009). PD-118057 contacts the pore helix of hERG1 channels to attenuate inactivation and enhance K+ conductance. *Proc. Natl. Acad. Sci. U. S. A* 106, 20075–20080. doi: 10.1073/pnas.0906597106

Pettersen, E. F., Goddard, T. D., Huang, C. C., Couch, G. S., Greenblatt, D. M., Meng, E. C., et al. (2004). UCSF Chimera–a visualization system for exploratory research and analysis. *J. Comput. Chem.* 25, 1605–1612. doi: 10.1002/jcc.20084

Poli, M. A., Mende, T. J., and Baden, D. G. (1986). Brevetoxins, unique activators of voltage-sensitive sodium channels, bind to specific sites in rat brain synaptosomes. *Mol. Pharmacol.* 30, 129–135.

Ragsdale, D. S., Mcphee, J. C., Scheuer, T., and Catterall, W. A. (1994). Molecular determinants of state-dependent block of Na+ channels by local anesthetics. *Science* 265, 1724–1728. doi: 10.1126/science.8085162

Raju, S. G., Barber, A. F., Lebard, D. N., Klein, M. L., and Carnevale, V. (2013). Exploring volatile general anesthetic binding to a closed membrane-bound bacterial voltage-gated sodium channel via computation. *PloS Comput. Biol.* 9, e1003090. doi: 10.1371/journal.pcbi.1003090

Rein, K. S., Baden, D. G., and Gawley, R. E. (1994). Conformational Analysis of the Sodium Channel Modulator, Brevetoxin A, Comparison with Brevetoxin B Conformations, and a Hypothesis about the Common Pharmacophore of the "Site 5". *Toxins. J. Organ. Chem.* 59, 2101–2106. doi: 10.1021/jo00087a027

Rundfeldt, C. (1997). The new anticonvulsant retigabine (D-23129) acts as an opener of K+ channels in neuronal cells. *Eur. J. Pharmacol.* 336, 243–249. doi: 10.1016/S0014-2999(97)01249-1

Sanchez-Chapula, J. A., Navarro-Polanco, R. A., Culberson, C., Chen, J., and Sanguinetti, M. C. (2002). Molecular determinants of voltage-dependent human ether-a-go-go related gene (HERG) K+ channel block. *J. Biol. Chem.* 277, 23587–23595. doi: 10.1074/jbc.M200448200

Sanchez-Chapula, J. A., Ferrer, T., Navarro-Polanco, R. A., and Sanguinetti, M. C. (2003). Voltage-dependent profile of human ether-a-go-go-related gene channel block is influenced by a single residue in the S6 transmembrane domain. *Mol. Pharmacol.* 63, 1051–1058. doi: 10.1124/mol.63.5.1051

Saxena, P., Zangerl-Plessl, E. M., Linder, T., Windisch, A., Hohaus, A., Timin, E., et al. (2016). New potential binding determinant for hERG channel inhibitors. *Sci. Rep.* 6, 24182. doi: 10.1038/srep24182

Schenzer, A., Friedrich, T., Pusch, M., Saftig, P., Jentsch, T. J., Grotzinger, J., et al. (2005). Molecular determinants of KCNQ (Kv7) K+ channel sensitivity to the anticonvulsant retigabine. *J. Neurosci.* 25, 5051–5060. doi: 10.1523/JNEUROSCI.0128-05.2005

Schreibmayer, W., and Jeglitsch, G. (1992). The sodium channel activator Brevetoxin-3 uncovers a multiplicity of different open states of the cardiac sodium channel. *Biochim. Biophys. Acta* 1104, 233–242. doi: 10.1016/0005-2736(92)90035-K

Schroeder, B. C., Hechenberger, M., Weinreich, F., Kubisch, C., and Jentsch, T. J. (2000). KCNQ5, a novel potassium channel broadly expressed in brain, mediates M-type currents. *J. Biol. Chem.* 275, 24089–24095. doi: 10.1074/jbc.M003245200

Sheridan, R. E., and Adler, M. (1989). The actions of a red tide toxin from Ptychodiscus brevis on single sodium channels in mammalian neuroblastoma cells. *FEBS Lett.* 247, 448–452. doi: 10.1016/0014-5793(89)81389-4

Stevens, M., Peigneur, S., and Tytgat, J. (2011). Neurotoxins and their binding areas on voltage-gated sodium channels. *Front. Pharmacol.* 2, 71. doi: 10.3389/fphar.2011.00071

Stock, L., Hosoume, J., Cirqueira, L., and Treptow, W. (2018). Binding of the general anesthetic sevoflurane to ion channels. *PloS Comput. Biol.* 14, e1006605. doi: 10.1371/journal.pcbi.1006605

Strachan, L. C., Lewis, R. J., and Nicholson, G. M. (1999). Differential actions of pacific ciguatoxin-1 on sodium channel subtypes in mammalian sensory neurons. *J. Pharmacol. Exp. Ther.* 288, 379–388.

Sun, J., and Mackinnon, R. (2017). Cryo-EM Structure of a KCNQ1/CaM Complex Reveals Insights into Congenital Long QT Syndrome. *Cell* 169, 1042–1050 e1049. doi: 10.1016/j.cell.2017.05.019

Sunami, A., Glaaser, I. W., and Fozzard, H. A. (2001). Structural and gating changes of the sodium channel induced by mutation of a residue in the upper third of IVS6, creating an external access path for local anesthetics. *Mol. Pharmacol.* 59, 684–691. doi: 10.1124/mol.59.4.684

Sutro, J. B. (1986). Kinetics of veratridine action on Na channels of skeletal muscle. *J. Gen. Physiol.* 87, 1–24. doi: 10.1085/jgp.87.1.1

Swartz, K. J. (2007). Tarantula toxins interacting with voltage sensors in potassium channels. *Toxicon : Off. J. Int. Soc. Toxinol.* 49, 213–230. doi: 10.1016/j.toxicon.2006.09.024

Thomas, D., Karle, C. A., and Kiehn, J. (2006). The cardiac hERG/IKr potassium channel as pharmacological target: structure, function, regulation, and clinical applications. *Curr. Pharm. Des.* 12, 2271–2283. doi: 10.2174/138161206777585102

Trainer, V. L., Thomsen, W. J., Catterall, W. A., and Baden, D. G. (1991). Photoaffinity labeling of the brevetoxin receptor on sodium channels in rat brain synaptosomes. *Mol. Pharmacol.* 40, 988–994.

Trainer, V. L., Baden, D. G., and Catterall, W. A. (1994). Identification of peptide components of the brevetoxin receptor site of rat brain sodium channels. *J. Biol. Chem.* 269, 19904–19909.

Uehara, A., and Moczydlowski, E. (1986). Blocking mechanisms of batrachotoxin-activated Na channels in artificial bilayers. *Membr. Biochem.* 6, 111–147. doi: 10.3109/09687688609065446

Ulbricht, W. (1969). The effect of veratridine on excitable membranes of nerve and muscle. *Ergeb. Physiol.* 61, 18–71. doi: 10.1007/BFb0111446

Vandenberg, J. I., Perry, M. D., Perrin, M. J., Mann, S. A., Ke, Y., and Hill, A. P. (2012). hERG K(+) channels: structure, function, and clinical significance. *Physiol. Rev.* 92, 1393–1478. doi: 10.1152/physrev.00036.2011

Vennekamp, J., Wulff, H., Beeton, C., Calabresi, P. A., Grissmer, S., Hansel, W., et al. (2004). Kv1.3-blocking 5-phenylalkoxypsoralens: a new class of immunomodulators. *Mol. Pharmacol.* 65, 1364–1374. doi: 10.1124/mol.65.6.1364

Wang, W., and Mackinnon, R. (2017). Cryo-EM Structure of the Open Human Ether-a-go-go-Related K(+) Channel hERG. *Cell* 169, 422–430 e410. doi: 10.1016/j.cell.2017.03.048

Wang, S. Y., and Wang, G. K. (1998). Point mutations in segment I-S6 render voltage-gated Na+ channels resistant to batrachotoxin. *Proc. Natl. Acad. Sci. U. S. A.* 95, 2653–2658. doi: 10.1073/pnas.95.5.2653

Wang, S. Y., and Wang, G. K. (1999). Batrachotoxin-resistant Na+ channels derived from point mutations in transmembrane segment D4-S6. *Biophys. J.* 76, 3141–3149. doi: 10.1016/S0006-3495(99)77465-5

Wang, G. K., and Wang, S. Y. (2003). Veratridine block of rat skeletal muscle Nav1.4 sodium channels in the inner vestibule. *J. Physiol.* 548, 667–675. doi: 10.1113/jphysiol.2002.035469

Wang, H. S., Pan, Z., Shi, W., Brown, B. S., Wymore, R. S., Cohen, I. S., et al. (1998). KCNQ2 and KCNQ3 potassium channel subunits: molecular correlates of the M-channel. *Science* 282, 1890–1893. doi: 10.1126/science.282.5395.1890

Wang, S. Y., Nau, C., and Wang, G. K. (2000). Residues in Na(+) channel D3-S6 segment modulate both batrachotoxin and local anesthetic affinities. *Biophys. J.* 79, 1379–1387. doi: 10.1016/S0006-3495(00)76390-9

Wang, S. Y., Barile, M., and Wang, G. K. (2001). Disparate role of Na(+) channel D2-S6 residues in batrachotoxin and local anesthetic action. *Mol. Pharmacol.* 59, 1100–1107. doi: 10.1124/mol.59.5.1100

Wang, S. Y., Tikhonov, D. B., Mitchell, J., Zhorov, B. S., and Wang, G. K. (2007). Irreversible block of cardiac mutant Na+ channels by batrachotoxin. *Channels (Austin)* 1, 179–188. doi: 10.4161/chan.4437

Wang, A. W., Yang, R., and Kurata, H. T. (2017). Sequence determinants of subtype-specific actions of KCNQ channel openers. *J. Physiol.* 595, 663–676. doi: 10.1113/JP272762

Wang, C. K., Lamothe, S. M., Wang, A. W., Yang, R. Y., and Kurata, H. T. (2018). Pore- and voltage sensor-targeted KCNQ openers have distinct state-dependent actions. *J. Gen. Physiol.* 150, 1722–1734. doi: 10.1085/jgp.201812070

Waterhouse, A. M, Procter, J. B., Martin, D. M. A., Clamp, M., and Barton, G. J. (2009). Jalview Version 2 - a multiple sequence alignment editor and analysis workbench. *Bioinformatics* 25 (9), 1189–1191. doi: 10.1093/bioinformatics/btp033

Waterhouse, A., Bertoni, M., Bienert, S., Studer, G., Tauriello, G., Gumienny, R., et al. (2018). SWISS-MODEL: homology modelling of protein structures and complexes. *Nucleic Acids Res.* 46, W296–W303. doi: 10.1093/nar/gky427

West, J. W., Patton, D. E., Scheuer, T., Wang, Y., Goldin, A. L., and Catterall, W. A. (1992). A cluster of hydrophobic amino acid residues required for fast Na (+)-channel inactivation. *Proc. Natl. Acad. Sci. U. S. A* 89, 10910–10914. doi: 10.1073/pnas.89.22.10910

Wickenden, A. D., Krajewski, J. L., London, B., Wagoner, P. K., Wilson, W. A., Clark, S., et al. (2008). N-(6-chloro-pyridin-3-yl)-3,4-difluoro-benzamide (ICA-27243): a novel, selective KCNQ2/Q3 potassium channel activator. *Mol. Pharmacol.* 73, 977–986. doi: 10.1124/mol.107.043216

Wrobel, E., Rothenberg, I., Krisp, C., Hundt, F., Fraenzel, B., Eckey, K., et al. (2016). KCNE1 induces fenestration in the Kv7.1/KCNE1 channel complex that allows for highly specific pharmacological targeting. *Nat. Commun.* 7, 1–13. doi: 10.1038/ncomms12795

Wulff, H., Castle, N. A., and Pardo, L. A. (2009). Voltage-gated potassium channels as therapeutic targets. *Nat. Rev. Drug Discovery* 8, 982–1001. doi: 10.1038/nrd2983

Xiong, Q., Sun, H., and Li, M. (2007). Zinc pyrithione-mediated activation of voltage-gated KCNQ potassium channels rescues epileptogenic mutants. *Nat. Chem. Biol.* 3, 287–296. doi: 10.1038/nchembio874

Xu, C. Q., Zhu, S. Y., Chi, C. W., and Tytgat, J. (2003). Turret and pore block of K+ channels: what is the difference? *Trends Pharmacol. Sci.* 24, 446–448author reply 448–449. doi: 10.1016/S0165-6147(03)00223-2

Yarov-Yarovoy, V., Mcphee, J. C., Idsvoog, D., Pate, C., Scheuer, T., and Catterall, W. A. (2002). Role of amino acid residues in transmembrane segments IS6 and IIS6 of the Na+ channel alpha subunit in voltage-dependent gating and drug block. *J. Biol. Chem.* 277, 35393–35401. doi: 10.1074/jbc.M206126200

Yazdi, S., Stein, E., Elinder, F., Andersson, M., and Lindahl, E. (2016). The Molecular Basis of Polyunsaturated Fatty Acid Interactions with the Shaker Voltage-Gated Potassium Channel. *PloS Comput. Biol.* 12, e1004704. doi: 10.1371/journal.pcbi.1004704

Yuki, T., Yamaoka, K., Yakehiro, M., and Seyama, I. (2001). State-dependent action of grayanotoxin I on Na(+) channels in frog ventricular myocytes. *J. Physiol.* 534, 777–790. doi: 10.1111/j.1469-7793.2001.00777.x

Zamponi, G. W., Doyle, D. D., and French, R. J. (1993). Fast lidocaine block of cardiac and skeletal muscle sodium channels: one site with two routes of access. *Biophys. J.* 65, 80–90. doi: 10.1016/S0006-3495(93)81042-7

Zhang, M., Korolkova, Y. V., Liu, J., Jiang, M., Grishin, E. V., and Tseng, G. N. (2003). BeKm-1 is a HERG-specific toxin that shares the structure with ChTx but the mechanism of action with ErgTx1. *Biophys. J.* 84, 3022–3036. doi: 10.1016/S0006-3495(03)70028-9

Zhang, X., Ren, W., Decaen, P., Yan, C., Tao, X., Tang, L., et al. (2012). Crystal structure of an orthologue of the NaChBac voltage-gated sodium channel. *Nature* 486, 130–134. doi: 10.1038/nature11054

Conflict of Interest: The authors declare that the research was conducted in the absence of any commercial or financial relationships that could be construed as a potential conflict of interest.

frontiers in Pharmacology

ORIGINAL RESEARCH
published: 15 May 2020
doi: 10.3389/fphar.2020.00721

Computational Insights Into Voltage Dependence of Polyamine Block in a Strong Inwardly Rectifying K^+ Channel

Xingyu Chen[†], *Michael Bründl*[†], *Theres Friesacher and Anna Stary-Weinzinger*[*]

Department of Pharmacology and Toxicology, University of Vienna, Vienna, Austria

Inwardly rectifying potassium (K_{IR}) channels play important roles in controlling cellular excitability and K^+ ion homeostasis. Under physiological conditions, K_{IR} channels allow large K^+ influx at potentials negative to the equilibrium potential of K^+ but permit little outward current at potentials positive to the equilibrium potential of K^+, due to voltage dependent block of outward K^+ flux by cytoplasmic polyamines. These polycationic molecules enter the K_{IR} channel pore from the intracellular side. They block K^+ ion movement through the channel at depolarized potentials, thereby ensuring, for instance, the long plateau phase of the cardiac action potential. Key questions concerning how deeply these charged molecules migrate into the pore and how the steep voltage dependence arises remain unclear. Recent MD simulations on GIRK2 (=Kir3.2) crystal structures have provided unprecedented details concerning the conduction mechanism of a K_{IR} channel. Here, we use MD simulations with applied field to provide detailed insights into voltage dependent block of putrescine, using the conductive state of the strong inwardly rectifying K^+ channel GIRK2 as starting point. Our µs long simulations elucidate details about binding sites of putrescine in the pore and suggest that voltage-dependent rectification arises from a dual mechanism.

Keywords: molecular dynamics simulation, charge movement, ion displacement, inward rectification, Kir3.2, putrescine

OPEN ACCESS

Edited by:
Gildas Loussouarn, Université de Nantes, France

Reviewed by:
Show-Ling Shyng, Oregon Health and Science University, United States
Mounir Tarek, Centre National de la Recherche Scientifique, France

***Correspondence:**
Anna Stary-Weinzinger
anna.stary@univie.ac.at

[†]*These authors have contributed equally to this work*

Specialty section:
This article was submitted to Pharmacology of Ion Channels and Channelopathies, a section of the journal Frontiers in Pharmacology

Received: *30 November 2019*
Accepted: *30 April 2020*
Published: *15 May 2020*

Citation:
Chen X, Bründl M, Friesacher T and Stary-Weinzinger A (2020) Computational Insights Into Voltage Dependence of Polyamine Block in a Strong Inwardly Rectifying K^+ Channel. Front. Pharmacol. 11:721. doi: 10.3389/fphar.2020.00721

INTRODUCTION

Inwardly rectifying potassium (K_{IR}) channels play important roles in controlling cellular excitability and K^+ ion homeostasis. Under physiological conditions, K_{IR} channels pass inward currents more easily than outward currents due to voltage-dependent block by intracellular cations such as Mg^{2+} and polyamines (Hibino et al., 2010). These polycationic molecules enter the K_{IR} channel pore from the intracellular side and block K^+ ion movement through the channel at depolarized potentials, thereby ensuring, for instance, the long plateau phase of the cardiac action potential (Nichols and Lee, 2018). The degree of inward rectification varies among the K_{IR} channel family. In strong inward rectifier channels, such as Kir2 and Kir3, very little outward current occurs at voltages positive to the K^+ equilibrium (E_K) potential. While in weak rectifier channels, e.g. Kir1 and Kir6 family members,

conductance at voltages positive to E_K is reduced relative to inward currents. Intermediate rectification properties are found in Kir4.x channels (Hibino et al., 2010).

Atomic and near-atomic resolution structures of different K_{IR} channels, albeit without polyamines bound, have been solved mainly in the closed state, revealing a conserved architecture of the K_{IR} channel family. Further, the transmembrane domain (TMD) is conserved throughout the whole K^+ channel superfamily (Doyle, 1998). It contains two transmembrane helices (M1 and M2), an extracellular turret region, a short P-helix and a selectivity filter region. A unique structural feature of K_{IR} channels is a long cytoplasmic domain (CTD), which contains another constriction, the so-called G-loop gate and extends the ion conduction pore to > 85 Å (Kuo et al., 2003).

Unlike voltage dependent gating of K_v channel proteins, voltage-dependent "inward rectification" in K_{IR} channels is not an intrinsic property. Voltage dependent rectification arises from voltage dependent channel blockade by cytoplasmic polycations, particularly polyamines, such as putrescine, spermine, and spermidine (Ficker et al., 1994; Lopatin et al., 1994; Fakler et al., 1995). Residues influencing rectification properties by polyamines have been identified in the CTD as well as the TMD. Two negatively charged residues in Kir2.1 (carrying I_{K1} current), E224 in the cytoplasm and D172, located in the transmembrane domain, have been shown to be critical for strong rectification. Interestingly, swapping residue D172 between strong and weak rectifier channels resulted in substantial transfer of rectification properties (Lopatin et al., 1994; Lu and MacKinnon, 1994; Stanfield et al., 1994; Wible et al., 1994). Due to the critical importance of this residue, this site has been referred to as rectification controller. Nevertheless, this position does not exert an all-or-nothing effect and surprisingly, channels such as Kir3.2, which exhibit relatively strong rectification lack this acidic residue (for alignment, see **Supplemental Figure 1**). Further, mutating D172 to N (Kir2.1) does weaken but not abolish polyamine binding (Wible et al., 1994; Yi et al., 2001; Guo et al., 2003). Importantly it has been shown that introducing a negative charge in the transmembrane domain is not position dependent (Kurata et al., 2004). This is in line with a computational study by the Roux group (Robertson et al., 2008), revealing that many of the residues influencing rectification interact with ions over very long distances up to 40 Å, likely affecting blocker energetics over the entire pore.

The CTD contributes to rectification to a lesser extent than the TMD. For example, interchanging the cytoplasmic domains of Kir2.1 and Kir1.1 resulted in partial transfer of rectification properties (Taglialatela et al., 1995). Mutagenesis identified two negatively charged residues in Kir2.1 (E224 and E299), being important determinants of rectification (Taglialatela et al., 1995; Kubo and Murata, 2001; Guo et al., 2003). Importantly, neutralization of these charges slowed the kinetics and reduced the affinity of spermine block (Taglialatela et al., 1995; Guo et al., 2003; Fujiwara and Kubo, 2006). However, mutations also changed the biophysics of the channel, complicating interpretation of the results.

Despite the existence of more and more crystal and cryo-EM structures, none of the different eukaryotic structures could be solved in the presence of polyamines so far, leaving important questions concerning the location of the polyamine binding site(s) within the K_{IR} channel pore open. Further, the nature of the charge movement associated with block and the origin of the steepness of the voltage dependence of these compounds, which roughly correlates with the number of charges of the polyamines remain unresolved.

Recent MD simulations on K_{IR} crystal structures have provided unprecedented details concerning the K^+ conduction mechanism of Kir3.2 and 2.2 channels (Bernsteiner et al., 2019; Zangerl-Plessl et al., 2020) and can serve as excellent starting point to address inward rectification. Here, we perform multi-microsecond-timescale MD simulations with applied field to provide first atomistic insights into the voltage dependent block of putrescine (PUT^{2+}), using the conductive state of the strong inwardly rectifying Kir3.2 channel as a starting point.

RESULTS

Putrescine Block of Kir3.2 Channels Under Applied Field

Starting from a conductive snapshot from a previous simulation (Kir3.2 also known as GIRK2), a bona-fide strong rectifier, we addressed the dynamics of the "shortest" polyamine putrescine (PUT^{2+}), a 1,4- butanediamine, which has a net charge of +2 under physiological pH. **Figure 1** illustrates K^+ and PUT^{2+} movement along the z-axis, monitored in six one µs atomistic simulations with an applied field of 40 mV/nm, which amounts to 580 mV. In four out of six runs, the molecule rapidly permeated from the initial binding site in the CTD to the selectivity filter (position S_C or S4). In the other two runs, PUT^{2+} remained close to the initial binding site in the CTD. Interestingly, in all except one run, at least a second, and in the case of run six, a third molecule entered from the cytoplasm to bind to the negatively charged residues in the CTD, mainly E236, revealing that the cytoplasmic pore can accommodate more than one blocker molecule. However, in none of the runs, more than one PUT^{2+} traversed up to the selectivity filter (SF). K^+ permeation was effectively prevented only when the charged blocker reached its binding site at the SF but not when the polyamine was bound to the original binding region in the CTD. As illustrated in **Figure 1** in runs three, four and six, ions were observed to pass by PUT^{2+} when bound to the CTD (ion slippage examples are indicated by black arrows). This finding is in agreement with experimental data, suggesting a shallow blocked state for polyamines in the CTD (Kurata et al., 2007). The timescales for PUT^{2+} permeation to the SF varied from ~ 250 ns to ~650 ns, with the molecule remaining at its binding site for the rest of the simulation time. Binding to the CTD was reasonably stable when analyzing second and/or third PUT^{2+} molecules entering the CTD, with retention times of up to 850 ns, after accessing the binding site from the intracellular site. To

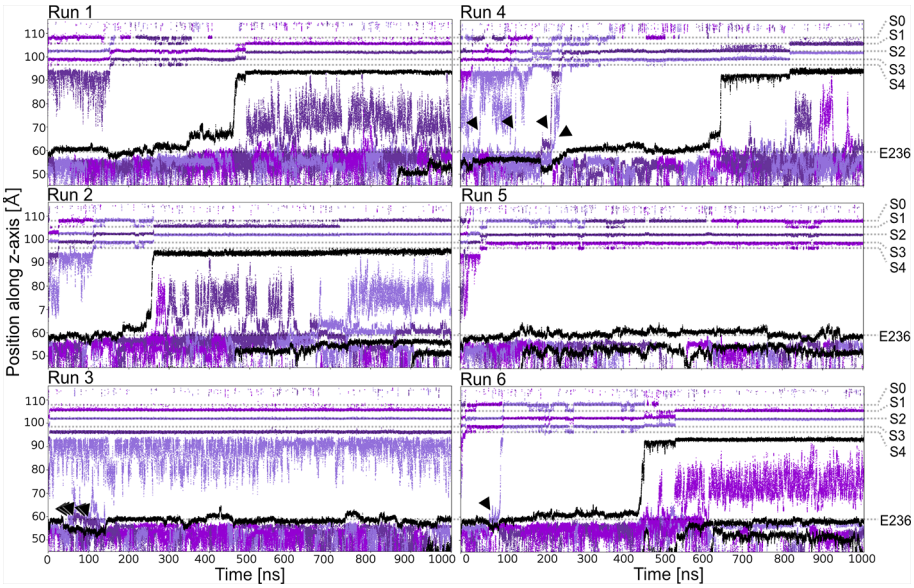

FIGURE 1 | PUT^{2+} blockage of Kir3.2 channels under an applied field. Positions of K^+ and PUT^{2+} molecules (center of mass) are plotted as function of time along the pore (z-axis). K^+ ions are colored in different shades of purple and PUT^{2+} molecules are shown in black. Slippage of K^+ ions is indicated with black arrows.

analyze binding at these different sites in more detail, PUT^{2+} and K^+ occupancies along the z-axis were plotted as function of time.

Binding Sites of Putrescine in Kir3.2

Based on analyzing PUT^{2+} and K^+ ion occupancies extracted from 4μs MD simulations (only from runs, where PUT^{2+} reached the SF binding site, compare **Figure 2B**), two binding areas emerged, one located close to E236 in the CTD, and a second, higher occupancy site close to T154 from the SF (**Figure 2A**). At the binding site in the CTD, frequent hydrogen bonds between the nitrogen atoms of PUT^{2+} and side-chains of E236 (equal to the known rectification-influencing residue E224 in Kir2.1) were observed. Less frequent hydrogen bond interactions to G318 and T320, close to the G-loop gate, were seen as well (see **Figure 2B**, right panel). When the molecule left this "shallow" blocking site, it rapidly passed the helix bundle-crossing gate (lined by residues F192) and the transmembrane cavity, without further intermediate binding sites. PUT^{2+} reached its final binding site at the bottom of the SF, where it oriented mainly perpendicular to the filter axis, which in one run was preceded by a horizontal orientation below the SF at site S_C (for representative snapshots, see **Figure 2B**, right panel). When PUT^{2+} was bound to the SF, it frequently formed hydrogen bonds with residue T154. Nitrogen atoms of the blocker interacted with the backbone carbonyl oxygen atoms as well as the side-chain of T154. Polyamine binding to the SF lead to displacement of a single K^+ ion from the SF (**Figure 1** and **Supplemental Movies 1–4**). Comparison of ion occupancies between apo (taken from Bernsteiner et al., 2019) and holo runs revealed important differences. While, binding sites S2 and S3 were predominantly occupied in the apo runs, with significant K^+ occupancy also observed in site S_C, PUT^{2+} binding to the SF or at site S_C lead to displacement of ions from site S_C, S4 or S3 upwards, expelling the uppermost K^+ ion from the filter. Interestingly, a water molecule frequently occupied the site subsequent to PUT^{2+}. K^+ occupancy in site S2 was similar between apo and holo runs, while sites S1 and S2 revealed higher occupancy when PUT^{2+} was bound to the SF, as shown in **Supplemental Figure 2**.

Simulations of Spermine Block (SPM^{4+})

Next, we performed μs MD simulations with spermine, a polyamine with a net charge of +4 under physiological pH. In contrast to simulations with PUT^{2+}, SPM^{4+} did not traverse up towards the SF, but remained bound at the CTD site. As illustrated in **Figure 3C**, the compound mainly interacts with residues E236, T320, G318, and T317. Interestingly, in contrast to simulations with PUT^{2+} no slippage of K^+ ions was observed in two times 1 μs runs. This suggests that SPM^{4+} completely blocks the channel already at this binding site. To probe if SPM^{4+} might be able to bind deep within the pore as observed for the much smaller PUT^{2+}, we performed pulling simulations as reported previously for polymine block in a Kainate receptor (Brown et al., 2016). SPM^{4+} was pulled into the transmembrane cavity up to the position at the SF, observed for PUT^{2+} binding by applying a harmonic force along the z-axis, as detailed in the *Methods* section. Subsequently, the molecule was pulled in the reverse direction, towards the intracellular solvent and the work involved in this process calculated as described previously (Brown et al., 2016). Similar pulling simulations were also performed with PUT^{2+}. As illustrated in **Figure 3**, the work needed for PUT^{2+} to traverse up to the SF binding site is much

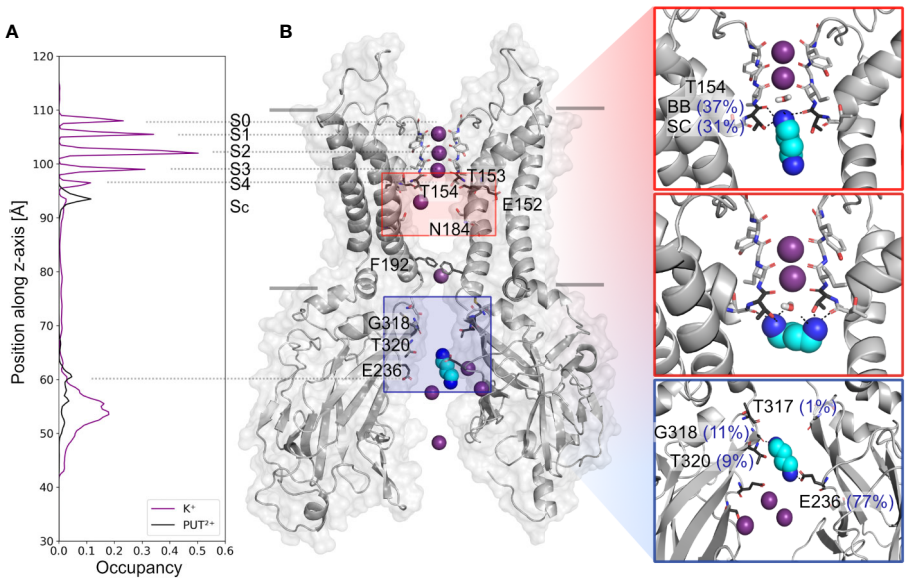

FIGURE 2 | Putrescine occupancies and interactions with Kir3.2. **(A)** Histograms of K^+ (purple line) and PUT^{2+} (black line) occupancies along the pore axis (z-axis) averaged from 4 μs MD simulations (runs 1, 2, 4, and 6). **(B)** Two opposing subunits of the equilibrated starting conformation of Kir3.2 (pdb: 3SYA), with K+ ions shown as purple spheres and PUT^{2+} shown as cyan spheres colored by atom name (nitrogen atoms colored in blue). Key residues for PUT^{2+} binding are labeled and shown in stick representation with oxygen atoms colored red and nitrogen atoms colored blue. Right panels: representative snapshots of PUT^{2+} binding sites at the SF (top and middle box) and the CTD (lower box) are shown, with hydrogen bond frequencies indicated in brackets (averaged over runs 1, 2, 4, and 6). BB, backbone; SC, sidechain.

smaller compared to the larger SPM^{4+} molecule. Overall, similar trends have been reported for the Kainate receptor, even though we did not attempt to pull the polyamines through the selectivity filter. These data suggest that SPM^{4+} might be able to reach a binding site deep in the pore, below the SF, as observed for PUT^{2+}. In the future, more extensive simulations will be required to assess SPM^{4+} block in Kir3.2 channels in more detail.

Where Does the Steep Voltage-Dependence of Polyamine Block Come From?

A long standing question in the field concerns the steepness of the voltage dependence of polyamine block. It roughly correlates with the charge of the polyamine molecules itself, ranging from +2 (in the case of the diamine PUT^{2+}) to +4 for SPM^{4+}, which contains four nitrogen atoms (Nichols and Lee, 2018). To assess the contribution that blocker charge migration through the electric field might have on the steepness of the voltage dependence, we calculated the electrostatic profile along the Kir3.2 channel pore, extracting 21 frames from a 1μs trajectory, using the PME method as implemented in VMD (Aksimentiev and Schulten, 2005), as detailed in the *Methods* section. The electrostatic contour plots shown in **Figure 4**, reveal a previously unappreciated feature of the open state of Kir3.2. In accordance to the much wider pore of the MthK channel (27.3 Å, measured at position L95) (Jiang et al., 2002), the membrane electrostatic profile of the narrower Kir3.2 channel pore (Cα-Cα distances of 17.7 Å measured at F192, which is equivalent to position L95 in MthK) is predominantly focused on

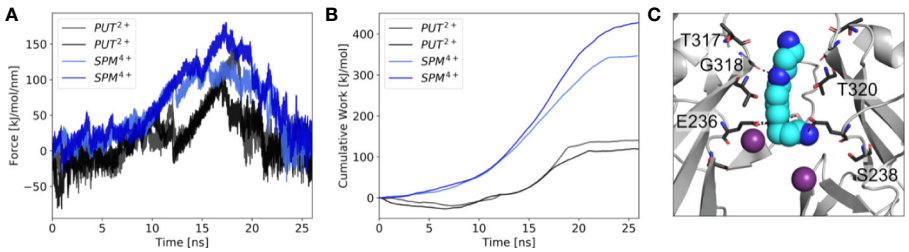

FIGURE 3 | Force probe simulations of PUT^{2+} and SPM^{4+} pulling. **(A)** Force profiles of the polyamines, when pulled along the pore axis of Kir3.2 **(B)** work profiles for pulling PUT^{2+} (black) and SPM^{4+} (blue). **(C)** Representative snapshot of SPM^{4+} binding site at the CTD. K^+ ions are shown as purple spheres, with interacting residues shown in stick representation.

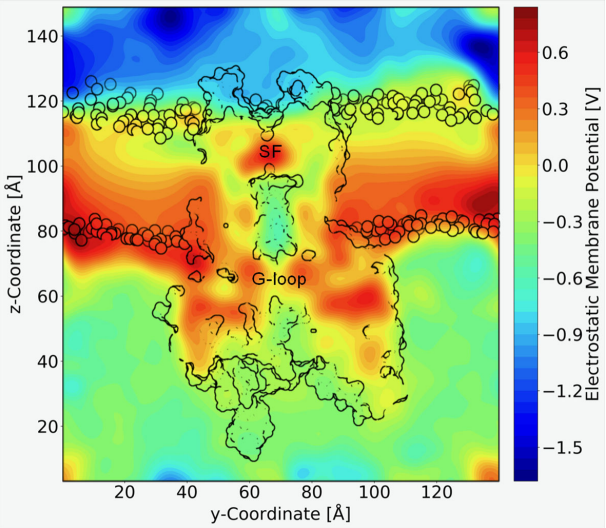

FIGURE 4 | Electrostatic profile of Kir3.2. An external electric field of 0.5 V was introduced, as applied in free MD simulations. 21 snapshots from the trajectory were extracted and smoothed electrostatic potential grids with a resolution of 1 Å per grid point are shown. The overall shape of the Kir3.2 channels (side view), as well has phospholipid head groups are outlined in black. The selectivity filter (SF) and G-loop area are indicated.

the SF region. Remarkably, however, there is also a significant fraction of the electric field focused on the narrow G-loop region (**Figure 4**). As previously reported, the region around residue G318, which forms the narrowest part of the G-loop gate, fluctuates between 5.9 to 6.8 Å, with oxygen atoms of G318 participating in K^+ coordination (Bernsteiner et al., 2019). This suggests that the access resistance for a K^+ ion diffusing between the cytoplasm and the SF might be higher in Kir3.2 compared to MthK. This agrees well with the much lower conductance rates in K_{IR} channels [~30 pS for Kir3.2 (Kofuji et al., 1996) vs. 170 pS for MthK channels (Li et al., 2007)]. Due to the narrower pore radius of the open K_{IR} channel, ions and other charged molecules such as PUT^{2+} experience a significant fraction of the membrane potential, when traversing from the CTD towards the SF. The electrostatic maps reveal that polyamine movement from the CTD towards a deep binding site below the SF might substantially contribute to the steepness of the voltage dependence of block (**Figure 3**). Further, partial binding to the SF, as observed for PUT^{2+} (**Figure 2**, left panel), contributes to voltage-dependence as well. This data also suggests that the electrical field distribution renders K^+ conduction through the channel voltage-dependent. Indeed, such behavior has been previously reported by Spassova and Lu (Spassova and Lu, 1998).

DISCUSSION

In this work, we aimed to obtain first structural insights into the mechanism of PUT^{2+} and SPM^{4+} interactions, two naturally occurring polyamines, with the strong inward rectifier K^+ channel Kir3.2. Polyamines are essential components in cells and bear ionisable amine moieties in their aliphatic chains. They play critical roles in protein synthesis, cell division and cell growth (Pegg, 2016; Handa et al., 2018). Their role in K_{IR} channel inhibition, due to pore block from the intracellular side was extensively studied (for detailed reviews see Nichols and Lopatin, 1997; Lu, 2004; Baronas and Kurata, 2014; Nichols and Lee, 2018), however, critical questions including the exact binding sites and the nature of the strong voltage-dependence are still unresolved.

We analysed blockade of the channel by performing multiple μs atomistic MD simulations on the GIRK2 crystal structure with an applied field to mimic a positive membrane potential, and performed pulling simulations to probe the work required for polyamines binding below the SF.

Two distinct, sequential polyamine binding sites were observed in our simulations with PUT^{2+}, in agreement with kinetic modelling studies (Lopatin et al., 1995). A "shallow" binding site in the CTD was predicted, where the drug mainly interacted with a negatively charged ring, formed by E236, which is equivalent to E224 in Kir2.1 (**Figure 2B**, right panel, **Supplemental Figure 1**, for alignment), the best studied strong inward rectifier channel. This residue has previously been implicated in polyamine block. Neutralization has been shown to slow the rate of block, and reduce the apparent affinity of a second deep site block (Taglialatela et al., 1995; Kubo and Murata, 2001). In contrast, in simulations with SPM^{4+}, only the CTD binding site was observed in the 1 μs runs, due to limited sampling. Thus, by applying enhanced sampling (pulling simulations) on the polyamines, we were able to sample binding of SPM^{4+} at the "deep" binding site, below the SF. Binding of this larger polyamine required three times more work, compared to the much smaller PUT^{2+}, suggesting that it is much easier for PUT^{2+} to move up to the SF site, compared to SPM^{4+}. A similar trend has previously been reported for Kainate receptor polyamine interactions (Brown et al., 2016).

Remarkably, our simulations revealed that PUT^{2+} could not completely inhibit ion conduction when interacting with the negatively charged residues in the CTD, since "slippage" of K^+ ions past the bound polyamine upwards into the transmembrane region was observed in several runs (**Figure 1**). This observation agrees with previous suggestions of incomplete block at the CTD, based on functional studies on Kir2.1 (Xu et al., 2009). Interestingly, no slippage was observed, when SPM^{4+} was bound to the same site in the CTD. However, longer sampling will be required to address, if this difference indeed holds true on longer simulation time scales.

Further, MD simulations revealed that PUT^{2+} could move through the electric field up to a steep binding site, at the SF where it stably interacted with T154, located at the base of the filter. This residue has not been tested experimentally for polyamine block, but it has been implicated in high-affinity block of Ba^{2+} in Kir2.1 channels (Hsieh et al., 2015). Support for blocker migration deep into the pore comes from blocker protection experiments with MTS reagents, suggesting that polyamines might bind above the rectification controller position D172 (Kurata et al., 2008).

Another important observation of our study is that PUT^{2+} migration to the SF binding site is coupled with displacement of a permeant K^+ ion. Such a scenario has recently been observed in CP-AMPAR channels, where polyamines with different tail length have been analyzed, using cryo-EM. Structures with short polyamines reveal that these molecules partially protrude into the SF, while longer molecules bind deep within the SF. The cryo-EM structure demonstrates that a combination of blocker entry into the filter and ion displacement can lead to steep voltage dependence (Twomey et al., 2018). Our simulations suggest a similar mechanism for inward rectifier channels. Further, such a mechanism has been previously envisioned, based on experimental observation, showing that the blocker dependence on the membrane voltage varied as a function of extracellular K^+ concentration (Spassova and Lu, 1998; Whorton and MacKinnon, 2011).

An important, previously largely unappreciated finding of our study concerns the nature of the electric field. In contrast to previous expectations, based on calculations of K^+ channel pores with wider gate diameters (e.g. Jiang et al., 2002), the membrane potential does not only drop over the selectivity filter, but there is a significant voltage drop over the G-loop area, as illustrated in **Figure 4**. Based on these qualitative calculations, polyamine binding to the CTD site is likely to depend on the prevailing voltage (without ion displacement from the SF), due to molecules traversing a fraction of the membrane potential, when passing through the G-loop gate area.

In addition, our simulations consistently predict that binding of PUT^{2+} to the SF site leads to outward displacement of a K^+ ion (**Figure 1** and **Supplemental Movies**). These predictions agree very well with functional studies, supporting sequential binding with weak and strong voltage dependence (Lopatin et al., 1995; Shin and Lu, 2005; Kurata et al., 2007).

The predicted differences in electrostatic potential along the pore further suggest that the access resistance for K^+ ions diffusing between the cytoplasm and the SF is higher in Kir3 channels, compared to ion channels with wider open pores such as MthK. This is in line with the different conductance rates reported for these channels, which amount to ~ 30 pS in Kir3.2 channels (Kofuji et al., 1996), but are much higher in MthK channels, where values of ~ 200 pS have been published (Li et al., 2007). The electrostatic data further suggests that the electrical field distribution should render K^+ conduction voltage dependent, which is in agreement with previous reports by Spassova and Lu (1998).

A clear limitation of our study is the fact that so far we tested only two polyamines PUT^{2+} and SPM^{4+} on an "atypical" strong inward rectifier channel that has been poorly studied in the homotetrameric form. Studies investigating polyamine block in Kir3 channels have almost exclusively focused on the heterotetrameric versions composed of Kir3.1 and Kir3.4 (carrying I_{KACh} currents) (Yamada and Kurachi, 1995; Salazar-Fajardo et al., 2018). However, strong inward rectification was confirmed for the crystal structure construct of Kir3.2 (Whorton and MacKinnon, 2011), justifying the use of this construct to study the mechanisms of inward rectification. Further, the open state structure of the extremely well characterized Kir2.1 channel is still not available.

Given the very recent success to crystallize Kir2.2 channels in an open, conductive conformation (Zangerl-Plessl et al., 2020) future studies will need to be performed to address polyamine block in the classic strong rectifier Kir2 family. Comparison of conductance studies on Kir3.2 and Kir2.2 channels reveal very interesting differences, which might affect polyamine block. While the inner (transmembrane) cavity of Kir3.2 contains on average only one K^+ ion (Bernsteiner et al., 2019), simulations on Kir2.2 channels revealed that the inner cavity in these channels can harbour up to five K^+ ions, located close to the acidic charges of the rectification controller, which is lacking in Kir3.2 channels. Thus, it might be envisioned that perhaps polyamine entry into the inner cavity would lead to different ion displacement between these different channels. Further, the diameter of the G-loop region is quite different in the two Kir families. While no Kir2.2 structure showing a narrow G-loop region has been reported so far, various constricted conformations have been reported for Kir3 structures. Our recent simulations on WT Kir3.2 channels (Bernsteiner et al., 2019) vs. Kir2.2 mutant channels (Zangerl-Plessl et al., 2020) support a different behaviour of this region in the two channels. Future studies will be necessary to address similarities and differences inward rectification mechanisms in other Kir channels in detail.

Summarizing our simulations predict that blocker amines can indeed interact with the SF, and that voltage dependence of inward rectification arises in part from the movement of the blocker through the electric field and energetic coupling between blocker binding and permeating K^+ ions.

MATERIAL AND METHODS

Molecular Dynamics Simulations

Gromacs (version 5.1.2) (Abraham et al., 2015) was used to perform molecular dynamics simulations, with the conductive state of the Kir3.2 channel, embedded in a lipid bilayer consisting of 588 POPC (1-palmitoyl-2-oleoyl-sn-glycero-3-phosphocholine) lipids, taken from Bernsteiner et al., (Bernsteiner et al., 2019). PIP_2 parameters were taken from our previous work (Lee et al., 2016). Berger lipid parameters (Berger et al, 1997) were used for the POPC lipids, the amber99sb forcefield (Hornak et al., 2006) for the protein, and corrected monovalent Lennard-Jones parameters (Joung and Cheatham, 2008) were used for K^+ ions. After neutralization with K^+ ions, 150 mM KCl was added to the simulation system. For Lennard-Jones and electrostatic interactions, a cut-off of 1.0 nm was employed, with long-range electrostatic interactions calculated with the Particle-Mesh Ewald algorithm (Essmann et al., 1995). Bonds were constrained using the LINCS algorithm (Hess et al., 1997), allowing for an integration timestep of 2 fs. Temperature was coupled to 310 K using the v-rescale thermostat (Bussi et al., 2007), with a coupling constant of 0.1 ps. The pressure was kept constant semi-isotropically at 1 bar by the Parrinello-Rahman (Parrinello and Rahman, 1981) barostat (τ = 2 ps). Putrescine was

parameterized using the Hartree-Fock geometry optimization with the 6–31G* basis set in Gaussian (Frisch et al, 2016) and the force field parameters are obtained from AmberTools (Case et al., 2018). All amine nitrogen atoms were treated as charged. Six times one μs runs with an applied electric field of 40 mV nm^{-1} along the z-axis of the simulation box were performed. With a z-axis box length of ~14.5 nm, this resulted in transmembrane potentials of 580 mV (Treptow et al., 2004; Roux, 2008). 20 putrescine molecules were added to the solvent, with one molecule initially placed at the entrance of the CTD, as shown in **Figure 2B** (left panel), using gromacs tools. PUT^{2+} and K^+ occupancies were calculated as described previously (Bernsteiner et al., 2019).

Force Probe (Steered) MD Simulations

The work needed to bind and unbind PUT^{2+} and SPM^{4+} from the Kir3.2 channel was assessed using force probe MD simulations. Polyamines were placed perpendicular to the z-axis and pulled into the transmembrane cavity towards position T154 (bottom of SF) and in the reverse direction towards the cytoplasm with a harmonic force of 100 kJ mol^{-1} nm^{-2} and a velocity of 0.25 nm ns^{-1}. The work was calculated from the force profiles as previously described (Brown et al., 2016) using the following equation:

$$W(t) = v\int_0^t f(t)dt$$

where v is the constant velocity, f(t) is the force at a specific time step given in the force probe output and dt is the time step between data points (100 fs).

Electrostatic Profile Calculations

The electrostatic profile along the Kir3.2 channel was calculated based on a 1 μs trajectory of a conductive WT Kir3.2 run taken from Bernsteiner et al., 2019. In total, 21 frames were extracted (one frame each 50 ns) and aligned at the selectivity filter backbone. We subsequently applied the VMD Plugin PME Electrostatics to each of the frames, which generates smoothed electrostatic potential grids by evaluating the reciprocal sum of the smooth particle-mesh Ewald method (PME) (Aksimentiev and Schulten, 2005; Treptow et al., 2009). By setting the size of the three dimensional grid to 144x144x160 points, we established a resolution of 1 Å per grid point. The Ewald factor was set to 0.25. Charge information was included by converting the PDBs to PSF files with Amber18 (Case et al., 2018) based on the Amber99sb force field with Berger lipids (see MD methods). Following the protocol for grid manipulation of the Aksimentiev group, an external electric field of 0.5 V was introduced to the system. The electrostatic profile was averaged over the 21 frames and plotted by extracting the y-z plane of the grid, which slices through the selectivity filter. A python script was kindly provided by Kumar Sarthak from the Aksimentiev group.

DATA AVAILABILITY STATEMENT

The datasets presented in this study can be found in online repositories. The names of the repository and accession number(s) are: Zenodo, http://doi.org/10.5281/zenodo.3760965.

AUTHOR CONTRIBUTIONS

AS-W designed the study. XC and MB performed simulations. XC, MB, TF, and AS-W analyzed the data. AS-W wrote the paper, which was edited by XC, MB, and TF.

FUNDING

This work was supported by the doctoral program "Molecular drug targets" W1232, from the Austrian Science Fund (FWF; http://www.fwf.ac.at).

ACKNOWLEDGMENTS

The computational results presented have been achieved in part using the Vienna Scientific Cluster (VSC).

SUPPLEMENTARY MATERIAL

The Supplementary Material for this article can be found online at: https://www.frontiersin.org/articles/10.3389/fphar.2020.00721/full#supplementary-material

REFERENCES

Abraham, M. J., Murtola, T., Schulz, R., Páll, S., Smith, J. C., Hess, B., et al. (2015). GROMACS: high performance molecular simulations through multi-level parallelism from laptops to supercomputers. *SoftwareX* 1, 19–25. doi: 10.1016/j.softx.2015.06.001

Aksimentiev, A., and Schulten, K. (2005). Imaging Alpha-Hemolysin with Molecular Dynamics: Ionic Conductance, Osmotic Permeability, and the Electrostatic Potential Map. *Biophys. J.* 88 (6), 3745–3761. doi: 10.1529/biophysj.104.058727

Baronas, V. A., and Kurata, H. T. (2014). Inward Rectifiers and Their Regulation by Endogenous Polyamines. *Front. Physiol.* 5. doi: 10.3389/fphys.2014.00325

Berger, O., Edholm, O., and Jähnig, F. (1997). Molecular Dynamics Simulations of a Fluid Bilayer of Dipalmitoylphosphatidylcholine at Full Hydration, Constant Pressure, and Constant Temperature. *Biophys. J.* 72 (5), 2002–2013. doi: 10.1016/S0006-3495(97)78845-3

Bernsteiner, H., Zangerl-Plessl, E.-M., Chen, X., and Stary-Weinzinger, A. (2019). Conduction through a Narrow Inward-Rectifier K+ Channel Pore. *J. Gen. Physiol.* 151 (10), 1231–1246. doi: 10.1085/jgp.201912359

Brown, P. M. G. E., Aurousseau, M. R. P., Musgaard, M., Biggin, P. C., and Bowie, D. (2016). Kainate Receptor Pore-Forming and Auxiliary Subunits Regulate Channel Block by a Novel Mechanism. *J. Physiol.* 594 (7), 1821–1840. doi: 10.1113/JP271690

Bussi, G., Donadio, D., and Parrinello, M.(2007). "Canonical sampling through velocity rescaling". *J. Chem. Phys.* 126 (1), 014101. doi: 10.1063/1.2408420

Case, D. A., Ben-Shalom, I. Y., Brozell, S. R., Cerutti, D. S., Cheatham, T. E., Cruzeiro, V. W. D., et al. (2018). *"AMBER 2018"* (San Francisco: University of California).

Doyle, D. A., Morais, C. J., Pfuetzner, R. A., Kuo, A., Gulbis, J. M., Cohen, S. L., et al. (1998). The structure of the potassium channel: molecular basis of K+ conduction and selectivity. *Science* 280 (5360), 69–77. doi: 10.1126/science.280.5360.69

Essmann, U., Perera, L., Berkowitz, M. L., Darden, T., Lee, H., and Pedersen, L. G. (1995). A smooth particle mesh Ewald method. *J. Chem. Phys.* 103 (19), 8577–8593. doi: 10.1063/1.470117

Fakler, B., Brändle, U., Glowatzki, E., Weidemann, S., Zenner, H. P., and Ruppersberg, J. P. (1995). Strong Voltage-Dependent Inward Rectification of Inward Rectifier K+ Channels Is Caused by Intracellular Spermine. *Cell* 80 (1), 149–154. doi: 10.1016/0092-8674(95)90459-x

Ficker, E., Taglialatela, M., Wible, B. A., Henley, C. M., and Brown, A. M. (1994). Spermine and Spermidine as Gating Molecules for Inward Rectifier K+ Channels. *Science* 266 (5187), 1068–1072. doi: 10.1126/science.7973666

Frisch, M. J., Trucks, G. W., Schlegel, H. B., Scuseria, G. E., Robb, M. A., Cheeseman, J. R., et al. (2016). *"Gaussian 09"* (Wallingford CT: Gaussian, Inc.).

Fujiwara, Y., and Kubo, Y. (2006). Functional Roles of Charged Amino Acid Residues on the Wall of the Cytoplasmic Pore of Kir2.1. *J. Gen. Physiol.* 127 (4), 401–419. doi: 10.1085/jgp.200509434

Guo, D., Ramu, Y., Klem, A. M., and Lu, Z. (2003). Mechanism of Rectification in Inward-Rectifier K+ Channels. *J. Gen. Physiol.* 121 (4), 261–275. doi: 10.1085/jgp.200208771

Handa, A. K., Fatima, T., and Mattoo, A. K. (2018). Polyamines: Bio-Molecules with Diverse Functions in Plant and Human Health and Disease. *Front. Chem.* 6, 10. doi: 10.3389/fchem.2018.00010

Hess, B., Bekker, H., Berendsen, H. J. C., and Fraaije, J. G. E. M. (1997). LINCS: A Linear Constraint Solver for Molecular Simulations. *J. Comput. Chem.* 18 (12), 1463–1472. doi: 10.1002/(SICI)1096-987X(199709)18:12<1463::AID-JCC4>3.0.CO;2-H

Hibino, H., Inanobe, A., Furutani, K., Murakami, S., Findlay, I., and Kurachi, Y. (2010). Inwardly Rectifying Potassium Channels: Their Structure, Function, and Physiological Roles. *Physiol. Rev.* 90 (1), 291–366. doi: 10.1152/physrev.00021.2009

Hornak, V., Abel, R., Okur, A., Strockbine, B., Roitberg, A., and Simmerling, C. (2006). Comparison of Multiple Amber Force Fields and Development of Improved Protein Backbone Parameters. *Proteins* 65 (3), 712–725. doi: 10.1002/prot.21123

Hsieh, C.-P., Kuo, C.-C., and Huang, C.-W. (2015). Driving Force-Dependent Block by Internal Ba(2+) on the Kir2.1 Channel: Mechanistic Insight into Inward Rectification. *Biophys. Chem.* 202, 40–57. doi: 10.1016/j.bpc.2015.04.003

Jiang, Y., Lee, A., Chen, J., Cadene, M., Chait, B. T., and MacKinnon, R. (2002). The open pore conformation of potassium channels. *Nature* 417 (6888), 523–526. doi: 10.1038/417523a

Joung, I. S., and Cheatham, T. E. (2008). Determination of Alkali and Halide Monovalent Ion Parameters for Use in Explicitly Solvated Biomolecular Simulations. *J. Phys. Chem. B* 112 (30), 9020–9041. doi: 10.1021/jp8001614

Kofuji, P., Hofer, M., Millen, K. J., Millonig, J. H., Davidson, N., Lester, H. A., et al. (1996). Functional Analysis of the Weaver Mutant GIRK2 K+ Channel and Rescue of Weaver Granule Cells. *Neuron* 16 (5), 941–952. doi: 10.1016/S0896-6273(00)80117-8

Kubo, Y., and Murata, Y. (2001). Control of Rectification and Permeation by Two Distinct Sites after the Second Transmembrane Region in Kir2.1 K+ Channel. *J. Physiol.* 531 (Pt 3), 645–660. doi: 10.1111/j.1469-7793.2001.0645h.x

Kuo, A., Gulbis, J. M., Antcliff, J. F., Rahman, T., Lowe, E. D., Zimmer, J., et al. (2003). Crystal Structure of the Potassium Channel KirBac1.1 in the Closed State. *Science* 300 (5627), 1922–1926. doi: 10.1126/science.1085028

Kurata, H. T., Phillips, L. R., Rose, T., Loussouarn, G., Herlitze, S., Fritzenschaft, H., et al. (2004). Molecular Basis of Inward Rectification: Polyamine Interaction Sites Located by Combined Channel and Ligand Mutagenesis. *J. Gen. Physiol.* 124 (5), 541–554. doi: 10.1085/jgp.200409159

Kurata, H. T., Cheng, W. W., Arrabit, C., Slesinger, P. A., and Nichols, C. G. (2007). The Role of the Cytoplasmic Pore in Inward Rectification of Kir2.1 Channels. *J. Gen. Physiol.* 130 (2), 145–155. doi: 10.1085/jgp.200709742

Kurata, H. T., Diraviyam, K., Marton, L. J., and Nichols, C. G. (2008). Blocker Protection by Short Spermine Analogs: Refined Mapping of the Spermine Binding Site in a Kir Channel. *Biophys. J.* 95 (8), 3827–3839. doi: 10.1529/biophysj.108.133256

Lee, S.-J., Ren, F., Zangerl-Plessl, E.-M., Heyman, S., Stary-Weinzinger, A., Yuan, P., et al. (2016). Structural Basis of Control of Inward Rectifier Kir2 Channel Gating by Bulk Anionic Phospholipids. *J. Gen. Physiol.* 148 (3), 227–237. doi: 10.1085/jgp.201611616

Li, Y., Berke, I., Chen, L., and Jiang, Y. (2007). Gating and Inward Rectifying Properties of the MthK K+ Channel with and without the Gating Ring. *J. Gen. Physiol.* 129 (2), 109–120. doi: 10.1085/jgp.200609655

Lopatin, A. N., Makhina, E. N., and Nichols, C. G. (1994). Potassium Channel Block by Cytoplasmic Polyamines as the Mechanism of Intrinsic Rectification. *Nature* 372 (6504), 366–369. doi: 10.1038/372366a0

Lopatin, A. N., Makhina, E. N., and Nichols, C. G. (1995). The mechanism of inward rectification of potassium channels: "long-pore plugging" by cytoplasmic polyamines. J Gen *Physiol.* 106 (5), 923–955. doi: 10.1085/jgp.106.5.923

Lu, Z., and MacKinnon, R. (1994). Electrostatic Tuning of Mg2+ Affinity in an Inward-Rectifier K+ Channel. *Nature* 371 (6494), 243–246. doi: 10.1038/371243a0

Lu, Z. (2004). Mechanism of Rectification in Inward-Rectifier K+ Channels. *Annu. Rev. Physiol.* 66 (1), 103–129. doi: 10.1146/annurev.physiol.66.032102.150822

Nichols, C. G., and Lee, S.-J. (2018). Polyamines and Potassium Channels: A 25-Year Romance. *J. Biol. Chem.* 293 (48), 18779–18788. doi: 10.1074/jbc.TM118.003344

Nichols, C. G., and Lopatin, A. N. (1997). Inward rectifier potassium channels. *Annu. Rev. Physiol.* 59 (1), 171–191. doi: 10.1146/annurev.physiol.59.1.171

Parrinello, M., and Rahman, A. (1981). "Polymorphic transitions in single crystals: A new molecular dynamics method". *J. Appl. Phys.* 52 (12), 7182–7190. doi: 10.1063/1.328693

Pegg, A. E. (2016). "Functions of Polyamines in Mammals". *J. Biol. Chem.* 291 (29), 14904–14912. doi: 10.1074/jbc.R116.731661

Robertson, J. L., Palmer, L. G., and Roux, B. (2008). "Long-Pore Electrostatics in Inward-Rectifier Potassium Channels". *J. Gen. Physiol.* 132 (6), 613–632. doi: 10.1085/jgp.200810068

Roux, B. (2008). "The Membrane Potential and Its Representation by a Constant Electric Field in Computer Simulations". *Biophys. J.* 95 (9), 4205–4216. doi: 10.1529/biophysj.108.136499

Salazar-Fajardo, P. D., Aréchiga-Figueroa, I. A., López-Serrano, A. L., Rodriguez-Elias, J. C., Alamilla, J., Sánchez-Chapula, J. A., et al. (2018). The Voltage-Sensitive Cardiac M2 Muscarinic Receptor Modulates the Inward Rectification of the G Protein-Coupled, ACh-Gated K+ Current. *Pflugers Archiv: Eur. J. Physiol.* 470 (12), 1765–1776. doi: 10.1007/s00424-018-2196-y

Shin, H. G., and Lu, Z. (2005). Mechanism of the voltage sensitivity of IRK1 inward-rectifier K+ channel block by the polyamine spermine. *J. Gen. Physiol.* 125 (4), 413–426. doi: 10.1085/jgp.200409242

Spassova, M., and Lu, Z. (1998). Coupled Ion Movement Underlies Rectification in an Inward-Rectifier K+ Channel. *J. Gen. Physiol.* 112 (2), 211–221. doi: 10.1085/jgp.112.2.211

Stanfield, P. R., Davies, N. W., Shelton, P. A., Sutcliffe, M. J., Khan, I. A., Brammar, W. J., et al. (1994). A Single Aspartate Residue Is Involved in Both Intrinsic Gating and Blockage by Mg2+ of the Inward Rectifier, IRK1. *J. Physiol.* 478 (Pt 1), 1–6. doi: 10.1113/jphysiol.1994.sp020225

Taglialatela, M., Ficker, E., Wible, B. A., and Brown, A. M. (1995). C-Terminus Determinants for Mg2+ and Polyamine Block of the Inward Rectifier K+ Channel IRK1. *EMBO J.* 14 (22), 5532–5541. doi: 10.1002/j.1460-2075.1995.tb00240.x

Treptow, W., Maigret, B., Chipot, C., and Tarek, M. (2004). Coupled Motions between Pore and Voltage-Sensor Domains: A Model for Shaker B, a Voltage-Gated Potassium Channel. *Biophys. J.* 87 (4), 2365–2379. doi: 10.1529/biophysj.104.039628

Treptow, W., Tarek, M., and Klein, M. L. (2009). Initial Response of the Potassium Channel Voltage Sensor to a Transmembrane Potential. *J. Am. Chem. Soc.* 131 (6), 2107–2109. doi: 10.1021/ja807330g

Twomey, E. C., Yelshanskaya, M. V., Vassilevski, A. A., and Sobolevsky, A. I. (2018). Mechanisms of Channel Block in Calcium-Permeable AMPA Receptors. *Neuron* 99 (5), 956–968.e4. doi: 10.1016/j.neuron.2018.07.027

Whorton, M. R., and MacKinnon, R. (2011). Crystal Structure of the Mammalian GIRK2 K+ Channel and Gating Regulation by G Proteins, PIP2, and Sodium. *Cell* 147 (1), 199–208. doi: 10.1016/j.cell.2011.07.046

Wible, B. A., Taglialatela, M., Ficker, E., and Brown, A. M. (1994). "Gating of Inwardly Rectifying K+ Channels Localized to a Single Negatively Charged Residue". *Nature* 371 (6494), 246–249. doi: 10.1038/371246a0

Xu, Y., Shin, H. G., Szép, S., and Lu, Z. (2009). Physical determinants of strong voltage sensitivity of K(+) channel block. *Nat. Struct. Mol. Biol.* 16 (12), 1252–1258. doi: 10.1038/nsmb.1717

Yamada, M., and Kurachi, Y. (1995). Spermine Gates Inward-Rectifying Muscarinic but Not ATP-Sensitive K+ Channels in Rabbit Atrial Myocytes. Intracellular Substance-Mediated Mechanism of Inward Rectification. *J. Biol. Chem.* 270 (16), 9289–9294. doi: 10.1074/jbc.270.16.9289

Yi, B. A., Lin, Y. F., Jan, Y. N., and Jan, L. Y. (2001). Yeast Screen for Constitutively Active Mutant G Protein-Activated Potassium Channels. *Neuron* 29 (3), 657–667. doi: 10.1016/s0896-6273(01)00241-0

Zangerl-Plessl, E.-M., Lee, S.-J., Maksaev, G., Bernsteiner, H., Ren, F., Yuan, P., et al. (2020). Atomistic Basis of Opening and Conduction in Mammalian Inward Rectifier Potassium (Kir2.2) Channels. *J. Gen. Physiol.* 152 (1). doi: 10.1085/jgp.201912422

Conflict of Interest: The authors declare that the research was conducted in the absence of any commercial or financial relationships that could be construed as a potential conflict of interest.

frontiers in Pharmacology

ORIGINAL RESEARCH
published: 30 June 2020
doi: 10.3389/fphar.2020.00914

Allosteric Coupling Between Drug Binding and the Aromatic Cassette in the Pore Domain of the hERG1 Channel: Implications for a State-Dependent Blockade

Meruyert Kudaibergenova[1,2], *Jiqing Guo*[2], *Hanif M. Khan*[1], *Farhan Zahid*[1], *James Lees-Miller*[2], *Sergei Yu. Noskov*[1]* *and Henry J. Duff*[2]*

[1] Centre for Molecular Simulation, Department of Biological Sciences, University of Calgary, Calgary, AB, Canada, [2] Cumming School of Medicine, Libin Cardiovascular Institute of Alberta, University of Calgary, Calgary, AB, Canada

OPEN ACCESS

Edited by:
Mounir Tarek,
Centre National de la Recherche Scientifique (CNRS), France

Reviewed by:
Christopher E. Dempsey,
University of Bristol, United Kingdom
Lucie Delemotte,
Royal Institute of Technology, Sweden

***Correspondence:**
Sergei Yu. Noskov
snoskov@ucalgary.ca
Henry J. Duff
hduff@ucalgary.ca

Specialty section:
This article was submitted to Pharmacology of Ion Channels and Channelopathies, a section of the journal Frontiers in Pharmacology

Received: *16 December 2019*
Accepted: *04 June 2020*
Published: *30 June 2020*

Citation:
Kudaibergenova M, Guo J, Khan HM, Zahid F, Lees-Miller J, Noskov SY and Duff HJ (2020) Allosteric Coupling Between Drug Binding and the Aromatic Cassette in the Pore Domain of the hERG1 Channel: Implications for a State-Dependent Blockade. Front. Pharmacol. 11:914. doi: 10.3389/fphar.2020.00914

Human-ether-a-go-go-related channel (hERG1) is the pore-forming domain of the delayed rectifier K^+ channel in the heart which underlies the I_{Kr} current. The channel has been extensively studied due to its propensity to bind chemically diverse group of drugs. The subsequent hERG1 block can lead to a prolongation of the QT interval potentially leading to an abnormal cardiac electrical activity. The recently solved cryo-EM structure featured a striking non-swapped topology of the Voltage-Sensor Domain (VSD) which is packed against the pore-domain as well as a small and hydrophobic intra-cavity space. The small size and hydrophobicity of the cavity was unexpected and challenges the already-established hypothesis of drugs binding to the wide cavity. Recently, we showed that an amphipathic drug, ivabradine, may favorably bind the channel from the lipid-facing surface and we discovered a mutant (M651T) on the lipid facing domain between the VSD and the PD which inhibited the blocking capacity of the drug. Using multi-microseconds Molecular Dynamics (MD) simulations of wild-type and M651T mutant hERG1, we suggested the block of the channel through the lipid mediated pathway, the opening of which is facilitated by the flexible phenylalanine ring (F656). In this study, we characterize the dynamic interaction of the methionine-aromatic cassette in the S5-S6 helices by combining data from electrophysiological experiments with MD simulations and molecular docking to elucidate the complex allosteric coupling between drug binding to lipid-facing and intra-cavity sites and aromatic cassette dynamics. We investigated two well-established hERG1 blockers (ivabradine and dofetilide) for M651 sensitivity through electrophysiology and mutagenesis techniques. Our electrophysiology data reveal insensitivity of dofetilide to the mutations at site M651 on the lipid facing side of the channel, mirroring our results obtained from docking experiments. Moreover, we show that the dofetilide-induced block of hERG1 occurs through the intracellular space, whereas little to no block of ivabradine is observed during the intracellular application of the drug. The dynamic conformational rearrangement of the F656 appears to regulate the

translocation of ivabradine into the central cavity. M651T mutation appears to disrupt this entry pathway by altering the molecular conformation of F656.

Keywords: hERG1, dofetilide, ivabradine, docking, drug block

INTRODUCTION

The human-*ether-a-go-go*-related gene (hERG1) encodes a homo-tetrameric potassium channel found in excitable cells such as neurons in the brain (Wymore et al., 1997; Papa et al., 2003), adrenal glands, heart and smooth muscle tissues throughout the human body (Warmke and Ganetzky, 1994; Wymore et al., 1997; Farrelly et al., 2003). The function of the channel is most studied in the cardiovascular system, where hERG1 encodes for the α-subunit of the rapid delayed rectifier K^+ current (I_{kr}), contributing to phase 3 of the cardiac action potential and the QT interval observed in electrocardiograms (Trudeau et al., 1995). Most common congenital mutations in hERG1 result in reduced I_{kr} current, elongating the QT wave and potentially causing a Long QT Syndrome (Sanguinetti et al., 1995). Long QT syndrome is a serious condition related to *torsade de pointes* arrhythmias which may deteriorate into ventricular fibrillation and ultimately sudden cardiac death (Romano, 1965; Sanguinetti and Tristani-Firouzi, 2006). The promiscuous susceptibility of hERG1 block by structurally diverse drugs underpins an acquired Long QT syndrome, which was the cause of withdrawal of several medications from the market (Zimmermann et al., 1992). It was estimated that hundreds of patients suffered from sudden cardiac death and ventricular fibrillation due to the off-target block of hERG1, making the channel an object of intense pharmacological interest (Rampe et al., 1997). Mandatory hERG1 pre-screening protocols have been implemented in the early stages of drug development in attempt to prevent the dangerous cardiovascular side effects (Food and Drug Administration, 2005; Gintant et al., 2006). Elucidating the promiscuous block of the channel by drugs represents a major research question which may have a profound impact on human health and drug development.

Drug-induced susceptibility of the hERG1 block has historically been attributed to the presence of a high affinity binding site in the channel: *the wide water-filled intra-cellular cavity* (Drici and Barhanin, 2000; Mitcheson et al., 2000a; Mitcheson et al., 2000b; Sanguinetti and Tristani-Firouzi, 2006). For decades, it was believed that the unique, large size of the central cavity of the hERG1 allowed for the trapping of chemically diverse molecules after the closure of the activation gate (Drici and Barhanin, 2000). This large cavity was attributed to the lack of a *Pro-Val-Pro* motif, commonly found and conserved in other potassium family channels (Kv1–4). Instead, the motif in hERG1 is replaced with *Ile-Phe-Gly* (Vandenberg et al., 2012). The lack of prolines in the helix was believed to cause a wider central cavity in hERG1, contributing to drug trapping in the cavity (Fernandez et al., 2004). A plethora of site-directed mutagenesis and electrophysiology studies have demonstrated the importance of residues in the central cavity such as T623 and S624, which affect the high affinity binding of drugs (Helliwell et al., 2018). However, two aromatic residues in the central cavity have emerged as the most essential participants in the drug induced block of hERG1: Y652 and F656 (Lees-Miller et al., 2000; Mitcheson et al., 2000a; Perry et al., 2004). Mutagenesis studies have further shown that the aromatic rings and the hydrophobic surface area of F656 and not the hydroxyl groups of Y652 were a determining factor in the drug induced block of the channel (Sanguinetti et al., 2005). Both Y652 and F656 are part of the K^+ conduction pathway below the selectivity filter. These aromatic residues were shown to contribute to high-affinity drug binding in a variety of structural models developed over the years using mammalian or bacterial K^+ channels with known crystal structures as templates for modeling (Mitcheson et al., 2000a; Osterberg and Aqvist, 2005; Stary et al., 2010). Many drugs with a positively charged amino group were proposed to bind in the cavity presumably stabilized with cation-π or π- π interactions with the aromatic rings of Y652 and F656 (Vandenberg et al., 2001; Mitcheson, 2003). However, drug sensitivity to the mutations in positions 652 and 656 varied greatly. For instance: mexiletine (Gualdani et al., 2015), flecainide (Melgari et al., 2015b), vesnarinone (Kamiya et al., 2001), propafenone (Witchel et al., 2004), bepridil (Kamiya et al., 2006), thioridazine (Milnes et al., 2006), show more acute sensitivity to mutations at site F656 than at replacements made at the site Y652.

In 2017, the cryo-EM structure of hERG1 (PDB id: 5VA2) was resolved at 3.8 Å resolution revealing completely new and different domain arrangements: hERG1 features a striking non-swapped topology of the Voltage-Sensor Domain (VSD) packed against the Pore-Domain (PD) (Wang and Mackinnon, 2017). While previous homology models of Shakers/Kv1.4 chimeras predicted swapped topology between the VSD and PD due to the presence of a long alpha-helical S4-S5 linker (~10 amino acids), the new structure shows a short, few amino acids long, S4–S5 linker (Wang and Mackinnon, 2017). Surprisingly, the cryo-EM structure also revealed a constricted hydrophobic intra-cavity space in striking contrast to the large cavity proposed in the past, hence challenging the already-established hypothesis discussed earlier (Wang and Mackinnon, 2017). Moreover, studies on hERG1 blockers such as quinidine, dofetilide, and terfenadine have unexpectedly shown that cation-π interactions in the hERG1 induced block are not critical determinants in channel block implying that π stacking of the aromatic residues with the drugs is the major contributing factor (Macdonald et al., 2018). The additional stabilization of bound drugs may be aided by the aromatic side-chain of F557 located in the S5 helix (Saxena et al., 2016). The potential importance of the cation-π interactions due to the positive charge in blockers are yet to be considered. Shagufta et al. used targeted chemical modifications of

dofetilide to create a library of analogs with increased the basicity of the tertiary amine, which leads in increased block potency (Shagufta et al., 2009). Wang et al. reported an enhanced hERG blockade at acidic pH values, which can also be attributed to the protonated (cationic) state of the blocker (Wang et al., 2016).

In 2015, a newly-released heart-rate reducing drug-ivabradine was shown to display off-target effects by blocking hERG1 at physiologically relevant concentrations and prolonging phase 3 repolarization in the heart (Melgari et al., 2015a; Lees-Miller et al., 2015). Lees-Miller et al. suggested that in addition to the already established high-affinity intra-cavity site, hERG1 might potentially have a lipid-facing binding pocket located near the position of M651 (Lees-Miller et al., 2015). The follow-up study investigated WT-hERG1 and M651X-hERG1 mutants to test the potential role of the protein-lipid interface between the VSD and the PD in the selective binding of ivabradine. Interestingly, the well-known hERG1 blocker dofetilide was insensitive to the M651T mutation (Perissinotti et al., 2019). It was proposed that ivabradine was accessing and blocking the intra-cellular cavity of the channel through a lipid mediated pathway whereas dofetilide was directly targeting and interacting with the intra-cellular cavity (Kudaibergenova et al., 2019; Perissinotti et al., 2019). There are striking differences between the measured water-hexane partitioning coefficients of ivabradine and dofetilide, providing additional support of the lipid-mediated pathway for ivabradine. The partition free energy for ivabradine favors its solubilization in a hydrophobic environment, whereas dofetilide partitions more favorably into the aqueous phase (Perissinotti et al., 2019). Other hydrophobic molecules such as ceramide, which is a secondary messenger of the sphingolipid family, and ω-3 and ω-6 polyunsaturated fatty acids tend to block hERG1, revealing potential importance of the lipid-mediated block of the channel (Guizy et al., 2005; Ganapathi et al., 2010). Machine-learning based analysis performed on hundreds of hERG1 blockers have further corroborated the importance of the lipophilicity of drugs in determining the hERG1-targeting properties (Wacker and Noskov, 2018).

In this work, we explore in further detail the dynamics of the hydrophobic cassette (F656, F557, Y652, and M651) in WT-hERG1 and M651T-hERG1 channels. We propose that F656 acts as a flexible gate that allows a passage of drugs into the central cavity of the channel in a drug-specific manner. To illustrate the importance of the conformational plasticity of F656 in drug induced hERG1 blockade, we performed experimental studies of dofetilide and ivabradine binding to WT-hERG1 and a number of single and double mutations testing role of the residues comprising hydrophobic cassette in WT-hERG1 channel. We also compared the pharmacologic potency of dofetilide and ivabradine when applied to the intracellular domain *via* the patch-clamp pipette experiments. In addition, we performed molecular docking of these drugs to the WT-hERG1 and the M651T mutant to elucidate the specific binding modes for ivabradine and dofetilide. These combined structural and functional studies strongly endorse an allosteric mechanism that couple the drug blockade of hERG1 currents and the conformational dynamics of the hydrophobic cassette. The proposed coupling between conformational dynamics of aromatic cassette may lend a structural support to the well-known state-dependence of the drug blockade of hERG1 (Stork et al., 2007).

METHODS

Molecular Dynamics Simulations

The development and relaxation of the explicit membrane-embedded systems (open-states for WT-hERG1 and M651T-hERG1 based on the atomic coordinates deposited to PDB:5VA2) were described in our previous work (Perissinotti et al., 2019). The structure was truncated before the PAS and after the CNBD domains and the missing residues were modeled using a 3-step protocol utilizing ROSETTA (Bender et al., 2016; Perissinotti et al., 2019). The Anton 2 software version 1.27.0 from D. E. Shaw Research was used for production runs (1.2–3.5 μs) using the purpose-built Anton 2 supercomputer (Shaw et al., 2014a; Shaw et al., 2014b). A 2.5 fs time step was used with nonbonded long-range interactions computed every 6 fs using the RESPA multiple-time-step algorithm (Tuckerman et al., 1992). The protein-membrane system was equilibrated for 250 ns and then subjected to 1.2 to 3.5 μs MD runs. The CHARMM36m (Huang et al., 2017) force-field were implemented for protein dynamics and the latest CHARMM36 lipid parameters were used to describe lipid membrane dynamics (Klauda et al., 2010; Klauda et al., 2012). The protein was embedded in the 1-palmitoyl-2-oleoyl-sn-glycero-3-phosphocholine (POPC) lipid bilayer using CHARMM-GUI (Jo et al., 2008). The POPC lipid bilayer was composed of 380 lipids in total: 188 in the upper leaflet and 192 in the lower leaflet. CHARMM-NBFIX Lennard-Jones parameters for K^+ and Cl^- were used to simulate counterions dynamics with the standard TIP3P model used for water molecules (Jorgensen et al., 1983; Noskov and Roux, 2008). The production runs were executed at 313.15 K in a semi-isotropic (NPat) ensemble. The multi-integrator (multigrator) algorithm (Lippert et al., 2013) developed in-house by D. E. Shaw Research was used for temperature and semi-isotropic pressure coupling (Shaw et al., 2014a; Shaw et al., 2014b). The time step for the production runs was set to 2 fs and trajectories were saved every 240 ps. Non-bonded and long-range electrostatic interactions were evaluated every 2 and 6 fs, respectively. Long-range electrostatics was calculated using the k-Gaussian Ewald method implemented to enhance performance on the ANTON2 platform (Shan et al., 2005; Shaw et al., 2014a; Shaw et al., 2014b). The original MD trajectories should become available to the public through the Pittsburgh Supercomputing Center ANTON2 program for WT and mutant forms of the hERG1 channel under Project #PSCA17021P (the release form has been completed and submitted by the authors of the current study).

Molecular Drug Docking

Structure Preparations

The analysis of the equilibrium trajectories for WT-hERG1 and the M651T-hERG1 mutant identified several well-defined and well-populated conformational states of F656 (Perissinotti et al., 2019) in WT-hERG1 and M651T-hERG1 systems. This observation of F656 re-packing was corroborated in other studies (Negami et al., 2019; Yang et al., 2020). Distinct conformational states of F656 are represented by four WT-hERG1 and three M651T-hERG1 structures (Perissinotti et al., 2019) which were extracted from the production phase of the MD trajectories for molecular docking calculations. The WT-hERG1 system state 1 represents the relaxed cryo-EM equilibrated structure (MD production time: 0 μs). For the cryo-EM state relaxation, the harmonic constraints were applied to heavy atoms in protein backbone and side-chains as defined in the CHARMM-GUI membrane builder protocol with gradual release (steps 1 to 6 in CHARMM-GUI membrane builder) (Jo et al., 2008). The gradual relaxation in presence of harmonic constraints allows optimization of the side-chains positions and protein-lipid interactions while preserving overall fold of the protein captured in the cryo-EM state. After the relaxation, the structure features all four F656 in the same configuration (RMSD < 1.0 Å for Cα atoms) as observed in the original cryo-EM structure e.g. facing upwards (**Figure 1**). Accordingly, state 2 represents one of the preferred F656 orientations observed during multi micro-seconds MD simulation with two F656 facing the side of the cavity, one pointing upwards and one facing the central cavity (**Figure 1**). State 3 represents well-populated conformation with two F656 pointing upwards and two F656 facing the side of the cavity. Finally, structure used as state 4 contains one F656 pointing to the side of the cavity, one F656 facing the inside of the cavity, and two F656 pointing upwards (**Figure 1**). The MD simulations of M651T system features three distinct conformational states for F656 packing. State 1 of M651T system shows all four F656 in the same configuration, facing upwards (**Figure 2**). State 2 represents the structural ensemble with three F656 pointing upwards and one F656 facing side of the central cavity (**Figure 2**). State 3 is structural representative of the intracellular cavity with four F656 facing upwards (**Figure 2**). The receptor structures for each of the states were optimized using the Schrödinger's restrained minimization Protein Preparation Wizard (Sastry et al., 2013) and the positions of the hydrogen atoms were re-optimized.

Ligands for docking (dofetilide and ivabradine) were prepared using the Ligprep Wizard application available in the Schrödinger suites (Schrödinger, 2016). Ligprep restrained bond length, bond angles, converted 2D representation into 3D, added hydrogens, sampled ring conformations, minimized and optimized structures based on the OPLS force field (Jorgensen et al., 1996; Jorgensen and Tirado-Rives, 1988). Multiple ionization states of drugs and their relative abundance at a given pH have been proposed as an important factor for understanding the pH-dependent block of hERG1 (Wang et al., 2016). Charged states of ivabradine and dofetilide were generated using EPIK at a pH of 7 for drugs and using PROPKA at pH 7 for each of the conformational states considered for WT-hERG1 and M651T-hERG1. Neutral and charged states of both drugs yielded similar results within the uncertainties of the docking calculations used in this work and are shown in **Table S1** for both ionization states of the drug. Since the primary focus of this work was to investigate dynamics at the protein-lipid interface, we decided to focus on the neutral form of both compounds. The focus on the neutral state of two drugs is also in agreement with recent studies by Clancy and co-workers where the neutral states of two hERG blockers (dofetilide and moxifloxacin) were found to be more stable than the charged ones in the narrow intra-cavity space in the study employing exhaustive Umbrella-Sampling simulations (Yang et al., 2020). It is important to stress that computational and experimental studies showed that various charged-states of the blockers exist in a highly dynamical equilibrium, where preference for a specific charge state of the drug can be shifted by the environment (membrane, binding pocket, or aqueous phase) (Shagufta et al., 2009; Carvalho et al., 2013; Demarco et al., 2018; Perissinotti et al., 2019; Yue et al., 2019).

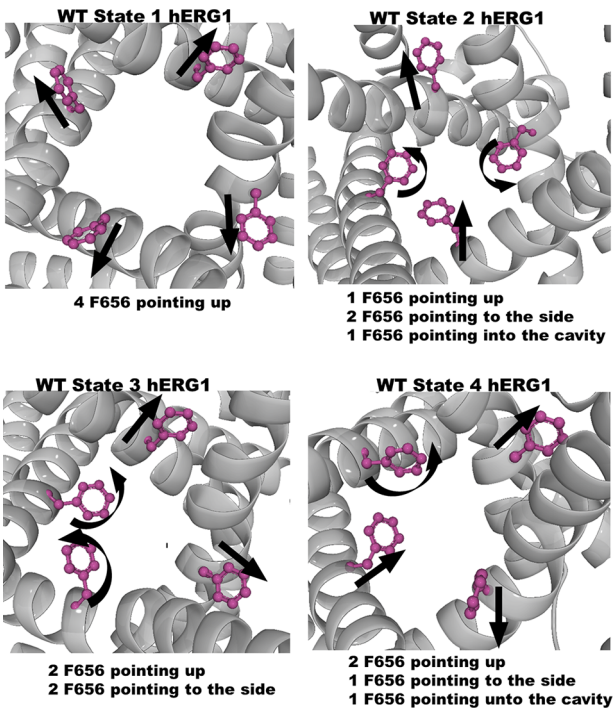

FIGURE 1 | Four states of the WT-hERG1 extracted from the MD simulations based on the F656 geometric position in the central cavity. Top-down perspective of the central cavity is shown for each state. The channel is represented as a gray cartoon, F656 is shown as sticks and balls in purple. These states were used in the docking simulation of ivabradine and dofetilide to explore the differences in the binding affinity to the central cavity.

Docking Protocol

The Glide-XP (extra-precision) (Friesner et al., 2006) cross-docking modules of the Maestro suit in Schrödinger were used for all docking calculations with a ligand vdW scale factor of 0.80 and a RMSD cut-off of 2.0 Å. Ivabradine and dofetilide were docked to two locations in all receptors: the internal central cavity (defined by a geometric center between four F656 residues) and the lipid facing

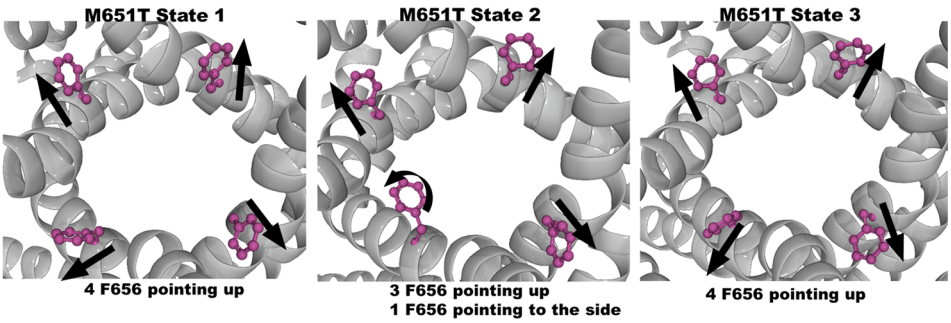

FIGURE 2 | Three states of the M651T-hERG1 extracted from the MD simulations based on the F656 geometric position in the central cavity. Top-down perspective of the central cavity is shown for each state. The channel is represented as a gray cartoon, F656 is shown as sticks and balls in purple. These states were used in the docking simulation of ivabradine and dofetilide to explore the differences in the binding affinity to the central cavity.

residues (between S6 helices) (**Figure S1**). For the internal cavity dockings, the Glide Grids for WT and M651T states were generated by selecting F656 and Y652, which have been implicated in the drug block of hERG1, of all four subunits as the centroid of the docking perimeter (**Figure S1**). As the channel is tetrameric, all four subunits were considered for each of the receptor states. The receptor grid dimensions are divided into inner and outer cubes. The length of the inner cube box edge was set to 10 Å and represents the space explored by Glide as acceptable positions for the geometrical center of the drugs. The outer box edge, representing the space all atoms of the drug must occupy, was set to 26 Å. The same receptor grid dimensions were used for dockings at the lipid facing surface residues (between the S6/S6 helices) (**Figure S1**). The coordinates used for the generation of the receptor grids for docking to the lipid facing surface was defined as a central point between the S5 and S6 helices (at F557 and M651T) for each four subunits. The GLIDE output provides a GScore (kcal/mol) which accounts for energy contributions from hydrophobic interactions, π-π stacking interactions between aromatic rings, root mean square deviation (RMSD), desolvation, protein-ligand interaction, and hydrogen bond formations. Only poses with energy score of ≤ −3 kcal/mol were used in further analysis. The absence of the membrane phase in docking studies represents a natural challenge to the direct interpretations of the binding scores and therefore we only use these scores to assess a relative likelihood (relative to the most favorable binding score) of different binding poses. The coordinates for the hERG1-dofetilide and hERG1-ivabradine complexes from docking studies are provided in the **Supplementary Information** section (receptor_drugs.zip). The full sets of docked conformations are available upon request.

Molecular Biology Protocols

The site-directed mutagenesis methods utilized in this work have been previously reported (Lees-Miller et al., 2015; Wang et al., 2016). The hERG1 constructs were transfected into mammalian HEK cells. Conventional overlap PCR with primers were synthesized by Sigma Genosys (Oakville, Ontario, Canada) and sequenced by using Eurofins MWG Operon (Huntsville, AL) to create the single- and double-point mutant constructs of hERG1. Following this, *XbaI* restriction endonuclease was used to linearize and the cRNA was transcribed *in vitro* using the mMessage mMachine T7 Ultra cRNA transcription kit (Ambion, Austin, TX).

General Setup for Electrophysiological Recordings

All experiments were performed under room temperature (295 K). The extracellular solution contained (mM) NaCl 140, KCl 5.4, $CaCl_2$ 1, $MgCl_2$ 1, HEPES 5, glucose 5.5; the pH of the solution was adjusted and kept at 7.4 with NaOH solution. Micropipettes were pulled from borosilicate glass capillary tubes using a programmable horizontal puller (Sutter Instruments, Novato, CA). The "intracellular" pipette solution contained the following: 10 mM KCl, 110 mM K-aspartate, 5 mM $MgCl_2$, 5 mM Na_2ATP, 10 mM EGTA [ethylene glycol-bis(-aminoethyl ether)-N,N,N,N tetraacetic acid], 5 mM HEPES, and 1mM $CaCl_2$. The internal solution was then adjusted to pH 7.2 with KOH solution. Transfected HEK cells were patched to record the hERG1 currents. Standard patch-clamp methods were used to measure the whole cell currents of hERG1 mutants expressed in HEK 293 cells using the AXOPATCH 200B amplifier (Axon Instruments). Tail currents were recorded when the voltage was returned to −100 mV from +50 mV. Ivabradine was dissolved in Tyrode solution immediately before the experiments and the solutions were used for the next 2 h during the experiments. The stock solution of 100 μM ivabradine was prepared in the extracellular solution and fresh stock solutions of ivabradine were prepared weekly. To test the effect of intracellular application of dofetilide and ivabradine, drugs were applied to the intracellular space *via* the pipette. Dofetilide at 0.5 μM (~12 times greater than its IC50 value when applied extracellularly [0.04 μM]) was incorporated into the pipette solution. The intracellular block produced by dofetilide was compared to that of ivabradine at 100 μM, a value 17-fold greater than its IC50 value when applied extracellularly. The changes of hERG1 currents during the intracellular dialysis of the drug were monitored each minute right after forming the whole cell configuration.

Statistical Analysis of Electrophysiological Experiments

Statsview (Abacus Concepts, Berkeley, CA), QTI plot (Vasilef, 2013), and Grace (http://plasma-gate.weizmann.ac.il/Grace/) were

used to analyze the data. The null hypothesis of this study predicted no difference between the IC50 values comparing single to the double mutations. The null hypothesis was rejected at $p < 0.05$ as evaluated by a One-way Analysis of Variance with Tukey test. All variance measures (bars) for electrophysiological data are shown as Standard Deviation (SD). The study was exploratory; there was no *a priori* reason to consider whether there was an additive or subtractive interaction. The *n* values for each experiment are shown in **Figure 7**.

RESULTS

While the wild type hERG1 channel demonstrated dynamic F656 fluctuations in the cavity in micro-seconds long simulations, the M651T mutant "locked" the F656 residue in a specific configuration. We extracted several WT and M651T hERG1 structures from these simulations and explored the effects of the F656 conformation on drug binding. We also investigated the binding routes of dofetilide and ivabradine by combining mutagenesis and electrophysiology *in-vitro* data with docking to the MD-derived hERG1 structures (**Figures 1** and **2**). We demonstrate that dofetilide blocks the channel through the intracellular side of the membrane, indicating that the drug directly targets and blocks the central cavity, which is exposed to the intracellular fluid (**Figure 3**). In contrast, the preferential block of the WT-hERG1 by ivabradine occurs through the extracellular side of the membrane and little to no block of the channel is observed during the application of the drug from the intracellular side (**Figure 3**). Instead, ivabradine may be blocking the channel by partitioning from the extracellular leaflet towards the lipid-facing residues of the channel and then accessing and blocking the central cavity. We interrogated the *in-vitro* data presented here through docking simulations to unlock the residues involved in stabilizing the lipid-mediated pathway of ivabradine induced block of the channel.

Bridging Docking With Electrophysiology

Dofetilide and ivabradine were docked to the various pore-domain conformations of the WT and M651T hERG1 states identified in the analysis of MD simulations (**Figures 1** and **2**). We selected four states for WT-hERG1 and three states for the M651T mutants based on the side chain conformations adopted by F656 through time (**Figures 1** and **2**). Results of the energy scores (kcal/mol) from the docking of dofetilide and ivabradine to all states for all three binding locations are listed in **Table 1**. Our docking results consistently show that dofetilide binds to the MD derived WT-hERG1 states with lower energy scores in comparison to the starting cryo-EM equilibrated structure (state 1) (**Table 1**). The docking results with the cryo-EM equilibrated structure (state 1) yielded higher energy scores revealing unfavorable binding poses, most likely due to the upright F656 conformation in the structure (**Table 1**), in general agreement with the observations of Helliwell and colleagues (Helliwell et al., 2018). Dofetilide was consistently docked in a vertical

TABLE 1 | Docking results of neutral ivabradine and dofetilde to four WT-hERG1 states to the central cavity and the lipid facing domain (between S6-S6 helices) are shown below. Drugs were found in the pore domain, lipid facing area or in-between S6-S6 helices.

		Pore domain	Lipid facing	In-between S6/S6
State 1	**IVA**	**–7.4**	**–5.9**	**–5.5**
	DOF	**–5.1**	**–5.7**	**—**
State 2	***IVA***	***–5.8****	***–5.3***	***–4.6***
	DOF	***–7.0***	***–7.9***	**—**
State 3	**IVA**	**—**	**–4.6**	**—**
	DOF	**–7.1**	**–5.5**	**—**
State 4	**IVA**	**–8.1**	**–6.9**	**—**
	DOF	**–8.4**	**–5.0**	**—**

All numerical values are in (kcal/mol), Dashes represent poses undetected during the docking. State 2 is italicized as it is the most representative of the highest affinity open state hERG1.

**The best-scored ivabradine pose for state 2 corresponds to the position in the central cavity but slightly lower than a classical Y652–F656 pocket.*

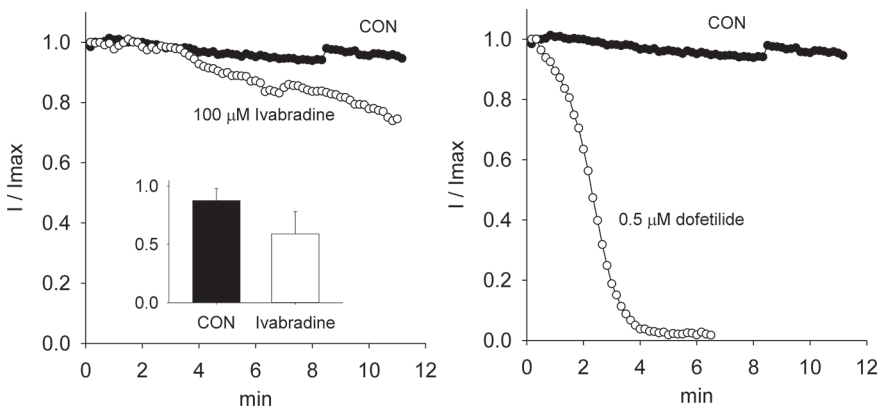

FIGURE 3 | Ivabradine produces little block when applied intracellularly, *via* the pipette, even at concentrations 15-fold greater than its IC50 value when applied extracellularly. On the other hand, dofetilide when applied intracellularly managed to completely block the hERG1 current at 0.5 μM (a value of approximately 12-fold greater than its IC50 value, 0.04 μM, when applied extracellularly).

position, which is too distant to interact with the aromatic rings of F656. Instead, the amine group of dofetilide was stabilized through interactions with the Y652 hydroxyl (-OH) groups (**Figure 4**). Drug docking outcomes to state 1 of the hERG1 channel do not parallel the results of the numerous experimental studies as F656 is crucial for dofetilide induced block of the hERG1 (Lees-Miller et al., 2000; Perry et al., 2004; Milnes et al., 2006; Saxena et al., 2016). Thus, poses of dofetilide found between the two S6 helices are highly unlikely. State 3 does not show binding of ivabradine in the cavity which does not correlate with experimental results reported in this paper and published previously (Melgari et al., 2015a; Lees-Miller et al., 2015), as the drug is sensitive to the mutations in the central cavity. State 4 demonstrates the nearly identical binding affinity for both drugs which also does not reflect our experimental data. Dofetilide is a "gold standard" hERG1 blocker, thus docking results are expected to yield a higher affinity to the cavity compared to ivabradine (Saxena et al., 2016). The docking results of the dofetilide and ivabradine to state 2 of hERG1 parallel and complement mutagenesis experiments in contrast to the cryo-EM equilibrated state 1 and the rest of the MD derived states suggesting that the F656 conformation of state 2 yields the highest affinity for the dofetilide induced block (**Table 1**). The following sections present our docking results to state 2 of hERG1 as it appears to be the most representative of the experimentally observed trends.

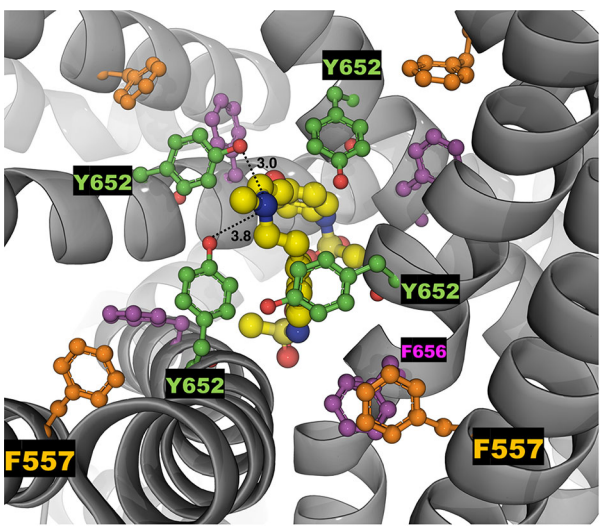

FIGURE 4 | The top-ranked docked pose of neutral dofetilide (energy score of -5.1 kcal/mol) to the central cavity of the cryo-EM hERG1 (referred as state 1 in the text) is shown from the top perspective. The docked drug is shown in sticks and balls mode, while the receptor structure is shown as a gray cartoon. Key residues of the central cavity are labeled and represented as balls and sticks in different colors: Y652 (green), F557 (orange) and F656 (purple). The drug docked to the relaxed Cryo-EM state does not interact with F656 or F557. Distances between the -OH groups of Y652 and a central amine group of the dofetilide are measured in angstroms (Å) and shown as dashed lines.

The Central Cavity of the WT-hERG1 Is Flexible and Dynamic

Next, we assessed individual behaviors of F656, Y652, F557, and M651 for each chain of the protein from long MD simulations to analyze dynamics of individual residues involved in the formation of the hydrophobic cassettes in WT-hERG1 and M651T-hERG1. We measured side-chain χ_1 dihedral angles (between C-Cα-Cβ-Cγ atoms) of the F656 and distances to Y652, F557, and M651 in all four chains. We observed that F656 is the most dynamic residue in the cavity contributing to the overall volume of the central cavity. The χ_1 dihedral angles of the WT F656 shows that the F656 shifts from the upright position (c1 of ~ 175° or -185°) and bends towards Y652 in the central cavity, (c1 ~50°) for chains B, C, and D (**Figure 5**). The side chain of F656 of chain A of the WT-hERG1 exhibited significantly less mobility: it only rotated around its axis resulting in dihedral angles fluctuating between ~175° or −185° (**Figure 5**). These findings demonstrate the dynamic nature of the F656 conformational arrangement and how the F656 is coordinated by the surrounding residues.

The M651T-hERG1 Mutant Rigidifies Central Cavity Due to Stabilization of F557–F656 Aromatic Stacking

We investigated the effect of M651 mutation on the cavity dynamics by checking the surrounding residues. The frequency of the flipping of F656 is decreased in the M651T-hERG1 structure (**Figure 5D**). F656 is stabilized in an upright conformation through T-state π-π interactions with the aromatic rings of the F557 (**Figures 5A** and **6**). Distances of 4.5 Å between aromatic ring centers correspond to the most stable stacking interaction between the aromatic rings. The distance between the centers of the aromatic rings of the WT-hERG1 F656 and F557 remained at ~6–7 Å after a few nanoseconds of the equilibration. For the M651T-hERG1, a distance greater than 8 Å between F656 and F557 correlated with the bending of the F656 towards the inside of the central cavity and to significantly weaken interactions between the aromatic rings. The average distance between F557 and F656 was consistently shorter compared to the WT-hERG1 ~6.5 Å (**Figure 6B**). The interaction between the two residues (M651–F557) showed no correlation with F656 fluctuation dynamics as the distances for the residues in chains A, C, and D remained on average ~5 Å, and in chain B fluctuated between 5 Å and 10 Å (**Figure S2B**).

Dofetilide Blocks Intracellularly by Binding to the Cavity of the WT-hERG1 and the M651T-hERG1

We next examined the impact of the single F557L, F656C and the double mutation (F557L/F656C) on the concentration-response relationships to ivabradine and dofetilide (**Figure 7**). We noted that the double mutation fully eliminated block by both dofetilide and ivabradine. In order to further establish the extent of loss of block, we applied suprapharmacologic concentrations of two drugs. We have previously reported both a high (100 nM) and a low affinity (1 μM) for binding of dofetilide (Duff et al., 1995). For the suprapharmacologic

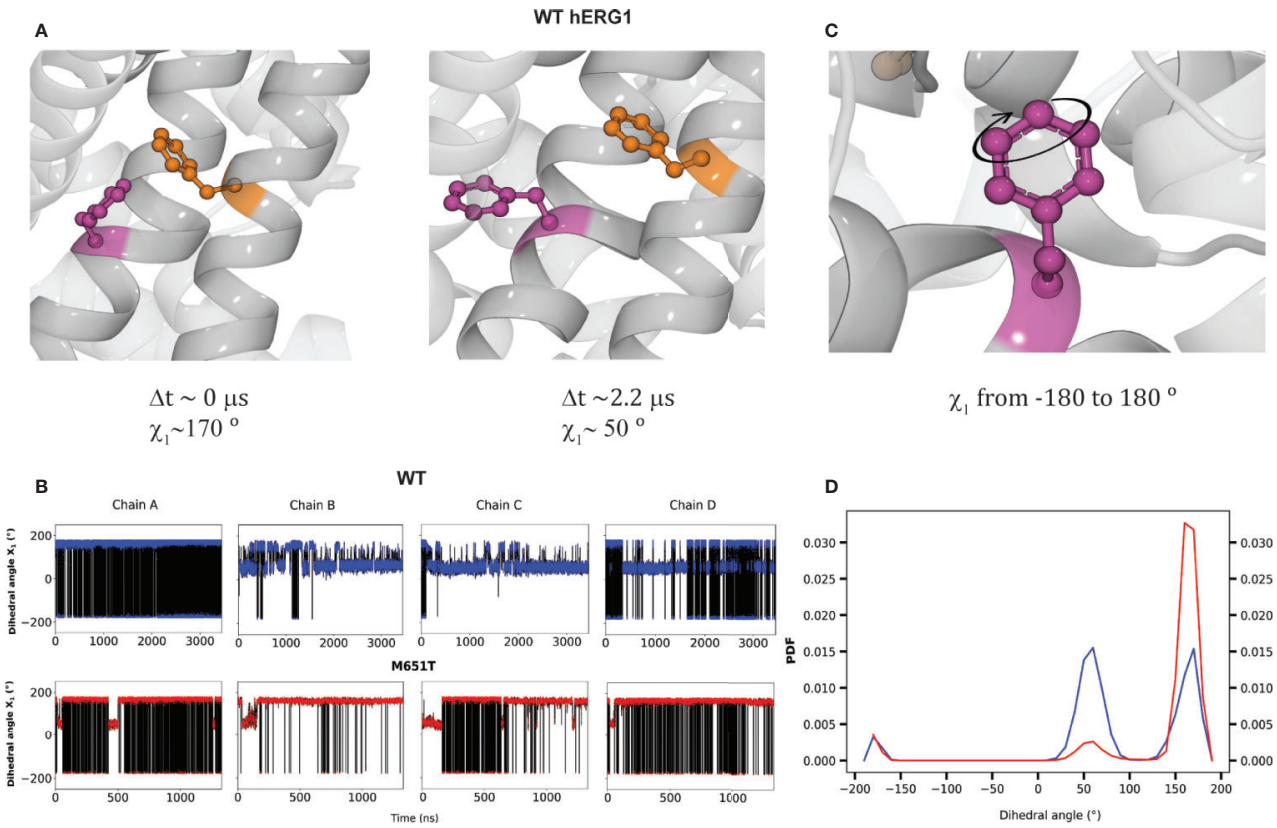

FIGURE 5 | F656 flexibility is impaired in the M651T-hERG1. Two distinct conformational states of F656 (shown in purple sticks) interacting with F557 (orange sticks) are shown in **(A)**. The F656 is shown from the side perspective in a T-shaped interaction arrangement with the F557 at the time (Δt) ~0 μs corresponding to F656 side-chain torsional angle of χ_1 ~170°. In the course of MD simulation F656 adopts "bent" into the central cavity conformation breaking T-shaped interaction with F557 illustrated with a state collected at the time (Δt) ~2.2μs. F656 side-chain torsional angle corresponding to this state is a χ_1~50°. The time-traces of F656 χ_1 for individual monomers in M651T and WT-hERG1 channels are shown in **(B)**. The total rotation of the F656 around its axis corresponding to changes in between χ_1 ~−175° to χ_1 ~+180° is illustrated in **(C)**. The Probability Distribution Function (PDF) for F656 dihedral angles show equal distribution of the "bent" (c1 ~170°) and "upright" (c1 ~50°.) F656 configurations for the WT hERG1, whereas for the mutant, the bent configuration is almost diminished **(D)**.

concentration of dofetilide, we applied a concentration of 20 μM (20-fold greater than the low affinity IC50 value) to be certain that near complete block would be seen for the wild type hERG1 channel. We also applied suprapharmacologic concentrations of ivabradine (100 μM). This concentration of ivabradine is 15-fold greater than its IC50 value (6.7 μM). Even at these very high concentrations, drug-induced block was eliminated in the double F557L/F656C mutation (**Figure 7**). Importantly, identical results were observed when dofetilide was applied at lower concentrations; either 0.5 μM or 2 μM (still suprapharmacologic). There is an additive effect of the double mutant F557L/F656C resulting in impaired blockade by dofetilide (~15% blocking compared to ~80% blocking for single mutants of F557 and F656). A similar trend is observed for ivabradine, resulting in ~15% blocking to the double mutant F557L/F656C (**Figure 7A**). In review, both dofetilide and ivabradine generated similar patterns of block in the F557L, F656C, and F557L/F656C hERG1 mutants. These results indicate that ivabradine and dofetilide interact similarly with F557 and F656 in the central cavity of the channel.

DISCUSSION

F656 Flexibility Is Impaired in the M651T-hERG1

MD simulations have revealed that F656 exhibits several well-defined rotameric states alternating between the upright position observed in the initially equilibrated cryo-EM, a bent state in which the residue points into the central cavity and an outward pose where F656 is closer to the surrounding lipids (**Figures 1** and **2**). Our analysis suggests that the F656 dynamics in the WT-hERG1 are complex and depend on the intricate interplay of the aromaticity of the pocket with its surrounding residues including F557, M651, and Y652. During the simulation, direct interaction of F557, M651, and Y652 with F656 are observed. F557 forms π-π stacking interactions with F656 rings, and the sulfur atom of the M651 also may interact with the aromatic rings of the F656. Y652, which is located above the F656, may contribute to weak π-π stacking interactions with the F656 side chain. Together, these residues compete for interactions with F656. Another factor

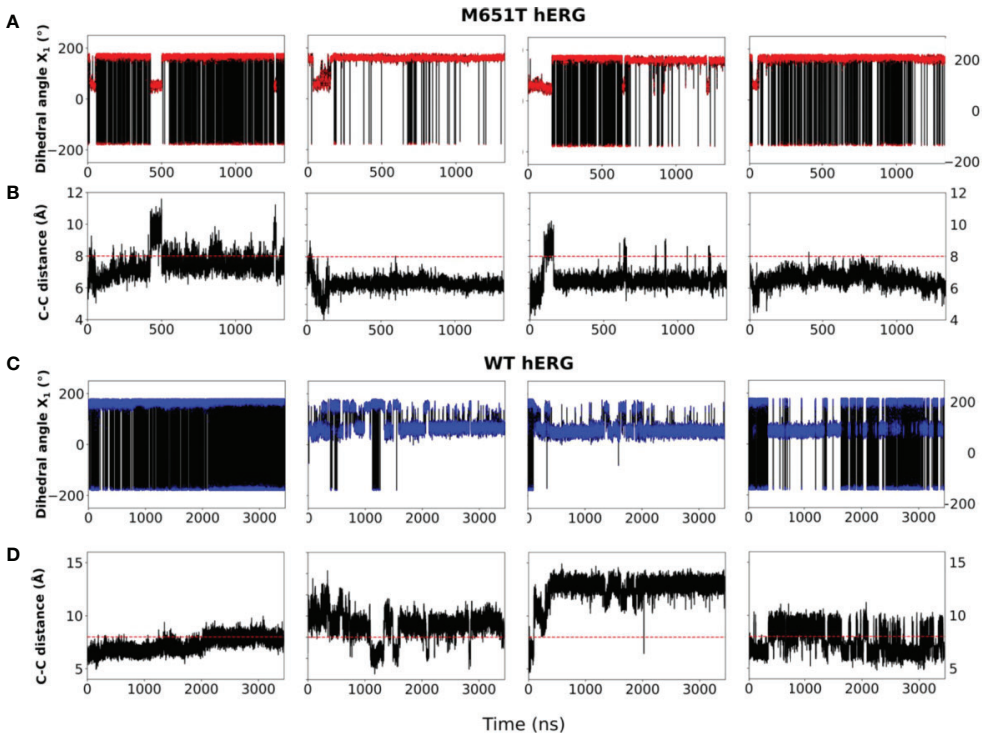

FIGURE 6 | The F656-F557 stacking interaction between the aromatic rings is dominant in the M651T-hERG1 but not in the WT-hERG1. **(A–D)** Comparisons of time traces for F656 χ_1 and F556–F656 C-C distances for the M651T-hERG1 (**A**, **B**, respectively) and the WT-hERG1 are shown (**C**, **D**, respectively). The time traces are averaged over all four monomers. The C-C distances corresponds to the distance between the two aromatic ring centers in F656 and F557. Dashed red line is at ~8 Å for ring-to-ring C-C distance corresponds to the state with F656 bent towards the water-filled intra-cellular cavity and T-shaped interaction between F656 and F557 is destabilized.

that contributes to the F656 geometric position in the central cavity is the limiting volume of the cavity. As the F656 and Y652 rings rotate and bend into the central cavity, steric hindrance may also be another contributing factor resulting in specific F656 configurations observed in states 2, 3, and 4. Overall, the interplay between these residues on the lipid facing domain (M651) and the S6 helices (F557, Y652) contribute to the fluctuating dynamic properties of the F656. The M651T-hERG1 results in more stable π-π interactions between F656 and F557 which maybe contributing to the loss of F656 flexibility (**Figure S3**). The cryo-EM configuration of the open-state hERG1 has been identified as a "low-affinity open state." Some publications have reported attempts to manually shift the F656 from the upright position into the cavity-oriented state in order to obtain docking results that align with the experimental data. Even so, the cryo-EM structure only partly recapitulated the modelling data (Helliwell et al., 2018; Cernuda et al., 2019). Structures derived from the MD simulation may provide a reasonable docking model which does not require artificial manipulation of the structure and may illuminate possible drug binding poses as the structure of the channel naturally adopts a higher affinity open state as the flexible nature of F656 causes the residue to point towards the central cavity thereby allowing for stronger interactions with the blockers as shown in our work.

Binding Pocket Aromaticity Is the Key Determinant in Dofetilide Block of the hERG1

Dofetilide is sensitive to the mutation in the central cavity (F656, Y652), and to the F557 mutation in the S5. Our experimental results show that the double-point mutation F656C/F557L results in an almost complete loss of dofetilide block compared to the single-point mutations of F656 or F557, indicating an additive effect (**Figure 7**). The docking of dofetilide to the pore domain of the WT channel revealed the presence of two main binding sites: 1) hydrophobic pocket below the selectivity filter, near F557, F656, and Y652 and 2) a binding site below the F656 aromatic rings in a wider space (**Figure 8**). MD-derived states are better predictors of experimental measurements than the starting cryo-EM structure (**Figure 7**, **Table 1**). In the central cavity, dofetilide adopts a configuration in which the drug bends at the tertiary amine and the sulfonamide functional groups of the drug

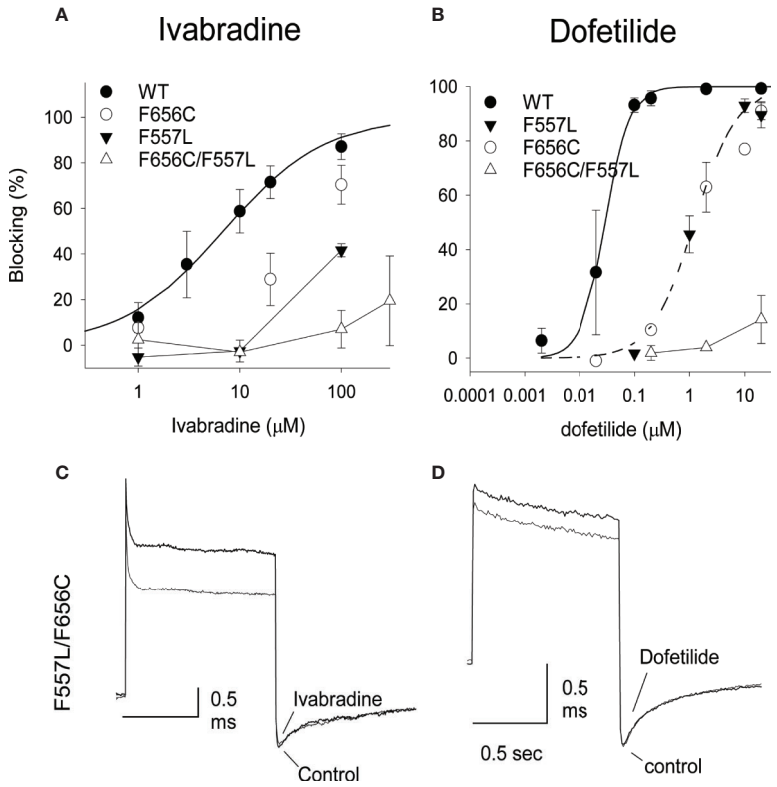

FIGURE 7 | Concentration-response relationships for block produced by ivabradine and dofetilide for WT, F656C, F557L and for the double mutation F656C/F557L. The smooth curves were the successful fitting to Hill's equation. IC50 for ivabradine were 6.8 and 45 mM on WT and F656C, respectively **(A)**. IC50 for dofetilide were 0.029, 1.47, and 1.22 μM on WT, F656C, and F557L, respectively **(B)**. The n values for the experimental numbers shown in **(A)** were: n = 5, 5, 5, 5, 5 on WT in concentrations of 1, 3, 10, 20, 100 μM; n = 5, 5, 5 on F656C in 1, 20, 100 μM; n = 3, 4, 5 on F557L in 1, 10, 100 μM; n = 4, 2, 5, 2 on F656C/F557L in 1, 10, 100, 300 μM. The n values for the experimental numbers shown in **(B)** were n = 5, 5, 2, 6, 6, 4 on WT in 0.002, 0.02, 0.1, 0.2, 2, 20 μM; n = 1, 2, 6, 1, 3 on F656C in 0.002, 0.2, 2, 10, 20 μM; n = 3, 3, 3, 5 on F557L in 0.1, 1, 10, 20 μM; n = 2, 2, 4 on F656C/F557L in 0.2, 2, 20 μM, respectively. **(C, D)** Raw current traces. The superimposed current traces of F557L/F656C in control and 100 μM Ivabradine **(C)** or 2 mM dofetilide **(D)**. Note that since there was no block by these drugs that the control and drug traces overlap.

extend horizontally into the hydrophobic pockets, below the selectivity filter and above Y652 directly interacting with F557 (**Figure 9**). The flexibility of dofetilide at the tertiary amine is essential for the snug fit of the drug into this hydrophobic pouch. Interestingly, dofetilide analogues with higher rigidity around the aliphatic amino group of the drug resulted in reduced hERG1 block. The drug may potentially be losing the ability to fit into this binding site (Carvalho et al., 2013). Surrounding aromatic moieties in the cavity, specifically F656, mediate the direct interaction of dofetilide with F557. Sulfonamide groups of the drug interact with two of the F557 rings (~4 Å away), whereas the F656 aromatic rings (~5 Å away) stabilize the drug in the pocket (**Figure 9**). There are two F557 and two F656 residues that are involved in dofetilide stabilization in this pocket. The interplay between these residues contributes to the favorability of this configuration of the drug in this hydrophobic pouch. Ergo, aromaticity of this pocket was determined essential for drug stabilization in this binding spot. The multiple and stable rotameric states of F656 allow dofetilide to interact with the F557 and F656 simultaneously in support with the experimental data on dofetilide block through the intracellular milieu. Experimentally, the drug targets and finds the central cavity very quickly and favorably interacts with F656 and F557 (**Figures 3** and **9**).

Ivabradine Block of the WT-hERG1 Occurs Through the Extracellular Milieu

In this work, we show the ivabradine block of the hERG1 occurs from the extracellular milieu and little block of the channel is observed during the intracellular application of the drug (**Figure 3**). Ivabradine does not target the central cavity of the hERG1 directly from the intracellular side as efficiently as dofetilide, as shown by our experimental results (**Figure 3**). Instead, our docking results suggest ivabradine's block of the channel is mediated by the membrane facing residues of the channel (**Figure 10**). During the docking, the resulting poses

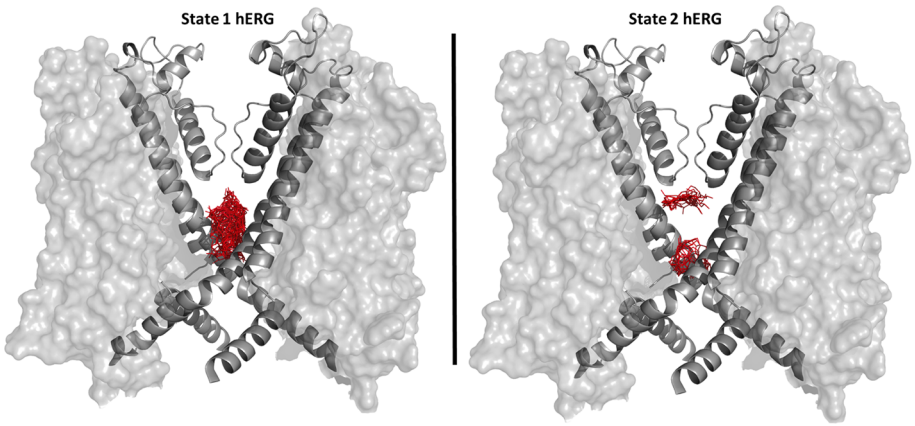

FIGURE 8 | Distributions of docked poses for dofetilide is shown as sticks in red for the state 1 hERG1 (cryo-EM equilibrated) on the left side and state 2 MD derived hERG1 on the right side. For clarity purposes only the pore domain S6 helices of two subunits are shown as cartoons, the voltage sensing domain is represented as a transparent surface.

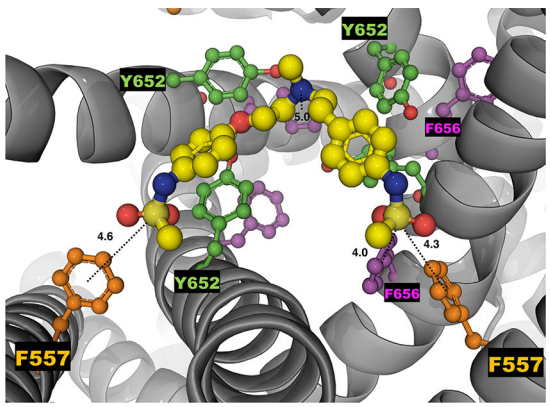

FIGURE 9 | The top-ranked docked pose of neutral dofetilide (shown in yellow as sticks and balls) to the hERG1 state 2. The central cavity is shown from the top perspective. The top-ranked binding pose yielded an energy score of −7.0 kcal/mol. Sulfonamide groups of dofetilide extend towards the F557 from two subunits, measured distances in angstroms **(Å)** as dashed lines of 4.6 and 4.3 Å. The distance between the sulfur atom and the F656 on the right side is ~4.0 Å and the F656 with the central amine ~5 Å. Relevant residues are also shown as balls and sticks and labeled. Y652 is shown in green, F557 is in orange and F656 is in purple.

were either in the pore, in the lipid facing surface, or in some cases, in-between the S6 helices (**Figure 10**). Residues that were in contact with the drugs within 5 Å of the lipid binding interface of the S5 and S6 include: M651, F557, L550, V549, Y667, I663, S654, N658, M554, G669, I647, F551. Ivabradine was also found to preferentially target a location between the segments of the S6-helices, we call the "in-between" pose (**Figure 10**). The plausible mechanism inferred from these data suggests a transition of the drug from the lipid-facing domain of the channel into central cavity as previously explored (**Figure S4**) (Perissinotti et al., 2019). The F656 stabilizes the aromatic ring of the ivabradine *via* π-π stacking interactions for the "in-between" poses. The drug was also interacting with the Y667 and Q664 from the adjacent subunits, as the drug was en-route to the central cavity.

Lipophilic Binding Pathway of Ivabradine Is Disrupted by the M651T Mutant

The molecular simulations indicate that the M651T mutation affects the dynamics of F656, causing dramatically decreased instances of the "bent" configuration of χ_1 ~50° (**Figure 5A**). Therefore, the cavity size of the M651T-hERG1 is larger than the WT-hERG1 as F656 does not point into the central cavity. The larger cavitary space of the mutant results in more energetically favorable binding of ivabradine in the cavity of the channel, as there are reduced instances of steric hindrance (**Table 2**). Given that the drug can favorably fit in the cavity, the binding route must be blocked in the M651T mutant as our previous experiments show (Perissinotti et al., 2019). Our docking showed no poses for the interface binding between the S6 for the M651T mutant states, suggesting the M651T mutant disturbs the entrance into the central cavity from the lipid facing side. Ivabradine is no longer "stabilized" in between the two S6 helices (**Figures 5** and **10**) because, the "bent" configuration of the aromatic ring in the WT-hERG1 is lost in the M651T mutant, and F656 is locked in the predominantly stationary conformation.

CONCLUSIONS

Our experimental and computational results suggest that ivabradine and dofetilide appear to block the central cavity of the channel *via* different paths. Our MD simulations

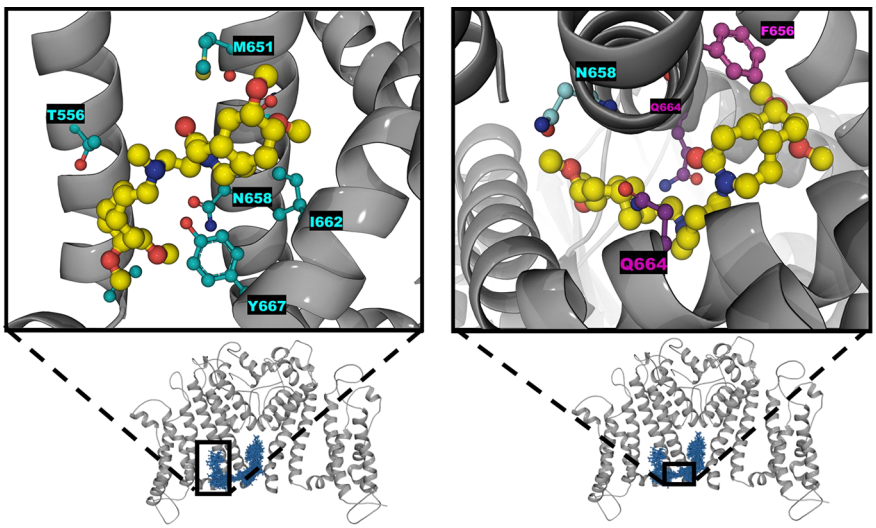

FIGURE 10 | Zoomed-in configuration of ivabradine represented as sticks and balls (yellow) in the black boxes found on the lipophilic side shown on the left and inbetween the two S6 helices shown on the right. The overall protein is shown as cartoon alpha helices in gray with two subunits removed for clarity purposes. Distributions of the ivabradine poses are shown in blue as lines and sticks.

TABLE 2 | The docking results for neutral states of ivabradine and dofetilide to three different states of M651T-hERG1 mutant to the central pore domain and the lipid facing domains (between S6-S6 helices). Poses of drugs were found either in the pore domain or the lipid facing domain and no drugs were in-between S6/S6 helices.

		Pore domain	Lipid facing	In-between S6/S6
State 1	**IVA**	**−8.7**	**−5.8**	**—**
	DOF	**−8.4**	**−4.5**	**—**
State 2	**IVA**	**−7.6**	**−4.7**	**—**
	DOF	**−7.4**	**−5.6**	**—**
State 3	**IVA**	**−10.0**	**−5.4**	**—**
	DOF	**−8.8**	**−4.4**	**—**

All numerical values are in kcal/mol.

coupled with docking and patch-clamp pipette experiments strongly support the notion that the aromaticity of the cavity governs the binding of dofetilide, whereas ivabradine requires fine-tuned conformational arrangement of the central cavity and utilizes the cavity's flexible nature for accessing the lipophilic pathway. Ivabradine is a larger molecule which requires a fine-tuned configuration of the central cavity to yield a favorable binding compared to dofetilide. The molecular modeling lend support to an idea that conformational plasticity of F656 is one of the determining factors in the cavity adaptation to a specific blocker. The conformational dynamics of aromatic cassette may play an important role in regulation of drug access to the main intracavity site. The conformational plasticity of the F656 residue is proposed to regulate the lipophilic entry pathway, which is lost in the mutant, M651T. The loss of conformational adaptation at F656 site in the mutant results in a significant decrease of ivabradine blockade.

DATA AVAILABILITY STATEMENT

The datasets generated for this study are available on request to the corresponding authors.

AUTHOR CONTRIBUTIONS

Participated in research design: JG, MK, JL-M, SN, and HD. Conducted experiments: JG, MK, FZ. Performed data analysis: JG, MK, HK, SN, and HD. Wrote or contributed to writing the manuscript: JG, MK, HK, SN, and HD.

FUNDING

The work in SN's group was partially supported by the National Institutes of Health (USA) (Grant R01HL128537-03). SN and HD were supported by the Canadian Institutes for Health Research (Project Program FRN-CIHR: 156236). HK is supported by the Eyes-High Post-Doctoral Fellowship from the University of Calgary. FZ would like to acknowledge support from Summer 2019 Markin Undergraduate Student Research Program (USRP) in Health & Wellness. MK was supported by Bettina Bahlsen Memorial graduate scholarship, Queen Elizabeth II graduate scholarship and Jake Duerksen Memorial scholarship. Anton 2 computer time was provided by the Pittsburgh Supercomputing

Center (PSC) through Grant R01GM116961 from the National Institutes of Health. The Anton 2 machine at PSC was generously made available by D.E. Shaw Research.

ACKNOWLEDGMENTS

We would like to thank Drs. M. Madrid and P. Blood of Pittsburgh Supercomputer Center (PSC) for their valuable assistance with running molecular dynamics simulations for ANTON2 platform. We also would like to express our gratitude to Professor Martin Karplus and CHARMM project for waiving license fees for CHARMM program package used for analysis of simulation data. In addition, we thank Dr. H. Zhekova for providing insights and edits to the manuscript.

SUPPLEMENTARY MATERIAL

The Supplementary Material for this article can be found online at: https://www.frontiersin.org/articles/10.3389/fphar.2020.00914/full#supplementary-material

REFERENCES

Bender, B. J., Cisneros, A.3rd, Duran, A. M., Finn, J. A., Fu, D., Lokits, A. D., et al. (2016). Protocols for Molecular Modeling with Rosetta3 and RosettaScripts. *Biochemistry* 55, 4748–4763. doi: 10.1021/acs.biochem.6b00444

Carvalho, J. F., Louvel, J., Doornbos, M. L., Klaasse, E., Yu, Z., Brussee, J., et al. (2013). Strategies to reduce HERG K+ channel blockade. Exploring heteroaromaticity and rigidity in novel pyridine analogues of dofetilide. *J. Med. Chem.* 56, 2828–2840. doi: 10.1021/jm301564f

Cernuda, B., Fernandes, C. T., Allam, S. M., Orzillo, M., Suppa, G., Chia Chang, Z., et al. (2019). The molecular determinants of R-roscovitine block of hERG channels. *PloS One* 14, e0217733. doi: 10.1371/journal.pone.0217733

Demarco, K. R., Bekker, S., Clancy, C. E., Noskov, S. Y., and Vorobyov, I. (2018). Digging into Lipid Membrane Permeation for Cardiac Ion Channel Blocker d-Sotalol with All-Atom Simulations. *Front. Pharmacol.* 9, 26. doi: 10.3389/fphar.2018.00026

Drici, M. D., and Barhanin, J. (2000). Cardiac K+ channels and drug-acquired long QT syndrome. *Therapie* 55, 185–193.

Duff, H. J., Feng, Z. P., and Sheldon, R. S. (1995). High- and low-affinity sites for [3H]dofetilide binding to guinea pig myocytes. *Circ. Res.* 77 (4), 718–725.

Farrelly, A. M., Ro, S., Callaghan, B. P., Khoyi, M. A., Fleming, N., Horowitz, B., et al. (2003). Expression and function of KCNH2 (HERG) in the human jejunum. *Am. J. Physiol. Gastrointest. Liver Physiol.* 284, G883–G895. doi: 10.1152/ajpgi.00394.2002

Fernandez, D., Ghanta, A., Kauffman, G. W., and Sanguinetti, M. C. (2004). Physicochemical features of the HERG channel drug binding site. *J. Biol. Chem.* 279, 10120–10127. doi: 10.1074/jbc.M310683200

Food and Drug Administration, H. H. S. (2005). International Conference on Harmonisation; guidance on E14 Clinical Evaluation of QT/QTc Interval Prolongation and Proarrhythmic Potential for Non-Antiarrhythmic Drugs; availability. Notice. *Fed. Regist.* 70, 61134–61135.

Friesner, R. A., Murphy, R. B., Repasky, M. P., Frye, L. L., Greenwood, J. R., Halgren, T. A., et al. (2006). Extra precision glide: docking and scoring incorporating a model of hydrophobic enclosure for protein-ligand complexes. *J. Med. Chem.* 49, 6177–6196. doi: 10.1021/jm051256o

Ganapathi, S. B., Fox, T. E., Kester, M., and Elmslie, K. S. (2010). Ceramide modulates HERG potassium channel gating by translocation into lipid rafts. *Am. J. Physiol. Cell Physiol.* 299, C74–C86. doi: 10.1152/ajpcell.00462.2009

Gintant, G. A., Su, Z., Martin, R. L., and Cox, B. F. (2006). Utility of hERG assays as surrogate markers of delayed cardiac repolarization and QT safety. *Toxicol. Pathol.* 34, 81–90. doi: 10.1080/01926230500431376

Gualdani, R., Tadini-Buoninsegni, F., Roselli, M., Defrenza, I., Contino, M., Colabufo, N. A., et al. (2015). Inhibition of hERG potassium channel by the antiarrhythmic agent mexiletine and its metabolite m-hydroxymexiletine. *Pharmacol. Res. Perspect.* 3, e00160. doi: 10.1002/prp2.160

Guizy, M., Arias, C., David, M., Gonzalez, T., and Valenzuela, C. (2005). {Omega}-3 and {omega}-6 polyunsaturated fatty acids block HERG channels. *Am. J. Physiol. Cell Physiol.* 289, C1251–C1260.

Helliwell, M. V., Zhang, Y., El Harchi, A., Du, C., Hancox, J. C., and Dempsey, C. E. (2018). Structural implications of hERG K(+) channel block by a high-affinity minimally structured blocker. *J. Biol. Chem.* 293, 7040–7057. doi: 10.1074/jbc.RA117.000363

Huang, J., Rauscher, S., Nawrocki, G., Ran, T., Feig, M., De Groot, B. L., et al. (2017). CHARMM36m: an improved force field for folded and intrinsically disordered proteins. *Nat. Methods* 14, 71–73. doi: 10.1038/nmeth.4067

Jo, S., Kim, T., Iyer, V. G., and Im, W. (2008). CHARMM-GUI: a web-based graphical user interface for CHARMM. *J. Comput. Chem.* 29, 1859–1865. doi: 10.1002/jcc.20945

Jorgensen, W. L., and Tirado-Rives, J. (1988). The Opls Potential Functions for Proteins - Energy Minimizations for Crystals of Cyclic-Peptides and Crambin. *J. Am. Chem. Soc.* 110, 1657–1666. doi: 10.1021/ja00214a001

Jorgensen, W. L., Chandrasekhar, J., Madura, J. D., Impey, R. W., and Klein, M. L. (1983). Comparison of Simple Potential Functions for Simulating Liquid Water. *J. Chem. Phys.* 79, 926–935. doi: 10.1063/1.445869

Jorgensen, W. L., Maxwell, D. S., and Tirado-Rives, J. (1996). Development and testing of the OPLS all-atom force field on conformational energetics and properties of organic liquids. *J. Am. Chem. Soc.* 118, 11225–11236. doi: 10.1021/ja9621760

Kamiya, K., Mitcheson, J. S., Yasui, K., Kodama, I., and Sanguinetti, M. C. (2001). Open channel block of HERG K+ channels by vesnarinone. *Mol. Pharmacol.* 60, 244–253. doi: 10.1124/mol.60.2.244

Kamiya, K., Niwa, R., Mitcheson, J. S., and Sanguinetti, M. C. (2006). Molecular determinants of HERG channel block. *Mol. Pharmacol.* 69, 1709–1716. doi: 10.1124/mol.105.020990

Klauda, J. B., Venable, R. M., Freites, J. A., O'connor, J. W., Tobias, D. J., Mondragon-Ramirez, C., et al. (2010). Update of the CHARMM all-atom additive force field for lipids: validation on six lipid types. *J. Phys. Chem. B* 114, 7830–7843. doi: 10.1021/jp101759q

Klauda, J., Monje, V., Kim, T., and Im, W. (2012). Improving the CHARMM Force Field for Polyunsaturated Fatty Acid Chains. *J. Phys. Chem. B* 116, 9424–9431. doi: 10.1021/jp304056p

Kudaibergenova, M., Perissinotti, L. L., and Noskov, S. Y. (2019). Lipid roles in hERG function and interactions with drugs. *Neurosci. Lett.* 700, 70–77. doi: 10.1016/j.neulet.2018.05.019

Lees-Miller, J. P., Duan, Y. J., Teng, G. Q., and Duff, H. J. (2000). Molecular determinant of high-affinity dofetilide binding to HERG1 expressed in Xenopus oocytes: Involvement of S6 sites. *Mol. Pharmacol.* 57, 367–374.

Lees-Miller, J. P., Guo, J., Wang, Y., Perissinotti, L. L., Noskov, S. Y., and Duff, H. J. (2015). Ivabradine prolongs phase 3 of cardiac repolarization and blocks the hERG1 (KCNH2) current over a concentration-range overlapping with that required to block HCN4. *J. Mol. Cell Cardiol.* 85, 71–78. doi: 10.1016/j.yjmcc.2015.05.009

Lippert, R. A., Predescu, C., Ierardi, D. J., Mackenzie, K. M., Eastwood, M. P., Dror, R. O., et al. (2013). Accurate and efficient integration for molecular dynamics simulations at constant temperature and pressure. *J. Chem. Phys.* 139, 164106. doi: 10.1063/1.4825247

Macdonald, L. C., Kim, R. Y., Kurata, H. T., and Fedida, D. (2018). Probing the molecular basis of hERG drug block with unnatural amino acids. *Sci. Rep.* 8, 289. doi: 10.1038/s41598-017-18448-x

Melgari, D., Brack, K. E., Zhang, C., Zhang, Y., El Harchi, A., Mitcheson, J. S., et al. (2015a). hERG potassium channel blockade by the HCN channel inhibitor bradycardic agent ivabradine. *J. Am. Heart Assoc.* 4, e001813. doi: 10.1161/JAHA.115.001813

Melgari, D., Zhang, Y. H., El Harchi, A., Dempsey, C. E., and Hancox, J. C. (2015b). Molecular basis of hERG potassium channel blockade by the class Ic

antiarrhythmic flecainide. *J. Mol. Cell Cardiol.* 86, 42–53. doi: 10.1016/j.yjmcc.2015.06.021

Milnes, J. T., Witchel, H. J., Leaney, J. L., Leishman, D. J., and Hancox, J. C. (2006). hERG K+ channel blockade by the antipsychotic drug thioridazine: An obligatory role for the S6 helix residue F656. *Biochem. Biophys. Res. Commun.* 351, 273–280. doi: 10.1016/j.bbrc.2006.10.039

Mitcheson, J. S., Chen, J., Lin, M., Culberson, C., and Sanguinetti, M. C. (2000a). A structural basis for drug-induced long QT syndrome. *Proc. Natl. Acad. Sci. U. S. A.* 97, 12329–12333. doi: 10.1073/pnas.210244497

Mitcheson, J. S., Chen, J., and Sanguinetti, M. C. (2000b). Trapping of a methanesulfonanilide by closure of the HERG potassium channel activation gate. *J. Gen. Physiol.* 115, 229–239. doi: 10.1085/jgp.115.3.229

Mitcheson, J. S. (2003). Drug binding to HERG channels: evidence for a 'non-aromatic' binding site for fluvoxamine. *Br. J. Pharmacol.* 139, 883–884. doi: 10.1038/sj.bjp.0705336

Negami, T., Araki, M., Okuno, Y., and Terada, T. (2019). Calculation of absolute binding free energies between the hERG channel and structurally diverse drugs. *Sci. Rep.* 9, 16586. doi: 10.1038/s41598-019-53120-6

Noskov, S. Y., and Roux, B. (2008). Control of ion selectivity in LeuT: two Na+ binding sites with two different mechanisms. *J. Mol. Biol.* 377, 804–818. doi: 10.1016/j.jmb.2008.01.015

Osterberg, F., and Aqvist, J. (2005). Exploring blocker binding to a homology model of the open hERG K+ channel using docking and molecular dynamics methods. *FEBS Lett.* 579, 2939–2944. doi: 10.1016/j.febslet.2005.04.039

Papa, M., Boscia, F., Canitano, A., Castaldo, P., Sellitti, S., Annunziato, L., et al. (2003). Expression pattern of the ether-a-gogo-related (ERG) K+ channel-encoding genes ERG1, ERG2, and ERG3 in the adult rat central nervous system. *J. Comp. Neurol.* 466, 119–135. doi: 10.1002/cne.10886

Perissinotti, L., Guo, J., Kudaibergenova, M., Lees-Miller, J., Ol'khovich, M., Sharapova, A., et al. (2019). The Pore-Lipid Interface: Role of Amino-Acid Determinants of Lipophilic Access by Ivabradine to the hERG1 Pore Domain. *Mol. Pharmacol.* 96, 259–271. doi: 10.1124/mol.118.115642

Perry, M., Degroot, M., Helliwell, R., Leishman, D., and Mitcheson, J. (2004). Structural determinants of HERG potassium channel block by ibutilide and clofilium. *Mol. Pharmacol.* 66, 240–249. doi: 10.1124/mol.104.000117

Rampe, D., Roy, M. L., Dennis, A., and Brown, A. M. (1997). A mechanism for the proarrhythmic effects of cisapride (Propulsid): high affinity blockade of the human cardiac potassium channel HERG. *FEBS Lett.* 417, 28–32. doi: 10.1016/S0014-5793(97)01249-0

Romano, C. (1965). Congenital Cardiac Arrhythmia. *Lancet* 1, 658–659. doi: 10.1016/S0140-6736(65)91761-7

Sanguinetti, M. C., and Tristani-Firouzi, M. (2006). hERG potassium channels and cardiac arrhythmia. *Nature* 440, 463–469. doi: 10.1038/nature04710

Sanguinetti, M. C., Jiang, C., Curran, M. E., and Keating, M. T. (1995). A mechanistic link between an inherited and an acquired cardiac arrhythmia: HERG encodes the IKr potassium channel. *Cell* 81, 299–307. doi: 10.1016/0092-8674(95)90340-2

Sanguinetti, M. C., Chen, J., Fernandez, D., Kamiya, K., Mitcheson, J., and Sanchez-Chapula, J. A. (2005). Physicochemical basis for binding and voltage-dependent block of hERG channels by structurally diverse drugs. *Novartis Found Symp.* 266, 159–166; discussion 166-170. doi: 10.1002/047002142X.ch13

Sastry, G. M., Adzhigirey, M., Day, T., Annabhimoju, R., and Sherman, W. (2013). Protein and ligand preparation: parameters, protocols, and influence on virtual screening enrichments. *J. Comput. Aided Mol. Des.* 27, 221–234. doi: 10.1007/s10822-013-9644-8

Saxena, P., Zangerl-Plessl, E. M., Linder, T., Windisch, A., Hohaus, A., Timin, E., et al. (2016). New potential binding determinant for hERG channel inhibitors. *Sci. Rep.* 6, 24182. doi: 10.1038/srep24182

Schrödinger, L. (2016). Schrödinger Suite 2018-2 Induced Fit Docking protocol; Glide, Schrödinger, LLC. LLC. New York: Schrodinger LLC.

Shagufta, G.D., Klaasse, E., De Vries, H., Brussee, J., Nalos, L., Rook, M. B., et al. (2009). Exploring chemical substructures essential for HERG k(+) channel blockade by synthesis and biological evaluation of dofetilide analogues. *ChemMedChem* 4, 1722–1732. doi: 10.1002/cmdc.200900203

Shan, Y. B., Klepeis, J. L., Eastwood, M. P., Dror, R. O., and Shaw, D. E. (2005). Gaussian split Ewald: A fast Ewald mesh method for molecular simulation. *J. Chem. Phys.* 122 (5), 54101. doi: 10.1063/1.1839571

Shaw, D. E., Grossman, J. P., Bank, J. A., Batson, B., Butts, J. A., Chao, J. C., et al. (2014a). Anton 2: Raising the bar for performance and programmability in a special-purpose molecular dynamics supercomputer. *Int. Conf. High Perfor.*, 41–53. doi: 10.1109/SC.2014.9

Shaw, D. E., Grossman, J. P., Bank, J. A., Batson, B., Butts, J. A., Chao, J. C., et al. (2014b). *Anton 2: Raising the Bar for Performance and Programmability in a Special-Purpose Molecular Dynamics Supercomputer* (IEEE Press), 41–53.

Stary, A., Wacker, S. J., Boukharta, L., Zachariae, U., Karimi-Nejad, Y., Aqvist, J., et al. (2010). Toward a Consensus Model of the hERG Potassium Channel. *ChemMedChem* 5, 455–467. doi: 10.1002/cmdc.200900461

Stork, D., Timin, E. N., Berjukow, S., Huber, C., Hohaus, A., Auer, M., et al. (2007). State dependent dissociation of HERG channel inhibitors. *Br. J. Pharmacol.* 151, 1368–1376. doi: 10.1038/sj.bjp.0707356

Trudeau, M. C., Warmke, J. W., Ganetzky, B., and Robertson, G. A. (1995). HERG, a human inward rectifier in the voltage-gated potassium channel family. *Science* 269, 92–95. doi: 10.1126/science.7604285

Tuckerman, M., Berne, B. J., and Martyna, G. J. (1992). Reversible multiple time scale molecular dynamics. *J. Chem. Phys.* 97, 1990–2001. doi: 10.1063/1.463137

Vandenberg, J. I., Walker, B. D., and Campbell, T. J. (2001). HERG K+ channels: friend and foe. *Trends Pharmacol. Sci.* 22, 240–246. doi: 10.1016/S0165-6147(00)01662-X

Vandenberg, J. I., Perry, M. D., Perrin, M. J., Mann, S. A., Ke, Y., and Hill, A. P. (2012). hERG K(+) channels: structure, function, and clinical significance. *Physiol. Rev.* 92, 1393–1478. doi: 10.1152/physrev.00036.2011

Vasilef, I. (2013). *Data Analysis and Scientific Visualization* (Utrecht, Netherlands: Universiteit Utrecht).

Wacker, S., and Noskov, S. Y. (2018). Performance of Machine Learning Algorithms for Qualitative and Quantitative Prediction Drug Blockade of hERG1 channel. *Comput. Toxicol.* 6, 55–63. doi: 10.1016/j.comtox.2017.05.001

Wang, W., and Mackinnon, R. (2017). Cryo-EM Structure of the Open Human Ether-a-go-go-Related K(+) Channel hERG. *Cell* 169, 422–430 e410. doi: 10.1016/j.cell.2017.03.048

Wang, Y. B., Guo, J. Q., Perissinotti, L. L., Lees-Miller, J., Teng, G. Q., Durdagi, S., et al. (2016). Role of the pH in state-dependent blockade of hERG currents. *Sci. Rep.* 6, 32536. doi: 10.1038/srep32536

Warmke, J. W., and Ganetzky, B. (1994). A family of potassium channel genes related to eag in Drosophila and mammals. *Proc. Natl. Acad. Sci. U. S. A.* 91, 3438–3442. doi: 10.1073/pnas.91.8.3438

Witchel, H. J., Dempsey, C. E., Sessions, R. B., Perry, M., Milnes, J. T., Hancox, J. C., et al. (2004). The low-potency, voltage-dependent HERG blocker propafenone–molecular determinants and drug trapping. *Mol. Pharmacol.* 66, 1201–1212. doi: 10.1124/mol.104.001743

Wymore, R. S., Gintant, G. A., Wymore, R. T., Dixon, J. E., Mckinnon, D., and Cohen, I. S. (1997). Tissue and species distribution of mRNA for the IKr-like K+ channel, erg. *Circ. Res.* 80, 261–268. doi: 10.1161/01.RES.80.2.261

Yang, P. C., Demarco, K. R., Aghasafari, P., Jeng, M. T., Dawson, J. R. D., Bekker, S., et al. (2020). A Computational Pipeline to Predict Cardiotoxicity. *Circ. Res.* 126, 947–964. doi: 10.1161/CIRCRESAHA.119.316404

Yue, Z., Li, C., Voth, G. A., and Swanson, J. M. J. (2019). Dynamic Protonation Dramatically Affects the Membrane Permeability of Drug-like Molecules. *J. Am. Chem. Soc.* 141, 13421–13433. doi: 10.1021/jacs.9b04387

Zimmermann, M., Duruz, H., Guinand, O., Broccard, O., Levy, P., Lacatis, D., et al. (1992). Torsades de Pointes after treatment with terfenadine and ketoconazole. *Eur. Heart J.* 13, 1002–1003. doi: 10.1093/oxfordjournals.eurheartj.a060277

Conflict of Interest: The authors declare the research was conducted in the absence of any commercial or financial relationships that could be construed as a potential conflict of interest.

frontiers in Pharmacology

ORIGINAL RESEARCH
published: 21 July 2020
doi: 10.3389/fphar.2020.01091

Evidence for the Effectiveness of Remdesivir (GS-5734), a Nucleoside-Analog Antiviral Drug in the Inhibition of $I_{K(M)}$ or $I_{K(DR)}$ and in the Stimulation of I_{MEP}

Wei-Ting Chang[1,2,3], *Ping-Yen Liu*[3,4], *Zi-Han Gao*[5], *Shih-Wei Lee*[5], *Wen-Kai Lee*[5] *and Sheng-Nan Wu*[5,6,7*]

[1] College of Medicine, Institute of Clinical Medicine, National Cheng Kung University, Tainan, Taiwan, [2] Division of Cardiovascular Medicine, Chi-Mei Medical Center, Tainan, Taiwan, [3] Department of Biotechnology, Southern Taiwan University of Science and Technology, Tainan, Taiwan, [4] Division of Cardiovascular Medicine, Department of Internal Medicine, College of Medicine, National Cheng Kung University Hospital, Tainan, Taiwan, [5] Department of Physiology, National Cheng Kung University Medical College, Tainan, Taiwan, [6] Institute of Basic Medical Sciences, National Cheng Kung University Medical College, Tainan, Taiwan, [7] Department of Medical Research, China Medical University Hospital, China Medical University, Taichung, Taiwan

OPEN ACCESS

Edited by:
Mounir Tarek,
Centre National de la Recherche Scientifique (CNRS), France

Reviewed by:
Mark Alan Zaydman,
Washington University in St. Louis, United States
Valentin K. Gribkoff,
Yale University, United States

***Correspondence:**
Sheng-Nan Wu
snwu@mail.ncku.edu.tw

Specialty section:
This article was submitted to Pharmacology of Ion Channels and Channelopathies, a section of the journal Frontiers in Pharmacology

Received: *23 April 2020*
Accepted: *06 July 2020*
Published: *21 July 2020*

Citation:
Chang W-T, Liu P-Y, Gao Z-H, Lee S-W, Lee W-K and Wu S-N (2020) Evidence for the Effectiveness of Remdesivir (GS-5734), a Nucleoside-Analog Antiviral Drug in the Inhibition of $I_{K(M)}$ or $I_{K(DR)}$ and in the Stimulation of I_{MEP}. Front. Pharmacol. 11:1091. doi: 10.3389/fphar.2020.01091

Remdesivir (RDV, GS-5734), a broad-spectrum antiviral drug in the class of nucleotide analogs, has been particularly tailored for treatment of coronavirus infections. However, to which extent RDV is able to modify various types of membrane ion currents remains largely uncertain. In this study, we hence intended to explore the possible perturbations of RDV on ionic currents endogenous in pituitary GH_3 cells and Jurkat T-lymphocytes. The whole-cell current recordings of ours disclosed that upon membrane depolarization in GH_3 cells the exposure to RDV concentration-dependently depressed the peak or late components of $I_{K(DR)}$ elicitation with effective IC_{50} values of 10.1 or 2.8 μM, respectively; meanwhile, the value of dissociation constant of RDV-induced blockage of $I_{K(DR)}$ on the basis of the first-order reaction was yielded to be 3.04 μM. Upon the existence of RDV, the steady-state inactivation curve of $I_{K(DR)}$ was established in the RDV presence; moreover, the recovery became slowed. However, RDV-induced blockage of $I_{K(DR)}$ failed to be overcome by further addition of either α,β-methylene ATP or cyclopentyl-1,3-dipropylxanthine. The RDV addition also lessened the strength of M-type K^+ current with the IC_{50} value of 2.5 μM. The magnitude of voltage hysteresis of $I_{K(M)}$ elicited by long-lasting triangular ramp pulse was diminished by adding RDV. Membrane electroporation-induced current in response to large hyperpolarization was enhanced, with an EC_{50} value of 5.8 μM. Likewise, in Jurkat T-lymphocytes, adding RDV declined $I_{K(DR)}$ amplitude concomitantly with the raised rate of current inactivation applied by step depolarization. Therefore, in terms of the RDV molecule, there appears to be an unintended activity of the prodrug on ion channels. Its inhibition of both $I_{K(DR)}$ and $I_{K(M)}$ occurring in a non-genomic

fashion might provide additional but important mechanisms through which *in vivo* cellular functions are seriously perturbed.

Keywords: remdesivir (GS-5734), delayed-rectifier K^+ current, electroporation-induced current, voltage hysteresis, pituitary cell, lymphocyte, M-type K^+ current

INTRODUCTION

Remdesivir (RDV, GS-5734), a broad-spectrum antiviral agent, is recognized as a mono-phosphoramidate prodrug of an adenosine analog that metabolizes into its active form GS-441524 which is a C-adenosine nucleoside analog (Warren et al., 2016; Lo et al., 2017; Sheahan et al., 2017; Tchesnokov et al., 2019; Gordon et al., 2020). This compound, a nucleotide-analog inhibitor of RNA-dependent RNA polymerase, is thought to be highly active against coronaviruses (CoVs), including MERS-Cov and SARS-CoV-2 (Lo et al., 2017; Sheahan et al., 2017; Agostini et al., 2018; Beigel et al., 2019; Brown et al., 2019; De Clercq, 2019; Ferren et al., 2019; Hoenen et al., 2019; Al-Tawfiq et al., 2020; de Wit et al., 2020; Dong et al., 2020; Khot and Nadkar, 2020; Ko et al., 2020; Lai et al., 2020; Li and De Clercq, 2020; Li Y. C. et al., 2020; Lu, 2020; Martinez, 2020; Morse et al., 2020; Sheahan et al., 2020; Wang et al., 2020). It has been recently recognized as a promising antiviral drug against an array of RNA viruses, predominantly through the targeting of the viral RNA dependent RNA polymerase. The active form GS-441524, into which RDV is metabolized, could inhibit cellular RNA polymerase to a lesser extent than viral polymerase (Agostini et al., 2018; Wang et al., 2020).

Recent studies have disclosed that RDV and chloroquine (or hydroxychloroquine) could be highly efficacious in control of the SARS-CoV-2 infection *in vitro* (Dong et al., 2020; Gao et al., 2020; Lai et al., 2020; Li and De Clercq, 2020; Wang et al., 2020). There are human studies of RDV efficacy for the treatment of SARS-CoV-2 infection (Beigel et al., 2020). However, none of the noticeable studies have been available with regard to the perturbing actions of RDV on membrane ion channels.

The voltage-gated K^+ (K_V) channels are essential in determining the membrane excitability in electrically excitable or non-excitable cells. Specifically, K_V3 (KCNC) and K_V2 (KCNB), two delayed-rectifier K^+ channels, are widespread in different excitable cells such as endocrine cells (Lien and Jonas, 2003; Wang et al., 2008; Fletcher et al., 2018; Kuo et al., 2018; Lu et al., 2019; So et al., 2019). The causal link between the delayed-rectifier K^+ current ($I_{K(DR)}$) and K_V3/K_V2 channels has been previously disclosed (Yeung et al., 2005; Wang et al., 2008; Huang et al., 2013; Chang et al., 2019; Lu et al., 2019). The biophysical characteristics of $K_V3.1$-$K_V3.2$ channels, which are the dominant factors of $I_{K(DR)}$ identified in pituitary tumor (GH_3) cells (Chang et al., 2019; Lu et al., 2019; So et al., 2019), show a positively shifted voltage dependency as well as fast deactivation rate. However, whether and how RDV effects the adjustments on the amplitude and kinetic gating of above-stated types of K^+ currents still requires investigations.

Furthermore, the KCNQ2, KCNQ3, and KCNQ5 genes have been noticed to encode the main subunits of $K_V7.2$, $K_V7.3$, and $K_V7.5$ channels, respectively; and among them, the augmented activity produces the M-type K^+ current ($I_{K(M)}$), which is characterized by a slowly activating and deactivating property (Brown and Adams, 1980; Sankaranarayanan and Simasko, 1996; Wang et al., 1998; Selyanko et al., 1999; Shu et al., 2007; Lu et al., 2019; So et al., 2019; Yang et al., 2019). With growing recognition, targeting $I_{K(M)}$ is regarded as a treatment of various neurologic diseases. How this compound acts on these types of K^+ currents, however, remains largely uncertain.

Membrane electroporation (MEP) applies an external electrical field in situations where an increase in the electrical conductivity and permeability of the plasma membrane could be produced. Such maneuvers have been applied to the electrotransferation of membrane-impermeant molecules which include DNAs, anti-cancer drugs, and antibodies, into the internal milieu of cells (Liu et al., 2012; Napotnik and Miklavčič, 2018). Of notice, through applying an electrical field to the cells which exceed the electric capacity of surface membrane, it transiently and temporarily turns to be permeable and destabilized. Consequently, the molecules could readily and efficiently get into the cell (Wu et al., 2012; So et al., 2013; Napotnik and Miklavčič, 2018). In this scenario, to facilitate the uptake of antineoplastic or antiviral agents with difficulty in passing the cell membrane, MEP-induced current (I_{MEP}) has been viewed as a novel therapeutic maneuver. However, as far as we are aware, none of studies have investigated whether the presence of RDV exerts any effects on I_{MEP}.

For the considerations elaborated above, we attempted to inquire into the actions of RDV on different types of ionic currents (e.g., $I_{K(DR)}$, $I_{K(M)}$ and I_{MEP}) in GH_3 cells. Whether the $I_{K(DR)}$ identified in Jurkat T-lymphocytes is subject to any modification by RDV was also tested. Noticeably, the present observations unveiled that, in GH_3 cells, RDV is presumably not a prodrug, and that it is virtually effective in inhibiting $I_{K(DR)}$ and $I_{K(M)}$ with similar potency; however, it was noticed to increase the strength of I_{MEP}. These actions demonstrated presently are prone to be acute in onset and will resultantly summate to affect electrical behaviors of different cell types. Findings from the present observations may conceivably contribute to its

Abbreviations: AMPCPP, α,β-methylene-ATP; ATP, adenosine triphosphate; CoV, coronavirus; DPCPX, 8-cyclopentyl-1,3-dipropylxanthine; EC_{50}, concentration required for half-maximal stimulation; IC_{50}, concentration required for half-maximal inhibition; I-V, current versus voltage; MEP, membrane electroporation; $I_{K(DR)}$, delayed-rectifier K^+ current; I_{MEP}, membrane electroporation-induced current; $I_{K(erg)}$, erg-mediated K^+ current; K_D, dissociation constant; $NMDG^+$, N-methyl-D-glucamine$^+$; RDV, remdesivir (GS-5734); SEM, standard error of mean; τ, time constant; K_V channel, voltage-gated K^+ channel; $I_{K(M)}$, M-type K^+ current.

toxicological and pharmacological actions of RDV occurring *in vitro* or *in vivo*.

MATERIALS AND METHODS

Chemicals, Drugs, and Solutions Used in This Study

Remdesivir (RDV, development code: GS-5734, $C_{27}H_{35}N_6O_8P$, 2-ethylbutyl (2*S*)-2-[[[(2*R*,3*S*,4*R*,5*R*)-5-(4-aminopyrrolo[2,1-f][1,2,4]triazin-7-yl)-5-cyano-3,4-dihydroxyoxolan-2-yl]methoxy-phenoxyphosphoryl]amino]propanoate) was from MedChemExpress (Bio-genesis Technologies, Taipei, Taiwan), while α,β-methylene ATP (AMPCPP), cyclopentyl-1,3-dipropylxanthine (DPCPX), ivabradine, nonactin, and tetrodotoxin were from Sigma-Aldrich (Merck, Taipei, Taiwan). Chorotoxin was a gift of Professor Woei-Jer Chuang (Department of Biochemistry, National Cheng Kung University Medical College, Tainan, Taiwan). In this study, we obtained the reagent water by using a Milli-Q Ultrapure Water Purification System (18.2 MΩ-cm) (Merck Millipore, Taipei, Taiwan) in all experiments.

The composition of bath solution (i.e., HEPES-buffered normal Tyrode's solution) used in this study was (in mM): 136.5 NaCl, 5.4 KCl, 1.8 $CaCl_2$, 0.53 $MgCl_2$, 5.5 glucose, and 5.5 HEPES, adjusted with NaOH to pH 7.4. In attempts to check $I_{K(M)}$ or $I_{K(erg)}$, we substituted the bath solution for a high-K^+, Ca^{2+}-free solution (in mM): 130 KCl, 10 NaCl, 3 $MgCl_2$, and 5 HEPES, adjusted with KOH to pH 7.4. To judge different types of K^+ currents or I_{MEP}, we backfilled the patch electrode with a solution (in mM): 130 K-aspartate, 20 KCl, 1 KH_2PO_4, 1 $MgCl_2$, 0.1 EGTA, 3 Na_2ATP, 0.1 Na_2GTP, and 5 HEPES, adjusted with KOH to pH 7.2. To minimize any contamination of Cl^- currents, Cl^- ions inside the examined cell were mostly replaced with aspartate. In a different set of recordings for measuring the cation selectivity of ion channels, K^+ ions inside the internal solution were replaced with $NMDG^+$ ions.

Cell Culture

GH_3, originally acquired from the Bioresources Collection and Research Center ([BCRC-60015]; Hsinchu, Taiwan), were cultured in Ham's F-12 medium added on with 15% (v/v) horse serum, 2.5% (v/v) fetal calf serum and 2 mM L-glutamine; while the Jurkat T cell line, a human T cell lymphoblast-like cell line (clone E6-1), was also from the Bioresource Collection and Research Center ([BCRC-60255]; HsinChu, Taiwan), and Jurkat T cells were grown in RPMI-1640 medium added on with 10% (v/v) fetal bovine serum. GH_3 or Jurkat T cells were maintained at 37°C in a 95% air and 5% CO_2 humidified atmosphere. The viability of these cells was often judged with the trypan blue dye-exclusion test. The electrical recordings were undertaken five or six days after cells had been cultured (60–80% confluence).

Electrophysiological Studies

Briefly before the recordings, we harvested GH_3 or Jurkat T cells and rapidly resuspended an aliquot of cell suspension to a custom-made cubicle mounted on the fixed stage of CKX-41 inverted microscope (Olympus; YuanLi, Kaohsiung, Taiwan). We the immersed cells at room temperature (20–25°C) in normal Tyrode's solution, the composition of which has been described above in detail. We exploited either a P-97 Flaming/Brown horizontal puller (Sutter Instruments, Novato, CA) or a PP-83 vertical puller (Narishige; Taiwan Instrument, Taipei, Taiwan) to fabricate the recording pipette electrodes, which were made of Kimax-51 glass capillaries (Kimble; Dogger, New Taipei City, Taiwan), and we then fire-polished electrode tips with an MF-83 microforge (Narishige). The patch electrodes, in which different internal solutions were filled up, had a tip resistance of 3 to 5 MΩ. In this study, we undertook standard patch-clamp whole cell recordings at room temperature by applying either an RK-400 (Bio-Logic, Claix, France) or an Axopatch-200B patch-amplifier (Molecular Devices, Sunnyvale, CA). To measure whole-cell data, the junctional voltage between the pipette and bath solution was set as zero once the electrode was bathed but shortly before the giga-seal (>1 GΩ) formation. The details of data recordings and analyses achieved in the present work were described in **Supplementary Material**.

Curve Fitting Procedures and Statistical Analyses

Curve parameter estimation was achieved either by a non-linear (e.g., Hill and Boltzmann equation or single-exponential function) or by linear fitting routine, in which the Solver add-in bundled with Excel 2013 (Microsoft, Redmond, WA) was undertaken. The experimental data in the present study are presented as the mean ± standard error of the mean (SEM), with sample sizes (n) representing the number of cells (e.g., GH_3 or Jurkat T cells) collected. Student's *t*-test and a one-way analysis of variance (ANOVA) were implemented and *post-hoc* Fisher's least-significance difference test was applied for multiple comparison procedures. However, assuming that the results might violate the normality underlying ANOVA, the nonparametric Kruskal-Wallis test was thereafter performed. Statistical significance was regarded as $P < 0.05$.

RESULTS

Inhibitory Effect of RDV on Depolarization-Evoked Delayed-Rectifier K^+ Current ($I_{K(DR)}$) Identified in GH_3 Cells

In the first stage of experiments, we undertook the whole-cell configuration of standard patch-clamp technique applied to these cells. The experiments were conducted in cells bathed in Ca^{2+}-free, Tyrode's solution which contained 1 μM tetrodotoxin and 10 μM $CdCl_2$, and we afterwards backfilled the recording electrode by utilizing K^+-containing solution. Tetrodotoxin or $CdCl_2$ in bathing solution was employed to block voltage-gated Na^+ or Ca^{2+} currents, respectively. As depicted in **Figure 1A**, when we voltage-clamped the examined cells at −50 mV and then applied depolarizing command potential to +50 mV with a duration of 1 sec, the delayed-rectifier K^+ current ($I_{K(DR)}$) was

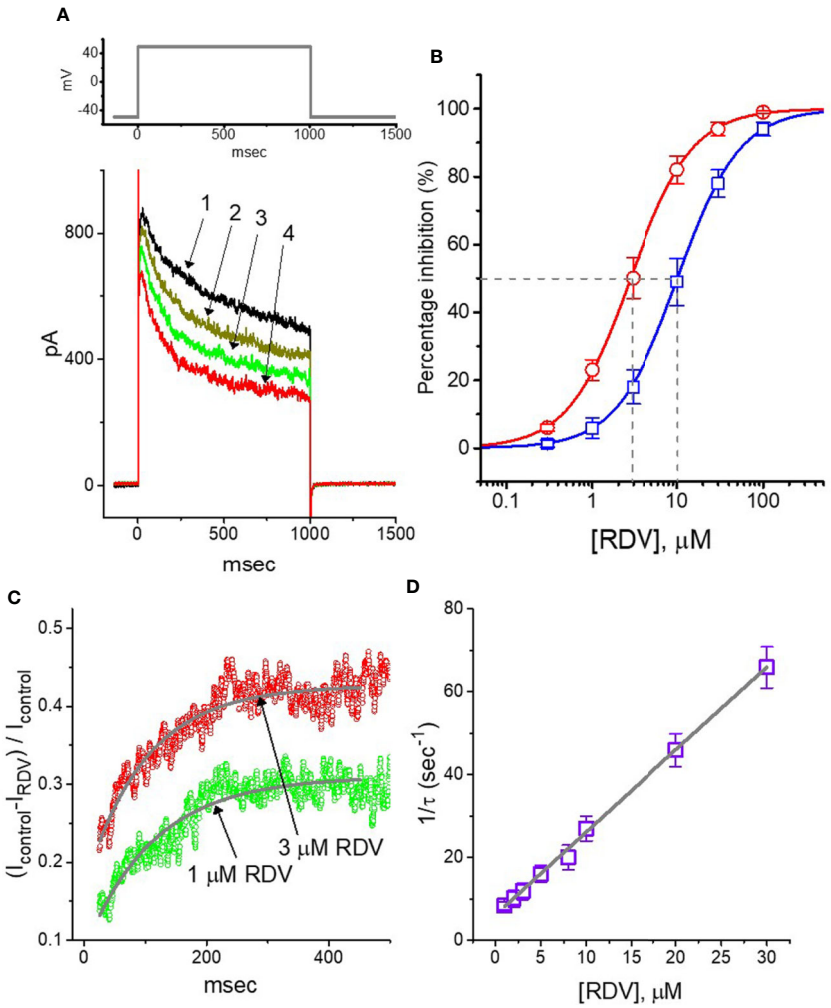

FIGURE 1 | Effect of RDV on delayed-rectifier K^+ current ($I_{K(DR)}$) in pituitary GH_3 cells. Cells were bathed in Ca^{2+}-free, Tyrode's solution and the recording electrode was backfilled up with K^+-containing solution. **(A)** Superimposed $I_{K(DR)}$ traces obtained in the control (**1**, i.e., RDV was not present), and during the exposure to 0.3 μM RDV (**2**), 1 μM RDV (**3**) or 3 μM RDV (**4**). The upper part is the voltage-clamp protocol applied to the cell. **(B)** Concentration-dependent inhibition of RDV on $I_{K(DR)}$ amplitude measured at the beginning (□) and end (○) of depolarizing command potential (mean ± SEM; n=8 for each point). $I_{K(DR)}$ amplitudes (i.e., transient or late component) in different RDV concentrations were taken at the beginning or end of depolarizing pulse for 1 sec from −50 to +50 mV. Continuous lines were well fitted with Hill equation as detailed in **Materials and Methods**. The IC_{50} value (as indicated by the vertical dashed line) measured in initial peak or late component of $I_{K(DR)}$ was yielded to be 10.1 or 2.8 μM, respectively. **(C)** Relative block (i.e., $(I_{control}-I_{RDV})/I_{control}$) of $I_{K(DR)}$ in the presence of 1 or 3 μM RDV. Smooth line in the presence of 1 or 3 μM RDV denotes the exponential fit with the time constant of 113.5 or 98.9 ms, respectively. **(D)** Relationship of the RDV concentration as a function of the rate constant ($1/\tau$) (mean ± SEM; n=8 for each point). Based on minimal kinetic scheme described in **Materials and Methods**, the value of $k_{+1}{}^*$ or k_{-1} was estimated to be 2.01 $s^{-1}\mu M^{-1}$ and 6.12 s^{-1}, respectively; and the K_D value ($k_{-1}/k_{+1}{}^*$, i.e., dissociation constant) was resultantly yielded to be 3.04 μM.

able to be robustly evoked, as elaborated previously (Wang et al., 2008; Lu et al., 2019). Of notice, As exposed to RDV at various concentrations, the strength of $I_{K(DR)}$ evoked by the corresponding depolarizing pulse was dose-dependently declined; however, the initial peak component of $I_{K(DR)}$ was measurably decreased to a less extent as compared with the late component of the current. Depending on the modified Hill equation elaborated in *Materials and Methods* section, the IC_{50} value entailed for its inhibitory effects on initial peak or late components of $I_{K(DR)}$ was yielded to be 10.1 or 2.8 μM, respectively (**Figure 1B**). As such, the experimental observations disclosed that during GH_3-cell exposure to this compound, the late component of $I_{K(DR)}$ by step depolarization applied from −50 to +50 mV was manifestly lessened to a greater extent than the initial peak component of the current.

Beyond the decreased strength of $I_{K(DR)}$, as the cells exposed to different RDV concentrations, the increase of $I_{K(DR)}$ inactivation relaxation responding to protracted depolarization was noticeably observed in a time-dependent manner. That is, the relaxation time course of $I_{K(DR)}$ inactivation in the presence of this compound likely became strengthened, though the activation one of the current was unchanged. What is more, we measured the time

constants of $I_{K(DR)}$ inactivation in different RDV concentrations, as illustrated in **Figure 1C**, the time courses of relative block of $I_{K(DR)}$, namely, $(I_{control}-I_{RDV})/I_{control}$, in the presence of different RDV concentrations were appropriately fitted to a single exponential process. Under minimal reaction scheme elaborated in the **Supplementary Material**, the estimated K_D value in the existence of RDV amounted to 3.06 μM (as indicated in **Figure 1D**), which is noticeably near the IC_{50} value warranted for RDV-mediated blockade of the late (or sustained) component of $I_{K(DR)}$; however, it was noticeably lower than that for its depressant action on the initial peak component of the current.

Inhibitory Effect of RDV on Averaged Current-Voltage (I-V) Relationship of $I_{K(DR)}$

In another separate series of measurements, we voltage-clamped at −50 mV and then delivered command voltage pulses from −60 to +70 mV in 10-mV increments with a duration of 1 sec to the examined cells. Under these experimental voltage protocols, a family of $I_{K(DR)}$ could be robustly elicited and the currents were noticeably manifested by an outwardly rectifying property with a reversal potential of −74 ± 2 mV (n = 13) (Wang et al., 2008; Lu et al., 2019; So et al., 2019). Of notice, one minute after exposure to 10 μM RDV, the $I_{K(DR)}$ strength was depressed particularly at the potentials ranging between −20 and +70 mV. **Figures 2A–C** depict the *I-V* relationships of $I_{K(DR)}$ measured at the beginning (initial peak) and end (late or sustained) of each potential in the control and during cell exposure to 10 μM RDV. The magnitude for RDV-induced block of $I_{K(DR)}$ measured at the end of depolarizing pulses (i.e., late $I_{K(DR)}$) noticeably became greater than that achieved at the beginning of pulses (i.e., peak $I_{K(DR)}$). For instance, at the level of +50 mV, RDV (10 μM) lessened the peak component of $I_{K(DR)}$ by 46 ± 2% from 976 ± 178 to 527 ± 114 pA (n = 8, $P<0.05$). However, at the same level of voltage pulse, RDV at the same concentration distinctly declined the $I_{K(DR)}$ amplitude attained at the end of depolarizing pulse by 74 ± 3% from 748 ± 121 to 194 ± 42 pA. After washout of RDV, the peak or late amplitude of $I_{K(DR)}$ was back to 956 ± 168 or 732 ± 114 pA, respectively (n = 7). Meanwhile, from the current experimental conditions, the presence of 10 μM RDV significantly declined initial or late component of macroscopic $I_{K(DR)}$ conductance (measured at the voltage from +30 to +70 mV) to 9.2 ± 0.2 or 3.5 ± 0.2 nS from the control values of 12.7 ±

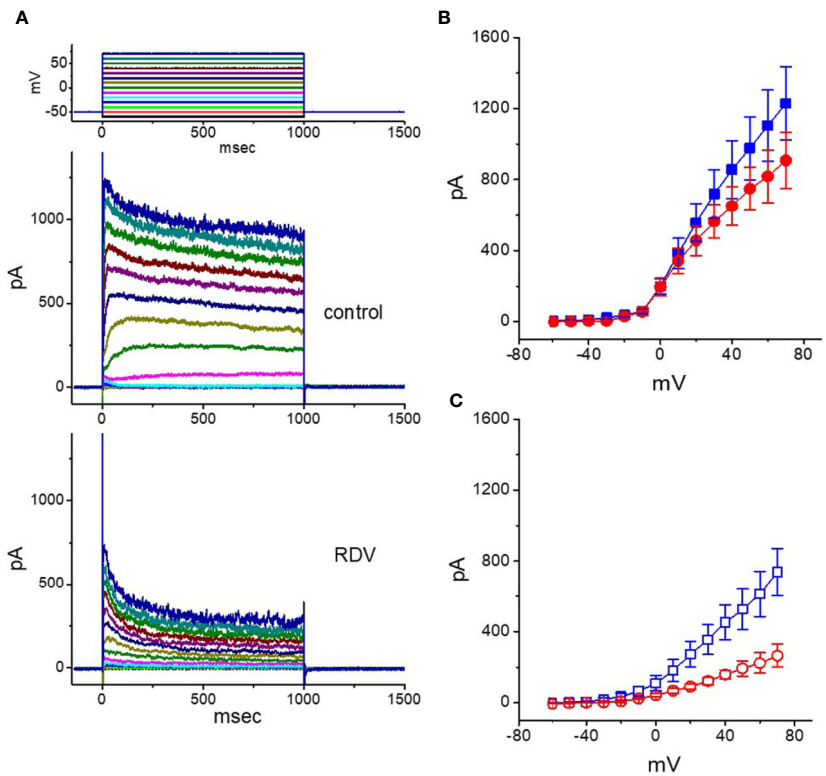

FIGURE 2 | Effect of RDV on the current-voltage (*I-V*) relationship of $I_{K(DR)}$ in GH_3 cells. In the experiments on the elicitation of $I_{K(DR)}$, the cell was maintained at −50 mV and 1-sec depolarizing command pulse to a series of voltage steps ranging between −60 to +70 mV in 10-mV increments was thereafter applied. **(A)** Representative $I_{K(DR)}$ traces obtained in the control (upper) and during cell exposure to 10 μM RDV (lower). The uppermost part shows the voltage protocol delivered. In **(B, C)**, the averaged *I-V* relationships of $I_{K(DR)}$ obtained in the absence (filled symbols) and presence (open symbols) of 10 μM RDV are illustrated, respectively (mean ± SEM; n=8 for each point). The data points in **(B, C)** were collected at the beginning (initial peak component, square symbols) or end (late component, circle symbols) of 1-sec depolarizing pulse.

0.6 or 8.5 ± 0.5 nS (n = 8), respectively. In consequence, the strength for RDV-induced block of late or steady-state $I_{K(DR)}$ in dealing with step depolarizations was pronouncedly larger than that of instantaneous peak components of the current.

Comparison Among the Effects of RDV, RDV Plus α,β-Methylene ATP (AMPCPP) and RDV Plus Cyclopentyl-1,3-Dipropylxanthine (DPCPX) on $I_{K(DR)}$ Amplitude

It has been noticed that the binding of muscarinic or purinergic receptors to GH_3 cells is likely to activate K^+-channel activity through a G-protein modulation (Yatani et al., 1987). We hence examined whether adding AMPCPP or DPCPX, but still in the continued exposure to RDV, was able to adjust RDV-perturbed inhibition of $I_{K(DR)}$ detected in GH_3 cells. Of surprise, as depicted in **Figure 3**, neither further application of AMPCPP (30 μM) nor DPCPX (1 μM) effectively modified the inhibition of $I_{K(DR)}$ produced by 10 μM RDV, in spite of the ability of RDV alone to depress $I_{K(DR)}$ and to fasten current inactivation. AMPCPP, a non-degradable ATP analog, is previously reported to be a P_{2X}-purinergic-receptor agonist, whereas DPCPX is an antagonist of adenosine A_1 receptor (Wu et al., 1998). Alternatively, in the continued presence of 10 μM RDV, further application of 10 μM nonactin, known to be a K^+ ionophore, could effectively reverse RDV-induced decrease of current amplitude. Therefore, RDV-perturbed strength of $I_{K(DR)}$ observed in GH_3 cells is most unlikely to be connected with its preferential binding to the purinergic or adenosine receptors, although the RDV molecule was thought to be a prodrug of an adenosine nucleoside analog (Lo et al., 2017; Brown et al., 2019; Tchesnokov et al., 2019; Gordon et al., 2020).

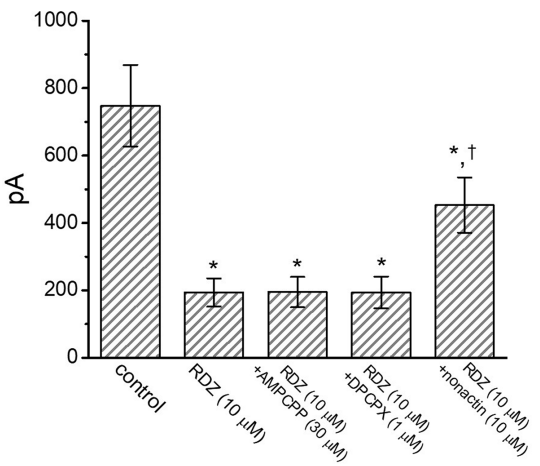

FIGURE 3 | Comparisons among the effect of RDV, RDV plus α,β-methylene ATP (AMPCPP), RDV plus cyclopentyl-1,3-dipropylxanthine (DPCPX) and RDV plus nonactin on $I_{K(DR)}$ amplitude in GH_3 cells (mean ± SEM; n=8 for each bar). GH_3 cells were bathed in Ca^{2+}-free, Tyrode's solution and the electrode was filled with K^+-containing internal solution. Current amplitude from −50 mV depolarizing pulse to +50 mV depolarization with a duration of 1 sec was measured at the end of depolarizing command potential. In this set of experiments on RDZ plus each agent, the tested compound was subsequently added in the continued presence of RDV (10 μM). *Significantly different from control (P<0.05).

The Inactivation of $I_{K(DR)}$ Modified by RDV

As cells were exposed to different RDZ concentrations, the $I_{K(DR)}$ in response to membrane depolarization noticeably exhibited an evident peak followed by an exponential decline to a steady-state level. Hence, we further explored the quasi-steady-state inactivation curve of $I_{K(DR)}$ attained in the absence or presence of RDV by using a two-step voltage protocol. In this series of experiments, we immersed cells in Tyrode's solution (Ca^{2+}-free), and then filled the electrode with K^+-containing solution, during electrical recordings. Once whole-cell configuration has been tightly established, we applied a two-pulse protocol, under analog-to-digital conversion, to the examined cells in which different RDV concentrations were present. From the least-squares minimization, the inactivation parameters of $I_{K(DR)}$ were appropriately derived in the presence of 3 or 10 μM RDV. As illustrated in **Figures 4A, B**, we constructed the normalized strength of $I_{K(DR)}$ (i.e., I/I_{max}) against the conditioning command potentials, and the continuous sigmoidal curve was well fitted with a modified Boltzmann function elaborated under *Materials and Methods*. In the presence of 3 μM RDZ, $V_{1/2}$ = −33.4 ± 1.8 mV, q = 4.7 ± 0.3 e (n = 8), whereas in the presence of 10 μM RDZ, $V_{1/2}$ = −18.5 ± 1.7 mV, q = 4.5 ± 0.3 e (n = 8). Observations from this set of experiments disclosed that during GH_3-cell exposure to different RDV concentrations, the $V_{1/2}$ value of $I_{K(DR)}$ inactivation curve attained from these cells could be measurably altered, although modification in the gating charge was not noticed.

RDV on the Recovery of $I_{K(DR)}$ Blockage Identified in GH_3 Cells

Recovery from block by RDV was additionally undertaken with another two-step voltage-clamp protocol which comprises an initial (i.e., the first conditioning) depolarizing pulse sufficiently long to allow block to reach block to reach a steady-state level. The membrane voltage was thereafter stepped to +50 mV from −50 mV for a variable time, after a second depolarizing pulse (test pulse) was applied at the same potential as the conditioning pulse (**Figure 5A**). The ratios (2^{nd} pulse/1^{st} pulse) of the peak amplitude of $I_{K(DR)}$ evoked in response to the test and the conditioning pulse were employed for a measure of recovery from block, and the values were constructed and then plotted versus interpulse interval (**Figure 5B**). The time course for the recovery of $I_{K(DR)}$ block with or without RDV addition was noticed to be described by a single-exponential function. The time constant for current recovery from inactivation in the control was measured to be 453 ± 17 ms (n = 7), whereas the addition of 1 or 3 μM RDV to the examined cells prolonged the time constant to 687 ± 23 (n = 7, P<0.05) or 867 ± 37 ms (n = 7, P<0.05), respectively. These observations prompted us to indicate that the slowing of recovery caused by adding RDV might be principally owed to the block in open or inactivated state.

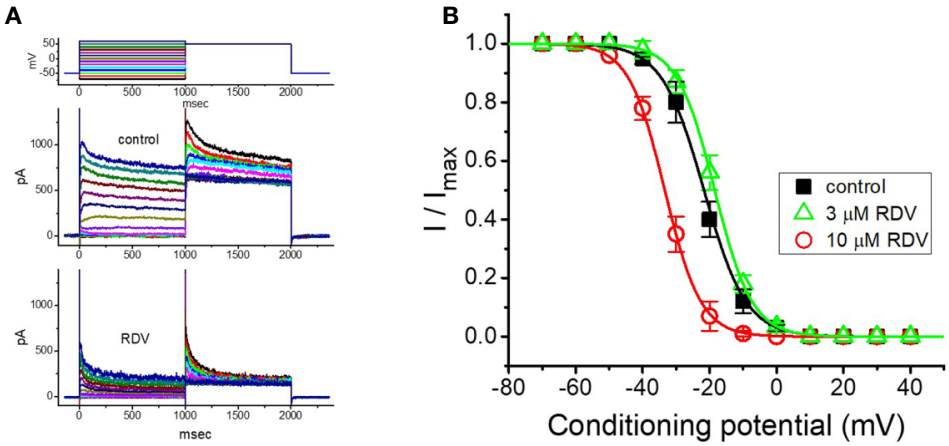

FIGURE 4 | Effect of RDV on the steady-state inactivation curve of $I_{K(DR)}$ in GH_3 cells. This set of experiments was undertaken with a two-step voltage protocol (as indicated in the uppermost part of **(A)**. **(A)** Representative $I_{K(DR)}$ traces obtained in the absence (upper) and presence (lower) of 10 μM RDV. The voltage protocol applied is illustrated in the uppermost part. **(B)** Steady-state inactivation curve of $I_{K(DR)}$ in the control (■) and during exposure to 3 μM RDV (△) or 10 μM RDV (○) (mean ± SEM; n=8 for each point). Each curve noticeably overlaid on the data was fitted by Boltzmann equation detailed in **Materials and Methods**.

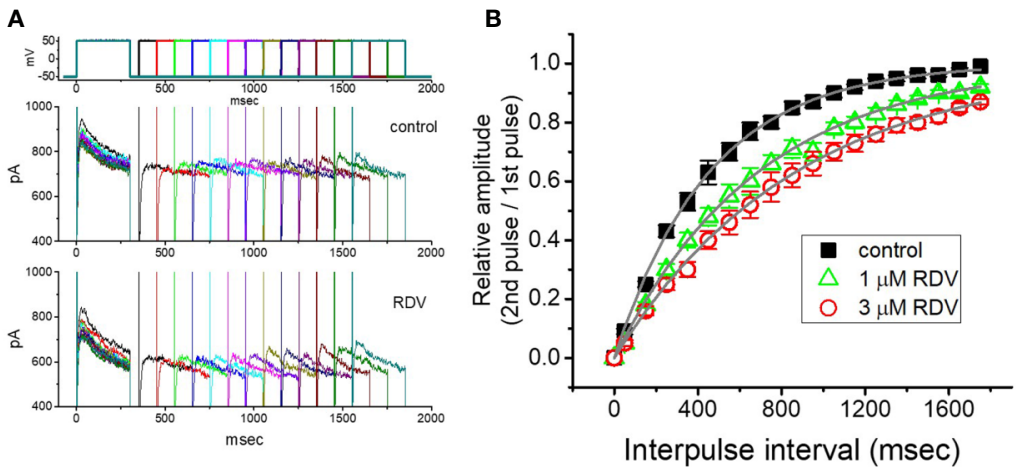

FIGURE 5 | Recovery from $I_{K(DR)}$ block produced by RDV. In this set of whole-cell recording experiments, GH_3 cells, bathed in Ca^{2+}-free, Tyrode's solution, were depolarized from –50 to +50 mV with a duration of 300 ms and different interpulse durations were thereafter applied. **(A)** Superimposed $I_{K(DR)}$ traces in the absence (upper) and presence (lower) of 1 μM RDV. Voltage protocol used is denoted in the uppermost part of (A). **(B)** Time course of recovery from $I_{K(DR)}$ inactivation achieved in the control (■) and during exposure to 1 μM RDV (△) or 3 μM RDV (○). The recovery time course in the control, during exposure to 1 μM RDV, and that to 3 μM RDV was satisfactorily fitted to a single exponential with a time constant of 453, 687, and 867 ms, respectively. Each point in this Figure is the mean ± SEM (n=7 for each point).

RDV on M-type K^+ Current ($I_{K(M)}$) in GH_3 Cells

In another separate measurements, we further checked whether the effect of RDV on the amplitude or gating of another type of K^+ current (i.e., M-type K^+ current [$I_{K(M)}$]) endogenously in GH_3 cells (Sankaranarayanan and Simasko, 1996; Selyanko et al., 1999; Yang et al., 2019). The cells were bathed in high-K^+, Ca^{2+}-free solution, and the K^+-containing solution was used to fill up the recording electrode. Of notice, within 1 min of RDV exposure, the $I_{K(M)}$ strength of GH_3 cells was considerably declined (**Figure 6A**). For example, at as the cells were depolarized from −50 to −10 mV, the addition of 3 μM RDV decreased $I_{K(M)}$ amplitude from 176 ± 25 to 78 ± 19 pA (n=9, P<0.05), and after removal of RDV, current amplitude returned to 169 ± 24 pA (n=9). We consequently constructed the association between the RDV concentration and the degree of $I_{K(M)}$ suppression. The half-maximal concentration (i.e., IC_{50}) needed for depressant effect of RDV on $I_{K(M)}$ was yielded to

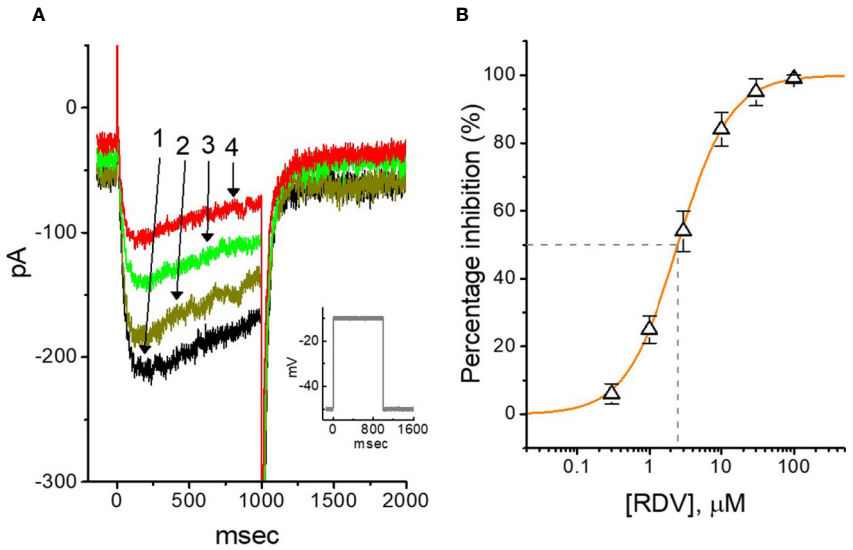

FIGURE 6 | Effect of RDV on M-type K^+ current ($I_{K(M)}$) in GH_3 cells. The experiments were conducted in cells immersed in high-K^+, Ca^{2+}-free solution and the pipette used was filled with K^+-containing solution. **(A)** Representative $I_{K(M)}$ traces elicited by 1-sec membrane depolarization from −50 to −10 mV (indicated in the Inset). Current trace labeled 1 is control and that labeled 2, 3 or 4 was obtained after the addition of 0.3 μM RDV, 1 μM RDV or 3 μM RDV, respectively. **(B)** Concentration-dependent relation of RDV effect on $I_{K(M)}$ amplitude in GH_3 cells (mean ± SEM; n=9 for each point). The continuous line was accordingly fitted by a Hill function as described under **Materials and Methods**. The IC_{50} value (as indicated in the vertical dashed line) needed for RDV-induced depression of $I_{K(M)}$ was identified to be 2.5 μM.

be 2.5 μM, and at a concentration of 100 μM, it nearly fully depressed current strength (**Figure 6B**). It is apparent, therefore, that RDV can exert a pronounced action on the inhibition of $I_{K(M)}$ identified in GH_3 cells.

Effect of RDV on $I_{K(M)}$ Triggered by Triangular Ramp Pulse With Varying Durations

Previous experiments disclosed the capability of $I_{K(M)}$ strength to modulate the patterns of bursting firing in central neurons (Brown and Passmore, 2009). Therefore, we wanted to evaluate how RDV could have any propensity to perturb $I_{K(M)}$ responding to long-lasting triangular ramp pulse with varying durations, which were achieved by digital-to-analog conversion. In the presence experiments, the examined cell was voltage-clamped at −50 mV and the upsloping (forward) limb from −50 to 0 mV followed by the downsloping (backward) limb back to −50 mV with varying durations (40–940 ms) was thereafter applied. As demonstrated in **Figure 7A**, once the slope of ramp pulse was declined, the maximal strength of $I_{K(M)}$ triggered by the upsloping limb of triangular ramp pulse was progressively raised, whereas the peak amplitude of $I_{K(M)}$ was initially elevated and followed by gradual decline. However, once 3 μM RDV was added, the strength of the current responding to both rising and falling ramp pulse was noticeably decreased (**Figure 7A**). For instance, as the duration of triangular ramp pulse applied was set at 940 ms (i.e., slope= ± 0.1 V/sec), the addition of 3 μM RDV decreased current amplitude measured at the upsloping or downsloping limbs from 150 ± 12± to 83 ± 9 pA (n=8, P<0.05), or from 294 ± 23 to 131 ± 11 pA (n=8, P<0.05). The experimental results illustrated that the strength of $I_{K(M)}$ in the upsloping lime was considerably raised as the duration of triangular ramp pulse elevated, while that in the downsloping limb was gradually declined, and that adding RDV contributed to a decline of $I_{K(M)}$ by a time-dependent manner in GH_3 cells.

The voltage hysteresis of ionic currents has been demonstrated to have an impact on electrical behaviors of action-potential firing (Männikko et al., 2005; Fürst and D'Avanzo, 2015; Hsu et al., 2020). The $I_{K(M)}$ amplitude triggered by the upsloping limb of triangular voltage ramp was considerable lower that that by the downsloping limb, strongly indicating a voltage-dependent hysteresis for $I_{K(M)}$ as depicted in **Figure 7B**, according to the relationship of $I_{K(M)}$ versus membrane voltage. As the duration of triangular pulse raised from 40 to 940 ms (i.e., the slope became decreased), the hysteresis degree for $I_{K(M)}$ was decreased. Of notice, by adding RDV (3 μM), $I_{K(M)}$ evoked in the upsloping limb of long-lasting triangular ramp decreased to a less extent than which measured from the downsloping ramp. For instance, in controls (i.e., RDV was not present), $I_{K(M)}$ at the level of −20 mV elicited upon the upsloping and downsloping ends of triangular ramp pulse were 78 ± 9 and 301 ± 23 pA (n=8), respectively, the values of which were noticed to differ significantly between them (P<0.05). Furthermore, by adding 3 μM RDV, the strength of forward

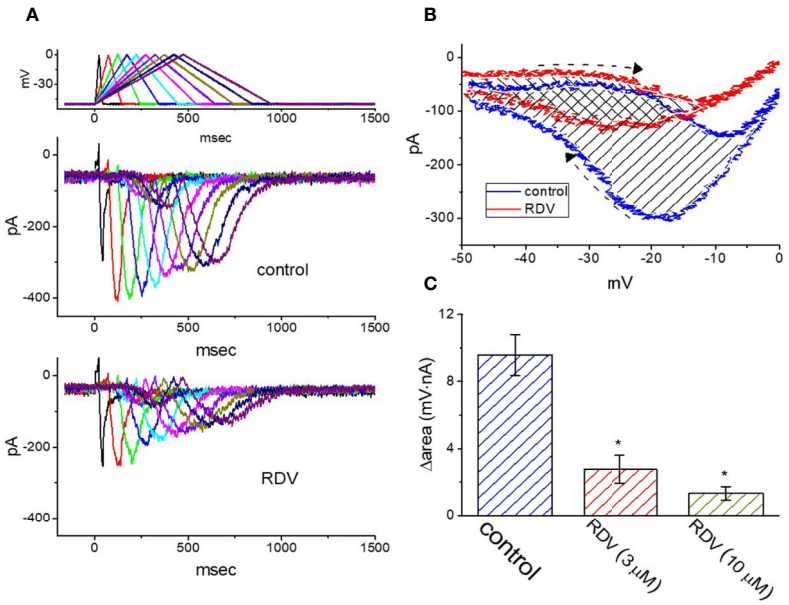

FIGURE 7 | Effect of RDV on $I_{K(M)}$ in response to isosceles-triangular ramp pulse with different durations (40–940 ms) which was particularly designed to mimic different depolarizing and repolarizing slope of bursting pattern. **(A)** Superimposed $I_{K(M)}$ traces in response to the uppermost voltage protocol obtained in the absence (upper) and presence (lower) of 3 μM RDV. The uppermost part is the voltage profile delivered. **(B)** Effect of RDV (3 μM) on voltage dependent hysteresis (i.e., the relationship of forward and reverse current versus membrane voltage) of $I_{K(M)}$ elicited by triangular ramp pulse with a duration of 940 ms. Blue or red current trajectory indicates the absence or presence of 3 μM RDV, respectively. Dashed arrows indicate the direction of $I_{K(M)}$ in which time passes during the elicitation by 940-ms triangular ramp pulse. **(C)** Summary bar graph showing the effect of RDV on the Δarea (as indicated in shaded area in **(B)** (mean ± SEM; n=9 for each bar). The Δarea with respect to the voltage-dependent hysteresis of $I_{K(M)}$ taken with or without 3 μM RDV addition is indicated as shaded area in **(B)**. *Significantly different from control (P<0.05).

and backward $I_{K(M)}$ at the same membrane voltage was evidently declined to 65 ± 6 and 135 ± 18 pA. Therefore, the strength of RDV-induced current inhibition at the upsloping (forward) and downsloping (reverse) limbs of triangular ramp differ significantly. The addition of 3 μM RDV decreased $I_{K(M)}$ amplitude evoked at the upsloping or downsloping limb of triangular ramp pulse by about 17% or 55%, respectively.

As described by the dashed arrows in **Figure 7B**, upon the difference (i.e., Δarea) in area under the curve in the forward (upsloping) and backward (downsloping) direction, furthermore, we quantified the degree of voltage-dependent hysteresis of $I_{K(M)}$. It showed that the amount of voltage hysteresis responding to 940-ms triangular ramp pulse was considerably lessened in the presence of RDV. **Figure 7C** summarized the data demonstrating the effects of RDV (3 or 10 μM) on the area under such curve. For instance, in addition to its depression of $I_{K(M)}$ amplitude, the presence of 3 μM RDV decreased the area responding to long-lasting triangular ramp, as illustrated by a specific reduction of Δarea from 9.6 ± 1.2 to 2.8 ± 0.8 mV·nA.

Mild Inhibition by RDV of erg-Mediated K^+ Current ($I_{K(erg)}$) in GH_3 Cells

Further, we investigated the potential modifications of RDV on another K^+ current (i.e., $I_{K(erg)}$) also endogenously in these cells. Under our experimental conditions, the deactivating inwardly directed $I_{K(erg)}$ could be robustly elicited from −10 mV holding potential to a range of voltage pulses from −100 to −10 mV within 1 sec (Wu et al., 2000; Huang et al., 2011; Hsu et al., 2020). When GH_3 cells were exposed to RDV at a concentration of 30 μM, the amplitude of deactivating $I_{K(erg)}$ was mildly but significantly depressed throughout the entire voltage-clamp pulses applied (**Figure 8**). For example, at the level of −90 mV, the peak amplitude of $I_{K(erg)}$ was noticeably decreased from 565 ± 59 to 383 ± 42 pA (n=9, P<0.05), as cells were exposed to 30 μM RDV. After the agent was washed out, the strength was back to 554 ± 51 pA (n=8). Alternatively, adding 30 μM RDV lessened whole-cell conductance of peak $I_{K(erg)}$ measured between −50 and −90 mV from 8.7 ± 0.8 to 5.8 ± 0.7 nS. Therefore, as compared with $I_{K(DR)}$ or $I_{K(M)}$, the $I_{K(erg)}$ in these cells is relatively resistant to being blocked by RDV. However, the RDV effect on $I_{K(erg)}$ tends to be rapid in onset, and it should be independent of its perturbing effect on the activity of RNA-polymerase.

Stimulation by RDV of I_{MEP} in GH_3 Cells

It has been reported that I_{MEP} elicited in response to large membrane hyperpolarization (Dyachok et al., 2010; Liu et al., 2012; Wu et al., 2012; So et al., 2013; Chiang et al., 2014; Chang et al., 2020a). To study whether RDV possibly perturb this type of ionic current, we bathed cells in Tyrode's solution (Ca^{2+}-free) and

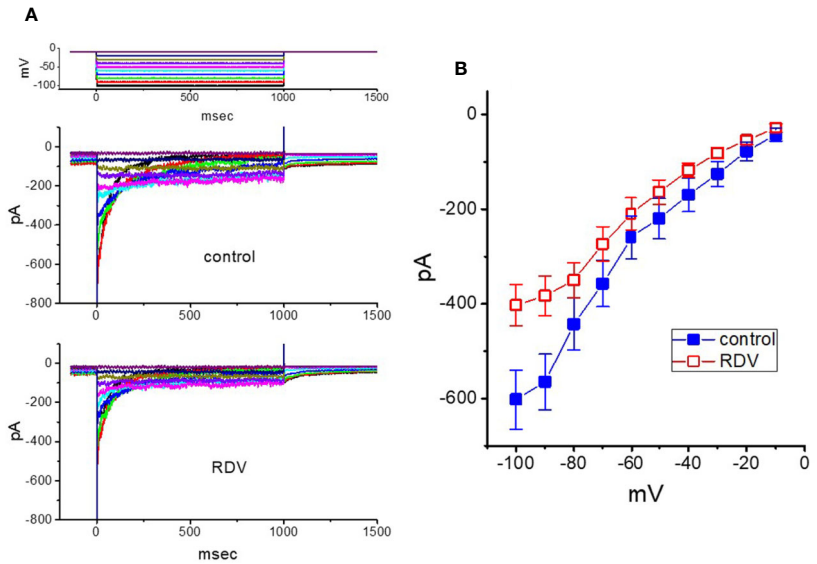

FIGURE 8 | Effect of RDV on *erg*-mediated K^+ current ($I_{K(erg)}$) enriched in GH_3 cells. The experiments were undertaken in cells bathed in high-K^+, Ca^{2+}-free solution, and we filled the electrode using K^+-containing solution. **(A)** Superimposed $I_{K(erg)}$ traces elicited by a series of voltage pulse as indicated in the uppermost part of **(A)**. The traces in the upper part are controls (i.e., RDV was not present), and those in the lower part was obtained 2 min after application of 30 μM RDV. **(B)** Averaged *I-V* relationships of $I_{K(erg)}$ obtained in the absence (■) and presence (□) of 30 μM RDV (mean ± SEM; n=9 for each point). Current amplitude was obtained at the beginning of each hyperpolarizing command pulse.

performed whole-cell current recordings. As described in previous observations (Dyachok et al., 2010; Wu et al., 2012; Chang et al., 2020a; Chang et al., 2020b), when the cell was voltage-clamped at −80 mV and the 300-ms hyperpolarizing pulse to −200 mV was applied to evoke I_{MEP}. As depicted in **Figures 9A, B**, when cells were continually exposed to RDV, the amplitude of I_{MEP} elicited by such large hyperpolarization was progressively raised. For instance, 3 μM RDV conceivably elevated I_{MEP} amplitude from 112 ± 21 to 238 ± 35 pA (n=8, P<0.05) at the level of −200 mV. After washout, current amplitude was back to 124 ± 24 pA (n=8). Additionally, as K^+ ions in the internal solutions were replaced with equimolar concentrations of $NMDG^+$, this current could still be enhanced through adding 3 μM RDV; however, current magnitude tended to be smaller. **Figure 9B** shows the association between the concentration of RDV and the degree of I_{MEP} increase. RDV could concentration-dependently elevate the amplitude of I_{MEP} activated during large step hyperpolarization. The half-maximal concentration (EC_{50}) needed for the stimulatory effect of RDV on I_{MEP} was noticed to be 5.8 μM. Our findings disclosed the effectiveness of RDV in generating a stimulatory action on I_{MEP} in GH_3 cells. **Figure 9C** depicts summary bar graph showing the effect of RDV, RDV plus ivabradine or RDV plus $LaCl_3$ on I_{MEP}. The results indicate that RDV-stimulated I_{MEP} was overcome by subsequent addition of $LaCl_3$ (5 mM), but not by ivabradine (3 μM). Ivabradine or hydroxychloroquine was demonstrated to be an inhibitor of hyperpolarization-activated cation current (Capel et al., 2015; Hsiao et al., 2019). Subsequent addition of chlorotoxin (1 μM), a blocker of Cl^- channels, was unable to reverse RDV-induced I_{MEP} (242 ± 38 pA [in the presence of 3 μM RDV] versus 239 ± 41 pA [in the presence of 3 μM RDV plus 1 μM chlorotoxin]; n=8, P>0.05). In consequence, the RDV-stimulated I_{MEP} identified in GH_3 cells is unlikely to result from its activation of hyperpolarization-activated cation current.

DISCUSSION

In this study, we noticed that in a time- and concentration-dependent fashion the presence of RDV depressed the strength of delayed-rectifier K^+ current ($I_{K(DR)}$) in pituitary tumor (GH_3) cells. The rate of current inactivation apparently became fastened as the RDV concentration increased. In another perspective, the suppression of RDV on $I_{K(DR)}$ is evidently associated with an increasing inactivation rate of the current responding to membrane depolarization. Specifically, the relative block of $I_{K(DR)}$ induced by the RDV concentrations could be hence fitted in an exponential fashion. From the minimal reaction scheme (as shown in **Supplementary Material (1)**), the value of dissociation constant (K_D) required for RDV-induced block of $I_{K(DR)}$ in GH_3 cells was yielded to be 3.04 μM, which is close to effective IC_{50} value (2.8 μM) for RDV-mediated inhibition of late $I_{K(DR)}$, but is lower than that (10.1 μM) for its block of initial peak $I_{K(DR)}$.

Alternatively, during cell exposure to different RDV concentrations, the inactivation parameter (i.e., $V_{1/2}$ value) for the inactivation curve of $I_{K(DR)}$ emerging from GH_3 cells can be

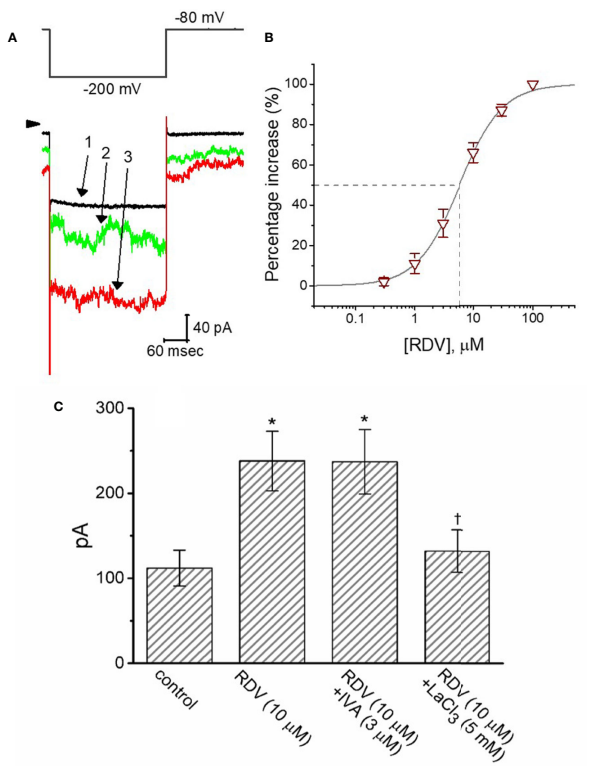

FIGURE 9 | The stimulatory effect of RDV on membrane electroporation-induced current (I_{MEP}) identified in GH_3 cells. In this separate set of experiments, we bathed cells in Ca^{2+}-free, Tyrode's solution and the recording pipette was filled with K^+-containing solution. **(A)** Representative I_{MEP} traces obtained in the control (**1**) and during cell exposure to 3 μM RDV (**2**) or 10 μM RDV (**3**). The voltage-clamp protocol applied is denoted in the upper part, arrowhead is the zero current level and the calibration mark at the right lower part applies all current traces. Noticeably, the addition of RDV causes a measurable increase in the amplitude of I_{MEP} elicited by large membrane hyperpolarization from –80 to –200 mV with a duration of 300 ms. **(B)** Concentration-dependent stimulation of I_{MEP} produced by RDV in GH_3 cells (mean ± SEM; n=8 for each point). Current amplitude was measured at the end of hyperpolarizing pulse from –80 to –200 mV with a duration of 300 ms, and the vertical dashed line is placed at the IC_{50} value required for RDV-stimulated I_{MEP}. **(C)** Summary bar graph showing effect of RDV, RDV plus ivabradine (IVA) and RDV plus $LaCl_3$ on I_{MEP} amplitude (mean ± SEM; n=8 for each bar). Current amplitude was taken at the end of hyperpolarizing voltage pulse from –80 to –200 mV with a duration of 300 ms. *Significantly different from control (P<0.05) and †significantly different from ZDV (10 M) alone group (P<0.05).

evidently adjusted, with no modifications of the gating charge. The presence of RDV (1 and 3 μM) induced $I_{K(DR)}$ block from the inactivation could be also noticeably recovered with single exponential of 687 and 867 ms, respectively. In this scenario, the present observations disclose that the RDV molecules tend to accelerate $I_{K(DR)}$ inactivation in a concentration- and state-dependent fashion, implying that they reach the blocking site of the channel, only when the channel involved resides in the open conformational state. The EC_{50} value of RDV against SARS-CoV-2 existing in Vero E6 cells was noticeably measured to be 1.76 μM, indicating that its working concentration is more than likely achieved *in vivo* (Wang et al., 2020). In the present study, the RDV presence was also observed to inhibit $I_{K(DR)}$ in Jurkat T-lymphocytes in a time- and concentration-dependent fashion (**Supplementary Material (2)** and **Supplementary Figure 1**). Besides its antiviral activity, similar to chloroquine, RDV per se might to some extent effect an immune-modulating activity possibly through the inhibition of K_V channels.

The current observations pointed out that with effective IC_{50} of 2.5 μM in GH_3 cells, RDV was capable of depressing the strength of $I_{K(M)}$. Moreover, the voltage-dependent hysteretic changes of ionic currents are hypothesized to play an essential characteristic in the behaviors of different types of electrically excitable cells. In the current study, echoing previous observations (Männikko et al., 2005; Fürst and D'Avanzo, 2015; Hsu et al., 2020), the $I_{K(M)}$ endogenously in GH_3 cells was also observed to go either through a voltage-dependent hysteresis, or a mode-shift in the conditions of which the voltage sensitivity of gating charge movements is dependent on the previous state. By long-lasting triangular ramp pulse, RDZ noticeably suppressed the strength of voltage-dependent hysteresis for $I_{K(M)}$ elicitation. As such, we provide the experimental results strongly demonstrating that there is a perturbing effect of RDZ on such non-equilibrium property in M-type K^+ channels in electrically excitable cells such as GH_3 cells, although how RDZ-induced changes in voltage hysteresis of $I_{K(M)}$ are connected with the behaviors of electrically excitable cells is unclear.

The present study discloses that RDV can directly inhibit $I_{K(M)}$ and $I_{K(DR)}$ in pituitary GH_3 cells, suggesting that this compound per se presumably is not an inactive prodrug. The depression of these K^+ currents would be expected to be potentially charged with its actions on activities in various types of cell including GH_3 cells. A current report noticeably demonstrated the occurrence of hypokalemia present in the patients with coronavirus disease 2019 (Chen et al., 2020). It is reasonable to presume that, apart from its effects on the viral polymerase and the proofreading exoribonuclease (Agostini et al., 2018; Brown et al., 2019; Tchesnokov et al., 2019; Gordon et al., 2020), to what extent RDV-induced perturbations of ion channels unexpectedly identified in this study participates in its antiviral actions has yet to be further delineated.

Our results are in accordance with previous findings demonstrating that the large hyperpolarization induced inward currents (i.e., I_{MEP}) occur in glioma cells, heart cells, pituitary cells, and macrophages (Dyachok et al., 2010; Liu et al., 2012; So et al., 2013; Chiang et al., 2014; Chang et al., 2020a; Chang et al., 2020b). Such hyperpolarization-induced activation followed by irregular time course indicates that I_{MEP} was produced by transient rupture of cell membrane caused by the electrical field tied to large hyperpolarization (Dyachok et al., 2010; Wu et al., 2012; So et al., 2013; Chang et al., 2020a; Chang et al., 2020b). In the current study, the presence of RDV was effective at

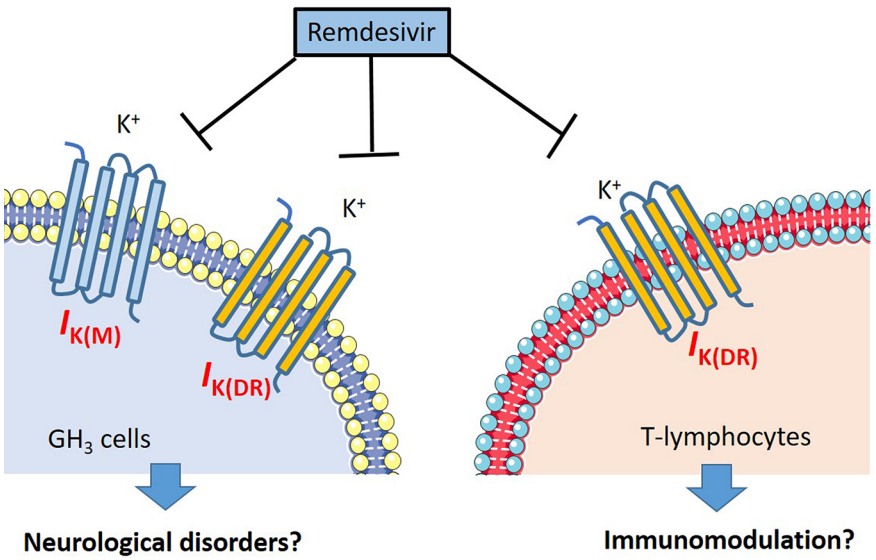

FIGURE 10 | The illustration of possible mechanism regarding the RDV induced perturbations on neurons and lymphocytes.

increasing I_{MEP} dose-dependently with EC_{50} value of 5.8 μM. Further addition of $LaCl_3$, yet not that of chlorotoxin or ivabradine, was noticed to reverse RDV-stimulated I_{MEP}. Previous observations have reported the effectiveness of AUY922, a small-molecule inhibitor of heat-shock protein 90 (HSP90), in stimulating I_{MEP} in glioblastoma cells through a mechanism independent of HSP90 inhibition (Chiang et al., 2014). As a corollary, stimulation by RDV of I_{MEP} in GH_3 cells also tends to be direct and is unlikely to be mediated through a mechanism linked to its prevailing actions on RNA polymerases.

The MEP-perturbed portion of the surface membrane can initiate ion fluxes into and out of the cell, hence producing a massive change in the ionic milieu of the cytosol. This effect has applications in biotechnology and medicine and, hence, has been the subject of both experimental and theoretical work (Gehl, 2003; So et al., 2013; Napotnik and Miklavčič, 2018). Due to high conductance of MEP-induced channels, even at low probability that would be open, significant currents have the propensity to flow, thereby altering the electrical behavior of cells (Vernier et al., 2009; Kaminska et al., 2012). Alternatively, previous studies have shown that the activity of MEP-elicited channels could act as a component of trans-plasma membrane electron transport, to which the targeting of mitochondrial permeability transition pore (mPTP) is closely linked (Del Principe et al., 2011; Bagkos et al., 2015). Therefore, whether RDV-stimulated perturbations of I_{MEP} in different types of cells can account for its antiviral effectiveness is worth further investigation.

Aconitine, a material agent with potential cardiotoxicity, has been described to modify the gating of $I_{K(DR)}$ in lymphocytes, neural, and cardiac cells (Lin et al., 2008). Aconite alkaloids from *Aconitum carmichaelii* were recently demonstrated to exert antiviral activity against cucumber mosaic virus (Xu et al., 2019). Additionally, curcuminoids have been demonstrated to depress $I_{K(DR)}$ as well as to fasten $I_{K(DR)}$ inactivation in insulin-secreting cells (Kuo et al., 2018), as well as to possess potent antiviral activities against coronavirus (Wen et al., 2007). Though additional experiments are required to verify the current results, RDV-induced effects on ionic currents demonstrated could be a confounding factor and the notable ionic mechanism underlying its modifications on cell behaviors occurring *in vitro* or *in vivo*. The summary of our findings regarding the possible perturbations of RDV is illustrated in **Figure 10**.

RDV-perturbed suppression of $I_{K(DR)}$ or $I_{K(M)}$ demonstrated is independent of its possible actions on RNA polymerase (Agostini et al., 2018; Brown et al., 2019; Gordon et al., 2020). in another perspective, it is intriguing to investigate whether the modification by RDV of RNA polymerase would attribute to its blocking of membrane $I_{K(DR)}$ or $I_{K(M)}$, as well as from its stimulation of I_{MEP} in different cell types. To what extent RDV-induced perturbations on membrane ionic currents confers its effectiveness in antiviral activities thus remains to be resolved. Following intravenous administration of RDV can readily pass across the blood-brain barriers (Warren et al., 2016; Ferren et al., 2019; Lucey, 2019). Recent studies have demonstrated that CoVs might exert neuro-invasive potential (Ferren et al., 2019; Li H. et al., 2020). Findings from the present observations might shed the light to the notion that the effect of RDV on the gating of the currents are intimately tied to its antiviral actions or variable forms of neurological effects (Ferren et al., 2019); however, the present observations do not preclude

the further investigations and uses of RDV in the treatment of SARS-CoV-2 infection.

DATA AVAILABILITY STATEMENT

The raw data supporting the conclusions of this article will be made available by the authors, without undue reservation.

AUTHOR CONTRIBUTIONS

S-NW designed the experiments. Z-HG, S-WL, W-KL, and S-NW carried out the experiments. P-YL provided the resources. W-TC and S-NW analyzed the data. W-TC and S-NW wrote the paper. All authors contributed to the article and approved the submitted version.

FUNDING

This study was financially supported by the grants from Ministry of Science and Technology (MOST-108-2314-B-006-094) and National Cheng Kung University (NCKUH-10709001 and D107-F2519), Taiwan. The funders are not involved in the study design, data collection, analyses, or interpretation.

ACKNOWLEDGMENTS

The authors are indebted to Kaisen Lee for enabling cell preparations in earlier experiments.

SUPPLEMENTARY MATERIAL

The Supplementary Material for this article can be found online at: https://www.frontiersin.org/articles/10.3389/fphar.2020.01091/full#supplementary-material

REFERENCES

Agostini, M. L., Andres, E. L., Sims, A. C., Graham, R. L., Sheahan, T. P., Lu, X., et al. (2018). Coronavirus susceptibility to the antiviral remdesivir (GS-5734) is mediated by the viral polymerase and the proofreading exoribonuclease. *mBio* 9, e00221–e00218. doi: 10.1128/mBio.00221-18

Al-Tawfiq, J. A., Al-Homoud, A. H., and Memish, Z. A. (2020). Remdesivir as a possible therapeutic option for the COVID-19. *Travel Med. Infect. Dis*. 34, 101615. doi: 10.1016/j.tmaid.2020.101615

Bagkos, G., Koufopoulos, K., and Piperi, C. (2015). Mitochondrial emitted electromagnetic signals mediate retrograde signaling. *Med. Hypotheses* 85, 810–818. doi: 10.1016/j.mehy.2015.10.004

Beigel, J. H., Nam, H. H., Adams, P. L., Krafft, A., Ince, W. L., El-Kamary, S. S., et al. (2019). Advances in respiratory virus therapeutics – a meeting report from the 6th isirv antiviral group conference. *Antiviral Res.* 167, 45–67. doi: 10.1016/j.antiviral.2019.04.006

Beigel, J. H., Tomashek, K. M., Dodd, L. E., Mehta, A. K., Zingman, B. S., Kalil, A. C., et al. (2020). ACTT-1 Study Group Members. Remdesivir for the treatment of Covid-19-preliminary report. *N Engl. Med. J.* 10, 383. doi: 10.1056/NEJMc2022236

Brown, D. A., and Adams, P. R. (1980). Muscarinic suppression of a novel voltage-sensitive K^+ current in a vertebrate neurone. *Nature* 283, 673–676. doi: 10.1038/283673a0

Brown, D. A., and Passmore, G. M. (2009). Neural KCNQ (Kv7) channels. *Br. J. Pharmacol.* 156, 1185–1195. doi: 10.1111/j.1476-5381.2009.00111.x

Brown, A. J., Won, J. J., Graham, R. L., Dinnon, K. H. 3., Sims, A. C., Feng, J. Y., et al. (2019). Broad spectrum antiviral remdesivir inhibits human endemic and zoonotic deltacoronaviruses with a highly divergent RNA dependent RNA polymerase. *Antiviral Res.* 169, 104541. doi: 10.1016/j.antiviral.2019.104541

Capel, R. A., Herring, N., Kalla, M., Yavari, A., Mirams, G. R., and Douglas, G. (2015). Hydroxychloroquine reduces heart rate by modulating the hyperpolarization-activated current If: Novel electrophysiological insightsand therapeutic potential. *Heart Rhythm*. 12 (10), 286–294. doi: 10.1016/j.hrthm.2015.05.027

Chang, W. T., Lo, Y. C., Gao, Z. H., and Wu, S. N. (2019). Evidence for the capability of roxadustat (FG-4592), an oral HIF prolyl-hydroxylase inhibitor, to perturb membrane ionic currents: an unidentified yet important action. *Int. J. Mol. Sci.* 20, 6027. doi: 10.3390/ijms20236027

Chang, W. T., Gao, Z. H., Li, S. W., Liu, P. Y., Lo, Y. C., and Wu, S. N. (2020a). Characterization in dual activation by oxaliplatin, a platinum-based chemotherapeutic agent of hyperpolarization-activated cation and electroporation-induced currents. *Int. J. Mol. Sci.* 21, 396. doi: 10.3390/ijms21020396

Chang, W. T., Liu, P. Y., Lee, K., Feng, Y. H., and Wu, S. N. (2020b). Differential inhibitory actions of multitargeted tyrosine kinase inhibitors on different ionic current types in cardiomyocytes. *Int. J. Mol. Sci.* 21, 1672. doi: 10.3390/ijms21051672

Chen, D., Li, X., Song, Q., Hu, C., Su, F., Dai, J., et al. (2020). Assessment of hypokalemia and clinical implications in patients with coronavirus disease 2019 in Wenzhou, China. *JAMA Netw. Open* 3, e2011122. doi: 10.1001/jamanetworkopen.2020.11122

Chiang, N. J., Wu, S. N., Kao, C. A., Huang, Y. M., and Chen, L. T. (2014). Stimulation of electroporation-induced inward currents in glioblastoma cell lines by the heat shock protein inhibitor AUY922. *Clin. Exp. Pharmacol. Physiol.* 41, 830–837. doi: 10.1111/1440-1681.12273

De Clercq, E. (2019). New nucleoside analogues for the treatment of hemorrhagic fever virus infections. *Chem. Asian J.* 14, 3962–3968. doi: 10.1002/asia.201900841

de Wit, E., Feldmann, F., Cronin, J., Jordan, R., Okumura, A., Thomas, T., et al. (2020). Prophylactic and therapeutic remdesivir (GS-5734) treatment in the rhesus macaque model of MERS-CoV infection. *Proc. Natl. Acad. Sci. U.S.A.* 117, 6771–6776. doi: 10.1073/pnas.1922083117

Dong, L., Hu, S., and Gao, J. (2020). Discovering drugs to treat coronavirus disease 2019 (COVID-19). *Drug Discov. Ther.* 14 (1), 58–60. doi: 10.5582/ddt.2020.01012

Dyachok, O., Zhabyeyev, P., and McDonald, T. F. (2010). Electroporation-induced inward current in voltage-clamped guinea pig ventricular myocytes. *J. Membr. Biol.* 238, 69–80. doi: 10.1007/s00232-010-9320-z

Ferren, M., Horvat, B., and Mathieu, C. (2019). Measles encephalitis: towards new therapeutics. *Viruses* 11, 1017. doi: 10.3390/v11111017

Fletcher, P. A., Sherman, A., and Stojilkovic, S. S. (2018). Common and diverse elements of ion channels and receptors underlying electrical activity in endocrine pituitary cells. *Mol. Cell Endocrinol.* 463, 23–36. doi: 10.1016/j.mce.2017.06.022

Fürst, O., and D'Avanzo, N. (2015). Isoform dependent regulation of human HCN channels by cholesterol. *Sci. Rep.* 5, 14270. doi: 10.1038/srep14270

Gao, J., Tian, Z., and Yang, X. (2020). Breakthrough: Chloroquine phosphate has shown apparent efficacy in treatment of COVID-19 associated pneumonia in clinical studies. *BioSci. Trends* 14, 72–73. doi: 10.5582/bst.2020.01047

Gehl, J. (2003). Electroporation. Theory and methods, perspectives for drug delivery, gene therapy and research. *Acta Physiol. Scand.* 177, 437–447. doi: 10.1046/j.1365-201X.2003.01093.x

Gordon, C. J., Tchesnokov, E. P., Feng, J. Y., Porter, D. P., and Götte, M. (2020). The antiviral compound remdesivir potently inhibit RNA-dependent RNA polymerase from Middle East respiratory syndrome coronavirus. *J. Bio Chem.* 295, 4773–4779. doi: 10.1074/jbc.AC120.013056

Hoenen, T., Groseth, A., and Feldmann, H. (2019). Therapeutic strategies to target the Ebola virus life cycle. *Nat. Rev. Microbiol.* 17, 593–606. doi: 10.1038/s41579-019-0233-2

Hsiao, H. T., Liu, Y. C., Liu, P. Y., and Wu, S. N. (2019). Concerted suppression of I_h and activation of $I_{K(M)}$ by ivabradine, an HCN-channel inhibitor, in pituitary

cells and hippocampal neurons. *Brain Res. Bull.* 149, 11–20. doi: 10.1016/j.brainresbull.2019.03.016

Hsu, H. T., Lo, Y. C., and Wu, S. N. (2020). Characterization of convergent suppression by UCL-2077 (3-(triphenylmethylaminomethyl)pyridine), known to inhibit slow afterhyperpolarization, of *erg*-mediated potassium currents and intermediate-conductance calcium-activated potassium channels. *Int. J. Mol. Sci.* 21, 1441. doi: 10.3390/ijms21041441

Huang, M. H., Shen, A. Y., Wang, T. S., Wu, H. M., Kang, Y. F., Chen, C. T., et al. (2011). Inhibitory action of methadone and its metabolites on *erg*-mediated K^+ current in GH_3 pituitary tumor cells. *Toxicology* 280, 1–9. doi: 10.1016/j.tox.2010.10.010

Huang, C. W., Hung, T. Y., Liao, Y. K., Hsu, M. C., and Wu, S. N. (2013). Underlying mechanism of regulatory actions of diclofenac, a nonsteroidal anti-inflammatory agent, on neuronal potassium channels and firing: an experimental and theoretical study. *J. Physiol. Pharmacol.* 64, 269–280. doi: 10.1016/S0301-0082(02)00004-7

Kaminska, I., Kotulska, M., Stecka, A., Saczko, J., Drag-Zalesinska, M., Wysocka, T., et al. (2012). Electroporation-induced changes in normal immature rat myoblasts (H9c2). *Gen. Physiol. Biophys.* 31, 91–25. doi: 10.4149/gpb_2012_003

Khot, W. Y., and Nadkar, M. Y. (2020). The 2019 novel coronavirus outbreak – a global threat. *J. Assoc. Phys. India* 68, 67–71. doi: 10.1016/S0140-6736(20)30185-9

Ko, W. C., Rolain, J. M., Lee, N. Y., Chen, P. L., Huang, C. T., Lee, P. I., et al. (2020). Arguments in favor of remdesivir for treating SARS-Cov-2 infections. *Int. J. Antimicrob. Agents* 55, 105933. doi: 10.5580/1650

Kuo, P. C., Yang, C. J., Lee, Y. C., Chen, P. C., Liu, Y. C., and Wu, S. N. (2018). The comprehensive electrophysiological study of curcuminoids on delayed-rectifier K^+ currents in insulin-secreting cells. *Eur. J. Pharmacol.* 819, 233–241. doi: 10.1016/j.ejphar.2017.12.004

Lai, C. C., Shih, T. P., Ko, W. C., Tang, H. J., and Hsueh, P. R. (2020). Severe acute respiratory syndrome coronavirus 2 (SARS-CoV-2) and coronavirus disease-2019 (COVID-19): the epidemic and the challenges. *Int. J. Antimicrob. Agents* 55, 105924. doi: 10.1016/j.ijantimicag.2020.105924

Li, G., and De Clercq, E. (2020). Therapeutic options for the 2019 novel coronavirus (COVID-19). *Nat. Rev. Drug Discov.* 19, 149–150. doi: 10.1038/d41573-020-00016-0

Li, H., Wang, Y. M., Xu, J. Y., and Cao, B. (2020). Potential antiviral therapeutics for 2019 novel coronavirus. *Zhonghua Jie He He Hu Xi Za Zhi* 43, E002. doi: 10.1007/978-0-387-31047-3_15

Li, Y. C., Bai, W. Z., and Hashikawa, T. (2020). The neuroinvasive potential of SARS-CoV2 may be at least partially responsible for the respiratory failure of COVID-19 patients. *J. Med. Virol.* doi: 10.1186/1471-2407-14-669

Lien, C. C., and Jonas, P. (2003). K_V3 potassium conductance is necessary and kinetically optimized for high-frequency action potential generation in hippocampal interneurons. *J. Neurosci.* 23, 2058–2068. doi: 10.1523/JNEUROSCI.23-06-02058.2003

Lin, M. W., Wang, Y. J., Liu, S. I., Lin, A. A., Lo, Y. C., and Wu, S. N. (2008). Characterization of aconitine-induced block of delayed rectifier K^+ current in differentiated NG108-15 neuronal cells. *Neuropharmacology* 54, 912–923. doi: 10.1016/j.neuropharm.2008.01.009

Liu, Y. C., Wu, P. C., Shieh, D. B., and Wu, S. N. (2012). The effects of magnetite (Fe_3O_4) nanoparticles on electroporation-induced inward currents in pituitary tumor (GH_3) cells and in RAW 264.7 macrophages. *Int. J. Nanomed.* 7, 1687–1696. doi: 10.2147/IJN.S28798

Lo, M. K., Jordan, R., Arvey, A., Sudhamsu, J., Shrivastava-Ranjan, P., Hotard, A. L., et al. (2017). GS-5734 and its parent nucleoside analog inhibit Filo-, Pneumo-, and Paramyxoviruses. *Sci. Rep.* 7, 43395. doi: 10.1038/srep43395

Lu, T. L., Chang, W. T., Chan, C. H., and Wu, S. N. (2019). Evidence for effective multiple K^+-current inhibitions by tolvaptan, a non-peptide antagonist of vasopressin V_2 receptor. *Front. Pharmacol.* 10:76. doi: 10.3389/fphar.2019.00076

Lu, H. (2020). Drug treatment options for the 2019-new coronavirus (COVID-19). *Biosci. Trends* 14, 69–71. doi: 10.5582/bst.2020.01020

Lucey, D. R. (2019). New treatments for Ebola virus disease. *BMJ* 366, I5371. doi: 10.1136/bmj.l5371

Männikko, R., Pandey, S., Larsson, H. P., and Elinder, F. (2005). Hysteresis in the voltage dependence of HCN channels: conversion between two modes affects pacemaker properties. *J. Gen. Physiol.* 125, 305–326. doi: 10.1085/jgp.200409130

Martinez, M. A. (2020). Compounds with therapeutic potential against novel respiratory 2019 coronavirus. *Antimicrob. Agents Chemother.* 64, e00399–e00320. doi: 10.1128/AAC.00399-20

Morse, J. S., Lalonde, T., Xu, S., and Liu, W. R. (2020). Leaning from the past: possible urgent prevention and treatment options for severe acute respiratory infections caused by 20190-nCoV. *Chembiochem* 21, 730–738. doi: 10.1002/cbic.202000047

Napotnik, T. B., and Miklavčič, D. (2018). In vitro electroporation detection methods-an overview. *Bioelectrochemistry* 120, 166–182. doi: 10.1016/j.bioelechem.2017.12.005

Sankaranarayanan, S., and Simasko, S. M. (1996). Characterization of an M-like current modulated by thyrotropin-releasing hormone in normal rat lactotrophs. *J. Neurosci.* 16, 1668–1678. doi: 10.1523/JNEUROSCI.16-05-01668.1996

Selyanko, A. A., Hardley, J. K., Wood, I. C., Abogadie, F. C., Delmas, P., Buckley, N. J., et al. (1999). Two types of K^+ channel subunit, Erg1 and KCNQ2/3, contribute to the M-like current in a mammalian neuronal cell. *J. Neurosci.* 19, 7742–7756. doi: 10.1523/JNEUROSCI.19-18-07742.1999

Sheahan, T. P., Sims, A. C., Graham, R. L., Menachery, V. D., Gralinski, L. E., Case, J. B., et al. (2017). Broad-spectrum antiviral GS-5734 inhibits both epidemic and zoonotic coronaviruses. *Sci. Transl. Med.* 9, eaal3653. doi: 10.1126/scitranslmed.aal3653

Sheahan, T. P., Sims, A. C., Leist, S. R., Schäfer, A., Won, J., Brown, A. J., et al. (2020). Comparative therapeutic efficacy of remdesivir and combination lopinavir, ritonavir, and interferon beta against MERS-CoV. *Nat. Commun.* 11, 222. doi: 10.1038/s41467-019-13940-6

Shu, Y., Yu, Y., Yang, J., and McCormick, D. A. (2007). Selective control of cortical axonal spikes by a slowly inactivating K^+ current. *Proc. Natl. Scad. Sci. U. S. A.* 104, 11453–11458. doi: 10.1073/pnas.0702041104

So, E. C., Tsai, K. L., Wu, F. T., Hsu, M. C., Wu, K. C., and Wu, S. N. (2013). Identification and minuscule inward currents as precursors to membrane electroporation-induced currents: real-time prediction of pore appearance. *Cell Physiol. Biochem.* 32, 402–416. doi: 10.1159/000354447

So, E. C., Liu, P. Y., Lee, C. C., and Wu, S. N. (2019). High effectiveness in actions of carfilzomib on delayed-rectifier K^+ current and on spontaneous action potentials. *Front. Pharmacol.* 10:1163. doi: 10.3389/fphar.2019.01163

Tchesnokov, E. P., Feng, J. Y., Porter, D. P., and Götte, M. (2019). Mechanism of inhibition of Ebola virus RNA-dependent RNA polymerase by remdesivir. *Viruses* 11, 326. doi: 10.3390/v11040326

Vernier, P. T., Levine, Z. A., Wu, Y. H., Joubert, V., Ziegler, M. J., Mir, L. M., et al. (2009). Electroporating fields target oxidatively damaged areas in the cell membrane. *PLoS One* 4, e7966. doi: 10.1371/journal.pone.0007966

Wang, H. S., Pan, Z., Shi, W., Brown, B. S., Wymore, R. S., Cohen, I. S., et al. (1998). KCNQ2 and KCNQ3 potassium channel subunits: molecular correlates of the M-channel. *Science* 282, 1890–1893. doi: 10.1126/science.282.5395.1890

Wang, Y. J., Lin, M. W., Lin, A. A., Peng, H., and Wu, S. N. (2008). Evidence for state-dependent block of DPI 201-106, a synthetic inhibitor of Na^+ channel inactivation, on delayed-rectifier K^+ current in pituitary tumor (GH_3) cells. *J. Physiol. Pharmacol.* 59, 409–423.

Wang, M., Cao, R., Zhang, L., Yang, X., Liu, J., Xu, M., et al. (2020). Remdesivir and chloroquine effectively inhibit the recently emerged novel coronavirus (COVID-19) in vitro. *Cell Res.* 30, 269–271. doi: 10.1038/s41422-020-0282-0

Warren, T. K., Jordan, R., Lo, M. K., Ray, A. S., Mackman, R. L., Soloveva, V., et al. (2016). Therapeutic efficacy of the small molecule GS-5734 against Ebola virus in rhesus monkeys. *Nature* 531, 381–385. doi: 10.1038/nature17180

Wen, C. C., Kuo, Y. H., Jan, J. T., Liang, P. H., Wang, S. Y., Liu, H. G., et al. (2007). Specific plant terpenoids and lignoids possess potent antiviral activities against severe acute respiratory syndrome coronavirus. *J. Med. Chem.* 50, 4087–4095. doi: 10.1021/jm070295s

Wu, S. N., Liu, S. I., and Hwang, T. L. (1998). Activation of muscarinic K^+ channels by extracellular ATP and UTP in rat atrial myocytes. *J. Cardiovasc. Pharmacol.* 31, 203–211. doi: 10.1097/00005344-199802000-00005

Wu, S. N., Jan, C. R., Li, H. F., and Chiang, H. T. (2000). Characterization of inhibition by risperidone of the inwardly rectifying K^+ current in pituitary GH_3 cells. *Neuropsychopharmacology* 23, 676–689. doi: 10.1016/S0893-133X(00)00151-2

Wu, S. N., Yeh, C. C., Wu, P. Y., Huang, H. C., and Tsai, M. L. (2012). Investigations into the correlation properties of membrane electroporation-induced inward currents: prediction of pore formation. *Cell Biochem. Biophys.* 62, 211–220. doi: 10.1007/s12013-011-9284-3

Xu, W., Zhang, M., Liu, H., Wei, K., He, M., Li, X., et al. (2019). Antiviral activity of aconite alkaloids from *Aconitum carmichaelii* Debx. *Nat. Prod. Res.* 33, 1486–1490. doi: 10.1080/14786419.2017.1416385

Yang, C. S., Lai, M. C., Liu, P. Y., Lo, Y. C., Huang, C. W., and Wu, S. N. (2019). Characterization of the inhibitory effect of gastrogenin and gastrodin on M-type K^+ currents in pituitary cells and hippocampal neurons. *Int. J. Mol. Sci.* 21, 117. doi: 10.3390/ijms21010117

Yatani, A., Codina, J., Sekura, R. D., Birnbaumer, L., and Brown, A. M. (1987). Reconstitution of somatostatin and muscarinic receptor mediated stimulation of K^+ channels by isolated GK protein in clonal rat anterior pituitary cell membrane. *Mol. Endocrinol.* 1, 283–289. doi: 10.1210/mend-1-4-283

Yeung, S. Y., Thompson, D., Wang, Z., Fedida, D., and Robertson, B. (2005). Modulation of Kv3 subfamily potassium currents by the sea anemone toxin BDS: significance for CNS and biophysical studies. *J. Neurosci.* 25, 8735–8745. doi: 10.1523/JNEUROSCI.2119-05.2005

Conflict of Interest: The authors declare that the research was conducted in the absence of any commercial or financial relationships that could be construed as a potential conflict of interest.

frontiers in Pharmacology

ORIGINAL RESEARCH
published: 04 August 2020
doi: 10.3389/fphar.2020.01182

Gating Properties of Mutant Sodium Channels and Responses to Sodium Current Inhibitors Predict Mexiletine-Sensitive Mutations of Long QT Syndrome 3

*Gang Li[1], Ryan L. Woltz[2], Cheng-yu Wang[1], Lu Ren[2], Pei-xin He[1], Shan-dong Yu[1], Xue-qin Liu[3], Vladimir Yarov-Yarovoy[4], Dan Hu[5], Nipavan Chiamvimonvat[2,6] and Lin Wu[1,7]**

[1] Department of Cardiology, Peking University First Hospital, Beijing, China, [2] Division of Cardiovascular Medicine, Department of Internal Medicine, School of Medicine, University of California, Davis, Davis, CA, United States, [3] Department of Pediatrics, Peking University First Hospital, Beijing, China, [4] Department of Physiology and Membrane Biology, School of Medicine, University of California, Davis, Davis, CA, United States, [5] Department of Cardiology and Cardiovascular Research Institute, Renmin Hospital of Wuhan University and Hubei Key Laboratory of Cardiology, Wuhan, China, [6] Department of Veterans Affairs, Northern California Health Care System, Mather, CA, United States, [7] Key Laboratory of Medical Electrophysiology, Institute of Cardiovascular Research, Southwest Medical University, Luzhou, China

OPEN ACCESS

Edited by:
Mounir Tarek,
Centre National de la Recherche Scientifique (CNRS), France

Reviewed by:
Isabelle Baró,
Centre National de la Recherche Scientifique (CNRS), France
Jean-sebastien Rougier,
University of Bern, Switzerland

***Correspondence:**
Lin Wu
lin_wu@163.com

Specialty section:
This article was submitted to Pharmacology of Ion Channels and Channelopathies, a section of the journal Frontiers in Pharmacology

Received: 02 March 2020
Accepted: 20 July 2020
Published: 04 August 2020

Citation:
Li G, Woltz RL, Wang C-y, Ren L, He P-x, Yu S-d, Liu X-q, Yarov-Yarovoy V, Hu D, Chiamvimonvat N and Wu L (2020) Gating Properties of Mutant Sodium Channels and Responses to Sodium Current Inhibitors Predict Mexiletine-Sensitive Mutations of Long QT Syndrome 3. Front. Pharmacol. 11:1182. doi: 10.3389/fphar.2020.01182

Background: Long QT syndrome 3 (LQT3) is caused by *SCN5A* mutations. Late sodium current (late I_{Na}) inhibitors are current-specific to treat patients with LQT3, but the mechanisms underlying mexiletine (MEX) -sensitive (N1325S and R1623Q) and -insensitive (M1652R) mutations remains to be elucidated.

Methods: LQT3 patients with causative mutations were treated with oral MEX following i.v. lidocaine. Whole-cell patch-clamp techniques and molecular remodeling were used to determine the mechanisms underlying the sensitivity to MEX.

Results: Intravenous administration of lidocaine followed by MEX orally in LQT patients with N1325S and R1623Q sodium channel mutation shortened QTc interval, abolished arrhythmias, and completely normalized the ECG. In HEK293 cells, the steady-state inactivation curves of the M1652R channels were rightward shifted by 5.6 mV relative to the WT channel. In contrast, the R1623Q mutation caused a leftward shift of the steady-state inactivation curve by 15.2 mV compared with WT channel, and N1325S mutation did not affect steady-state inactivation (n = 5–13, $P < 0.05$). The extent of the window current was expanded in all three mutant channels compared with WT. All three mutations increased late I_{Na} with the greatest amplitude in the M1652R channel (n = 9–15, $P < 0.05$). MEX caused a hyperpolarizing shift of the steady-state inactivation and delayed the recovery of all three mutant channels. Furthermore, it suppressed late I_{Na} in N1325S and R1623Q to a greater extent compared to that of M1652R mutant channel. Mutations altered the sensitivity of $Na_v1.5$ to MEX through allosteric mechanisms by changing the conformation of $Na_v1.5$ to become more or less favorable for MEX binding. Late I_{Na} inhibitors suppressed late I_{Na} in N1325S and R1623Q to a greater extent than that in the M1652R mutation (n = 4–7, $P < 0.05$).

Conclusion: The N1325S, R1623Q, and M1652R mutations are associated with a variable augmentation of late I_{Na}, which was reversed by MEX. M1652R mutation changes the conformation of $Na_v1.5$ that disrupt the inactivation of channel affecting MEX binding, corresponding to the poor response to MEX. The lidocaine test, molecular modeling, and drugs screening in cells expressing mutant channels are useful for predicting the effectiveness of late I_{Na} inhibitors.

Keywords: LQT3, torsades de pointes, gene mutation, late sodium current, mexiletine

INTRODUCTION

Congenital long QT syndrome (LQTS) is a genetic disorder caused by ion channel mutations disrupting the electrical activity of the heart with a prevalence of approximately 1:2000 (Garcia-Elias and Benito, 2018) in apparently healthy live births. Patients with the mutation(s) may present with QT interval prolongation in ECG recordings with episodes of polymorphic ventricular tachycardia, specifically torsade de pointes (TdP), resulting in syncope, cardiac arrest, and sudden cardiac death. To date, at least 15 genes have been identified and are associated with LQTS. LQTS types 1 and 2 caused by K^+ channel mutations account for approximately two-thirds of genetically confirmed LQTS patients (Wilde et al., 2016; Bohnen et al., 2017; Wallace et al., 2019).

LQT3 is relatively rare accounting for 5 to 10% of LQTS patients but is more malignant than LQT1 or 2 with a 10-year survival rate of less than 50%. LQT3 is caused by gain-of-function mutations in the *SCN5A* gene encoding the α-subunit of $Na_v1.5$ sodium channel, leading to abnormal Na^+ channel activation and/or inactivation, resulting in a sustained or late inward sodium current (I_{Na}). The increased late I_{Na} during the plateau phase of the cardiac action potential (AP) leads to prolonged AP duration (APD) and QT interval, increased propensities to pro-arrhythmic events including early (EAD) and delayed (DAD) afterdepolarizations, and enhanced transmural dispersions of repolarization and QT dispersion (George, 2005; Chadda et al., 2017; Yu et al., 2018). Furthermore, increased late I_{Na} is also documented in patients with LQT types 4, 9, 10, and 12. Both endogenous and enhanced late I_{Na} exhibit a frequency-dependent increase resulting in reverse rate dependence in APD (Wu et al., 2011; Yu et al., 2018). This property may explain why cardiac events of LQT3 patients often present at rest or during sleep, which is different from LQT1 and LQT2 patients whose arrhythmic events are associated with increased sympathetic activity and triggered by physical/emotional stress or environmental stimuli.

Anti-adrenergic therapies, including β-blockers and left cardiac sympathetic denervation, are recommended in guidelines to treat patients with LQTS, which are more effective in patients with LQT1 and LQT2 than LQT3. β-blockers are less effective and even potentially pro-arrhythmic associated with additional sudden death in case reports of patients with LQT3 after heart rate was slowed by drugs (Moss et al., 2000; Shimizu et al., 2000). ICD implantation is a great challenge in developing countries, especially in children. Drugs blocking late I_{Na} are considered as current-specific therapies for LQT3, because they directly reduce late I_{Na}, shortens the QTc interval, and are antiarrhythmic, which are superior to β-blockers from the mechanistic point of view (Arbelo et al., 2016; Huang et al., 2020). Lidocaine (LID), mexiletine (MEX), ranolazine (RAN), and a novel late I_{Na} inhibitor eleclazine (ELE) have been reported to inhibit late I_{Na}. However, patients with some mutations including M1652R mutation of LQT3 was reported to respond to MEX poorly (Ruan et al., 2007).

In this study, two patients with LQT3 associated with either N1325S or R1623Q mutation in *SCN5A* and responded well to LID and MEX treatment were evaluated. The electrophysiological properties and responses to MEX were compared in human embryonic kidney cells (HEK293) expressing N1325S, R1623Q, and M1652R mutant channels. A molecular model of $Na_v1.5$ channel was also used to investigate the underlying mechanisms of their differences in sensitivity to MEX.

METHODS

Clinical Evaluation

The research protocols described were approved by the Ethics Committee of Peking University First Hospital (Beijing, China). A written informed consent was obtained from the minor(s)' legal guardian for the publication of any potentially identifiable image or data included in this article. LQTS was diagnosed based on standard clinical criteria and guidelines (Priori et al., 2013). Electrocardiogram (ECG) parameters were manually measured on standard 12-leads ECG recordings. The QT interval was measured in lead II or V5 on three consecutive beats and corrected by heart rate using Bazett's formula. The LID infusion test was performed with a bolus intravenous injection of 1–2 mg/kg LID followed by an infusion of 50 μg/kg/min for 2 h. ECG recordings at baseline and at 5, 15, 30, 90, and 120 min after LID administration were obtained. Following LID infusion, MEX was administered orally 150 mg or 3–5 mg/Kg, three times daily.

Site-Directed Mutagenesis and Transfection in HEK293 Cells

The mutations were engineered into wild-type (WT) *SCN5A* cDNA cloned in pcDNA3.1 by overlap extension with the following primer pairs: N1325S, forward: 5'-TGG TCA GTG

CCC TGG TGG GCG CCA TC-3', reverse: 5'-CAG GGC ACT GAC CAC CAC CCT CAT GC-3'; R1623Q, forward: 5'- TCT TCC AAG TCA TCC GCC TGG CCC G-3', reverse: 5'- ATG ACT TGG AAG AGC GTC GGG GAG-3'; and M1652R, forward: 5'-CTC ATG AGG TCC CTG CCT GCC CTC TTC-3', reverse: 5'- CAG GGA CCT CAT GAG GGC AAA GAG CAG C-3'. The mutations were confirmed by direct sequencing. Transient transfection was carried out using lipofectamine 3000 (Invitrogen) according to the manufacture's instruction. A total of 2.0 μg of WT, N1325S, R1623Q, or M1652R *SCN5A* cDNA with *SCN1B* cDNA (encodes a β-1 subunit of the sodium channel) was used with equal amount of α and β subunits, and 0.2 μg of GFP plasmid as a report gene were transfected into HEK293 cells. GFP-positive cells were patch-clamped at least 24 h after transfection.

In Vitro Electrophysiology Experiments

Whole-cell patch-clamp experiments were performed at room temperature (20–22°C) with an EPC-10 USB amplifier. Experiments were conducted with the following internal solution (in mM): 120 CsF, 10 CsCl, 10 NaCl, 10 EGTA, and 10 HEPES (pH 7.35) adjusted with CsOH (Wang et al., 1996). The bath solution contained (in mM): 137 NaCl, 4 KCl, 1.8 $CaCl_2$, 1 $MgCl_2$, 10 glucoses, 10 HEPES (pH 7.4) adjusted with CsOH. In experiments designed to measure parameters of peak I_{Na}, external Na^+ concentration was reduced to 60 mM with CsCl used as a Na^+ substitute. Electrodes (3–5 MΩ) were pulled from 1.5 mm Sutter Instrument BF150-86-10 borosilicate glasses with filament using a PP-830 puller (NARISHIGE, Japan). After whole-cell configuration was achieved, only cells with seal resistance over 500 MΩ and access resistance less than 10 MΩ were recorded. Capacitance and series resistance compensation (80–90%) were carried out using analog techniques with patch-clamp amplifier. Pulse protocols are presented in each result figure. Currents were filtered at 2.9 kHz of Bessel filter and digitized at 10 kHz. Recordings were generally initiated at least 5 min after establishment of whole-cell configuration. Membrane potentials were not corrected for junction potentials that arose between the pipette and bath solution. All drugs were prepared as stock solutions in DMSO; concentrations of DMSO never exceeded 0.1% v/v in the final experimental solutions.

Late I_{Na} was measured as the tetrodotoxin (TTX; 30 μM)-sensitive current measured at 200 ms after a depolarization (a voltage step) from -90 mV to −20 mV was induced. Current densities (pA/pF) were obtained by dividing the peak or late I_{Na} by cell capacitance. Data for voltage dependence of activation and inactivation were fitted to a Boltzmann equation, $y = 1/\{1 + \exp[(V_{1/2} - V_m)/\kappa]\}$, in which y is the normalized current or conductance, $V_{1/2}$ is the voltage at which half of the channels are activated or inactivated, V_m is the membrane potential, and κ is the slope factor. Data for the time course of recovery from inactivation were fitted with functions of two exponentials, $P_2/P_1 = A_1[1 - \exp(-t/\tau_{fast})] + A_2[1 - \exp(-t/\tau_{slow})]$, where P_1 and P_2 are the peak sodium current of test pulse and pre-pulse and τ_{fast} and τ_{slow} are the fast and slow recovery time constants, respectively.

Molecular Model of $Na_v1.5$

A molecular model of $Na_v1.5$ channel in a partially open and presumably inactivated state was previously generated using Rosetta structural modeling software and the cryoEM structure of the eeNav1.4-beta1 complex (Nguyen et al., 2019). The three LQTS3 mutations (N1325S, R1623Q, and M1652R) were generated in $Na_v1.5$ channel using UCSF Chimera developed by the Resource for Biocomputing, Visualization, and Informatics at the University of California, San Francisco, with support from NIH P41-GM103311 (Pettersen et al., 2004). Molecular docking of MEX to wild-type $Na_v1.5$ channel was performed using Rosetta Ligand (Bender et al., 2016). 1,000 models were generated. The top 200 models were selected using the highest DSASA values. From these top 200 models, the top 10 models were selected based on the lowest LigInterface values (Wisedchaisri et al., 2019). Visual analysis and images were generated using UCSF Chimera. Amino acids from $Na_v1.5$ that are directly interacting with MEX binding site 1 or MEX binding site 2 were indicated using a 4.0 Å cutoff distance from the MEX molecules.

Statistical Analysis

FitMaster (HEKA Elektronik, Lambrecht/Pfalz Germany), Excel (Microsoft, Seattle, WA), and GraphPad Prism5 (GraphPad Software, Inc., La Jolla, CA) were used for data acquisition and analysis. Data were presented as mean ± SEM. An unpaired Student's *t* test, and one-way analysis of variance (ANOVA) followed by Newman-Keuls multiple comparison test and Kruskal-Wallis followed by Dunn's *post hoc* test were used for the comparison of parametric and non-parametric data, respectively. $P < 0.05$ was considered statistically significant.

RESULTS

Characterization of the LQT3 Patients

A 15-year-old female was admitted because of recurrent transient loss of consciousness over 9 years. She has a family history of sudden cardiac death in three relatives, and another live relative had documented syncope but was not willing to accept any evaluation. The proband had been diagnosed with epilepsy during the past 5 years and was prescribed with lamotrigine and phenytoin, with reduced frequency of syncope from several times a year to one to two times a year. At presentation, her ECG showed remarkable prolonged corrected QT (QTc) intervals of 487–640 ms in sinus rhythm with ventricular rate of 50–72 beats per minute (bpm) and periodic atrioventricular (AV) block with 2:1 AV conduction (**Figure 1A**). A 24-h Holter monitoring documented 2:1 AV block with a ventricular rate of 42 bpm and 723 premature ventricular contractions (PVCs) with two morphologies and one episode of TdP. Her electroencephalogram was normal. Following intravenous administration of LID, the QTc interval was shortened from 487 to 454 ms (**Figure 1A**), and the 2:1 AV block disappeared. The patient was preliminarily diagnosed with congenital LQT3 based on the baseline ECG and the response to

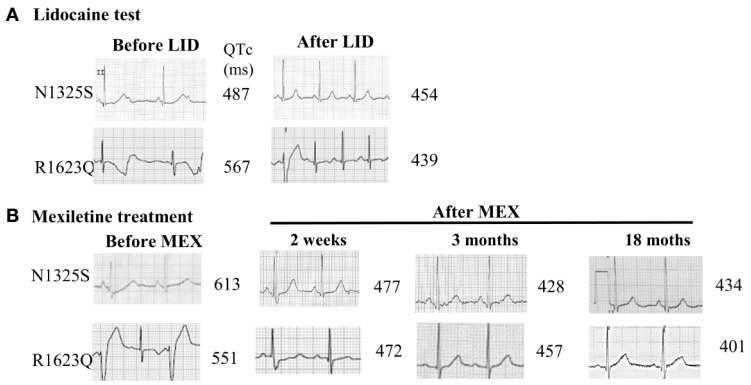

FIGURE 1 | ECG records from lead II in LQT3 patients before and after lidocaine test and oral mexiletine treatment. **(A)** ECG records from lead II in LQT3 patients before treatment showed prolonged QTc interval and combined with a 2:1 atrioventricular conduction block (upper panel), the lidocaine test shortened the QTc interval. **(B)** After treatment with oral mexiletine, ECG showed a gradually shortening and normalized QTc interval in follow-up period.

LID, and was treated with oral MEX alone at 200 mg daily. She refused implantable cardioverter defibrillator (ICD) therapy. This patient was followed up for 5 years with no episode of syncope and normal ECG recordings. Her QTc intervals in regular ECG and Holter monitoring remained between 477 to 434 ms (**Figure 1B**). AN1325S mutation of *SCN5A* gene, which was previously reported as a LQT3 causative mutation, was confirmed by molecular genetics.

A 6-year-old boy was admitted for frequent episodes of syncope in last 7 months, which often occurred at rest, and there was no family history of syncope or sudden cardiac death. The 24-h Holter monitoring documented a total of 69,388 ventricular ectopic beats with 55,067 single PVC, 1,880 paired PVCs, and 2,526 episodes of ventricular tachycardia (the longest episode of TdP lasted for 80.3 s). His ECG showed prolonged QTc intervals of 551–567 ms with frequent PVCs (**Figures 1A, B**). Following intravenous administration of LID, the QTc interval was shortened from 567 to 439 ms, and ventricular arrhythmias were decreased (**Figure 1A**). He was treated with oral MEX at 300 mg combined with 40 mg propranolol daily. During 2 years' follow-up, no syncope occurred, and his QTc intervals showed a gradually shorter trend from 472 to 401 ms (**Figure 1B**). Furthermore, the 24-h Holter recordings after 1, 4, and 18 months showed 1,962, 18, and 0 PVCs, respectively, without any ventricular tachycardia. Genetics test indicated an R1623Q mutation of *SCN5A* gene, which was reported as a LQT3 causative mutation.

Biophysical Properties of the WT and Mutant Channels

Though MEX may inhibit late I_{Na} in LQT3 patients carrying *SCN5A* mutations, some LQT3 patients with life-threatening arrhythmias were reported to be non-responsive to MEX, and the QTc intervals were not shortened by MEX in some mutations, including M1652R (Ruan et al., 2007). Here, the biophysical properties of three *SCN5A* mutations, i.e., N1325S and R1623Q (identified as MEX-sensitive mutations in the LQT3 patients in this study) and a previously reported MEX-insensitive missense mutation, M1652R, were investigated and compared. WT, N1325S, R1623Q, and M1652R mutant sodium channels were expressed in HEK293 cells, and their biophysical properties were measured by whole-cell patch-clamp techniques. Typical voltage-gated sodium currents were elicited in all channels and rapidly activated and inactivated by a series of depolarizing test potentials (**Figures 2A, B**). No significant differences in maximal peak sodium current density were observed among these channels. As shown in **Figure 2** and **Table 1**, there was a significant negative shift of steady-state inactivation curves of R1623Q mutant channel, i.e., more channels are inactivated at the holding potential of -90 mV, suggesting that R1623Q mutation may alter the expression or stability of $Na_v1.5$ channel.

In contrast, compared to the WT channel, the steady-state activation curve of the N1325S channel was shifted by 7.9 mV toward more negative potentials (**Figure 2C** and **Table 1**), suggesting that N1325S mutant channels open at more negative membrane potentials, resulting in increased availability of the channels (Olesen et al., 2012). No significant differences in steady-state activation were observed between the WT and R1623Q or M1652R channels (**Figure 2C** and **Table 1**). However, both R1623Q and M1652R changed the steady-state inactivation curves of the channel. The R1623Q caused a negative shift of steady-state inactivation curves by 15.2 mV compared with WT channel. In contrast, the steady-state inactivation curves of the M1652R channels were positively shifted by 5.6 mV relative to the WT channel. No significant change was observed between the WT and N1325S channel in the steady-state inactivation (**Figure 2D** and **Table 1**).

The time course of recovery from inactivation was investigated by a two-pulse protocol. A 500 ms conditioning pulse (-20 mV) was used to induce inactivation followed by a test pulse (-20 mV) after returning to -90 mV for a variable interval to allow channels to transit from the inactivated state. There were no significant differences in the recovery kinetics among the four different channels (**Figure 2E** and **Table 1**). Finally, the window current of peak sodium current, resulting from the overlap of the activation and inactivation curves, was larger in all three mutant channels than that in WT ($P < 0.05$, **Figures 2F–H**).

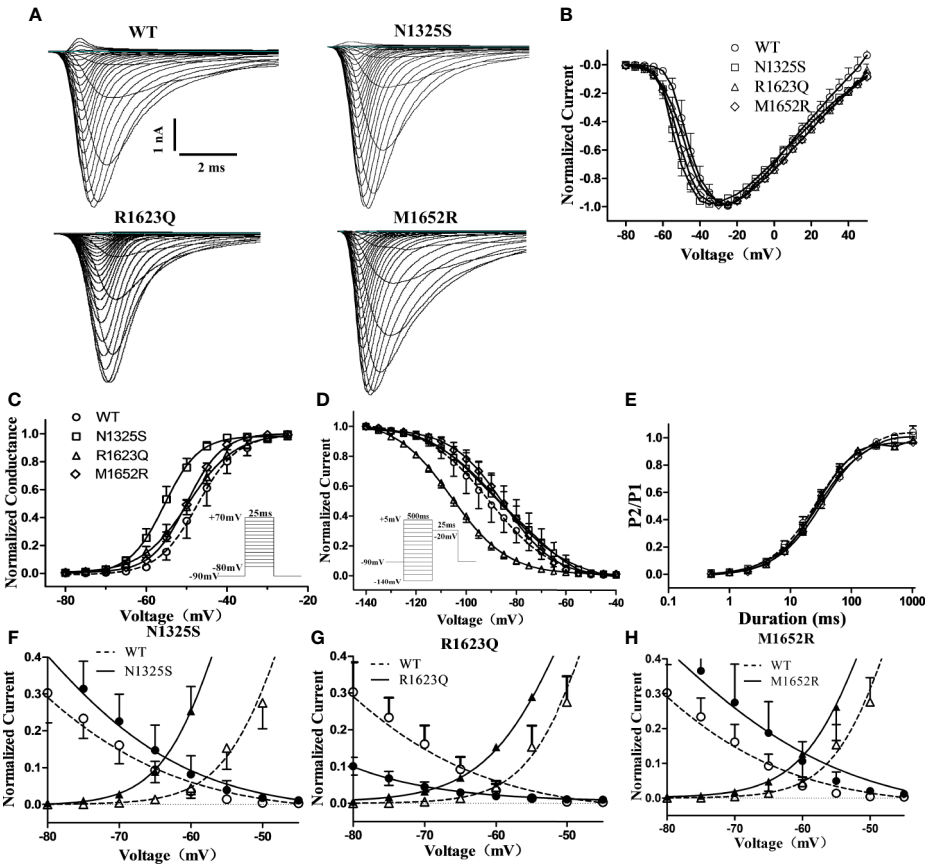

FIGURE 2 | Electrophysiological characterization of WT and mutant SCN5A channels' peak sodium current. **(A)** Represent traces of sodium current of WT and mutant channels. **(B)** Normalized I–V relationships of WT and mutant channels. Steady-state activation **(C)** and inactivation **(D)** curves of peak sodium current were determined with the inset protocol and fitted with a Boltzmann. **(E)** Time course of recovery from inactivation was fitted with a bi-exponential function. **(F–H)** Overlapping of activation and inactivation curve enlarged to show the window current of peak sodium current of mutant channels.

TABLE 1 | Biophysical properties of mutant channels and inhibition of late I_{Na} by drugs.

	Activation			Inactivation			Recovery			
	$V_{1/2}$ (mV)	Slope, κ (mV)	n	$V_{1/2}$ (mV)	Slope, κ (mV)	n	A1	τ_{fast} (ms)	τ_{slow} (ms)	n
WT	-47.3 ± 1.0	4.8 ± 0.8	7	-90.7 ± 1.8	-12.9 ± 1.8	6	0.32	24.0	164.0	7
N1325S(control)	-55.2 ± 0.5*	4.1 ± 0.6	13	-86.1 ± 1.3	-14.3 ± 2.8	13	0.35	23.6	170.0	13
N1325S(MEX)	-55.3 ± 0.5	4.9 ± 0.4	6	-95.62 ± 0.5†	-10.6 ± 0.5	5	0.09	67.2†	762.2†	6
R1623Q(control)	-49.6 ± 0.6	5.8 ± 0.6	7	-105.9 ± 0.7*	-11.3 ± 0.6	6	0.16	35.3	2356.3	9
R1623Q(MEX)	-51.7 ± 0.7	6.3 ± 0.7	6	-110.0 ± 0.8†	-11.0 ± 0.7	6	0.16	52.3	5007.5†	7
M1652R(control)	-49.9 ± 0.8	4.4 ± 0.3	6	-85.1 ± 1.0*	-14.4 ± 2.2	6	0.12	37.7	370.8	8
M1652R(MEX)	-52.2 ± 0.7	5.6 ± 0.6	6	-91.4 ± 2.0†	-16.0 ± 2.2	6	0.16	49.1	904.2†	8

*$P < 0.05$ compared with WT; †$P < 0.05$ compared with control.

Since late I_{Na} plays a critical role in LQT syndrome, we investigated the amplitude of late I_{Na} in these three mutant channels. Compared with the WT channel, all three mutations, N1325S, R1623Q, and M1652R channels, displayed a significantly increased late I_{Na} measured at 200 ms after depolarizing to -20 mV, with the greatest amplitude of late I_{Na} in the M1652R channel (**Figure 3**, -0.41 ± 0.14, -1.33 ± 0.11, -1.44 ± 0.27, and -2.23 ± 0.31 pA/pF, respectively, for WT, N1325S, R1623Q, and M1652R. n = 13, 15, 7, and 9. P < 0.05 vs. WT and M1652R, respectively).

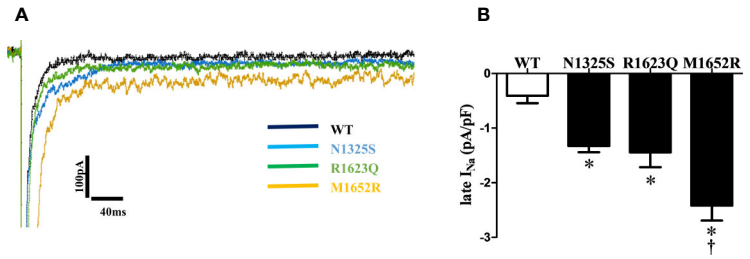

FIGURE 3 | N1325S, R1623Q, and M1652R mutations increased late I_{Na}. **(A)** Representative traces of late I_{Na} in WT, N1325S, R1623Q and M1652R mutant channels. **(B)** Bar graph summarized late I_{Na} at 200 ms, and showed that all three mutations increased late I_{Na} but with the greatest amplitude of late I_{Na} in the M1652R channel. Late I_{Na} was measured at 200 ms after a voltage step from -90 to -20 mV. *P < 0.05, compared with WT; †P < 0.05, M1652R value versus N1325S and R1623Q.

Electrophysiological Effects of MEX on Mutant Channels

The effects of MEX on electrophysiological properties of N1325S, R1623Q, and M1652R channels were determined at a clinically relevant concentration of 10 μM (Wang et al., 1997). Though the steady-state activation of N1325S, R1623Q, and M1652R channels was not significantly affected by MEX (**Figure 4A** and **Table 1**), MEX caused a significant hyperpolarizing shift of steady-state inactivation curves in N1325S, R1623Q, and M1652R mutant channels by 11.6, 4.1, and 6.3 mV, respectively (P < 0.05, **Figure 4B** and **Table 1**). In addition, MEX delayed recovery process (**Figure 4C**) and reduced peak

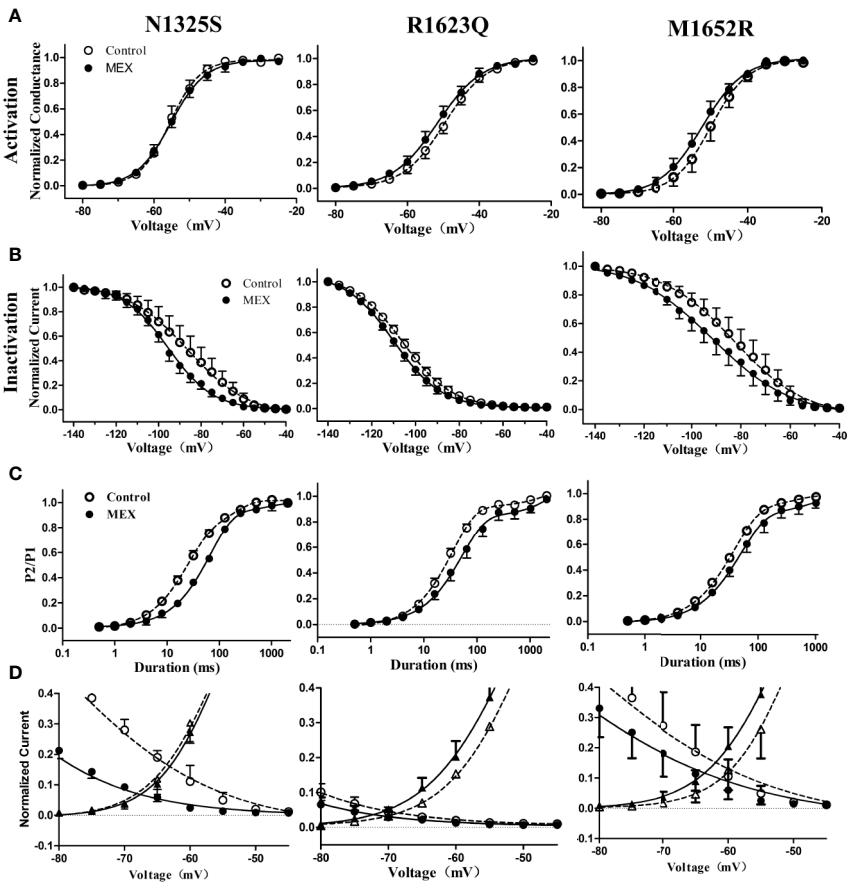

FIGURE 4 | Effects of mexiletine (MEX) on the activation, inactivation, and recovery of mutant channels' peak sodium current. Voltage dependence of activation **(A)** and inactivation **(B)** for mutant sodium channels in the absence and presence of MEX (10 μM). **(C)** Time course of recovery from inactivation under control and MEX was fitted using a bi-exponential function. **(D)** Window currents of peak sodium current in the absence (open symbols) or presence (filled symbols) of MEX (10 μM).

sodium's window currents of all three mutant channels (**Figure 4D**). Thus, these effects could collaborate to reduce the availability of sodium channels

The effects of MEX on late I_{Na} were further investigated. Shown in **Figure 5** are the representative records of I_{Na} (primarily late I_{Na}, a and b) and summarized data of late I_{Na} before and after MEX (n = 5–9, c) in N1325S, R1623Q and M1652R mutant channels (A, B, and C). Although MEX had differential clinical efficacy in patients with these mutations, MEX (10 μM) inhibited late I_{Na} in all three mutations. Furthermore, MEX exhibited a stronger inhibitory effect on the late I_{Na} of N1325S and R1623Q (by 68.12 ± 2.94% and 63.28 ± 4.29%, respectively) than that of M1652R mutant channels (by 38.82 ± 6.38%, $P < 0.05$ compared to that of N1325S and R1623Q). These results are consistent with the clinical response that MEX exhibited diminished effects on the MEX-insensitive mutant, M1652R, compared with the other two mutations.

A gradually shortened QTc interval and reduced number of PVCs were observed over time with MEX treatment, esp. in the severe case of R1623Q mutation. Late I_{Na} in cells expressing the three mutant channels was measured after incubation with MEX (10 μM) for 10 min, and 3-, 12-, 24-, and 48-h. Compared to the control (no MEX), MEX (10 μM) suppressed the augmented late I_{Na} of all mutant channels after incubated with MEX for 10 min or longer (n = 5–9, **Figure 6**). Furthermore, the inhibitory effects were greater in N1325S and R1623Q mutant channels than in M1652R mutation with longer incubation time. Thus, MEX

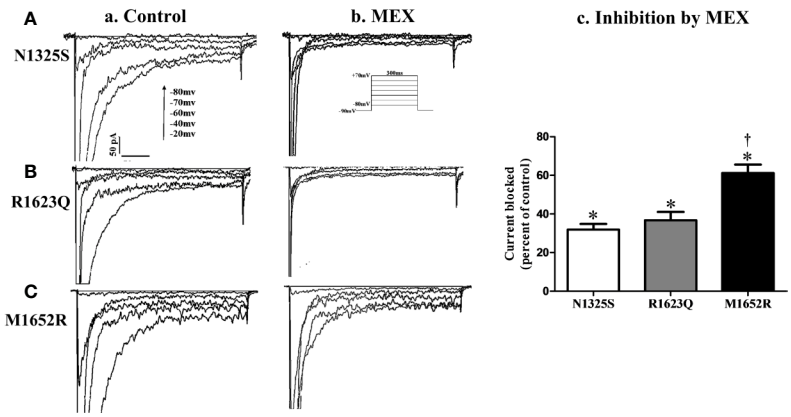

FIGURE 5 | Effects of mexiletine (MEX) on late I_{Na} of mutant channels. Representative traces of late I_{Na} recorded in the absence **(a)** or presence **(b)** of MEX (10 μM) at various depolarization voltages for N1325S **(A)**, R1623Q **(B)**, and M1652R **(C)** mutant channels, respectively. Summarized data of the percentage block of late I_{Na} by MEX was presented in panel **(c)**. Late I_{Na} was recorded at 10 min after MEX application and measured at 200 ms after a voltage step from -90 to -20 mV. Control values (no MEX) of late I_{Na} for N1325S, R1623Q, and M1652R were -1.33 ± 0.13, -1.22 ± 0.20, and -2.06 ± 0.21 pA/pF, respectively. N = 5–9. $^{*}P < 0.05$ compared with control; $^{\dagger}P < 0.05$ compared with N1325S and R1623Q.

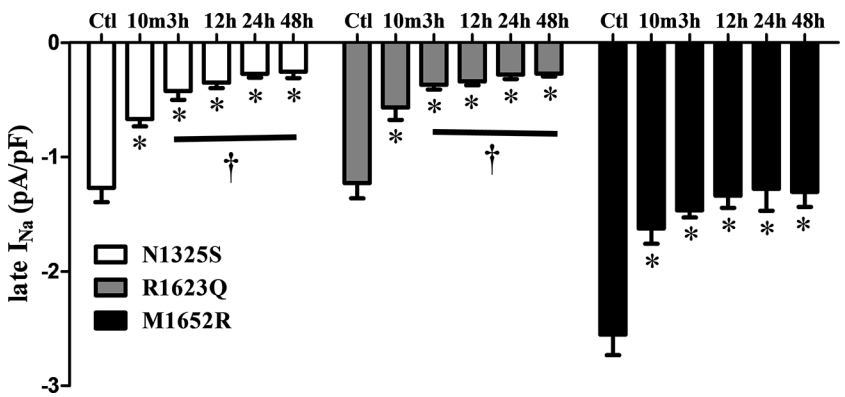

FIGURE 6 | Mexiletine (MEX) inhibited late I_{Na} of N1325S and R1623Q mutant channels in a time-dependent manner. Late I_{Na} was measured from the cells with three individual mutations either without MEX treatment (control) or after incubation with 10 μM MEX for 10 min, and 3, 12, 24, and 48 h, respectively. MEX (10 μM) suppressed late I_{Na} of all three mutant channels after incubated with MEX for 10 min. The inhibition effects were more pronounced in N1325S and R1623Q mutant channels than that in M1652R mutation with the increases in incubation time. N = 5–9. $^{*}P < 0.05$ compared with control; $^{\dagger}P < 0.05$ compared with 10 min' exposure of MEX.

inhibited late I_{Na} in a time-dependent manner, suggesting that with longer incubation time, the inhibitory effect increased in MEX-sensitive mutations.

Structural Modeling of MEX Binding to Mutant $Na_v1.5$

Structural modeling of MEX binding to $Na_v1.5$ provided important molecular insights into how MEX interacts with the channel. The top 10 energetically favorable MEX - $Na_v1.5$ models were analyzed revealing two possible binding sites within the Na_v channel pore. **Figures 7A, B** show both of the MEX binding sites occupied, with each site predicted by five models of the top 10 MEX - $Na_v1.5$ models, making both sites equally possible. MEX is depicted in dark blue space filling model to illustrate the size of MEX molecule when bound to the channel. For orientation purposes, MEX binding site 1 is located in **Figure 7A** above MEX binding site 2. Amino acid residues (N1325 and R1623) are shown in red, and amino acid residue (M1652) is shown in magenta. Domain (D)I, DII, DIII, and DIV are shown as ribbons in cyan, green, brown, and yellow, respectively. The voltage-sensing domain (VSD) and pore-forming domain (PD) regions of each domain are labeled. Currently, there are no high-resolution structures of an open and conductive state of $Na_v1.5$ channel; therefore, MEX binding to $Na_v1.5$ was based on a partially open and presumably inactivated state of $Na_v1.5$ channel (Nguyen et al., 2019).

The two MEX binding sites were formed by residues within the PD. **Figures 7C, D** shows a closer view of MEX binding site 1 and 2. Amino acid residues that directly contact binding site 1, 2, or both are shown in red, orange, and magenta, respectively (note that the amino acids colored in panels A and B are not the same as in panels C and D). MEX 1 and 2 molecules are shown in purple and pink, respectively while the heteroatoms on MEX 1, MEX 2, and amino acid cysteine are colored as follows: O = red, N = blue, S = yellow. The three mutations discussed in this paper are out of frame. MEX binding site 1 is formed by the S6 segments from all four domains (D) of the channel. The residues that directly contacted MEX include V405 and I408 (DI-S6), F934, L935, and L938 (DII-S6); I1466 and I1470 (DIII-S6); and V1764, Y1767, I1768, and I1771 (DIV-S6) (**Figure 7C**). MEX binding site 2 was located within the fenestration between DIII and DIV and formed by I1334, V1337, L1338, and C1341 (DIII-S5); T1461, L1462, and F1465 (DIII-S6); I1751, F1760, L1761, and V1764 (DIV-S6) (**Figure 7D**). We observed no evidence of two MEX molecules clashing with each other, despite a single residue (V1764) that binds both MEX molecules. Therefore, it is possible that both sites could be simultaneously occupied by two MEX molecules (**Figures 7C, D**).

Based on predicted MEX binding sites in our MEX - $Na_v1.5$ models, there were no direct interactions between MEX and the three LQT3 mutated amino acid residues (N1325S, R1623Q, and M1652R). The findings suggested that these mutations altered the sensitivity of $Na_v1.5$ to MEX through allosteric mechanisms by changing the conformation of $Na_v1.5$ to become more or less favorable for MEX binding. N1325S in S4-S5 linker in DIII resulted in the substitution from large to smaller side chain. In addition, the side chain of N1325 residue is exposed to solvent in the inactivated state of $Na_v1.5$ channel. Substitutions of side chains that are exposed to solvent are not likely to significantly impact the overall structure of the channel. **Figure 7E** shows the wild type N1325 residue, while **Figure 7F** shows the optimal position of the N1325S substitution. There is no evidence that the inactivated state of N1325S $Na_v1.5$ channel would be disrupted (**Figures 7E, F**).

R1623 is the first arginine in the S4 segment in DIV VSD of $Na_v1.5$. The model suggests that the R1623Q substitution, a smaller and polar amino acid, might affect the S4 movement during channel gating and therefore affect inactivated state of $Na_v1.5$ (**Figures 7G, H**). The M1652 residue (in S4-S5 linker in DIV) has direct interactions with the α-helix immediately downstream from the isoleucine-phenylalanine-methionine (IFM) motif, the intracellular linker between DIII and DIV, which contributed to the fast inactivation gating mechanism of the channel. Specifically, M1652 was seen to interact with an aromatic amino acid Y1495 from the α-helix. This interaction is very favorable and allows for π stacking between the sulfur atom in M1652 and the aromatic ring of Y1495. Substitution of methionine to arginine (M1652R) resulted in the loss of this interaction. In addition, M1652R substitution is predicted to be disruptive as arginine has a much larger side chain that exhibits steric hindrance with residues Y1495 to K1500 in the α-helix (**Figures 7I, J**). This could be observed by the cloud of possible rotamer positions of the arginine side chain, whereby in the optimal position, it is very close to the α-helix backbone. The model suggests that M1652R mutation would be disruptive of the inactivated state and results in MEX-insensitive mutant $Na_v1.5$ channel. These findings suggest that, from the perspective of the channel structure, mutations exhibit variable effects on the inactivated state of $Na_v1.5$ channels, thus resulting in various affinity of MEX to sodium channels.

Distinct Drug Responses of Mutant Channels

RAN and ELE, novel sodium channel inhibitors that exhibit greater potency and selectivity than class Ib antiarrhythmic agents for late I_{Na}, have been shown to shorten the QTc interval in animal models and in patients with LQT3 (Chorin et al., 2016; Rajamani et al., 2016). Herein, we chose LID, MEX, RAN and ELE, as well as β blockers, propranolol, metoprolol, nadolol, to investigate their effects on these three mutant channels. As shown in **Figure 8** and **Table 2**, MEX, LID, RAN, ELE, and the β blocker propranolol, but not metoprolol and nadolol, significantly inhibited late I_{Na} *in vitro*. Inhibitory potency for late I_{Na} was quantified as the IC_{50} values calculated from the dose-response curves. Compared with the N1325S or R1623Q channel, the M1652R channel was much less sensitive to late I_{Na} inhibitors with greater IC_{50} values for MEX, LID, ELE, RAN, and propranolol.

DISCUSSION

In the present study, two severe cases of LQT3 were successfully treated with MEX and mechanisms underlying

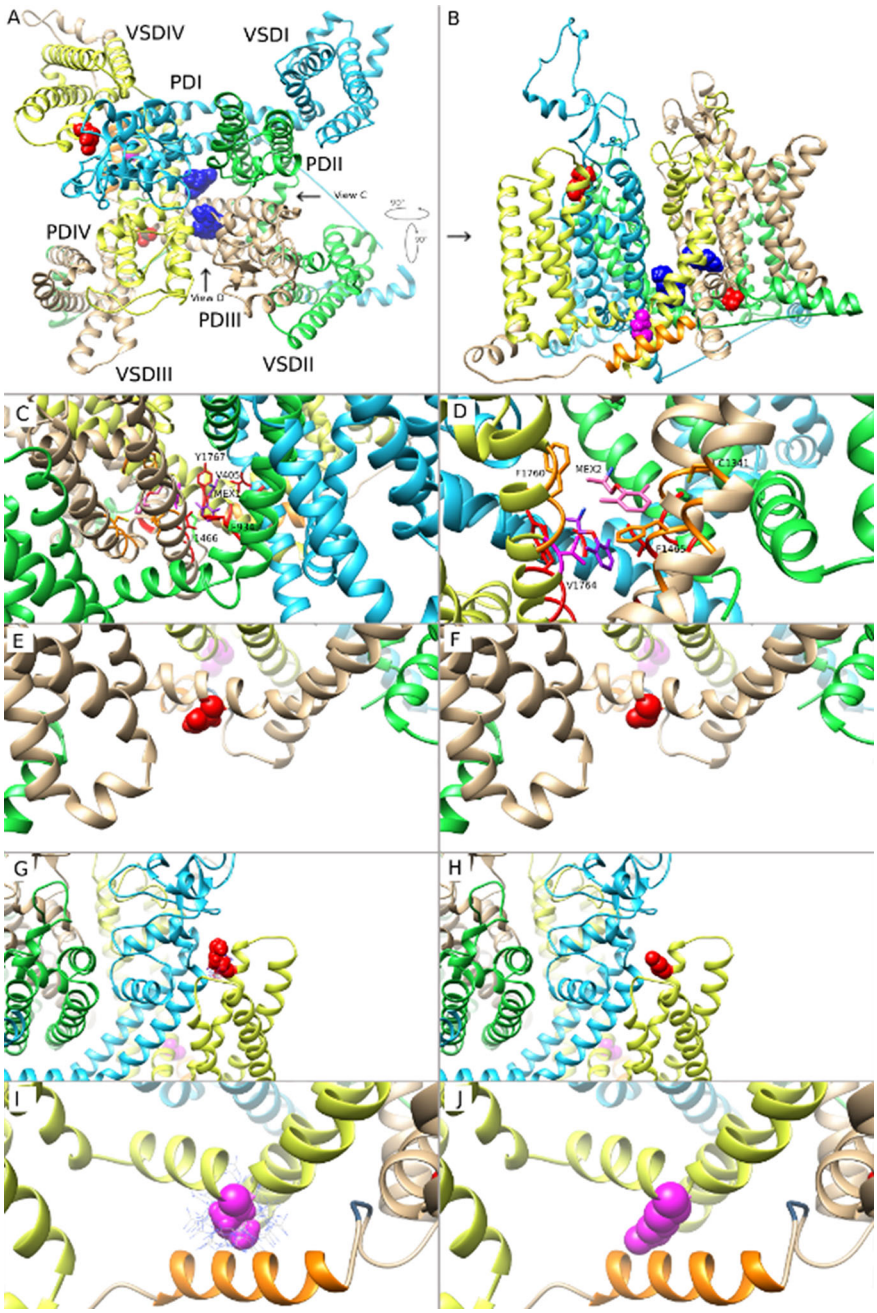

FIGURE 7 | Molecular modeling of mexiletine (MEX) binding to MEX-sensitive (N1325S, R1623Q) and -insensitive (M1652R) mutant channels. **(A)** A molecular model of wild-type (WT) $Na_v1.5$ in inactivated state, viewed from the extracellular side of the channel with MEX bound at two possible positions. **(B)** Side view of the channel with the three amino acids of interest facing the reader for clarity. **(C)** Closer view of MEX binding site 1. A single amino acid side chain in each binding region (S6 segments from all 4 domains) are labeled and colored. **(D)** Closer view of MEX binding site 2. Labels are specific to MEX binding site 2. A single amino acid side chain in each binding region (DIII-S5, DIII-S6, and DIV-S6) is labeled and shown. **(E**, **G**, **I)** Closer view of the three amino acid residues N1325, R1623, and M1652, respectively. **(F**, **H**, **J)**. Closer view of the optimal orientation for N1325S, R1623Q, and M1652R substitutions, respectively. Blue dots in panels **(I, J)** represent possible orientations of the M1652R substitution.

the phenotype and responsiveness to MEX were investigated. The prolonged QTc interval, recurrent syncope, and documented episode of TdP in the young girl with N1325S mutation in *SCN5A* were reversed completely after MEX administration. Lamotrigine and phenytoin were partially effective, probably due to their inhibitory effects on I_{Na}, specifically late I_{Na} (Chavez et al., 2015). LQTS is likely to be misdiagnosed with epilepsy because of the presentation of

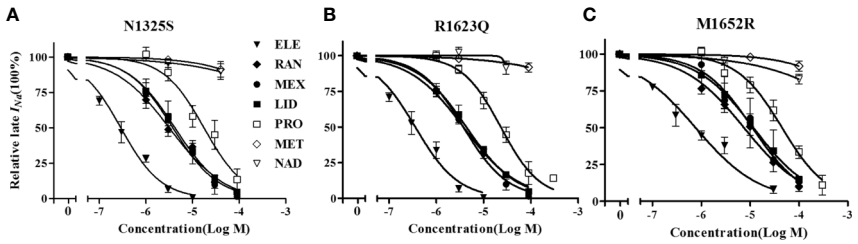

FIGURE 8 | The concentration-response relationships of drugs on late I_{Na} of mutant channels. **A-C**: Percentage inhibition of late INa in N1325S **(A)**, R1623Q **(B)** and M1652R **(C)** mutant channels in absence (0) and presence of increased concentrations of drugs. Late I_{Na} was measured at 200 ms after a voltage step from -90 mV to -20 mV. ELE, eleclazine; RAN, ranolazine; MEX, mexiletine; LID, lidocaine; PRO, propranolol; MET, metoprolol; NAD, nadolol.

TABLE 2 | Inhibition of late I_{Na} by drugs in mutant channels.

Drugs	N1325S		R1623Q		M1652R	
	IC_{50} (μM)	κ	IC_{50} (μM)	κ	IC_{50}(μM)	κ
MEX	3.77 ± 0.33	0.90 ± 0.07	3.27 ± 0.30	0.93 ± 0.06	11.14 ± 1.18*	0.84 ± 0.08
LID	4.14 ± 0.53	0.90 ± 0.11	4.32 ± 0.39	0.82 ± 0.06	11.66 ± 2.82*	0.74 ± 0.18
ELE	0.27 ± 0.05	0.92 ± 0.09	0.34 ± 0.04	0.89 ± 0.11	0.74 ± 0.12*	0.61 ± 0.08
RAN	3.14 ± 0.36	0.73 ± 0.08	3.73 ± 0.36	0.74 ± 0.07	7.47 ± 0.75*	0.69 ± 0.05
PRO	17.60 ± 1.81	1.00 ± 0.12	23.11 ± 2.35	1.06 ± 0.14	45.04 ± 5.69*	0.93 ± 0.11
MET	~11.56 mM	0.60 ± 0.64	~20.98 mM	0.44 ± 0.33	~4.20 mM	0.65 ± 0.49
NAD	~2.03 mM	0.38 ± 0.32	~0.51 mM	0.89 ± 0.44	~3.80 mM	0.43 ± 0.17

$P < 0.05$ compared with N1325S and R1623Q.

seizures, caused by cerebral hypoperfusion during ventricular arrhythmias. Indeed, mutations of *KCNQ1*, *KCNE1*, and *SCN5A* could also be found in certain epilepsy patients (Lupoglazoff et al., 2001). The AV block with 2:1 AV conduction block has been reported in patients with LQT2, LQT3, and LQT8 with an incidence of 4% in pediatric series and a greater than 50% probability of lethal arrhythmias within 6 months, regardless of the treatment (Lupoglazoff et al., 2001). The 2:1 AV conduction is likely due to the dramatic prolongation of ventricular repolarization, especially in His-Purkinje system, resulting in P wave falling on or before the preceding T wave, i.e. the effective refractive period in the AV junctional or His-Purkinje system (Rosenbaum and Acunzo, 1991; Pruvot et al., 1999). Hence, after shortening the QT interval with either LID or MEX, the functional AV block was reversed, as occurred in this patient. The boy harboring R1623Q mutation of *SCN5A* presented with not only extremely prolonged QTc interval but also large number of PVCs and episodes of TdP.

Utility of Intravenous Infusion of I_{Na} Blockers in Different LQT Syndrome Subtypes

Intravenous infusion of I_{Na} blockers, if available, may be a quick tool to differentiate patients with LQT3, and to predict the efficacy of long-term treatment with I_{Na} blockers. Moritoshi et al. reported that MEX induced greater QTc shortening in LQT3 patients than in LQT1 and LQT2 patients and concluded that MEX infusion test is a useful tool to distinguish LQT3 from LQT1 or LQT2 (Funasako et al., 2016). LID test was reported to be useful in distinguishing pathogenic LQT3 mutations from other *SCN5A* variants of uncertain significance (Anderson et al., 2017). Our study demonstrates that QTc interval was remarkably shortened and the arrhythmic activities were abolished with the intravenous injection of LID, suggesting that LID test may be useful in determining the efficacy of MEX and to provide a rapid control of TdP in severe cases. Considering the similarity between LID and MEX (Dumaine et al., 1996), these two patients were treated with oral MEX, which shortened the QTc interval to normal range and abolished ventricular arrhythmias and syncope associated with QT prolongation without the need of ICD implantation. Additionally, the QTc interval and PVCs of the patient with R1623Q mutation reduced gradually over the treatment period. It may suggest that MEX has an accumulation effect on late I_{Na}, possibly due to remodeling of the late I_{Na}, as shown in the two patients. Finally, future studies are required to further support that the use of LID test in identifying MEX-sensitive mutations in LQT3 patients.

Gating Changes in LQT3 Mutations

N1325S mutation in *SCN5A* is one of the earliest mutations reported to be associated with LQTS (Wang et al., 1995), in which asparagine is substituted by serine at position 1325 in the DIII/S4-S5 intracellular linker of $Na_v1.5$. The R1623Q mutation is located in the S4 segment in DIV VSD of $Na_v1.5$. The M1652R mutation, a MEX-insensitive mutation, is located in the DIV/S4-

S5 intracellular linker of the channel. Similar to previous studies (Ruan et al., 2007), gating defects were demonstrated in all three mutations.

In the current study, the gating properties of N1325S, R1623Q, and M1652R channels were studied in HEK293 cells. Typical voltage-gated sodium currents were elicited in all channels, though no significant differences in maximal peak sodium current density were observed among these channels. For R1623Q mutant channel, more channels are inactivated at a physiological holding potential (-90 mV) compared to the other two mutant channels. Therefore, R1623Q mutation may alter the expression or stability of $Na_v1.5$ channel. However, similar expression of WT and R1623Q channels was previously reported (Makita et al., 1998). Nonetheless, the use of heterologous expression system may not be the most suitable system to determine the expression, trafficking, and stability of the channels. Future studies in iPSC-derived cardiomyocytes or transgenic animals are needed to further interrogate for possible changes in the mutant channels.

A previous study has shown that MEX preferentially binds to the inactivated state of the sodium channel (Desaphy et al., 2001); therefore, mutations that favor the inactivated state may facilitate MEX binding to the channel with an increased clinical efficacy. Accordingly, MEX-sensitive mutation, R1623Q, causes a hyperpolarizing shift of the steady-state inactivation curve, which would favor the presence of the sodium channel in the inactivated state. In contrast, the MEX-insensitive mutation, M1652R, causes a depolarizing shift of steady-state inactivation curve. Therefore, our study supports the notion that the inactivated state of sodium channel may be an important factor that determines MEX sensitivity and the clinical response of MEX treatment. Indeed, this is consistent with the previous report (Ruan et al., 2007; (Moreno et al., 2019). The N1325S mutation, another MEX-sensitive mutation, causes a hyperpolarizing shift in the steady-state activation curve, increasing the activation of the channel.

Molecular Insights Into MEX Sensitivity

Molecular modeling of N1325S, R1623Q and M1652R mutations provides structural insights into possible mechanisms for how these mutations may alter the sensitivity of the $Na_v1.5$ channel to MEX. In addition, it also emphasizes the critical importance of future studies to resolve an open structure of human Na_v channel. Consistent with the electrophysiological findings, the molecular modeling suggests that the M1652R mutation affects the inactivated state of the channel (**Figure 7**). Based on the computational modeling, one possible mechanism of how M1652R results in MEX-insensitive channel is by not allowing the channel to fully inactivate and thus increasing the transition time from open to inactivated state. Mutation of R1623Q from a large basic amino acid to a smaller polar amino acid may affects the S4 movement during channel activation. The findings are consistent with our patch-clamp analyses where the R1623Q resulted in a hyperpolarizing shift of the steady-state inactivation curve and thus favoring the inactivated state. N1325S mutation may not significantly disrupt the inactivated state and the transition time from open to inactivated state is predicted to be faster. Thus, these two mutant channels favor inactivation state of channels and remain sensitive to MEX. However, $Na_v1.5$ structure in an open state channel is needed to provide further support. In addition, future studies are needed to reveal conformational changes of the channel between the drug-free and drug-bound states.

One previous report (Ruan et al., 2007) also reported that inactivated state of sodium channel favors inhibition by MEX, however, the peak, but not late I_{Na} was studied. Since the late I_{Na} plays critical roles in LQT3, we investigated the relationship of late I_{Na} and the patient's sensitivity to MEX. Multiple mechanisms may result in an increase in late I_{Na}. Single-channel records have revealed that channel bursting and late reopening are responsible for the generation of late I_{Na} in various mutations (Bennett et al., 1995; Dumaine et al., 1996). An additional mechanism for a sustained late current is the overlap between the channel activation and inactivation (Wang et al., 1996), resulting in a fraction of channels remaining open. Other mechanisms that may contribute to the late current include non-equilibrium gating processes causing channel re-opening due to more rapid recoveries from inactivation (Chadda et al., 2017). In our study, we found that all three mutations increased window currents of peak I_{Na} and late I_{Na} compared with the WT channel, with the largest late I_{Na} in M1652R compared to the two MEX-sensitive mutations (**Figure 3**). In view of the critical role of late I_{Na} in LQT3, this effect may account for the patients' phenotypes. There is no sign of mechanism of changes of channel re-opening, and late I_{Na} generated at -20 mV is out of voltage "window", so the augmented late I_{Na} are probably due to slower inactivation kinetics.

MEX has been shown to be effective in suppressing malignant ventricular arrhythmias and reducing the risk of sudden cardiac death in LQT3 patients and animal models. In addition, the prolonged APD and late I_{Na} of N1325S transgenic mice could be reversed by MEX (Tian et al., 2004). Although these three mutations showed distinct clinical responses to MEX, our results demonstrate that MEX has similar effects on all three mutations *in vitro*, including significant hyperpolarizing shift of steady-state inactivation curves, reduced window currents, and delayed recovery of channels into activated state (**Figure 4**). In accordance with these results, the augmented late I_{Na} in all three mutant channels was suppressed by MEX. Therefore, it can be concluded that MEX could suppressed late I_{Na} by stabilizing the inactivated state of the channel as evidenced by a hyperpolarizing shift in the steady-state inactivation curve and the slow recovery from inactivation.

A gradually shortened QT interval and reduced PVCs with treatment time for MEX-sensitive mutations, indicating that MEX might have an accumulation effect on late I_{Na}. MEX could suppress late I_{Na} of all three mutant channels after incubated with MEX for 10 min, but the inhibitory effects were more pronounced in N1325S and R1623Q mutant channels with longer incubation time. MEX may penetrant into the cell in a slow fashion through the membrane, possibly leading to the required longer incubation time and slower action in inhibiting late I_{Na}.

Effects of beta-blockers on LQT3 are controversial as they decrease the heart rate, which may result in the augmentation of

late I_{Na} (Wu et al., 2011). Propranolol blocks I_{Na} in a manner similar to local anesthetic drugs, which may contribute to its anti-arrhythmic effects in LQT3 patients (Bankston and Kass, 2010). In this study, we tested the effects of several clinical relevant medicines on late I_{Na} *in vitro*. As shown in **Figure 8** and **Table 2**, propranolol, but not metoprolol or nadolol, inhibited late I_{Na}. Therefore, if second drug is needed, non-selective beta-blockers with inhibitory effects on late I_{Na}, such as propranolol, rather than metoprolol and nadolol, would be preferred in patients with LQT 3.

The drug responses of different LQT3-causative mutations and the use-dependent block of peak I_{Na} was associated with the clinical efficacy of MEX in LQT3 (Ruan et al., 2007). As shown in **Table 2**, sodium channel blockers (LID, MEX, ELE, and RAN) and propranolol suppressed late I_{Na}, with ELE having the highest potency. In addition, the M1652R mutant channel showed reduced responsiveness to I_{Na} blockers and propranolol with IC_{50s} being about three times greater than that of N1325S and R1623Q. Though the patient with M1652R responded poorly to MEX treatment, MEX inhibited late I_{Na} of M1652R mutant channel *in vitro*. The IC_{50} of M1652R is ~3–4 fold higher than that of the other two mutations. In addition, M1652R exhibits greater amplitude of late I_{Na} with larger residual late I_{Na} after MEX application compared to N1325S and R1623Q. All these effects may account for the less clinical efficacy in patients harboring M1652R mutation. Thus, these findings suggested that drug screening in cells expressing disease-causing mutant channels would be helpful to predict the efficacy of drugs in LQT3 patients. Selective late I_{Na} blockers with a greater potency in inhibiting late I_{Na}, such as ELE, may be effective in patients with MEX-insensitive mutations, e.g., M1652R.

Na^+ channel inhibitors are supposed to bind to a local anesthetic site of Phe1760 and Tyr1767 in Nav1.5 (Kass and Moss, 2006). Mutations located in close to this binding site such as F1760A/Y1767A would disrupt the binding of drugs such as MEX, ELE, and propranolol (Sasaki et al., 2004; El-Bizri et al., 2018). The gating state of sodium channels also plays an important role in drug interaction (Desaphy et al., 2001). Furthermore, besides the gating properties, other factors such as therapeutic adherence, pharmacokinetic and metabolic factors of drugs, interaction among cardiac ion channels, and other modulators are also important determinants for the response to therapy. These factors may alone or in combination with each other contribute to the variable response to drug therapy. Development of more potent late I_{Na} inhibitors may be beneficial to patients with MEX insensitive mutations. Further large-scale investigations on these factors and whether this kind of current-specific treatment could reduce the need or delivery of shocks for ICD implantation are needed.

CONCLUSION

MEX suppresses late I_{Na} of N1325S, R1623Q, and M1652R mutations with abnormal gating properties of mutant channels and stabilizes the inactivated state of the channels through a hyperpolarizing shift of the steady-state inactivation curve and a slowed recovery from inactivation with greater potencies in N13255S and R1623Q than that in M1652R, which is consistent with the clinical response to MEX in patients. LID test, molecular modeling, and screening for more potent drugs are useful for the treatment of patients with different mutations of LQT3.

DATA AVAILABILITY STATEMENT

The raw data supporting the conclusions of this article will be made available by the authors, without undue reservation, to any qualified researcher.

ETHICS STATEMENT

The studies involving human participants were reviewed and approved by Ethics Committee of Peking University First Hospital. Written informed consent to participate in this study was provided by the participants' legal guardian/next of kin. Written, informed consent was obtained from the minor(s)' legal guardian for the publication of any potentially identifiable images or data included in this article.

AUTHOR CONTRIBUTIONS

GL, NC, and LW constructed the concept and designed the experimental protocol. GL, RW, C-YW, LR, and VY-Y performed experiments and molecular model. P-XH, S-DY, and X-QL collected clinical data. GL, RW, and DH analyzed data and interpreted results of experiments. GL and RW prepared figures and drafted this manuscript. GL, RW, LR, VY-Y, DH, NC, and LW edited and revised this manuscript. All authors contributed to the article and approved the submitted version.

FUNDING

This work was supported in part by grants from the National Natural Science Foundation of China (81270253, 81670304, 81430098, 81170156, 81770325 and 81930105), NIH R01 HL085727, NIH R01 HL085844, and NIH R01 HL137228 (NC), VA Merit Review Grant I01 BX000576 and I01 CX001490 (NC), NIH R01 HL137228-S1 (RW) and American Heart Association Predoctoral Fellowship Award 18PRE34030199 (LR).

REFERENCES

Anderson, H. N., Bos, J. M., Kapplinger, J. D., Meskill, J. M., Ye, D., Ackerman, M. J., et al. (2017). Lidocaine attenuation testing: An in vivo investigation of putative LQT3-associated variants in the SCN5A-encoded sodium channel. *Heart Rhythm*. 14 (8), 1173–1179. doi: 10.1016/j.hrthm.2017.04.020

Arbelo, E., Sarquella-Brugada, G., and Brugada, J. (2016). Gene-Specific Therapy for Congenital Long QT Syndrome: Are We There Yet? *J. Am. Coll. Cardiol.* 67 (9), 1059–1061. doi: 10.1016/j.jacc.2015.12.030

Bankston, J. R., and Kass, R. S. (2010). Molecular determinants of local anesthetic action of beta-blocking drugs: Implications for therapeutic management of long QT syndrome variant 3. *J. Mol. Cell Cardiol.* 48 (1), 246–253. doi: 10.1016/j.yjmcc.2009.05.012

Bender, B. J., Cisneros, A.3rd, Duran, A. M., Finn, J. A., Fu, D., Lokits, A. D., et al. (2016). Protocols for Molecular Modeling with Rosetta3 and RosettaScripts. *Biochemistry* 55 (34), 4748–4763. doi: 10.1021/acs.biochem.6b00444

Bennett, P. B., Yazawa, K., Makita, N., and George, A. L. Jr (1995). Molecular mechanism for an inherited cardiac arrhythmia. *Nature* 376 (6542), 683–685 doi: 10.1038/376683a0

Bohnen, M. S., Peng, G., Robey, S. H., Terrenoire, C., Iyer, V., Sampson, K. J., et al. (2017). Molecular Pathophysiology of Congenital Long QT Syndrome. *Physiol. Rev.* 97 (1), 89–134. doi: 10.1152/physrev.00008.2016

Chadda, K. R., Jeevaratnam, K., Lei, M., and Huang, C. L. (2017). Sodium channel biophysics, late sodium current and genetic arrhythmic syndromes. *Pflugers Arch.* 469 (5-6), 629–641. doi: 10.1007/s00424-017-1959-1

Chavez, P., Casso Dominguez, A., and Herzog, E. (2015). Evolving Electrocardiographic Changes in Lamotrigine Overdose: A Case Report and Literature Review. *Cardiovasc. Toxicol.* 15 (4), 394–398. doi: 10.1007/s12012-014-9300-0

Chorin, E., Hu, D., Antzelevitch, C., Hochstadt, A., Belardinelli, L., Zeltser, D., et al. (2016). Ranolazine for Congenital Long-QT Syndrome Type III: Experimental and Long-Term Clinical Data. *Circ. Arrhythm Electrophysiol.* 9 (10), e004370. doi: 10.1161/CIRCEP.116.004370

Desaphy, J. F., De Luca, A., Tortorella, P., De Vito, D., George, A. L.Jr, and Conte Camerino, D. (2001). Gating of myotonic Na channel mutants defines the response to mexiletine and a potent derivative. *Neurology* 57 (10), 1849–1857. doi: 10.1212/WNL.57.10.1849

Dumaine, R., Wang, Q., Keating, M. T., Hartmann, H. A., Schwartz, P. J., Brown, A. M., et al. (1996). Multiple mechanisms of Na+ channel–linked long-QT syndrome. *Circ. Res.* 78 (5), 916–924. doi: 10.1161/01.RES.78.5.916

El-Bizri, N., Xie, C., Liu, L., Limberis, J., Krause, M., Hirakawa, R., et al. (2018). Eleclazine exhibits enhanced selectivity for LQT3-associated late INa. *Heart Rhythm*. 15 (2), 277–286. doi: 10.1016/j.hrthm.2017.09.028

Funasako, M., Aiba, T., Ishibashi, K., Nakajima, I., Miyamoto, K., Inoue, Y., et al. (2016). Pronounced Shortening of QT Interval With Mexiletine Infusion Test in Patients With Type 3 Congenital Long QT Syndrome. *Circ. J.* 80 (2), 340–345. doi: 10.1253/circj.CJ-15-0984

Garcia-Elias, A., and Benito, B. (2018). Ion Channel Disorders and Sudden Cardiac Death. *Int. J. Mol. Sci.* 19 (3), 692. doi: 10.3390/ijms19030692

George, A. L.Jr. (2005). Inherited disorders of voltage-gated sodium channels. *J. Clin. Invest.* 115 (8), 1990–1999. doi: 10.1172/JCI25505

Huang, C. L., Wu, L., Jeevaratnam, K., and Lei, M. (2020). Update on antiarrhythmic drug pharmacology. *J. Cardiovasc. Electrophysiol.* 31, 579–592. doi: 10.1111/jce.14347

Kass, R. S., and Moss, A. J. (2006). Mutation-specific pharmacology of the long QT syndrome. *Handb. Exp. Pharmacol.* 171, 287–304. doi: 10.1007/3-540-29715-4_11

Lupoglazoff, J. M., Cheav, T., Baroudi, G., Berthet, M., Denjoy, I., Cauchemez, B., et al. (2001). Homozygous SCN5A mutation in long-QT syndrome with functional two-to-one atrioventricular block. *Circ. Res.* 89 (2), E16–E21. doi: 10.1161/hh1401.095087

Makita, N., Shirai, N., Nagashima, M., Matsuoka, R., Yamada, Y., Tohse, N., et al. (1998). A de novo missense mutation of human cardiac Na+ channel exhibiting novel molecular mechanisms of long QT syndrome. *FEBS Lett.* 423, 5–9. doi: 10.1016/S0014-5793(98)00033-7

Moreno, J. D., Zhu, W., Mangold, K., Chung, W., and Silva, J. R. (2019). A Molecularly Detailed NaV1.5 Model Reveals a New Class I Antiarrhythmic Target. *JACC Basic Transl. Sci.* 4, 736–751. doi: 10.1016/j.jacbts.2019.06.002

Moss, A. J., Zareba, W., Hall, W. J., Schwartz, P. J., Crampton, R. S., Benhorin, J., et al. (2000). Effectiveness and limitations of beta-blocker therapy in congenital long-QT syndrome. *Circulation* 101 (6), 616–623. doi: 10.1161/01.CIR.101.6.616

Nguyen, P. T., DeMarco, K. R., Vorobyov, I., Clancy, C. E., and Yarov-Yarovoy, V. (2019). Structural basis for antiarrhythmic drug interactions with the human cardiac sodium channel. *Proc. Natl. Acad. Sci. U.S.A.* 116 (8), 2945–2954. doi: 10.1073/pnas.1817446116

Olesen, M. S., Yuan, L., Liang, B., Holst, A. G., Nielsen, N., Nielsen, J. B., et al. (2012). High prevalence of long QT syndrome-associated SCN5A variants in patients with early-onset lone atrial fibrillation. *Circ. Cardiovasc. Genet.* 5 (4), 450–459. doi: 10.1161/CIRCGENETICS.111.962597

Pettersen, E. F., Goddard, T. D., Huang, C. C., Couch, G. S., Greenblatt, D. M., Meng, E. C., et al. (2004). UCSF Chimera–a visualization system for exploratory research and analysis. *J. Comput. Chem.* 25 (13), 1605–1612. doi: 10.1002/jcc.20084

Priori, S. G., Wilde, A. A., Horie, M., Cho, Y., Behr, E. R., Berul, C., et al. (2013). HRS/EHRA/APHRS expert consensus statement on the diagnosis and management of patients with inherited primary arrhythmia syndromes: document endorsed by HRS, EHRA, and APHRS in May 2013 and by ACCF, AHA, PACES, and AEPC in June 2013. *Heart Rhythm* 10 (12), 1932–1963. doi: 10.1016/j.hrthm.2013.05.014

Pruvot, E., De Torrente, A., De Ferrari, G. M., Schwartz, P. J., and Goy, J. J. (1999). Two-to-one AV block associated with the congenital long QT syndrome. *J. Cardiovasc. Electrophysiol.* 10 (1), 108–113. doi: 10.1111/j.1540-8167.1999.tb00647.x

Rajamani, S., Liu, G., El-Bizri, N., Guo, D., Li, C., Chen, X. L., et al. (2016). The novel late Na (+) current inhibitor, GS-6615 (eleclazine) and its anti-arrhythmic effects in rabbit isolated heart preparations. *Br. J. Pharmacol.* 173 (21), 3088–3098. doi: 10.1111/bph.13563

Rosenbaum, M. B., and Acunzo, R. S. (1991). Pseudo 2:1 atrioventricular block and T wave alternans in the long QT syndromes. *J. Am. Coll. Cardiol.* 18 (5), 1363–1366. doi: 10.1016/0735-1097(91)90560-V

Ruan, Y., Liu, N., Bloise, R., Napolitano, C., and Priori, S. G. (2007). Gating properties of SCN5A mutations and the response to mexiletine in long-QT syndrome type 3 patients. *Circulation* 116 (10), 1137–1144. doi: 10.1161/CIRCULATIONAHA.107.707877

Sasaki, K., Makita, N., Sunami, A., Sakurada, H., Shirai, N., Yokoi, H., et al. (2004). Unexpected mexiletine responses of a mutant cardiac Na+ channel implicate the selectivity filter as a structural determinant of antiarrhythmic drug access. *Mol. Pharmacol.* 66 (2), 330–336. doi: 10.1124/mol.66.2.330

Shimizu, W., and Antzelevitch, C. (2000). Differential effects of beta-adrenergic agonists and antagonists in LQT1, LQT2 and LQT3 models of the long QT syndrome. *J. Am. Coll. Cardiol.* 35 (3), 778–786. doi: 10.1016/S0735-1097(99)00582-3

Tian, X. L., Yong, S. L., Wan, X., Wu, L., Chung, M. K., Tchou, P. J., et al. (2004). Mechanisms by which SCN5A mutation N1325S causes cardiac arrhythmias and sudden death in vivo. *Cardiovasc. Res.* 61 (2), 256–267. doi: 10.1016/j.cardiores.2003.11.007

Wallace, E., Howard, L., Liu, M., O'Brien, T., Ward, D., Shen, S., et al. (2019). Long QT Syndrome: Genetics and Future Perspective. *Pediatr. Cardiol.* 40 (7), 1419–1430. doi: 10.1007/s00246-019-02151-x

Wang, Q., Shen, J., Li, Z., Timothy, K., Vincent, G. M., Priori, S. G., et al. (1995). Cardiac sodium channel mutations in patients with long QT syndrome, an inherited cardiac arrhythmia. *Hum. Mol. Genet.* 4 (9), 1603–1607. doi: 10.1093/hmg/4.9.1603

Wang, D. W., Yazawa, K., George, A. L.Jr, and Bennett, P. B. (1996). Characterization of human cardiac Na+ channel mutations in the congenital long QT syndrome. *Proc. Natl. Acad. Sci. U. S. A.* 93 (23), 13200–13205. doi: 10.1073/pnas.93.23.13200

Wang, D. W., Yazawa, K., Makita, N., George, A. L. Jr, and Bennett, P. B. (1997). Pharmacological targeting of long QT mutant sodium channels. *J. Clin. Invest.* 99 (7), 1714–1720. doi: 10.1172/JCI119335

Wilde, A. A., Moss, A. J., Kaufman, E. S., Shimizu, W., Peterson, D. R., Benhorin, J., et al. (2016). Clinical Aspects of Type 3 Long-QT Syndrome: An International Multicenter Study. *Circulation* 134 (12), 872–882. doi: 10.1161/CIRCULATIONAHA.116.021823

Wisedchaisri, G., Tonggu, L., McCord, E., Gamal El-Din, T. M., Wang, L., Zheng, N., et al. (2019). Resting-State Structure and Gating Mechanism of a Voltage-Gated Sodium Channel. *Cell* 178 (4), 993–1003 e12. doi: 10.1016/j.cell.2019.06.031

Wu, L., Ma, J., Li, H., Wang, C., Grandi, E., Zhang, P., et al. (2011). Late sodium current contributes to the reverse rate-dependent effect of IKr inhibition on ventricular repolarization. *Circulation* 123 (16), 1713–1720. doi: 10.1161/CIRCULATIONAHA.110.000661

Yu, S., Li, G., Huang, C. L., Lei, M., and Wu, L. (2018). Late sodium current associated cardiac electrophysiological and mechanical dysfunction. *Pflugers Arch.* 470 (3), 461–469. doi: 10.1007/s00424-017-2079-7

Conflict of Interest: The authors declare that the research was conducted in the absence of any commercial or financial relationships that could be construed as a potential conflict of interest.

frontiers in Pharmacology

REVIEW
published: 02 November 2020
doi: 10.3389/fphar.2020.579596

Hysteretic Behavior in Voltage-Gated Channels

Carlos A. Villalba-Galea and Alvin T. Chiem*

Department of Physiology and Pharmacology, Thomas J. Long School of Pharmacy, University of the Pacific, Stockton, CA, United States

An ever-growing body of evidence has shown that voltage-gated ion channels are likely molecular systems that display hysteresis in their activity. This phenomenon manifests in the form of dynamic changes in both their voltage dependence of activity and their deactivation kinetics. The goal of this review is to provide a clear definition of hysteresis in terms of the behavior of voltage-gated channels. This review will discuss the basic behavior of voltage-gated channel activity and how they make these proteins into systems displaying hysteresis. It will also provide a perspective on putative mechanisms underlying hysteresis and explain its potential physiological relevance. It is uncertain whether all channels display hysteresis in their behavior. However, the suggested notion that ion channels are hysteretic systems directly collides with the well-accepted notion that ion channel activity is stochastic. This is because hysteretic systems are regarded to have "memory" of previous events while stochastic processes are regarded as "memoryless." This review will address this apparent contradiction, providing arguments for the existence of processes that can be simultaneously hysteretic and stochastic.

Keywords: hysteresis, voltage-gated channels, voltage-sensing domain, voltage-sensitive phosphatases, modal gating, mode shift, voltage-sensing domain relaxation

OPEN ACCESS

Edited by:
Mounir Tarek,
Centre National de la Recherche Scientifique (CNRS), France

Reviewed by:
David Fedida,
University of British Columbia, Canada
Roope Mannikko,
University College London, United Kingdom

****Correspondence:***
Carlos A. Villalba-Galea
cvillalbagalea@pacific.edu

Specialty section:
This article was submitted to Pharmacology of Ion Channels and Channelopathies, a section of the Frontiers in Pharmacology

Received: *02 July 2020*
Accepted: *21 September 2020*
Published: *02 November 2020*

Citation:
Villalba-Galea CA and Chiem AT (2020) Hysteretic Behavior in Voltage-Gated Channels. Front. Pharmacol. 11:579596. doi: 10.3389/fphar.2020.579596

INTRODUCTION

When thinking about a physical or chemical system that responds to a "stimulus," it is commonly assumed that such system would display a constant activity-vs.-stimulus relationship. For instance, imagine a ligand-activated receptor with one binding site and an affinity of 1 μM for an agonist ligand. Adding 100 μM of such ligand will result in 99% of ligand-bound receptors, leading to their activation. On the other hand, decreasing the concentration to 0.01 μM of the agonist will result in less than 1% of ligand-bound receptors, deactivating these proteins. In theory, the level of activity of the receptor will only depend on the current concentration of the agonist ligand. This will always be the case regardless of how the ligand concentration changes. In other words, the receptor does not "remember" what happened before the ligand was at the current concentration, what the concentration of the ligand had been in the past, or what levels of activation were previously reached. This lack of "memory" of the receptors is the consequence of the ligand binding and activation being stochastic processes, unaffected by previous exposures of the receptor to the ligand.

In the case of voltage-gated channels, an analogous scenario is established when considering that the electrical field across the plasma membrane acts as the "stimulus" that drives channel activation and deactivation. As an example, let us consider a tetrameric voltage-gated cation-selective channel that has three effective sensing charges per subunit and that reaches half of its maximum activity at 0 mV. Assuming that it does not inactivate, this channel will be at 0.1% of its maximum activity when the membrane potential is −60 mV, while reaching about 99% of its maximum at a membrane

potential of +40 mV. These activity levels will be reached at the respective membrane potential levels regardless of the history of the channel's activity. This voltage sensitivity remains unaltered over time.

Like in the example of the hypothetical receptor discussed above, it is commonly thought that the activity-vs.-voltage relationship that describes the behavior of voltage-gated channels is a static function of the membrane potential. However, a growing body of evidence shows that the electrical sensitivity of voltage-gated channels can be dynamic rather than static. This dynamic character of the voltage dependence seems to be rooted in the hysteretic behavior of channels and has important consequences on the physiology and pharmacology of these proteins. Therefore, hysteresis seems to play a critical role in the generation and modulation of electrical signal events in neurons, muscles, and other excitable tissues.

HOW COULD HYSTERESIS AFFECT ELECTRICAL SIGNALING IN CELLS?

Let us consider the simple case of an excitable cell that expresses a prototypic sodium-selective voltage-gated (Na_V) channel and a prototypic potassium-selective voltage-gated (K_V) channel. In addition, let us also consider that the cell has a basal, non-voltage-dependent conductance that is mostly selective for K^+ ions. Upon reaching a threshold potential following a depolarizing stimulus, the action of Na_V channels will further depolarize the membrane. Then, while Na_V channels inactivate, the activity of K_V channels will start to repolarize the membrane, counteracting the Na_V-driven depolarization. As the membrane gradually returns to more negative voltages, K_V channels start to close. This decreases the voltage-dependent K^+ conductance of the membrane as it crawls back to its resting potential. In this case, the basal conductance of the membrane becomes critical in completing the repolarization process. This is the classical view of the development of an action potential (AP), derived from the outstanding work of Hodgkin and Huxley (1952).

On the other hand, in a more modern view, the voltage dependence of K_V channels is dynamic and shifts to more negative potentials following activation. In this case, hysteresis manifests as Dynamic Voltage Dependence (DVD) of K_V channel activity and makes the repolarization a more robust process. This is because transiently shifting the K_V channel's voltage dependence to more negative potentials would provide a steadier K^+ conductance as the membrane potential nears its resting values and beyond. Therefore, it is likely that this hysteretic behavior is essential for the generation and stability of cellular electrical signaling. Hysteresis in their behavior can make the deactivation of K_V-related conductance more resilient to closing at resting and to developing hyperpolarized potentials during repolarization.

Based on the previous example, it is clear that hysteresis is an important property of voltage-gated channels. Thus, understanding the mechanism of this phenomenon will be essential for a comprehensive study of channel activity. To start, this review will provide a definition of hysteresis in terms of voltage-gated channel activity.

WHAT IS HYSTERESIS?

The term hysteresis derives from the Greek ὑστέρησις, meaning "lagging behind." The term was used in 1881 by Sir James Alfred Ewing to describe the effect of magnetization on current induction in a conductor (Ewing, 1882). Subsequent studies showed one of today's best-known examples of hysteresis: the magnetization of a ferromagnetic material. Let us consider a sample of a ferromagnetic material (e.g., iron, a screwdriver) and impose a magnetic field across the sample. This results in magnetization of the sample, which will remain magnetically polarized even when the external field is removed. This means that the material "remembers" that it was magnetized. If the sample is allowed to rest for a long time or if it is heated up, then the magnetization will be lost. Overall, once the external field is removed, the material will still remember that it has been magnetized and remain magnetized for a finite time.

Extending the previous example, let us consider the following steps in a thought experiment: 1) apply a magnetic external field, 2) remove the field, and 3) reapply the external magnetic field in the reverse direction. Respectively, the outcomes of each step in this experiment will be that: 1) the material will be magnetically polarized, 2) it will remain magnetized, and 3) the magnetization will be reverted. As it can be seen by the outcome of step 2, the material will resist giving up its magnetization, even when the external magnetic field has been removed. Yet, this magnetic polarity can be reverted by applying a magnetic field in the reverse direction. Further extending this example, let us consider cyclically imposing the external magnetic field in one direction and then the reverse direction. Because the material resists giving up its polarity, what would be observed is that the amplitude and direction of the magnetization will be trailing behind with respect to the external magnetic field. The observance of this lagging response resulted in the coinage of the term "hysteresis."

PHYSIOLOGICAL ROLE OF HYSTERESIS

Ion channels are a critical component of the plasma membrane in all known living beings. These proteins are responsible for the generation of electrical activity in cells, which is essential for many biological processes. The physiological relevance of hysteresis remains elusive. However, the voltage dependence of several K_V channels shifts to more negative potentials following activation, displaying a behavior analogous to that of ferromagnetic materials. This lagging change in voltage dependence can be seen as an "on-demand" fine-tuning of channels' responsiveness during the generation of electrical signals. So, K_V channel closing happens when the membrane potential goes to further negative voltages, guaranteeing that the membrane's K^+ conductance will remain activated during repolarization.

Another interesting consequence of DVD is that the voltage dependence for activation is shifted towards more positive potentials while the K_V channels are closed at the resting potential. This may likely facilitate the triggering of an electrical signal by keeping the voltage-dependent K^+

conductance of the membrane relatively low as the depolarizing conductances are initiated (i.e., Na^+ and Ca^{2+} conductance). Therefore, DVD may constitute a molecular strategy that has evolved to facilitate the initial triggering of fast electrical signals and to ensure their prompt termination. Furthermore, if Na_V channels were to display hysteresis, this will also contribute to preventing reactivation of the Na^+ conductance during the inactivation process (since recovering from inactivation of the Na_V channels would require further repolarization of the membrane).

The observed "inertia" in the responsiveness of K_V channels, which is driven by changes in their electrical sensitivity, resembles that of ferromagnetic materials displaying hysteresis. In this case, the term "sensitivity" refers to the range of potential at which the channel changes, rather than the amount of change. So, it can be argued that hysteresis in the activity of K_V channels can make them harder to open when they are closed and harder to close when they are open. One example of this behavior is that of the potassium channel K_V3. These channels have a half-maximum potential for current activation above 0 mV (Kaczmarek and Zhang, 2017). Also, K_V3 channels have very fast deactivation kinetics that make them particularly suitable for high frequency firing of APs (Rudy et al., 1999; Rudy and McBain, 2001; Lien and Jonas, 2003; Kaczmarek and Zhang, 2017). In addition to these properties, it has been shown that $K_V3.1b$ channels display a remarkable shift in their voltage dependence for sensing charge movement (gating currents) of about −60 mV following activation (Labro et al., 2015). This shift favors channel opening during repolarization. This shift in the voltage-dependence of the channels results in a notable decrease in the deactivation rate kinetic of their conduction, guaranteeing a quick and efficient repolarization of the membrane (Labro et al., 2015).

In summary, hysteresis in the activity of voltage-gated channels can have remarkable consequences in the generation of APs. Thus, comprehensive study on the fundamentals of this process could lead to a novel perspective on the understanding of voltage-gated channel activity in cellular electrical signaling.

CANDIDATE MECHANISMS FOR HYSTERESIS IN S4-VOLTAGE-SENSING DOMAIN PROTEINS

The activity of ion channels can be defined by at least the following two general parameters: 1) the probability of channels to be open and 2) their ability to conduct and discriminate ions. This review will focus on the first of these general parameters.

Voltage-gated channels are so called because the probability of these channels to be open (open probability, P_O) is a function of the difference in electrical potential across the membrane. There are several types of voltage-gated channels. Here, the focus of the review will be on channels containing a voltage-sensing domain (VSD) made of four transmembrane helical segments (S1–S4), with the fourth segment (S4) bearing the main voltage-sensing charges. This type of voltage-gated channels are referred to as "S4-based voltage-gated channels," or "S4-VSD channels."

Evidence for hysteresis in S4-VSD channels dates from the early 1980s, when it was described for the sodium conductance that is observed in the squid giant axon (Bezanilla et al., 1982). It was shown that the voltage dependence for sensing charge movement is dependent on the holding potential, shifting to more negative potentials when the membrane was held at 0 mV instead of −70 mV. Analogous to the case of magnetization of a ferromagnetic material, the return of gating charges back to their resting state required bringing the membrane to more negative potentials when the membrane was initially held at 0 mV.

Similar observations were made over a decade later with the potassium-selective voltage-gated channel known as "Shaker" (Olcese et al., 1997; Lacroix et al., 2011). Like that of the squid axon's sodium conductance, the voltage-dependence for charge movement of Shaker was sensitive to the holding potential. In this case, the voltage dependence for gating charge movement was displaced approximately 25 mV towards more negative voltages when the holding potential was set at 0 mV instead of −90 mV (Olcese et al., 1997). Later research showed that the change in voltage dependence was overestimated due to a remarkable decrease in the rate of deactivation (Lacroix et al., 2011). Nonetheless, at that time, it was proposed that the channels could either be in a "permissive" or "reluctant" conformation (Olcese et al., 1997). In the "permissive" conformation, the channel was able to be activated and charges were readily moved. In the "reluctant" conformation, the channel was inactivated and charge movement was slow, requiring further hyperpolarization of the membrane. Adopting the "reluctant" state was associated with the slow inactivation of Shaker (Olcese et al., 1997). As the inactivated state is reached after the open state, it becomes more thermodynamically stable. This would make the open state a "transitory" or "meta-stable" state. From this idea, it can be concluded that bringing the channel out of a stable state could require more energy than was needed to move the charges in the first place (Villalba-Galea, 2017).

Another interesting aspect of Shaker is that the channels in the "permissive" and "reluctant" conformations are considered to be in separate interconvertible populations, where the fraction of channels in each of those populations are dependent on the holding potential (Olcese et al., 1997). The fact that there are two populations means that the activity of the VSD can adopt to "modes of operation." To illustrate this idea, let us consider a voltage-dependent channel that has two states: closed and open (**Figure 1A**, top). Following activation from an initial holding potential ($V_{0.1,ini}$) to a given potential that will bring it to 90% of activity (V_{90}), the channels can switch to another "mode of activity" with a different sensitivity to the membrane potential (**Figure 1A**, bottom). In this new mode, the membrane must be set at a potential ($V_{0.1,switched}$) that is more negative than $V_{0.1,ini}$ in order to bring the channel to the initial activity level (**Figure 1B**).

For many years, changes in the voltage dependence for charge movement in Shaker was linked to slow inactivation, which was thought to be due to conformational rearrangements in the pore domain. However, studies of charge movement in the voltage-

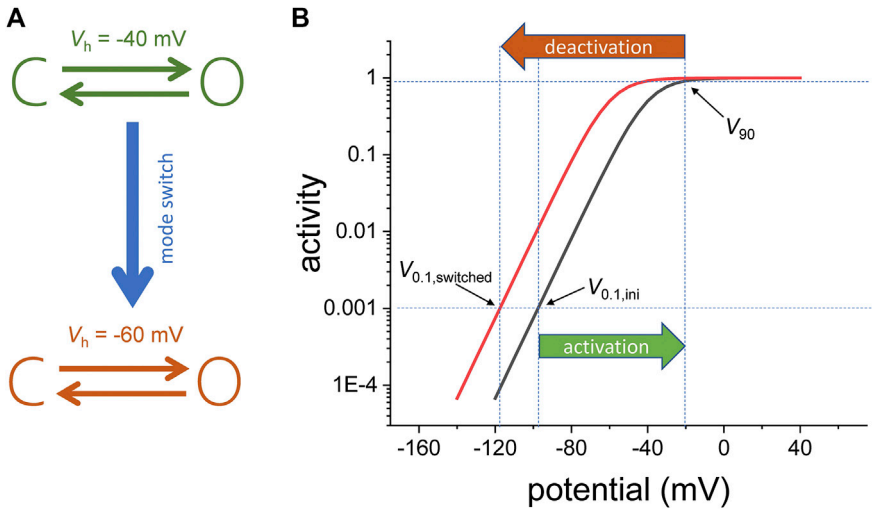

FIGURE 1 | (A) Voltage dependence model for a channel consisting of one closed (C) and one open (O) state. Following activation, the two-state model switches from one mode of activity to another. For the initial mode, the voltage the half-maximum potential (V_h) is –40 mV. For the final mode, V_h is –60 mV. **(B)** Semi-log plot of the activity (fraction of the open channels). Due to the mode switch, the change in the potential needed to drive the fraction of open channels from 0.001 to 0.9 ($|V_{90}–V_{0.1,ini}|$) is smaller in magnitude that the change in potential required to bring the fraction of open channels back to 0.001($|V_{0.1,switched}–V_{90}$). The indices 0.1 and 90 refer to 0.1 and 90% of the channel population, respectively.

sensitive phosphatase isolated from *Ciona intestinalis* (Ci-VSP) provided evidence demonstrating that DVD can be a phenomenon intrinsic of a S4-VSD (Villalba-Galea et al., 2008; Akemann et al., 2009; Villalba-Galea et al., 2009b). The voltage-controlled enzyme Ci-VSP is a dimeric protein that is made of a S4-VSD that is homologous to that of voltage-gated channels (Murata et al., 2005; Murata and Okamura, 2007; Sakata and Okamura, 2019). The VSD is linked to the phosphoinositide phosphate domain through a phospholipid/phosphoinositide binding motif (Villalba-Galea et al., 2009a; Kohout et al., 2010; Hobiger et al., 2012; Hobiger et al., 2013). The action of the VSD confers voltage sensitivity to the VSP's enzymatic activity through a mechanism that remains under debate (Villalba-Galea, 2012a; Villalba-Galea, 2012b; Sakata and Okamura, 2019).

Under voltage-clamp, sensing currents can be observed during the activation of a VSD. These currents are due to the movement of sensing charges in the VSD, analogous to gating currents in voltage-gated channels (Sakata and Okamura, 2019). In the case of Ci-VSP, the voltage dependence for charge movement shifts about −50 mV when holding the membrane potential at +80 mV instead of −60 mV or more negative voltages. Furthermore, deletion of the phosphoinositide phosphate domain of Ci-VSP causes a larger shift in voltage dependence for sensing charge movement following relaxation. Such shift that nearly doubled that of the intact enzyme (Villalba-Galea et al., 2008). This observation indicates that an isolated VSD can shift its voltage dependence without being coupled to another domain. Determining whether the interaction between the two VSDs causes a shift in voltage dependence has yet to be ruled out. Yet, more recent studies expressing the isolated VSD of Shaker shows that this type of domain can display an intrinsic hysteretic behavior (Zhao and Blunck, 2016).

VOLTAGE-SENSING DOMAIN RELAXATION

Another important aspect of the DVD concept is that changes in the voltage-dependence do not occur instantaneously. Instead, the displacement of the activity-vs.-potential relationship towards negative voltages is a process that can take time (Villalba-Galea et al., 2008; Villalba-Galea et al., 2009b; Villalba-Galea, 2017). In the case of Ci-VSP, the shift in voltage dependence has been proposed to occur through a process termed "VSD relaxation" (Villalba-Galea et al., 2008). In Ci-VSP, VSD relaxation can take seconds, indicating that it continues even after sensing currents have ended. This suggests that VSD relaxation is an intrinsically voltage-independent process.

VSD relaxation is not unique to Ci-VSP or Shaker—it can be observed in other S4-VSD proteins such as Hyperpolarization-activated Cyclic Nucleotide-gated (HCN) channels (Mannikko et al., 2005; Elinder et al., 2006; Bruening-Wright and Larsson, 2007) and the human Ether-à-go-go-Related Gene channel (Pennefather et al., 1998; Piper et al., 2003; Thouta et al., 2017; Shi et al., 2019; Shi et al., 2020). In these cases, VSD relaxation has been proposed to play an important role in the remarkable hysteretic behavior observed in these proteins. For HCN channels, hysteresis is manifested as a process called "mode shift" (Mannikko et al., 2005; Elinder et al., 2006). As the term implies, the concept is that channels can adopt one of at least two discrete modes of activity as a function of the membrane potential. The same idea seems to apply to VSD relaxation.

For Shaker, the charge-vs.-potential (Q-V) curves show two populations of charges moving with distinct voltage sensitivity (Olcese et al., 1997). Furthermore, the fraction of the total charge in each mode is a function of the holding membrane potential. This indicates that modes of activity in a VSD also are likely discrete sets of states, that channel activity can have more than one of these modes of activity, and that channels can adopt any of these modes one at a time.

VOLTAGE-SENSING IN S4-VOLTAGE-SENSING DOMAIN CHANNELS

The prototypic S4-based voltage sensor consists of four transmembrane (S1–S4) segments with S2, S3, and S4 segments containing charged residues (Islas, 2016). Typically, S2 and S3 segments bear 1 or 2 negative charges each, in the form of aspartate or glutamate residues. In contrast, the S4 segment contains positive charges in the form of arginine, lysine, and histidine residues. The current understanding is that the VSD charges, mainly those of the S4 segment, are displaced as a function of the membrane potential. In other words, the electrical gradient across the membrane does work on the VSD charges, leading to the rearrangement of the VSD. On this idea, let us consider the electrical field across the plasma membrane that does electrical work on the sensing charges, which can be calculated as:

$$W_{ELECT} = \sum_i \int_{a_i}^{b_i} Q_i E(r_i) dr \tag{1}$$

This means that the total electrical work (W_{ELECT}) is the sum of the work done on each charge. The work done by the electrical field on the *i*-th charge (Q_i) is given by the integral of the magnitude of that charge multiplied by the electrical field $E(r_i)$ as a function of the position of the charge (r_i). The integral is calculated between position a_i and b_i, which respectively represent the initial and final positions of the i-th charge.

$$W_{ELECT} = \int_{a_1}^{b_1} Q_1 E(r_1) dr + \int_{a_2}^{b_2} Q_2 E(r_2) dr + \ldots + \int_{a_n}^{b_n} Q_n E(r_n) dr \tag{2}$$

This equation seems difficult to resolve, as the electrical field E is a function of the position of the charge. However, it can be simplified when making some assumptions on the structure and functioning of a prototypic S4-VSD. These assumptions are as follows:

In terms of the VSD structure, the prototypical S4-based VSD consists of the four transmembrane helices arranged in a bundle that forms two crevices—one on each side of the membrane. These two crevices are separated by a small hydrophobic volume (Starace et al., 1997; Starace and Bezanilla, 2001; Starace and Bezanilla, 2004; Ahern and Horn, 2005). This region is commonly referred to as the "hydrophobic plug," also known more precisely as the "hydrophobic gasket." Structural evidence shows that the hydrophobic gasket is a few Angstroms thick, only hosting one charge residue at a time. Consequently, it can be assumed that some of the S4 segment charge residues can cross the entire electrical field.

In terms of the VSD functioning, several S4-VSD proteins have been shown to have a conductance through their VSD when some of their residues are replaced. To illustrate this, let us consider the case of Shaker. Replacing the S4-segment arginine located at positions 362, 365, 368, and 371 with histidine results in voltage-dependent proton conductance through the channel's VSD itself (Starace et al., 1997; Starace and Bezanilla, 2001; Starace and Bezanilla, 2004). In the particular case of mutation R362H and R371H, proton currents are observed only at the resting and activated conformations of the VSD, respectively. In contrast, the mutants R365H and R368H mediate a proton conductance when the VSD is residing in intermediate states between the fully rested or fully activated positions. These implies that residues R362 through R371—hereafter R1 through R4—can reside in the hydrophobic gasket, having access to both the intracellular and extracellular side of the membrane. Furthermore, this also implies that R365H and R368H—hereafter R2 and R3—cross the entire field. Therefore, in a channel like Shaker, the total number of charges per VSD on which the electrical field is acted on is between 2 and 4 elementary charges. Using **Eq. 2**, we can state that,

$$W_{ELECT} = \int_{a_1}^{b_1} Q_1 E(r_1) dr + \int_{a_2}^{b_2} Q_2 E(r_2) dr + \int_{a_3}^{b_3} Q_3 E(r_3) dr + \int_{a_4}^{b_4} Q_4 E(r_4) dr \tag{3}$$

Since each charge is an elementary charge, all Q_i are equal and will be called Q_e. Replacing and rearranging **Eq. 3** yields:

$$W_{ELECT} = Q_e \left(\int_{a_1}^{b_1} E(r_1) dr + \int_{a_2}^{b_2} E(r_2) dr + \int_{a_3}^{b_3} E(r_3) dr + \int_{a_4}^{b_4} E(r_4) dr \right) \tag{4}$$

If the field across the hydrophobic gasket is assumed to be constant, each of the terms within the parenthesis would be:

$$\int_{a_i}^{b_i} E(r_i) dr = \delta_i \Delta V_M \tag{5}$$

In **Eq. 5**, ΔV_M is the difference between the initial and the final membrane potential; δ corresponds to the fraction of the electric field that each charge crossed. In the case of charges R2 and R3, assume that they both cross the entire electric field, resulting in the term δ_i equal to 1. In the case of charges R1 and R4, the term would be within 0 and 1. Taking these assumptions into account, replacing **Eq. 5** into **Eq. 4** yields:

$$2Q_e \Delta V_M < W_{ELECT} < 4Q_e \Delta V_M \tag{6}$$

To put this in the context of a typical voltage-clamp experiment, let us consider that the membrane is held at

−90 mV and an activating pulse is applied to +10 mV. This will make ΔV_M equal to +100 mV. Note that the range of potential considered for this example allows for a meaningful displacement of the sensing charges that are driven by the electric field—if the charges do not move, then no electrical work is done. The activation of four VSDs will result in an overall electrical work ranging between 7.71 × 104 and 1.15 × 105 J/mol (between 18 and 37 kCal/mol). Since both R1 and R4 can gain access to both the intracellular and extracellular crevice of the VSD, it is unproven but likely that these residues cross at least half of the electric field. For this reason, it can be stated that the electric field does work on the equivalent of three elementary charge per VSD, meaning that the total electrical work is approximately $3Q_e\Delta V_M$. Consistently, experimental data, kinetic modeling, and estimation of the free energy show that the activation of Shaker involves at least 13 charges, or 3.25 charges per VSD. This translates into a total work of about 30 kCal/mol during activation (or deactivation) of the four VSDs.

To put this in perspective, let us consider that gating currents for Shaker are a simple two-state system, with R being the resting state and A being the activated state. Assuming this system, we calculate the equilibrium constant (also known as the Boltzmann distribution) for R and A as follows:

$$k_{eq} = \frac{A}{R} = e^{\frac{-W_{ELECT}+\Delta G_C}{k_B T}} \tag{7}$$

Assuming that the free energy of activation ΔG_C is −14 kCal/mol and that there are 3.25 charges per VSD, the ratio R/A that is given by the Boltzmann distribution (**Eq. 7**) will be 8.6 × 10−^{4} and 4.2 × 102 at −100 and 0 mV, respectively. This involves a 5.7-order-of-magnitude increase in the activity of each VSD. Putting this observation in more familiar terms, the fraction of activated VSD can be calculated as,

$$f_A = \frac{A}{A+B} \;\Rightarrow\; f_A = \frac{k_{eq}}{k_{eq}+1} \tag{8}$$

Replacing and rearranging **Eq. 7** into **Eq. 8** yields a Fermi-Dirac distribution:

$$\frac{k_{eq}}{k_{eq}+1} = \frac{1}{1+e^{\frac{-W_{ELECT}+\Delta G_C}{k_B T}}} \tag{9}$$

Because W_{ELECT} is proportional to the sensing charge (**Eq. 6**) and ΔG_C is proportional to the total charge, **Eq. 9** can be re-written as,

$$f_A = \frac{1}{1+e^{\frac{-zQ_e(\Delta V-\Delta V_C)}{k_B T}}} \tag{10}$$

Notice that the Fermi-Dirac distribution is transformed into what is commonly referred to as the "Boltzmann distribution." It is important to highlight that the term "Boltzmann distribution," which has been used in electrophysiology for many years, is a misnomer. The ratio between the active and resting states is the correct way to refer to a Boltzmann distribution for a 2-state model (like in **Eq. 7**). The fraction of the distribution representing the open state is the correct way to refer to a Fermi-Dirac distribution (like in **Eq. 10**).

The exponential term $zQ_e\Delta V_C$ in **Eq. 10** represents the magnitude of the free energy of activation for a VSD, where z represents the number of elementary charges and Qe represents the elementary charge. This is only true if the VSD behaves as a two-state system—an elegant procedure that has been described by Chowdhury and Chanda (2012). The basic Boltzmann and Fermi-Dirac distributions alluded here formally describe systems with two discrete states. However, in the case of voltage-gated channels, the existence of multiple interconnected states has been well-established. Thus, describing their behavior requires more elaborate functions. Yet, these equations can provide meaningful approximations when using a suitable charge value. So, the change in free energy following VSD relaxation is given by:

$$\Delta G_{RELAX} = zQ_e\left(\Delta V_{C,ACT} - \Delta V_{C,RELAX}\right) \tag{11}$$

According to **Eq. 11**, when considering a total of 3.25 elementary charges per VSD, there is a change of −2.98 kCal/mol for every 10 mV of voltage-dependence displacement.

DYNAMIC KINETICS AND HYSTERESIS

The HCN channel isolated from the sea urchin *Strongylocentrotus purpuratus* (spHCN) shows activity with at least two modes, which are populated as a function of the holding potential and a function of the duration of activation (Mannikko et al., 2005; Bruening-Wright and Larsson, 2007). In either mode, channels undergo a mode shift. Another important observation is that the deactivation becomes slower as the channels are kept activated. Likewise, the activation becomes faster as a function of how recently they were last activated. In both cases, "remembering" the event in the near past conditions the behavior of the channel—a hallmark of hysteresis. This shows that it is possible to observe a voltage-dependent conformational change in the channel, which can bring it to a short-lived transient state referred to as a "meta-stable state." Particularly, in channels with slow inactivation, the open/activated set of states reached following activation corresponds to meta-stable states. On the other hand, prolonging the activation of the channels lead to a set of inactivated or low-activity states which corresponds to stable states.

From a meta-stable state, a channel can transition into a more stable state, reaching steady state. To illustrate this idea, consider a deactivated channel in steady state at a given holding potential (e.g., human Ether-à-go-go-Related Gene and −90 mV or spHCN at 0 mV). Then, change the potential to a voltage that activates the channel. Focusing on the gating currents, the VSD will first be brought out of its steady state conformation arrangement as the electric field does work on the sensing charges. If this process is thermodynamically reversible in infinitesimal steps, then returning to its original resting state will occur with no changes to its surroundings. Thus, the path back to the resting state will be unaltered. This is likely not the case for voltage-gated channels, because the sudden change in the electrical field (e.g.,

~1 × 108 V/m for a 100-mV change) would result in a rapid rearrangement of the protein—a product that would not be in thermodynamic equilibrium (approx. 1 megawatts, assuming a 20 ms charge movement). In addition, it is likely that many intramolecular and intermolecular interactions are to take place, given that the channel and its surroundings are composed of condensed matter. In this view, the activation could lead the channel into a meta-stable open conformation, from which it would eventually "relax" into a stable arrangement. If this is the case, it would then be expected that deactivation will also be slower from the stable state compared to the meta-stable state.

Although the existence of such conformations remains a matter of debate, electrophysiological studies have provided examples of supporting evidence. In fact, several voltage-gated channels demonstrate this feature in their respective activity. For instance, prolonging the activation of HCN, Shaker, and K_V3.1b leads to a decrease in the rate of deactivation for both gating currents and ionic currents (Mannikko et al., 2005; Elinder et al., 2006; Bruening-Wright and Larsson, 2007; Lacroix et al., 2011; Labro et al., 2012; Priest et al., 2013; Labro et al., 2015; Zhao and Blunck, 2016). Others, like K_V7.2 and K_V7.2/K_V7.3 channels, undergo remarkable decreases in their rate of deactivation as a function of activation (Corbin-Leftwich et al., 2016). This indicates that the activated/open state that is observed in the study of any voltage-gated channel immediately after depolarization may not be in a thermodynamically stable state.

IMPLICATIONS OF HYSTERESIS TO THE CURRENT UNDERSTANDING OF S4-VOLTAGE-SENSING DOMAIN PROTEIN FUNCTION

One remarkable instance is K_V3.1b, which undergoes a fast VSD relaxation that enables a resurgent current during deactivation ("hooked tail") (Labro et al., 2015). Under voltage-clamp, activation by a pulse to positive values readily activates the channel. Then, returning to a moderate negative potential (−40 or −50 mV) results in a transient increase in the conductance. This occurs because the VSD quickly relaxes as it is activated, shifting its voltage-dependence to more negative potentials. This phenomenon has strong physiological implications because the rising of a "hooked tail" current during deactivation yields a transient increase in repolarizing power, securing the repolarization of the plasma membrane even after a brief depolarization (Labro et al., 2015). From a generalizing angle, it can be said that this kind of mechanism prevents K_+-selective voltage-gated channels from rapidly closing, since their own activity repolarized the membrane and caused them to deactivate themselves.

As another example, mode shift in HCN channels seems to be essential to their role in pace-making. In essence, the activation of HCN currents leads to the depolarization of the membrane and eventual triggering of an electrical event (e.g., an AP in the sinoatrial node) (Elinder et al., 2006). As the AP develops, the voltage-dependence of HCN channels shifts mode to one in which activation occurs at more negative potentials. Thus, HCN currents are not readily activated during repolarization. Instead, the activation of the channels is delayed. In the meantime, as the membrane becomes negative, the voltage-dependence for HCN-current activation switches to more positive voltages. At this point, HCN reactivates and currents drive depolarization, so the cycle starts anew.

In the previous two cases, the observance of DVD in the activity of K_V3.1b and HCN channels guarantees that they are activated when they are "most needed." A slightly different strategy seems to have evolved with members of the K_V7 family. For both the homomeric K_V7.2 and the heteromeric K_V7.2/K_V7.3 channels, the deactivation rate decreases as the channels are held activated. However, the response of these channels to depolarization is slower than the duration of the stereotypical neuronal AP (Corbin-Leftwich et al., 2016). Furthermore, the time required to observe a change in the deactivation rate is in the order of tens of milliseconds. Thus, it seems that hysteresis would not have a major role in the response of these channels to the AP under physiological conditions. Instead, the role of hysteresis seems to be at steady state. K_V7.2 and K_V7.2/K_V7.3 channels display meaningful activity at the typical resting membrane potentials (between −40 and −60 mV) (Jentsch, 2000; Cooper, 2012). In steady state at these potentials, the homomeric K_V7.2 and the heteromeric K_V7.2/K_V7.3 channels change their mode of activation so that their deactivation becomes much slower (~7-fold) than that of channels activated by depolarizing pulses, even those as strong as +40 mV in amplitude with a duration of 100 ms (Corbin-Leftwich et al., 2016). Thus, hysteresis plays a role in stabilizing open channels so that they will be resilient to deactivation when they are the most needed.

STOCHASTICITY, REVERSIBILITY, AND HYSTERESIS

Since the future behavior of a hysteretic system is affected by the past, this implies that voltage-gated channels displaying hysteresis will "remember" what happened in the past. As a result, they are said to have a short-term "memory." The idea that hysteresis confers "memory" to a system directly collides with two well-accepted concepts in ion channel function: 1) that channels seems to behave stochastically, and 2) that channel activity is thermodynamically reversible (except for the fibrosis transmembrane conductance regulator and similar molecules) (Csanady et al., 2010). One of the fundamental assumptions regarding the first concept is that channels adopt discrete states—transitions between these states depend only on the current state (Colquhoun and Hawkes, 1977). In other words, transitions are "memoryless" events. This property seems to sit diametrically opposite from the process of hysteresis that have been discussed above.

However, these two types of process are compatible. The "lack of memory" of a stochastic process suggests that the current state

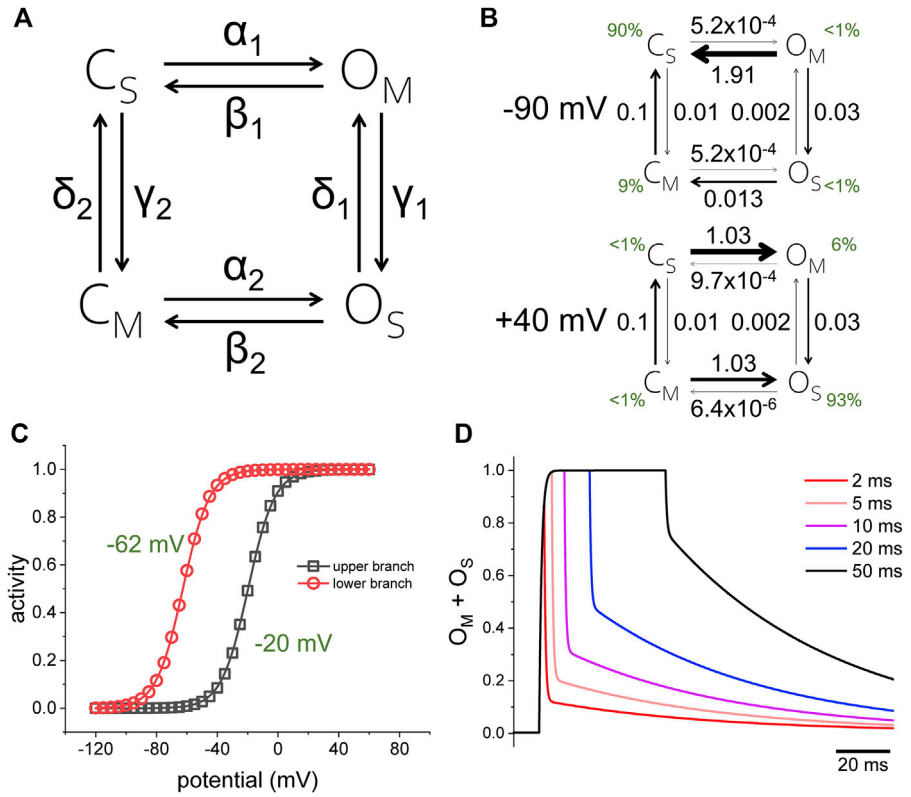

FIGURE 2 | (A) Four-state model for channel activity displaying hysteresis. The rates α and β are functions of the membrane potential; the rates γ and δ are voltage independent. The top and bottom branches of the model as partially isolated from each other by making the rates γ and δ small and constant. **(B)** Voltage-dependence for the top and bottom branch when calculated in isolation (making rates γ and δ equal to zero). **(C)** Rate constants for the model when the membrane potential was either −90 mV **(top)** or +40 mV **(bottom)**. Rate coefficients can be found in **Table 1**. **(D)** Simulation of the model applying +40-mV pulses of different duration (2, 5, 10, 20, and 50 ms). As the activation was prolonged, the temporal profile of deactivation changed, becoming slower. The rates α_i and β_i were defined by the functions $\alpha_i = \alpha_{0,i}e^{1.5FV/RT}$ and $\beta_i = \beta_{0,i}e^{-1.5FV/RT}$, respectively. The model assumes a charge of 1.5 e- associated with each voltage-dependent rate.

TABLE 1 | Rate coefficients for the four-state model in **Figure 2**.

Coefficient	Value (ms^{-1})	Coefficient	Value (ms^{-1})
$\alpha_{0,1}$	0.100	$\alpha_{0,2}$	0.1000
$\beta_{0,1}$	0.010	$\beta_{0,2}$	0.0001
γ_1	0.030	γ_2	0.0100
δ_1	0.002	δ_2	0.1000

is the only influence on the probability of a channel to transition states and on what that new state would be—what happened in the past is irrelevant (Colquhoun and Hawkes, 1977). However, the presence of hysteresis does not rely on whether the transition possesses memory or not. Instead, hysteresis exists when there is more than one pathway from one set of states to another, where one set of states can be made of a single state (Villalba-Galea, 2017).

To illustrate how a stochastic process can also display hysteresis, let us consider a model containing two sets of closed and open states, C and O, which are alternatingly stable (subscripted with a "S") and meta-stable (subscripted with a "M") (**Figure 2A**, rate coefficients in **Table 1**). The potential of half-maximum activity (V_h) for the top branch of the model is −20 mV; for the bottom branch, V_h is −65 mV (**Figures 2A,B**). Both branches are connected through voltage independent transitions. In steady state at −90 mV, the rates favor the population of states C_S and C_M, with C_S constituting 90% of the population (**Figure 2C**, top, green digits). On the other hand, in steady state at +40 mV, state O_M and O_S are most favored, with O_S making up 93% of the population (**Figure 2C**, bottom, green digits). To reach state O_S during activation, the model must go through either C_M or O_M. At +40 mV, the rate α_1 is 2 orders of magnitude larger than the rate γ_1, thus the activation preferentially proceeds through the top branch. When returning to −90 mV, the rate β_2 is six times larger than $\delta 1$, thus deactivation proceeds preferentially through the lower branch in a 1 to 7 ratio. This indicates that this stochastic model follows a preferred direction. This explanation applies only to channels that are in steady state. The situation is different in channels before reaching steady state. To illustrate this idea, let us consider that deactivation in the top branch is 146 times faster than in the bottom branch. Following activation at +40 mV, the overall speed of deactivation changes as a function of the time that the model was kept activated. This model shows that prolonging the duration of the activation results in a decrease in the deactivation kinetics, as deactivation from O_M is faster than from O_S.

Another important issue is reversibility. In the case of the hypothetical model considered here (**Figure 2**), reversibility is guaranteed, as the product of the coefficient rates in one direction of the cycle is equal to the coefficient rate in the opposite direction (Onsager, 1931). In addition, the total sensing charge mobilized in the top branch is equal to the total sensing charge mobilized in the bottom branch. Therefore, the example presented here is a stochastic reversible model that presents a preferred directing and changing kinetic of deactivation as a function of the duration of activation.

HYSTERESIS AND CHANNEL STRUCTURES

Structural models of voltage-gated channels obtained from crystallography studies likely represent stable conformations of these proteins in the absence of an electric field (at 0 mV). Furthermore, the VSD in such models may likely be in a relaxed state of the domain. This implies that structures which are commonly regarded to be representing voltage-gated channels in activated states may likely instead be representing channels in a conformation that is not the "short-lived" (meta-stable) open state. This would have implications in our understanding of the intramolecular interactions governing the activity of channels and of the intermolecular interactions of channels with modulatory subunits, signaling molecules, drugs, and other factors affecting their activity.

A FINAL THOUGHT

In general, hysteresis seems to dynamically adjust the voltage-sensitivity and kinetics to optimize channel function to match its physiological role. DVD, an example of hysteresis, may be mechanistically rooted in VSD relaxation and other processes found in the pore domain, intracellular domains, and auxiliary subunits. Although discussing these instances is beyond the scope of this review, it is important to mention a few examples for a more complete understanding. These examples include: hysteresis in the proton-dependent activation of KcsA (Tilegenova et al., 2017), hysteresis in the binding of nucleotides in CNG channels (Nache et al., 2013), and hysteresis in the activity of TRP channels (Liu et al., 2011).

AUTHOR CONTRIBUTIONS

CV-G wrote the review article. AC contributed additional research content and improved interpretation of the writing.

ACKNOWLEDGMENTS

The authors thank Dr. Robert "Bob" Eisenberg for many interesting conversations, including those on the misnomering of equations, condense matter, and other concepts.

REFERENCES

Ahern, C. A., and Horn, R. (2005). Focused electric field across the voltage sensor of potassium channels. *Neuron* 48 (1), 25–29. doi:10.1016/j.neuron.2005.08.020

Akemann, W., Lundby, A., Mutoh, H., and Knöpfel, T. (2009). Effect of voltage sensitive fluorescent proteins on neuronal excitability. *Biophys. J.* 96 (10), 3959–3976. doi:10.1016/j.bpj.2009.02.046

Bezanilla, F., Taylor, R. E., and Fernández, J. M. (1982). Distribution and kinetics of membrane dielectric polarization. 1. Long-term inactivation of gating currents. *J. Gen. Physiol.* 79 (1), 21–40. doi:10.1085/jgp.79.1.21

Bruening-Wright, A., and Larsson, H. P. (2007). Slow conformational changes of the voltage sensor during the mode shift in hyperpolarization-activated cyclic-nucleotide-gated channels. *J. Neurosci.* 27 (2), 270–278. doi:10.1523/JNEUROSCI.3801-06.2007

Chowdhury, S., and Chanda, B. (2012). Estimating the voltage-dependent free energy change of ion channels using the median voltage for activation. *J. Gen. Physiol.* 139 (1), 3–17. doi:10.1085/jgp.201110722

Colquhoun, D., and Hawkes, A. G. (1977). Relaxation and fluctuations of membrane currents that flow through drug-operated channels. *Proc. R. Soc. Lond. B Biol. Sci.* 199 (1135), 231–262. doi:10.1098/rspb.1977.0137

Cooper, E. C. (2012). "Potassium channels (including KCNQ) and epilepsy," in *Jasper's basic mechanisms of the epilepsies*. 4th Edn. Editors J. L. Noebels, M. Avoli, M. A. Rogawski, R. W. Olsen, and A. V. Delgado-Escueta (Bethesda, MD: National Center for Biotechnology Information (US)). Available from: https://www.ncbi.nlm.nih.gov/books/NBK98164/

Corbin-Leftwich, A., Mossadeq, S. M., Ha, J., Ruchala, I., Le, A. H. N., and Villalba-Galea, C. A. (2016). Retigabine holds KV7 channels open and stabilizes the resting potential. *J. Gen. Physiol.* 147 (3), 229–241. doi:10.1085/jgp.201511517

Csanady, L., Vergani, P., and Gadsby, D. C. (2010). Strict coupling between CFTR's catalytic cycle and gating of its Cl^- ion pore revealed by distributions of open channel burst durations. *Proc. Natl. Acad. Sci. U. S. A.* 107 (3), 1241–1246. doi:10.1073/pnas.0911061107

Elinder, F., Männikkö, R., Pandey, S., and Larsson, H. P. (2006). Mode shifts in the voltage gating of the mouse and human HCN2 and HCN4 channels. *J Physiol.* 575 (Pt 2), 417–431. doi:10.1113/jphysiol.2006.110437

Ewing, J. A. (1882). On the production of transient electric currents in iron and steel conductors by twisting them when magnetised or by magnetising them when twisted. *Proc. R. Soc. Lond.* 33, 21–23. doi:10.1098/rspl.1881.0067

Hobiger, K., Utesch, T., Mroginski, M. A., and Friedrich, T. (2012). Coupling of Ci-VSP modules requires a combination of structure and electrostatics within the linker. *Biophys. J.* 102 (6), 1313–1322. doi:10.1016/j.bpj.2012.02.027

Hobiger, K., Utesch, T., Mroginski, M. A., Seebohm, G., and Friedrich, T. (2013). The linker pivot in Ci-VSP: the key to unlock catalysis. *PLoS One.* 8 (7), e70272. doi:10.1371/journal.pone.0070272

Hodgkin, A. L., and Huxley, A. F. (1952). A quantitative description of membrane current and its application to conduction and excitation in nerve. *J. Physiol.* 117 (4), 500–544. doi:10.1113/jphysiol.1952.sp004764

Islas, L. D. (2016). Functional diversity of potassium channel voltage-sensing domains. *Channels* 10 (3), 202–213. doi:10.1080/19336950.2016.1141842

Jentsch, T. J. (2000). Neuronal KCNQ potassium channels: physislogy and role in disease. *Nat. Rev. Neurosci.* 1 (1), 21–30. doi:10.1038/35036198

Kaczmarek, L. K., and Zhang, Y. (2017). Kv3 channels: enablers of rapid firing, neurotransmitter release, and neuronal endurance. *Physiol. Rev.* 97 (4), 1431–1468. doi:10.1152/physrev.00002.2017

Kohout, S. C., Bell, S. C., Liu, L., Xu, Q., Minor, D. L., Jr., and Isacoff, E. Y. (2010). Electrochemical coupling in the voltage-dependent phosphatase Ci-VSP. *Nat. Chem. Biol.* 6 (5), 369–375. doi:10.1038/nchembio.349

Labro, A. J., Lacroix, J. J., Villalba-Galea, C. A., Snyders, D. J., and Bezanilla, F. (2012). Molecular mechanism for depolarization-induced modulation of Kv channel closure. *J. Gen. Physiol.* 140 (5), 481–493. doi:10.1085/jgp.201210817

Labro, A. J., Priest, M. F., Lacroix, J. J., Snyders, D. J., and Bezanilla, F. (2015). Kv3.1 uses a timely resurgent K^+ current to secure action potential repolarization. *Nat. Commun.* 6, 10173. doi:10.1038/ncomms10173

Lacroix, J. J., Labro, A. J., and Bezanilla, F. (2011). Properties of deactivation gating currents in Shaker channels. *Biophys. J.* 100 (5), L28–L30. doi:10.1016/j.bpj.2011.01.043

Lien, C.-C., and Jonas, P. (2003). Kv3 potassium conductance is necessary and kinetically optimized for high-frequency action potential generation in hippocampal interneurons. *J. Neurosci.* 23 (6), 2058–2068. doi:10.1523/jneurosci.23-06-02058.2003

Liu, B., Yao, J., Zhu, M. X., and Qin, F. (2011). Hysteresis of gating underlines sensitization of TRPV3 channels. *J. Gen. Physiol.* 138 (5), 509–520. doi:10.1085/jgp.201110689

Männikkö, R., Pandey, S., Larsson, H. P., and Elinder, F. (2005). Hysteresis in the voltage dependence of HCN channels: conversion between two modes affects pacemaker properties. *J. Gen. Physiol.* 125 (3), 305–326. doi:10.1085/jgp.200409130

Murata, Y., Iwasaki, H., Sasaki, M., Inaba, K., and Okamura, Y. (2005). Phosphoinositide phosphatase activity coupled to an intrinsic voltage sensor. *Nature* 435 (7046), 1239–1243. doi:10.1038/nature03650

Murata, Y., and Okamura, Y. (2007). Depolarization activates the phosphoinositide phosphatase Ci-VSP, as detected in *Xenopus* oocytes coexpressing sensors of PIP_2. *J. Physiol.* 583 (Pt 3), 875–889. doi:10.1113/jphysiol.2007.134775

Nache, V., Eick, T., Schulz, E., Schmauder, R., and Benndorf, K. (2013). Hysteresis of ligand binding in $CNGA_2$ ion channels. *Nat. Commun.* 4, 2866. doi:10.1038/ncomms3866

Olcese, R., Latorre, R., Toro, L., Bezanilla, F., and Stefani, E. (1997). Correlation between charge movement and ionic current during slow inactivation in Shaker K^+ channels. *J. Gen. Physiol.* 110 (5), 579–589. doi:10.1085/jgp.110.5.579

Onsager, L. (1931). Reciprocal relations in irreversible processes. I. *Phys. Rev.* 37 (4), 405–426. doi:10.1103/PhysRev.37.405

Pennefather, P. S., Zhou, W., and DeCoursey, T. E. (1998). Idiosyncratic gating of HERG-like K^+ channels in microglia. *J. Gen. Physiol.* 111 (6), 795–805. doi:10.1085/jgp.111.6.795

Piper, D. R., Varghese, A., Sanguinetti, M. C., and Tristani-Firouzi, M. (2003). Gating currents associated with intramembrane charge displacement in HERG potassium channels. *Proc. Natl. Acad. Sci. U. S. A.* 100 (18), 10534–10539. doi:10.1073/pnas.1832721100

Priest, M. F., Lacroix, J. J., Villalba-Galea, C. A., and Bezanilla, F. (2013). S3-S4 linker length modulates the relaxed state of a voltage-gated potassium channel. *Biophys. J.* 105 (10), 2312–2322. doi:10.1016/j.bpj.2013.09.053

Rudy, B., Chow, A., Lau, D., Amarillo, Y., Ozaita, A., Saganich, M., et al. (1999). Contributions of Kv3 channels to neuronal excitability. *Ann. N. Y. Acad. Sci.* 868, 304–343. doi:10.1111/j.1749-6632.1999.tb11295.x

Rudy, B., and McBain, C. J. (2001). Kv3 channels: voltage-gated K^+ channels designed for high-frequency repetitive firing. *Trends Neurosci.* 24 (9), 517–526. doi:10.1016/s0166-2236(00)01892-0

Sakata, S., and Okamura, Y. (2019). Dynamic structural rearrangements and functional regulation of voltage-sensing phosphatase. *J. Physiol.* 597 (1), 29–40. doi:10.1113/JP274113

Shi, Y. P., Thouta, S., Cheng, Y. M., and Claydon, T. W. (2019). Extracellular protons accelerate hERG channel deactivation by destabilizing voltage sensor relaxation. *J. Gen. Physiol.* 151 (2), 231–246. doi:10.1085/jgp.201812137

Shi, Y. P., Thouta, S., and Claydon, T. W. (2020). Modulation of hERG K^+ channel deactivation by voltage sensor relaxation. *Front. Pharmacol.* 11, 139. doi:10.3389/fphar.2020.00139

Starace, D. M., and Bezanilla, F. (2001). Histidine scanning mutagenesis of basic residues of the S4 segment of the Shaker K^+ channel. *J. Gen. Physiol.* 117 (5), 469–490. doi:10.1085/jgp.117.5.469

Starace, D. M., and Bezanilla, F. (2004). A proton pore in a potassium channel voltage sensor reveals a focused electric field. *Nature* 427 (6974), 548–553. doi:10.1038/nature02270

Starace, D. M., Stefani, E., and Bezanilla, F. (1997). Voltage-dependent proton transport by the voltage sensor of the Shaker K^+ channel. *Neuron* 19 (6), 1319–1327. doi:10.1016/s0896-6273(00)80422-5

Thouta, S., Hull, C. M., Shi, Y. P., Sergeev, V., Young, J., Cheng, Y. M., et al. (2017). Stabilization of the activated hERG channel voltage sensor by depolarization involves the S4-S5 linker. *Biophys. J.* 112 (2), 300–312. doi:10.1016/j.bpj.2016.12.021

Tilegenova, C., Cortes, D. M., and Cuello, L. G. (2017). Hysteresis of KcsA potassium channel's activation- deactivation gating is caused by structural changes at the channel's selectivity filter. *Proc. Natl. Acad. Sci. U. S. A.* 114 (12), 3234–3239. doi:10.1073/pnas.1618101114

Villalba-Galea, C. A. (2012a). New insights in the activity of voltage sensitive phosphatases. *Cell. Signal.* 24 (8), 1541–1547. doi:10.1016/j.cellsig.2012.03.013

Villalba-Galea, C. A. (2012b). Voltage-controlled enzymes: the new *Janus Bifrons*. *Front. Pharmacol.* 3, 161. doi:10.3389/fphar.2012.00161

Villalba-Galea, C. A. (2017). Hysteresis in voltage-gated channels. *Channels* 11 (2), 140–155. doi:10.1080/19336950.2016.1243190

Villalba-Galea, C. A., Miceli, F., Taglialatela, M., and Bezanilla, F. (2009a). Coupling between the voltage-sensing and phosphatase domains of Ci-VSP. *J. Gen. Physiol.* 134 (1), 5–14. doi:10.1085/jgp.200910215

Villalba-Galea, C. A., Sandtner, W., Dimitrov, D., Mutoh, H., Knöpfel, T., and Bezanilla, F. (2009b). Charge movement of a voltage-sensitive fluorescent protein. *Biophys. J.* 96 (2), L19–L21. doi:10.1016/j.bpj.2008.11.003

Villalba-Galea, C. A., Sandtner, W., Starace, D. M., and Bezanilla, F. (2008). S4-based voltage sensors have three major conformations. *Proc. Natl. Acad. Sci. U. S. A.* 105 (46), 17600–17607. doi:10.1073/pnas.0807387105

Zhao, J., and Blunck, R. (2016). The isolated voltage sensing domain of the Shaker potassium channel forms a voltage-gated cation channel. *Elife* 5, e18130. doi:10.7554/eLife.18130

Conflict of Interest: The authors declare that the research was conducted in the absence of any commercial or financial relationships that could be construed as a potential conflict of interest.

Advantages of publishing in Frontiers

OPEN ACCESS
Articles are free to read for greatest visibility and readership

FAST PUBLICATION
Around 90 days from submission to decision

HIGH QUALITY PEER-REVIEW
Rigorous, collaborative, and constructive peer-review

TRANSPARENT PEER-REVIEW
Editors and reviewers acknowledged by name on published articles

Frontiers
Avenue du Tribunal-Fédéral 34
1005 Lausanne | Switzerland

Visit us: www.frontiersin.org
Contact us: frontiersin.org/about/contact

REPRODUCIBILITY OF RESEARCH
Support open data and methods to enhance research reproducibility

DIGITAL PUBLISHING
Articles designed for optimal readership across devices

FOLLOW US
@frontiersin

IMPACT METRICS
Advanced article metrics track visibility across digital media

EXTENSIVE PROMOTION
Marketing and promotion of impactful research

LOOP RESEARCH NETWORK
Our network increases your article's readership